



ordan Journal of



Biological Sciences

An International Peer-Reviewed Scientific Journal

Financed by the Scientific Research and Innovation Support Fund



http://jjbs.hu.edu.jo/

المجلة الأردنية للعلوم الحياتية Jordan Journal of Biological Sciences (JJBS)

http://jjbs.hu.edu.jo

Jordan Journal of Biological Sciences (JJBS) (ISSN: 1995–6673 (Print); 2307-7166 (Online)): An International Peer- Reviewed Open Access Research Journal financed by the Scientific Research and Innovation Support Fund, Ministry of Higher Education and Scientific Research, Jordan and published quarterly by the Deanship of Scientific Research , The Hashemite University, Jordan.

Editor-in-Chief

Professor Atoum, Manar F.

Molecular Biology and Genetics,

The Hashemite University

Assistant Editor

Dr. Muhannad, Massadeh I.

Microbial Biotechnology,

The Hashemite University

Editorial Board (Arranged alphabetically)

Professor Al-Eitan, Laith

Biotechnology and Genetic Engineering

Jordan University of Science and Technology

Professor Al-Khateeb, Wesam M.

Plant Genetics and Biotechnology

Yarmouk University

Professor Al-Ghzawi, Abdul Latief A.

Plant biotechnology

The Hashemite University

Professor Al-Najjar, Tariq Hasan Ahmad.

Marine Biology

The University of Jordan/ Agaba

Professor Khleifat, Khaled M.

Microbiology and Biotechnology

Mutah University

Professor Odat, Nidal

Plant biodiversity

Al Balqa Applied University

Associate Editorial Board

Professor Al-Hindi, Adnan I.

Parasitology

The Islamic University of Gaza, Faculty of Health

Sciences, Palestine

Dr Gammoh, Noor

Tumor Virology

Cancer Research UK Edinburgh Centre, University of Edinburgh, U.K.

Professor Kasparek, Max

Natural Sciences

Editor-in-Chief, Journal Zoology in the Middle East,

Germany

Editorial Board Support Team

Language Editor

Dr. Shadi Neimneh

Submission Address

Professor Atoum, Manar F

The Hashemite Universit y

P.O. Box 330127, Zarqa, 13115, Jordan

Phone: +962-5-3903333 ext.4147

E-Mail: jjbs@hu.edu.jo

Professor Krystufek, Boris

Conservation Biology

Slovenian Museum of Natural History,

Slovenia

Dr Rabei, Sami H.

Plant Ecology and Taxonomy

Botany and Microbiology Department,

Faculty of Science, Damietta University, Egypt

Professor Simerly, Calvin R.

Reproductive Biology

Department of Obstetrics/Gynecology and

Reproductive Sciences, University of

Pittsburgh, USA

Publishing Layout Eng.Mohannad Oqdeh

المجلة الاردنية للعلوم الحياتية Jordan Journal of Biological Sciences (JJBS)

http://jjbs.hu.edu.jo

International Advisory Board (Arranged alphabetically)

Professor Ahmad M. Khalil

Department of Biological Sciences, Faculty of Science, Yarmouk University, Jordan

Professor Anilava Kaviraj

Department of Zoology, University of Kalyani, India

Professor Bipul Kumar Das

Faculty of Fishery Sciences W. B. University of Animal & Fishery Sciences, India

Professor Elias Baydoun

Department of Biology, American University of Beirut Lebanon

Professor Hala Gali-Muhtasib

Department of Biology, American University of Beirut Lebanon

Professor Ibrahim M. AlRawashdeh

Department of Biological Sciences, Faculty of Science, Al-Hussein Bin Talal University, Jordan

Professor João Ramalho-Santos

Department of Life Sciences, University of Coimbra, Portugal

Professor Khaled M. Al-Qaoud

Department of Biological sciences, Faculty of Science, Yarmouk University, Jordan

Professor Mahmoud A. Ghannoum

Center for Medical Mycology and Mycology Reference Laboratory, Department of Dermatology, Case Western Reserve University and University Hospitals Case Medical Center, USA

Professor Mawieh Hamad

Department of Medical Lab Sciences, College of Health Sciences , University of Sharjah, UAE

Professor Michael D Garrick

Department of Biochemistry, State University of New York at Buffalo, USA

Professor Nabil, A. Bashir

Department of Physiology and Biochemistry, Faculty of Medicine, Jordan University of Science and Technology, Jordan

Professor Nizar M. Abuharfeil

Department of Biotechnology and Genetic Engineering, Jordan University of Science and Technology, Jordan

Professor Samih M. Tamimi

Department of Biological Sciences, Faculty of Science, The University of Jordan, Jordan

Professor Ulrich Joger

State Museum of Natural History Braunschweig, Germany

Professor Aida I. El Makawy

Division of Genetic Engineering and Biotechnology, National Research Center. Giza, Egypt

Professor Bechan Sharma

Department of Biochemistry, Faculty of Science University of Allahabad, India

Professor Bogusław Buszewski

Chair of Environmental Chemistry and Bioanalytics, Faculty of Chemistry, Nicolaus Copernicus University Poland

Professor Gerald Schatten

Pittsburgh Development Center, Division of Developmental and Regenerative Medicine, University of Pittsburgh, School of Medicine, USA

Professor Hala Khyami-Horani

Department of Biological Sciences, Faculty of Science, The University of Jordan, Jordan

Professor James R. Bamburg

Department of Biochemistry and Molecular Biology, Colorado State University, USA

Professor Jumah M. Shakhanbeh

Department of Biological Sciences, Faculty of Science, Mutah University, Jordan

Dr. Lukmanul Hakkim Faruck

Department of Mathematics and Sciences College of Arts and Applied Sciences, Dhofar, Oman

Professor Md. Yeamin Hossain

Department of Fisheries, Faculty of Fisheries , University of Rajshahi, Bangladesh

Professor Mazin B. Qumsiyeh

Palestine Museum of Natural History and Palestine Institute for Biodiversity and Sustainability, Bethlehem University, Palestine

Professor Mohamad S. Hamada

Genetics Department, Faculty of Agriculture, Damietta University, Egypt

Professor Nawroz Abdul-razzak Tahir

Plant Molecular Biology and Phytochemistry, University of Sulaimani, College of Agricultural Sciences, Iraq

Professor Ratib M. AL- Ouran

Department of Biological Sciences, Faculty of Science, Mutah University, Jordan

Professor Shtaywy S. Abdalla Abbadi

Department of Biological Sciences, Faculty of Science, The University of Jordan, Jordan

Professor Zihad Bouslama

Department of Biology, Faculty of Science Badji Mokhtar University, Algeria

Instructions to Authors

Scopes

Study areas include cell biology, genomics, microbiology, immunology, molecular biology, biochemistry, embryology, immunogenetics, cell and tissue culture, molecular ecology, genetic engineering and biological engineering, bioremediation and biodegradation, bioinformatics, biotechnology regulations, gene therapy, organismal biology, microbial and environmental biotechnology, marine sciences. The JJBS welcomes the submission of manuscript that meets the general criteria of significance and academic excellence. All articles published in JJBS are peer-reviewed. Papers will be published approximately one to two months after acceptance.

Type of Papers

The journal publishes high-quality original scientific papers, short communications, correspondence and case studies. Review articles are usually by invitation only. However, Review articles of current interest and high standard will be considered.

Submission of Manuscript

Manuscript, or the essence of their content, must be previously unpublished and should not be under simultaneous consideration by another journal. The authors should also declare if any similar work has been submitted to or published by another journal. They should also declare that it has not been submitted/ published elsewhere in the same form, in English or in any other language, without the written consent of the Publisher. The authors should also declare that the paper is the original work of the author(s) and not copied (in whole or in part) from any other work. All papers will be automatically checked for duplicate publication and plagiarism. If detected, appropriate action will be taken in accordance with International Ethical Guideline. By virtue of the submitted manuscript, the corresponding author acknowledges that all the co-authors have seen and approved the final version of the manuscript. The corresponding author should provide all co-authors with information regarding the manuscript, and obtain their approval before submitting any revisions. Electronic submission of manuscripts is strongly recommended, provided that the text, tables and figures are included in a single Microsoft Word file. Submit manuscript as e-mail attachment to the Editorial Office at: <a href="https://dx.doi.org/10.1016/journal.org/10.101

Peer-review Process

It is requested to submit, with the manuscript, the names, addresses and e-mail addresses of at least 4 potential reviewers. It is the sole right of the editor to decide whether or not the suggested reviewers to be used. The reviewers' comments will be sent to authors within 6-8 weeks after submission. Manuscripts and figures for review will not be returned to authors whether the editorial decision is to accept, revise, or reject. All Case Reports and Short Communication must include at least one table and/ or one figure.

Preparation of Manuscript

The manuscript should be written in English with simple lay out. The text should be prepared in single column format. Bold face, italics, subscripts, superscripts etc. can be used. Pages should be numbered consecutively, beginning with the title page and continuing through the last page of typewritten material.

The text can be divided into numbered sections with brief headings. Starting from introduction with section 1. Subsections should be numbered (for example 2.1 (then 2.1.1, 2.1.2, 2.2, etc.), up to three levels. Manuscripts in general should be organized in the following manner:

Title Page

The title page should contain a brief title, correct first name, middle initial and family name of each author and name and address of the department(s) and institution(s) from where the research was carried out for each author. The title should be without any abbreviations and it should enlighten the contents of the paper. All affiliations should be provided with a lower-case superscript number just after the author's name and in front of the appropriate address.

The name of the corresponding author should be indicated along with telephone and fax numbers (with country and area code) along with full postal address and e-mail address.

Abstract

The abstract should be concise and informative. It should not exceed **350 words** in length for full manuscript and Review article and **150 words** in case of Case Report and/ or Short Communication. It should briefly describe the purpose of the work, techniques and methods used, major findings with important data and conclusions. No references should be cited in this part. Generally non-standard abbreviations should not be used, if necessary they should be clearly defined in the abstract, at first use.

Keywords

Immediately after the abstract, **about 4-8 keywords** should be given. Use of abbreviations should be avoided, only standard abbreviations, well known in the established area may be used, if appropriate. These keywords will be used for indexing.

Abbreviations

Non-standard abbreviations should be listed and full form of each abbreviation should be given in parentheses at first use in the text.

Introduction

Provide a factual background, clearly defined problem, proposed solution, a brief literature survey and the scope and justification of the work done.

Materials and Methods

Give adequate information to allow the experiment to be reproduced. Already published methods should be mentioned with references. Significant modifications of published methods and new methods should be described in detail. Capitalize trade names and include the manufacturer's name and address. Subheading should be used.

Results

Results should be clearly described in a concise manner. Results for different parameters should be described under subheadings or in separate paragraph. Results should be explained, but largely without referring to the literature. Table or figure numbers should be mentioned in parentheses for better understanding.

Discussion

The discussion should not repeat the results, but provide detailed interpretation of data. This should interpret the significance of the findings of the work. Citations should be given in support of the findings. The results and discussion part can also be described as separate, if appropriate. The Results and Discussion sections can include subheadings, and when appropriate, both sections can be combined

Conclusions

This should briefly state the major findings of the study.

Acknowledgment

A brief acknowledgment section may be given after the conclusion section just before the references. The acknowledgment of people who provided assistance in manuscript preparation, funding for research, etc. should be listed in this section.

Tables and Figures

Tables and figures should be presented as per their appearance in the text. It is suggested that the discussion about the tables and figures should appear in the text before the appearance of the respective tables and figures. No tables or figures should be given without discussion or reference inside the text. Tables should be explanatory enough to be understandable without any text reference. Double spacing should be maintained throughout the table, including table headings and footnotes. Table headings should be placed above the table. Footnotes should be placed below the table with superscript lowercase letters. Each table should be on a separate page, numbered consecutively in Arabic numerals. Each figure should have a caption. The caption should be concise and typed separately, not on the figure area. Figures should be self-explanatory. Information presented in the figure should not be repeated in the table. All symbols and abbreviations used in the illustrations should be defined clearly. Figure legends should be given below the figures.

References

References should be listed alphabetically at the end of the manuscript. Every reference referred in the text must be also present in the reference list and vice versa. In the text, a reference identified by means of an author's name should be followed by the year of publication in parentheses (e.g.(Brown, 2009)). For two authors, both authors' names followed by the year of publication (e.g.(Nelson and Brown, 2007)). When there are more than two authors, only the first author's name followed by "et al." and the year of publication (e.g. (Abu-Elteen et al., 2010)). When two or more works of an author has been published during the same year, the reference should be identified by the letters "a", "b", "c", etc., placed after the year of publication. This should be followed both in the text and reference list. e.g., Hilly, (2002a, 2002b); Hilly, and Nelson, (2004). Articles in preparation or submitted for publication, unpublished observations, personal communications, etc. should not be included in the reference list but should only be mentioned in the article text (e.g., Shtyawy, A., University of Jordan, personal communication). Journal titles should be abbreviated according to the system adopted in Biological Abstract and Index Medicus, if not included in Biological Abstract or Index Medicus journal title should be given in full. The author is responsible for the securacy and completeness of the references and for their correct textual citation. Failure to do so may result in the paper being withdraw from the evaluation process. Example of correct reference form is given as follows:-

Reference to a journal publication:

Bloch BK. 2002. Econazole nitrate in the treatment of Candida vaginitis. S Afr Med J., 58:314-323.

Ogunseitan OA and Ndoye IL. 2006. Protein method for investigating mercuric reductase gene expression in aquatic environments. *Appl Environ Microbiol.*, **64**: 695-702.

Hilly MO, Adams MN and Nelson SC. 2009. Potential fly-ash utilization in agriculture. *Progress in Natural Sci.*, **19**: 1173-1186.

Reference to a book:

Brown WY and White SR.1985. The Elements of Style, third ed. MacMillan, New York.

Reference to a chapter in an edited book:

Mettam GR and Adams LB. 2010. How to prepare an electronic version of your article. In: Jones BS and Smith RZ (Eds.), **Introduction to the Electronic Age**. Kluwer Academic Publishers, Netherlands, pp. 281–304.

Conferences and Meetings:

Embabi NS. 1990. Environmental aspects of distribution of mangrove in the United Arab Emirates. Proceedings of the First ASWAS Conference. University of the United Arab Emirates. Al-Ain, United Arab Emirates.

Theses and Dissertations:

El-Labadi SN. 2002. Intestinal digenetic trematodes of some marine fishes from the Gulf of Aqaba. MSc dissertation, The Hashemite University, Zarqa, Jordan.

Nomenclature and Units

Internationally accepted rules and the international system of units (SI) should be used. If other units are mentioned, please give their equivalent in SI.

For biological nomenclature, the conventions of the *International Code of Botanical Nomenclature*, the *International Code of Nomenclature of Bacteria*, and the *International Code of Zoological Nomenclature* should be followed.

Scientific names of all biological creatures (crops, plants, insects, birds, mammals, etc.) should be mentioned in parentheses at first use of their English term.

Chemical nomenclature, as laid down in the *International Union of Pure and Applied Chemistry* and the official recommendations of the *IUPAC-IUB Combined Commission on Biochemical Nomenclature* should be followed. All biocides and other organic compounds must be identified by their Geneva names when first used in the text. Active ingredients of all formulations should be likewise identified.

Math formulae

All equations referred to in the text should be numbered serially at the right-hand side in parentheses. Meaning of all symbols should be given immediately after the equation at first use. Instead of root signs fractional powers should be used. Subscripts and superscripts should be presented clearly. Variables should be presented in italics. Greek letters and non-Roman symbols should be described in the margin at their first use.

To avoid any misunderstanding zero (0) and the letter O, and one (1) and the letter I should be clearly differentiated. For simple fractions use of the solidus (/) instead of a horizontal line is recommended. Levels of statistical significance such as: ${}^*P < 0.05$, ${}^{**}P < 0.01$ and ${}^{***}P < 0.001$ do not require any further explanation.

Copyright

Submission of a manuscript clearly indicates that: the study has not been published before or is not under consideration for publication elsewhere (except as an abstract or as part of a published lecture or academic thesis); its publication is permitted by all authors and after accepted for publication it will not be submitted for publication anywhere else, in English or in any other language, without the written approval of the copyright-holder. The journal may consider manuscripts that are translations of articles originally published in another language. In this case, the consent of the journal in which the article was originally published must be obtained and the fact that the article has already been published must be made clear on submission and stated in the abstract. It is compulsory for the authors to ensure that no material submitted as part of a manuscript infringes existing copyrights, or the rights of a third party.

Ethical Consent

All manuscripts reporting the results of experimental investigation involving human subjects should include a statement confirming that each subject or subject's guardian obtains an informed consent, after the approval of the experimental protocol by a local human ethics committee or IRB. When reporting experiments on animals, authors should indicate whether the institutional and national guide for the care and use of laboratory animals was followed.

Plagiarism

The JJBS hold no responsibility for plagiarism. If a published paper is found later to be extensively plagiarized and is found to be a duplicate or redundant publication, a note of retraction will be published, and copies of the correspondence will be sent to the authors' head of institute.

Galley Proofs

The Editorial Office will send proofs of the manuscript to the corresponding author as an e-mail attachment for final proof reading and it will be the responsibility of the corresponding author to return the galley proof materials appropriately corrected within the stipulated time. Authors will be asked to check any typographical or minor clerical errors in the manuscript at this stage. No other major alteration in the manuscript is allowed. After publication authors can freely access the full text of the article as well as can download and print the PDF file.

Publication Charges

There are no page charges for publication in Jordan Journal of Biological Sciences, except for color illustrations,

Reprints

Ten (10) reprints are provided to corresponding author free of charge within two weeks after the printed journal date. For orders of more reprints, a reprint order form and prices will be sent with article proofs, which should be returned directly to the Editor for processing.

Disclaimer

Articles, communication, or editorials published by JJBS represent the sole opinions of the authors. The publisher shoulders no responsibility or liability what so ever for the use or misuse of the information published by JJBS.

Indexing

JJBS is indexed and abstracted by:

DOAJ (Directory of Open Access Journals)

Google Scholar

Journal Seek

HINARI

Index Copernicus

NDL Japanese Periodicals Index

SCIRUS

OAJSE

ISC (Islamic World Science Citation Center)

Directory of Research Journal Indexing (DRJI)

Ulrich's

CABI

EBSCO

CAS (Chemical Abstract Service)

ETH- Citations

Open J-Gat

SCImago

Clarivate Analytics (Zoological Abstract)

Scopus

AGORA (United Nation's FAO database)

SHERPA/RoMEO (UK)

المجلة الأردنية للعلوم الحياتية

Jordan Journal of Biological Sciences (JJBS)

ISSN 1995-6673 (Print), 2307-7166 (Online)

http://jjbs.hu.edu.jo

The Hashemite University

Deanship of Scientific Research TRANSFER OF COPYRIGHT AGREEMENT

Journal publishers and authors share a common interest in the protection of copyright: authors principally because they want their creative works to be protected from plagiarism and other unlawful uses, publishers because they need to protect their work and investment in the production, marketing and distribution of the published version of the article. In order to do so effectively, publishers request a formal written transfer of copyright from the author(s) for each article published. Publishers and authors are also concerned that the integrity of the official record of publication of an article (once refereed and published) be maintained, and in order to protect that reference value and validation process, we ask that authors recognize that distribution (including through the Internet/WWW or other on-line means) of the authoritative version of the article as published is best administered by the Publisher.

To avoid any delay in the publication of your article, please read the terms of this agreement, sign in the space provided and return the complete form to us at the address below as quickly as possible.

Article entitled:
Corresponding author:
To be published in the journal: Jordan Journal of Biological Sciences (JJBS)
I hereby assign to the Hashemite University the copyright in the manuscript identified above and any supplemental tables, illustrations or other information submitted therewith (the "article") in all forms and media (whether now known or hereafter developed), throughout the world, in all languages, for the full term of copyright and all extensions and renewals thereof, effective when and if the article is accepted for publication. This transfer includes the right to adapt the presentation of the article for use in conjunction with computer systems and programs, including reproduction or publication in machine-readable form and incorporation in electronic retrieval systems. Authors retain or are hereby granted (without the need to obtain further permission) rights to use the article for traditional scholarship communications, for teaching, and for distribution within their institution.
I am the sole author of the manuscript
I am signing on behalf of all co-authors of the manuscript
The article is a 'work made for hire' and I am signing as an authorized representative of the employing company/institution
Please mark one or more of the above boxes (as appropriate) and then sign and date the document in black ink.
Signed:Name printed: Title and Company (if employer representative) : Date:
Data Protection: By submitting this form you are consenting that the personal information provided herein may be used by the Hashemite University and its affiliated institutions worldwide to contact you concerning the publishing of your article.
Please return the completed and signed original of this form by mail or fax, or a scanned copy of the signed original by e-mail, retaining a copy for your files, to:

Hashemite University Jordan Journal of Biological Sciences Zarqa 13115 Jordan

Fax: +962 5 3903338 Email: <u>jjbs@hu.edu.jo</u>

EDITORIAL PREFACE

Jordan Journal of Biological Sciences (JJBS) is a refereed, quarterly international journal financed by the Scientific Research and Innovation Support Fund, Ministry of Higher Education and Scientific Research in cooperation with the Hashemite University, Jordan. JJBS celebrated its 12th commencement this past January, 2020. JJBS was founded in 2008 to create a peer-reviewed journal that publishes high-quality research articles, reviews and short communications on novel and innovative aspects of a wide variety of biological sciences such as cell biology, developmental biology, structural biology, microbiology, entomology, molecular biology, biochemistry, medical biotechnology, biodiversity, ecology, marine biology, plant and animal biology, plant and animal physiology, genomics and bioinformatics.

We have watched the growth and success of JJBS over the years. JJBS has published 11 volumes, 45 issues and 479 articles. JJBS has been indexed by SCOPUS, CABI's Full-Text Repository, EBSCO, Clarivate Analytics- Zoological Record and recently has been included in the UGC India approved journals. JJBS Cite Score has improved from 0.18 in 2015 to 0.7 in 2019 (Last updated on 1 March, 2021) and with Scimago Institution Ranking (SJR) 0.18 (Q3) in 2019.

A group of highly valuable scholars have agreed to serve on the editorial board and this places JJBS in a position of most authoritative on biological sciences. I am honored to have six eminent associate editors from various countries. I am also delighted with our group of international advisory board members coming from 15 countries worldwide for their continuous support of JJBS. With our editorial board's cumulative experience in various fields of biological sciences, this journal brings a substantial representation of biological sciences in different disciplines. Without the service and dedication of our editorial; associate editorial and international advisory board members, JJBS would have never existed.

In the coming year, we hope that JJBS will be indexed in Clarivate Analytics and MEDLINE (the U.S. National Library of Medicine database) and others. As you read throughout this volume of JJBS, I would like to remind you that the success of our journal depends on the number of quality articles submitted for review. Accordingly, I would like to request your participation and colleagues by submitting quality manuscripts for review. One of the great benefits we can provide to our prospective authors, regardless of acceptance of their manuscripts or not, is the feedback of our review process. JJBS provides authors with high quality, helpful reviews to improve their manuscripts.

Finally, JJBS would not have succeeded without the collaboration of authors and referees. Their work is greatly appreciated. Furthermore, my thanks are also extended to The Hashemite University and the Scientific Research and Innovation Support Fund, Ministry of Higher Education and Scientific Research for their continuous financial and administrative support to JJBS.

Jordan Journal of Biological Sciences

CONTENTS

Original Ar	ticles
347 – 352	Molecular Evaluation of <i>Cordyline fruticosa</i> (L.) A.Chev. Behavior Affected by Different Chemical Mutagens Eman Tawfik and Mohamed Fathy Ahmed
353 – 359	Evaluation of the Genetic Diversity of Antibiotic-Resistant <i>Klebsiella Pneumoniae</i> Isolated from Diarrheal Humans and Poultry using Multilocus Sequence Typing <i>Shaimaa Obaid Hasson and Walaa Farhan Obaid</i>
361 - 364	Prokaryotic Expression of Murine Cellular Prion Protein for in Vitro Evaluation Hoang-Anh Le-Dao, Yen-Vy Le-Nguyen, Hieu Tran-Van
365 – 372	Impact of Diabetic Retinopathy on Vulnerability of Atherosclerosis in Type 1 Diabetes: the Role of Lipid Ratios as a Metabolic Biomarker
373 – 380	Walid Hassene Hamri, Mustapha Diaf, Noria Harir Biological Control of Tomato Damping-off and Potato Black Scurf by Seed Treatment with Trichoderma harzianum Naffaa Walid, Lubana Al-Jaramany, Ahed Elbenay, Reema Al-Mhethawi
381 – 386	Bioconversion of Pear Pomace by Strains of <i>Pleurotus Ostreatus</i> During Mycelial Development María B. Buglione, Marta S. Agüero, Daniel A. Martínez, Marcela V. Filippi, Jorge F. Maldonado, Gustavo E. Rodríguez
387 – 394	DNA Paternity Testing with Two Mismatches: Our Experience Belma Jusic, Amela Pilav, Mirela Dzehverovic, Jasmina Cakar
395 – 404	Imaging Aspects (Chest Radiographic and CT Scan Findings) of COVID-19 with Clinical Classifications Ammar A. Oglat, Mohammad A. Oqlat, Ahmad A. Oqlat, Lo'ai Alanagreh, Pegah Moradi Khaniabadi, Mohammed Ali Dheyab, Hawraa Khaleel, Omar Althalji
405 – 411	Understanding the Medicinal Prospects of Methanolic Extract from a Recently Explored Mushroom of Tribal Delicacy
413 – 421	Somanjana Khatua, Krishnendu Acharya A Pilot Study: Ground and Aqueous Extract of Leptadenia Pyrotechnica Modulate the Immune System Affecting White Blood Cell Counts and Increasing Red Blood Cell Counts Sawsan H. Mahassni, Bushra S. Alsahafi
423 – 429	Role of IFN-γ, TNF-α, IL-6 and C-Reactive Protein in Newly Diagnosed Iraqi Corona Patients
431 – 440	Israa Qusay Falih, Noor Thair Tahir, Mithal R. Alkubaisi In-silico Genome Editing Identification and Functional Protein Change of Chlamydomonas reinhardtii Acetyl-CoA Carboxylase (CrACCase) Mentari Putri Pratami, Miftahul Huda Fendiyanto, Rizky Dwi Satrio, Isna Arofatun Nikmah, Mo Awwanah, Nadya Farah, Nastiti Intan Permata Sari, Nurhadiyanta
441 – 448	Potential for Crude Oil and Diesel Biodegradation by the Indigenous <i>Pseudomonas</i> sp. Strain LGMS7 Using GC-MS and GC-FID Analyses Abdelkrim Chaida, Farid Bensalah1, Belhadj Trari
449 – 456	Preliminary Studies on the Potential Antioxidant and Antidiabetic Activities of Sargassum polycystum C. Agardh (Phaeophyceae, Ochrophyta) Eldrin DLR. Arguelles
457 – 461	Biodegradation of Doxycycline Hyclate by Local <i>Purpureocillium lilacinum</i> strain PlHN17 and <i>Trichoderma asperellum</i> isolate Tullur: Monitoring by Antimicrobial Activity. Fathin Fashihah Kamaruddin, Maslinda Musa, Mohd Muzamir Mahat, Shahrul Hisham Zainal Ariffin, Muhd Fauzi Safian and Zaidah Zainal Ariffin
463 – 467	Utility of SPC25 as a Biological Biomarker in Colorectal Adenocarcinoma AbdulFattah Salah Fararjeh

469 – 473	Modeling and Allometric Analysis of two Butterfly Species of the Genus Colotis Ali Elkarmi and Lina Shaheen
	Evaluation of Coffee Pulp Waste from Coffee Cultivation Areas in Indonesia as Iron Booster
475 – 488	Roy Hendroko Setyobudi, Manar Fayiz Mousa Atoum, Damat Damat,Erkata Yandri, Yogo Adi Nugroho, Mardiana Sri Susanti, Satriyo Krido Wahono, Wahyu Widodo, Lili Zalizar, Ahmad Wahyudi, Elfi Anis Saati, M. Maftuchah, Zahid Hussain, Dwi Yono, Soni Sisbudi Harsono, Rangga Kala Mahaswa, Herry Susanto, Praptiningsih Gamawati Adinurani, Ida Ekawati, Ahmad Fauzi, and Susi Mindarti
489 – 500	Infraspecific Identity of the Wild Brassica Nigra (L.) Koch. Using Morphological, Cytogenetics and Molecular (Nuclear and Chloroplast) Approaches Wafaa M. Amer, Mahmoud A. Shoulkamy, Hadeer D. Abd El-Baset and Ahmed M. Faried
501 – 509	Molecular Genetic Identificatin of Plants of the Genus Artemisia L. Growing in Southern Regions of Kazakhstan
	Zhanar Rakhimberdiyeva, Anar Kaliyeva , Ahmet Aksoy, Bekbossyn Kassymbayev, Galiya Medeuova
511 – 522	Response Surface Method for Optimizing the Biosynthesis of Silver Nanoparticles Using <i>Talaromyces stipitatus</i> and Their Antimicrobial Activity Nada M. Elmayah, Amira A. El-Fallal, Mohamed I. Abou-Dobara, Mahmoud E. Khalifa
	Anti-malarial Effect of <i>Momordica charantia</i> Involved Modulation of Cytokine
523 -529	Mediated via GSK3β Inhibition in <i>Plasmodium berghei</i> - Infected Mice
	Mayada Hussain Ali, Izyanti Ibrahim, Malina Jasamai,Noor Embi, Hasidah Sidek

Short Communication

531 -535 Assessing Factors that Shape Neonatal Gut Microbiota in Erbil Province /Iraq *Muayad Ahmed Mahmud*

Jordan Journal of Biological Sciences

Molecular Evaluation of *Cordyline fruticosa* (L.) A.Chev. Behavior Affected by Different Chemical Mutagens

Eman Tawfik^{1,*} and Mohamed Fathy Ahmed²

¹Lecturer of Genetics and Genetic Engineering, Botany and Microbiology Department, Faculty of Science, Helwan University, Egypt; ²Master Degree, Horticulture Department, Faculty of Agriculture, Ain Shams University, Egypt

Received: May 4, 2021; Revised: July 27, 2021; Accepted: October 4, 2021

Abstract

Cordyline fruticosa is a medicinal plant that is also ornamental due to its variegated coloured leaves. Some traits benefit from mutation. Guanidine hydrochloride and sodium azide were the chemical mutagens used in this study. For each, concentrations of 30, 40, and 50 mM were used. The plantlets were exposed to these mutagens, and the explants were cultured in vitro using micropropagation. To estimate the effect of mutagens in comparison to non-mutant (control), different 8 morphological characters were measured. In the case of guanidine hydrochloride, all of the treatments are nearly identical to control, with no significant differences except for 30 mM, which is lower than the others. Cordyline fruticosa genetic variation resulted in a wide range of polymorphism percentages. In the case of sodium azide, it was 74.66 %, while in the case of guanidine hydrochloride, it was 37.77 %. All morphological parameters decreased in sodium azide comparing to control, with the exception of the number of branches, which increased more at 50 mM than at other concentrations and control. All morphological parameters increased in mutants rather than controls, unlike guanidine hydrochloride. For photosynthetic pigmentations, all pigments decreased with sodium azide treatments. As a result, chemical mutagens cause genetic instability and variation, which manifests itself in morphological and physiological characteristics.

Keywords: Cordyline fruticose; Guanidine hydrochloride; Sodium azide; photosynthetic pigmentations; RAPD-PCR.

1. Introduction

Cordyline fruticosa is a medicinal, ornamental, and woody plant native to the southern hemisphere and tropical areas of the world. It is a monocotyledonous ornamental plant with evergreen flowers in family Asparagaceae. It is also known for its medicinal treatments for human diseases such as hemostatic, toothache, sore throat, and neck pain. C. fruticosa has antioxidant activity and nutritional value in its leaves and roots, among other organs. It also has cytotoxic and antimicrobial properties microorganisms due to the presence of steroidal saponins. In some traditions and cultures, C. fruticosa was thought to ward off evil spirits and bring good luck (Fouedjou et al., 2014, 2016).

Induced chemical mutation produces genetic diversity, which results in new varieties with improved traits. Induced mutations also have a mechanism for abiotic and biotic stress resistance, allowing the creation of a new resistant strain (El-Mokadem and Mostafa, 2013; Suprasanna et al., 2015).

The chemical mutagen sodium azide (NaN₃) is a potent mutagen in plants. The application of a mutagen to a plant is simple and cheap, and it allows for mutation to enhance the plant's characteristics. The efficiency of mutant production is influenced by a number of factors, including azide concentration and treatment time. This causes point mutations, damages chromosomes, and results in plant

tolerance to various conditions (El-Mokadem and Mostafa, 2013). These changes lead to increase in seed germination percentage, seedling height and root length (El Kaaby et al., 2015).

Chemical mutagens known as guanidine hydrochlorides alkylate the structure of DNA nitrogen bases. Three categories of guanidine hydrochlorides were identified: Phenylethylbi-guanidide, even at relatively high concentrations, causes only partial inhibition. About 70 % of malate respiration is inhibited by Decamethylenediguanidide (e.g., succinate respiration and ascorbate-tetramethyl-p-phenylenediamine). Finally, all three phosphorylation sites and cyanide-insensitive respiration are inhibited by octyl-guanidine hydrochloride, but to varying degrees and concentrations (Wilson and Bonner, 1970).

The goal of that study was to see how two chemical mutagens (sodium azide and guanidine hydrochloride) affected *Cordyline fruticosa* growth. It also aimed to generate genetic diversity in the content of morphology and chlorophyll detected by RAPD-PCR.

2. Materials and Methods

2.1. Plant Materials

Cordyline fruticosa is a medicinal plant found in the cultivated gardens of Ain Shams University's Faculty of Agriculture.

^{*}Corresponding author. e-mail: emantawfik@science.helwan.edu.eg.

2.2. Mutagens

Two chemical mutagens were used in this study, guanidine hydrochloride and sodium azide. They were prepared in concentrations of (0, 30, 40, and 50 mM).

2.3. In Vitro Culture (Micropropagation)

The standard sterilization conditions were the elimination of stacked dust/soil practices. The explants were de-foliated and washed thoroughly in tap water. 20% Clorox + 0.1% HgCl₂ was used for 20 minutes and washed 4 to 5 times with sterile ddH₂O with surface sterilization of the explants. Under the sterilized condition, excision and culture procedures for stem nodal ex-plants were performed. Nodal explants of this ornamental plant were sterilized to be cultured on full power MS-free media, according to (Murashige and Skoog. 1962). After that, the resulting plantlets were twice regenerated multiplication on 3/4 MS-free media. The plantlets of both ornamental plants were then cut into nodal segments and incubated for 3 hours in various mutagenic concentrations. The cells were cleared in sterile dH2O and moved to clear MS jars then incubated for five weeks at 25°C (16 h light/8 h dark) with light intensity of 2000 lux.

2.4. Morphological Measurements

Compared with control, the measured parameters were estimated for the mutant plants. The parameters were fresh weight, shoot length, length of roots, number of lateral roots, number of branches, number of leaves, leaf length and leaf width.

2.5. Photosynthetic Pigments Estimation

Chlorophyll pigmentation is an essential physiological parameter that determines and controls most of the plant cell pathways. Chlorophylls compared with control plants were estimated for both mutants. Chlorophyll a, b, and carotenoids were measured in the plantlets' fresh leaves (Metzener et al., 1965). A solution of 85 % acetone was used to homogenize 0.5 g of fresh leaves. The supernatant, which contained the pigments, reached to 7 ml of 85 % acetone after centrifugation. The extract was compared to a blank of pure 85 % aqueous acetone using a colorimeter at different 3 wavelengths (452, 645, and 664 nm). The concentrations of chlorophyll a, b, and carotenoid were calculated in g/ml as follow:

Chl.
$$a = 10.3 \text{ A}664 - 0.918 \text{ A}645$$
 (1)

Chl.
$$b = 19.7 \text{ A}645 - 3.87 \text{ A}664$$
 (2)

After that, the fractions were used as mg/g fresh weight:

$$\frac{fraction \times dilution}{1000} \quad mg/g \tag{4}$$

2.6. Molecular marker

2.6.1. DNA isolation and RAPD-PCR bioassay

Cordyline fruticosa's total genomic DNA (mutagens and control) was extracted by CTAB protocol (Doyle and

Doyle, 1990). With 800 μ l of 2 % CTAB buffer, half g of leaves was ground and incubated for 30 min at water bath (65°C) with vortex 10 min intervals. The Eppendorf tubes were centrifuged for 10 minutes at 12,000 rpm, with the supernatant transferred to new tubes. Each tube was filled with an equal volume of chloroform: isoamyl alcohol (24:1) and centrifuged for 10 minutes at 4°C at 12,000 rpm. Move the upper aqueous layer to another Eppendorf's with addition of 900 μ l of isopropanol and left 2h at -20°C. DNA pellets were formed after centrifugation and wash using 70% ice-cold ethanol, then the air-dried pellets were resuspended in 50 μ l TE buffer and stored at -20°C.

Only five of eight RAPD primers performed (Table 3), gave reproducible clear bands. Biometra thermocycler machine was applied for the RAPD-PCR reaction. A total volume of 25 μl was used, which included 12.5 μl of master mix (COSMO PCR RED M. Mix), 3 μl of DNA (50ng), 1 μl of each primer (100 nanomole) (Willowfort), and 8.5 μl of ddH₂O. A 35 cycles reaction program was run and included of 30-second denaturation at 94°C, 30-sec annealing (Table 3), and 1-min extension at 72°C. Then a final extension step at 72°C for 10 min, followed by cooling at 4°C. The amplified products were checked on 1.4 % agarose gel.

2.7. Statistical Analysis

Electrophoresis of the gel resulted in analyzed images. A band's presence was scored as 1, while the absence of the band was coded as 0 using Bio-Rad Quantity one (4.6.2). Jaccard's coefficient of similarity, a similarity matrix was generated. Cluster analysis was applied to obtain a dendrogram by using the unweighted pair group method with the arithmetic averaging algorithm (UPGMA). These computations were carried out (Shuaib et al., 2997).

The data collected was analyzed for variance tests in SPSS 21. Estimated mean average and standard deviations. Using Tukey test multivariate analysis, significant means have been separated. For the 25 different treatments, Tukey homogeneous Subsets were used with one-way ANOVA, where Tukey homogeneous Subsets were used with multivariate analysis for the two factors.

3. Results

Different concentrations of guanidine hydrochloride and sodium azide were prepared (0, 30, 40, 50 mM). They were used to treat the explants of *Cordyline fruticosa* plantlets. The following parameters were recorded.

3.1. Morphological Parameters

Eight morphological parameters were estimated to respond to these plants to the different mutagens' concentrations (Fig. 1). The data in Table (1) showed significant differences compared to control for Cordyline fruticosa affected by sodium azide and guanidine hydrochloride. The high concentration of sodium azide (50 mM) showed branching in both *C. fruticosa*. In the case of guanidine hydrochloride mutagen, it causes stimulation in growth and morphology.





Figure 1. Phenological responses of Cordyline fruticosa to different mutagens; a) with sodium azide, b) with guanidine

Table 1. Phenological means estimation of Cordyline fruticosa in response to different mutagens

Species	Cordyline	Cordyline fruticosa						
Mutagens	Sod. azide	e			Guanidine hy	drochloride		
Conc. mM	0	30	40	50	0	30	40	50
Fresh wt. (g)	0.5143	0.2731	0.2852	0.2604	0.4223	0.6184	0.4195	0.5412
Shoot length cm	8.9000	6.1333	4.4667	4.6000	8.1333	9.5000	8.4000	7.6667
Root length cm	5.2333	1.9667	1.7000	1.7000	5.1500	6.8833	16.9000	4.4083
No. of roots	4.6667	2.3333	2.0000	2.3333	3.0000	5.0000	4.0000	4.6667
No. of leaves	2.6667	2.6667	2.3333	2.6667	4.3333	5.6667	4.3333	4.3333
No. of branches	2.0000	1.0000	1.6667	2.3333	1.0000	1.3333	1.0000	1.3333
Leaf length cm	5.2200	3.4200	2.5800	3.0000	4.1000	5.1875	4.9813	5.2063
Leaf width cm	0.7300	0.4800	0.3200	0.3500	0.6375	0.7250	0.6625	0.7063
F-value	16.059**	53.364**	12.904**	15.698**	25.576**	36.760**	1.083**	14.937**

^{*} highly significant

3.2. Photosynthetic Pigments

Chlorophyll content (chlorophyll a, b and carotenoids) was measured for response of *C. fruticosa* to the mutagens' concentrations. These were shown in Table (2) for sod. azide and guanidine. In the case of sodium azide mutagen, compared to control, the concentrations of the mutants' pigments decrease. Still, at a 50 mM concentration, the

pigmentations are significantly increasing more than the other concentrations (30 and 40 mM). In the case of guanidine hydrochloride mutagen, the pigmentations are less affected than sodium azide. At a concentration of 30 mM guanidine hydrochloride, the pigmentation is inhibited more than others, where the control, 40, and 50 mM are not significantly different.

Table 2. Means of chlorophyll content estimation of Cordyline fruticosa with different mutagens

Species	Cordyline fruticosa							
Mutagens	Sod. azide	Sod. azide				Guanidine hydrochloride		
Conc. mM	0	30	40	50	0	30	40	50
Chl. a	0.30618	0.13515	0.18170	0.19692	0.27834	0.20023	0.24840	0.24245
Chl. b	0.43028	0.08340	0.11298	0.30852	0.39116	0.31673	0.38181	0.37985
Cart.	1.39506	0.12159	0.11936	0.99555	0.12682	0.10472	0.12230	0.12257
F-value	198265.83**	1149.23**	771.199**	26653.80**	13941.31**	26820.43**	48600.6**	61297.2**

^{*}highly significant

3.3. Molecular Markers

In order to measure the genetic diversity resulting from treated mutagens, RAPD-PCR was performed after total

genomic DNA was extracted. Results on agarose gel (Fig. 2 and 3) for sodium azide and guanidine hydrochloride were shown for selected oligonucleotide decamers. The table (3) below shows the polymorphism data from these

primers. *Cordyline fruticosa's* total polymorphism percentage affected by sodium azide was 74.66 percent, with 37.77 percent of the polymorphism percentage resulting from the treatment of guanidine hydrochloride. Table 4 and 5 showed a matrix of similarities between the various concentrations of sod. azide and guanidine, respectively. Figure (4) illustrated a dendrogram of the

sodium azide impact on *Cordyline fruticose* on genetic variation. Control has been shown to be separated on its own from other mutants, where 40 and 50 mM are genetically similar. The effect of hydrochloride guanidine on genetics was demonstrated in (Fig. 5). This revealed that control is distinct, with 30 and 40 mM being genetically equivalent.

Table 3 List of primers used in the RAPD-PCR of Cordyline fruticosa with both mutagens, including their names (ID), nucleotide sequences, and polymorphism percentage

N-	No. Primer name	D.	GC	Т	Sodium azide		Guanidine hydrochloride	
NO.		Primers sequence	%	Tm	Total bands	Polymorphism %	Total bands	Polymorphism %
1	OPA-12	5'-TCGGCGATAG-3'	60	34	5	40	6	50
2	OPB-17	5'-AGGGAACGAG-3'	60	33.1	4	75	4	0
3	OPZ-07	5'-CCAGGAGGAC-3'	70	34.6	4	75	4	50
4	RFu-25	5'-CCGGCTGGAA-3'	70	39.8	6	83.33	6	33.33
5	Deca-11	5'-ATCGGCTGGG-3'	70	39.3	5	100	9	55.55
Total					24	74.66	29	37.77

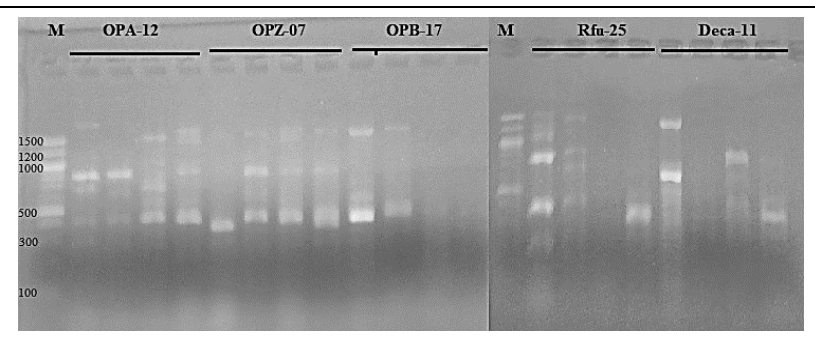


Figure 2. RAPD-PCR product pattern of Corydaline fruticosa with sodium azide

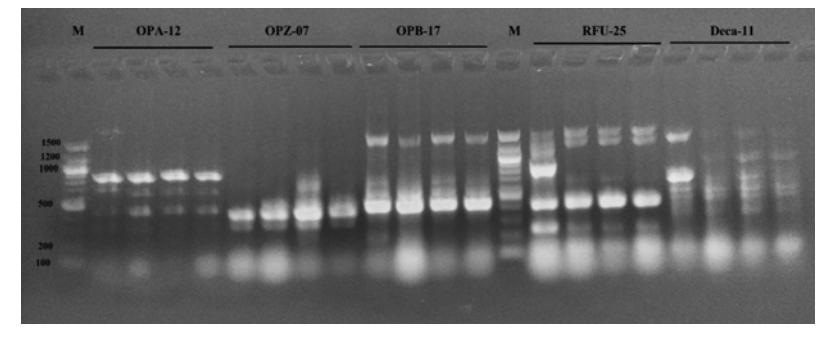
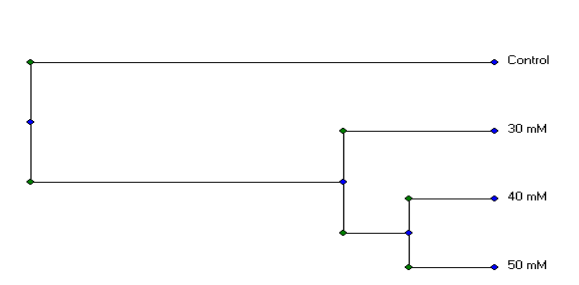


Figure 3. RAPD-PCR product pattern of Corydaline fruticosa with guanidine hydrochloride



5.85E3

3.31E3

1.79E4

Figure 4. Dendogram based on RAPD patterns for *Cordyline fruticosa* treated with sodium azide

Table 4 Similarity matrix based on RAPD-PCR for *Cordyline fruticosa* treated with sodium azide mutagen

	Control	30 mM	40 mM	50 mM
Control	100	32.86	21.98	10.06
30 mM	32.86	100	49.96	48.9
40 mM	21.98	49.96	100	60.18
50 mM	10.06	48.9	60.18	100

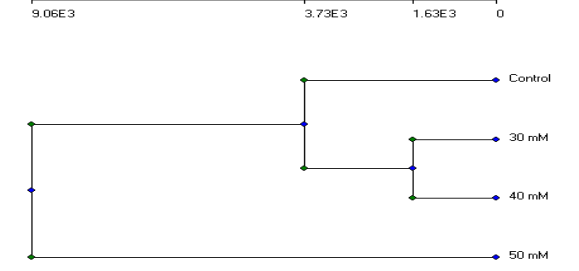


Figure 5. Dendogram based on RAPD pattern for *Cordyline fruticosa* treated with guanidine hydrochloride mutagen

Table 5 Similarity matrix based on RAPD-PCR for *Cordyline fruticosa* treated with guanidine hydrochloride mutagen

	Control	30 mM	40 mM	50 mM
Control	100	57.06	67.74	36.04
30 mM	57.06	100	72.56	40.30
40 mM	67.74	72.56	100	43.3
50 mM	36.04	40.30	43.3	100

4. Discussion

Cordyline fruticosa is a medicinal and ornamental plant. We can make some changes by mutations to enhance these ornamental characters and increase their medicinal value. Two chemical mutagens were used in this study: sodium azide and guanidine hydrochloride to cause these mutants' changes compared to control plant individuals. Many mutagens were used for the improvement of several ornamental plants. Research on the enhancement of ornamental and medicinal plants using induced chemical or physical mutations has been started by the Malaysian Nuclear Agency. The new varieties were moved to different users and private government agencies (Ahmad et al., 2012). As found in Amaranthus caudatus (El-Nashar, 2006), Mirabilis jalapa (Al-Gawwad, and Makka, 2009), and Helianthus annuus (Mostafa, 2011), sodium azide has been used to induce mutations in many types of research. Eruca sativa was mutated by sodium azide by Al-Qurainy (2009) and nine morphological traits and photosynthetic pigmentation were estimated. Also, proved that important differences are caused by sodium azide. El-Nashar and Asrar (2016) applied two mutagens for diversity estimation in Calendula officinalis. Many morphological and physiological parameters were calculated, and significant mutant differences comparing to control parameters were discovered. El Kaaby et al. (2015) mentioned that application of sodium azide to tomato lead to increase in seed germination percentage, seedling height and root length. Also, Eze and Dambo (2015) mentioned that sod. Azide treatment in maize enhance growth rate and seed size. The application of guanidine hydrochloride was confirmed by Tawfik and Fathy (2020) to enhance several morphological parameters comparing to control.

Several molecular markers have been applied to evaluate genetic diversity in many plants responded to different mutagens. Here, this work introduced RAPD technique to estimate genetic polymorphism in *Cordyline fruticosa* from to the action of guanidine and sod. azide.

Wannajindaporn et al. (2014) used tissue culture to estimate the effect of sodium azide on *Dendrobium*, using ISSR molecular markers to compare mutants with controls. This is consistent with numerous studies that have discovered genetic variation in plants as a result of chemical mutagen treatments.

5. Conclusion

Cordyline fruticosa is a medicinal and ornamental monocot plant. Two chemical mutagens were used in this study: guanidine hydrochloride and sodium azide. They were used in concentrations of 30, 40, and 50 mM for each one. Eight morphological traits were measured. They were fresh weight, roots and shoot lengths, number of branches, lateral roots and leaves, leaf length and leaf width. Sodium azide inhibited all of the morphological parameters (except the branching and leaves number). So, we can use sodium azide to obtain C. fruticosa individuals with more branching and leaves. Unlike, guanidine hydrochloride which promotes morphological behavior except in 30 mM, which is less than others. The genetic polymorphism percentage resulted from genetic variation of Cordyline fruticosa varied. It was 74.66% in sodium azide, 37.77% in the case of guanidine hydrochloride.

Acknowledgment

The authors would like to thank Agricultural center for genetic engineering and biotechnology "ACGEB", Faculty of Agriculture, Ain Shams University, for the facilitation of working in tissue culture labs.

References

Ahmad Z, Hassan AB, Salleh S, Ariffin SN, Shamsudin S, Basiran MN, Tan SG, Zainudin NA and Yusoh OM 2012. Improvement of Malaysian ornamental plants through induced mutation. *Plant Biotech*, *Pertanika J Trop Agric*, **35(3)**: 631–636.

Al Gawwad A and Makka AH 2009. Effect of chemical mutagens on *Mirabilis jalapa*. M.Sc. Thesis, Floriculture, Faculty of Agriculture, Alexandria University, Alexandria, Egypt.

Al-Qurainy F 2009. Effects of Sodium Azide on Growth and Yield Traits of Eruca sativa (L.). World Appl Sci J, 7(2): 220–226.

Doyle JJ and Doyle JL 1990. Isolation of Plant DNA from Fresh Tissue. Focus. 12: 13–15.

El Kaaby EAJ, Al-Ajeel SA, Al-Anny JA, Al-Aubaidy AA and Ammar K 2015. Effect of the Chemical Mutagens Sodium Azide on Plant Regeneration of Two Tomato Cultivars under Salinity Stress Condition in vitro. *J Life Sci*, **9:** 27–31.

El-Mokadem HE and Mostafa GG 2013. Induction of mutations in *Browallia speciosa* using sodium azide and identification of the genetic variation by peroxidase isozyme. *Afr J Biotechnol*, **13(1)**: 106–111.

El-Nashar YI and Asrar AA 2016. Phenotypic and biochemical profile changes in calendula (*Calendula officinalis* L.) plants treated with two chemical mutagenesis. *Genet Mol Res*, **15(2)**: gmr.15028071.

El-Nashar YIA 2006. Effect of chemical mutagens (sodium azide and diethyl sulphate) on growth, flowering and induced variability in *Amaranthus caudatus* L. and *A. hypochondriacus* L. Ph.D. Thesis, Floriculture, Faculty of Agriculture, Alexandria University. Egypt.

Eze JJ and Dambo A 2015. Mutagenic Effects of Sodium Azide on the Quality of Maize Seeds. *J Adv Lab Res Biol*, **6(3):** 76-82.

Fouedjou RT, Nguelefack-Mbuyo EP, Ponou PK, Nguelefack TB, Barboni L and Tapondjou LA 2016. Antioxidant Activities and Chemical Constituents of Extracts from *Cordyline fruticosa* (L.) A. Chev. (Agavaceae) and *Eriobotrya japonica* (Thunb) Lindl, (Rosaceae), *Pharmacologia*, **7(2-3)**: 103–113.

Fouedjou RT, Teponno RB, Quassinti L, Bramucci M, Petrelli D, Vitali LA, Fiorini D, Tapondjou LA and Barboni L 2014. Steroidal saponins from the leaves of *Cordyline fruticose* (L.) A. Chev. and their cytotoxic and antimicrobial activity, *Phytochem Lett*, 7: 62 – 68.

Metzener H, Rau H and Senger H 1965. Untersuchungen zur Synchronisierbarkeit einzelner PigmentmangelMutanten von Chlorella. *Planta*, **65**: 186–194.

Murashige T and Skoog FK 1962. A revised medium for rapid growth and bioassays with tobacco tissue cultures. *Physiol Plant*, **15**: 473–497.

Mostafa GG 2011. Effect of sodium azide on the growth and variability induction in Helianthus annuus L. *Int. J. Plant Breed Genet*, **5(1)**: 76–85.

Shuaib M, Zeb A, Ali Z, Ali W, Ahmad T and Khan I 2007. Characterization of Wheat Varieties by Seed Storage Protein Electrophoresis. *Afr J Biotechnol*, **6**: 497–500.

Suprasanna P, Mirajkar SJ and Bhagwat SG 2015. Induced Mutations and Crop Improvement. *Plant Bio. Biotech*, **1:** 593–617.

Tawfik E and Fathy M 2020. Chemical Mutagens Affecting in vitro Behavior of *Gardenia jasminoides*. *Plant Tissue Cult & Biotech*, **30(2)**: 209–218.

Wilson SB and Bonner WD 1970. Effects of Guanidine Inhibitors on Mung Bean Mitochondria, *Plant Physiol*, **46:** 21–24.

Wannajindaporn A, Poolsawat O, Chaowiset W and Tantasawat PA 2014. Evaluation of genetic variability in *in vitro* sodium azide-induced Dendrobium 'Earsakul' mutants. *Genet Mol Res*, **13(3)**: 5333–5342.

Jordan Journal of Biological Sciences

Evaluation of the Genetic Diversity of Antibiotic-resistant Klebsiella pneumoniae Isolated from Diarrheal Humans and Poultry using Multilocus Sequence Typing

Shaimaa Obaid Hasson^{1,*} and Walaa Farhan Obaid²

¹ Department of Biotechnology, Faculty of Biotechnology, Al-Qasim Green University, Babylon, Iraq ² Department of Microbiology, Faculty of veterinary medicine, Al-Qasim Green University, Babylon, Iraq

Received: April 1, 2022; Revised: June 6, 2022; Accepted June, 6, 2022

Abstract

Background: *Klebsiella pneumoniae* is an opportunistic pathogen usually responsible for healthcare-associated infections. Multilocus sequence typing (MLST) analysis utilized four housekeeping genes among *Klebsiella pneumonia* isolated from diarrheal humans and poultry to determine the extent of genetic diversity.

Material and methods: Seventy-five fecal samples from both human and poultry sources were cultured and diagnosed with the bacterial isolates by the VITEK-2 system as well as an Antibiotic sensitivity test (AST).

Results: Antibiotic susceptibility profile of Human's *K. pneumoniae* revealed all isolates bacteria were absolute resistant against Ampicillin and highly resistant toward Cefazolin 86%. Poultry's *K. pneumoniae* was highly resistant to Ampicillin at 100% and to Cefazolin at 46.6%. MLST results of all four housekeeping genes together revealed that humans *K. pneumoniae* (K1-K6) and poultry *K. pneumoniae* (K7-K11) were similar, specifically isolates K6 and K11, and different in (K1, K5, and K7).

Conclusion: The present study is considered the first in Iraq to determine the genetic relationship between *K. pneumonia* isolates from humans and poultry. *K. pneumonia* has a high rate of antibiotic resistance and high genetic diversity as a result of the sequencing of (*rpoB*, *gapA*, *phoE* and *tonB* genes) of human and poultry isolates. The genetic association (similarity) of antibiotic resistance *K. pneumoniae* strain between both sources where all isolates are resistant to most antibiotic agents in significant differences is evidence of the transmission of isolates from an animal source (poultry) to humans which poses a public health threat.

Keywords: Antibiotic resistance, Diarrheal poultry, Genetic diversity, Klebsiella pneumoniae, Multilocus sequence typing.

1. Introduction

K. pneumoniae is an important opportunistic bacteria, causing many diseases such as septicemia, liver abscesses, diarrhea, pneumonia and a few infectious diseases in humans (Riley, 2020). A variety of virulence factors are displayed by K. pneumoniae, including capsules, endotoxins, ferrous ferrites, iron removal mechanisms, binders, and antibiotic resistance that have been found to play major roles in pathogenesis (Zhang et al., 2018).

K. pneumonia is frequently found in food, including raw vegetables, milk powder, fish, and meat. It is reported to have a significant increase in foodborne outbreaks among different countries (Davis et al., 2015, Abu-Zaid et al., 2016, Hajikarim et al., 2020).

K. pneumoniae develops antibiotic resistance more easily than most bacteria by producing enzymes such as Extended Spectrum β-lactamase (ESBLs) and Carbapenemase (Padmini *et al.*, 2017). These bacteria develop resistance to antibiotics largely due to the evolution of bacterial enzymes of the superfamilies as a result of the diversity of genes (SHV-1., TEM-1, TEM-2,

TEM-12) that they encode (Egorov et al., 2018, Sukhum et al., 2019).

Antimicrobial resistance genes are passed from environmental bacteria through *K. pneumonia* (Wyres and Holt, 2018). Food consumption is one of the most common ways that transmit antibiotic-resistant bacteria and genes into the human digestive system (Verraes *et al.*, 2013). Antibiotics are mainly used in the poultry industry for treatment, prevention, and growth promotion to boost farm animal productivity (Kiambi *et al.*, 2021). In many countries of the world, antibiotics are given daily to food-producing animals to make them grow faster and prevent sickness (Milanović *et al.*, 2017).

Multifocal sequencing (MLST) has emerged as an effective new DNA typing tool for assessing genetic relatedness between species (Robles *et al.*, 2004). MLST is a molecular method that relies upon comparing sequenced portions of several housekeeping genes (genes that encode basic metabolic proteins processes functions), and identification of the "type of sequence" (ST) for each strain based on the existing alleles, phylogenetic analysis using the analyzed sites DNA sequence (Maiden *et al.*, 1998). MLST scheme for *K. pneumonia* was developed by Laure

^{*} Corresponding author e-mail: shaimaaobaid@vet.uoqasim.edu.iq, shaimaaobead@gmail.com.

Diancourt; using inner fragments housekeeping genes. These genes encode proteins essential for cellular metabolisms, such as RNA polymerase beta-subunit (*rpoB*), glyceraldehyde 3-phosphate dehydrogenase (*gapA*), phosphorine E (*phoE*), initiation, and periplasmic energy transducer (*tonB*). These were selected because they show a low level of mutation (Diancourt *et al.*, 2005).

This study aims to establish the extent of genetic diversity among *K. pneumonia* isolates that were isolated from diarrheal human and poultry using MLST analysis. This study, for the first time, determined the genetic diversity among *K. pneumonia* (*rpoB*), (gapA), (*phoE*) and (*tonB*) and provide evidence of antibiotic-resistant transmission between poultry and human.

2. Materials and Methods

2.1. Identification of K. pneumoniae from Fecal Samples

Seventy-five *K. pneumoniae* isolates were isolated and identified from fecal diarrheal humans and poultry samples and according to (Obaid and Hasson, 2021).

2.2. Antibiotic Resistance testing by VITEK-2 Compact

Antibiotic resistance testing (AST) was carried out using the VITEK-2 compact system based on the identification of Minimum inhibitory concentration technology using the AST-N222 card (Biomerieux/ France). This card contained the following Ampicillin, Piperacillin/tazobactam, Cefazolin, Cefoxitin, Ceftazidime, Ceftriaxone, Cefepime, Ertapenem, Imipenem, Amikacin, Gentamicin, Ciprofloxacin, Levofloxacin, Tigecycline, Nitrofurantoin, Trimethoprim/sulfamethoxazole. results interpreted according to (Wayne, 2011).

2.3. DNA extraction

Genomic DNA of *K. pneumoniae* isolates was extracted using PrestoTM Mini gDNA Bacteria Kit supplied from Geneaid Company as per manufacturer's instructions (Geneaid, USA). The extracted Chromosomal DNAs were used as DNA templates for MLST.

2.4. PCR amplification

PCR reactions were carried out according to Diancourt et al. 2005 using the following cycling conditions 94°C for 30 s; followed by 30 cycles of 95°C for 30 s; 45°C, or 50°C, or 60 °C for 30 s (annealing Tm was different to each gene according to (Diancourt et al., 2005) and 72°C for 30 s, with a final extension of 72°C for 10 min followed by the hold at 4°C. A 5 µl of the PCR products were loaded into 2% agarose gels with loading dye in 1 X TAE, and runs at 1X TAE for 7V/cm, 45min. The gels Images were captured using a gel documentation system (Genosens 2000 series, Japan).

Table 1. Primers used in the study according to (Diancourt *et al.*, 2005)

Gene name	Primer sequence (5'-3')	Size
(Locus)		(bp)
	F:gapA173: TGAAATATGACTCCACTCACGG	450
gapA	R:gapA181: CTTCAGAAGCGGCTTTGATGGCTT	430
	F:phoE604.1: ACCTACCGCAACACCGACTTCTTCGG	420
phoE	R:phoE604.2: TGATCAGAACTGGTAGGTGAT	
rpoB	F: Vic3: GGCGAAATGGCWGAGAACCA	501
	R: Vic2: GAGTCTTCGAAGTTGTAACC	
ton B	F:tonB1F: CTTTATACCTCGGTACATCAGGTT	414
	R:tonB2R: ATTCGCCGGCTGRGCRGAGAG	

F: forward R: reveres

2.5. PCR product sequencing

All the PCR products were cleaned and sequenced as follows: The Gel/PCR DNA Fragments extraction kit (Geneaid, USA) was used to remove the amplification primer from the PCR product, as directed by the manufacturer. Purified DNA was sequenced at Macrogen (Korea) using sequencing primers for each gene as described by Diancourt *et al.*, (2005), (Applied Biosystems, Foster City, CA, USA.

2.6. Multilocus sequence typing (MLST) analysis

The data from the raw sequences were edited and linked to the sequence of control. The Multi Locus Sequence Typing database provided the standard sequences for alignment. Multiple alignments were performed using ClustalW (Thompson et al., 1994) of Geneious Prime Software V2021.1 (Biomatters, Inc., North America). Identification of ST and allele profile was carried out by interrogation of gene sequences against the international MLST database at https://pubmlst.org/ and http://www.genomicepidemiology.org/. Regarding the identification of phylogenetic relationships among K. pneumoniae isolates, the merged edited sequences were used to generate phylogenetic tree using the PhyML maximum likelihood and the unweighted pair group method with arithmetic averages (UPGMA) (Kumar et al., 2018).

2.7. Statistical analysis

The Differences in data percentage values were analyzed by chi-square (X^2) test with the SPSS Statistics 25 software. The P < 0.05 Values were considered a statistical significance.

3. Results

3.1. Profile of Antibiotic Susceptibility of K. pneumoniae Isolates from diarrheal Human and Poultry

Human *K pneumoniae* were resistant to Ampicillin by 100%. The results revealed a high resistance rate (86%) to Cefazolin and, (60%) to each Ceftriaxone, Ceftazidime, Cefepime, and Trimethoprim/Sulfamethoxazole, but they showed a low level of resistance to Nitrofurantoin,

Cefoxitin, Gentamicin (46.6%), (33.3%), and (20%) respectively (Table 1).

Poultry *K pneumoniae* were resistant to Ampicillin (100%) and highly resistant to Cefazolin (46.6%) as well as it revealed resistance to Ciprofloxacin, Levofloxacin, and Trimethoprim/ Sulfamethoxazole (40%), followed by Ceftriaxone, Ceftazidime, Cefepime (33.3%).

Table (2) showed all these results, where the antibiotics resistance rate against K. pneumoniae isolates appeared as highly significantly different with a p-value (< 0.001).

Table 2: Antibiotic resistance of *K. pneumonia* isolated from diarrheal humans and poultry.

Classes	Members	Number and % of Resistant rate (Human)	Number and % of Resistant rate (poultry)	X^2	P-value
	Ampicillin	75(100)	75(100)		
	Piperacillin/Tazobactam	0(0)	5 (6.6)		
B-Lactam	Cefazolin	65(86.6)	35(46.6)	27	0.001*
	Ceftriaxone	45(60)	25(33.3)	10.71	0.001*
	Cefoxitin	25(33.3)	10(13.3)	8.38	0.004*
C 1	Ceftazidime	45(60)	25(33.3)	10.71	0.001*
Cephems	Cefepime	45(60)	25(33.3)	27 10.71 8.38	0.001*
	Ertapenem	0(0)	0(0)		
Carbapenems	Imipenem	0(0)	10(13.3)		
A	Amikacin	0(0)	10(13.3)		
Aminoglycoside	Gentamicin	15(20)	20(26.6)	0.932	0.001*
E1	Ciprofloxacin	5(6.6)	30(40)	23.29	0.001*
Fluor quinolones	Levofloxacin	5(6.6)	30(40)	23.29	0.001*
Glycylcycline	Tigecycline	0(0)	0(0)	0	
Nitro furans	Nitrofurantion	35(46.6)	20(26.6)	6.45	0.001*
Sulfonamides	Trimethoprim/Sulfamethoxazole	45(60)	30(40)	6	0.014*

X²: the test of chi-square, * significant difference (P<0.05).

3.2. Multilocus Sequence Typing Analysis (MLST)

3.2.1. Detection of Housekeeping genes using PCR:

The four K. pneumonia housekeeping genes were detected using PCR, sequenced and then analyzed by

MLST to determine the extent of genetic diversity and relation among human's *K. pneumoniae* (K1, K2, K3, K5, and K6), (K4 excluded from the study) and poultry's *K. pneumoniae* isolates (K7, K8, K9, K10 and K11).

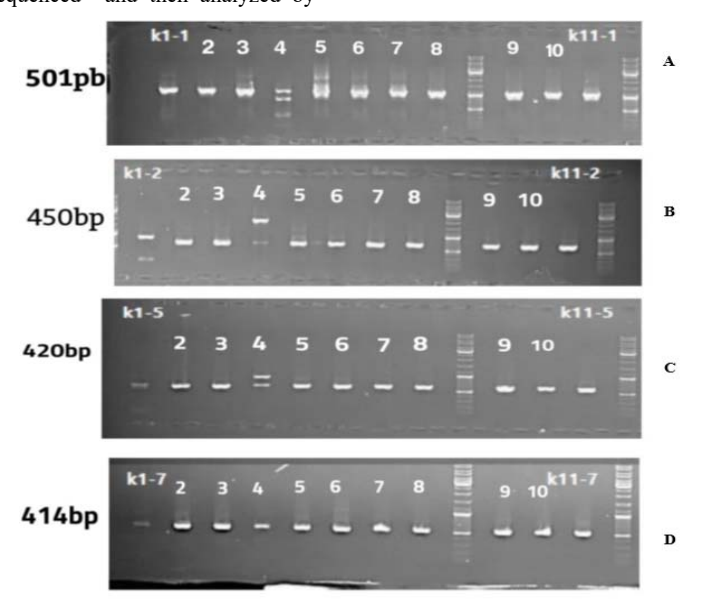


Figure 2. Electrophoresis the PCR product for A:rpoB (501 bp), B: gapA gene (450 bp), C:phoE gene (420 bp), and D:tonB gene (414 bp) of K. pneumoniae isolated from diarrheal human and poultry.

3.2.2. rpoB gene

Using UPGMA, the sequenced *rpoB* gene shows the phylogenetic Cladogram figures (2,3). There was no similarity detected in human *K. pneumoniae* isolates, but one group resemblance was found in poultry *K. pneumoniae* isolates (K9 and K10), while the link between *K. pneumoniae* in humans and poultry indicated two groups of commonalities (K6 with K7) samples and (K2 with K8) isolates.

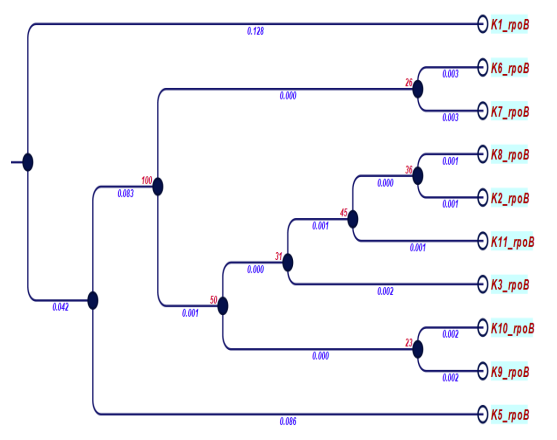


Figure 3. Phylogenetic Cladogram for *rpoB* gene of *K. pneumoniae* isolates from diarrhea human and poultry by using UPGMA, the blue text represents branch length and red text represents bootstrap values. (K1, K2, K3, K5, and K6) represent human *K. pneumonia* and (K7, K8, K9, K10, and K11) represent poultry *K. pneumoniae*.

3.2.3. The gap A gene

The outcomes of gap A sequence using UPGMA method showed phylogenetic cladogram figures (2,4). Except for one group, there are no similarities among all K pneumoniae isolates of human and poultry. The association between humans and poultry is reflected by similarities between isolates (K6 with K9).

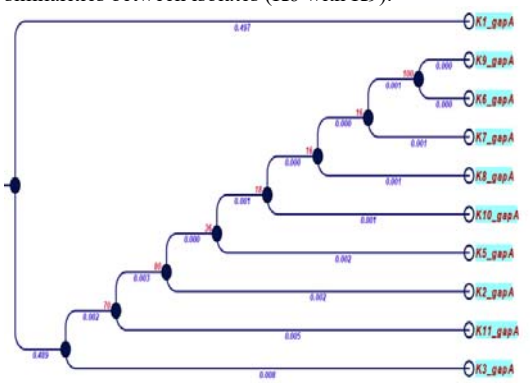


Figure 4. Phylogenetic Cladogram for *gapA* gene of isolates *K. pneumoniae* by using UPGMA, the blue text represents branch length and red text represents bootstrap values. (K1, K2, K3, K5, and K6) represent human *K. pneumonia* while (K7, K8, K9, K10, and K11) represent poultry *K. pneumoniae*.

3.2.4. The phoE gene

The phylogenetic tree of the *phoE* gene was shown in Figures 2 and 5. All human *K pneumoniae* isolates were different, while one group of poultry *K pneumoniae* isolates had similarities to one human K pneumoniae

isolate (K7 with K9). At the same time, two parallels between humans and poultry emerged in (K5-K11) and (K5-K12) (K6-K10).

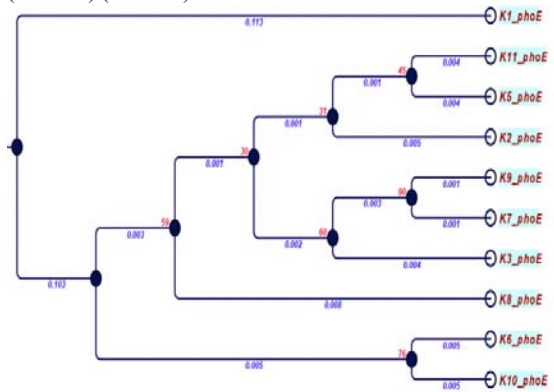


Figure 5. Phylogenetic Cladogram for *phoE* gene of isolates *K. pneumoniae* by using UPGMA, the blue text represents branch length and red text represents bootstrap values. (K1, K2, K3, K5, and K6) represent human *K. pneumonia* while (K7, K8, K9, K10, and K11) represent poultry *K. pneumoniae*.

3.2.5. The tonB gene

Phylogenetic tree of *tonB* gene (Fig 2 and 6) revealed there are differences in all humans and poultry *K. pneumoniae*. Three groups showed similarities between humans and poultry in (K2-K9), (K3-K10), and (K5-K8).

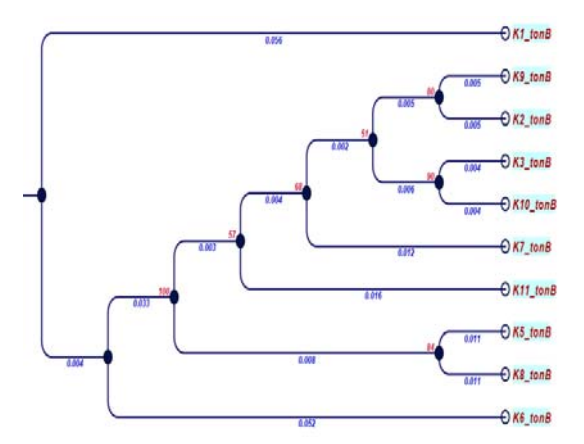


Figure 6. Phylogenetic Cladogram for *tonB* gene of isolates *K. pneumoniae* by using UPGMA, the blue text represents branch length and red text represents bootstrap values. (K1, K2, K3, K5, and K6) represent human *K. pneumonia* while (K7, K8, K9, K10, and K11) represent poultry *K. pneumoniae*.

MLST result of Diarrheal Human and Poultry based on locus gene and Allelic profile

Using the housekeeping genes, multilocus sequence typing was used to analyze the genetic diversity of *K. pneumoniae* isolates from diarrheal humans and poultry. Multiple sequence alignment of the four gene sequences from ten isolates revealed nucleotide sequence similarities and variations, as well as unique alleles (Table 3).

Multilocus sequence typing with four housekeeping genes and allelic profiles of 10 *K. pneumoniae* isolates from human and poultry feces were new sequence types of all isolates from both sources for all studied housekeeping genes as was generating many unique and novel alleles for the genes utilized in this investigation, particularly *tonB* gene alleles.

•							
Sample	Sours	ST	Nearest ST	All	Allelic profile		
				rpoB	gap A	pho E	ton B
K. pneumoniae 1	Human	New	1877	24	1*	72*	38*
K. pneumoniae 2	Human	New	857	24	2	56	19*
K. pneumoniae 3	Human	New	1300	1	4*	7	12*
K. pneumoniae 5	Human	New	2419 Or 4370	258*	10*	12	38*
K. pneumoniae 6	Human	New	1352	1*	2	191*	664*
K. pneumoniae 7	Poultry	New	3050 Or 1701	260	10*	275*	39*
K. pneumoniae 8	Poultry	New	15	1	1	1*	1*
K. pneumoniae 9	Poultry	New	3044 Or 4465	45*	2	275*	65*
K. pneumoniae 10	Poultry	New	3127	45	204*	334*	12*
K. pneumoniae 11	Poultry	New	3403 Or 1537	1	2	12	408

Table 3. MLST analysis to Identify MLST sequence types (STs), nearest ST, and allelic profiles of ten *K. pneumoniae* isolates from the fecal specimen of humans and poultry with four housekeeping genes.

Note: * represent Novel allele.

3.3. Genetic Relatedness of K. pneumoniae by MLST analysis among Diarrheal Humans and Poultry

The Multi- drug resistance B- Lactamase K. pneumoniae sequences of the four housekeeping genes revealed strong links between humans and poultry K pneumoniae (Figure 7). A tight association was discovered between K6 (human K. pneumoniae) and K11 (poultry K. pneumoniae), whereas a distance relationship was discovered (K1, K5, and K7) revision. A comprehensive tree based on a cladogram is presented as a method to determine the efficiency of K. pneumoniae isolated from fecal samples of people and poultry using the high potential of these genetically determined sections to give a realistic picture of the possibility of human infection with bacteria of animal origin such as chicken through identical or close genetic linkage.

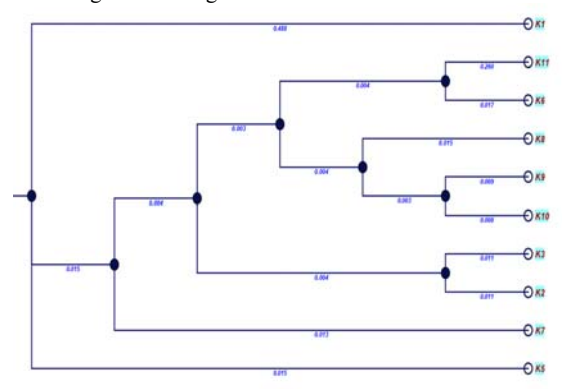


Figure 7. Cladogram Phylogenetic analysis of *K. pneumoniae* isolates from diarrheal human and poultry serotypes using PhyML maximum likelihood. (K1, K2, K3, K5, and K6) represent Human *K. pneumonia* also (K7, K8, K9, K10, and K11) represent Poultry *K. pneumoniae*.

4. Discussion

K. pneumoniae is a gastrointestinal commensal bacteria that occasionally causes diarrhea in humans. Some of the diarrhea traces carried the thermostable or thermolabile toxin (Forsythe et al., 2015). Identifying illness infection pathogenic mechanisms of Klebsiella can explain the interaction between bacterial cells and the host (Bengoechea and Sa Pessoa, 2019). K. pneumoniae

pathology has been attributed to many virulence genes that allow it to evade the host's innate defense responses such as *rpoB* (Beta-subunit of RNA polymerase B) *gapA* (Glyceraldehyde 3- Phosphate dehydrogenase), *tonB* (Periplasmic energy transducer) and *phoE* (Phosphoporine E) were responsible for the essential metabolic process in addition to pathogenicity and virulence activity related to antibiotic resistance (Alcántar-Curiel *et al.*, 2013, Blin *et al.*, 2017).

The production of a wide range of beta-lactamase or changing the permeability barrier or at the target site represented by the penicillin-binding protein, or a change in the outer membrane protein, are the most important problems of increasing infection in hospitals and the main causes of *K. pneumoniae* antibiotic resistance (beta-lactamase) (Aghamohammad *et al.*, 2020).

K. pneumoniae possesses many pumps that circulate and eject the antibiotic, especially Beta-lactam antibiotics including penicillin with cephalosporin, Alcarpinimat, and Monobactam among others (Smith and Kendall, 2021). Antimicrobial resistance is a global danger to food security, animal welfare, long-term therapy, and public health. Many variables contribute to the irrational use of antibiotics, including policymakers' perceptions of their expertise, manufacturers' prescriptions, consumers' perceptions of their knowledge, and dispensers' perceptions of their knowledge (Wall, 2019). rpoB gene, which codes for the RNA polymerase β -subunit, has emerged as a core gene candidate for phylogenetic analysis, allowing for the separation of closely related isolates (Michodigni et al., 2021). K. pneumoniae and other Klebsiella species can be correctly identified and differentiated using phylogenetic analysis of the rpoB gene. Urbaniak et al., (2018) recommended using the rpoB gene rather than the 16S rRNA gene to categorize Klebsiella. Both NAD-dependent phosphorylation and NAD-dependent conversion of Derythrose 4-phosphate are encoded by the gapA gene. phosphorylation NAD-dependent oxidative glyceraldehyde 3-phosphate to 1,3-bisphosphoglycerate is catalyzed by glyceraldehyde-3-phosphate dehydrogenase, while the NAD-dependent conversion of D-erythrose 4phosphate to 4-phosphoerythronate is catalyzed by erythrose-4-phosphate dehydrogenase. The periplasmic energy transducer is encoded by the tonB gene. phoE gene

(phosphoporine E), is a controller ion transmembrane transporter that regulates the expression of porins were present in the outer membrane of *K. pneumoniae* which responsible for antibiotic entry and actually associated with antibiotic resistance (Kaczmarek *et al.*, 2006).

Genotyping of rpoB. gapA, tonB and phoE is critical for identifying K. pneumoniae infections and determining the source and incidence of infections. MLST is a useful method for determining genetic diversity and population organization in epidemiological settings (Guo et al., 2016). The isolates K6 and K11 (which reflect the human-poultry interaction) were comparable in that they lacked ESBL and were resistant to Ampicillin, which was a novel finding in this investigation. The formation of extended spectrum beta-lactamase (ESBL), which is one of the most severe concerns of rising infection in hospitals, or modifying the permeability barrier or at the target site represented by a binding protein were the major causes of antibiotic resistance in K. pneumoniae (Tilahun et al., 2021). ESBL product due to continuous exposure of K. pneumoniae to b-lactam antibiotic resulted in a dynamic and persistent production and mutation of b-lactamases, which expanded their resistance activity (Shaikh et al., 2015).

In addition, new data in K6 and K11 (which represent the human-poultry interaction) show the same rate of resistance to tested antibiotics. As a result, the strain of antibiotic-resistant bacteria can be transmitted from animals to humans directly, such as through direct contact with farmers or veterinarians, or indirectly, through the consumption of contaminated animal feed, contaminated groundwater or surface water, and methods of animal waste treatment (Daniel et al., 2015). Antibiotic-resistant or vulnerable persons can be infected not just via direct contact but also through animal-derived food items. (Lekshmi et al., 2017). Furthermore, antibiotic-resistant bacteria in food are a major public health concern because they can transmit antibiotic resistance features to pathogenic bacteria, making it difficult to treat bacterial infections in the medical environment (Imran et al., 2019). However, when compared to gene-based phylogenetic methods, the multilocus sequence typing (MLST) analysis demonstrated a high detection specificity. As a result, the currently available PCR sequencing procedures, as well as phylogenetic tools, revealed surprisingly relationships between some of the isolated K. pneumoniae studied. MLST is thought to be a good method for characterizing the genetic links between bacterial isolates as well as identifying and tracking the global spread of drug-resistant strains (Adwan et al., 2020). In commercial cultures, antibiotics are used extensively in chickens, even with modest quantities of hormones, which may be one of the contributors to generating germ resistance in some people (Waters et al., 2022). It has a major influence and may increase the risk of cancer and premature puberty (Pérez-Rodríguez and Mercanoglu, 2019). The similarities of K11, K6, and differences between K1, K5, and K7 among the isolates categorized by MLST suggested that K. pneumoniae might be transmitted in the community from animal sources throughout time. Isolated K. pneumoniae could produce a significant signal of drug resistance among a considerable signal of drug resistance in the community. One of the most essential strategies for the rapid deployment of a substantial multi-drug resistance among bacteria is the horizontal transfer of drug resistance genes (Blin *et al.*, 2017).

5. Conclusions

The current study is considered the first in Iraq and the world on the genetic relationship between *K. pneumoniae* isolates from humans and poultry. *K. pneumoniae* has a high rate of antibiotic resistance and high genetic diversity as a result of the sequencing of (*rpoB*, *gapA*, *phoE* and *tonB* genes) of human and poultry isolates. The genetic association (similarity) of antibiotic resistance *K. pneumoniae* strain between both sources where all isolates are resistant to most antibiotic agents in significant differences is evidence of the transmission of isolates from an animal source (poultry) to humans which poses a public health threat. As a result, control measures for *K. pneumoniae* transmission between humans and poultry, as well as cautious antibiotic use in human therapeutic strategies and poultry production, are required.

Acknowledgments

This study was supported by the Veterinary Medicine College, Al-Qasim Green University, Veterinary Teaching Hospital, and Private Clinics in Babylon Province, Iraq.

Conflict of Interest

"The authors declare that there are no conflicts of interest regarding the publication of this manuscript."

References

Abu-Zaid A A, Sehrawy M, Mahmoud H and A H Nemari. 2016. Detection of Klebsiella pneumonia in raw food and their antibiotic resistance. *Adv Env Biol.*, **10(4)**: 80-92.

Adwan G M, Owda D M and Abu-Hijleh A A. 2020. Prevalence of Capsular Polysaccharide Genes and Antibiotic Resistance Pattern of Klebsiella pneumoniae in Palestine. *Jordan J Biol Sci.*, **13(4).**

Aghamohammad S, Badmasti F, Solgi H, Aminzadeh Z, Khodabandelo Z and Shahcheraghi F. 2020. First report of extended-spectrum beta-lactamase-producing Klebsiella pneumoniae among fecal carriage in Iran: high diversity of clonal relatedness and virulence factor profiles. *Microb Drug Resis*, 26(3): 261-269.

Alcántar-Curiel MD, Blackburn D, Saldaña Z, Gayosso-Vázquez C, Iovine NM, De la Cruz MA, Girón JA. 2013. Multi-functional analysis of Klebsiella pneumoniae fimbrial types in adherence and biofilm formation. Virulence. 15;4(2):129-38. doi: 10.4161/viru.22974.

Bengoechea J A and Pessoa J Sa. 2019. Klebsiella pneumoniae infection biology: living to counteract host defenses. FEMS *Microbiol Rev*, **43(2)**: 123-144.

Blin C, Passet V, Touchon M, Rocha E P and Brisse S. 2017. Metabolic diversity of the emerging pathogenic lineages of Klebsiella pneumoniae. *Env Microbiol*, **19(5)**: 188-1898-1.

Daniel D S, Lee S M, Dykes G A and Rahman S. 2015. Public health risks of multiple-drug-resistant Enterococcus spp. in Southeast Asia. *App Env Microbiol*, **81(18)**: 6090-6097.

Davis, G S, Waits K, Nordstrom L, Weaver B, Aziz M, Gauld L, Grande H, Bigler R, Horwinski J and Porter S. 2015. Intermingled Klebsiella pneumoniae populations between retail meats and human urinary tract infections. *Clin Inf Dis.*, **61(6):** 892-899.

Diancourt L, Passet V, Verhoef J, Grimont P A and Brisse S. 2005. Multilocus sequence typing of Klebsiella pneumoniae nosocomial isolates. *J Clin Microbiol*, **43(8)**: 4178-4182.

Egorov A, Ulyashova M and Rubtsova M Y. 2018. Bacterial enzymes and antibiotic resistance. *Acta Naturae*, **104** (**39**): 33-48.

Forsythe S J, Abbott S L and Pitout J. 2015. Klebsiella, enterobacter, citrobacter, cronobacter, serratia, plesiomonas, and other enterobacteriaceae. *Manual Clin Microbiol*, 714-737.

Guo Y, Zhou H, Qin L, Pang Z, Qin T, Ren H, Pan Z and Zhou J. 2016. Frequency, antimicrobial resistance and genetic diversity of Klebsiella pneumoniae in food samples. *PLoS One.*, 11(4): e0153561.

Hajikarim F, Dallal M M S, Pourmand M R and Abdi M. 2020. An investigation of extended-spectrum β -lactamases (ESBLs) in Klebsiella isolated from foodborne outbreaks in Iran. *Gene Rep*, **19**: 100632.

Imran M, Das K R and Naik M M. 2019. Co-selection of multiantibiotic resistance in bacterial pathogens in metal and microplastic contaminated environments: An emerging health threat. Chemosphere., 215: 846-857.

Kaczmarek FM, Dib-Hajj F, Shang W and Gootz T. 2006. High-level carbapenem resistance in a Klebsiella pneumoniae clinical isolate is due to the combination of bla(ACT-1) beta-lactamase production, porin OmpK35/36 insertional inactivation, and down-regulation of the phosphate transport porin phoe. *Antimicrob Agents Chemother.*, **50(10)**:3396-406. doi: 10.1128/AAC.00285-06.

Kiambi, S, Mwanza R, Sirma A, Czerniak C, Kimani T, Kabali E, Dorado-Garcia A, Eckford S, Price C and Gikonyo S. 2021. Understanding Antimicrobial Use Contexts in the Poultry Sector: Challenges for Small-Scale Layer Farms in Kenya. *Antibiotics*, **10(2)**: 106.

Kumar S, Stecher G, Li M, Knyaz C and Tamura K. 2018. MEGA X: molecular evolutionary genetics analysis across computing platforms. *Mol Biol Evol*, **35(6)**: 1547.

Lekshmi M, Ammini P, Kumar S and Varela M F. 2017. The food production environment and the development of antimicrobial resistance in human pathogens of animal origin. *Microorganisms*, **5(1)**: 11.

Maiden M C, Bygraves J A, Feil E, Morelli G, Russell J E, Urwin R, Zhang Q, Zhou J, K and Caugant D A. 1998. Multilocus sequence typing: a portable approach to the identification of clones within populations of pathogenic microorganisms. *Proc Nat Academy Sci*, **95(6)**: 3140-3145.

Michodigni N F, Nyacheo A, Akhwale J K, Magoma G and Kimang'a A N. 2021. Molecular Identification of Co-Existence of Carbapenemase and Extended-Spectrum β-Lactamase Genes in Klebsiella pneumoniae Clinical Isolates, and Their Phylogenetic Patterns in Kenya. *Adv Microbiol*, **11(8):** 399-415.

Milanović V, Osimani A, Aquilanti L, Tavoletti S, Garofalo C, Polverigiani S, Litta Mulondo A, Cocolin L, Ferrocino I and Di Cagno R. 2017. Occurrence of antibiotic resistance genes in the fecal DNA of healthy omnivores, ovo-lacto vegetarians and vegans. *Mol Nut Food Res*, **61(9)**: 1601098.

Obaid W F and Hasson S O. 2021. Pattern of Multi Drug Resistance with Biofilm Formation among Klebsiellapneumoniaisolated from Fecal Samples of Diarrheal Iraqi Patients. Annals of the Romanian Society for Cell Biology, 5350-5360.

Padmini N, Ajilda AK, Sivakumar N and Selvakumar G. 2017. Extended spectrum β -lactamase producing Escherichia coli and Klebsiella pneumoniae: critical tools for antibiotic resistance pattern. *J Basic Microbiol.*, **57(6):** 460-470.

Pérez-Rodríguez F and Mercanoglu Taban B. 2019. A state-of-art review on multi-drug resistant pathogens in foods of animal origin: risk factors and mitigation strategies. *Front Microbiol*, 2091.

Riley LW 2020. Extraintestinal foodborne pathogens. Annual review of food science and technology, 11: 275-294.

Robles JC, Koreen L, Park S and Perlin DS. 2004. Multilocus sequence typing is a reliable alternative method to DNA fingerprinting for discriminating among strains of Candida albicans. *J Clin Microbiol*, **42(6)**, 2480–2488.

Shaikh S, Fatima J, Shakil S, Rizvi SM, Kamal MA. 2015. Antibiotic resistance and extended spectrum beta-lactamases: Types, epidemiology and treatment. *Saudi J Biol Sci*, **22(1)**:90-101. doi: 10.1016/j.sjbs.2014.08.002.

Smith HZ and Kendall B. 2021. Carbapenem Resistant Enterobacteriaceae." StatPearls [Internet]

Sukhum KV, Diorio-Toth L and Dantas G 2019. Genomic and metagenomic approaches for predictive surveillance of emerging pathogens and antibiotic resistance. *Clin Pharmacol Therap*, **106(3)**: 512-524.

Tilahun M, Kassa Y, Gedefie A, and Ashagire M. 2021. Emerging Carbapenem-Resistant Enterobacteriaceae Infection, Its Epidemiology and Novel Treatment Options: A Review. *Inf Drug Resis*, **14**:4363–4374. https://doi.org/10.2147/IDR.S337611

Thompson J, Higgins DG and Gibson TJ. 1994. CLUSTAL W: improving the sensitivity of progressive multiple sequence alignment through sequence weighting, position-specific gap penalties and weight matrix choice. *Nuc Acids Res*, **22(22)**: 4673-4680.

Urbaniak C, Sielaff AC, Frey K, Allen J, Singh N, Jaing C, Wheeler K and Venkateswaran K. 2018. Detection of antimicrobial resistance genes associated with the International Space Station environmental surfaces. *Scientific Rep*, 8(1): 1-13.

Verraes C, Van Boxstael S, Van Meervenne E, Van Coillie E, Butaye P, Catry B, de Schaetzen A, Van Huffel X, Imberechts H, Dierick K, Daube G, Saegerman C, De Block J, Dewulf J and Herman L. 2013. Antimicrobial resistance in the food chain: a review. *Int J Env Res Public Health*, **10(7)**: 2643–2669. https://doi.org/10.3390/ijerph10072643

Wall S. 2019. Prevention of antibiotic resistance—an epidemiological scoping review to identify research categories and knowledge gaps. Global Health Action., 12(sup1): 1756191.

Waters F, Baca M, Graham P. 2022. Antibiotic use by backyard food animal producers in Ecuador: a qualitative study. *BMC Public Health* **22**:685. https://doi.org/10.1186/s12889-022-13073-4

Wayne P 2011. Clinical and laboratory standards institute. Performance standards for antimicrobial susceptibility testing.

Wyres KL. and Holt KE. 2018. Klebsiella pneumoniae as a key trafficker of drug resistance genes from environmental to clinically important bacteria. *Curr Opinion Microbiol*, **45**: 131-139.

Zhang S, Yang G, Ye Q, Wu Q, Zhang J and Huang Y. 2018. Phenotypic and genotypic characterization of Klebsiella pneumoniae isolated from retail foods in China. *Front Microbiol*, **9**:289

Jordan Journal of Biological Sciences

Prokaryotic Expression of Murine Cellular Prion Protein for In vitro Evaluation

Hoang-Anh Le-Dao^{1,2,3,+}, Yen-Vy Le-Nguyen^{1,2,3,+}, Hieu Tran-Van^{1,2,3,*}

¹Department of Molecular and Environmental Biotechnology, Faculty of Biology and Biotechnology, University of Science, Ho Chi Minh City 700000, Vietnam; ²Laboratory of Biosensors, Faculty of Biology and Biotechnology, University of Science, Ho Chi Minh City 700000, Vietnam; ³Vietnam National University, Ho Chi Minh City 700000, Vietnam

Received: June 4, 2021; Revised: August 2, 2021; Accepted: August 25, 2021

Abstract

M cell (Microfold cell) targeting is a potential strategy for oral vaccine development due to its role in presenting antigen to mucosal lymphoid tissue. Numerous researches have focused on directing vaccine antigens to M cell receptors, based on their affinity with specific ligands. This study was aimed to biosynthesize murine cellular prion protein (mPrP^C), a highly expressed receptor on the M cell apical surface. The mPrP^C coding sequence was obtained by PCR for construction of pGEX-5X-1-mprpc plasmid. Then, recombinant plasmid was induced for expression in E. coli BL21(DE3) cells by IPTG. The overexpression of mPrP^C was confirmed by SDS-PAGE and Western blotting. Since the expressed protein was found to remain mostly in insoluble fraction, DTT and glycerol were used to improve the solubility. This soluble, recombinant mPrP^C could be used for in vitro evaluation, and also on further research for developing antigen targeting M cell.

Keywords: cellular prion protein, gene expression, M cells, microfold cells, SDS-PAGE.

1. Introduction

Gastrointestinal mucus is the largest surface of the human body frequently exposed to microbial pathogens from the environment. The most effective treatment for the infection is antibiotic which can cause antibiotic-resistance (Ventola, 2015). This is a serious global concern that requires an alternative solution for these pathogens. Oral vaccine protects against mucosal infection because of its efficiency in inducing mucosal immune responses, inclusively elicit antigen-specific secretory IgA, or even inducing systemic immune responses (Baumann, 2008). However, the number of oral vaccines is still limited due to some disadvantages. For example, vaccine antigens resist the harsh conditions, large-area surface in the gastrointestinal tract resulting in antigen dispersion; moreover, the intestine tends to become immune-tolerance because of continuously being exposed to numerous external antigens (Pabst and Mowat, 2012). To overcome these challenges, multiple strategies for targeting vaccines to gut-associated lymphoid tissue (GALT), where the antigen sampling takes place and immune responses induced, have been implemented. A specialized cell that has an important role in antigen sampling is M cell (Microfold cell), which is found overlying Peyer's patches (PP) and containing lymphoid follicles of GALT (Sansonetti and Phalipon, 1999). Current knowledge on M cell has shown that antigen uptake occurs via surface receptors, and antigen transports through dorm structure to beneath lymphoid tissue and present to PP's immunocytes, leading to the production of specific IgA (Neutra et al., 2001, Azizi et al., 2010). Because of these characteristics, orientating vaccine antigen to M cell receptors is a promising strategy and has been carried out in many studies (Huynh et al., 2019, Shima et al., 2014). For research on this strategy, it is necessary to identify the ligands of M cell receptors and verify the interaction between them. PrP^C is a highly expressed receptor on M cell apical membrane and proved to have interactions with Heat shock protein (Hsp)60 from Brucella abortus (Nakato et al., 2012), which is found to be an immunodominant antigen of many pathogenic bacteria (Kaufmann, 1990). These features make PrP^C-Hsp60 a potential receptor-ligand for M cell targeting vaccine antigen.

In this present study, we proceeded on expressing the recombinant murine PrPC receptor fused with GST-tag in E. coli prokaryotic expression system in which GST tag would enhance solubility and support for in vitro interaction evaluation with recombinant Hsp60 ligand in further study; moreover, this result was a prerequisite for studies on the application of this receptor-ligand in oral vaccine development.

2. Materials and Methods

Isolation of mprpc gene: mprpc gene corresponding to 1792-2415 of Mus musculus prion protein (Prnp) mRNA (NM_001278256.1) was amplified by PCR using a DNA

CO-IIIst authorship

⁺ Co-first authorship

^{*} Corresponding author. e-mail: tvhieu@hcmus.edu.vn.

Engine Tetrad thermal cycler (MJ Research, USA) with forward primer (5'-ggatccccaaaaageggccaaagcctgg-3') containing a *Bam*HI restriction site underlined, and reverse primer (5'-ctcgagctaggatcttctcccgtcgtaatag-3') containing a *Xho*I restriction site underlined. The PCR reaction (50 μl total volume) contains 2x MyTaq Red Mix (Bioline, Canada), 25 μl; 15 μM primer (PhuSa Biochem, Vietnam), 1 μl each; 200 ng template plasmid pET-*mprpc* from our previous work (Truong-Ha *et al.*, 2019), 1 μl; and sterile distilled water, 22 μl. PCR conditions were performed: initial denaturation 2 min at 95°C, followed by 30 cycles of 15 sec at 95°C, annealing for 15 sec at 65°C, extension for 15 sec at 72°C, and final extension at 72°C for 10 min before cooling to 30°C.

2.1. Recombinant plasmid construction:

mprpc gene and cloning vector pGEX-5X-1 containing GST were treated with the same restriction enzymes BamHI and XhoI (Thermoscientific, USA) to produce compatible sticky ends. Subsequently, the treated gene was ligated to digested plasmid using T4 DNA ligase (Thermoscientific, USA).

2.2. Cloning procedure

the competent E. coli DH5a cells (New England Biolabs, USA) was prepared by ice-cold CaCl₂ 100 mM buffers using the Hanahan Method (Green and Sambrook, 2018). The ligated product was transformed into E. coli DH5 α by incubating the mixture of competent cells and ligated product on ice for 10 min, then placing at 45°C for 90 sec, and cooling down on ice for 10 min (heat-shock method) (Sambrook and Russell, 2001). The transformed cells were screened onto Luria-Bertani (LB) agar plate containing ampicillin (LB-Amp) for selection of recombinant clones. Transformants grown on plate were screened by colony PCR using the same thermal cycler and condition, which was mentioned in isolation of mprpc. PCR product was showed on 1.5% agarose gel. The sequence of inserted gene from positive colonies was confirmed by sequencing alignment with the obtained sequence gene. Successfully constructed recombinant plasmid pGEX-5X-1-mprpc was purified using EZ-10 Spin Column Plasmid DNA Minipreps Kit (Biobasic, Canada). Purified plasmid was transformed into E. coli BL21(DE3) (New England Biolabs, USA) chemically competent cells for overexpression of recombinant protein. The colonies grown on LB-Amp agar plate were confirmed for carrying recombinant plasmid by colony PCR using same setting mentioned above with pGEX5 primer (5'-ggcaagccacgtttggtg-3') and pGEX3 primer (5'ggagctgcatgtgtcagagg-3').

Protein expression and Western blotting: the positive *E. coli* BL21(DE3) colony was cultivated in LB broth supplemented with ampicillin (100 ug/ml) overnight at 37°C. On the following day, a subculture was made by transferring the inoculum into fresh LB-Amp with a ratio of 1:10 (v/v), and it was then incubated in shaker until OD₆₀₀ reached 0.6-0.8. The expression was induced by IPTG at final concentration of 0.1 mmol/L at 16°C for 16 h in a 200-rpm shaker incubator. The culture was

centrifuged to obtain cell pellet, which was dissolved in lysis buffer, PBS which composed of 137 mM of NaCl. 2.7 mM KCl, 10 mM Na₂HPO₄, 1.8 mM KH₂PO₄, pH 7.4. To increase soluble fraction, DTT (2 mM) and glycerol (10%) were added to cell lysis buffer. Suspended cells were lysed by sonication (15 cycles, pulse for 10 sec on and 10 sec off) and then were centrifuged at 10,000 rpm for 10 min to separate soluble and insoluble fractions. The protein expression analysis of recombinant mPrPC-GST was conducted simultaneously with the GST protein expressed from cloning plasmid pGEX-5X-1 with the same procedure. Total cellular protein, soluble and insoluble protein phase was subjected to a SDSpolyacrylamide gel electrophoresis (SDS-PAGE method) according to standard protocol (Sambrook and Russell, 2006) and Coomassie Brilliant Blue staining. Protein separated after SDS-PAGE was then transferred onto a nitrocellulose membrane via Trans-Blot SD Semi-Dry Transfer Cell (Biorad, USA). The membrane was blocked with skim milk 5% in PBS + Tween20 (0.05%) (PBS-T). Blocked membrane was incubated with antibody (Anti-GST monoclonal mouse HRP (Proteintech, USA)) (1:50 000) for 30 mins. The protein bands were visualized by adding TMB substrate (Thermoscientific, USA).

3. Results

The pGEX-5X-1-mprpc plasmid construction was described in Fig. 1A. The insertion of mprpc was identified by nucleotide sequencing on positive clone to confirm that the cloned gene was matched with designed sequence and correct direction.

The recombinant plasmid was isolated and transformed to *E. coli* BL21(DE3) expression host and recombinant clones were screened by colony PCR. The difference in fragment length in Fig. 1B, lane 2-4 after PCR using pGEX5/pGEX3 primers identified the positive clone containing pGEX-5X-1-*mprpc* recombinant plasmid.

mPrPC-GST expression was induced with IPTG at low temperature. The expression was analyzed by SDS-PAGE, simultaneously with the expression of GST protein in the same condition. The result showed that the expression of mPrP^C fused GST-tag was seen as a band at approximately 49 kDa size, corresponding with the sum of the 23 kDa mPrP^C protein and the 26 kDa GST-tag (Fig. 2A, lane 4), and this band was not seen in total cellular protein of controls (Fig. 2A, lane 1-3). When analyzing soluble and insoluble fractions of induced cell lysate, the mPrPC-GST protein band was seen mostly in insoluble fraction (Fig 2A, lane 5, 6). After adding DTT 2 mM and glycerol 10% to cell lysis buffer, the solubility of expressed protein was improved by about 147.8% (analyzed using ImageJ software) and could be clearly observed in Fig. 2A, lane 8. In addition, the expression of target protein was confirmed by Western blot using specific anti-GST antibody. Figure 2B showed that the antibody bound to GST-fused protein. These results confirmed that the mPrPC was expressed successfully and can be obtained from soluble fraction of cell lysate in the presence of DTT and glycerol.

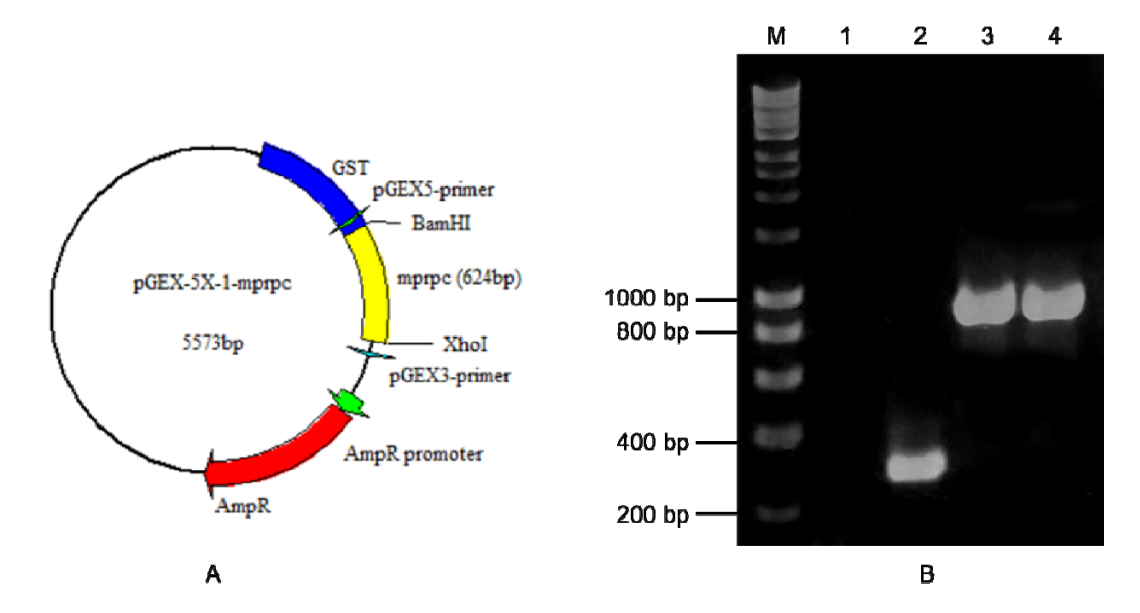


Figure 1. Construction of E. coli BL21(DE3) harboring pGEX-5X-1-mprpc. A: recombinant vector map pGEX-5X-1-mprpc. B: Bacterial colony screening by PCR. M: DNA HyperLadder, lane 1: negative control, lane 2: colony PCR with pGEX-5X-1 transformant, lane 3-4: colony PCR with pGEX-5X-1-mprpc transformants.

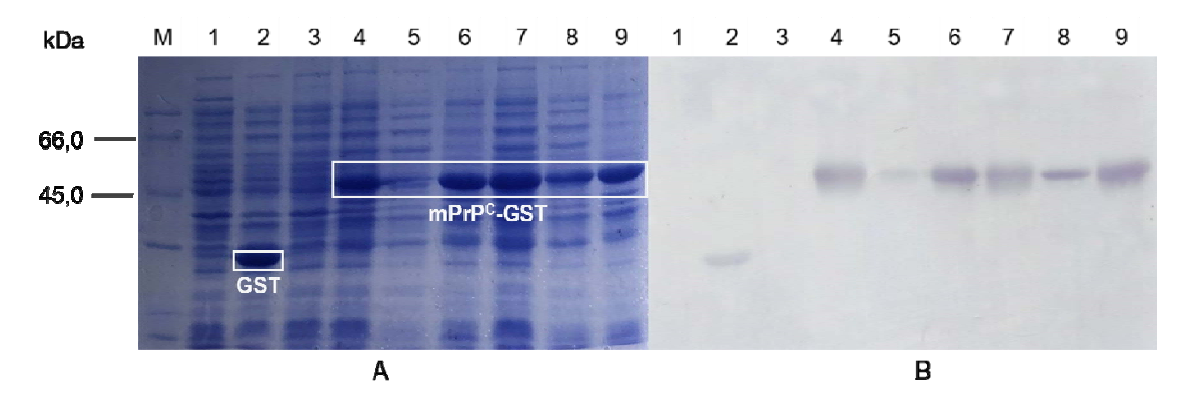


Figure 2. SDS-PAGE (A) and Western blotting (B) analysis of mPrP^C-GST expression. M: protein molecular weight standard, lane 1: E. coli BL21(DE3) cell lysate, lane 2: total cellular protein of induced E. coli BL21(DE3)/pGEX-5X-1, lane 3: non-induced E. coli BL21(DE3)/pGEX-5X-1-mprpc, lane 4-6: total cellular protein, soluble fraction, insoluble fraction of clone expressing mPrP^C-GST, lane 7-9: total cellular protein, soluble fraction of clone expressing mPrP^C-GST with DTT and glycerol supplemented in lysis buffer.

4. Discussion

M cell is a promising target in the development of oral vaccine, an effective prevention method for mucosal infectious diseases (Wang *et al.*, 2014, Kim *et al.*, 2012). Due to the important role of M cell in antigen entry to the mucosal immune system, we have been currently focusing on M cell targeting strategies. Many studies have shown that PrP^C membrane receptor of M cell has an affinity for Hsp60 protein from *Brucella abortus* (Edenhofer *et al.*, 1996, Nakato *et al.*, 2012). Therefore, we conducted to express recombinant murine PrP^C (mPrP^C) for being used as a source for *in vitro* interaction evaluation with recombinant Hsp60. The result of this study was a prerequisite for further studies.

Expressed mPrP^C-GST was aggregated in insoluble fraction of cell lysate. This was a disadvantage for the next steps of interaction evaluation. We considered using several chemical agents to improve soluble protein yield.

DTT and glycerol were seen to have the most effectiveness leading to a deductive explanation as follows: mPrP^C-GST was expressed and formed non-classical inclusion bodies containing insoluble proteins encapsulated correctly folded proteins (Peternel *et al.*, 2006), in *E. coli* cytoplasm. The presence of glycerol in lysis buffer inhibited protein aggregation and DTT has the ability to break disulfide bonds between surrounding precipitated, misfolded protein, helped release proper folded soluble protein.

As many other specific proteins from animal organisms, isolation of PrP^C from gut is a time-consuming and intensive laboratory procedure (Lee, 2017, Pan *et al.*, 1993). Hence, attempts of overexpressing high-yield PrP^C were described. In Weiss *et al.* work (Weiss *et al.*, 1995), cellular prion protein from Syrian golden hamster fusion GST was synthesized using three different systems including *E. coli*. To compare with solubilizing method of this study, DTT and glycerol were used as described below, while recombinantly expressed Syrian golden hamster PrP^C was soluble only in the presence of 2%

sarcosyl since it has the ability to encapsulate proteins and disrupt aggregates (Tao *et al.*, 2010). As mentioned, we used several chemical agents to solubilize fusion protein, and it was found that the solubilizing effect of sarcosyl was lower than that of DTT and glycerol combination (data not shown), which led us to use these reagents for protein solubility improvement.

5. Conclusion

In summary, the soluble form of murine cellular prion protein was successfully biosynthesized and could play a vital role as a potential receptor of M cell for targeting oral vaccine development. *In vitro* interaction evaluating with Hsp60 ligand, *ex vivo* and *in vivo* evaluation could be performed as a premise for further researches on Hsp60 ligand application as a vaccine orientating tag.

Acknowledgements

This research did not receive any specific grant from funding agencies in the public, commercial, or not-forprofit sectors.

Conflict of Interest

Authors declare that there is no conflict of interest.

References

Azizi A et al. 2010. Enhancing oral vaccine potency by targeting intestinal M cells. PLoS Pathog., 6(11): e1001147.

Baumann U. 2008. Mucosal vaccination against bacterial respiratory infections. Expert Rev Vaccines., 7(8): 1257-1276.

Edenhofer F *et al.* 1996. Prion protein PrPc interacts with molecular chaperones of the Hsp60 family. *Journal of virology.*, **70(7):** 4724-4728.

Green MR and Sambrook J. 2018. The Hanahan Method for Preparation and Transformation of Competent Escherichia coli: High-Efficiency Transformation. *Cold Spring Harb Protoc*, **2018(3)**.

Huynh K-Q et al. 2019. Cloning, expression, purification and interaction evaluation of 30 amino acids in C terminus of Clostridium perfringens toxin with its receptor Claudin-4. Science and Technology Development Journal - Natural Sciences., 2: 47-55.

Kaufmann SH. 1990. Heat shock proteins and the immune response. *Immunol Today.*, **11(4):** 129-136.

Kim S-H, Lee K-Y and Jang Y-S. 2012. Mucosal Immune System and M Cell-targeting Strategies for Oral Mucosal Vaccination. *Immune network.*, **12(5)**: 165-175.

Lee CH. 2017. A Simple Outline of Methods for Protein Isolation and Purification. *Endocrinology and metabolism (Seoul, Korea)*. **32(1)**: 18-22.

Nakato G et al. 2012. Cutting Edge: Brucella abortus exploits a cellular prion protein on intestinal M cells as an invasive receptor. J Immunol., 189(4): 1540-1544.

Neutra MR, Mantis NJ and Kraehenbuhl JP. 2001. Collaboration of epithelial cells with organized mucosal lymphoid tissues. *Nat Immunol.*, **2(11)**: 1004-1009.

Pabst O and Mowat AM. 2012. Oral tolerance to food protein. *Mucosal Immunol.*, **5(3)**: 232-239.

Pan KM et al. 1993. Conversion of alpha-helices into beta-sheets features in the formation of the scrapie prion proteins. Proceedings of the National Academy of Sciences of the United States of America., 90(23): 10962-10966.

Peternel Š *et al.* 2006. Nonclassical inclusion bodies in *Escherichia coli. Microbial Cell Factories.*, **5(1):** P23.

Sambrook J and Russell DW. 2006. SDS-Polyacrylamide Gel Electrophoresis of Proteins. *CSH protocols.*, **2006**.

Sambrook J and Russell DW. 2001. **Molecular cloning: a laboratory manual**. Cold Spring Harbor Laboratory Press, New York

Sansonetti PJ and Phalipon A. 1999. M cells as ports of entry for enteroinvasive pathogens: mechanisms of interaction, consequences for the disease process. *Semin Immunol.*, **11(3)**: 193-203

Shima H *et al.* 2014. A novel mucosal vaccine targeting Peyer's patch M cells induces protective antigen-specific IgA responses. *Int Immunol.*, **26(11)**: 619-625.

Tao H et al. 2010. Purifying natively folded proteins from inclusion bodies using sarkosyl, Triton X-100, and CHAPS. Biotechniques., 48(1): 61-64.

Truong-Ha M-N, Huynh K-Q and Tran-Van H. 2019. Cloning, expression, and refolding prion protein (PrPC) from murine fused with GST-tag. *Can Tho University Journal of Science.*, **55:** 16-22.

Ventola CL. 2015. The antibiotic resistance crisis: part 1: causes and threats. *Pharmacy and Therapeutics.*, **40(4):** 277-283.

Wang M et al. 2014. Roles of M cells in infection and mucosal vaccines. Human vaccines & immunotherapeutics., 10(12): 3544-3551.

Weiss S *et al.* 1995. Overexpression of active Syrian golden hamster prion protein PrPc as a glutathione S-transferase fusion in heterologous systems. *J Virol.*, **69(8)**: 4776-4783.

Jordan Journal of Biological Sciences

Impact of Diabetic Retinopathy on Vulnerability of Atherosclerosis in Type 1 Diabetes: the Role of Lipid Ratios as a Metabolic Biomarker

Walid Hassene Hamri^{1.2}, Mustapha Diaf ^{1,*}, Noria Harir^{1.2}

¹Department of Biology, Faculty of Natural and Life Sciences, Djillali Liabes University of Sidi-bel-Abbes, Algeria; ²Laboratory of Molecular Microbiology, Proteomics and Health, Department of Biology, Faculty of Natural and Life Sciences, Djillali Liabes University of Sidi-bel-Abbes, Algeria.

Received: April 14, 2021; Revised: September 18, 2021; Accepted: September 25, 2021

Abstract

This study aims to examine the correlation between diabetic retinopathy (DR) and early atherosclerotic changes in type 1 diabetics. We conducted a cross-sectional and observational study of 293 type 1 diabetic patients who attended the Diabetes Center from January 2015 to December 2019 in Sidi-bel-Abbès province, northwest Algeria. The patients were segregated into the following groups: patients with DR and patients without DR. Our study revealed a definite preponderance of males (52.60%). The mean age was 28.26±10.52 years, whereas the diabetes duration was 10.15±9.06 years. The overall prevalence of DR was 32.1%. TC/HDL ratio was a strong indicator for atherosclerotic disease (sensitivity of 66.0%, a specificity of 64.8%, and diagnostic accuracy of 0.653). Our results reported that the 4th quartiles (OR= 2.15 [1.08-4.27]; p=<0.02) of TC/HDL ratio was markedly greater in DR patients. Likewise, the fourth quartile of TG/HDL ratio was significantly greater in DR patients (OR= 2.06 [1.03-4.13]; p=0.03). In contrast to females who developed DR, lipid ratios and lipid profiles were significantly greater in male patients. Patients who develop DR are characterized by dyslipidemia and a higher risk of atherosclerotic disease. Thus, early detection of DR accompanied by a more careful cardiovascular assessment in these patients is crucial to prevent premature cardiovascular morbidity and mortality.

Keywords: Diabetic retinopathy, type 1 diabetes, atherosclerosis, dyslipidemia.

1. Introduction

Endothelial dysfunction and increased arterial stiffness are linked to the development of atherosclerosis in type 1 diabetes (T1D), both of which may contribute to an increase in cardiovascular (CV) mortality. (Jenkins et al., 2019). Cardiovascular disease (CVD) caused by atherosclerosis is considered a significant cause of morbimortality in patients with T1D. Among the risk factors linked with the development of CV risk in diabetics are age, smoking, proteinuria, glomerular dysfunction, deteriorated glycemic control, obesity, hypertension, lipid values and the duration of diabetes (de Ferranti et al., 2014). Even in patients who maintain acceptable glycemic control, the risk of mortality from CVD remains higher than that of non-diabetic people (Lind et al., 2014). Patients with T1D usually do have higher incidences of hypertension and hypercholesterolemia compared with the overall population (Livingstone et al., 2012). Thus, the underlying pathways following the escalated risk of mortality from CVD among patients with T1D who have good glycemic control are not well explained. Recently, it has been reported that there is a shared background for the progression of endothelial complications of T1D related to mutual pathogenic mechanisms in all types of complications (Garofolo et al., 2019). Diabetic retinopathy

(DR) remains a prevalent and distinct microvascular complication of diabetes leading to vision impairment and blindness globally, with an estimated prevalence of 30% among people with T1D (Cheung et al., 2010). The association of hyperglycemia, hypertension, dyslipidemia and albuminuria with DR is well known (Long and Dagogo-Jack, 2011). Several of these risk factors of DR have also been shown to be linked with atherosclerosis (Jenkins et al., 2019; Long and Dagogo-Jack, 2011). Many studies have shown that DR is an independent indicator of CV accidents and all-cause of death among diabetic patients. (Kramer et al., 2011). Many possible mechanisms have been suggested to be implicated in the pathological link between diabetic micro- and macroangiopathy. These comprise oxidative and glycemic stress, chronic low-grade inflammation and dysfunctional endothelial restoration mechanisms (Garofolo et al., 2019). In the action to regulate CV risk in T1D, the severity of DR has been proven to be linked with the risk of incidental CV events in patients with T1D (Carbonell et al., 2018). In patients with T1D, severe types of DR have been stated to be associated with the existence of coronary artery calcification (Almeida et al., 2011), along with developed carotid intima-media thickness (Rema et al., 2004). While there is a scarcity of data on atherosclerotic plaques in T1D patients, limited evidence exists on whether the atherosclerotic disease and DR in patients with T1D are

^{*} Corresponding author. e-mail: diafmustapha@gmail.com.

related. Therefore, the purpose of this study was to determine the relationship between the presence of DR and elevated risk of atherosclerosis in patients with T1D, whose free of any CVD, by evaluating blood lipid ratios.

2. Patients and Methods

2.1. Study design

This was a retrospective study reporting data from January 1, 2015, to December 30, 2019, on type 1 diabetics who visited the Diabetes Center in Sidi-Bel-Abbes, northwestern Algeria. Our study included 293 type 1 diabetics (52.60%) diagnosed in their pubertal period (according to the WHO guideline) who were over 13 years old during this study. All the medical records of the participants were revised for the following: status of the diabetic disease, biochemical parameters, other associated diseases and complications. Inclusion criteria were defined as: (1) type 1 diabetic patient aged between (13-65 years), (2) performed a proper full eye examination by direct ophthalmoscopy, (3) underwent routine examinations at the Diabetes Center at least one time a year, (4) free from any cardiovascular disease. On this basis, according to retinal function, patients with retinal dysfunction were included in the DR group, and those with normal retinal function were included in the without DR group. Exclusion criteria: (1) history of cardiovascular disease or taking cardiovascular-related drugs, (2) missing medical record on the disease status, (3) incomplete clinical data, (4) missing informed consent.

2.2. Study protocol

2.2.1. Anthropometric parameters

For all patients, the anthropometric measures including body height, weight, waist circumference and body mass index (BMI) were taken from the patient's medical record. BMI was calculated as weight (kg)/Height² (m), and the patients were classified into the following categories: underweight (BMIs of <18.5 kg/m²), normal (18.5–24.9 kg/m²), overweight (25–29.9 kg/m²), and obese (BMIs \geq 30 kg/m²).

2.2.2. Blood pressure

A sphygmomanometer was used to measure blood pressure in the supine position, followed by a standing measurement (after a few minutes). A systolic blood pressure (SBP) of 140 mmHg and diastolic blood pressure (DBP) of 90 mmHg or more are considered hypertension.

2.2.3. Hematological parameters

The latest biochemical measurement including fasting blood glucose, glycated hemoglobin (HbA1c), Hemoglobin (Hb), high-sensitivity C-reactive protein (hs-CRP), urea, urinary albumin excretion rate (UAER), serum creatinine, and lipid parameters, namely high-density lipoprotein cholesterol (HDL), low-density lipoprotein cholesterol (LDL), total cholesterol (TC), and triglycerides (TG), were available on the patients' medical records.

2.2.4. Complication assessment

The presence and severity of DR were assessed by retinal photography using a wide-angle (45°) mydriatic camera (Aldington *et al.*, 1995), and the eye with the critical retinal condition including prior photocoagulation

or surgical approach was used for DR staging (absent, mild, moderate, or severe non-proliferative, proliferative) according to the Global DR Project Group criteria (Wilkinson *et al.*, 2003). For additional classification, patients with a non-proliferative, mild, or moderate stage were categorized as nonadvanced DR while those with severe non-proliferative, proliferative DR, or blindness were assembled into the advanced, sight-threatening DR category. Furthermore, lipid ratios (TC/HDL, LDL/HDL, and TG/HDL) were measured as indicators of atherogenic risk.

2.3. Ethical approval

The Ethics Committee of Diabetic Center granted approval AAU-3/2019 of this research and since its retrospective research, ethical approval was acquired from the center in which the research was conducted.

2.4. Statistical analysis

Data are shown as mean \pm SD with its respective 95% CI for continuous variables, whereas percentages (%) with its relative frequencies for categorical variables. The differences between groups with and without DR were analyzed by the Chi-square test for qualitative variables, and the Student t-test was used for quantitative variables. After adjusting for quartiles of lipid ratios, multivariate logistic regression analysis was utilized to measure odds ratios (OR) and 95% CI for lipid ratios to examine the correlation between DR and atherosclerotic disease. Receiver operator characteristics (ROC) curves were applied to identify the predictive values of lipid ratios for atherosclerosis. A p-value of 0.05 or less ($p \le 0.05$) was maintained as statistically significant. SPSS software package (SPSS 22.0; IBM Corporation; Chicago, IL, USA. August 2013) was employed for statistical analyses of data.

3. Results

The baseline characteristics of the enrolled participants are summarized in Table 1. A total of 293 type 1 diabetics (52.60% males and 47.40% females) were included in this research. Purposely, participants were segregated into two groups according to the existence of DR. Of the 293 diabetics, 94 (32.10%) of them had DR. The mean age of the patients was 28.26±10.52 years, whereas the mean of diabetes duration was 10.15±9.06 years. The mean age of DR patients was statistically greater than in those without DR $(34.76\pm11.30 \text{ years } vs. 25.19\pm8.59 \text{ years, } p<10^{-3};$ respectively). Likewise, the mean duration of T1D was statistically greater among those who had DR (17.21±8.74 years vs. 6.82 ± 7.10 years, $p<10^{-3}$; respectively) (Table 2). The most affected age group was the "30-39 years" (36.20%). Conversely, the least affected age group was the "> 60 years". In addition, smoking history was strongly correlated with the occurrence of DR (23.40%, p=0.02) while there were no statistical differences between the various weight classes (Table 1).

In our study, the most commonly known complications in the two groups were low visual acuity (33.80%), followed by Anemia (28.30%). However, Ketosis on diabetes (60.60%, p=<10⁻³), diabetic foot (37.20%, p=<10⁻³), hypertension (28.70%, p=<10⁻³), diabetic nephropathy (26.60%, p=<10⁻³), and dyslipidemia (6.40%, p=10⁻³) were all significantly higher in DR patients (Table 1).

Table 1. Basic characteristics of the participants

Table 1. Basic characteristics of the participan	All Patients, n=293	Without DR, n=199	With DR, n=94	
Variables	Number (%)	Number (%)	Number (%)	<i>p</i> -value
Gender				
Male	154 (52.60)	101 (50.80)	53 (56.40)	0.369
Female	139 (47.40)	98 (49.20)	41 (43.60)	
Age groups, years				
[13-19]	68 (23.20)	62 (31.20)	6 (6.40)	
[20-29]	110 (37.60)	83 (41.70)	27 (28.70)	
[30-39]	73 (24.90)	39 (19.60)	34 (36.20)	<10-3*
[40-49]	28 (9.60)	14 (7.00)	14 (14.90)	
[50-59]	13 (4.40)	1 (0.50)	12 (12.90)	
≥ 60	1 (0.30)	0 (0.00)	1 (1.10)	
Smoking history				
Male	48 (16.40)	26 (13.10)	22 (23.40)	0.02*
Female				
Prevalence of weight categories,				
Underweight, BMI <18.5 Kg/m ²	84 (28.70)	63 (31.60)	21 (22.30)	
Normal weight, BMI=18.5-24.9Kg/m ²	166 (56.70)	112 (56.30)	54 (57.50)	0.06
Overweight, BMI=25.0-29.9Kg/m ²	30 (10.20)	18 (9.00)	12 (12.80)	
Obesity, BMI ≥30 Kg/m ²	13 (4.40)	6 (3.00)	7 (7.40)	
Other associated complications				
Low visual acuity	99 (33.80)	15 (7.50)	84 (89.40)	<10-3*
Diabetic nephropathy	25 (8.50)	0 (0.00)	25 (26.60)	<10-3*
Hypertension	29 (9.90)	2 (1.00)	27 (28.70)	<10-3*
Hypothyroidism	20 (6.80)	11 (5.50)	9 (9.60)	0.20
Hyperthyroidism	4 (1.40)	2 (1.00)	2 (2.10)	0.44
Anemia	83 (28.30)	47 (23.60)	36 (38.30)	0.009*
Dyslipidemia	6 (2.00)	0 (0.00)	6 (6.40)	<10-3*
Diabetic foot	44 (15.00)	9 (4.50)	35 (37.20)	<10-3*
Ketosis on diabetes	79 (27.00)	22 (11.10)	57 (60.60)	<10-3*
Symptoms and signs				
Weight loss	159 (54.30)	123 (61.80)	36 (38.30)	<10-3*
Polyuria-Polydipsia	273 (93.20)	190 (95.50)	83 (88.30)	0.02*
Asthenia	117 (39.90)	89 (44.70)	28 (29.80)	0.07
Overeating	153 (52.20)	101 (50.70)	52 (55.30)	0.14

^(*) percentages were compared with Chi-square test, p≤0.05 was considered as significant; DR: Diabetic retinopathy; BMI: body mass index.

Table 2: Comparison of clinical characteristics between patients with and without diabetic retinopathy

	All Patients, n=293		Without DR, n=199		With DR, n=94		p-	
Variables	Mean±SD	95% CI	Mean±SD	95% CI	Mean±SD	95%CI	value	
Mean age (years)	28.26 ± 10.52	27.05-29.47	25.19 ± 8.59	23.99-6.39	34.76 ± 11.30	32.44-37.07	<10-3*	
Diabetes duration (years)	10.15 ± 9.06	9.11-11.20	6.82 ± 7.10	5.82-7.81	17.21 ± 8.74	15.42-19.00	<10-3*	
Age at 1st diagnosis (years)	18.17 ± 8.59	17.19-19.16	18.46 ± 8.39	17.29-9.64	17.56 ± 9.02	15.72-19.41	0.40	
Body height (m)	1.68 ± 0.08	1.67-1.69	1.68 ± 0.09	1.67-1.69	1.67 ± 0.08	1.66-1.69	0.67	
Body weight (Kg)	58.94 ± 11.23	57.65-60.24	$58.06{\pm}10.76$	56.55-9.56	60.88 ± 12.02	58.38-63.39	0.04*	
BMI (Kg/m²)	20.82 ± 3.71	20.39-21.25	20.50 ± 3.66	19.98-1.01	21.54 ± 3.75	20.76-22.32	0.02*	
Waist circumference (cm)	80.66 ± 9.70	78.62-82.69	79.02 ± 9.36	76.68-1.36	84.69 ± 9.52	80.85-88.54	0.01*	
SBP (mmHg)	112.8 ± 12.9	111.4-114.3	110.1 ± 11.0	108.76-111.6	118.7 ± 14.7	115.7-121.7	<10-3*	
DBP (mmHg)	66.7 ± 8.7	65.7-67.7	65.5 ± 7.7	64.4-66.6	69.4 ± 10.0	67.3-71.4	<10-3*	
Fasting plasma glucose g/L)	2.98 ± 0.92	2.88-3.09	2.87 ± 0.86	2.75-2.99	3.23 ± 1.00	3.02-3.43	0.002*	
HbA1c (%)	9.63 ± 2.11	9.38-9.87	9.25 ± 1.95	8.97-9.52	10.45 ± 2.24	9.98-10.92	<10-3*	
Hb (g/L)	12.63 ± 2.01	12.37-12.90	13.01 ± 1.88	12.71-3.31	11.80 ± 2.03	11.31-12.28	<10-3*	
hs CRP (mg/L)	35.73 ± 50.18	18.99-52.46	7.99 ± 6.38	4.13-11.84	50.75 ± 57.01	26.68-74.83	0.01*	
Total cholesterol (g/L)	1.57 ± 0.36	1.53-1.61	1.56 ± 0.35	1.51-1.61	1.58 ± 0.38	1.50-1.66	0.73	
HDL-c (g/L)	0.42 ± 0.11	0.41-0.43	0.43 ± 0.10	0.42-0.45	0.40 ± 0.11	0.38-0.43	0.02*	
LDL-c (g/L)	0.90 ± 0.28	0.86-0.93	0.90 ± 0.28	0.86-0.94	0.89 ± 0.29	0.83-0.95	0.84	
Triglycerides (g/L)	0.95 ± 0.57	0.88-1.02	0.91 ± 0.52	0.84-0.99	1.03 ± 0.67	0.89-1.17	0.12	
TC/HDL-c	3.88 ± 1.17	3.74-4.02	3.75 ± 1.09	3.60-3.91	4.15 ± 1.30	3.88-4.41	0.008*	
LDL/HDL-c	2.25 ± 0.90	2.15-2.36	2.20 ± 0.90	2.07-2.32	2.37 ± 0.91	2.18-2.56	0.13	
TG/HDL-c	2.48 ± 1.88	2.26-2.69	2.31 ± 1.71	2.07-2.55	2.82 ± 2.17	2.38-3.27	0.03*	
Creatinine (mg/L)	11.65 ± 11.50	9.73-13.57	7.32 ± 1.76	6.92-7.72	16.95 ± 15.52	13.04-20.86	<10-3*	
Urea (g/L)	0.38 ± 0.33	0.32-0.44	0.23 ± 0.07	0.21-0.25	0.56 ± 0.43	0.45-0.67	<10-3*	
UAER (mg/24h)	130.69±371.75	70.92-90.47	7.71 ± 6.16	6.31-9.11	258.66±501.38	142.50-74.82	<10-3*	

(*) means were compared with independent sample Student's t-test, a p<0.05was considered as significant; DR: Diabetic retinopathy; SD: standard deviation; CI: confidence interval; HbA1c: glycosylated hemoglobin; BMI: body mass index; SBP: systolic blood pressure; DBP: diastolic blood pressure; Hb: Hemoglobin; hs-CRP: high-sensitivity C-reactive protein; TC: total cholesterol; HDL-c: high-density lipoprotein cholesterol; LDL-c: low-density lipoprotein cholesterol; TG: triglycerides; UAER: Urinary albumin excretion rate.

The clinic characteristics and laboratory indexes are described in Table 2. Regarding the anthropometric measurements on admission, significant differences were highlighted in body weight (p=0.04), waist circumference (p=<0.01) and BMI (p=<0.02), whereas there was no significant difference in body height. Furthermore, in respect to blood pressure, significant differences were revealed in diabetics who developed DR (SBP, p=<10⁻³; DBP, p=<10⁻³) (Table 2).

Remarkably, fasting plasma glucose and HbA1c levels were statistically increased in DR patients (p=<0.002, p=<10⁻³; respectively). A significant difference was maintained in terms of hemoglobin (p=<10⁻³). Concerning renal function, patients who developed DR had higher plasma values of creatinine and urea and microalbuminuria (16.95±15.52 mg/L, p=<10⁻³; 0.56±0.43 g/L, p=<10⁻³; and 258.66±501.38 mg/24h, p=<10⁻³; respectively).

Interestingly, hs-CRP was significantly increased in DR patients (patients with DR: 50.75 ± 57.01 mg/L vs. patients without DR: 7.99 ± 6.38 mg/L, p=0.01; respectively).

In terms of lipid values, as described in Table 2, HDL-c values statistically differed among the two groups (p=<0.02). Moreover, it was revealed that lipid ratios

(TC/HDL-c and TG/HDL-c) were statistically higher in the DR group (p=0.008, p=0.008).

The multivariate regression was utilized to identify independent determinants of atherosclerosis according to lipid ratios quartiles. The results showed that the 4th quartile (OR= 2.15 [1.08-4.27]; p=<0.02) of TC/HDL ratio was statistically greater in DR patients as shown in Table 3. Likewise, the 4th quartile of TG/HDL ratio was significantly greater in DR group (OR= 2.06 [1.03-4.13]; p=0.03). ROC curve for lipid ratios showed strong discriminatory power for detecting atherosclerotic disease. TC/HDL ratio was a strong indicator with an optimal cutoff level of \geq 4.0 (sensitivity of 66.0%, specificity of 64.8%, positive predictive value "PPV" of 64.5%, and negative predictive value "NPV" of 58.7% with a diagnostic accuracy of 0.653). On the other hand, TG/HDL ratio was a moderate indicator for atherosclerotic disease. The optimal cut-off level was ≥ 3.0 (sensitivity of 65.5%, specificity of 62.3%, PPV of 72.0%, and NPV of 62.7% with a diagnostic accuracy of 0.619) (Figure 1B, 1D).

As displayed in Figure 2A-2F, In contrast to females who developed DR, when comparing all lipid parameters (lipid ratios, and conventional lipid parameters) between the two genders, superior values were found in male patients with DR.

Table 3: Crude "Odds Ratio" of blood lipid ratios quartiles associated with diabetic retinopathy presence

Variables	Without DR, n=199	With DR, n=94	Odds ratio (95% CI OR)	p-value
variables	Number (%)		Odds fatio (55% Cf OK)	p-varue
TC/HDL ratio				
1st quartile (1.56-3.01)	52 (26.1)	21 (22.3)	Reference	
2 nd quartile (3.02-3.69)	56 (28.1)	17 (18.1)	0.75 [0.35-1.58]	0.45
3 rd quartile (3.70-4.56)	52 (26.1)	22 (23.4)	1.04 [0.51-2.13]	0.89
4 th quartile (4.57-8.10)	39 (19.6)	34 (36.2)	2.15 [1.08-4.27]	0.02*
LDL/HDL ratio				
1st quartile (0.35-1.53)	54 (27.1)	20 (21.3)	Reference	
2 nd quartile (1.54-2.12)	55 (27.6)	18 (19.1)	0.88 [0.42-1.85]	0.74
3 rd quartile (2.13-2.75)	46 (23.1)	27 (28.7)	1.58 [0.78-3.18]	0.19
4th quartile (2.76-5.93)	44 (22.1)	29 (30.9)	1.78 [0.88-3.56]	0.10
TG/HDL ratio				
1st quartile (0.22-1.28)	53 (26.6)	20 (21.3)	Reference	
2 nd quartile (1.29-1.97)	56 (28.1)	17 (18.1)	0.80 [0.38-1.69]	0.56
3 rd quartile (1.98-2.98)	49 (24.6)	25 (26.6)	1.35 [0.66-2.73]	0.40
4 th quartile (2.99-8.10)	41 (20.6)	32 (34.0)	2.06 [1.03-4.13]	0.03*

(*) multivariate logistic regression significant at p = 0.05; DR: Diabetic retinopathy; CI, confidence interval; OR, Odd ratio; TC: total cholesterol (g/L); LDL: low-density lipoprotein cholesterol (g/L); HDL: high-density lipoprotein cholesterol (g/L); TG: triglycerides (g/L).

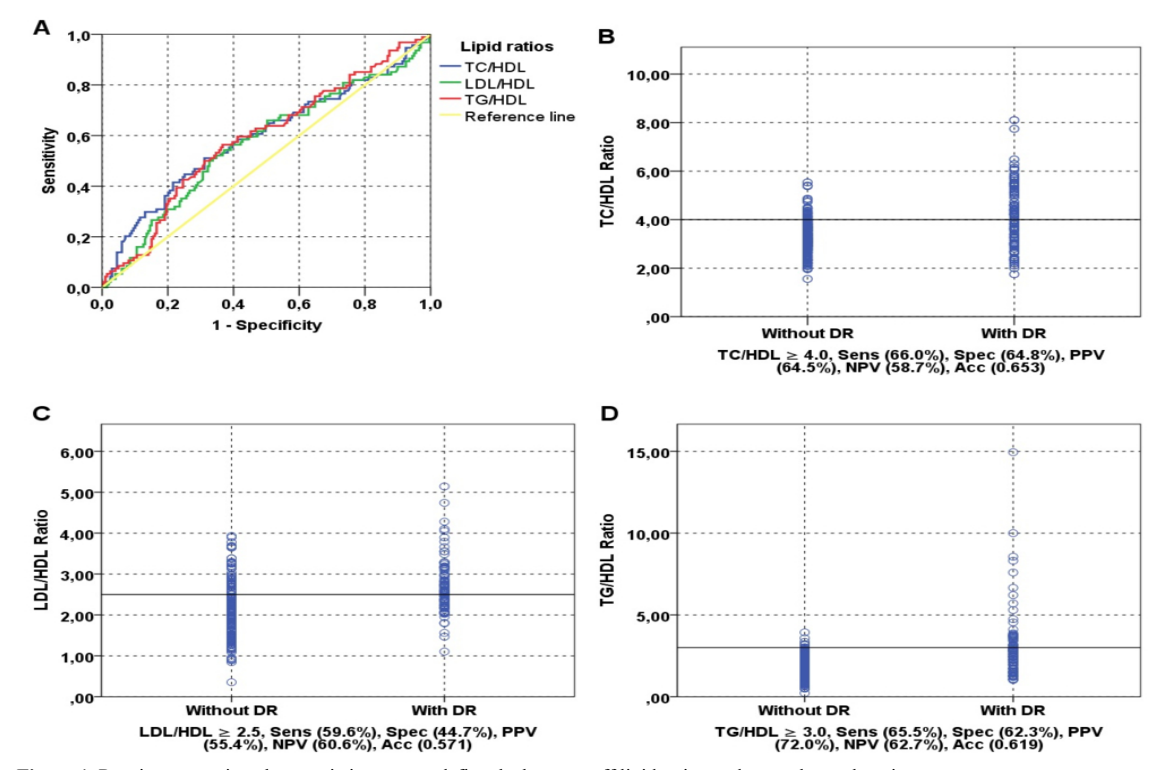


Figure 1. Receiver operating characteristic curve to define the best cut-off lipid ratios to detect atherosclerosis

DR: Diabetic retinopathy; Sens: Sensitivity; Spec: Specificity; PPV: Negative Predictive Value; NPV: Positive Predictive Value; Acc: Accuracy; TC: total cholesterol; LDL: low-density lipoprotein cholesterol; HDL: high-density lipoprotein cholesterol; TG: triglycerides

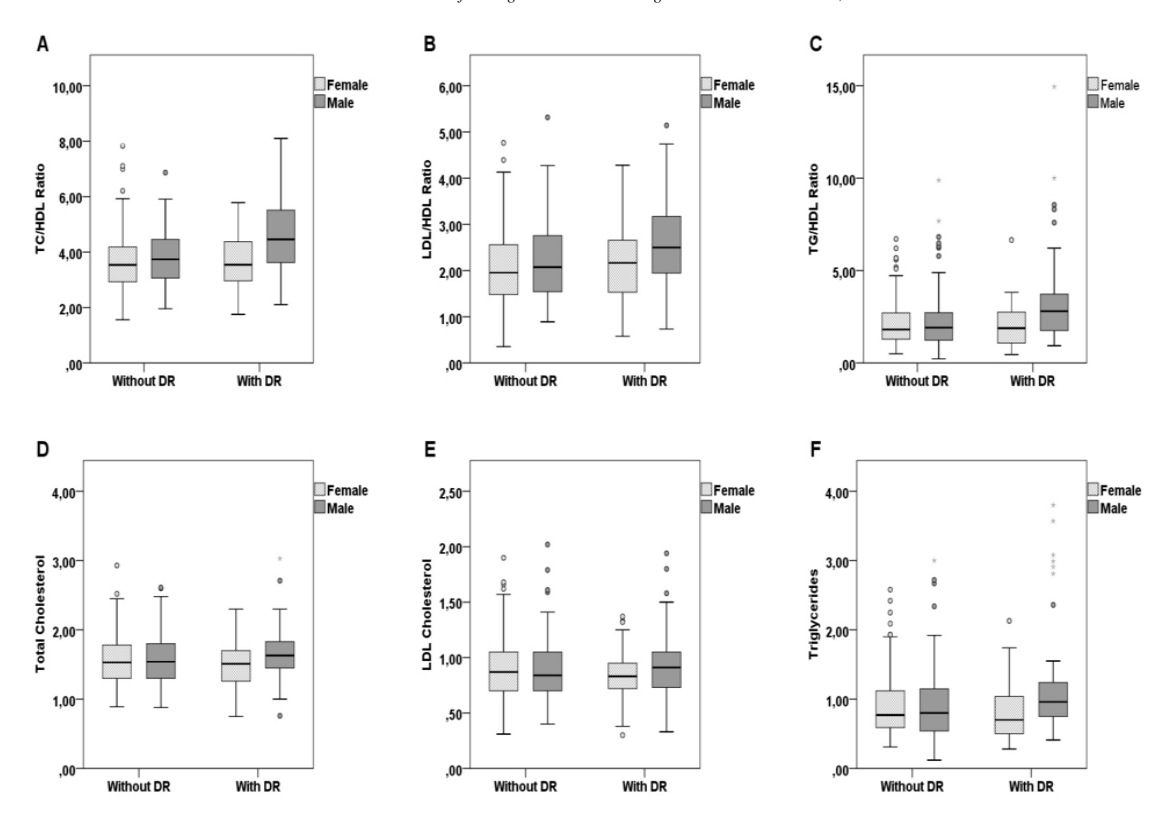


Figure 2. Comparison of lipid ratios levels between patients with and without diabetic retinopathy according to their gender DR: Diabetic retinopathy; TC: total cholesterol; LDL: low-density lipoprotein cholesterol; HDL: high-density lipoprotein cholesterol; TG: triglycerides

4. Discussion

The current study assessed the potential role of biological and clinical features in diabetics with and without DR in order to establish the factors related with the existence of DR in this population. Surprisingly, in addition to several well-known CV risk factors, this study supports the idea that microvascular disease such as DR may promote the formation of the atherosclerotic plaques in type 1 diabetics. Thus, we examine the link between DR and atherosclerosis by comparing two groups of diabetics based on the existence of DR (patients with and without DR). We revealed that the distribution of diabetics by gender was inequitable, emphasizing a clear male preponderance over females (52.60% - 47.40%) with a sex ratio of 1.10. Compared to patients who developed DR, the proportion of men was higher than that of women among type 1 diabetics. A prospective study conducted by Rajalakshmi et al., (2014), demonstrated that 80 patients with T1D had DR; of those, 48 (60.0%) were men, whereas, in the Araszkiewicz's study group, 39 (44.8%) had DR; of those, 22 (56.4%) were men (Araszkiewicz et al., 2011). Our findings showed significant effects of age and duration of diabetes on the presence of DR. The findings concord with Matuszewski et al. who found that aged patients (≥ 30 years) with long-lasting diabetes (≥ 15 years) had higher risk to develop more severe DR (Matuszewski et al., 2020). The results are also consistent with previous studies in the literature (Carbonell et al., 2018; Rajalakshmi et al., 2014; Araszkiewicz et al., 2011).

In addition, our study also indicates that tobacco strongly advanced the progression of DR. A similar conclusion was found by Uruska et al., (2014) regarding patients with T1D. Other authors also established a causal link between smoking and the incidence of DR (Matuszewski et al., 2020; Campagna et al., 2019). Interestingly, body corpulence elevated the probability of DR in our study population. Authors studied the impact of BMI on the development of DR and concluded that DR is associated to BMI only in its correlation with HbA1c, cholesterol concentration and hypertension (Carbonell et al., 2018; Kaštelan et al., 2014). Price et al., (2014) hypothesized that obesity in subject with T1D may lead to the progression of DR and macrovascular complications. Our findings have shown strong and consistent correlations between diabetic nephropathy and DR. Statistically significant associations were highlighted in the Renin-Angiotensin-System investigation between DR and preclinical diabetic nephropathy in patients T1D (Klein et al., 2005). Same observations were made by Kaštelan et al. (2014). In our study, hypertension was identified in 29 patients, and 27 (28.70%) of them have developed DR. Our results are in agreement with the previous conclusions which indicate that the prevalence of resistant hypertension escalates with advanced retinopathy and define hypertension as the most significant risk factor for DR (Carbonell et al., 2018; Rajalakshmi et al., 2014; Araszkiewicz et al., 2011; Kaštelan et al., 2014). Notably, our study revealed an association of an increased prevalence of DR with low hemoglobin levels in patients with T1D. Our results are in line with the conclusions made by Li et al., (2020) who ascertained a similar correlation between an increased progression to DR and anemia. Our results demonstrated that ketosis on diabetes was associated with an increased incidence of DR, and this echoes with a former follow-up study of adults with T1D (Martin et al., 2005). We also detected a sustained increase in HbA1c levels in DR patients, proposing an early interaction between these two conditions. Previous studies reported impaired microvascular function in the retina (retinal arteriolar dilation response to flickering light) was associated with higher levels of HbA1c (Carbonell et al., 2018; Araszkiewicz et al., 2011; Matuszewski et al., 2020; Kaštelan et al., 2014). With regard to decreased glomerular filtration rate (known as diabetic nephropathy), we also noticed an incremental increase in UAER (≥ 30 mg/24h) in patients who developed DR, which may allow the findings to be more credible. Carbonell et al., (2018) ascertained that in patients with a urine albumin/creatinine ratio higher than 4 mg/g, DR was observed significantly more often. Additionally, in concordance with several studies in the literature (Carbonell et al., 2018; Araszkiewicz et al., 2011; Miljanovic et al., 2004), we further established that there were increased triglycerides decreased concentration and HDL-cholesterol concentration in patients who had developed DR compared to those who did not. Moreover, these findings suggest that implication of dyslipidemia may reflect underlying, as jet unidentified, mechanisms linked to vascular dysfunction (Chang et al., 2013). According to Melo et al. (2019), in both males and females, several clinical risk factors and pathophysiological features are shared between cardiovascular disease and diabetic (type 1 or type 2 collectively) retinopathy. However, even after controlling for the major risk factors, patients with DR have a higher probability of presenting with CVD. A strong association between DR and the atherosclerosis risk (screened through lipid ratios and traditional lipid parameters) was disclosed in our male T1D patients comparing to females. In their review study, Ozawa et al., (2015) suggest that basically, the difference in sex seems to modify the risk of developing T1D and vision-threatening retinopathy and further cardiovascular complications. Indeed, relationship between sex difference, DR cardiovascular risk is not unidirectional. The causal relationship can be explained in several ways. For at least two decades, the findings that elevated serum lipid levels and also the TC/HDL ratio have been associated to an increased risk of progression of DR, thus suggest a relationship with disruption of the blood-retinal barrier. At the same time, controlling retinal complications in diabetic patients can help prevent the onset or even worsening of CVD (Miljanovic et al., 2003).

To evaluate the CV risk linked with a microvascular complication, such as DR in diabetics, longitudinal studies are recommended, and to properly establish this risk, future inquiries should include type 1 diabetic subjects (with and without DR).

5. Conclusion

In conclusion, our data confirmed that type 1 diabetics with DR exhibit a higher risk of atherosclerotic disease, suggesting that dyslipidemia might play an important role in the development of macro-angiopathy in this

population. Moreover, our results established the usefulness of the employment of lipid ratios in the evaluation of subclinical atherosclerosis risk in this population. Thus, our findings could have both therapeutic and investigational implications that encourage extensive monitoring accompanied by a more careful cardiovascular assessment in patients with DR, in order to prevent the development of major adverse CVD.

Conflict of interest

The authors declared no conflicts of interest.

Funding statement

No funding was received for this study.

References

Aldington SJ, Kohner EM, Meuer S, Klein R and Sjølie AK. 1995. Methodology for retinal photography and assessment of diabetic retinopathy: the EURODIAB IDDM complications study. *Diabetologia.*, **38**:437–444.

Almeida FK, Esteves JF, Gross JL, Biavatti K and Rodrigues TC. 2011. Severe forms of retinopathy predict the presence of subclinical atherosclerosis in type 1 diabetes subjects. *Arq Bras Cardiol.*, **97**:346–349.

Araszkiewicz A, Rogowicz-Frontczak A, Zozulinska-Ziolkiewicz D, Pilacinski S, Wykretowicz A and Wierusz-Wysocka B. 2011. Presence of retinopathy in type 1 diabetic patients is associated with subclinical macroangiopathy. *Scand J Clin Lab Investig.*, 71:563–568.

Campagna D, Alamo A, Di Pino A, Russo C, Calogero AE and Purrello F. 2019. Smoking and diabetes: Dangerous liaisons and confusing relationships. *Diabetol Metab Syndr.*, **11**:85.

Carbonell M, Castelblanco E, Valldeperas X, Betriu À, Traveset A and Granado-Casas M. 2018. Diabetic retinopathy is associated with the presence and burden of subclinical carotid atherosclerosis in type 1 diabetes. *Cardiovasc Diabetol.*, **17**:1-10.

Chang YC and Wu WC. 2013. Dyslipidemia and diabetic retinopathy. *Rev Diabet Stud.*, **10**:121–132.

Cheung N, Mitchell P and Wong TY. 2010. Diabetic retinopathy. *Lancet.*, **376**:124–136.

de Ferranti SD, de Boer IH, Fonseca V, Fox CS, Golden SH and Lavie CJ. 2014. Type 1 diabetes mellitus and cardiovascular disease: a scientific statement from the American heart association and American diabetes association. *Circulation.*, **130**:1110–1130.

Garofolo M, Gualdani E, Giannarelli R, Aragona M, Campi F and Lucchesi D. 2019. Microvascular complications burden (nephropathy, retinopathy and peripheral polyneuropathy) affects risk of major vascular events and all-cause mortality in type 1 diabetes: a 10-year follow-up study. *Cardiovasc Diabetol.*, **18**:1-16.

Jenkins A, Januszewski A and O'Neal D. 2019. The early detection of atherosclerosis in type 1 diabetes: why, how and what to do about it. *Cardiovasc Endocrinol Metab.*, **8**:14-27.

Kaštelan S, Salopek Rabatić J, Tomić M, Antunica AG, Ljubić S and Kaštelan H. 2014. Body mass index and retinopathy in type 1 diabetic patients. *Int J Endocrinol.*, **2014**;387919.

Klein R, Zinman B, Gardiner R, Suissa S, Donnelly SM and Sinaiko AR. 2005. The relationship of diabetic retinopathy to preclinical diabetic glomerulopathy lesions in type 1 diabetic patients: the Renin-Angiotensin System Study. *Diabetes.*, **54**:527-533

Kramer CK, Rodrigues TC, Canani LH, Gross JL and Azevedo MJ. 2011. Diabetic retinopathy predicts all-cause mortality and cardiovascular events in both type 1 and 2 diabetes: meta-analysis of observational studies. *Diabetes Care.*, **34**:1238–1244.

Li Y, Yu Y and VanderBeek BL. 2020. Anaemia and the risk of progression from non-proliferative diabetic retinopathy to vision threatening diabetic retinopathy. *EYE.*, **34**:934–941.

Lind M, Svensson AM, Kosiborod M, Gudbjörnsdottir S, Pivodic A and Wedel H. 2014. Glycemic control and excess mortality in type 1 diabetes. *N Engl J Med.*, **371**:1972–1982.

Livingstone SJ, Looker HC, Hothersall EJ, Wild SH, Lindsay RS and Chalmers J. 2012. Risk of cardiovascular disease and total mortality in adults with type 1 diabetes: Scottish registry linkage study. *PLoS Med.*, 9:e1001321.

Long AN and Dagogo-Jack S. 2011. Comorbidities of diabetes and hypertension: mechanisms and approach to target organ protection. *J Clin Hypertens (Greenwich).*, **13**:244-251.

Martin SLA, Hoffman WH, Marcus DM, Passmore GG and Dalton RR. 2005. Retinal vascular integrity following correction of diabetic ketoacidosis in children and adolescents. *J Diabetes Complications.*, 19:233–237.

Matuszewski W, Stefanowicz-Rutkowska MM, Szychlińska M and Bandurska-Stankiewicz E. 2020. Differences in Risk Factors for Diabetic Retinopathy in Type 1 and Type 2 Diabetes Mellitus Patients in North-East Poland. *Medicina.*, **56**:177.

Melo LGN, Morales PH, Drummond KRG, Santos DC, Pizarro MH and Barros BSV. 2019. Diabetic retinopathy may indicate an increased risk of cardiovascular disease in patients with type 1 diabetes-A nested case-control study in Brazil. *Front Endocrinol.*, 10:689

Miljanovic B, Glynn RJ, Nathan DM, Manson JE and Schaumberg DA. 2003. Serum Lipid Levels and Diabetic Retinopathy in Type 1 Diabetes Mellitus. *Invest Ophthalmol Vis Sci.*, 44:3099.

Miljanovic B, Glynn RJ, Nathan DM, Manson JE and Schaumberg DA. 2004. A prospective study of serum lipids and risk of diabetic macular edema in type 1 diabetes. *Diabetes.*, **53**:2883–2892.

Ozawa GY, Bearse MA Jr and Adams AJ. 2015. Male-female differences in diabetic retinopathy?. *Curr Eye Res.*, **40**:234–246.

Price SA, Gorelik A, Fourlanos S, Colman PG and Wentworth JM. 2014. Obesity is associated with retinopathy and macrovascular disease in type 1 diabetes. *Obes Res Clin Pract.*, **8**:178–182.

Rajalakshmi R, Amutha A, Ranjani H, Ali MK, Unnikrishnan R and Anjana RM. 2014. Prevalence and risk factors for diabetic retinopathy in Asian Indians with young onset type 1 and type 2 diabetes. *J Diabetes Complications.*, **28**:291-297.

Rema M, Mohan V, Deepa R and Ravikumar R. 2004. Association of carotid intima-media thickness and arterial stiffness with diabetic retinopathy: the Chennai Urban Rural Epidemiology Study (CURES-2). *Diabetes Care.*, **27**:1962-1967.

Swärd P, Tofik R, Bakoush O, Torffvit O, Nilsson PM and Christensson A. 2020. Patterns of urinary albumin and IgM associate with markers of vascular ageing in young to middle-aged individuals in the Malmö offspring study. *BMC Cardiovasc Disord.*, 20:1-9.

Uruska A, Araszkiewicz A, Uruski P and Zozulinska-Ziolkiewicz D. 2014. Higher risk of microvascular complications in smokers with type 1 diabetes despite intensive insulin therapy. *Microvasc Res.*, **92**:79–84.

Wilkinson CP, Ferris FL, Klein RE, Lee PP, Agardh CD and Davis M. 2003. Global Diabetic Retinopathy Project Group. Proposed international clinical diabetic retinopathy and diabetic macular edema disease severity scales. *Ophthalmology*., **110**:1677–1682

Jordan Journal of Biological Sciences

Biological Control of Tomato Damping-off and Potato Black Scurf by Seed Treatment with *Trichoderma harzianum*

Naffaa Walid^{1,*}, Lubana Al-Jaramany², Ahed Elbenay², Reema Al-Mhethawi²

¹Damascus University, Faculty of Agriculture, Department of Plant Protection, 30621 Damascus – Syria; ²Damascus University, Second Faculty of Agriculture, Sweida – Syria

Received: April 17, 2021; Revised: August 20, 2021; Accepted: September 25, 2021

Abstract

During the present study, the antagonistic potential of *Trichoderma harzianum* Rifai against *Phytophthora infestans* (Mont.) de Bary and *Rhizoctonia solani* Ktihn. was evaluated by dual culture technique. Its efficacy to inhibit pathogenic effects caused by these two pathogens was also evaluated on tomato and potato, under artificial inoculation conditions. On PDA medium, *T. harzianum* showed high level of antagonistic activity against all tested isolates of two pathogens. Appressorium − like structures were observed on *R. solani* hyphae. Treatment of tomato seeds with spore suspension of *T. harzianum* showed considerable decrease in pre-emergence damping-off disease incidence caused by *P. infestans* and *R. solani*, with biological control efficacy of 49.3% and 64.33% respectively. Seed treatment with *T. harzianum* also showed biological control efficacy of 66.03% for stem canker disease of tomato seedlings caused by *R. solani*. *Trichoderma* treatment significantly (≤ 0.05) reduced black scurf disease incidence caused by *R. solani* on potato during pot test experiments by 77.95% over untreated control. Although 0.2% carbendazim treatment highly protected tomato and potato plants, but it had a phytotoxic effect, however *Trichoderma* treatments had a positive effect on growth parameters studied as compared to the untreated control.

Keywords: biological control, black scurf disease, Trichoderma, damping-off

1. Introduction

Tomato (Lycopersicon esculentum Mill.) is one of the most important and widespread vegetable crops in the world (FAOSTAT, 2019). Tomato production is very important in Syria as a cash crop due to its relatively low expenditure and high productivity. Moderate temperatures in Syria allow farmers to produce tomato in open fields. Also, due to the mild climate in the coastal area, greenhouses can be used with minimal heating in winter (Annual Agricultural Statistical group, 2016). Potato (Tuberosum solanum L.) is one of the most important food and industrial crops in the world. Potato production has increased enormously in developing countries in the past few decades, and has now overtaken that in the developed countries, underlining the growing importance of potato as a staple food crop to meet the demands of increasing human populations (Birch et al., 2012). In Syria, potato production was estimated to be 507,384 tons with a cultivated area of 22,369 hectares in 2016 (Annual Agricultural Statistical Group, 2016).

Damping off, a destructive disease of plant seedlings, is caused by a number of seed- and soil-borne fungi and fungus-like Oomycetes, including *Pythium* spp.,

Phytophthora sp. (Joo, 2005), Rhizoctonia solani (Asaka and Shoda, 1996), Sclerotium rolfsii (Errakhi et al., 2007), and Fusarium oxysporum (Getha and Vikineswary, 2002). Phytopthora infestans (Mont.) de Bary causes pre- and post-emergence damping-off and late blight of potato and tomato (Ston, 2009). The disease incidence varied and ranged from 0 to 85.71% in all survived areas throughout the interior of Syria (Naffaa et al., 2017). Rhizoctonia solani Kühn. [telemorph Thanatephorus cucumeris (A.B. Frank) Donk] infects many crops, including tomatoes, causing seed decay as well as pre- and post-emergence damping-off of tomato seedlings (Rehman et al., 2012). Stem canker and black scurf also caused by R. solani is a serious disease of potato grown in cooler regions of the world (Yanar et al., 2005). Yield losses of up to 50% caused by black scurf, in severely affected potato areas have been reported (Keiser, 2008). Studies have confirmed the spread of the disease in most potato cultivation areas in Syria, where the overall average incidence of the disease in autumn season reached 60.46%, while in the spring season, infection rate was higher than in autumn with an average incidence of 64.19% (Abdo et al., 2012).

The use of fungicides, besides being expensive and representing a potential risk for the environment and for human health, is not totally effective and may lead to the

^{*} Corresponding author. e-mail: walid1851966@yahoo.com or ray-dya@scs-net.org.

^{**} **Abbreviations used:** (RAM) rye agar medium, (PDA) potato dextrose agar, (AGs) anastomosis groups, (BCE) biological control efficacy, (CE) control efficacy, (T) treatment.

appearance of new resistant strains of pathogens (Alwathnani and Perveen 2012; Tomlin, 2006). It is therefore, necessary to explore alternative control strategies (Boogert Van der and Luttikholt, 2004; Rauf et al., 2007). One such alternative is biological control, in which living organisms are selected for their ability to prevent or reduce damage caused by pathogens. Species of the genus Trichoderma are considered as potential biological control agents (BCAs) (Vinale et al., 2014). Trichoderma is a fast growing, secondary opportunistic invader, with efficient sporulation rate, antibiotic and cell wall degrading enzyme producing ability (Francesco et al., 2008). The success of strains as bio-control agents may be attributed to their high reproductive ability, survival under adverse conditions, efficient utilization of nutrients, rhizosphere modifying capacity, aggressiveness against plant pathogenic fungi and plant growth promotion. Therefore, Trichoderma spp. are the most investigated fungal biocontrol agents, which are available commercially as bio-pesticides (Harman, 2000; Sawant, 2014).

The aim of this study was to determine the antagonistic potential of *T. harzianum* against *P. infestans* and *R. solani* by dual culture technique, and to evaluate the efficacy of seed treatment with *T. harzianum* in controlling diseases caused by two pathogens on tomato and potato in pot experiment under artificial inoculation conditions.

2. Materials and Methods

2.1. Isolation and identification of plant pathogenic fungi

Samples of tomato leaves showing late blight symptoms, and potato tubers showing typical symptoms of black scurf were collected from five different tomato and potato fields in Sweida governorate (southern of Syria). Infected leaves were superficially sterilized for 2 minutes in 1% sodium hypochlorite, washed 3 times with sterile water, cut into small pieces, dried between two sterilized filter papers, placed under potato slices in Petri dishes and incubated at 20 ± 2 °C for 7 days until abundant sporulation appeared on the upper side of the slice. The clean pure mycelium was placed on Rye Agar Medium (RAM) (60 g of rye grain, 15 g of agar and 20 g of dextrose in 1L of distilled water) amended with 12 mg/L of rifampicin in Petri dishes. Incubation was carried out for at least two weeks at 20°C (Jmour and Hamada, 2006). P. infestans identification was based on colony, sporangiophores and sporangia morphological characteristics.

Infected potato tubers were carefully washed under running tap water to remove the associated soil particles, surface sterilized with 1% sodium hypochlorite for 2 min, rinsed three times with sterile water and then dried on sterilized filter papers. Infected parts were cut using sterilized scalpel into small pieces (3-5 mm), transferred to plates of PDA supplemented with streptomycin sulfate (120 mg l⁻¹) to suppress bacterial growth, then incubated at 25±1°C for 7 days. Plates were observed daily for mycelial growth. Hyphal tips of mycelium emerging from the infected pieces were transferred to fresh plates of PDA. Pure cultures of *R. solani* isolates were identified microscopically as described by Ogoshi (1987).

2.2. Preparation of antagonistic fungus

Spore suspension of *Trichoderma harzianum* was prepared from a commercial product (1.15% BIO-TH WP, 1 x 10^7 cfu/g) obtained from the Trichoderma laboratory in Hama (Syria). 0.5 ml of the spore suspensions were added to each Petri dish containing PDA medium and incubated at $25 \pm 1^{\circ}$ C for 7 days.

2.3. Antagonistic test by dual culture technique

The antifungal activity of T. harzianum against 5 isolates of each plant pathogenic fungi was evaluated on PDA medium using a dual culture technique. An agar disc (0.5 cm) of 7 days-old colony of T. harzianum was placed on one end of the Petri dish (9 cm) and an agar disc with one of plant pathogenic isolates was placed on the opposite end. The control test was set up without placing the disc of the antagonist, only pathogen was kept for comparison. Experiment was carried out in three replicates. Paired cultures were incubated at 25 ± 1 °C till the fungal growth in the control test reached the edge of the plate. Scoring for the degree of antagonism was carried out on a scale of 1 -5 classes: class 1= Trichoderma completely overgrew the pathogen and covered the entire medium surface, class 2 = Trichoderma overgrew at least 2/3 of the medium surface, class 3 = Trichoderma and the pathogen each colonized approximately 1/2 of the medium surface (more than 1/3 and less than 2/3) and neither organism appeared to dominant the other, class 4 = the pathogen colonized at least 2/3 of the medium surface and appeared to withstand encroachment by Trichoderma, class 5 = the pathogen completely overgrew the Trichoderma and occupied the entire medium surface. Trichoderma was considered to be antagonistic to the pathogen if the mean score for a given comparison (when rounded to the nearest whole class number) was ≤ 2 , but considered less antagonistic if the mean score was ≥ 3 (Bell *et al.*, 1982).

2.4. Preparation of the plant pathogenic fungi inoculum

Culturing of pathogens was carried out according to Jayaraj *et al.* (2006) on broken maize-sand medium (broken maize 37.5 g; black sand 3550 g; tap water 360.0 ml), then sterilized at 121°C / 1.5 bar for 20 min and inoculated with mycelial discs (5 mm diameter) taken from 7 days-old PDA culture of the fungal pathogens. The inoculated medium was transferred to 500 ml flasks (300 g in each). The flasks were sealed with the help of cotton and incubated at 25±1°C for 15 days with periodical mixing to avoid formation of clump. When the medium were fully covered with test fungus, it was used in the biological control test.

2.5. Preparation of T. harzianum spore suspension and tomato seed treatment

10 ml of distilled water was added to each plate containing 15 days-old colony of T. harzianum. Plates were carefully sealed and incubated at room temperature about 2 h. The spores were harvested as previously described (Perelló et al., 2009). The spore concentration was measured with a hemocytometer and a suspension with a concentration of 5×10^8 spores per ml was selected and used immediately (Biam and Majumder, 2019). Tomato seeds (Marmande cv.) were surface disinfested in 1% sodium hypochlorite for 3 min, washed three times in sterilized distilled water, dried between filter papers and dipped into the spore suspension for 5 min. The treated

seeds were then spread on a cleaned blotting paper and allowed to air dry.

2.6. Efficacy of bio-control against R. solani and P. infestans on tomato in pot experiment

A biological control test against *P. infestans* isolated from tomato, and *R. solani* isolated from potato was performed for both the pathogens on tomato. Soil (clay, sand and peat 1: 1: 2 v) was sterilized twice in autoclave at 121°C for 30 min. Soil mix was inoculated with *P. infestans* and *R. solani* inoculum individually at the rate of 5 g/kg soil. Inoculated soil was shifted into 15 cm pots (1 kg/pot) and incubated at 28°C, subjected to darkness and watered for 4 days before sowing. Tomato seeds treated

with *T. harzianum* were sown in pots (5 seeds / pot). Treatment details are furnished as follows: T1 = treated seeds in inoculated soil, T2 = untreated seeds in inoculated soil (untreated control), T3 = untreated seeds in uninoculated soil (healthy control), T4 = seeds dipped into 0.2% carbendazim (Bavistin) for 1 min and sown in inoculated soil. Total eight replicates were set up for all treatments. Plants were watered as and when required. The disease incidence of pre-and post-emergence of tomato plants were recorded after 15 and 45 days respectively using the standard procedure (Omokhua, 2011). Percentage disease incidence was calculated using

following formula:

Percentageof diseaseincidence(pre-emergence)= Numberof seeds not germinated Total numberof seeds sown

 $Percentage of \ disease incidence (post-emergence) = \frac{Number of \ infected seed lings}{Total \ number of \ seeds \ germinated} \times 100$

Control efficacy was calculated by using the following formula (Zhang et al., 2012)

Control efficacy = $\frac{\text{Disease incidence of control - disease incidence of treatment}}{\text{Disease incidence of control}} \times 100$

The average plant lengths were calculated.

2.7. Efficacy of bio-control against black scurf disease on potato in pot experiment

Potato tubers (cv. "Spunta"), almost identical in size with 4-5 buds, were surface sterilized by soaking in 1% sodium hypochlorite for 3 min, washed three times with sterilized water, air dried and dipped into the Trichoderma spore suspension for 5 min. The treated tubers were then spread on a cleaned blotting paper and allowed to air dry. Soil (clay, sand and peat 1: 1: 2 v) was sterilized twice in autoclave at 121°C for 30 min, and inoculated with R. solani as described earlier. Three tubers were planted at a depth of approximately 5 cm in a 50-cm plastic pot containing 6 kg of soil mix. The treatments given in the pots were as follows: T1 = treated tubers in inoculated soil, T2 = untreated tubers in inoculated soil (untreated control), T3 = untreated tubers in un-inoculated soil (healthy control), T4 = tubers were dipped into 0.2% carbendazim (Bavistin) for 1 min and sown in inoculated soil. Eight pots were used as replicates for each treatment. The plants were grown in spring season at ambient temperature. The plants were fertilized with a balanced NPK (2-3g/ liter of water), and watered as and when needed. Average plant height at the beginning of flowering stage, stem canker incidence (%), number and weight of tubers and the ratio of infected progeny tubers were calculated 120 days after planting (Woodhall et al., 2008).

2.8. Statistical analysis

Analyses of variance were carried out using SPSS15 statistical program. The least significant difference (LSD) was employed to test significant differences between treatments at $P \le 0.05$ (Gomez & Gomez, 1984).

3. Results and Discussion

Five isolates of both pathogens *P. infestans* and *R. solani* were obtained and identified according to their morphological characteristics.

3.1. Antagonistic activity of T. harzianum

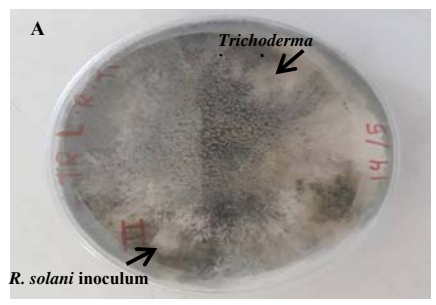
The dual culture method used to investigate the antagonistic potential of T. harzianum against P. infestans and R. solani indicated that T. harzianum had a high level of antagonism (rating ≤ 2) against all tested isolates of both pathogenic fungi. Different susceptibility patterns against the antagonism were observed between isolates of both pathogens with significant differences (≤ 0.05) (Table 1). Previous study showed that significant differences in antagonism susceptibility of R. solani to Trichoderma have been noticed between isolates from different anastomosis groups (AGs) and between isolates within an AG (Bell et In another study, T. harzianum was al., 1982). consistently found to be the effective inhibitor of radial growth of all isolates of P. infestans with the highest inhibition rate (85 %) for isolate P10 and less inhibition rate (57%) for isolate P19 (Kerroum et al., 2015). Elad et al. (1983) suggest that the lectin of the host plays a major role in the recognition of host hyphae by Trichoderma spp., and it may also be involved in the direct attachment of Trichoderma spp. to its host, so the differences in the antagonistic susceptibility between pathogens and isolates may be due to the lectin level in the host. The most antagonistic susceptible isolates R. solani (Rh 3) and P. infestans (P 5) were chosen for biological control tests.

Table 1. Antagonistic potential of *T. harzianum* against plant pathogenic fungi

Pathogen	Percentage (%) of the medium surface occupied by <i>T. harzianum</i>					
	Isolate1	Isolate 2	Isolate 3	Isolate 4	Isolate 5	Mean
P. infestans	ab96.67	°90	d83.33	^{bc} 91.67	a 100	92.33
R. solani	^b 90	^d 70	a100	°83.33	c80	82.67

*Values followed by the same letter in the same row do not differ significantly according to (LSD) least significant difference ($P \le 0.05$)

Microscopic examination showed that in dual culture plates, the hyphae of the two cultures grew towards each other, came into contact, and the *Trichoderma* hyphae overgrew the hyphae of the plant pathogens. The pathogen colony became entirely covered by the antagonistic fungi and was hardly visible (Figure 1A). The diameter of hyphae from *Trichoderma* was about 1.3 μm, where it ranged from 5.3 to 7.9 μm for *R. solani*, and from 4.8 to 7.1 μm for *P. infestans*. The differences in diameter made them easily distinguishable from each other. Furthermore, the hyphae of *T. harzianum* produced appressorium-like structures on *R. solani* hyphae (Figure 1B).



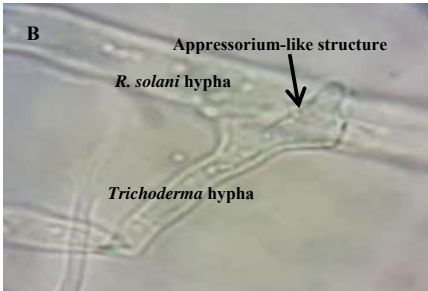


Figure 1. Antagonistic potential of *T. harizianum*: (A) antagonistic fungal hyphae overgrew hyphae of *R. solani*; (B) Appressorium-like structures formed by *T. harzianum* on *R. solani* hyphae.

The attachment of *Trichoderma* hyphae to the host hyphae occurred by numerous means. The formation of hyphal coiling by *Trichoderma* is common (Dennis and Webster, 1971). *T. harzianum* formed hooks, but their presence was infrequent (Murmanis *et al.*, 1988). The hyphae of *T. polysporum* formed appressorium-like structures, which pressed against the host hyphae. At the end of the parasitic activity, the cytoplasmic contents of host fungi appeared totally evacuated, and the hyphae looked almost "translucent" as if only the hyphal "exoskeleton" had remained (Murmanis *et al.*, 1988). Ibrahim (2017) showed that five isolates of *T. harzianum* were found antagonistic to the growth of *R. solani* in dual

culture on PDA. The method of myco-parasitism was sparse to intense coiling followed by disintegration, disorganization and death of *R. solani* mycelium.

Antagonistic activity of *Trichoderma* spp. could also be due to the secretion of antifungal substances, some enzymes that degrade the fungal cell walls including protease, β -1,3- glucanase and chitinase, various toxic and antibiotic metabolites (Limon *et al.*, 2004; Sood *et al.*, 2020) which are involved in the inhibition and lysis of pathogenic fungi. Singh and Islam (2010) affirmed that the *in vitro* culture of *Phytophthora nicotianae* and *T. harzianum* together led to a variety of interactions. *P. nicotianae* growth was inhibited and the hyphae severely parasitized by *T. harzianum* were lysed.

Isolates of *Trichoderma* spp. have been reported to produce fungicidal antibiotics, regarding their production there is a considerable variation among the isolates (Lee and Wu, 1984; Dennis and Webster, 1971). In this study, however we did not observe inhibition zones in any of the dual culture interactions, corroborating the absence of any antifungal substance in the medium, and hyphal interactions had taken place between the two fungi (Dennis and Webster, 1971; Tronsmo and Dennis, 1978; Murmanis *et al.*, 1988).

3.2. Biological control of pre-emergence damping-off of tomato seeds and seedlings

The effect of tomato seed treatment with T. harzianum on pre-emergence damping off and its ability to reduce the disease incidence caused by P. infestans and R. solani under artificially inoculated conditions was studied. The results showed that Trichoderma treatment (T1) significantly (≤ 0.05) reduced the disease incidence caused by P. infestans by 24.3%, where the pathogen caused seed decay before germination and pre-emergence seedling damping-off. Among the treatments, the lowest disease incidence was recorded in T4 (carbendazim seed treatment) that resulted in high percent of seed germination (92.3%) (Figure2). The biological control efficacy (BCE) was 49.3% compared with control efficacy (CE) of 84.38% in T4 (Table 2).

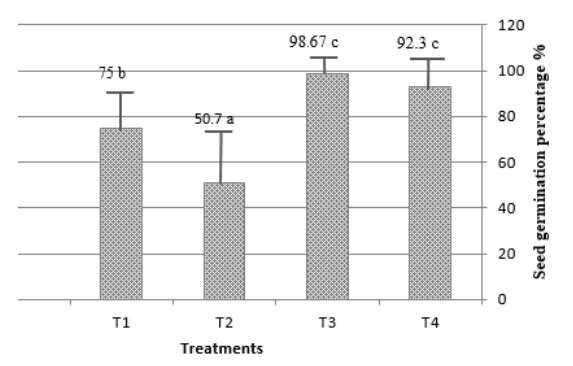


Figure 2. Efficacy of *T. harzianum* in controlling seed rot and damping-off diseases of tomato caused by *P. infestans* under artificial inoculation conditions. T1; *Trichoderma* treatment, T2; untreated control, T3; healthy control, T4; fungicide treatment. Values followed by the same letter do not differ significantly according to (LSD) least significant difference ($P \le 0.05$).

Likewise tomato seed treatment with spore suspension of *T. harzianum* (T1) significantly increased the seed germination rate from 41.67% (T2) to 79.33% under artificial inoculation by *R. solani*, with no significant

differences as compared to the fungicide treatment (T4) (87.6%%). The highest pre-emergence damping off incidence was recorded in the untreated control T2 (58.23%) (Figure 3). The biological control efficacy (BCE) was 64.56% compared to CE of 78.74% in T4 (Table 2).

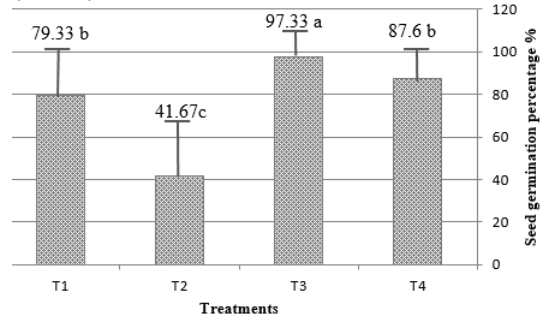


Figure 3. Efficacy of *T. harzianum* in controlling seed rot and damping-off diseases of tomato caused by *R. solani* under artificial inoculation conditions. T1; *Trichoderma* treatment, T2; untreated control, T3; healthy control, T4; fungicide treatment. Values followed by the same letter do not differ significantly according to (LSD) least significant difference ($P \le 0.05$).

Table 2. Effect of tomato seed treatment with *T. harzianum* on pre-emergence damping-off disease incidence and biological control efficacy against *P. infestans* and *R. solani* under artificial inoculation conditions.

Pathogen	Treatment	Percentage of pre-emergence disease incidence (%)	Control efficacy (CE) %
P. infestans	T. harzianum	25	49.3
	Carbenazim	7.7	84.38
R. solani	T. harzianum	20.67	64.56
	Carbendazim	12.4	78.74

This study showed that tomato seed treatment with *T. harzianum* decreased significantly the incidence of preemergence damping off disease caused by *P. infestans* and *R. solani* under artificial inoculation conditions. Our results are in accordance with those of Biam and Majumder (2019), where tomato seed treatment with four *Trichoderma* isolates showed considerable increase in germination percentage, and reduction in pre-emergence damping off incidence, with biological control efficacy ranged from 20.66% to 39.23% against *R. solani*, and from 32.39% to 64.46% against *Pythium* sp. depending on the *Trichoderma* isolate. Hassan *et al.* (2015) revealed a noticeable reduction in tomato damping off caused by *R. solani* in different substrates amended with *Trichoderma* spp.

Many studies revealed the efficacy of biological control against tomato pre-emergence damping off disease. When tomato and chilli seedlings that colonized with antagonistic *Streptomyces rubrolavendulae* S4 were grown in *P. infestans* artificially inoculated peat moss, the percentage of survival of tomato and chilli seedlings significantly increased from 51.42% to 88.57% and from 34.10% to 76.71% respectively (Loliam *et al.*, 2012). Other studies showed that *T. harzianum*, *Bacillus subtilis*, *Pseudomonas fluorescens*, and *Streptomyces* species were

reported as commercial biocontrol agents for controlling *Phytophthora* species (Xiao *et al.*, 2002; Lozoya-Saldana *et al.*, 2006; Fialho de Oliveira *et al.*, 2010). In one of the recent studies, *Bacillus subtilis* subsp. *subtilis*, and *T. harzianum* significantly enhanced tomato plant growth and immunity when exposed to *P. infestans* (Bahramisharif and Rose, 2019), and *T. harzianum* proved effective in controlling damping off disease of chilli (*Capsicum annuum* L.) caused by *Pythium aphanidermatum* (Tekale *et al.*, 2019).

It was observed that, in T2 (untreated seeds in inoculated soil), the post-emergence damping-off disease incidence was approximately 37.3% compared with 12.67% and 0% in the *Trichoderma* treatment (T1) and fungicide treatment (T4) respectively. The affected seedlings emerging from the soil have developed dark brown lesions (0.5 – 1.3 cm) at the collar region leading of seedlings death. The biological control efficacy of post-emergence damping off disease was 66.03%.

The effect of tomato seed treatment with T. harzianum on the plant growth was studied in pots under artificial inoculation with P. infestans and R. solani, and the results are presented in Figure 4. It was observed that both pathogens reduced the plant height significantly (≤ 0.05) by 15.9% and 30.1% respectively than in the healthy control. In contrast, Trichoderma treatment (T1) had a positive effect on tomato plant growth, where it increased the plant height significantly by 12.49% and 64.33% under artificial inoculation with P. infestans and R. solani respectively. T1 (Trichoderma / R. solani) had the highest plant lengths, with significant increase of 14.8% than the healthy plants. It was also observed that seed treatment with carbendazim reduced the plant growth significantly.

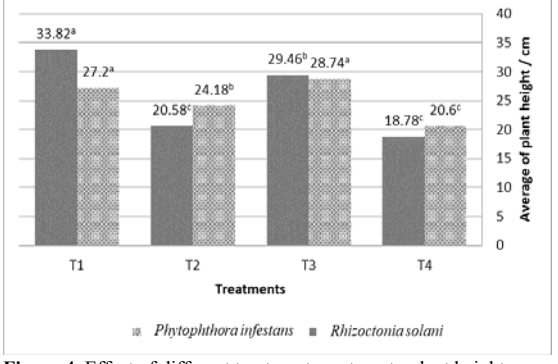


Figure 4. Effect of different treatments on tomato plant height under artificial infection by *R. solani* and *P. infestans*. Values followed by the same letter for each pathogen do not differ significantly according to (LSD) least significant difference ($P \le 0.05$).

Trichoderma spp. are known as a biocontrol agent against many plant pathogens, and improve the plant growth and yield by enhancing the growth hormones and increment of plant beneficial microbiome (Dubey et al., 2007; Khatabi et al., 2012; Hussein, 2019). Biam and Majumder (2019) showed that plant height, number of leaves and flowers per plant, dry and fresh weight, root length and yield of tomato was significantly superior in Trichoderma treated plants and low in control. T. harzianum improved the overall tomato plant growth in the presence of Pythium ultimum and Phytophthora capsici, while both pathogens reduced the plant height by 28.6% and 42% respectively than in the healthy control (Uddin et

al., 2018). Improvement in agronomic traits of host plant in the presence of pathogen was attributed to *T. harzianum* that increased water uptake and translocation of nutrients (Hoyos-Carvajal *et al.*, 2009).

On the contrary, beside tomato seed treatment with carbendazim almost completely protected the plants against the two pathogens, but it significantly decreased the plant height. It seems that carbendazim concentration (0.2%) used in this study was inappropriate for tomato seed treatment. Dhanamanjuri et al. (2013) showed that the plant growth was slightly affected according to the difference in crops and fungicide concentration used for seed treatment. The fungicide Bavistin (Carbendazim) at 10 ppm concentration was the best among the treatments of Cicer arietinum, while in case of Zea mays, 1ppm concentration of carbendazim has shown better stimulating effect on the plant growth as compared to control (Dhanamanjuri et al., 2013). Many studies showed that carbendazim could have some phytotoxic effects especially when used at dosage higher than recommended. It caused a decrease in dry weight and in all of the foliar pigments of tobacco plants Nicotiana tabacum L. cv. tennessee 86 (Garcia et al., 2002).

3.3. Efficacy of T. harzianum in controlling potato black scurf disease caused by R. solani

Black scurf incidence was significantly reduced by *T. harzianum* under artificial inoculation conditions.

Biocontrol treatment had significantly low black scurf incidence (12.7%), and low percent of stem canker (7.33%) compared with 57.6% and 47.3% in untreated control (T2). No sclerotia were observed on new tubers in the carbendazim treated pots, while 1.52% of plants showed stem canker symptoms.

Under artificial inoculation conditions, R. solani adversely affected the growth of host plant resulting in a significant decrease in number and weight of new tubers by 49.93% and 54.21% compared to 6.28% and 14.03% respectively in T1 (Trichoderma treatment). Although carbendazim showed high efficiency to prevent the potato black scurf disease, but it caused a significant decrease (17.19%) in tuber number compared to Trichoderma treatment (6.28%), and it also caused an obvious reduction in tuber weigh by 20.46% with no significant differences compared to 14.03% in T1 (biocontrol treatment). On the other hand, potato plant height was not significantly affected by the pathogen compared to the healthy plants, while T. harzianum (T1) increased significantly the plant height compared to T2 (pathogen alone), but this increase in plant height was not significant as compared to T3 (healthy control). T4 (carbendazim) significantly reduced 24.03% height (Table plant bv

Table 3. Efficacy of *T. harzianum* in controlling potato black scurf and stem canker diseases caused by *R. solani* under artificial inoculation conditions

Treatment	Percentage of progeny tubers infection (%)	Percentage of stem canker %	Number of tubers	Relative reduction in tubers Number %	Mean weight of tubers (g)	Relative reduction in tubers weight %	Mean length of plants (cm)	Relative reduction in plant length %
T1	b12.7	7.33 a	6.87	a6.28	337.55	14.03 b	41.29	+a 3.23
T2	57.6 c	47.3 b	3.67	c49.93	179.8	c54.21	39.33	b 1.68
T3	- a	- a	7.33	- a	392.65	- a	40.0	- ab
T4	a-	1.52 a	6.07	b17.19	312.33	b20.46	30.39	c 24.03
LSD at P=5%	9.63	12.8	-	8.95	-	6.54	-	4.8

T1; *Trichoderma* treatment, T2; untreated control (*R. solani*), T3; healthy control, T4; fungicide (carbendazim). Values followed by the same letter in the same column do not differ significantly according to (LSD) least significant difference (P = 0.05).

It appears that there are many factors affecting the effectiveness of biological control, among them the isolates of the fungus used in the biological control. It was determined that both *in vitro* and *in vivo* the isolates of *T. harzianum* and *T. virens* have shown different efficiency against *R. solani*. Some isolates of these two antagonistic fungi have significantly reduced the severity of the potato black scurf and stem canker diseases, and they raised the development of the plant (Durak, 2016).

Increased growth response of several plants, following the treatment of pathogen – free soil by *Trichoderma* has been documented (Baker, 1989; Chang *et al.*, 1986; Kleifeld and Chet, 1992). This was explained by the ability of *Trichoderma* to inhibit pathogens in the rhizosphere which might cause seed rots and pre-emergence damping off (Kleifeld and Chet, 1992). Some studies reported that the increased growth response caused by *Trichoderma* isolates resulted in large increase in the root area and root lengths and may be related to the effect

on root system. Yedidia *et al.* (1999) suggested a direct role for *T. harzianum* in mineral uptake by the plant at a very early stage of fungal-plant association. In addition, Harman (2000) demonstrated that *Trichoderma* spp. are opportunistic plant colonizers that affect plant growth by promoting healthy and abundant plant roots, probably via the production or control of plant hormones.

4. Conclusion

The present study clearly indicated that *T. harzianum* had strong antagonistic activity against *P. infestans* and *R. solani* on PDA medium. Tomato seed treatment with *T. harzianum* spore suspension showed higher seed germination, lower pre and post emergence damping off disease incidence caused by *P. infestans* and *R. solani*, and higher biological control efficacy than the untreated control. Seed treatment with *T. harzianum* also showed effective biological control for stem canker disease of

tomato seedlings caused by *R. solani. Trichoderma* treatment significantly reduced black scurf and stem canker disease incidence caused by *R. solani* on potato as compared to untreated control. From the present findings, recommendation could be made for further evaluation of local *Trichoderma* isolates under different climatic condition of Syria for development of effective Trichoderma formulation as a component of integrated disease management practice to manage damping-off of tomato and potato, and black scurf disease of potato.

Acknowledgment

The authors would like to thank Mr. Salama Rasheed, Sweida Agriculture Directorate, for providing the sample of *T. harzianum* commercial product.

References

Annual Agricultural Statistical Abstract. 2016. Agricultural Statistics Directorate, Ministry of Agriculture and Agrarian Reform, Damascus, Syria.

Abdo RH, Bayaa B and Abbas A. 2012. Determination of anastomosis groups within population of *Rhizoctonia solani* Kuhn in potato in Syria. *Arab J. Plant Prot.*, **30**: 1-10.

Alwathnani HA and Perveen K. 2012. Biological control of Fusarium wilt of tomato by antagonist fungi and cyanobacteria. *Afr. J. Biotechnol.*, **11(5)**:1100-1105.

Asaka O and Shoda M. 1996. Biocontrol of *Rhizoctonia solani* damping-off of tomato with *Bacillus subtilis* RB14. *Appl. Environ. Microbiol.*, **62(11)**: 4081–4085.

Bahramisharif A and Rose LE. 2019. Efficacy of biological agents and compost on growth and resistance of tomatoes to late blight. *Planta*, **249**:799–813. Doi.org/10.1007/s00425-018-3035-2

Baker R. 1989. Improved *Trichoderma* spp. for promoting crop productivity. *Trends Biotechnol.*, 7: 34-38.

Bell DK, Wells HD and Markham CR. 1982. *In vitro* antagonism of *Trichoderma* species against six fungal plant pathogens. *J. Phytopathol.*, **72:** 379-382.

Biam M and Majumder D. 2019. Biocontrol efficacy of *Trichoderma* isolates against tomato damping off caused by *Pythium* spp. and *Rhizoctonia solani* (Kuhn.). *Int. J. Chem. Stud.*, **7(3)**: 81-89.

Birch PRJ, Bryan G, Fenton B, Gilroy EM, Hein I, Jones JT, Prashar A, Taylor MA, Torrance L and Toth IK. 2012. Crops that feed the world 8: Potato: are trends of increased globa production sustainable? *Food Secur.*, **4:** 477-508.

Boogert van den H and Luttikholt AJG. 2004. Compatible biological and chemical control systems for *Rhizoctonia solani* in Potato. *Eur. J. Plant Pathol.*, **2:** 110. doi:10.1023/B:EJPP.0000015325. 33299.e0.

Chang YC, Chang YC, Baker R, Kleifeld O and Chet I. 1986. Increased growth of plants in presence of biological control agent *Trichoderma harzianum. Plant Dis.*, **70**: 145-148.

Dennis C and Webster J. 1971. Antagonistic properties of species groups of *Trichoderma*. Trans. Br. Mycol. Soc., **57**: 25-39.

Dhanamanjuri W, Thoudam R and Dutta BK. 2013. Effect of some pesticides (Fungicides) on the germination and growth of seeds/seedlings of some crop plants, (i.e. *Cicer arietinum* and *Zea mays*). *Middle East J. Sci. Res.*, **17:** 627-632. Doi: 10.5829/idosi.mejsr.2013.17.05.12221.

Dubey SC, Suresh M and Birendra SS. 2007. Evaluation of Trichoderma species against Fusarium oxysporum f. sp. ciceris for integrated management of chickpea wilts. *Biol. Control*, 40:118–127.

Durak E. 2016. Biological control of *Rhizoctonia solani* on potato by using indigenous *Trichoderma* spp. AIP Conference Proceedings 1726, 020020. Doi.org/10.1063/1.4945846

Elad Y and Kapat A. 1999. The role of *Trichoderma harzianum* protease in the bio-control of *Botrytis cinerea*. *Eur. J. Plant. Pathol.*, **105**:177-189.

Errakhi R, Bouteau F, Lebrihi A and Barakate M. 2007. Evidences of biological control capacities of *Streptomyces* spp. against *Sclerotium rolfsii* responsible for damping-off disease in sugar beet (*Beta vulgaris* L.). *World J. Microbiol. Biotechnol.*, 23(11): 1503–1509.

FAOSTAT, 2019. Food and Agriculture Organization of the United Nations (Syria).

Fialho de Oliveira M, Germano da Silva M and Van Der Sand ST. 2010. Anti-phytopathogen potential of endophytic actinobacteria isolated from tomato plants (*Lycopersicon esculentum*) in southern Brazil, and characterization of *Streptomyces* sp. R18(6), a potential biocontrol agent. *Res. Microbiol.*, **161(7)**: 565–572.

Francesco VK, Sivasithamparam EL, Ghisalberti RM, Sheridan L and Woo ML. 2008. *Trichoderma* plant pathogen interactions. *Soil Biol. Biochemist*, **40**: 1-10.

García P, Ruiz J, Rivero R, López-Lefebre L, Sánchez E and Romero L. 2002. Is the Application of Carbendazim Harmful to Healthy Plants? Evidence of Weak Phytotoxicity in Tobacco. *J. Agric. Food Chem.*, **50:** 279-83. Doi:10.1021/jf010748g.

Getha K and Vikineswary S. 2002. Antagonistic effects of *Streptomyces violaceusniger* strain G10 on *Fusarium oxysporum* f. sp. *cubense* race 4: indirect evidence for the role of antibiosis in the antagonistic process. *J. Ind. Microbiol. Biotechnol.*, **28**(6): 303–310.

Gomez KA and Gomez A. 1984. Statistical Procedure for Agricultural Research—Hand Book. John Wiley & Sons, New York.

Harman GE. 2000. Myths and dogmas of bio-control: changes in perceptions derived from research on *Trichoderma harzianum* T22. *Plant Dis.*, **84:** 377-393.

Hassan WA, Taher IE, Saido KA and Ali AS. 2015. Antagonistic succession of *Trichoderma* against Rhizoctonial damping- off on tomato in composted media. Bull. *Iraq nat. Hist. Mus.*, 13 (4): 41-49

Hussein SN. 2019. Biological control of root rot disease of cowpea *Vigna unguiculata* caused by the fungus *Rhizoctonia solani* using some bacterial and fungal species. *Arab J. Plant Prot.*, **37(1)**:31-39. Doi.org/10.22268/AJPP-037.1. 031039.

Hoyos-Carvajal L, Ordua S and Bissett J. 2009. Growth stimulation in bean (*Phaseolus vulgaris* L.) by *Trichoderma*. *Biol. Control*. **51**:409–416

Ibrahim ME. 2017. *In vitro* Antagonistic activity of *Trichoderma harzianum* against *Rhizoctonia solani* the causative agent of potato black scurf and stem canker. The 7th Inter. Conf."Plant & Microbial Biotech. & their Role in the Development of the Society"pp.173-185. Doi:10.21608/ejbo.2017. 903.1067.

Jayaraj J, Radhakrishnan NV and Velazhahan R. 2006. Development of formulations of *Trichoderma harzianum* strain M1 for control of damping-off of tomato caused by *Pythium aphanidermatum*. Arch. Phytopathol. Pflanzenschutz, **39(1)**:1-8.

Jmour W and Hamada W. 2006. First report of A2 mating type of *Phytophthora infestans* in Tunisia using molecular markers and some observations on its metalaxyl resistance. *Tunis. J. Plant Protect.*, 1: 85-91.

Joo GJ. 2005. Production of an anti-fungal substance for biological control of *Phytophthora capsici* causing phytophthora blight in red-peppers by *Streptomyces halstedii*. *Biotechnol*. *Lett.*, **27(3)**: 201–205.

Keiser A. 2008. *Rhizoctonia solani* a fungal disease with multiple symptoms: means of preventive and curative control. *In*: Potato Research for a Production of Quality. Information Day, February 2008, Changins

Kerroum F, Noureddine K, Henni J and Mebrouk K. 2015. Antagonistic effect of *Trichoderma harzianum* against *Phytophthora infestans* in the North-west of Algeria. *Int. J. Agric. Res.*, **6:** 44-53.

Khatabi B, Molitor A, Lindermayr C, Pfiffi S, Durner J, Wettstein D, Kogel KH and Schäfer P. 2012. Ethylene supports colonization of plant roots by the mutualistic fungus *Piriformospora indica*. PLoS One 7:e35502

Kleifeld O and Chet I. 1992. *Trichoderma harzianum* – interaction with plants and effect on growth response. *Plant Soil*, **144:** 267-272.

Lee ET, Lim SK, Nam DH, Khang YH and Kim SD. 2003. Pyoverdin 2112 of *Pseudomonas fluorescens* 2112 inhibits *Phytophthora capsici*, a red-pepper blight-causing fungus. *J. Microbiol. Biotechnol.*, **13(3):** 415–421.

Limón MC, Chacón MR, Mejías R, Delgado-Jarana J, Rincón AM, Codón AC and Benítez T. 2004. Increased antifungal and chitinase specific activities of *Trichoderma harzianum* CECT 2413 by addition of a cellulose binding domain. *Appl Microbiol Biotechnol*, **64(5)**:675-85. Doi: 10.1007/s00253-003-1538-6.

Loliam B, Morinaga T and Chaiyanan S. 2012. Biocontrol of *Phytophthora infestans*, fungal pathogen of seedling damping off disease in economic plant nursery. *Hindawi Publishing Corporation Psyche*. Doi:10.1155/2012/324317

Lozoya-Saldana H, Coyote-Palma MH, Ferrera-Cerrato R and Lara-Hernandez ME. 2006. Microbial antagonism against *Phytophthora infestans* (Mont) de Bary. *Agrociencia*, **40(4)**: 491–499

Murmanis L, Highley TL and Ricard J. 1988. Hyphal interaction of *Trichoderma harzianum* and *Trichoderma polysporum* with wood decay fungi. *Material Organismen*, **23**:271 – 279.

Naffaa W, Ibrahim S, Abou-Alfadil T and Dawood A. 2017. Incidence of the potato late blight pathogen, *Phytophthora infestans*, in Syria and its mating type. *J. Plant Dis. Prot.*, **124 (6)**: 533-537. Doi.org/10.1007/s41348-017-0130-8

Ogoshi A. 1987. Ecology and pathogenicity of anastomosis and intraspecific groups of *Rhizoctonia solani* Kühn. *Ann. Rev. Phytopathol.*, **25:** 125–143.

Omokhua GE. 2011. Pre and post-emergence damping-off of *Chrysophyllum albidum* in Port Harcourt. *Int. Multidiscip. J.*, **5(6**):411-421.

Perelló AE, Moreno MV, Mónaco C, Simón MR and Cordo C. 2009. Biological control of *Septoria tritici* blotch on wheat by *Trichoderma* spp. under field conditions in Argentina. *Biocontrol*, **54**:113–122. Doi.org/10.1007/s10526-008-9159-8

Rauf C, Ashraf M and Ahmad I. 2007. Management of black scurf disease of potato. *Pak. J. Bot.*, **39(4):** 1353.

Rehman SU, Lawrence R, Kumar EJ and Badri ZA. 2012. Comparative efficacy of *Trichoderma viride*, *T. harzianum* and carbendazim against damping-off disease of cauliflower caused by *Rhizoctonia solani* Kuhn. *J. Biopestic.*, **5(1)**:23-27.

Sawant I. 2014. Trichoderma- Foliar Pathogen Interactions. *Open Mycol. J.*, **8:** 58-70. Doi: 10.2174/1874437001408010058.

Singh A and Islam MN. 2010. *In vitro* evaluation of *Trichoderma* spp. against *Phytophthora nicotianae*. *Int. J. Expt. Agric*, **1(1)**: 20-25

Sood M, Kapoor D, Kumar V, Sheteiwy MS, Ramakrishnan M, Landi M, Araniti F and Sharma A. 2020. *Trichoderma*: The "Secrets" of a Multitalented Biocontrol Agent. *Plants*, 9: 762.

Ston A. 2009. Organic Management of Late Blight of Potato and Tomato (*Phytophthora infestans*). Sustainable Agriculture Research and Education. Oregon State University. Available on: http://www.extension.org/pages/18361/Accessed on 22/03/2014.

Tekale AG, Guldekar DD, Kendre VP, Deshmukh AP and Potdukhe SR. 2019. Efficacy of fungicides and bioagents against damping off in Chilli caused by *Pythium aphanidermatum*. *Int. J. Curr. Microbiol. App. Sci.*, **8(6):** 637-648. Doi. org/10. 20546

Tomlin CDS. 2006. The Pesticide Manual: A World Compendium, 14th ed.; British Crop Protection Council: Surrey, UK.

Tronsmo A and Dennis C. 1978. Effect of temperature on antagonistic properties of *Trichoderma* species. *Trans Brit. Mycol. Soc.*, **71(3)**:469-474.

Vinale F, Sivasithamparam K, Ghisalberti E, Woo S, Nigro M, Marra R, Lombardi N, Pascale A, Ruocco M, Lanzuise S, Manganiello G and Lorito M. 2014. *Trichoderma* secondary metabolites active on plants and fungal pathogens. *Open Mycol. J.*, **8**. 10.2174/1874437001408010127.

Uddin MN, Rahman UU, khan W. et al. 2018. Effect of Trichoderma harzianum on tomato plant growth and its antagonistic activity against Phythium ultimum and Phytopthora capsici. Egypt. J. Biol. Pest. Control, 28, 32. Doi.org/10.1186/s41938-018-0032-5

Woodhall JW, Lees AK, Edwards SG and Jenkinson P. 2008. Infection of potato by *Rhizoctonia solani*: effect of anastomosis group. *Plant Pathol.*, **57**:897-905.

Xiao K, Kinkel LL and Samac DA. 2002. Biological control of *Phytophthora* root rots on alfalfa and soybean with *Streptomyces*. *Biol. Control*, **23(3):** 285–295.

Yanar Y, Yilmaz G, Cesmeli I and Coskun S. 2005. Characterization of *Rhizoctonia solani* isolates from potatoes in Turkey and screening potato cultivars for resistance to AG-3 isolates. *Phytoparasitica*, **33**: 370-376.

Yedidia I, Benhamou N and Chet I. 1999. Induction of defense responses in cucumber plants (*Cucummis sativus* L.) by the Biocontrol agent *Trichoderma harzianum*. *Appl. Environ. Microbiol.*, **65**: 1061-1070.

Zhang RS, Liu YF, Luo CP, Wang XY, Liu YZ, Qiao JQ et al., 2012. Bacillus amyloliquefaciens Lx-11, A potential biocontrol agent against rice bacterial leaf streak. J. Plant Pathol., 94(3):609-619.

Jordan Journal of Biological Sciences

Bioconversion of Pear Pomace by Strains of *Pleurotus Ostreatus*During Mycelial Development

María B. Buglione^{1,*}, Marta S. Agüero¹, Daniel A. Martínez¹, Marcela V. Filippi², Jorge F. Maldonado¹, Gustavo E. Rodríguez³

¹Universidad Nacional de Río Negro. Sede Alto Valle y Valle Medio. Escuela de Veterinaria y Producción Agroindustrial. Centro de Investigaciones y Transferencia de Río Negro. Argentina; ²Universidad Nacional de Río Negro. Sede Alto Valle y Valle Medio. Escuela de Producción, Tecnología y Medio Ambiente. Centro de Investigaciones y Transferencia de Río Negro. Argentina; ³Universidad Nacional del Comahue. Facultad de Ciencias Agrarias. Laboratorio de Hongos Comestibles y Medicinales. Argentina.

Received: June 4, 2021; Revised: September 14, 2021; Accepted: December 28, 2021

Abstract

The cultivation of edible fungi is an ecological bioconversion system since it allows us to take advantage of lignocellulosic waste. In this way, the pear processing industries generate waste that is called pomace. Nevertheless, these kinds of residues could be considered the basement of substrate for these mushroom growths. Hence, the focus of this study was to analyse the modify of the content of different chemical components in pear pomace while the mycelial growth of Pl-P and Pl-J take place. These are two kinds of strains of *P. ostreatus*. Thus, the inoculated substrate was incubated in Petri dishes at 28°C in the dark for 8 weeks. A decrease in dry matter was observed, obtaining a 30% average bioconversion for the analysed strains. The chemical characterisation of the biodegraded pomace showed a significant decrease in all tested variables. The net content of non-structural carbohydrates had the greatest decrease (approximately 60%) in the analysed period. The content of dry matter, organic matter, crude protein, hemicellulose, and lignin was reduced to a lesser extent. The development of emerging end-of-pipe technologies and applications aimed at reducing the negative impact on the environment due to the accumulation of waste generated by industrial activities should be considered.

Keywords: biodegradation, agro-industrial by-products, lignocellulosic waste, ligninolytic microorganisms, Pleurotus ostreatus.

1. Introduction

The cultivation of edible mushrooms can be considered an ecological bioconversion system since it allows the production of food, enzymes, and physiologically active metabolites and provides technological tools to recycle agricultural and agro-industrial waste. Likewise, the biodegraded substrate can be used for animal feed and as organic fertiliser, thus reducing environmental pollution (Koutrotsios *et al.*, 2014; Barshteyn & Krupodorova, 2016; Bellettini *et al.*, 2019; Sadik *et al.*, 2021).

The capacity of *Pleurotus* for generating extracellular enzymes makes that they can be cultivated on a vast diversity of lignocellulosic by-products, and they classified into the group of white-rot fungi (WRF). In this way, WRF have unique capabilities to depolymerise, cleave carboncarbon linkages, and mineralise lignin to CO₂ and H₂O. Due to this capacity, WRF play a key role in carbon recycling in terrestrial ecosystems (Isroi *et al.*, 2011; Anike *et al.*, 2016; Yang *et al.*, 2020; Del Cerro *et al.*, 2021).

The raw material used as a substrate for the cultivation and production of these edible mushrooms includes cereal straw, leaves, plant crop residues destined for industrial use, and products result of agro-industries activities, such as oilseeds, distillation of different resources, sugar cane process, and factory of wood cut (Koutrotsios *et al.*, 2014; Martínez *et al.*, 2015; Barshteyn & Krupodorova, 2016; Rodríguez *et al.*, 2018).

As well the mushrooms employ the substrates as nutrients sources for this reason the degrades materials are called "spent" mushroom substrate (SMS). Meanwhile, these elements are exhausted, the fungi grow. SMS is a lignocellulosic biomass that contains fungal mycelium and the biodegraded substrate. Currently, it is considered a valuable waste, as a source of raw material for new processes, but it is still named SMS (Ribas *et al.*, 2009; Sánchez, 2010; Foluke *et al.*, 2014; Koutrotsios *et al.*, 2014; Hanafi *et al.*, 2018).

SMS has been successfully reused as a component of substrate mixtures in the production of horticultural seedlings, according to Lopes *et al.* (2015); Moraes *et al.* (2020) in tomato (*Solanum lycopersicum*) and Liu *et al.* (2018) in lettuce (*Lactuca sativa* L.). Other authors have investigated the use of SMS as a diet feed supplement for broilers (Foluke *et al.*, 2014, Cayolo *et al.*, 2019, Bandara *et al.*, 2021).

Previously, the authors of this work evaluated the mycelial growth of three strains of *Pleurotus ostreatus* and one strain of *Agrocybe aegerita* for their ability to colonize pear pomace generated by pear juice production plants from Río Negro (Argentina). In this study, the strains of *A*.

^{*} Corresponding author. e-mail: mbuglione@unrn.edu.ar.

aegerita analyzed showed a lower rate of colonisation than *P. ostreatus* (Martínez *et al.*, 2015).

The relationship between the physical and chemical factors has variable effects in the colonization and fructification phases due to the influence of some conditions such as pH, temperature, time of cultivation, substrate composition, kind of inoculated strain and others. For this reason, it is important to determine these technical aspects to achieve adequate substrate management and an efficient production system (Sánchez, 2009, 2010; Pineda-Insuasti *et al.* 2015; Heredia-Solís *et al.*, 2016; Bellettini *et al.*, 2019).

In the Patagonia of Argentina, just on the Valle Medio y Alto Valle of Río Negro province, there are food agroindustries systems destined to produce concentrated juice, cider, dehydrated products preserves and liqueurs. This industry generates a large amount of a by-product known as bagasse of apple and pear, which is the product obtained (25–30% of the total weight of the fresh fruit) mainly from the pulp / peel (95%), seeds (2–4%), and peduncle (1%), as described by Bhushan *et al.* (2008). The pomace or bagasse presents a high content of lignocellulosic carbon sources, in addition to soluble simple sugars.

The objective of this study was to evaluate the changes in the chemical composition of the pear pomace during mycelial growth by Pl-P and Pl-J which are two different strains of *P. ostreatus*.

2. Materials and Methods

2.1. Fungal strains

Two strains of *Pleurotus ostreatus* (Jacq.: Fr.) Kummer were used. The strains were obtained from Cepario FACA-UNCo, Laboratorio de Hongos Comestibles y Medicinales:

Pl-J: Misiones, Argentina. Collector: Rodríguez G. FACA Pl-J 07.

Pl-P: Paraje Abra Ancha, Neuquén, Argentina. Collector: Rodríguez G. FACA Pl-P 12.

The strains have been maintained in malt extract agar (10% w/v) at 4°C in the dark. Meanwhile, the multiplication to obtain active mycelium discs has carried on potato dextrose agar (PDA) which has been formulated by an infusion of potato, agar-agar and D (+) glucose. (Merck, 2005).

2.2. Substrate

The characterization of the biodegradation process by *P. ostreatus* took place over pear (*Pyrus communis* L.) v. 'Williams Bon Chretien' pulp as a substrate. The wet bagasse of pears produced by company Jugos S.A. was first sundried on a rectangular mesh. Afterwards, dried substrate was crushed in a commercial grain grinder until a particle size between 0.1 to 0.5 mm in diameter was obtained. This company is in the Alto Valle of Río Negro Province in the Patagonian region of Argentina.

2.3. Mycelial growth

The dried and ground pomace was hydrated at 70% (w/w) with distilled water and placed in Petri dishes (approximately 30 g/dish). The Petri dishes (90 mm diameter) were sterilised in an autoclave for 30 minutes at 1 atm of pressure and kept sealed in a refrigerator at 4°C

until inoculated. Subsequently, active mycelium discs with a diameter of 10 mm have inoculated into plates containing hydrated and sterile pomace. The inoculation process has carried on under a laminar flow cabinet, ensuring the environment and materials have been germfree. Later, the Petri dishes with inoculated substrate have incubated in a culture stove at 28°C and environmental darkness for eight weeks. Thus, after this time, the Petri dishes have been stored at -20°C until their chemical characterization.

2.4. Physicochemical analysis of pomace

The chemical composition of the pear pomace was analysed before inoculation with the PI-P and PI-J strains (initial) and after eight weeks of incubation (final). At the end of the incubation period, the substrate contained mainly degraded lignocellulosic materials impregnated with fungal mycelium.

The substrates (initial and final) were dried to a constant weight at 65°C to obtain the dry matter content. The final product has been ground to pass through an l-mm screen in a Wiley grinder (Thomas Scientific, Swedesboro, NJ, USA), and the samples of each substrate were analyzed.

The total ash content (Ash) was determined by incineration in a muffle at 550°C; non-structural carbohydrates (NSCH) were determined by the Antrona method (Koehler, 1952). The crude protein (CP) content was determined by the Kjeldahl method ($CP = N \times 6.25$) as well as acid and neutral detergent fibres (NDF and ADF) and acid detergent lignin (ADL = LIG) were determined by the sequential method of Van Soest et al. (Van Soest et al., 1991). The bioconversion efficiency was estimated as the decrease in the initial dry matter, expressed as a percentage. The organic matter content (OM) was obtained by the difference between dry matter (DM) and ash (OM = DM – Ash). Organic carbon (OC) was calculated as OM / 1.724 (AOAC, 2000). The net cellulose (CEL) and hemicellulose (HCEL) contents were calculated as CEL = ADF - ADL and HCEL = NDF - ADF, respectively (Van Soest et al., 1991).

2.5. Experimental design and statistical analyses

An experimental design with two factors and two levels was considered to characterise the biodegradation process during the mycelial development of two strains of *P. ostreatus*. For this, the following were considered:

- Strains: Pl-P and Pl-J
- Moments: Initial (not biodegraded) Final (biodegraded after eight weeks)

The tests were carried out with 5 replications of each sample.

The analysed variables were N (g); C (g), C/N; OM (g), CP (g), NSCH (g), HCEL (g), CEL (g), and LIG (g).

The means of the treatments or their linear combinations were evaluated by analysis of variance (ANOVA) and subsequently contrasted using the multiple comparisons method proposed by Fisher (LSD Fisher) with a significance level of $\alpha = 0.01$. The normal distribution of the data was previously verified by applying the Shapiro-Wilks test (Di Rienzo *et al.*, 2012).

3. Results

3.1. ANOVA model

A 2x2 full factorial experiment was considered in the treatment design; that is, two factors (Strain and Moment) with two levels each. In the first instance, the level of significance of each source of variation and the possible interaction (Strain * Moment) in the model for each of the response variables was evaluated using the value of p.

For each observation (Y), the model that was subjected to statistical analysis was:

$$Y_{ijk} = \mu + \alpha_i + \beta_j + \delta_{ij} + \epsilon_{ijk}$$

where
$$i = 1,2$$
; $j = 1,2$; $k = 1,...,5$

 Y_{ijk} represents the response of the k-th repetition at the i-th level of factor A (Strain) and the j-th level of factor B (Moment), μ represents a general mean, α_i is the effect produced by the i-th level of factor A, β_i corresponds to the effect of the j-th level of factor B, δ_{ij} is the additional effect (interaction) for the combination of levels i of factor A and j of factor B and ϵ_{ijk} is the associated random error to the ijk-th observation (Di Rienzo *et al.*, 2012).

Table 1 shows the results obtained from the statistical analysis by means of an ANOVA for one of the dependent variables, DM, using models with and without interaction. Similar results were observed for the rest of the variables (data not shown).

Table 1. Analysis of the variance (type III SoS) for the variable dry matter expressed in g (DM, g), considering the Moment of sampling as factors and Strains as classification variables, with the interaction Strain * Moment and without strain (additive bifactorial model). N = 20, $R^2 = 0.72$.

Variation source	Interaction	p value
Model	Yes	0.0001
Model	No	< 0.0001
Factor A: Strain	Yes	0.6018
ractor A: Strain	No	0.5912
Factor B: Moment	Yes	< 0.0001
ractor B: Moment	No	< 0.0001
Strain * Moment	Yes	0.7882

The p value <0.0001, less than the nominal significance level of the test ($\alpha=0.01$), for the effect of the Moment factor implies that it had a statistically different effect from zero on the average chemical composition of the substrate. The results obtained also suggest that there were no effects associated with the interaction of the Strain * Moment factors (p=0.7882) or the Strain factor (p=0.60187), since the value of p in both cases was greater than the chosen significance level.

In other words, the strain factor did not interact with the sampling moments, so a new ANOVA was carried out by applying an additive bifactorial model without the interaction term δ_{ij} . Table 1 shows the results obtained from the statistical analysis with this model for one of the dependent variables, DM. Similar results were observed for the rest of the variables (data not shown).

The biodegradation process (Moment factor) induced highly significant variation in the chemical composition of the substrate (p < 0.0001), and this variation did not depend on the genetic characteristics of the analysed strains (p = 0.5912).

3.2. Biodegradation of pear pomace during mycelial growth

Table 2 shows the results of the post-ANOVA analysis, using the LSD Fisher mean comparison test, for the net DM content, using the factors Strain (Pl-P and Pl-J) and Moment (initial and final) as classification variables. Similar effects were observed for the rest of the response variables (data not shown). Post-ANOVA analysis confirmed that the variation in each of the components examined in the substrate was exclusively due to the biodegradation process and not to the strain type.

Table 2. Post-ANOVA analysis for the variable dry matter (g) for the comparison of means by using the Fisher test.

Test: LSD Fisher $\alpha = 0.01$ LSD = 2.21816 error: 2.9288 df: 17

Strain	Mean	n	E.E.	Moment	Mean	n	E.E.
Pl-J	13.29 ^a	10	0.54	Initial	10.96 ^a	10	0.54
Pl-P	13.71 ^a	10	0.54	Final	16.04^{b}	10	0.54

Means with the same letter are not significantly different (p > 0.01).

Consequently, the results presented below (Table 3) correspond to the analysis of the variation in the chemical composition of the pear pomace associated only with the biodegradation process by *P. ostreatus*.

As can be seen in Table 3, the mycelial development of *P. ostreatus* on the substrate caused a significant decrease in all considered variables. To analyse the results in greater detail, the percentage of loss for each variable was also calculated.

Table 3. Chemical composition of pear pomace prior to inoculation (initial) with *Pleurotus ostreatus* strains (Pl-J and Pl-P) and after eight weeks of incubation (final). Results are expressed as net content per Petri dish in grams, and the percentage of loss was calculated.

	Initial	Final	Loss, %
Dry Matter, g	$16.04^a\pm1.91$	$10.96^b\pm1.41$	31.66 ± 3.70
Nitrogen, g	$0.11^a\!\pm0.01$	$0.08^\text{b} \pm 0.01$	25.41 ± 4.51
Carbon, g	$9.10^a \pm 1.08$	$6.18^{\text{b}}\pm0.79$	32.07 ± 3.64
C/N	$80.59^a \pm 0.01$	$73.62^b \pm 5.71$	11.37 ± 4.66
Organic Matter, g	$15.69^a\pm1.86$	$10.66^{b} \pm 1.36$	32.07 ± 3.64
Crude Protein, g	$0.71^a \pm 0.08$	$0.52^{\text{b}} \pm 0.06$	25.41 ± 4.51
Non-structural carbohydrates, g	$0.70^a \pm 0.08$	$0.30^b \pm 0.05$	57.03 ± 4.75
Cellulose, g	$4.93^a \pm 0.59$	$4.05^{\text{b}}\pm0.49$	17.85 ± 2.82
Hemicellulose, g	$3.05^a \pm 0.36$	$2.14^b \pm 0.24$	29.82 ± 2.95
Lignin, g	$3.54^a \pm 0.42$	$2.56^\text{b} \pm 0.42$	27.80 ± 7.90

The values correspond to the mean of 10 replications per treatment \pm SD. Means with the same letter for the same row are not significantly different (p > 0.01).

After allowing mycelial development on pear pomace for 8 weeks at 28°C in Petri dishes, a decrease in the dry matter (16.04 ± 1.91 g to 10.96 ± 1.41 g) was observed, indicating a 30% average bioconversion efficiency by *P. ostreatus*.

The net content of NSCH (0.70 g \pm 0.08 vs. 0.30 g \pm 0.05) was the one that presented the greatest decrease in the analysed period, approximately 60% on average for both strains. The biodegraded substrate impregnated with fungal mycelium showed a lower reduction in OM, CP,

HCEL, and LIG by almost 30%. The least fluctuation was observed in the fraction corresponding to CEL, which only decreased by about 20%.

4. Discussion

Due to the environmental problems related to the accumulation of solid waste with a high organic content, such as the generates in the food industries related to extraction of pear juice the authors of this work investigated alternatives to reuse these wastes and involve the agricultural and environmental sectors (Martínez et al., 2015; Maldonado et al., 2018; Rodríguez et al., 2018; Maldonado et al., 2021).

In this work, the biodegradation process of pear pomace during the stage of colonisation of the substrate by the Pl-P and Pl-J strains of *P. ostreatus* were chemically characterised, as these strains presented the best performance when analysing the mycelial growth curves in previous studies (Martínez *et al.*, 2015).

The variation in the chemical composition of the substrate was analyzed using an additive factorial model. Therefore, the terms in the model showed that the interaction between the classification variables, Moment and Strain, were absent (Table 1). This model was used to study the main effects associated with the biodegradation process, since ANOVA indicated that the Strain and Moment factors did not interact with each other (Di Rienzo *et al.*, 2012).

The obtained results indicated that the variation in the chemical composition of the substrate would be directly associated with the biodegradation process (Moment factor), regardless of the Strain type (p < 0.01).

The DM loss of the pear pomace substrate was 31.66%. This is a substantial mass reduction from the standpoint of lignocellulosic residue removal. Similar values were obtained by Zhang et al. (2002) in the cultivation of Pleurotus sajor-caju on rice and wheat straw. Sánchez et al. (2002) found that the bioconversion of vineyard pruning and grape pomace by Pleurotus spp. was from 16.7 to 38.8%, respectively. As demonstrated by Anike et al. (2016), the use of Pleurotus ostreatus for the bio convert of substrates as peanut shells and cornstalks during the stage of mycelial development in an array of proportions assayed is an encouraging and healthy environment way to the bioconversion of different substrates.

As shown in Table 3, the OM and C content of pear pomace used as a substrate was reduced by 32%. Several authors have reported that the loss of carbon from the resulting biomass (fungus and substrate) can be explained in part by its assimilation into the mycelium of the fungus and in part by its loss to the atmosphere as carbon dioxide due to the respiration of the fungus. The N loss might be due to volatilisation during the N mineralisation process (Zhang et al., 2002; Isroi et al., 2011; Anike et al., 2016; Del Cerro et al., 2021).

Principally, the loss of C and OM could be due to intracellular catabolism of central carbon metabolism (Del Cerro *et al.*, 2021) and not only to lignin degradation.

In this study, a statistically significant decrease in the C/N ratio from 80.6 to 73.6 (11% loss) was found in the mycelial development stage.

The analysis of this relationship was carried out due to the importance of the C/N ratio as one of the most important factors to balance biomass and biocomposite production. The excess or lack of nitrogen content in the substrate may be a limiting factor for fungal growth (D'Agostini et al., 2011). The decrease obtained during mycelial development is important to consider since according to Hoa et al. (2015), a higher C/N ratio favours mycelium growth and a lower C/N ratio favours fruiting body growth. Previously, in fruiting body production trials with the same substrate, the authors found that the Pl-P strain caused a significant decrease in the C/N ratio (26% loss), while Pl-J practically did not modify this variable (Rodríguez et al., 2018). This variation in the C/N ratio indicates that the substrate, even after biodegradation during the mycelial development of the analysed strains (SMS), could be used in productive cycles to obtain edible carpophores.

As can be seen in Table 3, NSCH were the carbohydrates that decreased the most (approximately 60%), while cellulose, hemicellulose, and lignin fibres had a decrease between 20 to 30%. This metabolic profile could be attributed to the fact that the expression of genes of enzymes related to the use of NSCH are constitutive, while the lignocellulolytic exoenzymes are inducible and would be expressed only when the levels of NSCH decrease. The presence of metabolised sugars could cause the analysed *P. ostreatus* strains to produce ligninolytic enzymes, thus obtaining the carbon source and inducers for enzymatic synthesis (Akpinar and Urek, 2012; Rouches *et al.*, 2016; Ergun and Urek, 2017).

Thereby, variation minimal in the fibre fraction was detected in the cellular wall correspondent to CEL. The result was similar to the findings of Zhang *et al.* (2002), implying that the fungi utilised a greater percentage of hemicellulose than cellulose. The fungi also used some lignin.

In previous studies (Rodríguez *et al.*, 2018), the authors evaluated the biological potential of different strains of *P. ostreatus* to develop on the same substrate, observing that pear pomace produced edible carpophores. They also evaluated the chemical composition during the substrate colonisation and fruiting phases. At the end of the productive period, similar results were obtained in terms of the variation of the chemical composition; the fibers (FDN, FDA, and LDA) decreased 10 to 20% while the crude protein content was not substantially modified.

At this time, the authors of this work are testing the use of agro-industrial wastes biodegraded by *P. ostreatus* as a feed supplement for broilers (Cayolo *et al.*, 2019) and as a substitute for non-renewable resources, such as peat, for seedling production.

5. Conclusion

This work showed that *Pleurotus* mycelial development on pear pomace is possible. This, together with the fruiting results published by the authors previously, indicates that it is possible to consider the cultivation of edible mushrooms of the genus *Pleurotus* over this substrate taking advantage of an agro-industrial waste product.

Acknowledgments

This work was funded by the SICADyTT, UNRN, Resolution 332/2018, PI 40-A-626 and PI 40-A-614.

The authors thank the company JUGOS S.A. (Villa Regina, Río Negro, Argentina) for the provision of the pomace used in this work.

Conflict of interest

The authors declare that there is no conflict of interests.

References

Akpinar M. and Urek R. 2012. Production of ligninolytic enzymes by solid-state fermentation using *Pleurotus* eryngii. *Prep Biochem Biotechnol.* 42(6): 582–597.

AOAC. 2000. Official methods of analysis Association of Official Analytical Chemists, 17th ed. AOAC, Washington.

Anike FN, Yusuf M and Isikhuemhen OS. 2016. Co-substrating of peanut shells with cornstalks enhances biodegradation by *Pleurotus ostreatus*. *J Bioremed Biodeg*, 7(1): 1–7.

Bandara A.R., Lian C.K., Xu J. and Mortimer P.E. 2021. Mushroom as a means of sustainable rural development in the Chin State, Myanmar. *Circular Agricultural System*, 1(1): 1–6.

Barshteyn V and Krupodorova T. 2016. Utilization of agroindustrial waste by higher mushrooms: modern view and trends. *J Microbiol Biotechnol Food Sci*, **5**: 563–577.

Bellettini MB, Fiorda FA, Maieves HA, Teixeira GL, Ávila S, Hornung PS, Maccari-Júnior A and Ribani RH. 2019. Factors affecting mushroom *Pleurotus* spp. *Saudi J Biol Sci*, **26**: 633–646.

Bhushan S, Kalia K, Sharma M, Singh B and Ahuja PS. 2008. Processing of apple pomace for bioactive molecules. *Crit Rev Biotechnol*, **28**(4): 285–296.

Cayolo F, Buglione MB, Filippi MV, Maldonado JF, Cáceres R, Peña S and Martínez D. 2019. Influencia de la dieta suplementada con bagazo de manzana sobre la calidad de la carne de *Gallus gallus*. Revista Argentina de Producción Animal, 39(S1): 95.

Del Cerro C, Erickson E, Dong T, Wong AR, Eder EK, Purvine SO, Mitchell HD, Weitz KK, Markillie LM, Burnet MC, Hoyt DW, Chu RK, Cheng J-F, Ramirez KJ, Katahira R, Xiong W, Himmel ME, Subramanian V, Linger JG and Salvachúa D. 2021. Intracellular pathways for lignin catabolism in white-rot fungi. *PNAS*, **118**(9): 1–10.

D'Agostini É, Mantovani TR, Valle JS, Paccola-Meirelles L, Colauto N and Linde GA. 2011. Low carbon/nitrogen ratio increases laccase production from basidiomycetes in solid substrate cultivation. *Sci Agric*, **68**: 295–300.

Di Rienzo JA, Casanoves F, Balzarini MG and González L, Tablada M and Robledo CW. 2012. "InfoStat User's Manual", https://es.slideshare.net/yeisonmendezortiz/manual-infostat-eng (April 24, 2021).

Ergun SO and Urek RO. 2017. Production of ligninolytic enzymes by solid state fermentation using *Pleurotus ostreatus*. *Ann Agrar Sci*, **15**: 273–277.

Foluke A, Olutayo A and Olufemi A. 2014. Assessing spent mushroom substrate as a replacement to wheat bran in the diet of broilers. *Am Int J Contemp Res*, **4**(4): 178–83.

Hanafi FHM, Rezania S, Taib SM, Din MFM, Yamauchi M, Sakamoto M, Hara H, Park J and Ebrahimi SS. 2018. Environmentally sustainable applications of agro-based spent mushroom substrate (SMS): an overview. *J Mater Cycles Waste Manag*, **20**(3): 1383–1396.

Heredia-Solís A, Esparza-Ibarra EL, Romero-Bautista L, Cabral-Arellano FJ, Echavarría-Chairez FG and Bañuelos-Valenzuela R. 2016. Evaluación de mezclas para sustrato y producción de *Pleurotus ostreatus* (Jacq. ex Fr.) P. Kumm. *Agroproductividad*, 9: 67–72.

Hoa HT, Wang CL and Wang CH. 2015. The effects of different substrates on the growth, yield, and nutritional composition of two oyster mushrooms (*Pleurotus ostreatus* and *Pleurotus cystidiosus*). *Mycobiology* **43**(4): 423–434.

Isroi I, Millati R, Niklasson C, Cayanto C, Taherzadeh MJ and Lundquist K. 2011. Biological treatment of lignocelluloses with white-rot fungi and its applications. *BioResources* **6**(4): 5224–5259.

Koehler LH. 1952. Differentiation of carbohydrates by anthrone reaction rate and color intensity. *Anal Chem*, **24**(10): 1576–1591.

Koutrotsios G, Mountzouris KC, Chatzipavlidis I and Zervakis GI. 2014. Bioconversion of lignocellulosic residues by *Agrocybe cylindracea* and *Pleurotus ostreatus* mushroom fungi—Assessment of their effect on the final product and spent substrate properties. *Food Chem,* **161:** 127–135.

Liu CJ, Duan YL, Jin RZ, Han YY, Hao JH and Fan SX. 2018. Spent mushroom substrates as component of growing media for lettuce seedlings. *IOP Conf Ser Earth Environ Sci*, **185**: 012016.

Lopes RX, Zied DC, Martos ET, de Souza RJ, da Silva R and Dias ES. 2015. Application of spent *Agaricus subrufescens* compost in integrated production of seedlings and plants of tomato. *Int J Recycl Org Waste Agric*, **4**(3): 211–218.

Maldonado JF, Agüero MS, Iturmendi F, Buglione MB, Filippi MV and Martínez DA. 2018. Effect of compost of pear pomace on the forage production of *Setaria italica* (L.) P. Beauv. *Semiárida*, 28: 45–50

Maldonado JF, Agüero MS, Buglione MB, Iturmendi F, Filippi MV and Martínez DA. 2021. Pear and apple pomace compost as an alternative to commercial substrates in the production of tomato seedlings. *Rev Fac Cienc Agrar*, **53** (1): 128–138.

Martínez DA, Buglione MB, Filippi MV, Reynoso L, Rodríguez GE and Agüero MS. 2015. Mycelial growth evaluation of *Pleurotus ostreatus* and *Agrocybe aegerita* on pear pomaces. *An Biol* 37: 1–10

Merck KgaA. 2005. The Merck Microbiology Manual. 12th ed. Merck, Germany.

Moraes TS, Costa LMAS, Souza TP, Collela CF and Dias ES. 2020. Fungal and bacterial population from spent mushroom substrate used to cultivate tomato plants. *Ciênc Agrotec*, **44**: 1–8.

Pineda-Insuasti JA, Ramos-Sánchez LB, Soto-Arroyave CP, Freitas-Fragata A and Pereira-Cruz L. 2015. Growth of *Pleurotus ostreatus* on non-supplemented agro-industrial wastes. *Rev Téc Ing Univ Zulia*, **38**: 41–49.

Ribas LCC, De Mendonça MM, Camelini CM and Soares CHL. 2009. Use of spent mushroom substrates from *Agaricus subrufescens* (syn. *A. blazei*, *A. brasiliensis*) and *Lentinula edodes* productions in the enrichment of a soil-based potting media for lettuce (*Lactuca sativa*) cultivation: Growth promotion and soil bioremediation. *Bioresour Technol*, **100**(20): 4750–4757.

Rodríguez GE, Martínez DA, Buglione MB, Filippi MV and Agüero MS. 2018. Cultivation of *Pleurotus ostreatus* (Jacq.: Fr.) Kummer on pear pomace: Evaluation of productivity and chemical composition of the biodegraded substrate. *An Biol*, **40**: 21–30.

Rouches E, Zhou S, Steyer JP and Carrere H. 2016. White-Rot Fungi pretreatment of lignocellulosic biomass for anaerobic digestion: Impact of glucose supplementation. *Process Biochem*, **51**: 1784–1792.

Sadik MW, Zohair MM, El-Beih AA, Hamed ER and Sedik MZ. 2021. Utilization of Agro-industrial wastes as carbon source in solid-state fermentation processes for the production of value-added byproducts. *Jordan J Biol Sci*, **14**(1): 157–161.

Sánchez C. 2009. Lignocellulosic residues: Biodegradation and bioconversion by fungi. *Biotechnol Adv*, **27**: 185–194.

Sánchez C. 2010. Cultivation of *Pleurotus ostreatus* and other edible mushrooms. *Appl Microbiol Biot*, **85**: 1321–1337.

Sánchez A, Ysunza F, Beltrán-García MJ and Esqueda M. 2002. Biodegradation of viticulture wastes by *Pleurotus*: A source of microbial and human food and its potential use in animal feeding. *J Agric Food Chem*, **50**: 2537–2542.

Van Soest PJ, Robertson JB and Lewis BA. 1991. Methods for dietary fiber, neutral detergent fiber and nonstarch polysaccharides in relation to animal nutrition. *J Dairy Sci*, **74**: 3583–3597.

Yang L, Yuan H, Yang Y, Wang R, Wang C, Wei X, Chen S, Yu J and Ma X. 2020. Enhanced lignin degradation in tobacco stalk composting with inoculation of white-rot fungi *Trametes hirsuta* and *Pleurotus ostreatus*. *Waste Biomass Valorization*, 11: 3525–3535.

Zhang R, Li X and Fadel JG. 2002. Oyster mushroom cultivation with rice and wheat straw. *Bioresour Technol*, **82**(3): 277–284.

Jordan Journal of Biological Sciences

DNA Paternity Testing with Two Mismatches: Our Experience

Belma Jusic*, Amela Pilav, Mirela Dzehverovic, Jasmina Cakar

University of Sarajevo-Institute for Genetic Engineering and Biotechnology, Zmaja od Bosne 8, Sarajevo, Bosnia and Herzegovina Received: June 4, 2021; Revised: December 2, 2021; Accepted: January 4, 2022

Abstract

In paternity testing, the adopted rule is to exclude paternity when mismatch at more than two STR loci is observed. Here we present two routine DNA paternity testing cases with two autosomal STR mismatches between the alleged father and female child, where we employed X-STR analysis to confirm or exclude paternity. Mismatches at D16S539 and D18S51 loci in the Case 1 and D8S1179 and FGA loci in the Case 2 were detected using PowerPlex® Fusion System. X-STR analysis using Investigator® Argus X-12 kit yielded one inconsistency at DXS10135 locus between the child and the alleged father in the Case 1, whereas we found a complete match at all 12 analysed X-STR loci in the Case 2. As a result, paternity was confirmed in both cases. Conclusively, this case study indicates that including an additional analysis has a great importance in solving paternity cases with inconclusive results of autosomal STR analysis.

Keywords: kinship testing, STR markers, PowerPlex® Fusion System, Investigator® Argus X-12, mutations

1. Introduction

Nowadays, STR (Short Tandem Repeat) markers represent a powerful tool in the field of forensic-genetic analyses, kinship and parentage testing as well as population-genetic studies (Li et al., 2015; Lee et al., 2017). Consisted of short repetitive units from two to six base pairs in length, STR markers are adequate for forensic analyses of biological samples (Canturk et al., 2014). Their high variability among individuals contributes to highly effectiveness for human identification (Butler, 2011). Unlike unique DNA sequences that exhibit low mutation rate around 10-9 nucleotides per generation, STR sequences have higher mutation rate from 10⁻⁶ to 10⁻² nucleotides per generation (Fan and Chu, 2007). Besides high heterozygosity, discriminating power, clearly defined repetitive units and precisely determined allelic variants, simple amplification and detection of STR markers make them ideal for forensic analyses (Khalil et al., 2008; Primorac et al., 2014; Gomes et al., 2020). STR markers located on the autosomal, X and Y chromosomes are highly informative, practical and reliable for all kinds of forensic-genetic analyses including parentage testing, what was strongly supported by many population-genetic studies focused on investigating allele frequencies and forensic parameters (such as heterozygosity, power of discrimination, power of exclusion, polymorphic information content, matching probability and typical paternity index) of autosomal STR (Al-Eitan and Tubaishat, 2016; Al-Eitan et al., 2019; Al-Eitan et al., 2020; Pilav et al., 2020; Takic Miladinov et al., 2020) and X-STR loci (Grskovic et al., 2013; Crnjac et al., 2017; Veselinovic et al., 2018) in different populations. Generally, parentage testing follows Mendelian inheritance law, according to which child receives one allele from the mother and the other allele from the father (Schanfield *et al.*, 2014).

In some cases, spontaneous mutations as non-Mendelian inheritance patterns of alleles lead to allelic mismatch, making paternity or maternity testing case complicated. Fan and Chu (2007) described several different mechanisms of STR mutations, highlighting the strand-slippage replication as a main pattern of STR mutation. Most of reported STR mutations observed in routine parentage testing cases are single-step mutations (Lu et al., 2012; Wojtas et al., 2013), while multi-step mutations occur rarely in a small number of mutation events (Wojtas et al., 2013; Jia et al., 2015; Liu et al., 2015). According to "two exclusion" rule, paternity cannot be excluded when a mismatch at two STR loci between the alleged father and child is observed (Deepak et al., 2019).

In a study of paternity testing reported by Aktheruzzaman et al. (2012), two incompatibilities at D2S1338 and vWA loci were observed. Paternity testing was repeated using PowerPlex®16 System and GenePhile G-Plex. Mismatch at vWA locus was observed with PowerPlex®16 System, while two mismatches between the alleged father and child were encountered at D3S1744 and D18S536 loci with GenePhile G-Plex kit. Since the child was a female, paternity was excluded with a set of 13 X-STR markers. In another study of paternity testing by Jha et al. (2013), two exclusions between the alleged father and male child were observed at loci D21S11 and D18S51 out of 15 autosomal loci. Then, paternity was excluded after Y-STR analysis using AmpFLSTR™ Yfiler which result showed a match at only three out of 16 loci. As can be seen from the above cited reports, disputed parentage cases not easily solved by routine autosomal STR analysis should be confirmed or excluded by employing an additional analysis (Akhteruzzaman et al., 2012). Analysis of the X-linked STR markers can be performed in disputed

^{*} Corresponding author. e-mail: belma.jusic@hotmail.com.

paternity cases involving female child (García et al., 2017) or disputed maternity (Chen et al., 2009), while the Y-linked STR analysis is appropriate in paternity testing cases with male child (Kayser, 2017). This paper reports two paternity testing cases involving female child, mother and the alleged father, where analysis of autosomal STR markers resulted in single-step mutation in two STR loci, thus X-STR analysis was performed in order to confirm or exclude paternity.

2. Materials and Methods

2.1. Materials

Written informed consents were obtained from each individual in two cases of disputed paternity. In the Case 1, buccal swab samples were taken from female child aged 5 years, mother aged 46 years and the alleged father aged 70 years. Information about the age of the child, mother and the alleged father from the Case 2 was not obtained before taking buccal swab samples. Samples were collected using sterile cotton swabs (CITOSWAB, Shanghai, China) and proceeded to DNA extraction or stored at +4°C until the extraction. Publishing of the results of paternity testing cases was approved by the Ethics Committee of the Institute for Genetic Engineering and Biotechnology, University of Sarajevo (No. 289/20).

2.2. DNA extraction

Genomic DNA was extracted using QiagenDneasyTM Tissue Kit (Qiagen, 2012) and amplified using the PowerPlex® Fusion System (PROMEGA, Wisconsin, USA) which includes 24 loci (Amelogenin, D3S1358, D1S1656, D2S441, D10S1248, D13S317, Penta E, D16S539, D18S51, D2S1338, CSF1PO, Penta D, TH01, vWA, D21S11, D7S820, D5S818, TPOX, DYS391, D8S1179, D12S391, D19S433, FGA and D22S1045). Also, Investigator® Argus X-12 kit (QIAGEN, GmbH, Hilden, Germany) which includes 13 loci (Amelogenin, DXS8378, DXS10103, DXS7132, DXS10134, DXS10074. DXS10101. DXS10135. DXS7423. DXS10146, DXS10079, HPRTB and DXS10148) was included in analysis. PCR amplification was carried out in GeneAmpTM **PCR** System 9700 (APPLIED BIOSYSTEMS, USA), following the manufacturer's recommendations. Fragment analysis of PCR products was carried out using an ABI PRISM® 310 Genetic Analyzer (Applied Biosystems, CA, USA). Data were collected

using 310 Data Collection Software. STRs analysis was performed applying GeneMapperTM v. 3.2 software (Applied Biosystems, USA).

2.3. Statistical analysis

Paternity Index (PI) was calculated for each STR locus, as a likelihood ratio generated by comparing probability that the alleged father contributed the obligate allele with probability that randomly chosen man contributed the allele. Combined Paternity Index (CPI) was calculated by multiplying PI values for each locus. Probability of Paternity (PP) was calculated using PP=CPI/CPI+1 formula, which represents the probability that the alleged father is a biological father of the child (Schanfield et al., 2014). Observing two inconsistencies between child and the alleged father, possibilities of mutations were taken into account. Mutation Index (MI) values were calculated according to formula MI= μ /2p (Brenner, 1998), where μ is the mutation rate for STR locus obtained from Short Tandem Repeat Internet DataBase DNA (https://strbase.nist.gov/mutation.htm) and p is a frequency of mutated allele in the population. For statistical analysis of results obtained by X-STR analysis was used FamLinkX v. 2.8 software, including calculation of Likelihood Ratio (LR), Total LR and Probability of Paternity (PP).

3. Results

3.1. Results of autosomal STR analysis

In the Case 1, out of 22 loci tested, a complete match at all autosomal STR loci in the child with the mother was observed. On the other hand, we found two incompatibilities between the alleged father and the child. Allelic variants detected at autosomal STR loci of the child, mother and the alleged father are displayed in Table 1.

Figure 1 shows genotypes of the child, mother and the alleged father, detected at D16S539 and D18S51 loci. At the D16S539, genotype of the child, mother and the alleged father was found to be 10/13, 10/12 and 14/14, respectively. At the D18S51 observed alleles were 18/20 for the child, 15/18 for the mother and 13/21 for the alleged father. With possibilities of mutation events incorporated into the calculation, CPI and PP values were 647157598 and 99,9999998 %, respectively.

Table 1. Autosomal STR profiles of the child, mother and the alleged father in the Case 1 (mutated alleles underlined)

Locus	Child	Mother	Alleged father	PI
D3S1358	15/17	14/17	15/16	1,78571
D1S1656	15/17	11/15	12/17	8,34585
D2S441	14/15	11/14	15/15	21,70139
D10S1248	13/16	12/16	13/17	2,17004
D13S317	9/12	12/12	8/9	6,66667
PENTA E	10/13	13/14	10/18	3,03030
D16S539	10/13	10/12	<u>14</u> /14	$0,00278^a$
D18S51	18/20	15/18	13/ <u>21</u>	$0,05500^{b}$
D2S1338	17/19	17/21	17/19	3,85713
CSF1PO	12/12	10/12	10/12	1,44928
PENTA D	13/13	9/13	10/13	3,33333
TH01	8/8	8/9.3	6/8	4,34783
VWA	15/18	18/18	15/19	4,16667
D21S11	28/30	28/30	30/30	2,66667
D7S820	8/8	8/11	8/12	3,22581
D5S818	11/11	11/12	11/11	2,66667
TPOX	8/11	8/8	11/11	3,84615
DYS391	-	-	10/10	-
D8S1179	12/15	12/13	13/15	6,25000
D12S391	22/23	22/23	22/23	2,41115
D19S433	14/14.2	13/14	13/14.2	19,72387
FGA	24/25	23.2/24	25/25	11,11111
D22S1045	15/16	15/15	16/16	3,03499
AMELOGENİN	XX	XX	XY	-
CPI				647157598
PP (%)				99,9999998

PI=Paternity Index; CPI=Combined Paternity Index;

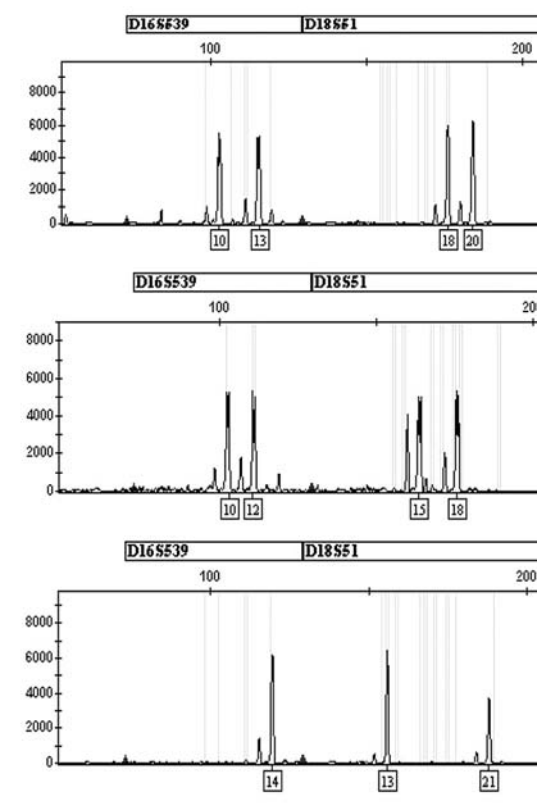


Figure 1. Electrophoretogram for the genotypes of the child (upper panel), mother (middle panel) and the alleged father (lower panel) at D16S539 and D18S51 loci in the Case 1

The results of autosomal STR analysis in the Case 2 are listed in Table 2. STR profile of the alleged father matched with the STR profile of the child in 20 out of 22 loci. All alleles of the child at all STR loci monitored were detected in the mother.

At locus D8S1179 alleles 13/16 for the child, 10/13 for the mother and 12/15 for the alleged father were scored (Figure 2). At locus FGA, genotype of the child, mother and the alleged father was found to be 21/21, 21/25 and 20/22, as depicts Figure 3. Absence of obligate paternal allele 16 at D8S1179 and allele 21 at FGA locus indicated to the possibility of mutation. Calculated CPI and PP values including mutation indices at these two loci were 286760481978 and 99,99999999 %.

PP=Probability of Paternity

 $^{^{\}mathrm{a}}\mathrm{MI}$ (Mutation Index) calculated including possibility of mutation at D16S539 locus

^b MI (Mutation Index) calculated including possibility of mutation at D18S51 locus

In above both cases, paternity could not be excluded or confirmed, since it is a practice to exclude paternity with three mismatches observed. Thus, we had taken support of X-linked STR markers in order to get more accurate and conclusive results.

Table 2. Autosomal STR profile of the child, mother and the alleged father in the Case 2 (mutated alleles underlined)

Locus	Child	Mother	Alleged father	PI
D3S1358	17/18	18/18	15/17	2,63158
D1S1656	12/15	12/15	12/15	3,44448
D2S441	11/11.3	11.3/14	10/11	1,65651
D10S1248	14/15	13/15	13/14	1,64393
D13S317	10/11	8/10	11/11	2,77778
Penta E	11/13	9/11	11/13	3,22581
D16S539	11/14	11/13	12/14	25,00000
D18S51	14/18	17/18	14/16	2,32558
D2S1338	19/19	16/19	17/19	3,85713
CSF1PO	9/10	10/13	9/12	10,00000
Penta D	9/16	11/16	9/12	2,04082
TH01	6/9	6/6	9/9	5,12821
vWA	17/18	18/18	17/17	3,63636
D21S11	28/32.2	28/28	30.2/32.2	5,88235
D7S820	10/11	10/11	11/12	1,05263
D5S818	11/13	11/11	10/13	2,85714
TPOX	8/11	8/11	8/8	1,20482
DYS391	-	-	10	-
D8S1179	13/16	10/13	12/ <u>15</u>	$0,0029^{c}$
D12S391	21/22	18/22	21/23	4,25496
D19S433	12/13	12/14	13/15	2,14850
FGA	21/21	21/25	<u>20/22</u>	$0,0083^{d}$
D22S1045	11/18	11/18	11/17	3,23897
Amelogenin	XX	XX	XY	-
CPI			286	6760481978
PP (%)			9	9,99999999

PI=Paternity Index; CPI=Combined Paternity Index;

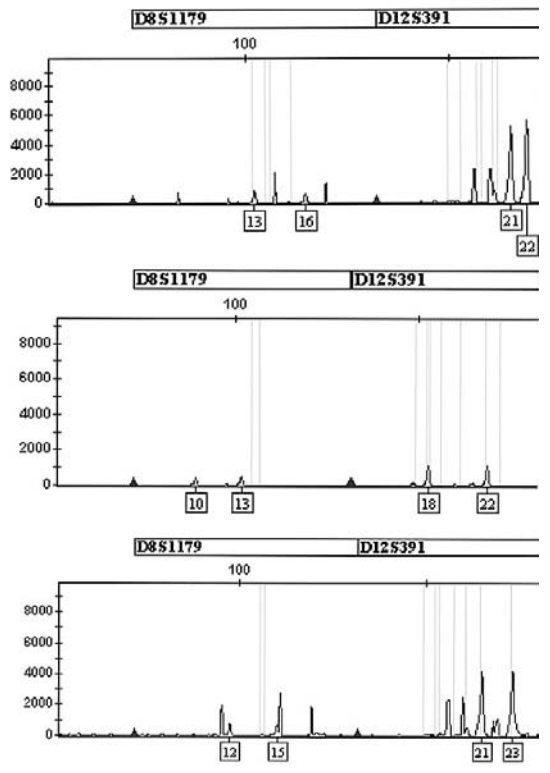


Figure 2. Electrophoretogram for the genotypes of the child (upper panel), mother (middle panel) and the alleged father (lower panel) at D8S1179 locus in the Case 2

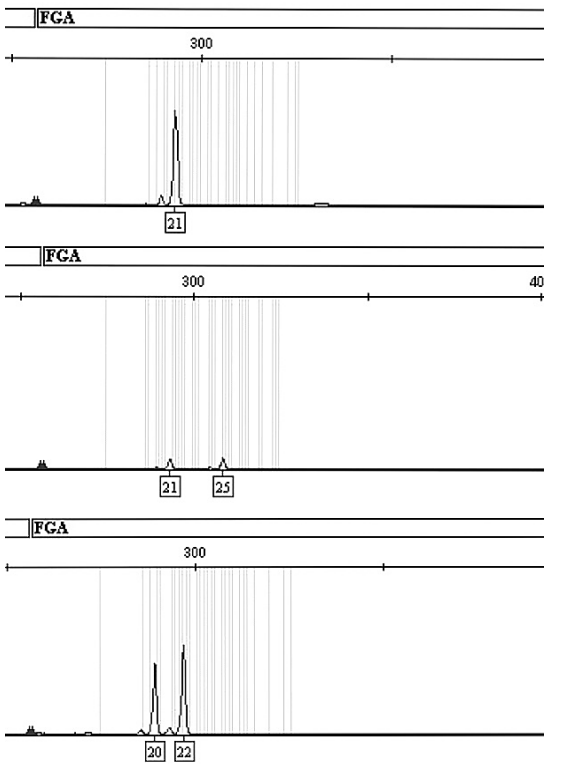


Figure 3. Electrophoretogram for the genotypes of the child (upper panel), mother (middle panel) and the alleged father (lower panel) at FGA locus in the Case 2

PP=Probability of Paternity

^eMI (Mutation Index) calculated including possibility of mutation at D8S1179 locus

^dMI (Mutation Index) calculated including possibility of mutation at FGA locus

3.2 Results of X-linked STR analysis

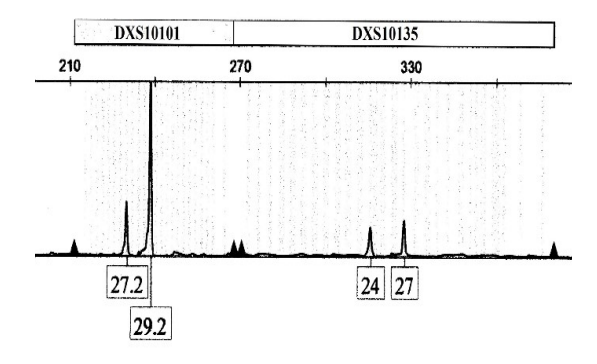
Table 3 displays observed allelic variants at 12 analysed X-STR loci in the Case 1. There was observed match at all analysed loci between the child and the mother, and match between the child and the alleged father at all analysed loci except DXS10135. Observed alleles for the child and the mother at DXS10135 locus were 24/27 and 20/24, while the alleged father was found to be homozygous for allele 28, as depicted in Figure 4. Total LR (Likelihood Ratio) and PP values calculated including mismatched paternal allele, were 20025200 and 99,99999501%, respectively.

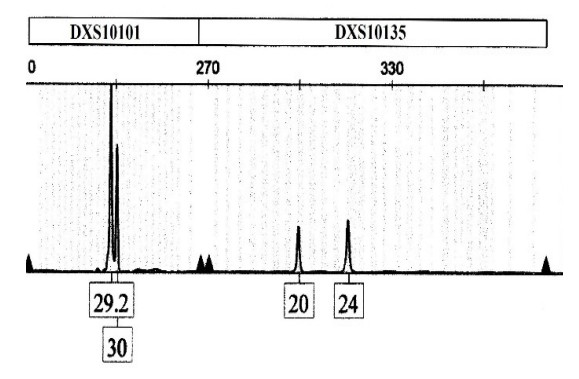
On the other hand, in the Case 2, all alleles of the child at all X-linked STR loci monitored were detected in both the mother and the alleged father. Total LR value was 1331298773, while the PP was 99,99999999 %. The results are summarized in **Table 4**.

Table 3. X-linked STR profile of the child, mother and the alleged father in the Case 1 (mutated allele underlined)

Locus	Child	Mother	Alleged father	LR
DXS10103	18/19	18/19	19	1,67501
DXS8378	11/12	10/11	12	5,61609
DXS7132	15/15	14/15	15	4,68189
DXS10134	35/36	35/36	35	2,24069
DXS10074	8/14	8/14	8	4,58464
DXS10101	27.2/29.2	29.2/30	27.2	8,70467
DXS10135	24/27	20/24	<u>28</u>	0,0215162e
DXS7423	14/15	14/14	15	6,51461
DXS10146	40.2/46.2	28/40.2	46.2	207,068
DXS10079	17/20	18/20	17	9,21573
<i>HPRTB</i>	12/12	12/12	12	2,57443
DXS10148	18/24.1	18/28.1	24.1	7,38388
Amelogenin	XX	XX	XY	-
Total LR				20025200
PP (%)				99,99999501

LR=Likelihood Ratio; PP=Probability of Paternity





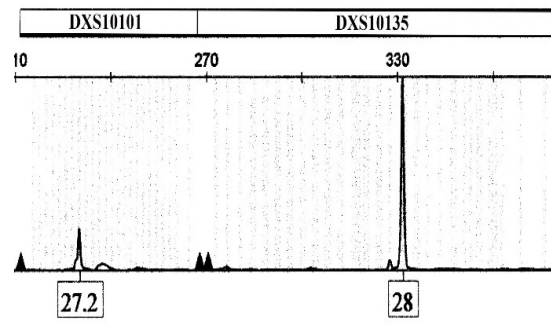


Figure 4. Electrophoretogram for the genotypes for the child (upper panel), mother (middle panel) and the alleged father (lower panel) at DXS10135 locus in the Case 1

^eMI (Mutation Index) calculated including possibility of mutation at DXS10135 locus

Table 4. X-linked STR profile of the child, mother and the alleged father in the Case 2

Locus	Child	Mother	Alleged father	LR
DXS10103	16/18	16/19	18	5,798
DXS8378	12/12	10/12	12	1,952
DXS7132	13/13	13/14	13	3,696
DXS10134	35/36	35/36	36	2,214
DXS10074	16/18	16/19	18	5,671
DXS10101	32/33	28/32	33	19,33
DXS10135	18/28	22/28	18	15,36
DXS7423	14/14	14/16	14	3,629
DXS10146	27/28	28/28	27	7,521
DXS10079	17/19	17/20	19	4,336
<i>HPRTB</i>	11/14	11/13	14	9,238
DXS10148	18/25.1	24/25.1	18	7,809
Amelogenin	XX	XX	XY	-
Total LR				1331298773
PP (%)				99,99999992

LR=Likelihood Ratio; PP=Probability of Paternity

4. Discussion

In this case study, two cases of routine DNA trio paternity testing with two inconsistencies between the child and the alleged father at autosomal STR loci were presented. The initial analysis was carried out using the PowerPlex® Fusion System (PROMEGA, Wisconsin, USA), which is routinely used in our laboratory. Typing of 22 autosomal STR loci revealed mismatches at D16S539 and D18S51 loci in the Case 1, and at D8S1179 and FGA loci in the Case 2. Within standard paternity testing procedure, paternity is excluded when more than two mismatches have been observed at all analysed loci, whereas the possibility of mutations must be included into account for calculation of CPI (Combined Paternity Index) and PP (Probability of Paternity) when one or two mismatches have been observed (Akhteruzzaman et al., 2012).

Generally, mutations occur at D16S539, D18S51, D8S1179 and FGA loci more frequently than at the other autosomal STR loci, according to referent Short Tandem Repeat DNA Internet DataBase (https://strbase.nist.gov/mutation.htm) and study mutation rates of autosomal STR loci in Bosnian and Herzegovinian population (Zametica et al., 2018). There are a few factors influencing STR mutations such as repeat number, length and base composition of STR repeat unit and interruptions in STR as well as sex and age of individual. Throughout replication of a repetitive region, incorrect reassociation of DNA strands leads to insertion or deletion of repeat units, which affects allele length. Besides unequal crossing over in meiosis and retrotransposition mechanism (Fan and Chu, 2007), a major STR mutational factor might be strand-slippage during replication, which causes increase or decrease in a repeat number (Qian et al., 2015), generating new allelic variants during cell division.

Therefore, we assumed that inconsistency in the Case 1 at D16S539 locus might be caused by a loss of one repeat from paternal allele 14, what was transmitted to the child as 13. In the same case, allele mismatch, observed at D18S51 locus, can be attributed to a single-step mutation where there was a loss of one repeat from 21 allele, what was transmitted to the child as allele 20. In the Case 2, obligate paternal allele 16 at D8S1179 locus was characterized as resulting from the mutation of allele 15 into allele 16 (a gain of one repetitive unit). Regarding the inconsistency between child and the alleged father at FGA locus, two hypothetical situations can be considered: 1. Child's allele 21 exists by loss of one repeat from allele 22 of the father. 2. Allele 21 was inherited from allele 20 of the father by gain of one repetitive unit.

Mutations detected in both cases were from paternal source, what was supported by the statement that the mutations occur more often in sperm cells compared to the female egg cells (Qian *et al.*, 2015). Other studies have also found that paternal mutations occur more frequently than maternal not only at autosomal STR loci (Huang *et al.*, 2021) but X-linked STR loci as well (Pinto *et al.*, 2020).

Length of repeat unit and rate of slippage are inversely related, which means that the rate of slippage is expected to be higher in dinucleotide than in trinucleotide or tetranucleotide STR units (Chakraborty *et al.*, 1997). On the other hand, D16S539, D18S51, D8S1179 and FGA loci affected with mutations have tetranucleotide units, as well as almost all of autosomal STR loci analysed in these two paternity testing cases.

Since autosomal STR analyses revealed the number of discrepant loci between the alleged father and female child less than three and left these paternity testing cases unsolved, additional X-linked STR analyses using Investigator®Argus X-12 kit (QIAGEN, GmbH, Hilden, Germany) were included for confirmation or exclusion of paternity. Studies proved usability and efficiency of this kit in kinship testing cases (Hering et al., 2015) and population-genetic researches (Crnjac et al., 2017). Analysis of 12 X-STR loci yielded only one mismatch between child and the alleged father, caused by a singlestep mutation at DXS10135 locus in the Case 1, and complete matching at all analysed X-STR loci in the Case 2. In both cases, result of X-STR analysis and PP value clearly indicate that the alleged father is a biological father of the child.

Studies conducted by Jia et al. (2015) and Qian et al. (2015) revealed that paternal age could contribute to the occurrence of mutations. In light of the fact that sperm cells of older men undergo more divisions than the cells of younger men (Fan and Chu, 2007; Qian et al., 2015), it is more likely that mutations will affect older cells. Since the father from the Case 1 was 65 years old at the birth of child, we assume that his age could be the cause of mutations occured in both autosomal and X-linked STRs. Considering all aforementioned, knowledge about mutation rates and possible mutational processes of different STR loci is important for accurate genetic profiles interpretation (Qian et al., 2015; Hamester et al., 2019). As previously mentioned in the Introduction section, a number of population-genetic studies, focused on evaluating of forensic efficiency parameters of STR markers (Grskovic et al., 2013; Al-Eitan and Tubaishat,

2016; Crnjac et al., 2017; Veselinovic et al., 2018; Al-Eitan et al., 2019; Al-Eitan et al., 2020; Pilav et al., 2020; Takic Miladinov et al., 2020) indicated a high degree of reliability of these markers important for all kinds of forensic-genetic analyses, including kinship and parentage testing. Finally, results from these two cases clearly demonstrate that X-STR markers have the potential to solve parentage cases not easily solved by standard analysis based on autosomal STR markers.

5. Conclusions

This case study emphasizes the importance and usefulness of supplementary analyses in parentage testing cases with inconclusive results obtained by routine autosomal STR analysis. Moreover, we consider that STRs located on the X chromosome might be superior to conventional autosomal STR markers in parentage testing cases involving at least one female individual, regarding the inheritance pattern of these markers. In the future, investigations focused on the advantages of supplementing the autosomal STR loci with X-STR in other kinds of kinship testing involving at least one female individual should be conducted.

Acknowledgment

None.

Conflict of interest

The authors declare that there is no conflict of interest.

References

Akhteruzzaman S, Majumder AK, Ferdous A and Ali ME. 2012. False paternity with one or two mismatches using commercial STR kits. *Aust J Forensic Sci.*, **44**(3): 253–259.

Al- Eitan LN and Tubaishat RR. 2016. Evaluation of forensic genetic efficiency parameters of 22 autosomal STR markers (PowerPlex® Fusion system) in a population sample of Arab descent from Jordan. *Aust J Forensic Sci.*, **50**(1): 97-109.

Al- Eitan LN, Darwish NN, Hakooz NM and Dajani RB. 2019. Assessing the forensic efficiency of the GlobalFiler STR loci among the genetically isolated Chechen subpopulation in Jordan. *Gene*, **720**: 144078.

Al- Eitan LN, Darwish NN, Hakooz NM and Dajani RB. 2020. Investigation of the forensic GlobalFiler loci in the genetically isolated Circassian subpopulation in Jordan. *Gene*, **733**: 144269.

Brenner, CH. 1998. Mutations in Paternity. Retrieved 30 May 2021 from http://dna-view.com/mudisc.htm

Butler JM. 2011. Advanced Topics in Forensic DNA Typing: Methodology. Academic Press, Elsevier, USA.

Canturk KM, Emre R, Kınoglu K, Başpınar B, Sahin F and Ozen M. 2014. Current Status of the Use of Single-Nucleotide Polymorphisms in Forensic Practices. *Genet Test Mol Biomarkers*, **18**(7): 455–460.

Chakraborty R, Kimmel M, Stivers DN, Davison LJ and Deka R. 1997. Relative mutation rates at di-, tri- and tetranucleotide microsatellite loci. *Proc Natl Acad Sci USA*, **94**(3): 1041-1046.

Chen DP, Tseng CP, Tsai SH, Wang MC, Lu SC, Wu TL, Chang PY and Sun CF. 2009. Use of X-linked short tandem repeats loci to confirm mutations in parentage caseworks. *Clin Chim Acta*, **408**(1-2): 29-33.

Crnjac J, Ozretic P, Merkas S, Ratko M, Lozancic M, Korolija M, Popovic M and Mrsic G. 2017. Investigator Argus X-12 study on the population of northern Croatia. *Genet Mol Biol.*, **40**(1): 80-83.

Deepak YK, Vaishali BM, Bhausaheb PM and Krishna VK. 2019. Paternity Disputes—Importance of Y DNA Profiling in Mutation Cases. *J Forensic Sci.*, **12**(1): 555829.

Fan H and Chu JY. 2007. A brief review of short tandem repeat mutation. *Genomics Proteomics Bioinformatics*, **5**(1): 7-14.

García MG, Gusmão L, Catanesi CI, Penacino GA and Pinto N. 2017. Mutation rate of 12 X-STRs from investigator Argus X-12 kit in Argentine population. *Forensic Sci Int Genet Suppl Ser.*, **6**: 562–564.

Gomes I, Pinto N, Antão-Sousa S, Gomes V, Gusmão L and Amorim A. 2020. Twenty Years Later: A Comprehensive Review of the X Chromosome Use in Forensic Genetics. *Front Genet.*, **11**: 926

Grskovic B, Zidkova A, Stenzl V, Popovic M, Primorac D and Mrsic G. 2013. Analysis of 8 X-chromosomal markers in the population of Central Croatia. *Croat Med J.*, **54**(3): 238-247.

Hamester F, da Silva DS, Leboute A, Motta C and Alho CS. 2019. Slippage mutation rates in 15 autosomal short tandem repeat loci for forensic purposes in a Southeastern Brazilian population. *Electrophoresis*, **40**(21): 2873–2876.

Hering S, Edelmann J, Haas S and Grasern N. 2015. Paternity testing of two female siblings with Investigator Argus X-12 kit: A case with several rare mutation and recombination events, *Forensic Sci Int Genet Suppl Ser.*, **5**:341-343.

Huang Y, Liu C, Xiao C, Chen X, Han X, Yi S and Huang D. 2021. Mutation analysis of 28 autosomal short tandem repeats in the Chinese Han population. *Mol Biol Rep.*, **48**(6): 5363-5369.

Jha DK, Rijal JP, Tuladhar BS, Tuladhar BS and Pokharel BR. 2013. Mutations or exclusion: An uncommon parentage assessment case. *Scientific World*, **11**(11): 74-76.

Jia YS, Zhang L, Qi LY, Mei K, Zhou FL, Huang DX and Yi SH. 2015. Multistep microsatellite mutation leading to father-child mismatch of FGA locus in a case of non-exclusion parentage. *Leg Med.*, **17**(5): 364-365.

Kayser M. 2017. Forensic use of Y-chromosome DNA: a general overview. *Hum Genet.*, **136**: 624-635.

Khalil R, Yasin S, Hamad M, Sharieh A and Al-Jaber A. 2008. Virtual Reference Values for STR Genetic Loci Assignment in Forensic Arenas: A Jordanian-Based Study. *Jordan J Biol Sci.*, 1(2): 73-76.

Lee HJ, Lee JW, Jeong SJ and Park M. 2017. How many single nucleotide polymorphisms (SNPs) are needed to replace short tandem repeats (STRs) in forensic applications?. *Int J Legal Med.*, **131**(5):1203-1210.

Li L, Lin Y, Liu Y, Zhu R, Zhao Z and Que T. 2015. A case of false mother included with 46 autosomal STR markers. *Investig Genet.*, **6**:9.

Liu YX, Zhang WQ, Jia YS, Zhang L, Zhou FL, Mei K and Yi SH. 2015. Multistep microsatellite mutation in a case of non-exclusion parentage. *Forensic Sci Int Genet.*, **16**: 205-207.

Lu D, Liu Q, Wu W and Zhao H. 2012. Mutation analysis of 24 short tandem repeats in Chinese Han population. *Int J Legal Med.*, **126**(2): 331–335.

Pilav A, Pojskic N, Kalajdzic A, Ahatovic A, Dzehverovic M and Cakar J. 2020. Analysis of forensic genetic parameters of 22 autosomal STR markers (PowerPlex® Fusion System) in a population sample from Bosnia and Herzegovina. *Ann Hum Biol.*, 47(3): 273-283.

Pinto N, Pereira V, Tomas C, Loiola S, Carvalho FE, Modesti N, Maxzud M, Marcucci V, Cano H, Cicarelli R, Januario B, Bento A, Brito P, Burgos G, Paz-Cruz E, Díez-Juárez L, Vannelli S, Pontes M de L, Berardi G, Furfuro S, Fernandez A, Sumita D, Bobillo C, García MG and Gusmão L. 2020. Paternal and maternal mutations in X-STRs: A GHEP-ISFG collaborative study. Forensic Sci Int Genet., 46: 102258.

Primorac D, Schanfield M and Marjanovic D. 2014. Basic Genetics and Human Genetic Variation. In: Primorac D and Schanfield MS (Eds.), Forensic DNA applications: An interdisciplinary perspective. CRC Press, Boca Raton, FL, USA, pp. 3-53.

Qiagen. 2012. QIAmp DNA MiniKit Handbook. Qiagen, Hilden, Germany

Qian XQ, Yin C, Ji Q, Li K, Fan HT, Yu YF, Bu FL, Hu LL, Wang JW, Mu HF, Haigh S and Chen F. 2015. Mutation Rate Analysis at 19 Autosomal Microsatellites. *Electrophoresis*, **36**(14):1633-1639.

Schanfield MS, Primorac D and Marjanovic D. 2014. Forensic DNA Analysis and Statistics. In: Primorac D and Schanfield MS (Eds.), Forensic DNA applications: An interdisciplinary perspective. CRC Press, Boca Raton, FL, USA, pp. 55-83.

Takic Miladinov D, Vasiljevic P, Sorgic D, Axelsson Podovsovnik E and Stefanovic A. 2020. Allele frequency and forensic parameters of 22 autosomal STR loci in a population of 938 individuals from Serbia and comparison with 24 other populations. *Ann Hum Biol.*, 47(7-8): 632-641.

Veselinovic I, Vapa D, Djan M, Velickovic N, Veljovic T and Petric G. 2018. Genetic analysis of 12 X-STR loci in the Serbian population from Vojvodina Province. *Int J Legal Med.*, **132**(2): 405-408

Wojtas M, Piniewska D, Polańska N, Stawowiak A and Sanak M. 2013. Mutations of microsatellite autosomal loci in paternity investigations of the Southern Poland population. *Forensic Sci Int Genet.*, 7(3): 389–391.

Zametica B, Macar S, Kalajdzic A and Pilav A. 2018. Mutation Analysis of Autosomal STR loci Commonly Used in Paternity Testing in Bosnia and Herzegovina. *Genetics and Applications*, **2**(1):14.

Jordan Journal of Biological Sciences

Imaging Aspects (Chest Radiographic and CT Scan Findings) of COVID-19 with Clinical Classifications

Ammar A. Oglat ^{1,*}, Mohammad A. Oqlat ^{2,}, Ahmad A. Oqlat ³, Lo'ai Alanagreh ⁴, Pegah Moradi Khaniabadi⁵, Mohammed Ali Dheyab ^{5,6}, Hawraa Khaleel ⁵, Omar Althalji ⁷

¹Department of Medical Imaging, Faculty of Applied Medical Sciences, The Hashemite University, Zarqa, 13133, Jordan; ²Department of Biological Sciences, School of Science Engineering and environment, University of Salford Manchester, Salford, UK; ³Department of Emergency, Faculty of Medicine, JUST, Irbid, Jordan; ⁴Department of Laboratory Medical Sciences, Faculty of Applied Medical Sciences, The Hashemite University, Zarqa, 13133, Jordan; ⁵School of Physics, Universiti Sains Malaysia, 11800, Pulau Pinang, Malaysia; ⁶Nano-Biotechnology Research and Innovation (NanoBRI), Institute for Research in Molecular Medicine (INFORMM), Universiti Sains Malaysia, 11800, Pulau Pinang, Malaysia; ⁷Department of Medical Imaging, Higher Colleges of Technology, UAE, Emirates.

Received: June 12, 2021; Revised: July 15, 2021; Accepted: September 28, 2021

Abstract

Chest radiographic (CXR) and chest computed tomography (CT) scans have been used to diagnose coronavirus (COVID-19) disease as an important counterpart to the reverse transcription polymerase chain reaction (RT-PCR) diagnostic protocol. This work explores the application of CXR and CT scans as diagnostic instruments for COVID-19. Numerous databases were searched from 01/01/2020 till 2020 late for COVID-19 articles which documented the clinical features of CXR and CT scans. The documented cases were based on the evaluation of the imaging characteristics. Chest radiographic findings may be confirmed with the most basic CT scans. Peripheral, bilateral and primary ground-glass distortion are the most prominent CT results with COVID-19 infections. In conclusion, unique and ambiguous terms such as pneumonia, blurred opacities, airspace disease, patchy opacities, and infiltrates make it difficult to perceive the different chest radiographic findings.

Keywords: Coronavirus, World respiratory syndrome coronavirus, RT-PCR, Chest X ray, Chest CT.

1. Introduction

In January 2020, the world was shocked by the novel COVID-19 outbreak in Wuhan city (Hubei province, China). Molecular analyses discovered that the COVID-19 virus is closely related to the 2003 severe acute respiratory syndrome coronavirus (SARS-CoV-2) (Al Mutair and Ambani 2020, Kanne, Little et al. 2020, Ludvigsson 2020, Rodriguez-Morales, Cardona-Ospina et al. 2020). COVID-19 is a highly contagious disease that might sometimes lead to critical respiratory disorders requiring dedicated managing and supervision at hospital (Bastola, Sah et al. 2020, Chan, Yuan et al. 2020, Chen, Zhou et al. 2020, Huang, Wang et al. 2020, Lim, Jeon et al. 2020, The 2020, Wu, Liu et al. 2020, Xu, Shi et al. 2020, Zhu, Zhang et al. 2020). • Initially, COVID-19 patients typically have a fever, dry cough, dyspnea, fatigue, and anosmia. Some patients also report gastrointestinal (GI) symptoms(Sahu, Mehta et al. 2021). Moreover, it can cause neurological and enteric diseases, particularly in immunocompromised patients, such as Children, pregnant women, and older adults. Coronaviruses were initially recognized in the 1960s. Before in 2003, these viruses were known to cause flu-like mild symptoms (Bermingham, Chand et al. 2012, Zaki, Van Boheemen et al. 2012, de Groot, Baker et al.

2013, Mailles, Blanckaert et al. 2013, Raj, Farag et al. 2014, Al-Osail and Al-Wazzah 2017).

The COVID-19 pandemic is the third global epidemic caused by a Betacorovirus over the last 20 years. In 2003, the world was shocked by the severe acute respiratory syndrome in Asia (Drosten, Günther et al. 2003, Ksiazek, Erdman et al. 2003, Kuiken, Fouchier et al. 2003). Nine years later in Saudi Arabia, a new coronavirus emerged to the known Middle East Respiratory Syndrome coronavirus (MERS-CoV) (Haagmans, van den Brand et al. 2015, de Wit, van Doremalen et al. 2016, Baharoon and Memish 2019). There are many differences and similarities in the clinical feature, epidemiology, and strategies used in managing and controlling Influenza H1N1, SARS, MERS, and COVID-19 (Ratre, Vishvakarma et al. 2020) (Al-Tawfiq, Zumla et al. 2014, Baharoon and Memish 2019, Chen, Zhou et al. 2020, Huang, Wang et al. 2020, Organization 2020, Zhu, Zhang et al. 2020). Coronaviruses are a large group of viruses with a positive-strand RNA (+ssRNA) genome. Most of the studies revealed that these viruses originated in bats and transferred to humans through an intermediate animal host (Plowright, Parrish et al. 2017, Ruiz-Saenz, Bonilla-Aldana et al. 2019, Millán-Oñate, Rodriguez-Morales et al. 2020, Rodriguez-Morales, Bonilla-Aldana et al. 2020). Despite the similarities in the clinical features of SARS, MERS and COVID-19, there are notable differences ever since the initial accounts (Al-

^{*} Corresponding author. e-mail: ammar.oglat@yahoo.com.

Tawfiq, Zumla et al. 2014, Yin and Wunderink 2018). Therefore, comprehensive characterizations are required considering the clinical, laboratory as well as imaging features.

Pulmonary embolism is a pathologic condition, whether acute or chronic, causes both partial and complete intraluminal filling defects, which should have a sharp interface with intravascular contrast material. In acute pulmonary embolism that manifests as complete arterial occlusion, the affected artery may be enlarged. Partial filling defects due to acute pulmonary embolism are often centrally located, but when eccentrically located they form acute angles with the vessel wall. However, CT pulmonary angiography is becoming the standard of care at many institutions for the evaluation of patients with suspected pulmonary embolism. Patients with COVID-19 have an increased prevalence of pulmonary embolisms and most have moderate or severe lung involvement on CT studies (Chamorro, Ostolaza et al. 2021).

Typical COVID-19 pneumonia CT results exhibited consolidation and bilateral ground-glass opacities (GGOs) with a posterior and peripheral lung distribution. These findings consistently supported the early radiological studies (Chung, Bernheim et al. 2020, Pan, Ye et al. 2020, Song, Shi et al. 2020). Even though it is merely about three months after the outbreak of COVID-19, many articles have been published in the most reputable international medical and scientific journals, both from China and other international researchers. These published articles include case reports with travel- and non-travel-related circumstances (Ahmad, Khan et al. 2020, Arab-Mazar, Sah et al. 2020, Bastola, Sah et al. 2020, Bernard-Stoecklin, Rolland et al. 2020, Giovanetti, Benvenuto et al. 2020, Holshue, DeBolt et al. 2020, Nishiura, Kobayashi et al. 2020, Organization 2020, Pongpirul, Pongpirul et al. 2020, Reusken, Broberg et al. 2020, Rothe, Schunk et al. 2020). Many studies have begun to proffer solutions to the imaging results; however, there has been no single review to consolidate the knowledge learning from various studies or case reports to understand the authors. In this study, a literature review was conducted to offer the most recent synthesis of the radiographic portrait of the COVID-19 patients. This was achieved with the help of the CXR and CT chest results of several instances at different places. Clinical symptoms, findings, and CT/CXR follow-ups imaging are presented (Oglat 2020, Oglat, Alshipli et al. 2021).

2. Methods

2.1. Criteria of this Study

In the present study, peer-reviewed articles that reported cases with image features were considered. Article language was limited to English and the time span was open to several published during 2020. Furthermore, documents that did not contain the original data were omitted. The data used in the present study were obtained from the Web of Science, Scopus, and the Medline/PubMed. Novel coronavirus, Novel coronavirus 2019, 2019 nCoV, COVID-19, Wuhan coronavirus, Wuhan pneumonia, and SARS-CoV-2 were used as the search terms. The result was assessed by numerous different independent scholars.

2.2. Study Selection

Screenings by title and abstract on the outcomes of the preliminary search were firstly carried out. This was followed by retrieving of the relevant articles considered relevant in the present study. Documents that reported duplicate data were excluded and counted as a single case. Several published articles were incorporated for the study, and their findings were summarized. Data extraction procedures that include information on the publication type, the publication year, date, country, institution, and the amount of cases reported, were studied. Also, demographic information such as age and sex, as well as outcome such as death, complications such as acute respiratory distress syndrome, acute respiratory distress syndrome (ARDS), imaging such as chest X-ray, laboratory findings such as biochemistry, white blood cell counts (WBC), and clinical features such as cough, were studied. The articles list was checked two times to avoid duplication of records.

3. Results

Many patients having a lower pulmonary tract infection caused by COVID-19 were presented with cough, dyspnea, myalgia, and fever. Moreover, 17-29 % of them had ARDS (Chen, Zhou et al. 2020, Huang, Wang et al. 2020). More than 2.3 % fatality rate was estimated. In one retrospective study, the R0 was projected as the average figure of new cases of infection transfer from person to native population as 3.28, as opposed to estimated values of 1.4–2.5 by the World Health Organization (Liu, Gayle et al. 2020). Any value higher than 1.0 indicates the likelihood of the infection's spread instead of being diminished. Because of the improved intervention and awareness, R0 values from later studies were projected to be more dependable.

It was difficult to deduce the desired information from the diverse outcomes on chest radiographs due to the vague and special terms such as hazy opacities, patchy opacities, infiltrates, pneumonia, and airspace disease (Chang, Lin et al. 2020, Huang, Wang et al. 2020, Liu, Gayle et al. 2020). The most detailed reports on CT results can simplify chest radiographic findings. Consolidation, peripheral, basal ground-glass opacity and bilateral were among the predominant CT results of patients infected with COVID-19 (Bernheim, Mei et al. 2020, Pan, Ye et al. 2020). Opacities frequently show extensive geographical distributions. Numerous distinct areas of consolidation, GGO, or both take place in a subcategory of patients who repeatedly have a reversed halo or round morphology or a toll sign. Lymphadenopathy, extensive lung nodules, and pleural effusion, occur in a very small number of cases, suggesting another diagnosis or bacterial superinfection. CXR assessment involves the existence of interstitial involvement (mixed, nodular or reticular form), mediastinal lines, hilar expansion, pleural calcification, pleural effusion, etc.

CT scan estimation has four major categories: 1. GGO and consolidation which is classified as follows: lack of both consolidation and ground glass opacities, occurrence of pure ground glass, existence of ground glass opacities, existence of consolidation, existence of GGO with consolidation, and crazy paving (Huang, Wang et al. 2020); 2. Pleura that includes: existence of focal thicken,

pleural effusion, and existence of calcifications (Organization 2020); 3. Mediastinum which includes: existence of lymphadenopathy (defined as lymph node size of ≥10 mm in short-axis dimensions), existence of pericardial effusion; and ascending thoracic aorta diameter [49]; 4. Pulmonic vessels consisting of: perilesional vessels diameter and diameter of pulmonic artery trunk (Chan, Yuan et al. 2020).

3.1. Case 1.

Pt history: A 50-year-old male patient was admitted to a fever clinic. The patient indicated signs of shortness of breath, fatigue, cough, chills, and fever. The patient was also reported to have travelled to Wuhan city. Furthermore, he showed initial indications of dry cough and mild chills but kept working and only reported to the clinic after 14 days (Xu, Shi et al. 2020).

CXR/CT findings: The CXR exhibited many patchy shadows in both lungs (Figure 1). A throat swab sample was collected and on the 22nd of January, the patient was confirmed to have the COVID-19 infection by the Beijing Centre for Disease Control using the RT- PCR assay. Some differences between the right and left lungs and the swift advancement of pneumonia were observed, as evident from the CXR. Also, the liver tissues exhibited mild lobular movement and moderate micro vesicular steatosis; nevertheless, there was no convincing proof to establish that drug-induced liver damage or COVID infections are directly caused. Furthermore, no clear histological alterations were observed in heart tissues, signifying that COVID infection might not be the direct cause of the heart impairment. Even though corticosteroid is not formally endorsed as a treatment for COVID pneumonia, it has been suggested that appropriate and timely use of ventilator support, together with corticosteroids, should be used for the severe patient to avoid the development of ARDS.

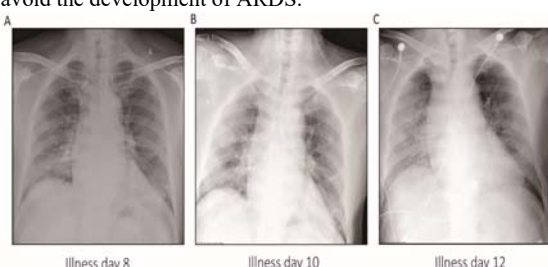


Figure 1. Chest radiographs on day 8, day 10 and day 12 since the onset of illness. (A) The brightness of both lungs was decreased, and multiply patchy shadows were observed. Heart shadow presents in the normal range roughly. The diaphragmatic surface was light and smooth; phrenic rib angle was sharp (illness day 8). (B) Diffuse ground-glass opacity was found in both lungs (illness day 10). (C) Chest radiograph showed progressive infiltrate, diffuse gridding shadow appeared in both lungs. Small area emphysemas were observed in the upper and lower lobes of the left lung (illness day 12) (Xu, Shi et al. 2020).

3.2. Case 2.

Pt history: A 54-year-old man from Korea and living in Wuhan, returned to Korea. The patient sensed the earliest symptom of muscle pain and chills and was isolated (by a negative pressurized room) at Myongji Hospital. After 2 days, the COVID-19 infection test was by RT-PCR and pan-coronavirus conventional PCR assay with a swab taken from the patient throat. The patient had

no major ailment and was without any record of drinking or smoking (Lim, Jeon et al. 2020).

CXR/CT findings: Upon admission, the patient did not show any respiratory symptoms and recorded blood pressure of 152/93 mmHg at 73 beats/minute. Moreover, his respiratory rate was 20 breaths per minute, and he recorded a body temperature of 37.0 °C. Clear lung sounds were observed upon physical examinations with clear CXR nor pharyngeal injection. On day 5 and 7 of the illness, the patient developed fever and dry cough respectively. Nevertheless, the patient had no severe respirational symptom such as chest pain, productive sputum, or shortness of breath. Upon high-resolution CT scan, GGOs in both lower lobes and minor consolidation in the right upper lobe were observed (Figure 2).

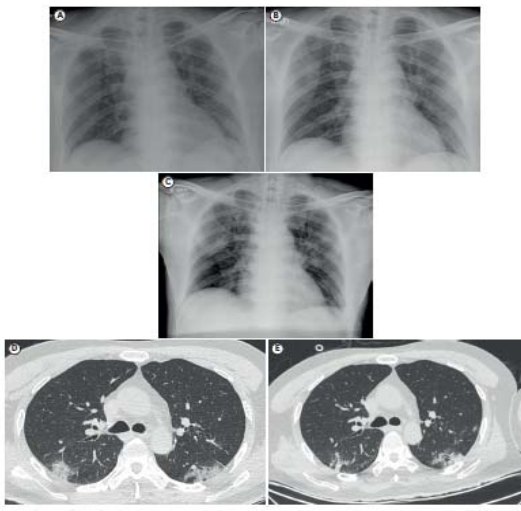


Figure 2. Radiologic findings of the patient. (A) Chest X-ray of illness day 3, hospital day 1. (B) Chest X-ray of illness day 9, hospital day 7. (C) Chest X-ray of illness day 15, hospital day 13. (D) HRCT scan of illness day 9, hospital day 7. (E) HRCT scan of illness day 15, hospital day 13. AP(P) = Anteroposterior (Portable X-ray), HRCT = high-resolution computed tomography (Lim, Jeon et al. 2020).

3.3. Case 3.

Pt history: All registered eighty patients, who were indicated to the Fifth People's Hospital of Wuxi, the Yancheng City was for the second People's Hospital, and the First People's Hospital of Yancheng City were sequentially analysed in retrospect. All the data were collected which include extent of hospitalization and stay at the intensive care unit, medical records, attending doctors, chest CT, laboratory parameters, prognosis from patients' demographic information, and clinical records. The patients were clinically grouped into four subcategories: mild, severe, moderate, and critically ill. At that time, 51% of the patients were female, and their median age was nearly 46.1 years. About thirty-three percent of the patients aged between 25 and 49 years, while about 24 % were between 50 and 64-years-old. Furthermore, about 11% of the patients were above 65 years while 13% below 18 years old, and 19% (15 patients) aged between 18 and 24-years-old (Figure 1). Three patients (3.75 %) were clinically classified as severe type, 49 patients were moderate, while 28 patients mild, and no one was classified as being critically ill (Wu, Liu et al. 2020).

CXR/CT findings: 55 of the 80 patients (68.75 %), indicated anomalous CT scans. These anomalies consisted of thirty-six (45.0 %) and nineteen (23.75 %) bilateral and unilateral pneumonia respectively. Away from both bilateral and unilateral GGOs (Figure 3A) and (Figure 3B) respectively, bilateral ground glass or sub-segmental consolidation regions, as well as bilateral lobular, subsegmental consolidation areas, were absent. About 31 % of the cases had normal density shadow in both lungs parenchyma (Figure 3C). Chest imagines are of great importance for diagnoses (Chung, Bernheim et al. 2020). At an early stage, numerous interstitial and mottling changes, particularly in the peripheral part were observed. Lungs consolidations can occur in severe cases; on the other hand, pleural effusions were uncommon. Compared to the cases reported from Wuhan, CT scans in which all the patients were odd with 98% of the patients having bilateral involvement; the abnormal rate of the present study was relatively lower. Total of 55 patients (68.75 %) displayed abnormalities in their chest CT images. 19 out of these abnormal CT images were unilateral pneumonia (23.75 %), while 36 were bilateral pneumonia (45.00 %). The first CT scans of the 25 patients were normal with 23 of them being diagnosed for over four days. It is therefore suggested that during the screening of patient for clinical manifestations, there is a need to combine the laboratory examination with chest imaging with for all-inclusive investigation.

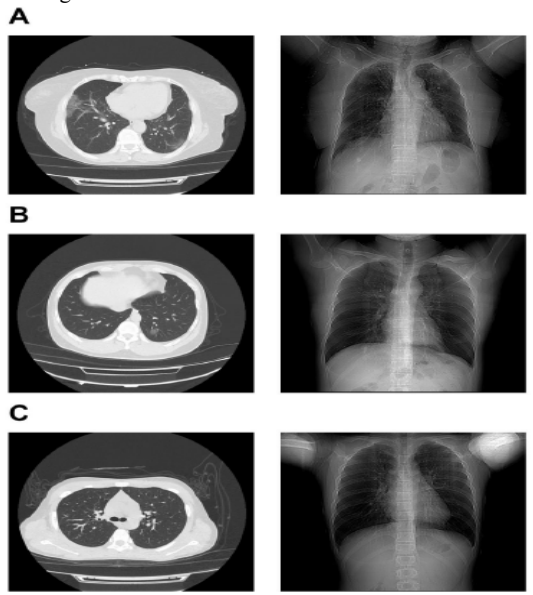


Figure 3. (A) a 71-year-old woman showing that there are scattered high-density shadows with fuzzy patches in the lower lobes of the two lungs, with ground glass, with clear hilar structure, unobstructed trachea, no displacement of mediastinum, no enlarged lymph node shadow (B) a 38-year-old man showing that there is small patchy ground glass like density increasing shadow in the upper and lower lobes of the left lung, with clear hilar structure (C) a 12-year-old boy showing that there was no abnormal density shadow in the parenchyma of both lungs, the structure of pulmonary hilus (Wu, Liu et al. 2020).

3.4. Case 4.

Patient history: A retrospective study of 25 dead persons with the COVID-19 pandemic was done in Renmin Hospital (Wuhan University). All 25 dead patients (fifteen females and ten males) were tested positive for COVId-19 using RT-PCR on their respiratory tract sample. In conclusion, the age of the patients ranged from 55 to 100-years-old. 100% of the dead persons had diseases, including hypertension (16/25, 64 %), which was the most common. Others include kidney diseases (20 %), cerebral infarction (16 %), Chronic Obstructive Pulmonary Disease (8 %), cancers (8 %), acute pancreatitis (4 %), heart diseases (32 %) and diabetes (40 %) (Li, Wang et al. 2020).

CXR/CT findings: Chest CT scans disclosed that the patients' pulmonic lesions were less well in the later stage than earlier ones (patients 3, 13, and 14) (Figure 4).

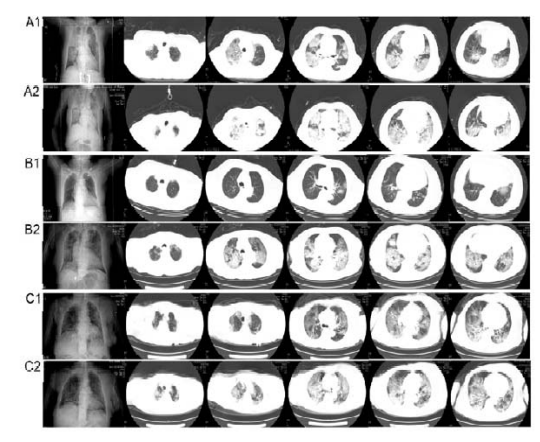


Figure 4. Chest CT scans of patient 3, patient 13 and patient 14. A1: the early stage Chest CT scan of Patient 3; A2: the late stage Chest CT scan of Patient 3; B1: the early stage Chest CT scan of Patient 13; B2: the late stage Chest CT scan of Patient 13; C1: the early stage Chest CT scan of Patient 14; C2: the late stage Chest CT scan of Patient 14 (Li, Wang et al. 2020).

3.5. Case 5.

Patient history: A 40-years-old woman was admitted to the hospital with fever, fatigue, and chest tightness. The patient had no travel history to Wuhan and had no contact with any COVID-19 infected patients. Her body-temperature on admission was elevated to 38.9 °C. The investigations indicated normal lymphocytes (30.9 %), neutrophils (59.6 %), and leukocyte (4170 /µL). There was an increase in the glucose (7.3 mmol/L) and hematocrit (0.456) levels (Wei, Xu et al. 2020).

CXR/CT findings: The Figure 5A indicated that the lungs were normal from the first chest radiograph was that obtained 3-days after the onset of the fever. Moreover, the unenhanced chest CT taken on the same day displayed that the left lung was normal, while GGOs in the sub-pleural zone of the right-lower lobe was observed (Figure 5B). The patient was treated with antibiotics for the obtainable symptoms.

No respiratory symptoms were observed initially; however, the patient begun to cough on day 6 following the commencement of the fever onset. A gained density of GGOs was observed in the right-lower lobe, upon a follow-up chest CT examination. Then this advanced into consolidations with perilobular condensing. Furthermore,

GGO lesions and multi-focal peripheral patchy regions of nodular consolidations were lately established in the subpleural zones of both lower lobes (Figure 5C-E). A repeat CT scan at the time of discharge revealed that the earlier GGOs and consolidations in the patient's lungs were virtually absorbed and only a small number of fibrous lesions that may signify lingering consolidating pneumonia were left (Figure 5F).

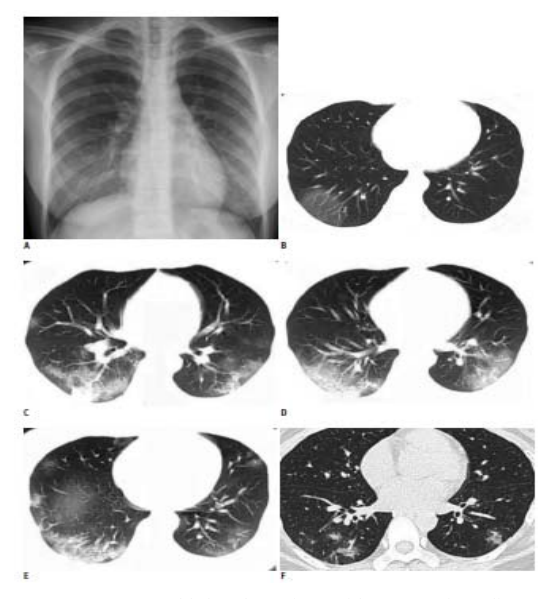


Figure 5. 40-year-old female patient with Coronavirus disease 2019 pneumonia. (A) shows no thoracic abnormalities. Axial CT scan (B) shows GGOs in subpleural area of right lower lobe. Left lung is normal. Multifocal peripheral patchy areas of nodular consolidations and nodular GGO lesions are newly developed in subpleural areas of both lower lobes. F. Progressive resolution of parenchymal lesions is seen in follow-up high-resolution CT scan obtained on day 12. Patchy consolidations and GGOs in both lungs were almost absorbed leaving a few fibrous lesions that may represent pneumonia (Wei, Xu et al. 2020).

The preliminary CT indicated GGOs in the right-lower lobe, the abnormality of which may indicate the formation of hyaline membrane or pulmonary edema (Chung, Bernheim et al. 2020). However, it is difficult to picture the lesions using conventional radiographs due to the subtle nature of their density. Hence, COVID-19 patients are recommended to undergo routine CT scans to lessen missed diagnoses. This patient's CT results contain GGOs in both right lungs and the left lung, particularly in the marginal regions of lower lobes that may signify alveolar damage, fibrous and cellular exudation, several patchy consolidation and the short-term progressions of lesion. After treatment, GGOs and consolidations were virtually absorbed, then leaving the fibrous cord like shades that denote fibrosis.

3.6. Case 6.

Pt history: Two residents of Wuhan a male and a female couple both in their 60s travelled to Italy for vacation. The male patient was seemingly healthy, while the female was taking treatment for oral hypertension. They had fever and respiratory symptoms, and they were received in the advanced isolation unit of the Lazzaro Spallanzani (National Institute of Infectious Diseases), Italy. Their RT-PCR oropharyngeal and nasopharyngeal

swabs tested were positive for COVID-19 (Corman, Landt et al. 2020). On their fourth day of admission, they developed progressive respirational failure and clinical proof of ARDS with mechanical ventilator in ICU (Albarello, Pianura et al. 2020).

CXR/CT findings: Chest X-Rays were achieved with conventional plain films with anteroposterior projection at bedsides. On the second day, baseline volumetric CT scans in the horizontal positions at full inspiration were achieved. On the 3rd and 4th day, follow-up scans were carried on these both patients in order to evaluate the level of progressive pulmonary injury. A multiple detector scanner was used for all the earlier and follow-ups CT scans (Albarello, Pianura et al. 2020). The CT images were studied by two skilful radiologists in thorax imaging to assess for any manifestation and spreading of abnormality, and a consensus was reached on the outcomes.

CXR/CT findings: Follow-ups CT scans of the lung were obtained in both abnormal patients; moreover, they were also used to evaluate and measure the residual pulmonic volume in an initial quantitative setting with the help of a thoracic volume by Reading imaging using a specific software (VCAR, GE, Milwaukee, Wis) (Figure 6a, b, c).

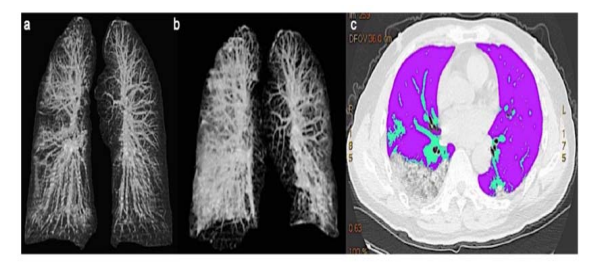


Figure 6. (a and b) Lung VCAR imaging displaying baseline CT and follow-up CT with progressive impairment of the lung parenchyma. (c) lung sparing analysis (Albarello, Pianura et al. 2020).

Two days later, the onset of the symptoms a CXR of the male patient was obtained and found to be inconsistent with lung alteration. However, crazy paving and GGOs were observed in the posterior-basal segment of the right-lower lobe, the lateral piece of the mid lobe, a day following the chest CT scan (Figure 7a and 8a). However, the lesion on the left side involved the posterior segment and superior basal segment of the lower lobes. Likewise, minor unilateral pleural effusions and mediastinal lymphadenopa- were found, and this was the largest with a short-axis of 12 mm (Figure 7b) (Albarello, Pianura et al. 2020).

The initial following-up CT scan was conducted on day 3, and pericardial and bilateral pleural effusions were observed (Figure 8b). The lymph nodes with a linear size ≥ 10 mm in the short-axis dimensions were found in the 4L, 4R, and 2R levels. Moreover, there was an increase in the diameter of the sub-segmentary vessels as revealed in the first CT scan and also after the third and the 6th day of the follow-ups, 5% and 10% increase in size were observed.

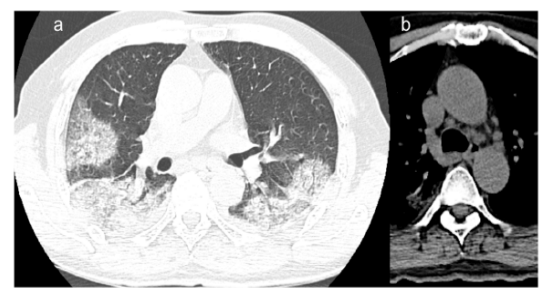


Figure 7. (a) Baseline chest CT images in a 66 years old man displaying multiple patchy ground glass opacities with reticular and interlobular septal thickening: crazy paving. The lesions are mostly distributed in the upper segment of right lower lobe and focal ground glass opacities in the superior segment of left inferior lobe. (b) Mediastinal lymphadenopathies the biggest with short axis of 12 mm (Albarello, Pianura et al. 2020).

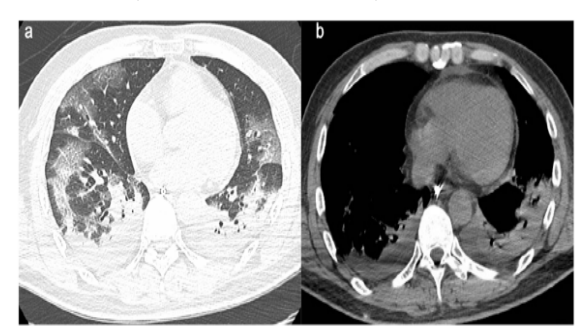


Figure 8. (a) Follow-up CT in a 66 years old man after 5 days, shows severe progression of pneumonia with increased of extension of ground glass opacities and consolidation. (b) Appearance of bilateral pleural effusion (Albarello, Pianura et al. 2020).

Two days later, the onset of the symptoms, a CXR was conducted for the female patient and interstitial lung alteration was evident. Ground glass and crazy pavement in the lateral basal segment of the right lower lobe, the middle-segments of the middle-lobes, the posterior and superior-basal, and the posterior and anterior of the right upper lobes, were observed on the third day following a chest CT scan. The lesions on the left side involved the superior and upper lobes as well as the posterior and lateral-basal sections of the lower-lobe (Figure 9a, 10a).

At third CT scan, pleural effusion at both sides (bilateral) appeared; however, at both 1^{st} and 2^{nd} CT scans, the non-pleural effusion appeared. There was no pericardial involvement (Figure 10b). Nodes having a longitudinal size ≥ 10 mm in the short-axis dimensions existed in the 10R level, 1R level, as well as the 6R, and level (Figure 9b). The first CT scan revealed an increase in the diameter size of the sub-segmentary vessels. Specifically, there was fourteen percent increase after the third follow-up as well as five percent rise after the 6th day of the following-up (Figure 11 a, b).

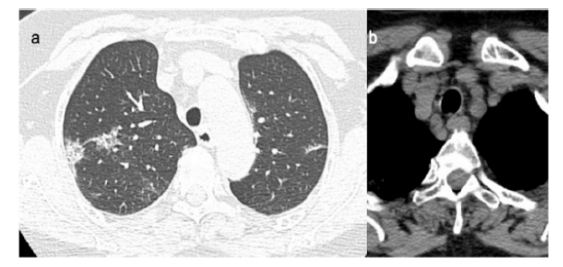


Figure 9. (a) Baseline CT images in a 65 years old woman shows patchy ground-glass opacities in the posterior segment of upper right lobe, with pleural contact. (b) Mediastinal lymphadenopathy with short axis of 10 mm (Albarello, Pianura et al. 2020).



Figure 10. (a) Follow-up CT after 3 days in a 65 years old woman shows increase size and density of the lesions (b) with bilateral pleural effusion (Albarello, Pianura et al. 2020).

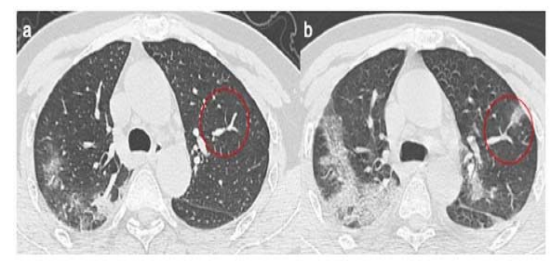


Figure 11. (a) Baseline chest CT shows tubular size increase of segmental vessel with normally ventilated adjacent lung parenchyma, (b) where after 3 days there is a ground-glass opacities (Albarello, Pianura et al. 2020).

Both patients exhibited a rise in the number of lung injury throughout their follow-ups. Enlargement in the lung lesion penetrates as well as an increase in the quantity of lung lesion with a comparative rise in consolidative zones in the posterior segments of the lower-lobes, comparative rise in GGO, and a decrease in interstitialreticular involvement. The lungs formed of both lung injury patients were hypertrophy of the pulmonic vessels that are enlarged, mainly in areas with further distinct and noticeable interstitial injury. Related to those perceived in the existing severe infectious diseases (Wong, Antonio et al. 2003, Ooi, Khong et al. 2004). The vasoconstriction of the pulmonic vessels was probably connected to the existence of vasoactive elements in the lesions. A changed configuration of lung association was suggested by new radiological evidence [58]. In these 2 patients, the enlarged breadth of the perilesional pulmonic vessels developed by outspreading the pulmonic variations. An enlarged and a tubular look of pulmonic vessels with an unexpected calibre decline was testified throughout the sequel investigations. They were principally established in the dichotomy tracts, where a new insurrectionary pulmonary lesion center was observed (Figure 11a, b).

Case 7.

Pt history: A woman visitor from Wuhan (China) with age of 74-year-old came to the hospital and suffered from losing appetite, malaise, and fever. However, she notified no dependent medical conditions, and there was no diarrhea, abdominal pain, dyspnea, myalgia, rhinorrhea, chest discomfort, sore throat, cough, or chillness. Physical examination disclosed blood pressure (129/68 mm Hg), with a respiratory rate of 18 breaths per min, heart rate of 79 beats per min, as well as a body temperature of 38.1 °C. CXR discovered a tiny-raised infiltration over two (bilateral) lower lungs. Peripheral WBC count was 3770 per mL cube (32.1 % lymphocytes and 62.3 % neutrophils). COVID-19 of nasopharyngeal swab was found positive via RT-PCR done at the Centres in Taiwan for Diseases Control (Huang, Teng et al. 2020).

Case 8.

Pt history: A 77-year-old female came to the hospital with poor appetite, malaise, fever, and dry cough. The patient denied diarrhea, abdominal pain, dyspnea, chest discomfort, sore throat, myalgia, rhinorrhea, or chillness. Her blood pressure was 117/47 mm Hg, with respiratory rate of 18 breaths per min, a heart rate of 82 beats per min, as well as body temperature of 38.7 °C. CXR investigated non-clear tiny raised infiltration over bilateral lower lung. Peripheral-blood white-cell count was 3420 per cubic millimetre (with 69.3 % neutrophils and 26.9 % lymphocytes).

CXR/CT findings: Following-up CXR discovered rising opacity at right centre and at the lower lung (Figure 12A). On day number 6 in the hospital, the ill person stayed febrile, with malaise and tiny appetite. However, she informed worsening of cough. Following-up chest x ray discovered patchy consolidation over bilateral lower lung (Figure 12B).

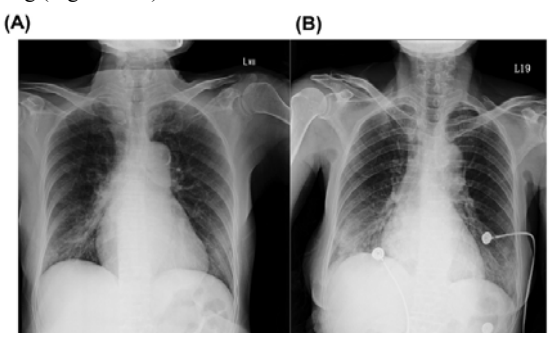


Figure 12. (a) Baseline chest CT shows tubular size increase of segmental vessel with normally ventilated adjacent lung parenchyma, (b) where after 3 days there is a ground-glass opacities (Huang, Teng et al. 2020).

The clinical utility of CXR in the early diagnosis of COVID-19 is questionable. Similar findings were reported in the first case of COVID-19 in the United States, and pulmonary patch/consolidation was not detected by CXR until day 5 in hospital (day 9 of illness) (Holshue, DeBolt et al. 2020). Equally, in a case series of SARS patients from the Amoy Gardens housing estate, 29.3 % (22/75) cases had normal CXR on admission; however, four of the 22 cases developed acute respiratory distress syndrome

(ARDS); afterwards, generally 80% (60/75) of the cases experienced radiological worsening at a mean of 7.4 days (Peiris, Chu et al. 2003). Both unifocal and bilateral lung infiltration could be observed. Of 99 COVID-19 cases in China, 25 and 75 % were presented with unilateral and bilateral pneumonia respectively (Chen, Zhou et al. 2020).

4. Discussion

An analysis of the latest work was carried out with the goal of collecting findings in a number of COVID-19 patients (almost 1,200 patients). Pathological and clinical results in a severe case of COVID-19 cannot only help to determine the cause of death but may also provide new insights into the pathogenesis of SARS-CoV-2-related pneumonia. It can allow medical professionals to come up with an effective treatment solution in a similar situation, resulting in a decrease in the death rate. It could be deduced from this event that COVID-19 can cause relatively mild symptoms, and that patient recovery can be accomplished with timely diagnosis of pneumonia. Reduced pathological loads and improved clinical symptoms were reported during treatment with ritonavir / lopinavir. Ritonavir / lopinavir may also be recommended to high-risk patients with COVID-19 at an early stage. However, further research was required to confirm the therapeutic effectiveness of lopinavir / ritonavir based on well-controlled clinical trials. In fact, there is also a need for an in-depth review of COVID-19 cases. Aging and primary conditions, such as diabetes, hypertension, etc., were found to be the most important risk mortality factors for COVID-19 infection. Nevertheless, bacterial infection can play a vital role in raising the death of the patient. In addition, malnutrition was also widespread among serious patients. There was also some multiple organ dysfunction, with the heart being the most affected organ in the lungs, followed by the liver and kidneys. Successive CT results have been recorded for a female COVID-19 patient. The CT scans revealed a fast-emerging number of patchy consolidations and GGOs in both the right and left lungs and were mainly scattered in peripheral areas. In addition, the use of high-resolution CT would make it easier to detect GGOs quickly. Furthermore, since there is potential similarity between the images of COVID-19 and pneumonia caused by other viruses, it is recommended that RT-PCR be adopted for rapid detection and treatment.

Finally, an early marker radiological indicator of lung failure may be identified on the basis of the growth of the expansion of the pulmonary vessel in places where the new lungs permeate as shown by the CT follow-up. As more reports are identified, the full spectrum of imaging findings in SARS-COV2 contaminated patients would be clearer. COVID-19 cannot be consistently differentiated from other causes of pneumonia by surgical, radiological or experimental requirements. There are also a number of cases not listed in this study due to the vast number of reported cases linked to this pandemic around. However, a summary of whole review article with a recap of several cases is shown at Table 1.

Table 1. Review article with summarizing of several cases

Case No.	Study date	Sample size/mean age	Common radiological findings/distributions	Conclusion
1	2020	A 50-year-old male patient	The CXR exhibited many patchy shadows in both lungs Some differences between the right and left lungs and the swift advancement of pneumonia were observed	Use of ventilator support together with corticosteroids should be used for the severe patient to avoid the development of ARDS.
2	2020	A 54-year-old man	Upon high-resolution CT scan, GGOs in both lower lobes and minor consolidation in the right upper lobe were observed	The patient did not show any respiratory symptoms and recorded blood pressure of 152/93 mmHg at 73 beats/minute. Moreover, his respiratory rate was 20 breaths per minute and recorded a body temperature of 37.0 °C. Clear lung sounds were observed upon physical examinations with clear CXR nor pharyngeal injection
3	2020	All registered eighty patients	Bilateral ground glass or sub-segmental consolidation regions, as well as bilateral lobular, sub-segmental consolidation areas, were absent. Total of 55 patients (68.75 %) displayed abnormalities	It is, therefore, suggested that during the screening of patient for clinical manifestations, there is the need to combine the laboratory examination with
			in their chest CT images. Nineteen out of these abnormal CT images were unilateral pneumonia (23.75 %), while 36 were bilateral pneumonia (45.00 %).	chest imaging with for all-inclusive investigation.
4	2020	A retrospective study of 25 dead persons with the COVID-19 pandemic	Chest CT scans disclosed that the patients' pulmonic lesions were less well in the later stage than earlier ones.	In conclusion, the age of the patients ranged from 55 to 100-years-old. 100% of the dead persons had diseases, including hypertension (16/25, 64 %), which was the most common. Others include kidney diseases (20 %), cerebral infarction (16 %), Chronic Obstructive Pulmonary Disease (8 %), cancers (8 %), acute pancreatitis (4 %), heart diseases (32 %) and diabetes (40 %).
5	2020	A 40-years-old woman	The lungs were normal from the first chest radiograph was that obtained 3-days after the onset of the fever. Moreover, the unenhanced chest CT taken on the same day, displayed that the left lung was normal while GGOs in the sub-pleural zone of the right-lower lobe was observed.	It is difficult to picture the lesions using conventional radiographs due to the subtle nature of their density. Hence, COVID-19 patients are recommended to undergo routine CT scans to lessen missed diagnoses.
			A gained density of GGOs was observed in the right- lower lobe, upon a follow-up chest CT examination.	
6	2020	Two residents of Wuhan a male and a female couple both in their 60s	Crazy paving and GGOs were observed in the posterior-basal segment of the right-lower lobe, the lateral piece of the mid lobe, the superior like the right upper lobe, a day afterward the chest CT scan. The lesion on the left side involved the posterior segment and superior basal segment of the lower lobes.	Both patients exhibited a rise in the number of lung injury throughout their follow-ups. Enlargement in the lung lesion penetrates as well as an increase in the quantity of lung lesion with a comparative rise in consolidative zones in the posterior segments of the lower-lobes, comparative rise in GGO, and a decrease in interstitial-reticular involvement.
			Minor unilateral pleural effusions and mediastinal lymphadenopa- were found and this was the largest with a short-axis of 12 mm.	
7	2020	A woman with age of 74-year- old	CXR discovered tiny raised infiltration over two (bilateral) lower lungs.	COVID-19 of nasopharyngeal swab found positive via RT-PCR done at the Centers in Taiwan for Diseases Control
8		A 77-year-old female	Following-up CXR discovered rising opacity at right centre and at the lower lung.	The clinical utility of CXR in the early diagnosis of COVID- 19 is questionable.
			Following-up chest x ray discovered patchy consolidation over bilateral lower lung.	Similar findings were reported in the first case of COVID-19 in the United States, and pulmonary patch/consolidation was not detected by CXR until day 5 in hospital (day 9 of illness).

5. Conclusion

In conclusion, several recent studies have presented descriptions of the results for common chest imaging of respiratory diseases instigated by COVID-19. It is concluded that the image results previously described in patients with SARS and MERS infection appeared similar to those recently reported for COVID-19. The analysis of the various results on chest radiographs proved to be difficult due to the unique and mysterious terms used, such as hazy opacities, patchy opacities, infiltrates, pneumonia, and airborne disease. Health care facilities have a strong responsibility in cases of COVID-19, particularly in situations where the patient suffers from other health problems.

Acknowledgments:

We would like to thank the Department of Medical Imaging, Faculty of Applied Medical Sciences, The Hashemite University, Jordan, for their efforts to make this work possible.

Funding:

Funding information is not available.

Competing Interests:

The authors declare that they have no conflicts of interest.

References

Ahmad, T., et al. (2020). "Are we ready for the new fatal Coronavirus: scenario of Pakistan?" Human Vaccines & Immunotherapeutics 16(3): 736-738.

Al-Osail, A. M., et al. (2017). "The history and epidemiology of Middle East respiratory syndrome corona virus." Multidisciplinary respiratory medicine **12**(1): 20.

Al-Tawfiq, J. A., et al. (2014). "Travel implications of emerging coronaviruses: SARS and MERS-CoV." Travel medicine and infectious disease 12(5): 422-428.

Al Mutair, A., et al. (2020). "Narrative review of Middle East respiratory syndrome coronavirus (MERS-CoV) infection: updates and implications for practice." Journal of International Medical Research **48**(1): 0300060519858030.

Albarello, F., et al. (2020). "2019-novel Coronavirus severe adult respiratory distress syndrome in two cases in Italy: An uncommon radiological presentation." International Journal of Infectious Diseases

Arab-Mazar, Z., et al. (2020). "Mapping the incidence of the COVID-19 hotspot in Iran–Implications for Travellers." Trav Med Infect Dis 101630.

Baharoon, S., et al. (2019). "MERS-CoV as an emerging respiratory illness: A review of prevention methods." Travel medicine and infectious disease: 101520.

Bastola, A., et al. (2020). "The first 2019 novel coronavirus case in Nepal." The Lancet Infectious Diseases **20**(3): 279-280.

Bermingham, A., et al. (2012). "Severe respiratory illness caused by a novel coronavirus, in a patient transferred to the United Kingdom from the Middle East, September 2012." Eurosurveillance 17(40): 20290.

Bernard-Stoecklin, S., et al. (2020). "First cases of coronavirus disease 2019 (COVID-19) in France: surveillance, investigations and control measures, January 2020." Eurosurveillance **25**(6).

Bernheim, A., et al. (2020). "Chest CT findings in coronavirus disease-19 (COVID-19): relationship to duration of infection." Radiology: 200463.

Chamorro, E. M., et al. (2021). "Pulmonary embolisms in patients with COVID-19: a prevalence study in a tertiary hospital." Radiología (English Edition) **63**(1): 13-21.

Chan, J. F.-W., et al. (2020). "A familial cluster of pneumonia associated with the 2019 novel coronavirus indicating person-toperson transmission: a study of a family cluster." The Lancet **395**(10223): 514-523.

Chang, D., et al. (2020). "Epidemiologic and clinical characteristics of novel coronavirus infections involving 13 patients outside Wuhan, China." Jama.

Chen, N., et al. (2020). "Epidemiological and clinical characteristics of 99 cases of 2019 novel coronavirus pneumonia in Wuhan, China: a descriptive study." The Lancet **395**(10223): 507-513

Chung, M., et al. (2020). "CT imaging features of 2019 novel coronavirus (2019-nCoV)." Radiology: 200230.

Corman, V. M., et al. (2020). "Detection of 2019 novel coronavirus (SARS-COV2) by real-time RT-PCR." Euro Surveill **25**(3)

de Groot, R. J., et al. (2013). "Commentary: Middle East respiratory syndrome coronavirus (MERS-CoV): announcement of the Coronavirus Study Group." Journal of virology **87**(14): 7790-7792.

de Wit, E., et al. (2016). "SARS and MERS: recent insights into emerging coronaviruses." Nature Reviews Microbiology 14(8): 523

Drosten, C., et al. (2003). "Identification of a novel coronavirus in patients with severe acute respiratory syndrome." New England journal of medicine **348**(20): 1967-1976.

Giovanetti, M., et al. (2020). "The first two cases of 2019-nCoV in Italy: Where they come from?" Journal of Medical Virology.

Haagmans, B. L., et al. (2015). "Asymptomatic Middle East respiratory syndrome coronavirus infection in rabbits." Journal of virology **89**(11): 6131-6135.

Holshue, M. L., et al. (2020). "First case of 2019 novel coronavirus in the United States." New England Journal of Medicine.

Huang, C., et al. (2020). "Clinical features of patients infected with 2019 novel coronavirus in Wuhan, China." The Lancet **395**(10223): 497-506.

Huang, W.-H., et al. (2020). "2019 novel coronavirus disease (COVID-19) in Taiwan: Reports of two cases from Wuhan, China." Journal of Microbiology, Immunology and Infection.

Kanne, J. P., et al. (2020). Essentials for radiologists on COVID-19: an update—radiology scientific expert panel, Radiological Society of North America.

Ksiazek, T. G., et al. (2003). "A novel coronavirus associated with severe acute respiratory syndrome." New England journal of medicine **348**(20): 1953-1966.

Kuiken, T., et al. (2003). "Newly discovered coronavirus as the primary cause of severe acute respiratory syndrome." The Lancet **362**(9380): 263-270.

Li, X., et al. (2020). "Clinical characteristics of 25 death cases with COVID-19: a retrospective review of medical records in a single medical center, Wuhan, China." International Journal of Infectious Diseases.

Lim, J., et al. (2020). "Case of the index patient who caused tertiary transmission of Coronavirus disease 2019 in Korea: the application of lopinavir/ritonavir for the treatment of COVID-19 pneumonia monitored by quantitative RT-PCR." Journal of Korean Medical Science 35(6).

Lim, J., et al. (2020). "Case of the index patient who caused tertiary transmission of COVID-19 infection in Korea: the application of lopinavir/ritonavir for the treatment of COVID-19 infected pneumonia monitored by quantitative RT-PCR." Journal of Korean medical science 35(6).

Liu, Y., et al. (2020). "The reproductive number of COVID-19 is higher compared to SARS coronavirus." Journal of travel medicine

Ludvigsson, J. F. (2020). "Systematic review of COVID-19 in children show milder cases and a better prognosis than adults." Acta Paediatrica.

Mailles, A., et al. (2013). "First cases of Middle East Respiratory Syndrome Coronavirus (MERS-CoV) infections in France, investigations and implications for the prevention of human-to-human transmission, France, May 2013." Eurosurveillance 18(24): 20502.

Millán-Oñate, J., et al. (2020). "A new emerging zoonotic virus of concern: the 2019 novel Coronavirus (COVID-19)." Infectio **24**(3).

Nishiura, H., et al. (2020). The rate of underascertainment of novel coronavirus (2019-nCoV) infection: Estimation using Japanese passengers data on evacuation flights, Multidisciplinary Digital Publishing Institute.

Oglat, A. A. (2020). "Acceptance experimentation and quality monitor of x-ray radiography units." Radiation Physics and Chemistry 172: 108810.

Oglat, A. A., et al. (2021). "Fabrication and characterization of epoxy resin-added Rhizophora spp. particleboards as phantom materials for computer tomography (CT) applications." The Journal of Adhesion: 1-18.

Ooi, G. C., et al. (2004). "Severe acute respiratory syndrome: temporal lung changes at thin-section CT in 30 patients." Radiology **230**(3): 836-844.

Organization, W. H. (2020). "Coronavirus disease 2019 (COVID-19): situation report, 59."

Organization, W. H. (2020). Laboratory testing for coronavirus disease 2019 (COVID-19) in suspected human cases: interim guidance, 2 March 2020, World Health Organization.

Organization, W. H. (2020). Novel coronavirus (2019-nCoV)-situation report-10-30 January 2020.

Pan, F., et al. (2020). "Time course of lung changes on chest CT during recovery from 2019 novel coronavirus (COVID-19) pneumonia." Radiology: 200370.

Peiris, J. S. M., et al. (2003). "Clinical progression and viral load in a community outbreak of coronavirus-associated SARS pneumonia: a prospective study." The Lancet **361**(9371): 1767-1772.

Plowright, R. K., et al. (2017). "Pathways to zoonotic spillover." Nature Reviews Microbiology 15(8): 502.

Pongpirul, W. A., et al. (2020). "Journey of a Thai taxi driver and novel coronavirus." New England Journal of Medicine **382**(11): 1067-1068.

Raj, V. S., et al. (2014). "Isolation of MERS coronavirus from a dromedary camel, Qatar, 2014." Emerging infectious diseases **20**(8): 1339.

Ratre, Y. K., et al. (2020). "Dynamic propagation and impact of pandemic influenza A (2009 H1N1) in children: a detailed review." Current Microbiology: 1-12.

Reusken, C. B., et al. (2020). "Laboratory readiness and response for novel coronavirus (2019-nCoV) in expert laboratories in 30 EU/EEA countries, January 2020." Eurosurveillance **25**(6).

Rodriguez-Morales, A. J., et al. (2020). "History is repeating itself: probable zoonotic spillover as the cause of the 2019 novel Coronavirus Epidemic." Infez Med **28**(1): 3-5.

Rodriguez-Morales, A. J., et al. (2020). "Clinical, laboratory and imaging features of COVID-19: A systematic review and meta-analysis." Travel medicine and infectious disease: 101623.

Rothe, C., et al. (2020). "Transmission of 2019-nCoV infection from an asymptomatic contact in Germany." New England Journal of Medicine.

Ruiz-Saenz, J., et al. (2019). "Brazil burning! What is the potential impact of the Amazon wildfires on vector-borne and zoonotic emerging diseases?-A statement from an international experts meeting." Travel medicine and infectious disease.

Sahu, T., et al. (2021). "Current understanding of the impact of COVID-19 on gastrointestinal disease: Challenges and openings." World Journal of Gastroenterology **27**(6): 449.

Song, F., et al. (2020). "Emerging 2019 novel coronavirus (2019-nCoV) pneumonia." Radiology: 200274.

The, L. (2020). "Emerging understandings of 2019-nCoV." Lancet (London, England) **395**(10221): 311.

Wei, J., et al. (2020). "2019 Novel Coronavirus (COVID-19) Pneumonia: Serial Computed Tomography Findings." Korean Journal of Radiology **21**(4): 501-504.

Wong, K., et al. (2003). "Thin-section CT of severe acute respiratory syndrome: evaluation of 73 patients exposed to or with the disease." Radiology **228**(2): 395-400.

Wu, J., et al. (2020). "Clinical characteristics of imported cases of COVID-19 in Jiangsu province: a multicenter descriptive study." Clinical Infectious Diseases.

Xu, Z., et al. (2020). "Pathological findings of COVID-19 associated with acute respiratory distress syndrome." The Lancet respiratory medicine.

Yin, Y., et al. (2018). "MERS, SARS and other coronaviruses as causes of pneumonia." Respirology **23**(2): 130-137.

Zaki, A. M., et al. (2012). "Isolation of a novel coronavirus from a man with pneumonia in Saudi Arabia." New England Journal of Medicine **367**(19): 1814-1820.

Zhu, N., et al. (2020). "A novel coronavirus from patients with pneumonia in China, 2019." New England Journal of Medicine.

Jordan Journal of Biological Sciences

Understanding the Medicinal Prospects of Methanolic Extract from a Recently Explored Mushroom of Tribal Delicacy

Somanjana Khatua^{1,2}, Krishnendu Acharya^{1,*}

¹Molecular and Applied Mycology and Plant Pathology Laboratory, Centre of Advanced Study, Department of Botany, University of Calcutta, 35, Ballygunge Circular Road, Kolkata 700019, West Bengal, India; ²Department of Botany, Krishnagar Government College, Krishnagar 741101, West Bengal, India.

Received: August 26, 2021; Revised: October 21, 2021; Accepted: November 6, 2021

Abstract

At present, wild edible mushrooms are experiencing a curious renaissance as they offer a range of functional benefits. In that connection, West Bengal, India constitutes a wealth of macrofungal flora where many species are being harvested by locals as food and medicine. One of such matrices has recently been reported by our team that in turn appeared as a novel species (*Russula pseudocyanoxantha* Paloi, K. Acharya & S. Khatua). The present study thus aimed to screen bioactive potential of the neglected tribal cuisine and explore related metabolite profile for downstream applications. For that the dried basidiocarps were subjected to methanolic extraction and the fraction was found to be mainly composed of phenolics (pyrogallol> cinnamic acid) along with ascorbic acid and carotenoids. Consequently, the preparation emerged as a potent radical scavenger, metal ion chelator and electron donor where EC₅₀ values ranged from 621 to 1491 μg/ml. Additionally, antimicrobial activity tests were also performed using microdilution technique against six bacterial strains where MIC values ranged from 88.65 to 1559 μg/ml. Besides, the extract was able to inhibit Hep3B cell proliferation as well, evident by cytotoxicity (IG₅₀ 376.21 μg/ml) and scratch assays. The findings thus suggest that *R. pseudocyanoxantha* may be used as a valuable resource of natural antioxidant, antibacterial and cytotoxic ingredients to control various human diseases.

Keywords: Hep3B, HPLC, Human pathogens, Radical scavenging activity, Wild edible mushroom.

1. Introduction

India is one of the most mega-diverse countries in the world where an appreciable portion of the total land area is under forest and tree cover (Krishna et al., 2015). The subcontinent includes virtually all the major climate zones of the globe cradling a large number of fungal species and their natural beauty. Indeed, scientists have suggested that one third of the universal myco-diversity exists in India, and thus presence of novel species in the nation, is not a rare event (Tripathi et al., 2017; Khatua et al., 2019). In this regard, it is worth mentioning that West Bengal, a state in eastern India, constitutes a wealth of macrofungal flora (Singha et al., 2017). The monsoon season makes the highly prized mushrooms to flourish on forest floors where many species play a key role in food security for tribals. Inherently, the local people value these nature derived resources, and the wisdom collected by forefathers is orally passed to the next generations (Khatua et al., 2017a; Khatua et al., 2019). During our recent foray, one of such matrices was fortunately being discovered growing under Shorea robusta at lateritic regions of West Bengal. The investigation based on morphological characters, DNA barcoding and phylogenetic analysis revealed novelty of the specimen which was further entitled as Russula pseudocyanoxantha Paloi, K. Acharya & S. Khatua. The mushroom is colloquially known as "Jam Patra" and enjoyed as seasonal health promoting food by locals indicating potential to be used as a functional nutrient. Despite that, city people have refrained from consuming the macrofungus due to lack of proper knowledge, and thus detailed study should be carried out to increase awareness, before the species disappears from the natural habitat (Khatua *et al.*, 2021a).

Nowadays, people are predisposed to various diseases due to modern lifestyle associated with exposure to a wide range of chemicals, processed food and lack of exercise (Sharifi-Rad et al., 2020). As a result, people are gradually moving towards functional foods that are purported to provide optimal nutrition and reduce the risk of disease occurrence (Granato et al., 2020). In this context, mushrooms are widely acknowledged for their tremendous nutritional value and pleasant taste. They have also been continually used in traditional Asian medical systems to treat many diseases and promote longevity (Ho et al., 2020). Current research has comprehended that macrofungi are the natural reservoirs of potent pharmaceuticals and new interface for drug discovery (Zeb and Lee, 2021). Basidiomycetes possess a variety of biologically active compounds such as phenolics that offer valuable therapeutic effects including antioxidant (Khatua et al., 2017c), antibacterial (Khatua and Acharya, 2021) and anticancer properties (Khatua et al., 2021b). There is thus an increasing interest with medicinal effects of mushroom extracts enriched in secondary metabolites and

^{*} Corresponding author. e-mail: krish_paper@yahoo.com.

potential for its use as functional foods (Abdelshafy et al., 2021). The present study henceforth was aimed to determine health beneficial effects of *R. pseudocyanoxantha*, and for that a methanol extract was isolated.

2. Materials and methods

2.1. Fungal material collection

Several field trips were conducted at the lateritic areas of West Bengal, and fruit bodies were collected. The fruit bodies were identified following macroscopic study, anatomical characterization, DNA barcoding and phylogenetic placement analysis. The voucher specimen is conserved at Calcutta University Herbarium under accession number of CUH AM652 (Khatua *et al.*, 2021a).

2.2. Preparation of crude methanol extract

Dried fruit bodies were first pulverized using an electric blender and sieved through 160 mesh. For extract preparation, 10 g of the powder was soaked in 200 ml of methanol for 24 h with frequent shaking. The fraction was then isolated using Whatman filter paper. The preparation was further dried by evaporation (Rotavapor R-3, Butchi, Switzerland) at 40°C (Khatua *et al.*, 2019).

2.3. Determination of major bioactive compounds

For estimation of total phenolic compounds, Folin-Ciocalteu (FC) assay was followed where the isolated methanol extract from R. pseudocyanoxantha was mixed with FC reagent and sodium carbonate solution. Further, absorbance was recorded at 725 nm and gallic acid (10-40 μg) was used as a standard (Khatua et al., 2019). The amount of total flavonoid was quantified by mixing the extract with aluminium nitrate and potassium acetate. Following 40 min incubation, absorbance was measured at 415 nm. Quercetin (5-20 µg) was considered as a reference. Further, the amount of ascorbic acid was quantified following a modified titration method where vitamin C was mixed with oxalic acid and titrated against 2,6-dichlorophenolindophenol dye (Khatua et al., 2017c). Contents of carotenoids were determined by mixing the extract with acetone-hexane solution and recording absorbance at three different wavelengths such as 453, 505 and 663 nm. Finally, the extract was analyzed for estimation of phenolic composition with the help of high performance liquid chromatography (HPLC) (Agilent, USA) (Khatua et al., 2015).

2.4. Evaluation of antioxidant activity

A revised version for reducing power assay was considered where variable doses of the preparation under investigation were mixed in 96 well plate and the absorbance at 750 nm was recorded (Bio-Rad iMarkTM Microplate Reader, USA). Nevertheless, ability of the fraction to chelate ferrous ions was also estimated in the microtiter plate using ferrozine, and ferrous chloride and absorbance at 595 nm was estimated (Dehimat *et al.*, 2021). Methanol solution of 2,2-diphenyl-1-picrylhydrazyl (DPPH) radical was evaluated against various dosages of the studied extract in 96 well plate and absorbance at 595 nm was determined (Thakur *et al.*, 2021; Khatua *et al.*, 2017b). The method of total antioxidant capacity was carried out in the present study and activity of the

methanol extract was expressed as a number of equivalents of ascorbic acid (Khatua *et al.*, 2018).

2.5. 2.5. Estimation of antibacterial action

Listeria monocytogenes ATCC[®] 19111[™], Bacillus subtilis ATCC[®] 6633[™], Staphylococcus aureus ATCC[®] 700699[™], Escherichia coli ATCC[®] 25922[™], Klebsiella pneumoniae ATCC[®] 15380[™] and Salmonella typhimurium ATCC[®] 23564[™] were cultured overnight in nutrient broth and used for the investigation. After 24 h incubation with the methanol extract, antibacterial effect was assessed by computing minimum inhibitory concentration (MIC) values (Khatua and Acharya, 2021).

2.6. Estimation of anti-proliferative activity

To determine cytotoxicity, Hep3B human liver cancer cells were seeded in 96-well plate overnight, and the studied methanolic extract dissolved in sterile DMSO was added at a range of concentrations. After 24 h incubation, 20 μl water-soluble tetrazolium (WST) reagent was added in each well and absorbance was measured at 450 nm (Khatua *et al.*, 2017c). Further, wound healing assay was performed by creating a scratch in Hep3B monolayer and incubation of the cells with the studied fraction. Healing of the wound was estimated after 24 h incubation and photographed (Khatua *et al.*, 2021b).

2.7. Statistical analysis

The results presented herein are expressed as mean \pm SD of three independent experiments. The analysis of statistical data was procured with Student's t-test by p<0.05 as the minimal level of significance using IBM SPSS Statistics, v. 23.0. (IBM Corp., Armonk, New York, United States).

3. Results and discussion

3.1. Determination of major bioactive compounds

The phenol content of an extract depends on the type of sample and solvent used for extraction. In general, methanol is identified as the most effective medium for the preparatory process, resulting in high extraction yield as well as appreciable content of phenolic compounds (Do et al., 2014). Keeping this in mind, the solvent was selected in the present study to isolate secondary metabolites from R. pseudocvanoxantha that in turn resulted satisfactory recovery percentage (21.07 ± 0.93%). Literature survey revealed that the yield was comparatively better than that of Auricularia polytricha, Tremella fuciformis and Auricularia fuscosuccinea (Lin et al., 2013). Spectroscopic analysis depicted that the studied preparation was enriched mainly with phenols (11.37 \pm 0.94 µg gallic acid equivalent/mg of extract) and the amount was found to be superior to alcoholic extract from Auricularia auricula (Yuwa-Amornpitak et al., 2020). Alongside, flavonoid was also detected in the fraction under investigation in moderate extent (7.14 \pm 3.33 μg quercetin equivalent/mg of extract) which was higher than the methanol fraction of Pleurotus ostreatus (González-Palma et al., 2016). In contrast, trace amount of ascorbic acid was recorded (0.83 \pm 0.28 µg/mg of extract) which was quantified lower than Pleurotus djamor (Acharya et al., 2017). Similar range of carotenoids including $0.55 \pm 0.08 \,\mu g$ β -carotene and $0.43 \pm$ 0.07 µg lycopene per mg of extract was also found in the studied preparation where the quantities were enumerated to be better than *Macrocybe lobayensis* (Khatua *et al.*, 2017c).

Further, HPLC was performed following a standardized protocol to procure a phenolic fingerprint of the methanolic preparation from *R. pseudocyanoxantha*. The chromatogram revealed presence of minimum five phenolics in the extract; amongst them two components were tentatively recognized. Comparatively, pyrogallol was detected as the chief component presented at the level of 3.96 ± 0.04 µg/mg of extract. Besides, cinnamic acid was also detected where the amount was calculated as 0.16 ± 0.03 µg/mg of extract. The observation was in contrast to Kouassi *et al.* (2016) reporting presence of a range of phenolic compounds in *Russula delica*, *Russula lepida* and *Russula mustelina*.

3.2. Evaluation of antioxidant activity

Free radicals, oxygen-containing molecules with an uneven number of electrons, are the natural by-product of chemical processes. As a result, they can react so easily with other molecules causing damage to cells, proteins and DNA (Neha *et al.*, 2019). These reactions can lead to a vast number of diseases including cancer, atherosclerosis, Alzheimer's disease, Parkinson's disease and many others. Antioxidants are molecules that can donate an electron to the highly reactive free radicals stabilizing them (Khatua *et al.*, 2017d). In this line, several synthetic antioxidants are available in market; however, they are prone to cause side-effects. At the same time, nature-derived antioxidants are gaining more and more attention due to food safety aspects (Lourenço *et al.*, 2019).

To determine the antioxidant potential, ferric reducing assay was executed as it delivers vital information regarding hydrogen atom donation capacity. The technique is based on the principle that antioxidative substances can react with potassium ferricyanide resulting formation of potassium ferrocyanide, which subsequently forms ferric-ferrous complex with λ_{max} of 750 nm. The study demonstrated that the fraction from *R. pseudocyanoxantha* owns effective reducing power that increased steadily with the increase of concentrations (Figure 1a). The preparation

at the concentrations of 1000 and 1500 µg/ml exhibited reducing power of 0.35 and 0.57 respectively which reached to 0.9 in presence of 2000 µg/ml dosage. In this connection, the studied formulation could be considered as a better reductant than methanol extract from Russula alatoreticula (Khatua et al., 2019). Further, a ferrozine based assay was followed to depict affinity of the studied fraction towards metal ion as excess amount of Fe2+ is prone to generate free radicals. The method is based on the formation of violet coloured ferrozine-Fe²⁺ complex which is disrupted in presence of antioxidative compound resulting decrease in colour. As presented in Figure 1b, the preparation under investigation exhibited 7.45%, 43.09% and 80.48% Fe²⁺ chelating abilities at the levels of 100, 500 and 1000 μg/ml respectively. Literature survey revealed that methanol extract from R. pseudocyanoxantha might possess higher affinity to metal ions than that of M. lobayensis (Khatua et al., 2017c). To confirm antioxidant potency of the studied methanol extract, DPPH. scavenging assay was performed being an accurate, easy and economic technique to estimate the bioactivity. The protocol is based on reduction of the violet-colored radical by antioxidative molecules via a hydrogen atom transfer mechanism ensuing formation of stable yellow-colored diphenylpicrylhydrazine. Our results showed a doseresponse curve of DPPH scavenging activity of the methanolic fraction from R. pseudocyanoxantha. At a concentration of 500 µg/ml, the preparation quenched 22.81% radicals that reached to 49.87% and 78% radical inhibition in presence of 1000 and 1500 µg/ml of the formulation respectively (Figure 1c). Comparatively, the effect was found to be inferior to the standard; but superior to methanol extract from Macrocybe crassa (Acharya et al., 2015b). Finally, phosphomolybdenum assay was implemented to determine reducing ability of the antioxidative compounds converting Mo(VI) to Mo(V). Result showed that the studied fraction did not respond well as presented in Table 1 and thus the outcome was found to be inferior to the organic preparation from Grifola frondosa (Acharya etal., 2015a).

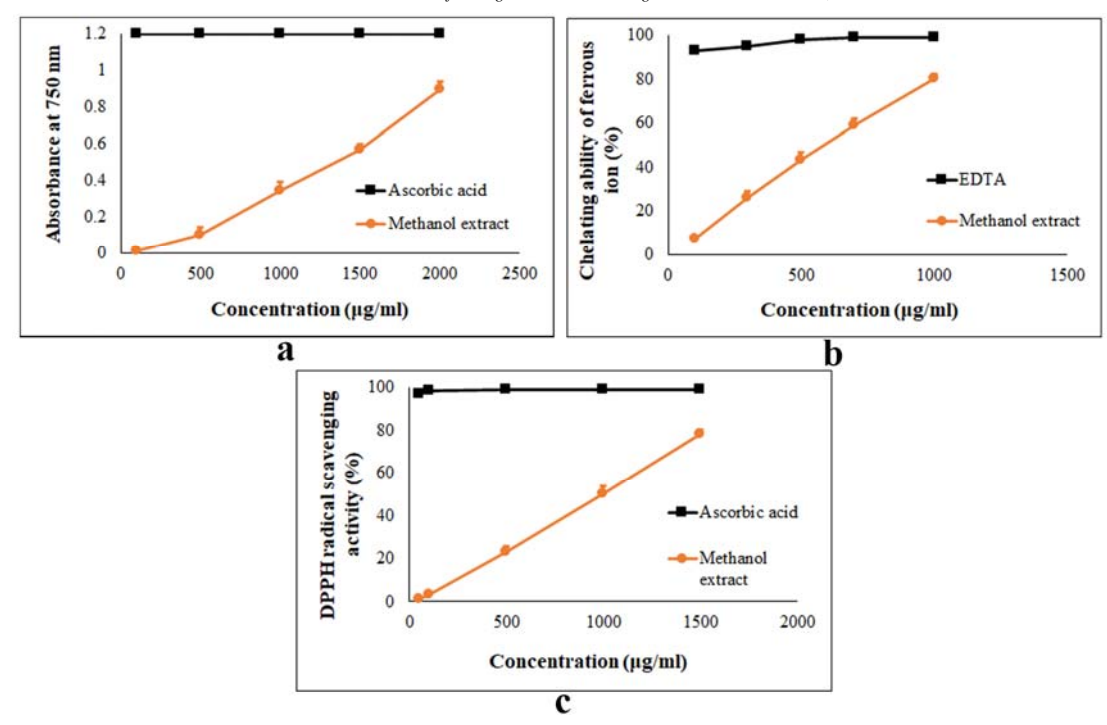


Figure 1. Antioxidant activity of *Russula pseudocyanoxantha* methanolic fraction. (a) Reducing power (b) Chelating ability of ferrous ion (c) DPPH radical scavenging activity.

Table 1. Antioxidant activity of *Russula pseudocyanoxantha* methanolic fraction. EDTA was used as standard in chelating ability of ferrous ion method, while ascorbic acid was considered as a reference for rest of the assays. Dissimilar letters in each row designate significant alterations between the sample and standard.

Antioxida	nt parameters	Methanol extract	Standard
EC50	Reducing power	1491 ± 45^a	17.92 ± 3.87^{b}
value (μg/ml)	Chelating ability of ferrous ion	621 ± 23^a	12.09 ± 1.67^{b}
	Scavenging ability of DPPH radical	1002 ± 28^a	8.21 ± 0.07^{b}
Total antioxidant activity (µg ascorbic acid equivalent/mg of dry extract)		0.31 ± 0.03	Not applicable

3.3. Estimation of antibacterial action

Today, microbial infection is considered as the biggest challenge worldwide that threatens the health of societies causing millions of deaths every year. Many factors are known to contribute to evolution of resistance including unnecessary prescription of antimicrobials and their use in agriculture (Chassagne *et al.*, 2021). In recent years, various strategies have been recommended to overcome the urgent danger. In this regard, phytochemicals have exhibited profound ability, and many researchers thus have focused on searching for natural products that can act against bacterial resistance (Khameneh *et al.*, 2019).

In this context, the present study was designed to explore antibacterial activity of the methanol extract from *R. pseudocyanoxantha* against three Gram positive and three Gram negative bacteria. Amongst the tasted microorganisms, *S. aureus* was found to be the most susceptible species as evident by the lowest MIC value (Table 2). Alongside, the fraction also inhibited cellular

growth of *E. coli*, *L. monocytogenes* and *B. subtilis* where the MIC data ranged from 125.63 to 350 µg/ml. On the other hand, *K. pneumoniae* appeared as the most resistant pathogen followed by *S. typhimurium* indicating more powerful activity of the fraction against Gram positive bacteria. The observation was in accord with previous publications describing difficulty to hinder growth of Gram negative pathogens by mushroom extracts (Gebreyohannes *et al.*, 2019). Literature survey also revealed that the studied fraction executed better antibacterial effect than methanol extracts from *Handkea utriformis*, *H. excipuliformis* and *Vascellum pratense* (Petrović *et al.*, 2016).

Table 2. Antibacterial activity of *Russula pseudocyanoxantha* methanolic fraction as determined by MIC values ($\mu g/ml$) (mean \pm standard deviation; n=3).

Type of bacteria	Name of bacteria	Methanol extract	Streptomycin
Gram positive	Listeria monocytogenes	276 ± 13.36^{a}	5.18 ± 0.02^{b}
	Staphylococcus aureus	88.65 ± 5.03^{a}	$5.98\pm0.43^{\rm b}$
	Bacillus subtilis	350 ± 25.05^a	$4.87\pm0.26^{\rm b}$
Gram	Escherichia coli	125.63 ± 31.59^a	$6.02\pm0.39^{\mathrm{b}}$
negative	Salmonella typhimurium	923 ± 27^a	4.75 ± 0.52^{b}
	Klebsiella pneumoniae	$1559 \pm 38.91^{\rm a}$	6.42 ± 0.69^{b}

3.4. Estimation of anti-proliferative activity

Cancer, abnormal cell proliferation, is the most feared ailment second only to heart disorder as a life-threatening disease. Every year, millions of people are diagnosed with cancer, often leading to death. In 2018, around 18 million

new cases of cancer were globally reported, ensuing around 10 million deaths (Khalifa *et al.*, 2019). Amongst the different types, liver cancer remains a universal health challenge, and its occurrence is in steep escalation (Balogh *et al.*, 2016). The majority of the anticancer agents used at clinical level are known to produce toxic effects, which limits their further usage. Scientists have suggested one realistic approach to deal with this problem in the use of natural products for effective drug development (Khazir *et al.*, 2014).

In this background, Hep3B cells were used in the present study to determine growth inhibitory activity of the methanol extract from *R. pseudocyanoxantha*. The treated and untreated cells were subjected to WST assay to determine effect of the fraction on cell proliferation. The results, as shown in Figure 2a, demonstrated that the preparation was able to inhibit hepatocellular carcinoma (HCC) in a dose dependent manner. After exposure to 100,

300 and 500 µg/ml of the extract, cell viability was reduced by 10.1%, 43.9% and 59.67% respectively within 24 h. Thus, IC₅₀ value was calculated as 376.21 ± 0.9 μg/ml which was found to be superior to the methanol extract from R. alatoreticula (Khatua et al., 2019). Further, wound healing or scratch assay was performed to analyze influence of the studied preparation on cell migration or invasion. As illustrated in Figure 2b, untreated HCC cells occupied the free space and filled the gap within 24 h. In contrast, wound enclosure of treated cells was suppressed upon exposure to the extract under investigation. Indeed, cells incubated with higher level i.e. 400 µg/ml failed to populate the wounded area indicating probable antiproliferative potency of the methanol fraction from R. pseudocyanoxantha towards the Hep3B liver cancer cell. The observation was in accordance to our previous reports (Khatua et al., 2017c; Khatua and Acharya, 2021; Khatua et al., 2021b).

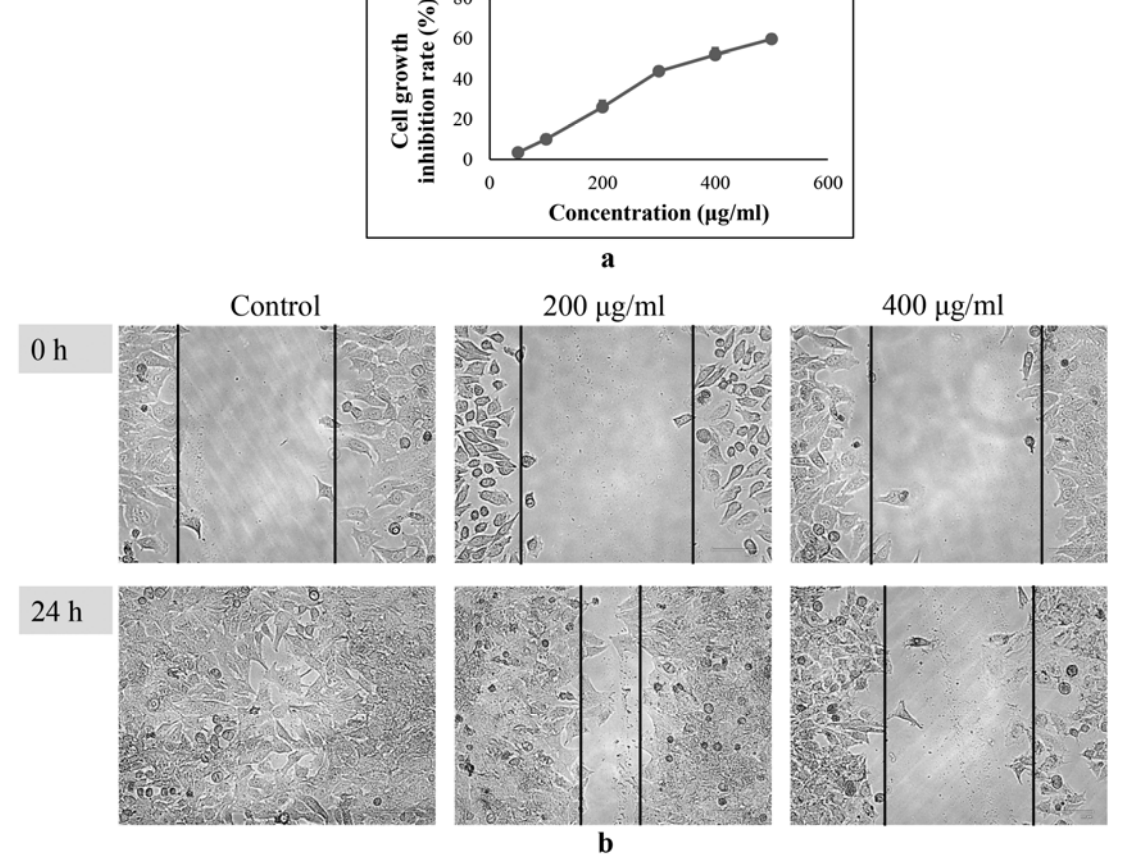


Figure 2. Anti-proliferative activity of methanol fraction isolated from *Russula pseudocyanoxantha* against Hep3B human liver cancer cells. (a) WST assay (b) Scratch assay.

4. Conclusion

In sum, the studied methanol extract exhibited potent antioxidant activity where the lowest EC₅₀ value was detected in case of chelating ability of metal ion and moderate effect was noted against DPPH scavenging, reducing power and total antioxidant assays. Alongside, strong antimicrobial property was also evident against the

targeted organisms where MIC values were in the decreasing order of *K. pneumoniae*> *S. typhimurium*> *B. subtilis*> *L. monocytogenes*> *S. aureus.* Further, the fraction was capable to inhibit Hep3B cell proliferation as well as migration within 24 h incubation. Such diverse outcomes might be related to the presence of a range of biomolecules in the fraction including phenols, flavonoids, ascorbic acid and carotenoids. Together, our results proved that the novel mushroom, *R. pseudocyanoxantha*, has a great potential in biomedical, nutraceutical and functional food applications. However, further investigation is needed

on bio-assay guided isolation of active compounds and confirmation of the therapeutic prospects *in vivo*.

Conflicts of interest

None.

Acknowledgment

The authors would like to acknowledge the facilities provided by the Department of Botany (UGC-CAS Phase VI, VII), University of Calcutta, and DST-FIST for instrumental support.

Reference

Abdelshafy AM, Belwal T, Liang Z, Wang L, Li D, Luo Z and Li L. 2021. A comprehensive review on phenolic compounds from edible mushrooms: Occurrence, biological activity, application and future prospective. *Crit Rev Food Sci Nutr.*, 1–21.

Acharya K, Bera I, Khatua S and Rai M. 2015. Pharmacognostic standardization of *Grifola frondosa*: A well-studied medicinal mushroom. *Der Pharm Lett.*, **7(7)**:72–78.

Acharya K, Khatua S and Ray S. 2017. Quality assessment and antioxidant study of *Pleurotus djamor* (Rumph. ex Fr.) Boedijn. *J Appl Pharma Sci.*, **7(6):** 105–110.

Acharya K, Khatua S and Sahid S. 2015. Pharmacognostic standardization of *Macrocybe crassa*: an imminent medicinal mushroom. *Research J Pharm Technol.*, **8**(7): 860–866.

Balogh J, Victor D3rd, Asham EH, Burroughs SG, Boktour M, Saharia A, Li X, Ghobrial RM and Monsour HPJr. 2016. Hepatocellular carcinoma: a review. *J Hepatocell Carcinoma*, 3: 41_53

Chassagne F, Samarakoon T, Porras G, Lyles JT, Dettweiler M, Marquez L, Salam AM, Shabih S, Farrokhi DR and Quave CL. 2021. A systematic review of plants with antibacterial activities: A taxonomic and phylogenetic perspective. *Front Pharmacol.*, **11**: 586548

Dehimat A, Azizi I, Baraggan-Montero V and Khettal B. 2021. *In vitro* antioxidant and inhibitory potential of leaf extracts of *Varthemia sericea* against key enzymes linked to type 2 diabetes. *Jordan J Biol Sci.*, 14(1): 97–104.

Do QD, Angkawijaya AE, Tran-Nguyen PL, Huynh LH, Soetaredjo FE, Ismadji S and Ju YH. 2014. Effect of extraction solvent on total phenol content, total flavonoid content, and antioxidant activity of *Limnophila aromatica*. *J Food Drug Anal.*, **22(3)**: 296–302.

Gebreyohannes G, Nyerere A, Bii C and Berhe Sbhatu D. 2019. Determination of antimicrobial activity of extracts of indigenous wild mushrooms against pathogenic organisms. *Evid Based Complement Alternat Med.*, **2019**: 6212673.

González-Palma I, Escalona-Buendía HB, Ponce-Alquicira E, Téllez-Téllez M, Gupta VK, Díaz-Godínez G and Soriano-Santos J. 2016. Evaluation of the antioxidant activity of aqueous and methanol extracts of *Pleurotus ostreatus* in different growth stages. *Front Microbiol.*, 7: 1099.

Granato D, Barba FJ, Bursać Kovačević D, Lorenzo JM, Cruz AG and Putnik P. 2020. Functional foods: Product development, technological trends, efficacy testing, and safety. *Annu Rev Food Sci Technol.*, **11**: 93–118.

Ho L-H, Asyikeen Zulkifli N and Tan T-C. 2020. Edible mushroom: Nutritional properties, potential nutraceutical values, and its utilisation in food product development. In: An Introduction to Mushroom; IntechOpen Limited: London, UK.

Khalifa SAM, Elias N, Farag MA, Chen L, Saeed A, Hegazy MF, Moustafa MS, Abd El-Wahed A, Al-Mousawi SM, Musharraf SG, Chang FR, Iwasaki A, Suenaga K, Alajlani M, Göransson U and El-Seedi HR. 2019. Marine natural products: A source of novel anticancer drugs. *Mar Drugs*, **17(9)**: 491.

Khameneh B, Iranshahy M, Soheili V and Fazly Bazzaz BS. 2019. Review on plant antimicrobials: a mechanistic viewpoint. Antimicrob Resist Infect Control, 8: 118.

Khatua S and Acharya K. 2021. Antioxidative and antibacterial ethanol extract from a traditional myco-food, *Russula senecis*, suppresses Hep3B proliferation by regulating ROS-driven intrinsic mitochondrial pathway. *Biointerface Res Appl Chem.*, **11(4):** 11202–11220.

Khatua S, Chandra S and Acharya K. 2019. Expanding knowledge on *Russula alatoreticula*, a novel mushroom from tribal cuisine, with chemical and pharmaceutical relevance. *Cytotechnology*, 71(1): 245–259.

Khatua S, Dutta AK and Acharya K. 2015. Prospecting *Russula senecis*: A delicacy among the tribes of West Bengal. *PeerJ*, 3: e810.

Khatua S, Dutta AK, Chandra S, Paloi S, Das K and Acharya K. 2017a. Introducing a novel mushroom from mycophagy community with emphasis on biomedical potency. *PloS ONE*, **12(5):** e0178050.

Khatua S, Ghosh S and Acharya K. 2017b. Chemical composition and biological activities of methanol extract from *Macrocybe lobayensis*. *J Appl Pharm Sci.*, **7(10)**: 144–151.

Khatua S, Ghosh S and Acharya K. 2017c. *Laetiporus sulphureus* (Bull.: Fr.) Murr. as food as medicine. *Pharmacogn J.*, **9(6):** s1–s15.

Khatua S, Ghosh S and Acharya K. 2017d. A simplified method for microtiter based analysis of *in vitro* antioxidant activity. *Asian J Pharm.*, **11(2):** S327–S335.

Khatua S, Paloi S and Acharya K. 2021a. An untold story of a new myco-resource from tribal cuisine: an ethno-medicinal, taxonomic, antioxidant and immune-potentiating approach. *Food Funct.*, **12:** 4679–4695.

Khatua S, Sen Gupta S, Ghosh M, Tripathi S and Acharya K. 2021b. Exploration of nutritional, antioxidative, antibacterial and anticancer status of *Russula alatoreticula*: towards valorization of a traditionally preferred unique myco-food. *J Food Sci Technol.*, **58(6)**: 2133–2147.

Khatua S, Sikder R and Acharya K. 2018. Chemical and biological studies on a recently discovered edible mushroom: a report. *FABAD J Pharm Sci.*, **43(3):** 151–157.

Khazir J, Riley DL, Pilcher LA, De-Maayer P and Mir BA. 2014. Anticancer agents from diverse natural sources. *Nat Prod Commun.*, **9(11)**: 1655–1669.

Kouassi KA, Kouadio EJP, Djè KM, Dué AE and Kouamé LP. 2016. Edible ectomycorrhizal mushrooms *Russula* spp. Of Côte d'Ivoire: total phenolic content, HPLC-profiles of phenolic compounds and organic acids, antioxidant activities. *J Agric Chem Environ.*, 5: 73–84.

Krishna G, Samatha B, Nidadavolu SVSSSLHB, Prasad MR, Rajitha B and Charaya MAS. 2015. Macrofungi in some forests of Telangana state, India. *J Mycol.*, **2015**: Article ID 382476.

Lin W-Y, Yang MJ, Hung L-T and Lin L-C. 2013. Antioxidant properties of methanol extract of a new commercial gelatinous mushrooms (white variety of *Auricularia fuscosuccinea*) of Taiwan. *African J Biotechnol.*, **12(43)**: 6210–6221.

Lourenço SC, Moldão-Martins M and Alves VD. 2019. Antioxidants of Natural Plant Origins: From Sources to Food Industry Applications. *Molecules*, **24(22)**: 4132.

Neha K, Haider MR, Pathak A and Yar MS. 2019. Medicinal prospects of antioxidants: A review. *Eur J Med Chem.*, **178**: 687–704

Petrović P, Vunduk J, Klaus A, Kozarski M, Nikšić M, Žižak Ž, Vuković N, Šekularac G, Drmanić S and Bugarski B. 2016. Biological potential of puffballs: a comparative analysis. *J Funct Foods*, **21**: 36–49.

Sharifi-Rad M, Anil Kumar NV, Zucca P, Varoni EM, Dini L, Panzarini E, Rajkovic J, Tsouh Fokou PV, Azzini E, Peluso I, Prakash Mishra A, Nigam M, El Rayess Y, Beyrouthy ME, Polito L, Iriti M, Martins N, Martorell M, Docea AO, Setzer WN, Calina D, Cho WC and Sharifi-Rad J. 2020. Lifestyle, oxidative stress, and antioxidants: Back and forth in the pathophysiology of chronic diseases. *Front Physiol.*, **11**: 694.

Singha K, Banerjee A, Pati BR and Das Mohapatra PK. 2017. Eco-diversity, productivity and distribution frequency of mushrooms in Gurguripal Eco-forest, Paschim Medinipur, West Bengal, India. *Curr Res Environ Appl Mycol.*, **7(1):** 8–18.

Thakur A, Singh S and Puri S. 2021. Nutritional evaluation, phytochemicals, antioxidant and antibacterial activity of *Stellaria monosperma* Buch.-Ham. ex D. Don and *Silene vulgaris* (Moench) Garcke: wild edible plants of Western Himalayas. *Jordon J Biol Sci.*, **14(1)**: 83–90.

Tripathi NN, Singh P and Vishwakarma P. 2017. Biodiversity of macrofungi with special reference to edible forms: a review. *J Indian Bot Soc.*, **96(3)**: 144–187.

Yuwa-Amornpitak T, Butkhup L and Yeunyaw P-N. 2020. Amino acids and antioxidant activities of extracts from wild edible mushrooms from a community forest in the Nasrinual District, Maha Sarakham, Thailand. *Food Sci Technol.*, **40(3):** 712–720.

Zeb M and Lee CH. 2021. Medicinal properties and bioactive compounds from wild mushrooms native to North America. *Molecules*, **26(2)**: 251.

Jordan Journal of Biological Sciences

A Pilot Study: Ground and Aqueous Extract of *Leptadenia* pyrotechnica Modulate the Immune System Affecting White Blood Cell Counts and Increasing Red Blood Cell Counts

Sawsan H. Mahassni*, Bushra S. Alsahafi

 $^{1}Department\ of\ Biochemistry,\ Faculty\ of\ Science,\ King\ Abdualziz\ University,\ Jeddah,\ Saudi\ Arabia$

Received: June 17, 2021; Revised: October 6, 2021; Accepted: October 27, 2021

Abstract

Leptadenia pyrotechnica (Forssk.) Decne. (LP) is used in local folk medicine for the treatment of different ailments. There are no published studies on the hematological and immune system effects of LP. This study is the first to determine the acute toxicity of LP extract and the effects of ground and aqueous LP extracts on red blood cell (RBC), and total and differential white blood cells counts in rats. Ground LP mixed with the regular diet at 25%, 50% and 75% LP weight/feed weight was administrated to six young adult Wistar albino rats (one female and one male rat per concentration), while control rats were fed the regular feed, daily for one week. Aqueous LP extracts were orally gavaged at 3, 9, 15 and 20 g/kg body weight to 16 rats (two female and two male rat per concentration), while control rats were gavaged with water, daily for two weeks. Blood samples were collected for the determination of blood cells counts and percents. Results were compared with the controls. The extract was safe up to a dose of 40 g/kg body weight. Rats that consumed ground LP had significantly higher neutrophil and monocyte counts and percents, and lower lymphocyte percent and eosinophil counts and percents. Rats that consumed extracts had significantly higher RBC counts and neutrophil counts and percents, and lower lymphocyte percent and eosinophil counts and percents. Therefore, ground and extracts of LP affect blood cells counts and may modulate the immune system, while only the extract increases RBC counts.

Keywords: Leptadenia pyrotechnica, Lymphocytes, Neutrophils, Red blood cells, White blood cells

1. Introduction

Leptadenia pyrotechnica (Forssk.) Decne. (LP), a desert plant of the family Asclepiadaceae, is a valuable medicinal plant. It is known as "markh" in Arabic, and it grows in equatorial regions of Asia, Africa and in the sandy plains in the nations of the Western Arabian Gulf (Khasawneh et al., 2015). It is a shrub, with a height of 0.5 to 2.6 meters, that has many green branches but no leaves. The season of flowering and fruiting begins in August and lasts to the end of January (Verma et al., 2014). There are five chief active compounds found in all parts of LP, namely cardiac glycosides (Youssef Moustafa et al., 2009), alkaloids, flavonoids, tannins and saponins (Munazir et al., 2015). The stem contains polyphenolic compounds (Mohammad et al., 2011; Preet and Chand Gupta, 2018), steroids, terpenes, fatty acids (Youssef Moustafa et al., 2007), and other chemical compounds

LP is used locally in Saudi Arabia and other Arab countries to add flavor to some foods and as a vegetable. Its stem has been used in traditional medicine to treat several diseases, including tuberculosis (using the water extract) (Patel *et al.*, 2014); smallpox, psoriasis and diabetes (using the sap of young stems) (Verma *et al.*, 2014); dermatitis, kidney disorders, cough, urinary retention, constipation, abortion and cancer (Bhabootra,

2016). Although there is no scientific evidence, LP may have some effects on the immune system since it is used for the treatment of wounds, (Upadhyay *et al.*, 2007), rheumatism (Bhabootra, 2016), the common cold, eczema and other skin diseases (Katewa and Galav, 2006).

The immune system is one of the most important and complex systems in the body, affecting other systems of the body and general health. The main function of the immune system is to protect the body from pathogens, while the functional failure of the immune system results in many diseases (Rasheed et al., 2016). The immune system is made up of different cells, molecules, and organs. The two main types of immune responses mediate their effects and actions through different molecules and cells. The cells that are important in innate immunity are most of the white blood cells (WBC), such as neutrophils, monocytes, eosinophils and basophils, while in the adaptive immunity the lymphocytes are the major WBC (Hillion et al. 2019). Therefore, it is possible to modify the activity of the immune response by affecting the counts of WBC by natural plants, which has received wide attention recently.

Presently, most suppressive immune modulators, such as chemotherapeutic drugs, have cytotoxic effects that limit their repeated use (Kumolosasi *et al.*, 2018). On the other hand, there are many plants and seeds that have been used in folk and traditional medicinal systems worldwide

^{*} Corresponding author. e-mail: sawsanmahassni@hotmail.com.

for thousands of years for the enhancement of the immune system. Some of these medicinal plants and seeds are black seeds, garden cress seeds, soybean, curcumin and Moringa oleifera (Osman, Shayoub and Babiker, 2012; Ghori et al., 2018). Most medicinal plants that have immunomodulatory activities are considered harmless, thus they can be used as alternative medicines for the treatment of a variety of diseases (Ghori et al., 2018) and for their useful effects (Mahassni and Al-Reemi, 2013; ; Mahassni and Khudauardi, 2017; Mahassni and Bukhari, 2019; ; Mahassni and Munshi, 2019; Mahassni and Nabulsi, 2020).

Research studies on LP are limited (Algasoumi et al., 2012; Munazir et al., 2012; Khasawneh et al., 2015), with the alcoholic extract being the form that has been used. In addition, there is only one study (Alsahafi and Mahassni, 2021) on the effects of LP aqueous extracts on the immune system, where it was found to suppress innate immune responses and enhance adaptive immune responses. The specific active components in LP that may be responsible for these effects are probably the alkaloids, which have immunostimulant activity, and the flavonoids, which possess anti-inflammatory and immunomodulatory effects. Other studies have been done on the antioxidant (Alqasoumi et al., 2012) and antibacterial activities (Munazir et al., 2012), and antiatherosclerotic and hypolipidemic effects (Jain et al., 2007) of the alcoholic extracts of LP. Additionally, the LP alcoholic extracts have been shown to have anticancer effects against human breast cancer cells (Khasawneh et al., 2011) and colon cancer cells (Khasawneh et al., 2015).

It is important to ensure the safety and efficacy of medicinal plants before utilizing them for the treatment of diseases and ills. A critical step to ensure the validity of medications is to perform acute toxicity testing in animal models. All toxicity studies on LP have been done on alcoholic extracts only (Watafua and Geidam, 2014; Rasheed *et al.*, 2016). The present study is the first to carry a toxicity study on the LP aqueous extract.

Thus, there are no published research studies using ground or aqueous extracts of LP, none on their effects on the immune system cells, and only one published study on the effects of LP aqueous extracts on the immune responses in rats (Alsahafi and Mahassni, 2021). This study aimed to determine the non-toxic doses of the aqueous LP extract, by using the acute toxicity assay, and the suitability of using ground or water extract of LP in rats. Using the optimal LP form (either ground or water extract), we aimed to investigate the effects of LP on the immune system cell counts and red blood cell (RBC) counts. This may aid in determining the best method for human use for the treatment of different ailments and if, in fact, LP affects the counts of cells of the immune system and red blood cells.

2. Materials and methods

2.1. Collection of LP stems and preparation of the LP aqueous extract

Young LP stems were collected from the Khulais governorate, Makkah, Saudi Arabia during the third week of September 2020. The plants collected was verified by a taxonomist to be *leptadenia pyrotechnica* (Forssk.) Decne.

The stems were cleaned thoroughly under running water and finally rinsed with distilled water.

The aqueous extract was prepared by boiling 500 g of young LP stems, that have been cut into small pieces, in 1 L of water for 5 minutes as per the previously described folk medicine method (Patel *et al.*, 2014). The hot water extract was filtered using cotton balls. The yield of the LP extraction was 0.476 ml extract/g LP (47.6%). Subsequently, the LP extract was allowed to air dry for two days resulting in a semisolid precipitate that is green to brown in color. The yield of the precipitate was 0.60 g LP precipitate/ml LP extract (60%). Finally, this precipitate was stored in an airtight bottle at 4°C for about one week. Fresh batches were prepared weekly.

2.2. Preparation of ground LP diets

Fresh young LP stems were collected and allowed to air dry for one week. The dry LP stems and the pellets of the standard animal diet (Grain Silos and Flour Mills Organization, Jeddah, KSA) were separately ground into powder using a seed grinder. Three different concentrations of ground LP (25%, 50% and 75%) were mixed with the ground animal diet separately. Subsequently, these diets were manually formed into pellets, by the addition of a small amount of water, and they were allowed to air dry in the shade for three days.

2.3. Acute toxicity assay of LP extract

Acute toxicity was determined for the LP aqueous extract according to the Organization for Economic Cooperation and Development (2001) Guidelines for testing of chemicals: acute oral toxicity–acute toxic class method-guideline 423, Paris.

Healthy female adult Wistar albino rats that were used for the assay were allowed to acclimate in the laboratory for one week. After this adaption period, rats were weighed (weights ranged 190-210 g), and they were divided into four groups with three rats for each group. The rats were denied feed for a fasting period of 12 hours. Subsequently, the control group rats were orally administered with a 3 ml of water once. The three remaining groups [toxicity concentrations groups (TC)] were each administered with a single dose of dried LP extract, dissolved in 3 ml of water, at concentrations of 5, 20 and 40 g LP/kg body weight. The rats were monitored daily for 14 days for any signs of toxicity. The body weights for all rats were measured before and after the start of the test. In addition, the feed and water intakes were measured daily for each group.

2.4. Pilot study design and collection of blood samples

Twenty-eight healthy Wistar albino rats (with an equal number of female and male rats), at weights of about 170-250 g, were used for this study. Rats were obtained from the in-house animal facility of the King Abdulaziz University, Jeddah, Saudi Arabia. Rats were given free access to water and the regular laboratory animal feed (Grain Silos and Flour Mills Organization, Jeddah, Saudi Arabia), and they were maintained at room temperature and exposed to the natural light-dark cycle. After an adaption period of one week, eight rats were equally divided into four groups (LPG 1, LPG 2, LPG 3, and control), with one female and one male rat per group. The groups were administered ground LP mixed with the regular rat diet at three different concentrations (25%,

50%, 75% ground LP), while the control group was given the regular diet without any LP. Fresh food was given daily for an experimental period of one week.

For the LP aqueous extract groups (LPE 1, LPE 2, LPE 3, LPE 4, and control), 20 rats were equally divided into the five groups, with two females and two males per group. Each group of rats was gavaged with one of four different concentrations of the extract (3, 9, 15, and 20 g/kg, respectively), while the control rats were gavaged with 3 ml of water, daily for 2 weeks. On the 7th and 14th days, whole blood samples were withdrawn from the rats, under anesthesia with diethyl ether, from the retro orbital plexus using heparinized capillary tubes. Blood samples were collected in ethylenediamine tetraacetic acid vacutainer test tubes for the determination of the total and differential WBC and RBC counts.

2.5. Complete and differential blood counts

Total and differential WBC and RBC counts were done manually at King Fahd Center for Medical Research, Jeddah, Saudi Arabia. RBC and WBC were counted by using a hemocytometer under 40x magnification. Blood samples were diluted (1:20) with Turk's solution for the WBC counts and Hayem's solution (1:200) for the RBC counts. The differential WBC counts were counted under 100x magnification by using frosted slides and Rapi-diff II

stain (Atom Scientific, Cheshire, Hyde, United States of America).

2.6. Statistical analysis

The MegaStat (Version 9.4, Butler University, Indianapolis, Indiana, United States of America) statistical program was used for the analysis of the data. The data were expressed as mean \pm standard deviation (SD). The pairwise *t*-test was used for the significance testing between groups for all of the parameters. The statistical difference was considered significant for P < 0.05, highly significant for P < 0.01 and non-significant for P > 0.05.

3. Results

3.1. Acute toxicity assay of LP extract

There was no evidence of toxicity for the extract doses used, and thus the extract is considered safe up to a dose of 40 g/kg body weight. Body weight, water and feed intakes for the groups are show in Table 1. Compared to the control group, there were no significant differences in the mean final and initial body weights, and water and feed intakes for the acute toxicity groups. Additionally, there were no significant differences between the mean final and initial body weights for all groups.

Table 1: Initial and final body weights, water and feed intakes, and toxicity signs for all experimental groups.

Variables	Groups	n	Mean ± SD	P-value ^a	P-value b
Initial body weight (g)	Control	3	200.01 ± 12.58		0.069 (NS)
	TC 1	3	201.00 ± 11.94	0.846 (NS)	0.836 (NS)
	TC 2	3	204.45 ± 15.01	0.700 (NS)	0.880 (NS)
Final body weight (g)	TC 3	3	212.33 ± 7.64	0.265 (NS)	0.188 (NS)
Timar oody weight (g)	Control	3	204.00 ± 7.28		
	TC 1	3	203.21 ± 11.39	0.831 (NS)	
	TC 2	3	205.00 ± 15.01	0.887 (NS)	
Water intake (ml)	TC 3	3	213.53 ± 8.74	0.351 (NS)	
	Control	3	81.68 ± 8.88		
	TC 1	3	83.00 ± 6.43	0.544 (NS)	
Feed intake (g)	TC 2	3	81.65 ± 8.12	0.759 (NS)	
	TC 3	3	80.00 ± 6.43	0.647 (NS)	
	Control	3	62.48 ± 1.24		
	TC 1	3	61.35 ± 2.56	0.399 (NS)	
	TC 2	3	62.12 ± 1.33	0.247 (NS)	
	TC 3	3	60.92 ± 3.41	0.247 (NS)	

Pairwise t-test was used for the significance testing; a: between the groups and the control; b: between final and initial body weights for each group

TC: Toxicity concentration group; NS: Non-significant; SD: Standard deviation

3.2. Pilot study

3.2.1. Complete and differential blood counts for the ground LP groups

Table 2 shows the mean total WBC and RBC counts for the ground LP groups. It is apparent that there were no significant differences in the mean counts of WBC and RBC for each group compared with the respective control.

Results in Table 3 show the effects of ground LP on the differential counts for the groups compared with the control. The percent and absolute count of neutrophils was

significantly higher for the LPG 3 group compared with the respective control. Lymphocytes percent for the LPG 3 group was significantly lower compared with the control. The percent and absolute count of monocytes were highly significantly higher for the LPG 3 group compared with the respective control. Eosinophils percent and absolute counts for all the experimental groups were highly significantly lower compared with the respective control. All other group comparisons were not significantly different compared to the respective controls.

Table 2: Mean total WBC and RBC counts for the ground LP groups.

Parameter	Group	n	$Mean \pm SD$	P-value
WBC	Control	2	10.22 ± 1.09	
$(\times 10^3 \text{ cell/}\mu\text{l})$	LPG 1	2	11.75 ± 3.04	0.696 (NS)
	LPG 2	2	12.07 ± 0.74	0.637 (NS)
	LPG 3	2	11.22 ± 6.47	0.796 (NS)
RBC	Control	2	9.61 ± 1.86	
$(\times 10^6 \text{ cell/}\mu\text{l})$	LPG 1	2	0.69 ± 8.40	0.570 (NS)
	LPG 2	2	9.76 ± 0.31	0.651 (NS)
	LPG 3	2	9.50 ± 1.41	0.796 (NS)

Pairwise *t*-test was used for the significance testing between the groups and the control

WBC: White blood cells; RBC: Red blood cells; LPG: Ground LP group; NS: Non-significant; SD: Standard deviation

Table 3: Differential mean WBC counts and percents for the ground LP groups.

Parameter	Group	n	Mean ± SD	P-value	
Neutrophils	Control	2	2.27 ± 0.20		
$(\times 10^3 \text{ cell/}\mu\text{l})$	LPG 1	2	2.16 ± 0.50	0.905 (NS)	
	LPG 2	2	2.55 ± 0.06	0.771 (NS)	
	LPG 3	2	4.34 ± 2.60	0.049 (S)	
Neutrophils	Control	2	23.50 ± 4.95		
(%)	LPG 1	2	24.50 ± 0.71	0.846 (NS)	
	LPG 2	2	31.00 ± 2.83	0.195 (NS)	
	LPG 3	2	38.50 ± 7.78	0.036 (S)	
Lymphocytes	Control	2	6.92 ± 1.17		
$(\times 10^3 \text{ cell/}\mu\text{l})$	LPG 1	2	6.25 ± 1.09	0.455 (NS)	
	LPG 2	2	5.47 ± 0.46	0.120 (NS)	
	LPG 3	2	5.66 ± 1.78	0.171 (NS)	
Lymphocytes	Control	2	70.00 ± 5.77		
(%)	LPG 1	2	71.50 ± 2.89	0.729 (NS)	
	LPG 2	2	66.00 ± 2.31	0.363 (NS)	
	LPG 3	2	56.50 ± 9.81	0.007 (HS)	
Monocytes	Control	2	0.24 ± 0.03		
$(\times 10^3 \text{ cell/}\mu\text{l})$	LPG 1	2	0.33 ± 0.21	0.315 (NS)	
	LPG 2	2	0.20 ± 0.03	0.649 (NS)	
	LPG 3	2	0.52 ± 0.09	0.006 (HS)	
Monocytes	Control	2	2.50 ± 0.58		
(%)	LPG 1	2	3.05 ± 1.73	0.294 (NS)	
	LPG 2	2	2.50 ± 0.58	0.294 (NS)	
	LPG 3	2	5.50 ± 1.73	0.006 (HS)	
Eosinophils	Control	2	0.33 ± 0.13		
$(\times 10^3 \text{ cell/}\mu\text{l})$	LPG 1	2	0.05 ± 0.05	0.000 (HS)	
	LPG 2	2	0.04 ± 0.04	0.000 (HS)	
	LPG 3	2	0.09 ± 0.07	0.002 (HS)	
Eosinophils	Control	2	3.50 ± 1.73		
(%)	LPG 1	2	0.50 ± 0.58	0.001 (HS)	
	LPG 2	2	0.50 ± 0.58	0.001 (HS)	
	LPG 3	2	0.80 ± 0.50	0.002 (HS)	
Basophils	Control	2	0.00 ± 0.00		
$(\times 10^3 \text{ cell/}\mu\text{l})$	LPG 1	2	0.00 ± 0.00	1.000 (NS)	
	LPG 2	2	0.00 ± 0.00	1.000 (NS)	
	LPG 3	2	0.00 ± 0.00	1.000 (NS)	
Basophils	Control	2	0.00 ± 0.00		
(%)	LPG 1	2	0.00 ± 0.00	1.000 (NS)	
	LPG 2	2	0.00 ± 0.00	1.000 (NS)	
	LPG 3	2	0.00 ± 0.00	1.000 (NS)	

Pairwise *t*-test was used for the significance testing between the groups and the control

LPG: Ground LP group; S: Significant; HS: Highly significant; NS: Non-significant; SD: Standard deviation

3.2.2. Complete and differential blood counts for the LP extract groups

The mean total WBC and RBC counts for the LP groups after 7 and 14 days compared with the respective controls are shown in Table 4. After 7 days, no significant differences were found between the mean WBC counts for all experimental groups and the control. On the other hand, the mean RBC counts were highly significantly higher for the LPE 4 group compared with the control. For the mean counts after 14 days, the WBC counts showed no significant differences between the groups and the control. However, the mean RBC counts were significantly higher for the LPE 2 and LPE 3 groups and highly significantly higher for the LPE 4 group compared to the control.

Table 5 shows the mean differential counts for the LP extract groups after 7 and 14 days, compared with the control. It was found that after 7 days only the mean neutrophil and eosinophil counts and percents showed significant differences compared to the respective controls. The absolute mean counts for neutrophils, compared to the

control, for the LPE 3 and LPE 4 groups were significantly higher. On the other hand, the mean percent of neutrophils was significantly higher for the LPE 4 group compared with the control. Mean eosinophil counts were significantly lower for the LPE 1, LPE 2 and LPE 3 groups compared with the control. The mean percent count for eosinophils was significantly lower for the LPE1 and LPE 2 groups compared to the control. All other group comparisons were not significantly different compared to the respective controls.

Results for effect of LP extract on differential counts for the groups after 14 day (Table 5) were fewer than after 7 days. The only significant differences were found for mean neutrophil counts and percents, and mean lymphocyte percents and only for the LPE 4 group compared to the control. The mean absolute count and percent of neutrophils for the LPE 4 group were highly significantly higher compared to the respective controls. The mean lymphocyte percent for the LPE 4 group was highly significantly lower compared to that of the control.

Table 4: Mean total WBC and RBC counts for the LP extract groups after 7 and 14 days.

			7 th day		14 th day	
Parameter	Group	n	$\text{Mean} \pm \text{SD}$	P-value	$Mean \pm SD$	P-value
WBC	Control	4	13.44 ± 1.07		15.85 ± 1.32	
$(\times 10^3 \text{ cell/}\mu\text{l})$	LPE 1	4	15.48 ± 9.37	0.282 (NS)	16.26 ± 3.47	0.488 (NS)
	LPE 2	4	14.88 ± 3.89	0.442 (NS)	15.96 ± 3.35	0.575 (NS)
	LPE 3	4	10.15 ± 0.72	0.092 (NS)	15.10 ± 4.61	0.817 (NS)
	LPE 4	4	10.45 ± 2.96	0.123 (NS)	14.25 ± 3.65	0.595 (NS)
RBC	Control	4	$8.06 \pm\ 0.952$		8.05 ± 1.04	
(×10 ⁶ cell/μl)	LPE 1	4	7.91 ± 0.593	0.892 (NS)	10.50 ± 1.39	0.050 (NS)
	LPE 2	4	9.80 ± 2.458	0.119 (NS)	11.11 ± 1.56	0.023 (S)
	LPE 3	4	9.36 ± 1.859	0.235 (NS)	10.95 ± 1.36	0.017 (S)
	LPE 4	4	11.03 ± 0.552	0.012 (HS)	11.88 ± 2.43	0.004 (HS)

Pairwise *t*-test was used for the significance testing between the groups and the control

WBC: White blood cells; RBC: Red blood cells; LPE: LP aqueous extract group; S: Significant; HS: Highly significant; NS: Non-significant; SD: Standard deviation

Table 5: Differential mean WBC counts for the LP extract groups after 7 and 14 days.

Group		7 th day		14 th day	14 th day	
	n	$Mean \pm SD$	P-value	Mean ± SD	P-value	
Control	4	1.48 ± 0.38		1.42 ± 0.27		
LPE 1	4	1.55 ± 0.12	0.798 (NS)	1.29 ± 0.56	0.798 (NS)	
LPE 2	4	1.82 ± 0.45	0.158 (NS)	1.62 ± 0.17	0.407 (NS)	
LPE 3	4	2.57 ± 0.40	0.000 (HS)	2.06 ± 1.15	0.143 (NS)	
LPE 4	4	2.91 ± 0.08	0.000 (HS)	2.47 ± 0.70	0.021 (HS)	
Control	4	19.70 ± 3.86		22.33 ± 2.31		
	4	24.00 ± 2.16	0.313 (NS)	25.50 ± 3.70	0.282 (NS)	
LPE 2	4	24.80 ± 6.95	0.238 (NS)	26.50 ± 4.04	0.163 (NS)	
LPE 3	4	26.00 ± 5.85	0.076 (NS)	27.00 ± 4.00	0.145 (NS)	
LPE 4	4	30.80 ± 9.88	0.016 (S)	34.33 ± 3.86	0.001 (HS)	
Control	4	5.40 ± 0.26		4.55 ± 0.26		
LPE 1	4	4.84 ± 0.83	0.611 (NS)	4.60 ± 1.28	0.957 (NS)	
LPE 2	4	5.05 ± 1.48	0.754 (NS)	4.13 ± 1.30	0.661 (NS)	
LPE 3	4	6.95 ± 0.68	0.169 (NS)	4.85 ± 1.44	0.773 (NS)	
LPE 4	4	6.98 ± 2.85	0.162 (NS)	4.29 ± 0.99	0.781 (NS)	
Control	4	72.66 ± 2.06		72.00 ± 2.16		
LPE 1	4	72.66 ± 0.96	1.000 (NS)	71.80 ± 5.65	0.936 (NS)	
LPE 2	4	71.25 ± 5.56	0.755 (NS)	68.50 ± 5.62	0.272 (NS)	
LPE 3	4	70.25 ± 6.13	0.604 (NS)	66.77 ± 3.69	0.108 (NS)	
LPE 4	4	64.70 ± 12.23	0.111 (NS)	59.80 ± 4.11	0.001 (HS)	
Control	4	0.44 ± 0.18		0.29 ± 0.14	` /	
LPE 1	4		0.053 (NS)		0.821 (NS)	
LPE 2			` ′		0.840 (NS)	
LPE 3					0.186 (NS)	
LPE4					0.363 (NS)	
Control			` ,		, ,	
LPE 1			0.063 (NS)		0.847 (NS)	
LPE 2					0.847 (NS)	
LPE 3					0.565 (NS)	
LPE 4	4				0.565 (NS)	
Control		0.10 ± 0.04	` ,	0.03 ± 0.02	,	
LPE 1		0.02 ± 0.03	0.022 (S)	0.02 ± 0.04	0.873 (NS)	
LPE 2					0.657 (NS)	
LPE 3	4		` ′		0.812 (NS)	
LPE 4	4		` ′		0.949 (NS)	
Control	4	1.66 ± 0.58	` ,		,	
LPE 1	4		0.040 (S)		0.832 (NS)	
LPE 2					1.000 (NS)	
LPE 3			` ′		0.832 (NS)	
LPE 4			` ′		0.497 (NS)	
Control			()		v. v, (- · -)	
LPE 1			0.134 (NS)		0.269 (NS)	
					0.293 (NS)	
					1.000 (NS)	
LPE 4					1.000 (NS)	
			0.13+ (113)		1.000 (113)	
			0.134 (NS)		1.000 (NS)	
LPE 2	4	0.00 ± 0.00 0.00 ± 0.00	0.134 (NS) 0.134 (NS)	0.30 ± 0.50 0.30 ± 0.50	1.000 (NS) 1.000 (NS)	
	4	0.00 ± 0.00	U.134 (NS)	0.50 ± 0.50	1.000 (113)	
LPE 3	4	0.00 ± 0.00	0.134 (NS)	0.00 ± 0.00	0.375 (NS)	
	Control LPE 1 LPE 2 LPE 3 LPE 4 Control LPE 1	N Control 4 LPE 1 4 LPE 2 4 LPE 3 4 LPE 4 Control 4 LPE 1 4 LPE 2 4 LPE 3 4 LPE 4 Control 4 LPE 1 4 LPE 2 4 LPE 3 4 LPE 4 Control 4 LPE 1 4 LPE 2 4 LPE 3 4 LPE 4 Control 4 LPE 1 4 LPE 2 4 LPE 3 4 LPE 4 Control 4 LPE 1 4 LPE 2 4 LPE 3 4 LPE 4 Control 4 LPE 1 4 LPE 2 4 LPE 3 4 LPE 4 Control 4 LPE 1 4 LPE 2 4 LPE 3 4 LPE 4 Control 4 LPE 1 4 LPE 2 4 LPE 3 4 LPE 4 Control 4 LPE 1 4 LPE 2 4 LPE 3 4 LPE 4 Control 4 LPE 1 4 LPE 2 4 LPE 3 4 LPE 4 Control 4 LPE 1 4 LPE 2 4 LPE 3 4 LPE 4 Control 4 LPE 1 4 LPE 2 4 LPE 3 4 LPE 4 Control 4 LPE 1 4 LPE 2 4 LPE 3 4 LPE 4 Control 4 LPE 1 4 LPE 2 4 LPE 3 4 LPE 4 Control 4 LPE 1 4 LPE 2 4 LPE 3 4 LPE 4 Control 4 LPE 1 4 LPE 2 4 LPE 3 4 LPE 4 Control 4 LPE 1 4 LPE 2 4 LPE 3 LPE 4 Control 4 LPE 1 4 LPE 2 4 LPE 3 LPE 4 Control 4 LPE 1 4 LPE 2 4 LPE 3 LPE 4 Control 4 LPE 1 4 LPE 2 4 LPE 3 LPE 4 Control 4 LPE 1 4 LPE 2 4 LPE 3 LPE 4 Control 4 LPE 1 4 LPE 2 4 LPE 3 LPE 4 Control 4 LPE 1 LPE 3 LPE 4 Control 4 LPE 2 LPE 3 LPE 4 LPE 3 LPE 4	N Mean ± SD Control 4 1.48 ± 0.38 LPE 1 4 1.55 ± 0.12 LPE 2 4 1.82 ± 0.45 LPE 3 4 2.57 ± 0.40 LPE 4 4 2.91 ± 0.08 Control 4 19.70 ± 3.86 LPE 1 4 24.00 ± 2.16 LPE 2 4 24.80 ± 6.95 LPE 3 4 26.00 ± 5.85 LPE 4 4 30.80 ± 9.88 Control 4 5.40 ± 0.26 LPE 1 4 4.84 ± 0.83 LPE 2 4 5.05 ± 1.48 LPE 3 4 6.95 ± 0.68 LPE 4 4 6.98 ± 2.85 Control 4 72.66 ± 2.06 LPE 3 4 72.66 ± 2.06 LPE 1 4 72.66 ± 2.06 LPE 2 4 71.25 ± 5.56 LPE 3 4 70.25 ± 6.13 LPE 4 4 64.70 ± 12.23 Control 4 0.	Control 4 1.48 ± 0.38 P-value LPE 1 4 1.55 ± 0.12 0.798 (NS) LPE 2 4 1.82 ± 0.45 0.158 (NS) LPE 3 4 2.57 ± 0.40 0.000 (HS) LPE 4 4 2.91 ± 0.08 0.000 (HS) Control 4 19.70 ± 3.86 LPE 1 LPE 1 4 24.00 ± 2.16 0.313 (NS) LPE 2 4 24.80 ± 6.95 0.238 (NS) LPE 3 4 26.00 ± 5.85 0.076 (NS) LPE 4 4 30.80 ± 9.88 0.016 (S) Control 4 5.40 ± 0.26 LPE 1 4 4.84 ± 0.83 0.611 (NS) LPE 2 4 5.05 ± 1.48 0.754 (NS) LPE 3 4 6.95 ± 0.68 0.169 (NS) LPE 3 4 6.95 ± 0.68 0.169 (NS) LPE 3 4 6.95 ± 0.68 0.169 (NS) LPE 4 4 6.98 ± 2.85 0.162 (NS) 0.162 (NS) Control 4 72.66 ± 2.06	Control 4 1.48 ± 0.38 1.42 ± 0.27 LPE I 4 1.55 ± 0.12 0.798 (NS) 1.29 ± 0.56 LPE 2 4 1.82 ± 0.45 0.158 (NS) 1.62 ± 0.17 LPE 3 4 2.57 ± 0.40 0.000 (HS) 2.06 ± 1.15 LPE 4 4 2.91 ± 0.08 0.000 (HS) 2.47 ± 0.70 Control 4 19.70 ± 3.86 22.33 ± 2.31 LPE 1 4 24.00 ± 2.16 0.313 (NS) 25.50 ± 3.70 LPE 2 4 24.80 ± 6.95 0.238 (NS) 26.50 ± 4.04 LPE 3 4 26.00 ± 5.85 0.076 (NS) 27.00 ± 4.00 LPE 4 4 30.80 ± 9.88 0.016 (S) 34.33 ± 3.36 Control 4 5.40 ± 0.26 4.55 ± 0.26 LPE 1 4 4.84 ± 0.83 0.611 (NS) 4.60 ± 1.28 LPE 2 4 5.05 ± 1.48 0.754 (NS) 4.13 ± 1.30 LPE 3 4 6.95 ± 0.68 0.169 (NS) 4.85 ± 1.44 LPE 3 4	

Pairwise *t*-test was used for the significance testing between the groups and the control

 $LPE: LP\ aqueous\ extract\ group;\ S:\ Significant;\ HS:\ Highly\ significant;\ NS:\ Non-significant;\ SD:\ Standard\ deviation$

4. Discussion

This research study is the first to determine the acute toxicity, RBC counts, and total and differential WBC counts in rats given ground or aqueous extract of LP. The ground and aqueous extract of LP were used since they are the most commonly used forms of LP in humans in folk and traditional medicinal systems, although there is no scientific evidence of their beneficial effects. In addition, they are the most easily accessible forms for self-healing and treatment at home. Additionally, the stem was the only part of the plant used for the study since only the stem is used in folk medicine and, more importantly, the stem contains more active ingredients than other parts of the plant. The acute toxicity assay and the pilot study were carried to determine whether the ground or aqueous extract of LP is more effective at inducing changes in the counts of the immune system cells in rats and to determine the appropriate concentrations to use.

There are no previous scientific studies on the effects of ground or aqueous extracts of LP on the counts of cells involved in the immune system in humans or laboratory animals. On the other hand, only one previous study used the aqueous extract of LP for immune response parameters, although the complete and differential blood counts were not determined (Alsahafi and Mahassni, 2021). In addition, there were only two studies (Watafua and Geidam, 2014; Rasheed *et al.*, 2016) that determined the acute toxicity of the alcoholic extracts of LP, while none used aqueous extracts. Therefore, we were unable to compare any of the current findings with those of other previous researchers.

In the acute toxicity study, it is recommended by the Organization for Economic Co-operation Development Guidelines (2002) to test any substance in laboratory animals at concentrations of 0.0005 g/kg body weight and up to 2 g/kg body weight. In some circumstances, it is allowed to use concentrations of 2-5 g/kg body weight. Therefore, in this study the toxicity of the LP extract was tested starting at 5 g/kg body weight, which is the recommended upper limit for the doses, and up to 40 g/kg body weight, with no detectable toxicity. This was expected since LP is commonly eaten by humans in large amounts with no adverse reactions. In addition, the rat dose, based on the recommended dose used for humans in folk medicine (Patel et al., 2014), is 1,86 g/kg. Thus, it was decided to use a little more than double this dose (3 g/kg body weight) for the lowest dose administered to the rats and to use 20 g/kg body weight as the highest dose, which is 11 times the rat dose.

In the acute toxicity assay, the mean initial and final body weights, and mean water and feed consumptions were not significantly different between all groups. Furthermore, there were no significant differences between the final and initial body weights for each group. Additionally, no signs of toxicity were observed in rats for all used extract concentrations. The signs of toxicity according to the Organization for Economic Co-operation and Development Guidelines (2002) that are commonly observed might be increased sleep, coma, salivation, mortality, convulsions, diarrhea, tremors, lacrimation, writhing reflex, and any changes in motor activity and patterns of behavior. These results are in agreement with

the previous acute toxicity study in mice (Rasheed *et al.*, 2016) using different doses of the methanol LP extract, which found that doses up to 10 g LP/kg body weight were safe. A study (Watafua and Geidam, 2014) that is in disagreement with the present results showed slight toxic effects of the ethanolic LP extract in rats at 50, 100 and 150 mg/kg body weight.

For the pilot study, it was planned that both the ground and aqueous LP extract would be administered for two weeks, but it was observed within the first few days of the experiment that the rats that were given the ground LP were not consuming the expected amount of feed, and they were scattering it in the cage. In addition, their body weights were decreasing daily. As for the rats that were orally gavaged with the LP extract, they were consuming their regular diet normally and their weights were not decreasing. Therefore, it was decided not to continue the ground LP groups for the second week.

For the ground LP groups, the total mean WBC and RBC counts were not significantly different ($P \geq 0.05$) between the groups after one week of feeding. The mean neutrophil and monocyte counts and percents for the rats that were fed the highest percent of LP were significantly higher (P < 0.05 and P < 0.01) compared to the respective mean counts and percents for the control. The mean lymphocyte percent for the highest ground LP group, and the mean eosinophil counts and percents for all LP groups were significantly lower (P < 0.01) compared to the respective mean controls counts and percents.

As for the LP extract groups after 7 days, the mean total WBC counts were not significantly different ($P \ge 0.05$) between the groups, while the mean RBC counts were significantly higher (P < 0.01) for the LPE 4 group compared to the respective control. As for the differential blood counts, the mean neutrophil counts for the LPE 3 and 4 groups (P < 0.01) and mean neutrophil percents for the LPE 4 group (P < 0.05) were all significantly higher than the respective mean counts and percents for the respective controls. The mean eosinophil counts for the LPE 1, 2 and 3 groups (P < 0.05) and mean percents for the LPE 1 and 2 groups (P < 0.05) were significantly lower than the respective mean counts and percents for the respective controls.

As for the LP extract groups after 14 days, the mean total WBC counts were not significantly different ($P \ge 0.05$) between the groups, while the mean RBC counts for LPE 2 (P < 0.05), LPE 3 (P < 0.05) and LPE 4 groups (P < 0.01) were significantly higher compared to the means for the respective controls. For the LPE 4 group, the mean neutrophil count and percent (P < 0.01) were significantly higher and the mean lymphocyte percent (P < 0.01) was significantly lower compared to the respective mean counts and percents for the respective controls.

Therefore, it is apparent that most significant differences were found for the highest concentration of the ground and extract groups. In addition, there were some differences in the types of cells effected by ground LP and its extracts. When comparing the significant changes for the ground and extracts of LP, mean neutrophil and eosinophil counts and percents, and mean lymphocyte percents all showed the same significant differences. On the other hand, mean monocyte counts and percents behaved differently in the ground and extracts groups. In addition, the effects of the extracts were different after one

and two weeks. Thus, the duration of LP consumption is important since different periods lead to different effects.

The high mean neutrophil and monocyte counts for both the ground LP and its extract, compared to the controls, may be due to specific components in the two forms that may have enhancing effects on the immune system. Thus, LP might stimulate the bone marrow to generate and release more neutrophils and monocytes, specifically, into the blood (Ofem, Ani and Eno, 2012). On the other hand, LP may have inhibitory effects on the bone marrow, thus leading to the lower mean lymphocyte and eosinophil percents and counts.

On the other hand, compared to the control, the mean WBC counts were not significantly different at the end of the experimental periods for both ground and extracts of LP, although some of the individual white blood cells were significantly higher while others were significantly lower. Thus, the non-significance found for the WBC counts may be due to the canceling effects of higher and lower counts and percents of the different types of WBC.

The LP extracts may have some effects on the kidney, which might lead to the increased production of erythropoietin leading to increased production of RBC, as found in the current study. In addition, the tannins and flavonoids in PL are known to protect RBC from oxidative damage (Jorum *et al.*, 2016), thereby possibly leading to higher RBC counts. Therefore, as expected and as found in the current findings, the higher the dose of LP extract the higher the mean count of RBC.

Studies on other medicinal plants show similar results to the results of the current study. Ofem et al. (2012) used the aqueous extract of Ocimum gratissimum in rats for 28 days and found higher RBC and neutrophil counts and lower lymphocyte counts, in agreement with the current findings. A study (Jorum et al., 2016) using varying doses of the methanolic extracts of Carissa edulis leaf administered to rats, for different time periods up to 21 days, found significant increases in the monocyte and neutrophil cell counts, in agreement with our findings. On the other hand, in contradiction to our findings of lower counts, they found (Jorum et al., 2016) increased counts for lymphocytes and eosinophils. Finally, they also found increased WBC and basophil cell counts, while in the present findings there were no significant differences. The previous research study of Antai et al. (2009) on the ethanolic root extract of Gonglonema latifolium, given to rats for 14 days, resulted in a significant increase in the counts of monocytes in agreement with the current study. On the other hand, they found a significant increase in the WBC counts contradicting the no significant change in the present study. Finally, in contradiction to our findings, they found increased eosinophil counts and no significant differences for RBC counts, while we found lower eosinophil counts and higher RBC counts.

5. Conclusions

In conclusion, LP seems to be completely safe for consumption since high doses of the LP extract did not cause any toxic effects in rats. It is apparent that both the ground and extracts of LP modulate both the innate and acquired immune systems, while only the extract may be beneficial for increasing RBC counts. Furthermore, the extract led to different effects for the different durations of

consumption. Thus, it may be assumed, pending further studies, that the same effects may be found in humans. It is recommended that further studies be done in rats using higher concentrations of the aqueous extract and investigating other parameters and effects on the major organs of the body.

Funding

There are no sources of funding for this study.

Conflicts of interest/Competing interests

Both authors have no conflicts of interest/competing interests.

Availability of data and material

Data is available upon request.

References

Alsahafi BS and Mahassni SH. 2021. Leptadenia pyrotechnica aqueous extract suppresses innate immunity and enhances adaptive immunity in rats. International Journal of Pharmaceutical and Phytopharmacological Research, 11: 25-33.

Alqasoumi SI, Soliman G, Awaad AS and Donia A. 2012. Antiinflammatory activity, safety and protective effects of *Leptadenia* pyrotechnica, Haloxylon salicornicum and Ochradenus baccatus in ulcerative colitis. Phytopharmacology, 2: 58-71.

Antai AB, Ofem OE, Ikpi DE, Ukafia S and Agiang EA. 2009. Phytochemistry and some haematological changes following oral administration of ethanolic root extract of *Gonglonema latifolium* in rats. *Niger J Physiol Sci*, 24:79-83.

Bhabootra R. 2016. Important uses of *Leptadenia pyrotechnica* of Bikaner. *IJASEAT*, 4: 26-28.

Ghori SS, Ruqsar A, Akram M, Fatima Z and Arafath, MIA. 2018. Evaluation of Immunomodulatory activity of *Ficus dalhousiae* Miq leaves Methanolic extract against Cyclophosphamide Induced Myelosuppression. *Research J Pharm and Tech*, **11**: 3427-3430.

Hillion S, Arleevskay MI, Blanco P, Bordron A, Brooks WH, Cesbron JY, Kaveri S, Vivier E and Renaudineau Y. 2019. The innate part of the adaptive immune system. *Clin rev in allergy immu*, **58**: 1-4.

Jain G, Jhalani S, Agarwal S and Jain K. 2007. Hypolipidemic and antiatherosclerotic effect of *Leptadenia pyrotechnica* extract in cholesterol fed rabbits. *Asian J Exp Sci*, **21**: 115-122.

Jorum OH, Piero NM and Machocho AK. 2016. Haematological effects of dichloromethane-methanolic leaf extracts of *Carissa edulis* (Forssk.) Vahl in normal rat models. *J Hematol Thromboembolic Dis*, 4: 2-3.

Katewa SS and Galav PK. 2006. Additions to the traditional folk herbal medicines from Shekhawati region of Rajasthan. *Indian J Tradit Knowl*, **5**: 494-500.

Khasawneh MA, Koch A, Elwy HM, Hamza AA. and Schneider-Stock R. 2015. *Leptadenia pyrotechnica* induces p53-dependent apoptosis in colon cancer cells. *Nat Prod Chem Res*, 3: 1-8.

Khasawneh MA, Elwy HM., Hamza AA, Fawzi NM and Hassan AH. 2011. Antioxidant, anti-lipoxygenase and cytotoxic activity of *Leptadenia pyrotechnica* (Forssk.) decne polyphenolic constituents. *Molecules*, **16**:7510-7521.

Kumolosasi E, Ibrahim SNA, Shukri SMA. and Ahmad W. 2018. Immunostimulant activity of standardised extracts of Mangifera indica leaf and Curcuma domestica rhizome in mice. *Trop J Pharm Res*, 17:77-84.

Mahassni SH and Al-Reemi R. M. 2013. Apoptosis and necrosis of human breast cancer cells by an aqueous extract of garden cress (Lepidium sativum) seeds. *Saudi journal of biological sciences*, **20**: 131-139.

Mahassni SH and Bukhari OA. 2019. Beneficial effects of an aqueous ginger extract on the immune system cells and antibodies, hematology, and thyroid hormones in male smokers and non-smokers. *Journal of Nutrition & Intermediary Metabolism*, **15**: 10-17.

Mahassni SH and Khudauardi ER. 2017. A pilot study: The effects of an aqueous extract of Lepidium sativum seeds on levels of immune cells and body and organs weights in Mice. *J. Ayurvedic. Herb. Med*, **3**: 27-32.

Mahassni SH and Munshi MA. 2019. Ground Lepidium Sativum Linn Seeds Mixed with The Regular Diet of Rats Lead to Higher Body Weight and Body Weight Gain. *Pharmacophore*, **10**: 49-56.

Mahassni S and Nabulsi K. 2020. Ground Lepidium sativum seeds affect immune system cells, IgM levels, body weights, and hematology in rats. *Journal of Pharmaceutical Negative Results*, 11: 35-41.

Mohammad AK, Hanan, ME, Alaaeldin, AH, Nael MF and Ahmed HH. 2011. Antioxidant, antilipoxygenase and cytotoxic activity of *Leptadenia pyrotechnica* (Forsk.) decne polyphenolic constituents. *Molecules*, **16**: 7510-21.

Munazir M, Qureshi R and Munir M. 2015. Preliminary phytochemical screening of roots and aerial parts of *Leptadenia* pyrotechnica. Pak J Bot, 47: 659-664.

Munazir M, Qureshi R, Arshad M and Gulfraz, M. 2012. Antibacterial activity of root and fruit extracts of *Leptadenia pyrotechnica* (Asclepiadaceae) from Pakistan. *Pak J Bot*, 44: 1209-1213.

Osman HM, Shayoub ME and Babiker EM. 2012. The effect of Moringa oleifera leaves on blood parameters and body weights of albino rats and rabbits. *Jordan J. Biol. Sci.*, **147**: 1-4.

Ofem OE, Ani EJ and Eno AE. 2012. Effect of aqueous leaves extract of *Ocimum gratissimum* on hematological parameters in rats. *Int J Appl Basic Med Res*, **2**:38-42.

OECD (2002), Test No. 423: Acute Oral toxicity - Acute Toxic Class Method, OECD Guidelines for the Testing of Chemicals, Section 4, OECD Publishing, Paris, https://doi.org/10.1787/9789264071001-en.

Patel SK, Desai PR and Pandey VB. 2014. Ethnomedicicinal plants used by the tribals in Bhiloda taluka of Sabarkantha district, *Gujarat. Indian J. Adv. Plant Res*, 1: 33-36.

Preet R and Chand Gupta R. 2018. Simultaneous Determination of Phenolic Compounds in Leptadenia pyrotechnica (Forssk.) Deene. by Using High-Performance Liquid Chromatography (HPLC-DAD-UV). *Adv. Pharmacol. Sci.*, **3**: 1-4.

Rasheed HMF, Rasheed F, Qureshi AW and Jabeen Q. 2016. Immunostimulant activities of the aqueous methanolic extract of *Leptadenia pyrotechnica*, a plant from Cholistan desert. *J Ethnopharmacol*, **186**: 244-250.

Upadhyay B, Roy S and Kumar A. 2007. Traditional uses of medicinal plants among the rural communities of Churu district in the Thar Desert, India. *J Ethnopharmacol*, **113**: 387-399.

Verma N, Jha KK, Chaudhary S, Singh O and Kumar A. 2014. Phytochemistry, pharmacology and traditional uses of *Leptadenia* pyrotechnica. *Indian J Pharm Biol Res*, **2**: 128-134.

Watafua M, Geidam MA. 2014. Effects of the Ethanolic Extract of aerials of *Leptadenia pyrotechnica* (Forsk.) Decnse. on the Liver function of Wister strain Albino Rats. *Int J Sci Res Manag*, 2: 605–610.

Youssef Moustafa AM, Khodair AI and Mahmoud AS. 2007. Phytochemical Investigation and Toxicological studies of lipid constituents isolated from *Leptadenia Pyrotechnic*. *J Pharm Toxicol*, 2: 681-697.

Youssef Moustafa AM, Khodair AI and Saleh MA. 2009. Structural elucidation and evaluation of toxicity and antitumor activity of cardiac glycosides isolated from *Leptadenia* pyrotechnica. Pharm Biol, 47: 826-834.

Jordan Journal of Biological Sciences

Role of IFN-γ, TNF-α, IL-6 and C-Reactive Protein in Newly Diagnosed Iraqi Corona Patients

Israa Qusay Falih^{1,*}, Noor Thair Tahir², Mithal R. Alkubaisi³

¹ Department of Chemistry, College of Science, University of Misan, Maysan, Iraq; ² National Diabetes center/ Mustansiriyah University, Baghdad, Iraq; ³College of Medicine, University of Anbar, Ramadi, Iraq

Received: June 24, 2021; Revised: October 2, 2021; Accepted: October 16, 2021

Abstract

The exceptional conditions sweeping the world due to the Corona virus epidemic have prompted researchers to race to study each of the symptoms, phenomena and relevant clinical biochemical parameters to provide science and scientists with valuable information to achieve victory over the virus. The aim of this investigation is to study the early inflammatory features caused by the immune system before a cell storm occurs in Iraqi Corona patients. The investigation was conducted at Yarmouk Teaching Hospital, Baghdad, Iraq, during the period from January 2021 until the end of March 2021. Our team obtained five milliliters of venous blood from 50 participants newly diagnosed with the Coronavirus (24 males and 26 females). Their ages ranged between (25-55) years compared to 38 individuals (18 males and 20 females). Corona virus patients had statistically significant higher (P<0.01) with Low density lipoproteins-cholesterol (LDL-C), urea, C-Reactive Protein (CRP), and (P<0.001) with D-dimer when they were compared with control group. There was a significant increase in the value of Interleukin-6(IL-6) in people infected with the virus compared to the reviewers whose swab results showed that they were not infected with the virus. For both interferon- γ (IFN) and Tumor necrosis factor - α (TNF- α), the data showed a significant decrease in morale of reviewers diagnosed with acute respiratory syndrome (COVID-19) against their non-infected peers. These data indicate that early intervention for IFN antiviral infection could be fundamental in inhibiting fibrosis to improve functional recovery. Any source of cytokine control, such as interferon- γ and Tumor necrosis factor - α combined with combination therapies for clinical treatment, will be important in the future for COVID-19 infection.

Keywords: Covid-19, Interleukins, Cytokine storm, C-reactive protein, Lung fibrosis.

1. Introduction

The emergence of a new strain of the respiratory syndrome SARS-Cov-2 in 2019 has been announced globally (Johnson et al.,2020). The World Health Organization has launched the term pandemic for this disease, as viruses have widely and rapidly moved from the source of the virus to the rest of the world. The disease has also been called Corona virus 2019 (Covid-19). This disease unknown origin, and it is believed that this virus was transmitted by eating animals that are believed to provide a suitable medium for the development of this strain (Elmasry et al., 2020). Infection with this disease occurs when the virus penetrates the human respiratory system and multiplies in the lung. Its speed of spread is due to its ability to remain effective on contaminated surfaces or to transmit through sneezing or coughing and direct contact with infected people (Mohadeseh et al.,2021). Coronavirus infection stimulates the body's immune system, at which point the cytokine storm begins, which is the most dangerous cause of acute respiratory distress syndrome (ARDS) and lung fibrosis. Many researchers have provided evidence confirming the association of the inflammatory effect with signs of lung fibrosis in people with coronavirus 2019 (Zhong-Jie et

al.,2020). The virus has been described as a very fine nanostructured structure surrounded by the lipid sheath of the nucleocapsid, and inside it there is the nucleoprotein (N) and the positive-sense single-stranded RNA ((+) RNA ss) that allows a virus to force human cells to produce virus particles. It binds to the N protein to (+) SSRNA from its N terminus and leads to viral transcription and repetition. Externally, the membrane protein (M) surrounds the surface of the virus more than once, as it works to stack its wallSARS-CoV-2. It also appears under the electron microscope of a spike-like glycoprotein (S). It is the last transmembrane protein that comes outside the surface and regulates its binding to the host cell receptor, leading to the entry of the virus in the host cell (Kirchdoerfer et al., 2016). (E) the envelope consists of tiny amino acids united parts . The minor part of the virus plays a critical role in synthesizing the virus. Fig. 1. shows a hypothetical drawing of the SARS-CoV-2 structure (Mohadeseh et al., 2021). The human immune system identifies the virus as soon as it enters the body, and then it summons immune factors such as immune cells or firstline receptors (Woo et al.,2010; Zhong et al.,2003; Drosten et al., 2003). Generally, most of prognostic factors related to the varieties of interleukins. Many of severe disease cases which led to death, was due to (proinflammatory innate immunity, anti-inflammatory system)

* Corresponding author. e-mail: israaqusai@uomisan.edu.iq, dr.noorthair.ndc@uomustansiriyah.edu.iq.

(Víctor et al., 2020), where the virus is identified through pathogen recognition receptors (PRRs) as well as by stimulating cells to interferon (IFN). The mechanisms of action of such viruses include reducing the activity of innate human immune cells by inducing variables in cytokine secretion so that the virus produces IgM and IgG. High IFN had a positive effect on patients' resistance to viral infections; but at low levels of this cytokine, symptoms occur and the complications of SARS-CoV-2 infection and death increase (Miriam and Jerome 2020). Tlymphocytes produce a cytokine that is necessary in cases of an immune response. IFN reduces the proliferation of viruses and acts as a wall of counterattacks. The production of cytokine by T cells increases the toxicity of these cells and thus increases the incidence of lymphocyte mortality (Dalia et al., 2021). The continuous rise in IFN results in a doubling of systemic inflammation, increased tissue injury, and organ failure (Lindsay 2016). Recent studies reported severe cases of Covid-19 as a result of

pulmonary and systemic thrombosis occurring at low levels of INFs, while moderate levels of IFN lead to a delay in SARS-Cov-2. That is, elevated immunoglobulins are interpreted as a positive therapeutic marker (Mohammed and Asmaa 2019). Besides, a cytokine storm is also present in severely ill patients with elevation of interleukins such as TNF-α and IL-6(Huang et al.,2020; Hahn et al.,2015). Thus, the host differences are immune responses playing a major role in the severity of COVID-19(Víctor et al.,2020). It is good to understand the effect of interleukins and their role as a diagnostic factor for the severity of Covid 19 patients, which is one of the objectives of this study. The aim of this study is to find the role of IFN-γ, TNF-α, IL-6, C-Reactive Protein and other biochemical parameters in Iraqi Corona Patients, and to demonstrate the early inflammatory features induced by the immune system before the occurrence of a cellular

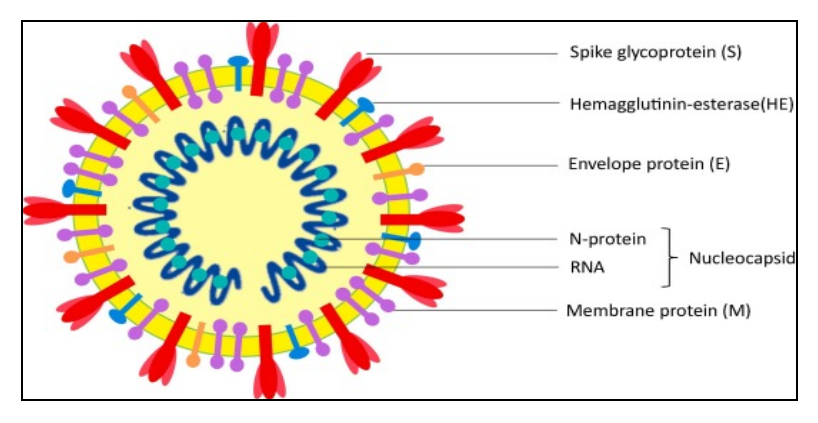


Figure 1. An illustration of the main components of SARS-CoV-2.

2. Materials and Methods

2.1. Patients and control

This investigation was conducted at Yarmouk Teaching Hospital, Baghdad, Iraq, during the period from January 2021 until the end of March 2021. Our team obtained five milliliters of venous blood from 50 participants newly diagnosed with the Coronavirus (24 males, 26 female). Their ages ranged between (25-55) years and compared to 38 people (18 males and 20 females), and it was proved by using a swab that they were not infected with the previously mentioned virus. It should be noted that all patients did not receive any treatment while conducting the research examinations. Patients' data were documented during a private medical interview along with their medical history.

2.2. Methods

2.2.1. Anthropometric Measurement:

Blood pressures were recorded according to the guidelines adopted by (WHO 2019), and body mass index was determined by dividing subjects' weight (Kg) by their height (m²). BMI= mass (kg)/ (height (m)²) (Simon et al.,2005).

2.2.2. Biochemical Assessment:

Glucose was determined by using the enzymatic colorimetric method (Trinder 1969), serum TC was measured by using an enzymatic method (Richmond1992), serum TG was measured by using method (Fossati and Prencipe 1982), and serum HDL-C was measured by HDL-C kit using an enzymatic method (Lopes-Virella et al.,1977). LDL-C was calculated, using (Nauck et al.,2002), the blood urea and serum creatinine were measured, according to an enzymatic method (Helmut and Yvette 1959). Furthermore, C-Reactive Protein (crp) was determined by using automated analyzer (BIOLABO), D - Dimer concentration measured according to minividas kits supplied by Bio Meriux-France., and Serum Biomarkers INF-γ, TNF-α and IL-6 concentrations were measured by the (Biosours) ELISA kit.

2.3. Statistical analysis

All data were expressed as (mean \pm SD). Statistical significance was considered at the level of (P<0.001),(P<0.01), and (P<0.05). Analysis of variance (ANOVA) for equality of means (testing of coincidence). Statistical analysis used (SPSS programs: Statistical Package for Social Sciences, version 22 (SPSS, Chicago, IL, USA).

3. Results

By tracking (Table 1) which shows the general characteristics and the parametric measurements of the patients who were received in the aforementioned hospital, it was found that the average age was 39.5 for those infected with COVID-19, while the average age of the control group was 29.5, and no significant differences were shown for the ages participating in this research. The number of infected women participating was 52%, while

the number of infected men participating was estimated at 48%. The data obtained from the aforementioned table did not record any significant differences between the comparison groups at the level of weight, height and body mass index. At the same time, a significant increase of (P< 0.05) was recorded in the DBP and SBP values, by comparing those infected with the virus and the group of healthy controls. The results obtained are similar to research conducted by researchers from Bangladesh (Syeda *et al.*,2021).

Table 1. Anthropometric Measurements between Patients of Corona Virus& Control

Parameters	COVID-19 Patients Positive	Control (COVID-19 Patients	P-value
	Mean ±SD N=50	Negative) Mean ±SD N=38	
Age (Years)	39.5±8.68	29.5± 5.71	0.156 NS
Sex (M/F)	(24/26)	(18/20)	/
Wights	73.3125 ± 10.77	68±12.11	0.143 NS
Height	168.875 ± 5.20	169±5.73	0.124 NS
$BMI\;(Kg/m^2)$	25.68±3.41	23.69±2.94	0.06 NS
SBP (mmHg)	136.875±6.29	123.75±5.18	0.05^{*}
DBP (mmHg)	86.25±5.63	77.5±4.6291	0.05^{*}

NS: Non-Significant, * (P< 0.05) Significant.

As inferred in Table 2, the serum of each of the FBS, TC, TG, HDL & Creatinine level have no significant between the competition groups. However, upon reaching the determination of LDL & Urea values, we found that they bear significance with significantly higher significant

differences for the affected patients compared to the healthy ones. Our results are consistent with other studies (Syeda *et al.*,2021; Abdulla *et al.*,2020; Isabella Marcia *et al.*,2020).

Table 2. Mean ±SD Characteristics of some Biochemical Parameters in both Covid-19 & Control Patients'

Parameters	COVID-19 Patients Positive	Control (COVID-19 Patients Nagative)	P-value
	Mean ±SD N=50	Mean ±SD N=38	
FBS (mg/dl)	98.438±4.24	90.25±4.77	0.106 NS
TC (mg/dl)	177.625±21.96	152.875±20.82	0.107 NS
TG (mg/dl)	111.9375±19.14	95.625±12.67	.0163 NS
HDL (mg/dl)	47.75±2.77	53.375±4.40	0.136 NS
LDL (mg/dl)	137.25±12.03	83.35±8.44	0.01**
urea(mg/dl)	66.875±5.40	29.375±2.06	0.01**
creatinine(mg/dl)	1.163±0.140	0.7±0.075	0.06 NS

NS: Non-Significant, **(P<0.01) and (P<0.001) high significant.

The biochemical measurements taken from Table 3 show an increase with a highly significant difference of (P<0.01) and (P<0.001) in both D-dimer & CRP for people who tested positive for coronavirus than for non-infected people.

Many studies give support to the phenomena that we obtained, such as the studies of each of (Zhu *et al.*,2020; Zhong-Jie *et al.*,2020; Moutchia *et al.*,2020).

Table 3. Comparative of CRPand D-Dimer concentration Covid-19 & Control Patients

Parameters	COVID-19 Patients Positive Mean ±SD N=50	Control (COVID-19 Patients Negative) Mean ±SD N=38	P-value
CRP (g/dl)	8.5±1.37	2.1875±0.56	0.01**
D-Dimer (ng/ml)	821.875±80.25	144.875±23.012	0.0001**

^{**(}P<0.01) and (P<0.001) high significant

Interleukin values are identical to some extent with other studies that included the same field, as there was a significant increase in the value of IL-6 in persons diagnosed with the virus compared to the reviewers whose

negative swab test results showed that they were not infected with the virus in question.

As for each of (IFN -γ& TNF- α), it is evident from the data a significant decrease in the morale of the auditors

diagnosed with acute respiratory syndrome (COVID-19) against their uninfected peers. All that has been mentioned

previously for the values of interleukin can be tracked by looking at Table 4.

Table 4. Comparative of Interleukins for Covid-19 & Control Patients

Parameters	COVID-19 Patients Positive	Control (COVID-19 Patients Negative)	P-Value	
	Mean ±SD N=50	Mean ±SD N=38		
IL-6(pg/ml)	46.056± 8.08	15.55±1.87	0.001**	
IFN- γ (pg/ml)	6.881±1.18	40.375 ± 9.04	0.0001**	
TNF- α (pg/ml)	27.544±5.2	44±4.9	0.001**	

^{**(}P<0.01) and (P<0.001) high significant

4. Discussion

We are currently facing the largest global health emergency in decades, the devastating outbreak of COVID-19(Wu and McGoogan 2020). Even with a preventive vaccine, it will be critical to determine whether exposed and /or infected people, especially those with mild or asymptomatic forms of the disease who are likely to unintentionally act as major carriers, develop a robust adaptive immunity against SARS-CoV-2(Long et al.,2020).

The reports approved by the World Health Organization based on the data collected from different countries, one third of the patients infected with the virus currently spreading have suffered from acute respiratory distress syndrome (ARDS), which is considered the greatest cause of death or may cause later pulmonary fibrosis in survivors (Hui *et al.*,2018). Aging, obesity, diabetes, cardiovascular disease, and high blood pressure are pre-existing factors that increase the risk of severe infection and death (Norbert *et al.*,2021).

Age is an influential factor that plays a very important role in overcoming infection with the emerging coronavirus, as the elderly are more likely to die when infected (Merad and Martin 2020). It has been shown that most of the elderly suffer from chronic diseases, problems such as diabetes, pressure, and other disorders (Norbert et al.,2021). An immune aging factor is an additional reason for the increasing of vulnerability of the elderly to complications from the infection (Roel et al,2020). The immune system changes dramatically and dramatically over time and behaves inconsistently in elderly people, in particular, because it either treats the infection excessively and thus leads to major infections, or it is too late to react to (Parmigiani et al.,2013). The danger is like the virus entering the body, getting worse, and then causing death. It has been revealed that the immune system changes dramatically and dramatically over time and behaves inconsistently in elderly people in particular, because it either treats the infection excessively and thus leads to major infections, or the uncontrol over it, therefore, the virus is intrusion through body. Hence, a fatal health problem could be reported. (Arne and Derek 2020). An irregular blood pressure is appeared as a result of infection, persistent physical complications and nervous tension. Ultimately, blood pressure has a greatly effects on the patient through the performance effective of the internal organs, including the kidney function efficiency, which it leads to an increase of blood urea level (Guyi et al., 2020).

A number of manuscripts confirming the fact of a disorder in metabolism of lipid during SARA-CoV-2

infection, wherefore an increase in the level of low-density lipoprotein (Eva et al., 2021), hence that a change in lipid levels had been occurring (Shen et al.,2020; Boikova et al.,2020). The high biological markers of Covid 19 patients have been observed (Shi et al., 2020); the cause is attributed to such a circumstance that the virus may cause direct damage to the organs as in the lungs, kidneys, small intestine, heart, and arteries due to lack of oxygenation and respiratory failure (Moutchia et al.,2020). We note in our study, for example, an increase in LDL and urea for patients diagnosed with a positive result of the virus. Or the reason for the increase in each of the inflammatory indicators, such as high D-dimer (a marker of intravascular thrombosis), CRP, and cytokines, the cause of the increase in the systemic hyperinflammation caused by cytokine is the innate immune system syndrome (Merza et al.,2021; Wang et al.,2020).

An elevated C-reactive protein is an indication of inflammation, and is very useful in that it shows the body's resistance to disease (Shang *et al.*,2020). Several studies have shown an increase in C-reactive protein levels in patients diagnosed with coronavirus (Javanian *et al.*, 2020; Ling 2020). This increase plays a role in the incidence of pneumonia and respiratory failure, and so the increase is associated with the development of ARDS (Terpos *et al.*,2020).

Signs of an overexpression of the innate immune system include an increase in a number of indicators, such as the IL-6A end CRP ratio, so that after a viral infection, the innate immune system will be activated early to limit the reproduction of the virus (Hwaiz *et al.*,2021; Luis 2019). D-dimer elevation indicates an increased risk of abnormal blood clotting (Hai-Han *et al.*,2020), as its measurements are used in clinical analyzes to diagnose deep vein thrombosis or pulmonary embolism (Querol-Ribelles *et al.*,2004). Studies have found that its rate is associated with higher deaths from pneumonia resulting from viral infection (Chen N. *et al.*,2020; Tang *et al.*,2020).

IL-6 is one of the main mediators of the inflammatory and immune response resulting from viral infection (Herold *et al.*,2020; Aziz *et al.*,2020). Therefore, many patients develop a fatal immune reaction with persistent damage by the action of cytokines leading to alveolar infiltration by macrophages and monocytes (Abbasifard and Khorramdelazad 2020).

When infection occurs, the affected cells specifically enhance both cytokines and chemokines, and in copious quantities, resulting in a cytostome that can infect endothelial cells and thin blood vessels with a lack of ischemia and oxygen, then the infection increases (Hu *et al.*,2020). Among the results of our study, it was noted that

the IFN and TNF values are lower in patients diagnosed with positive coronavirus test, which is identical to a study in 21 patients with severe COVID-19 compared to the moderate form of patients (Chen G. et al., 2020). It has been shown that there is an inverse relationship with results of IFN levels with cases of pulmonary fibrosis in people with COVID-19, so that IFN is produced by specific antigens or by T cells and natural killer cells. The action of IFN lies in the secretion of defensive macrophages in the host against viral infection, as well as activation of the protease maturation protein (POMP), which enhances antigen activity (Kate and Eileen 2014). IFN has been considered a risk factor for developing lung fibrosis in people with COVID-19 (Zhou, 2009). There is a consensus relationship linking a high level of IFN to the risk of developing cell inflammation caused by SARS-COV-2 infection. Inflammatory particles play a role in determining the type of ARDS and pulmonary fibrosis (Torres Acosta and Singer, 2020). The level of this cytokine is inversely related to lung fibrosis (Keane, 2019). The process of securing these molecules and inhibiting pulmonary fibrosis needs future studies.

5. Conclusion

In conclusion, SARS-CoV-2 infection elicited an inflammatory response and led to the formation of fibrosis in COVID-19 patients even after attenuation of clinical symptoms and negative results from an RT-PCR test for RNA extracted from nasopharyngeal swabs. By following the data of the analyzes conducted during the study, it was evident that there was an increase in the values of CRP, IL-6, Urea, LDL and D-dimer, and yet a decrease in the values of INF and TNF was recorded. Baseline IFN-levels were negatively associated with increased fibrosis volume in COVID-19 upon discharge. These data indicate that early intervention of antiviral infection with IFN- could be fundamental in inhibiting fibrosis to improve functional recovery. Any source of cytokine control, such as IFN-and TNF-α combined with combined therapies for clinical treatment will be important in the future for COVID-19 infection. (Main). It is also reasonable to use markers of immune function to predict disease severity, as a comparison of non-severe or severe Covid 19 is associated with increased signs of the immune response such as IL-6, CRP and increased signs of tissue damage and organ damage as in D-dimer and urea, among other signs.

References

Abbasifard M. and Khorramdelazad H. 2020. The bio-mission of interleukin-6 in the pathogenesis of COVID-19: A brief look at potential therapeutic tactics. *Life Sciences.*, **257**: 11809.

Abdulla Kamil Abdulla, Omar A Salman, Ahlam Ahmed Mahm. 2020. Study of Some Hematological, and Biochemical Parameters in Patients with SARS-CoV-2 in Kirkuk City/Iraq. *Sys Rev Pharm.*, **11(11)**: 515-522.

Arne N. Akbar and Derek W. Gilroy .2020.Aging immunity may exacerbate COVID-19. *Science.*, **369** (6501):256-257.

Aziz M., Fatima R., Assaly R. 2020. Elevated interleukin-6 and Severe COVID-19: a meta-analysis. *J Med Virol.*, 10.1002/jmv.25948Online ahead of print

Bojkova, D., Klann, K., Koch, B. 2020. Proteomics of SARS-CoV-2-infected host cells reveals therapy targets. *Nature.*, **583**: 469.472

Chen N., Zhou M., Dong X. 2020.Epidemiological and clinical characteristics of 99 cases of 2019 novel coronavirus pneumonia in Wuhan, China: a descriptive study, *Lancet.*, **395** (10223): 507–513.

Chen G, Wu D, Guo W. 2020.Clinical and immunological features of severe and moderate coronavirus disease 2019. *J Clin Invest.*, **130**: 2620–9.

Dalia A. Taha, Eman R. Mahfouz, Mona A. Bibars, Nagwa A. Hassan and Othman E. Othman. 2021. Cytokine genes expression in uteri of Bubalus bubalis associated with endometritis infection. *Jordan Journal of Biological Sciences.*, **14**(2):245-251.

Drosten C., Günther S., Preiser W. 2003. Identification of a novel coronavirus in patients with severe acute respiratory syndrome, *N. Engl. J. Med.*, **348**: 1967–1976.

El Masry, I., von Dobschuetz, S., Plee, L. 2020. Exposure of humans or animals to SARS-CoV-2 from wild, livestock, companion and aquatic animals: **Qualitative exposure assessment.** *FAO animal production and health*, Paper 181. Rome.

Eva Ko'car, Tadeja Re'zen, Damjana Rozman. 2021. Cholesterol, lipoproteins, and COVID-19: Basic concepts and clinical applications. *BBA - Molecular and Cell Biology of Lipids.*, **1866**: 158849.

Fossati. P and Prencipe L.1982 Serum triglycerides determined colorimetric ally with an enzyme that produces hydrogen peroxide. *Clin.Chem.*, **28(10)**: 2077-2080.

Guyi Wang, Quan Zhang, Xianmei Zhao. 2020. Low high-density lipoprotein level is correlated with the severity of COVID-19 patients: an observational study. *Lipids in Health and Disease*. **19**: 204.

Hahn JN, Kaushik DK, Yong VW. 2015. The role of EMMPRIN in T cell biology and immunological diseases. *J. Leukoc. Biol.*, **2** 98(1): 33–48.

Hai-Han Yu, Chuan Qin, Man Chen, Wei Wang, Dai-Shi Tian. 2020. D-dimer level is associated with the severity of COVID-19. *Thrombosis Research.*, **195**: 219–225.

Helmut JR. and Yvette SL. 1959. A simple method for the determination of blood urea nitrogen with special refences to automatic colorimetric analysis. *Clinical Chemistry.*, **5(6)**.

Herold T., Jurinovic V. and Arnreich C. 2020. Elevated levels of interleukin6 and CRP predict the need for mechanical ventilation in COVID-19 [published online ahead of print, 2020 May 18]. *J Allerey Clin Immunol.*

Huang C., Wang,Y. Li X., L. 2020. Clinical features of patients infected with 2019 novel coronavirus in Wuhan, China, *Lancet.*, **395**: 497–506.

Hu ZJ, Xu J, and Yin JM. 2020. Lower Circulating Interferon-Gamma Is a Risk Factor for Lung Fibrosis in COVID-19 Patients. *Front. Immunol.*, **11**: 585-647.

Hui DS, Azhar EI, Kim YJ, Memish ZA, Oh MD and Zumla A. 2018.Middle East respiratory syndrome coronavirus: risk factors and determinants of primary, household, and nosocomial transmission, *Lancet Infect Dis.*, **18**: 217-27.

Hwaiz R., Merza,M., Hamad B., HamaSalih S., Mohammed M. and Hama H. 2021. Evaluation of hepatic enzymes activities in COVID-19 patients, *International Immunopharmacology.*, **97**: 107701.

Isabella Marcia Soares Nogueira Teot 'onio, Juliana Lott de Carvalho and Luiz Claudio Castro.2020. Clinical 'and biochemical parameters of COVID-19 patients with prior or active dengue fever, *Acta Tropica.*, **214**: 105782.

Javanian M., Bayani M. and Shokri M.2020. Clinical and laboratory findings from patients with COVID-19 pneumonia in Babol North of Iran: a retrospective cohort study, *Romanian Journal of Internal Medicine.*, **58(3)**: 161–167.

Johnson Olaleye Oladele, Ebenezer Idowu Ajayi, Oyedotun Moses Oyeleke, Oluwaseun Titilope Oladele, Boyede Dele Olowookere, Boluwaji M Adeniyi. 2020. Curative Potential of Nigerian Medicinal Plants in COVID-19 Treatment: A Mechanistic Approach, *Jordan Journal of Biological Sciences.*, 13: 681 – 700.

Kate A. Redgrove and Eileen A. McLaughlin. 2014. The role of the immune response in Chlamydia trachomatis infection of the male genital tract: a double-edged sword, *Frontiers in Immunology Microbial Immunology*., **5** (534): 1-22.

Keane M.P. 2019. The role of chemokines and cytokines in lung fibrosis. *EUROPEAN RESPIRATORY REVIEW*. 17 (109): 151-156

Kirchdoerfer R.N., Cottrel C.A. and Wang, N. 2016. Pre-fusion structure of a human coronavirus spike protein. *Nature.*, **531**: 118–121.

Lindsay B. Nicholson.2016. The immune system, Portland Press. *Essays in Biochemistry*. **60**: 275–301.

Ling W.,2020. C-reactive protein levels in the early stage of COVID-19. *Médecine et Maladies Infectieuses.*, **50**: 332–334.

Long Q.X., Tang X.J. and Shi Q.L., 2020.Clinical and immunological assessment of asymptomatic SARS-CoV-2 infections, *Nat. Med.*, **26:** 1200–1204.

Lopes-Virella M., Ston P. and Ellis S.1977. Cholesterol dtermination in high density lipoprotein separated by three different methods. *Clinc. Chem.*, **23(5)**: 882-884.

Luis Perez. 2019. Acute phase protein response to viral infection and vaccination, *Archives of Biochemistry and Biophysics.*, **671**: 196–202.

Merad M. and. Martin J. C., 2020. Nat. Rev. Immunol., 20: 355.

Merza MY, Hwaiz RA, Hamad BK, Mohammad KA, Hama HA and Karim AY. 2021. Analysis of cytokines in SARS-CoV-2 or COVID-19 patients in Erbil city, Kurdistan Region of Iraq. *PLoS ONE.*, **16(4)**: 250330.

Miriam Merad and Jerome C. Martin.2020. Pathological inflammation in patients with COVID-19: a key role for monocytes and macrophages, PROGRESS *nature Reviews / Immunology.*, **20**: 355-362.

Mohadeseh Haji Abdolvahab, Shima Moradi-kalbolandi, *et al.* 2021.Review (Potential role of interferons in treating COVID-19 patients), *International Immunopharmacology.*, **90**: 107171.

Mohammed N. Maaroof and Asmaa E. Mahmood.2019. Determination of the Immunogenic and Hematologic Effects of Titanium Nanoparticles Manufactured from Aspergillus flavus in Vivo. Jordan *Journal of Biological Sciences.*, **12(2)**:135-140.

Moutchia J, Pokharel P, Kerri A, et al. 2020. Clinical laboratory parameters associated with severe or critical novel coronavirus disease 2019 (COVID-19): A systematic review and meta-analysis. PLoS ONE., 15(10): 239802.

Nauck, M., Warnick, G.R. and Rifai, N. 2002. Methods for measurement of LDL-cholesterol: a critical assessment of direct measurement0T 0Tby homogeneous assays versus calculation. *Clin Chem.*, **48**: 236-254.

Norbert Stefan, Andreas L. Birkenhead, and Matthias B. Schulze. 2021. Global pandemics interconnected — obesity, impaired metabolic health and COVID-19. *Nature Reviews Endocrinology.*, 17: 135-149.

Parmigiani, A., Alcaide, M. L., Freguja, R., Pallikkuth, S., Frasca, D., Fischl, M. A., & Pahwa, S. 2013. Impaired Antibody Response to Influenza Vaccine in HIV-Infected and Uninfected Aging Women Is Associated with Immune Activation and Inflammation. *PLoS ONE.*, **8**(11): 79816.

Querol-Ribelles J.M., Tenias J.M., Grau E. 2004.Plasma d-dimer levels correlate with outcomes in patients with community-acquired pneumonia, Chest., **126(4)**: 1087–1092.

Richmond W. 1992. Analytical reviews in clinical biochemistry: the quantitative analysis of cholesterol. Ann. *Clin.Biochem.*, **29(26)**: 577-597

Roel P. H. De Maeyer, Rachel C. van de Merwe, Rikah Louie, Olivia V. Bracken, Oliver P. Devine, Daniel R. Goldstein, Mohib Uddin, Arne N. Akbar and Derek W. Gilroy. 2020. Blocking elevated p38 MAPK restores efferocytosis and inflammatory resolution in the elderly. *Nature Immunology.*, 21: 615-625.

Shang, W., Dong, J., Ren, Y., Tian, M., Li, W., Hu, J., & Li, Y. 2020. The value of clinical parameters in predicting the severity of COVID-19. *J Med Virol.*, 1–5.

Shen, B., Yi, X., Sun, Y., Bi, X., Du, J., Zhang, C. and Guo, T. 2020 . Proteomic and Metabolomic Characterization of COVID-19 Patient Sera. Cell.

Shi, Y., Wang, Y., Shao, C., Huang, J., Gan, J., Huang, X and Melino, G. (2020). COVID-19 infection: the perspectives on immune responses. *Cell Death & Differentiation.*, **27**: 1451–1454.

Simon C., Everitt H. & Kendrick T. 2005. **Oxford Handbook of General Practice**. 2nd Edition. Oxford University Press, pp. 712-728.

Syeda Umme Fahmida Malik, Parveen Afroz Chowdhury, Al Hakim, Mohammad Shahidul Islam, Md Jahangir Alam and Abul Kalam Azad. 2021. Blood biochemical parameters for assessment *oCOVID*-19 in diabetic and non-diabetic subjects: a cross-sectional study, International Journal of Environmental Health Research

Tang N., Li D. and Wang X. 2020. Abnormal coagulation parameters are associated with poor prognosis in patients with novel coronavirus pneumonia, *J. Thromb. Haemost.*, **18** (4): 844–847.

Terpos, E., Ntanasis-Stathopoulos, I., Elalamy, I., Kastritis, E., Sergentanis, T. N., Politou, M. and Dimopoulos, M. A. (2020). Hematological findings and complications of COVID-19. *American Journal of Hematology.*, **95**: 834–847.

Trinder P.A.1969. Determination of glucose in blood using glucose oxidase with an alternative oxygen acceptor. *Clin.Biochem.*, **6**: 24-27.

Torres Acosta MA and Singer BD.2020. Pathogenesis of COVID-19-induced ARDS: implications for an ageing population. *Eur Respir J.*, **56**: 2002049.

Víctor J. Costela-Ruiz, Rebeca Illescas-Montes, Jose M. Puerta-Puerta, Concepción Ruiz and Lucia Melguizo-Rodríguez. 2020.SARS-CoV-2 infection: The role of cytokines in COVID-19 disease. *ScienceDirect.*, Cytokine and Growth Factor Review **54**: 62–75.

Wang, J., Hajizadeh, N., Moore, E. E., McIntyre, R. C., Moore, P. K., Veress, L. A. and Barrett, C. D. (2020). Tissue Plasminogen Activator (tPA) Treatment for COVID-19 Associated Acute Respiratory Distress Syndrome (ARDS): A Case Series. *Journal of Thrombosis and Haemostasis.*, **18**: 1752–1755.

Woo P.C.Y., Y. Huang, S.K.P. Lau and K.-Y. Yuen. 2010. Coronavirus genomics and bioinformatics analysis, *Viruses.*, **2**: 1804–1820.

World Health Organization. 2019.International Society of Hypertension: guideline for management of hypertension. Guideline subcommittee. *Journal of Hypertension.*, **17**: 151-183.

Wu, Z., and McGoogan, J.M. Characteristics of and Important Lessons from the Coronavirus Disease 2019 (COVID-19) Outbreak in China: Summary of a Report of 72314 Cases from the Chinese Center for Disease Control and Prevention. *JAMA*. Published online February 24, 2020.

Zhong-Jie Hu, Jia Xu, Ji-Ming Yin. 2020.Lower Circulating Interferon-Gamma Is a Risk Factor for Lung Fibrosis in COVID-19 Patients. *Frontiers in Immunology.*, **11**: 585647.

Zhong N.S., B.J. Zheng, Y.M. Li . 2003. Epidemiology and cause of severe acute respiratory syndrome (SARS) in Guangdong, People's Republic of China, *The Lancet.*, **362**: 1353–1358.

Zhou F. 2009.Molecular mechanisms of IFN-gamma to upregulate MHC class I antigen processing and presentation. *Int Rev Immunol.*, **28**: 239–60.

Zhu, Na; Zhang, Dingyu; Wang, Wenling; Li, Xinwang; Yang, Bo; Song, Jingdong; Zhao, Xiang; Huang, Baoying; Shi, Weifeng; Lu, Roujian; Niu, Peihua; Zhan, Faxian; Ma, Xuejun; Wang, Dayan; Xu, Wenbo; Wu, Guizhen; Gao, George F.; Tan, Wenjie. 2020. A Novel Coronavirus from Patients with Pneumonia in China, 2019. New England Journal of Medicine., 382(8): 727-733.



Jordan Journal of Biological Sciences

In-silico Genome Editing Identification and Functional Protein Change of Chlamydomonas reinhardtii Acetyl-CoA Carboxylase (CrACCase)

Mentari Putri Pratami¹, Miftahul Huda Fendiyanto^{1,2,*}, Rizky Dwi Satrio^{1,2}, Isna Arofatun Nikmah¹, Mo Awwanah¹, Nadya Farah¹, Nastiti Intan Permata Sari¹, Nurhadiyanta¹

¹Study Program of Biology, Faculty of Military Mathematics and Natural Sciences, The Republic of Indonesia Defense University. Kampus Universitas Pertahanan RI, Sentul-Bogor, Kawasan IPSC, 16810, West Java, Indonesia; ²Laboratory of Plant Physiology and Genetics, Department of Biology, Faculty of Mathematics and Natural Sciences, IPB University. Kampus IPB Darmaga Bogor 16680, West Java, Indonesia.

Received: July 28, 2021; Revised: January 4, 2022; Accepted: January 12, 2022

Abstract.

The Acetyl-Coa Carboxylase (CrACCase) in Chlamydomonas reinhardtii is a gene encoded triacylglyceride (TAG) and lipid (oil body) synthesis. The CrACCase gene was little studied and had not been genetically engineered either in-silico or invivo. In this study, we provide bioinformatic precision information for genome editing, especially in CrACCase. This study aimed to construct sgRNA and predict the functional region of the putative mutant protein of the CrACCase. Based on the results of molecular identification, the best CrACCase (GeneBank XM 001703135) can be genetically in-silico modified. potential sgRNA this study were GCGTCTGCTCAATCACACGGCGG, constructions in TTGAGGTCGGAACTCCAGCGG, and AGGCAATACCCTCAATTGGGTGG with efficiency values of 79.27, 68.25, and 65.17%, respectively. The best oligo sgRNA obtained has a protospacer adjacent motif (PAM) site with NGG especially in the form of CGG and TGG. The location of the engineered CrACCase gene mutation was found in the XM 001703135.1:1089 region in the Chlamydomonas reinhardtii genome, especially in the negative strand. CrACCase protein was predicted to have the structure of carboxyl transferase subunit of ACC, carboxyl transferase subunit of putative PCC, humanized carboxyltransferase domain of yeast Acetyl-CoA carboxylase, and Acetyl-CoA Carboxylase. Changes in frameshift mutations in the CrACCase gene influenced structural changes of the functional regions of the ligand-protein binding sites at residues D:C 92, 95, 111, and 114 where these sites are zinc ion binding sites. This structural change resulted in a change in the function of the CrACCase protein. This bioinformatics information is important to perform in-vivo genome editing on the CrACCase in the future so that mutants with the highest TAG production or the highest biodiesel (oil body) producer can be obtained. The manipulation of the CrACCase gene in Chlamydomonas reinhardtii can be applied to other microalgae organisms with the highest lipid percentages to increase future bioenergy production by molecular biologists and biotechnologists.

Keywords: Acetyl-CoA Carboxylase, Chlamydomonas reinhardtii, CRISPR/Cas 9, Genome Editing, Protospacer Adjacent Motif

1. Introduction

Microalgae can be used as an alternative energy source (renewable biofuel) to overcome the problem of energy difficulties in recent times (Alam et al., 2012; Jones and Mayfield, 2012; Suali and Sarbatly, 2012; Medipally et al., 2015). Microalgae are the best source of biofuels (Barqi, 2015; Eisentraut, 2010) when compared to palm oil, Jatropha, and lignocellulosic biomass (Milano et al., 2016) because the organisms have a very high lipid content, i.e in Nannochloropsis oculata it reaches 31-68%, while in Chlorella sp. reached 10-58% (Christi, 2007). However, the use of microalgae as a source of biofuel has not been carried out optimally and efficiently. This is due to the

limited identification of species and molecular characterization.

Microalgae can produce 150-200 times more lipids (Demirbas, 2011; Peng et al., 2013; Bouabidi et al., 2018) than lipid-producing plants (oil palm, jatropha) at the best conditions of silver per year. Microalgae have the greatest potential as a producer of biodiesel feedstock (Godhe et al., 2008; Khan et al., 2009) compared to other plants. In contrast to other plants, microalgae are able to produce very high lipids for biodiesel production with fast harvest times (Bligh and Dyer, 1959; Lee, 1980; Brown et al., 1994; Chisti, 2007; Bringezu et al., 2007; Ratha and Prasanna, 2012). Recently, mass microalgae culture with bioreactors (Peng et al., 2016) can be used as an alternative to meet bioenergy needs, especially biodiesel (Brennan and Owende, 2010; Sharma et al., 2018).

^{*} Corresponding author. e-mail: miftahul.fendiyanto@idu.ac.id.

However, the efficiency of lipid production through the triacylglyceride metabolic pathway (TAG) is vital to study to increase lipid production in microalgae (Cooksey et al., 1987; Duong et al., 2015; Sharma et al., 2018). Especially for the species Chlamydomonas reinhardtii, genome editing of the ACCase gene has not been reported; therefore, this study is the first step in carrying out genetic manipulation to increase lipid production. In addition to increased lipid production with biocatalysts (Rodolfi et al., 2009; Yun et al., 2014), a genome editing approach becomes important. This genetic engineering can be done by looking for markers both at the gene level (Diaz et al., 2010; Fendiyanto et al., 2019a; Miftahudin et al., 2021), genome (Countway et al., 2005; Zhu et al., 2005; Fendiyanto et al., 2019b; Pratami et al., 2020), mRNA (Satrio et al., 2019), or metabolites (Chini-Zittelli et al., 2006; Ramasamy et al., 2015; Fendiyanto et al., 2020; Fendiyanto et al., 2021).

Chlamydomonas reinhardtii is a microalga with great potential as a source of biofuels, but this species has not been studied or molecular characterized completely. Therefore, the potential of microalgae particularly Chlamydomonas reinhardtii as a renewable bioenergy source is necessary to study. In addition, C. reinhardtii was found to have the Acetyl-Coa Carboxylase (CrACCase) gene, which encodes for triacylglyceride (TAG) and lipid (oil body) synthesis. TAG is the main form of energy storage in microalgae cells and is contained in 60-70% of its dry weight (Hu et al., 2008; Scott et al., 2010; Shuba and Kifleb, 2018). Research on the CrACCase gene in Chlamydomonas reinhardtii has not been carried out comprehensively and has not been characterized either in-silico or in-vivo, even though this gene plays an important role in producing TAG.

Lipid metabolism is the synthesis and degradation of lipids in cells, which involves the breakdown or storage of fat for energy (Spolaore et al., 2006). These fats are obtained from consuming food and absorbing them or are synthesized by plants or animals. Lipogenesis is the process of synthesizing these fats. The types of lipids found in the body are fatty acids and membrane lipids in microalgae (Weldy and Huesemann, 2007). Lipid metabolism often begins with hydrolysis, which occurs with the help of various important enzymes. Lipid metabolism also occurs in microalgae, although the process is different than in animals. In microalgae organisms, lipid biosynthesis is carried out by involving the ACC and GPAT enzymes (Ummalyma et al., 2017) in the triacylglyceride (TAG) pathway starting from the acetyl-CoA precursor to oil bodies in the plastids and endoplasmic reticulum. One of the important enzymes analyzed in this study is ACCase, the protein encoded by the Acetyl-Coa Carboxylase gene. The gene can be found in Chlamydomonas reinhardtii and then we called CrACCase. We attempted to perform genome editing and search for mutation sites in silico in the CrACCase gene and predict changes in the functional structure of the protein. Therefore, this study aimed to construct oligo guide RNA and predict the functional region of the putative protein mutant of the CrACCase gene to engineer the increase in lipid content in Chlamydomonas reinhardtii.

2. Materials and Methods

2.1. CrACCase Gene Searching of Microalgae in GenBank Database

The Acetyl-Coa Carboxylase (CrACCase) gene was done by performing an advance search ((Acetyl-Coa Carboxylase)(OR Microalgae) OR Chlamydomonas reinhardtii) using Nucleotide Query in the NCBI database (https://www.ncbi.nlm.nih.gov/). Gene selection was done by filtering only for mRNA sequences and coding sequences for the CrACCase gene in the species Chlamydomonas reinhardtii. From 1244 accessions obtained, we selected the CrACCase gene with accession XM 001703135, specifically the gene that has a high level of confidence in Microalgae. The XM 001703135 accession was then downloaded in FASTA and GENEBANK formats to determine the area of the open reading frame (ORF), promoter, and coding sequence (CDS). Accession Data visualization was performed using the UGENE program (Okonechnikov et al., 2012). In addition, we also performed a BLASTn process to ensure the best access to the Acetyl-Coa Carboxylase gene in Chlamydomonas reinhardtii species. The selection of species of microalgae Chlamydomonas reinhardtii was carried out based on the reference of Sharma et al., (2018) which can be chosen as the main gene to regulate the synthesis of triacylglycerol (TAG) in producing oil bodies for biodiesel production in microalgae. Identification, characterization, and search for functional regions of genes were investigated with a precision tool using the UGENE program (Okonechnikov. et al., 2012).

2.2. sgRNA Design of the CrACCase using in-silico CRISPR/Cas 9 approaches

The design guide-RNA was carried out using a comparative approach for the initial study on genome editing CRISPR/Cas 9 (Sharma et al., 2018). The design of guide-RNA in bioinformatics in the CRISPR/Cas 9 approach was carried out by searching for the protospacer adjacent motif (PAM) region in the genome of Chlamydomonas reinhardtii, especially the CrACCase gene. This search process is carried out with the help of the CHOP-CHOP application (https://chopchop.cbu.uib.no/) with the 'KNOCK OUT' format in the hope that the target gene undergoes a frameshift mutation. The primers obtained were then statistically tested and genetically verified through the value of GC nucleotide ratio and potential for self-complementarity. Self-complementarity was avoided to eliminate the potential for hairpin structure formation in the RNA oligo-guide of the generated CrACCase gene. sgRNA sequences obtained were also designed based on the choice of PAM, especially the NGG site on the CrACCase genome of the species Chlamydomonas reinhardtii. The obtained oligos are then used as a benchmark to see the potential for frameshift mutations in the CrACCase gene and its protein.

2.3. Identification Genes and Proteins of CrACCase

Identification of the *CrACCase* gene was carried out using the BLASTn approach (Fendiyanto *et al.*, 2019a), while the search for CrACCase protein was carried out using the BLASTtn approach (Miftahudin *et al.*, 2021) on the NCBI database. We selected 50 genes with similar identity and query cover above 80% to identify the

CrACCase gene. The CrACCase gene with accession XM_001703135 was selected for further analysis because it is the only gene encoding the highest quality Acetyl-Coa Carboxylase in Chlamydomonas reinhardtii species. The gene with the accession was then searched for its protein sequence with the help of BLAST and characterization directly using the UGENE program. The protein obtained was then further analyzed for its 2-dimensional (2D), 3-dimensional (3D) structure, functional regions, protein sequence homology, and potential ligand binding to the active site of the CrACCase protein in Chlamydomonas reinhardtii species.

2.4. Confirmation of CrACCase Putative Protein and Prediction of Functional Region

The putative protein sequences obtained from the UGENE and BLAST tools were then confirmed and further characterized. We constructed a 3D and crystal structure of the CrACCase protein using the SWISS-MODEL program (Bienert et al., 2017; Waterhouse et al., 2018) based on homology modeling and functional structure. The homology predictions obtained were four putative proteins, and we chose only one protein using the protein template based on the highest residue sequence composition (QMEANDisCo) (Waterhouse et al., 2018). We also pay attention to the QMEAN Z-score value, local quality estimates, ligand interaction, amino acid composition, oligo state type, GMQE value, sequence identity, and structure assessment. Specifically for the study of ligand-protein interactions, we identified the ligands of the CrACCase protein in the chemical component summary description in the RCSB PDB database (https://www.rcsb.org/ligand/ZN) which includes identities, formulas, molecular weight, type, isomeric SMILES, InChl, InChlKey, formal charge, atom count,

chiral atom count, bond count, and aromatic bond count. The quality of protein homology and identification of functional regions were also carried out with the ORION tool (Altschul *et al.*, 1997; de Brevern *et al.*, 2000; Söding, 2005; Ghouzam *et al.*, 2015). Identification of changes in protein function was carried out by looking at the structure of amino acid residues and ligands using the MODELLER, I-TASSER, and SWISS MODEL programs (Waterhouse *et al.*, 2018).

3. Results and Discussion

3.1. In silico Genome Editing of CrACCase in Chlamydomonas reinhardtii

Based on the test for making oligo single-guide (sg) RNA, it was shown that the protospacer adjacent motif (PAM) region in the CrACCase gene, especially the Chlamydomonas reinhardtii genome, contained 188 regions spread from the 25th to 1300 bp nucleotides. The oligo sgRNA construction was carried out by randomly searching the PAM region of the CrACCase gene with nucleotide orientation either from the 5' to 3' end (positive thread) or vice versa from the 3' to 5' end (negative strand). There are three types of sgRNA in the CrACCase gene, namely green, red, and orange types. The different types of sgRNA regenerated in chop-chop tools depend on the type of PAM especially at the NGG site in the CrACCase genome. The most sgRNA was found in the red type, while the least in the green type. however, the green type SgRNA ranked 1st in statistical analysis, genome editing efficiency, and self-complementary. Green type SgRNA, rank 1, was found in the 1089 bp region with negativestrand (-).

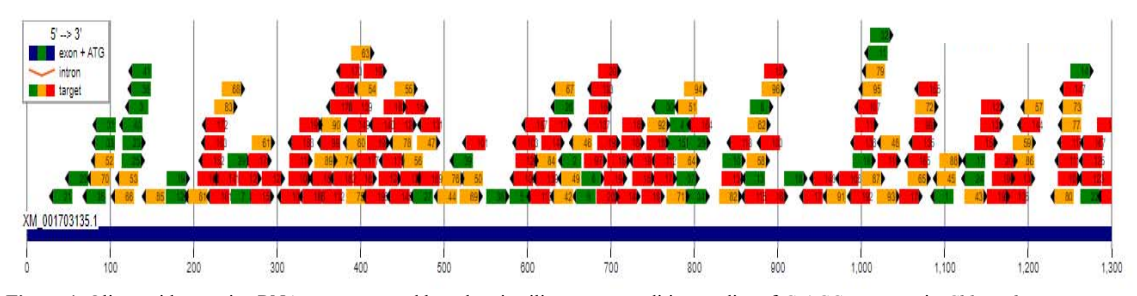


Figure 1. Oligo guide putative RNA was generated based on in silico genome editing studies of *CrACCase* genes in *Chlamydomonas reinhardtii*. There are three types of oligo-guide RNA based on genetic testing, namely type 1 (green), type 2 (orange), and type 3 (red). The black arrow indicates the NGG sequence at the protospacer adjacent motif (PAM) site in the *CrACCase* gene region. The accession number for the chop-chop program used in this study is XM_001703135.1. The size of the genome sequence was 1300 bp with an orientation from the 5' end to the 3' end.

A total of 50 selected top hits from a total of 188 sgRNAs were found in this study. The determination of the top 50 hits was mainly based on the efficiency of genome editing of the *CrACCase* gene, however, we also took into account the values of self complementarity, GC content, strand, and genomic location. Based on the parameters, the gene-editing efficiency value of fifty sgRNA Top hits showed a range of 65.98 to 79.27% and GC content of 35 to 65% (Table 1). In the preparation of primers for either sgRNA or ordinary PCR amplicon, it has high efficiency if the GC content value does not exceed 65%. The principle of targeting sgRNA sequences is basically similar to ordinary primer design (Galluzzi *et al.*, 2004; Galluzzi *et*

al., 2010), but this method pays attention to the PAM region in the genome/gene of interest.

Based on these parameters, the three best target sgRNA sequences are GCGTCTGCTCAATCACACGGCGG, TTGAGGTCGGAGAACTCCAGCGG, and AGGCAATACCCTCAATTGGGTGG. The sgRNAs formed was at 1089, 643, and 124 bp nucleotides. The NGG regions of the first and second rank sgRNAs are nucleotide type C, while the nucleotides of the third rank sgRNA are type T nucleotides. Regarding the second rank sgRNA, although it has a high potential for self-complementarity (as much as 2), the value of gene editing efficiency is relatively high at 68.25. % (Table 1). Based

on positive threads, oligo sgRNAs that have the highest efficiency value and have positive (+) threads, the best target sequences are ATGGATTTCACCTACATGGGTGG, ATCAACCACCTCATTGACGCCGG, and GTCTTACACCGACCGCATCAAGG. The three sgRNAs were in the fourth to sixth ranks, respectively, and were located at the 772, 580, and 666 bp nucleotides,

respectively. However, we used sgRNA with the First Rank at the 1089 bp location because it has the highest gene editing efficiency value in the *CrACCase* gene from *Chlamydomonas reinhardtii*. Therefore, we further studied the analysis of sequences that cause nucleotide changes/mutations at the protein level, especially in functional areas.

Table 1. Fifty top hits guide RNA design for genome editing in CrACCase gene region

Rank	Target sequence	Genomic location	Strand	GC content (%)	Self-complementarity	Efficiency
1	GCGTCTGCTCAATCACACGGCGG	XM_001703135.1:1089	-	60	0	79.27
2	TTGAGGTCGGAGAACTCCAGCGG	XM_001703135.1:643	-	55	2	68.25
3	AGGCAATACCCTCAATTGGGTGG	XM_001703135.1:124	-	50	0	65.17
4	ATGGATTTCACCTACATGGGTGG	XM_001703135.1:772	+	45	1	64.36
5	ATCAACCACCTCATTGACGCCGG	XM_001703135.1:580	+	50	0	62.68
6	GTCTTACACCGACCGCATCAAGG	XM_001703135.1:666	+	55	0	62.17
7	TGGTTGCAATGGAGTCAGGATGG	XM_001703135.1:246	+	50	1	62.59
8	ATCATTGTGTGCACCTCGGGCGG	XM_001703135.1:868	+	55	0	60.75
9	TGCGGTCGGTGTAAGACTTGAGG	XM_001703135.1:660	-	55	1	61.44
10	ATCGAGTACGCCACGCAGGAGGG	XM_001703135.1:835	+	60	0	60.23
11	GAACGAGGCCGTCACACCACCGG	XM_001703135.1:1010	-	65	0	60.2
12	TAGATTACTGATCTAACGCTCGG	XM_001703135.1:168	+	35	0	60.1
13	CGAGGTGCACACAATGATGACGG	XM_001703135.1:863	-	50	0	57.51
14	AAGCGCGGCATGATCCCCTTCGG	XM_001703135.1:1252	+	60	0	56.56
15	GTCATGGATTTCACCTACATGGG	XM_001703135.1:769	+	40	0	56.34
16	ATCCTCACCTCGCCTACCACCGG	XM_001703135.1:991	+	60	0	54.12
17	CTCCGCAGTCTGGAAGTCGTCGG	XM_001703135.1:1127	-	60	2	56.09
18	CATCTTTTCGCTCATGCAGATGG	XM_001703135.1:909	+	45	0	53.93
19	AGATTACTGATCTAACGCTCGGG	XM_001703135.1:169	+	40	0	53.55
20	GGTAAAAGTGCTCGCTGACAAGG	XM_001703135.1:52	-	50	0	53.26
21	AAGGTGTCAAAACTTGCGTTTGG	XM_001703135.1:33	-	40	0	53.18
22	ATCCCCTTCGGCGTGCAGCACGG	XM_001703135.1:1264	+	65	2	54.71
23	GCCAATTACCACCCAATTGAGGG	XM_001703135.1:116	+	45	0	52.43
24	TCCGCAGTCTGGAAGTCGTCGGG	XM_001703135.1:1126	-	60	2	54.26
25	CGCCAATTACCACCCAATTGAGG	XM_001703135.1:115	+	50	0	50.99
26	GAGAACTCCAGCGGGTCCACGGG	XM_001703135.1:634	-	65	0	50.54
27	ACTTGTCGCACCGGGTCCACAGG	XM_001703135.1:465	-	65	0	49.58
28	GGATCCATGGGCAGTGTGGTGGG	XM_001703135.1:793	+	60	0	49.36
29	AGCGTGGTTGCAATGGAGTCAGG	XM_001703135.1:242	+	55	1	50.04
30	ATCCATGACGCCCAGCGCCACGG	XM_001703135.1:755	-	65	0	48.38
31	GCACAAAAGCTGAGCTCGCGTGG	XM_001703135.1:85	-	60	1	48.95
32	GGTGGTGTGACGGCCTCGTTCGG	XM_001703135.1:1012	+	65	0	47.47
33	CACAAAAGCTGAGCTCGCGTGGG	XM_001703135.1:84	-	55	1	47.52
34	TGGATCCATGGGCAGTGTGGTGG	XM_001703135.1:792	+	60	0	44.25
35	AGCTCGCGTGGGGCAAGGATAGG	XM_001703135.1:73	-	65	0	44.23
36	GCAAGGCAATACCCTCAATTGGG	XM_001703135.1:127	-	45	0	43.63
37	CACCTACATGGGTGGATCCATGG	XM_001703135.1:780	+	55	2	43.78

38	CCATCTCAAGATGAGCTCTATGG	XM_001703135.1:552	+	45	1	41.41
39	AGATGTGGTGGTGCTCCTTCAGG	XM_001703135.1:513	-	55	0	37.42
40	ACCCTCAATTGGGTGGTAATTGG	XM_001703135.1:117	-	45	1	36.58
41	TGCAAGGCAATACCCTCAATTGG	XM_001703135.1:128	-	45	0	31.92
42	AGAACTCCAGCGGGTCCACGGGG	XM_001703135.1:633	-	65	0	69.11
43	GCCCGACGACTTCCAGACTGCGG	XM_001703135.1:1125	+	65	0	69.03
44	CAGGTGCTTGATGTACAGGATGG	XM_001703135.1:494	-	50	0	67.77
45	GCAGCGTCTGCTCAATCACACGG	XM_001703135.1:1092	-	55	1	67.63
46	GTCGGTGTAAGACTTGAGGTCGG	XM_001703135.1:656	-	50	1	66.82
47	TGGACCCGGTGCGACAAGTGCGG	XM_001703135.1:469	+	65	0	65.77
48	GTCTCCCAGCATGCCGAACGAGG	XM_001703135.1:1025	-	65	0	65.4
49	TGAGGTCGGAGAACTCCAGCGGG	XM_001703135.1:642	-	60	2	67.22
50	TGCAGCCAAAGCAGATGTGGTGG	XM_001703135.1:525	-	55	1	65.98

Note: XM_XM_001703135.1 is an accession of the *CrACCase* gene in chop-chop tools. The last nucleotide in the target sequence represents the NGG nucleotide in the protospacer adjacent motif (PAM) region of the *CrACCase* gene in *Chlamydomonas reinhardtii*. The + sign indicates the positive thread with the 5'-3' orientation, while the - sign indicates the negative thread with the 3'-5' orientation.

3.2. Crystal Structure Prediction of CrACCase Protein

Based on the information on the sgRNA construction of the *CrACCase* gene at the -1089 bp nucleotide region with a negative orientation, we tried to find the functional region and crystal structure of the CrACCase protein. We used the ORION, SWISS-MODEL, Modeller, and I-TASSER programs to search for information on changes in amino acid residues of the sgRNA regions we designed. We found four crystal structures of CrACCase which have a similarity (seq identity) reaching 49.62 %. We found four crystal structure models of putative proteins similar to CrACCase, namely models 1, 2, 3, and 4. Model 1 is a protein similar to the acetyl-coenzyme A carboxylase

carboxyl transferase beta subunit commonly found in *Staphylococcus aureus*. Model 2 is a protein similar to the hypothetical methyl malonyl-CoA decarboxylase alpha subunit commonly found in *Sulfolobus tokodaii*. Model 3 is a protein Acetyl-CoA carboxylase which is commonly found in Acetyl-CoA carboxylase in complex with compound 1, especially in yeast. Model 4 is the Acetyl-Coa Carboxylase protein ACC2 CT Domain in Complex with Inhibitor commonly found in Bovine (Figure 2). Based on the value of sequence identity, we chose the putative protein model 1 for further analysis and we made it a template for determining the functional regions of the CrACCase protein.

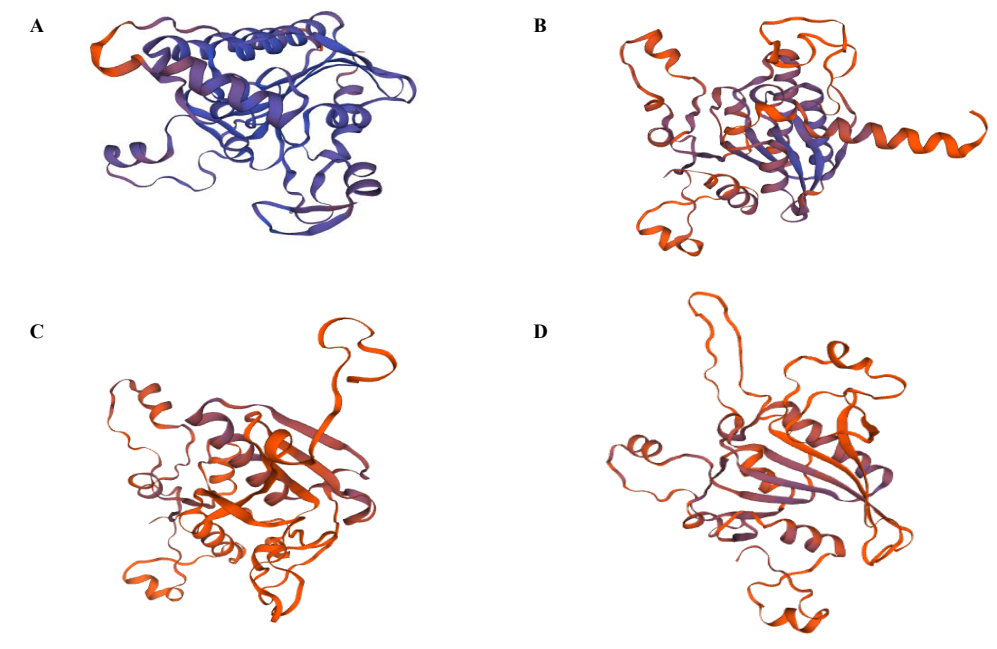


Figure 2. Prediction of the protein structure of CrACCase in *Chlamydomonas reinhardtii* using the SWISS-MODEL, I-TASSER, ORION, and MODELLER programs. The putative protein structures are acetyl-coenzyme A carboxylase carboxyl transferase subunit beta, Crystal Structure of the carboxyltransferase subunit of ACC (A). Hypothetical methyl malonyl-CoA decarboxylase alpha subunit, Crystal Structure of the carboxyl transferase subunit of putative PCC of *Sulfolobus tokodaii* (B). Acetyl-CoA carboxylase, Crystal Structure of the humanized carboxyltransferase domain of yeast Acetyl-CoA carboxylase in complex with compound 1 (C). Acetyl-Coa Carboxylase. Bovine ACC2 CT Domain in Complex with Inhibitor (D).

3.3. Functional Region Analysis of the CrACCase Protein

Analysis of functional areas of CrACCase protein can be studied in several ways, one of which is by identifying important amino acid residues. The putative CrACCase protein was analyzed by general composition, glycine composition, proline composition, and pre-proline composition. Based on the Ramachandran Plots, the composition of amino acid residues in CrACCase protein is found at three main centers, while in the composition of Glycine there are six main points with 2 main centers that are opposite the residue values. The amino acid residue composition of proline shows two central values of Ramachandran Plots, whereas pre-proline is located at one main center point (Figure 3).

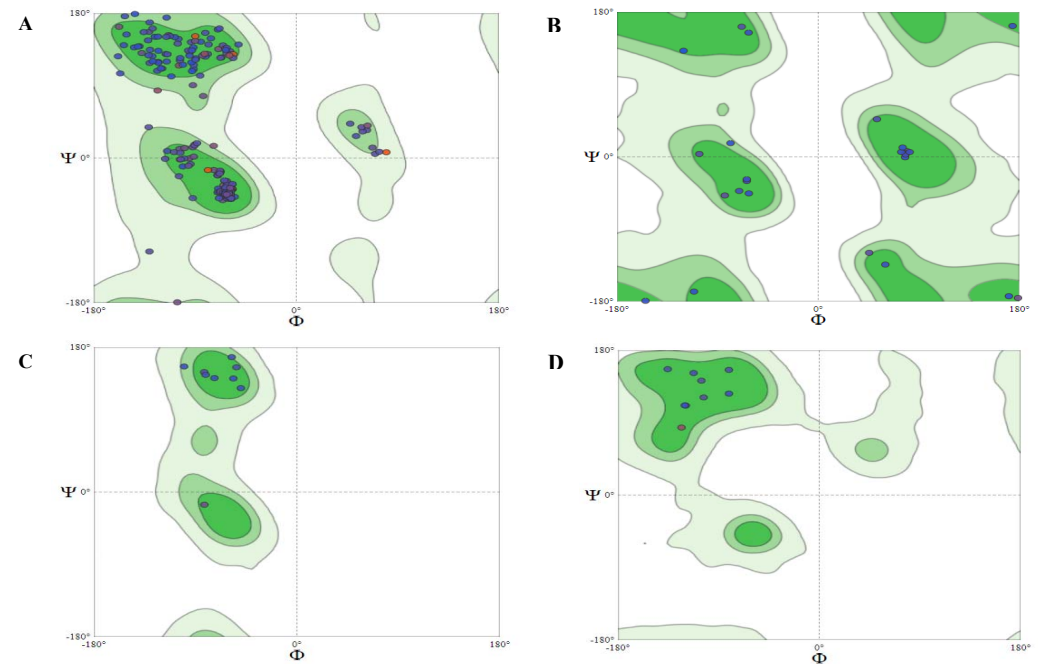


Figure 3. Ramachandran Plots of Amino Residue of putative protein CrACCase in *Chlamydomonas reinhardtii*. General (A), Glycine (B), Proline (C), Pre-Proline (D). Amino acid residues are generally concentrated at three main points. Amino acid residues were tested using the SWISS-MODEL program.

In addition to the composition of the amino acid residues, the functional regions of the CrACCase protein can be tested with local quality estimates, Z-scores of the non-redundant set of PDB structure, Global QMEANDisCo values, and QMEAN Z-scores (Figure 4). Based on local quality estimates, amino acid residues with values of 0.3-0.8 were found around the 150th and 260th residues. The majority of amino acid residues had predicted local similarity values of 0.7-0.9 at residues 90

to 340 (Figure 4A). The amino acid model constructed in this study showed a Z-score between 0.5 and 1.0, so the putative protein structure model tested in this study showed a high level of confidence (Figure 4B). Global QMEANDisCo value in this study also showed a value above 75 percent with details of QMEAN value of -0.76, C β of -0.88, All-atom of 0.41, solvation value of -0.34, and torsion of -0.54 (Figure 4C).

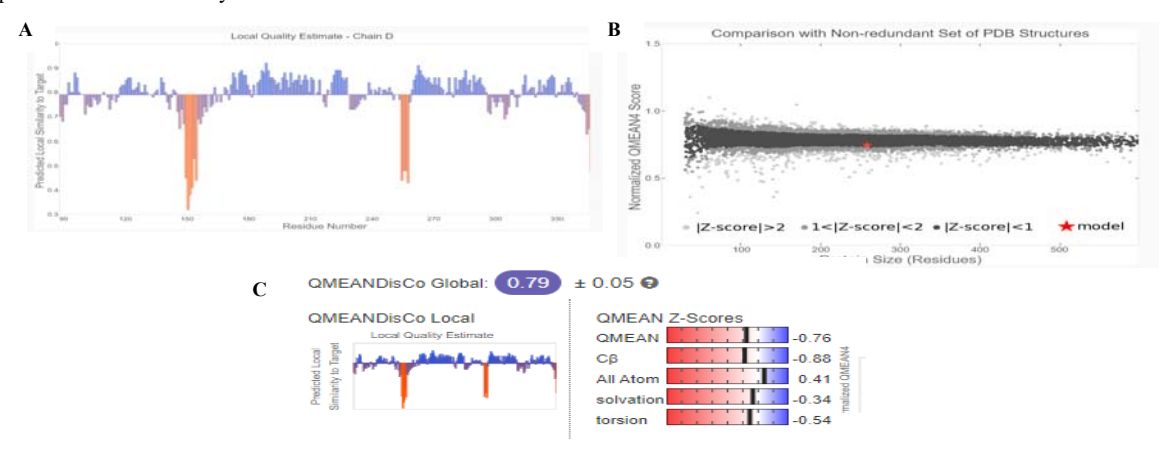


Figure 4. Quality estimates of the structure of the CrACCase protein in *Chlamydomonas reinhardtii*. Local quality estimates (A), Comparison PDB structure (B), and QMEANDisCo Global Value (C) of CrACCase protein structure.

3.4. Interaction between CrACCase Mutant Protein and Zinc Ligand

The putative sequence of CrACCase showed a structural similarity with the template at the 90th to 346th amino acids. Based on protein sequence investigations, putative proteins had relatively similar QMEAN values for almost all amino acid residues (Figure 5A). Changes in frameshift mutations in the *CrACCase* gene are located at the 1086 bp nucleotide and the amino acids after that change and result in changes in protein structure. In addition to the structure, it also resulted in a change in the functional area of the ligand-protein binding site at residues D:C 92, 95, 111, and 114 where this site is a zinc ion binding site. The D or C residues are amino acid residues that code for cysteine and aspartic acid. These two amino acids play an important role in the binding of

ligands in the form of zinc ions (Figure 5B, 5C). Four residues bind to zinc ions to form a D:C chain and four PLIP interactions form a metal complex structure. Based on the search of the ligand database on the RCSB PDB, we got information that the zinc ligand type in the putative protein CrACCase has a cation in the form of zinc⁺² cation, Zn formula, molecular weight 65.41, non-polymer type, isomeric smiles [Zn+2], InCHI = 1S /Zn/q+2, InChIKey PTFCDOFLOPIGGS-UHFFFAOYSA-N. In addition, the zinc ligand has a formal charge of 2, an atomic count of 1, and does not have a chiral atom count, bond count, and aromatic count. Thus, the bioinformatics construction of sgRNA can lead to changes in protein structure and changes in the binding of zinc ligands to the protein active site of CrACCase in *Chlamydomonas reinhardtii* species.

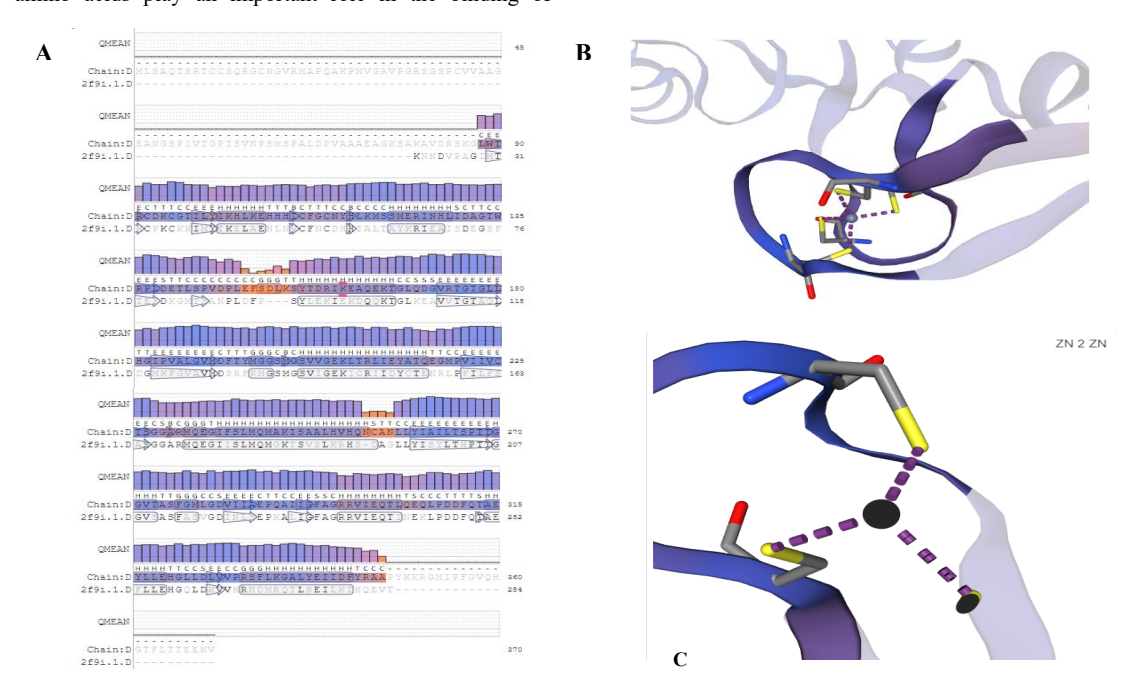


Figure 5. Amino acid residue analysis using SWISS-MODEL analysis. Alignment between CrACCase and protein template model (A), Ligand-amino acid residue interaction (PLIP/chain D interaction) in the active site of CrACCase protein (B), and Zinc-Zinc (ZN 2 ZN) binding (C).

4. Discussion

Chlamydomonas reinhardtii is a microalga belonging to the Division Chlorophyta, Classis Chlorophyceae, Ordo Volvocales, Family Chlamydomonadaceae, and Genus Chlamydomonas (Wilson and Loomis, 1962; Bold and Wynne, 1985; Barsanti and Gualtieri, 2006; Ghufran and Kordi, 2010). This organism is used very little as a source of biofuel even though Rengel et al., (2018) reported that the content of triacylglyceride (TAG) is 2.4 times more than other microalgae species (Hariyanti, 1994; Yani, 2003; Harada et al., 2007; Hubbard et al., 2008; Bellinger and Sigee, 2010; Joo et al., 2010). In recent studies, we developed the potential of the use of C. reinhardtii, especially as a resource of TAG content and Biofuel. We improved the in-silico method to find the potency of gene and protein of Acetyl-CoA Carboxylase (CrACCase) and predict their mutant. In this study, we provided Oligo

guide putative RNA to engineer or create mutant genes of *CrACCase*. Based on our investigation, the best target sgRNA sequences were GCGTCTGCTCAATCACA CGGCGG, TTGAGGTCGGAACTCCAGCGG, and AGGCAATACCCTCAATTGGGGG (Figure 1, Table 1).

Changes in DNA structure in the functional area of a gene can replace the function and structure of a protein (Sharma *et al.*, 2018) including *CrACCase*. Based on information on changes in the mutant sequence in genome editing of sgRNA, we found that there were changes in the secondary, tertiary, and quaternary structure of the CrACCase protein, especially in the complex structure of the domain, β -sheet, and number of α -helix (Figure 2). Changes in the functional area of the CrACCase protein are thought to affect the function of CrACCase in acting as a key enzyme in the fatty acid biosynthesis pathway (Sharma *et al.*, 2018; Miftahudin *et al.*, 2021; Halim *et al.*, 2021). The enzymes CrACCase, Acetyl CoA synthase (ACS), and Acyl-ACP reductase which change their

structure can enhance fatty acid biosynthesis in microalgae, especially C. reinhardtii (Sharma et al., 2018). We suspect that genetically modified mutations in the CrACCase mutant in-silico could alter the structure and function of the enzyme and further increase TAG production and lipid biosynthesis. The production of mutants and transgenic over-expression of genetic engineering has been shown to increase the production of TAG in Microalgae, i.e., C. cryptica, D. salina, Schizochytrium sp., and C. merolae (Sharma et al., 2018). Genetic engineering of the CrACCase gene can be carried out further by considering the bioinformatics test data that we have done. Bioinformatics prediction with genome editing CRISPR/Cas9 was also commonly used in other organisms such as rice in studying DLT and OsGERLP genes (Miftahudin et al., 2021; Halim et al., 2021). Insilico information on both genes was proven after genetic engineering resulted in mutants and transgenics that were different from their wild type especially in the mRNA gene expressions (Siska et al., 2017; Fendiyanto et al., 2021; Satrio et al., 2021; Miftahudin et al., 2021). Specifically for the microalgae C. reinhardtii, we examined the functional regions of the protein comprehensively and looked at the ligand-binding region, as well as changes in enzyme function.

Recently, mass microalgae culture with bioreactors (Peng et al., 2016) can be used as an alternative to meet bioenergy needs, especially biodiesel (Brennan and Owende, 2010; Sharma et al., 2018). However, the efficiency of lipid production through the triacylglyceride metabolic pathway (TAG), is vital to study to increase lipid production in microalgae (Cooksey et al., 1987; Duong et al., 2015; Sharma et al., 2018). Especially for the species Chlamydomonas reinhardtii, genome editing of the ACCase gene has not been reported; therefore, this study is the first step in carrying out genetic manipulation to increase lipid production. In addition to increased lipid production with biocatalysts (Rodolfi et al., 2009; Yun et al., 2014), a genome editing approach becomes important. This genetic engineering can be done by looking for markers both at the gene level (Diaz et al., 2010; Fendiyanto et al., 2019a; Miftahudin et al., 2021), genome (Countway et al., 2005; Zhu et al., 2005; Fendiyanto et al., 2019b; Pratami et al., 2020), mRNA (Satrio et al., 2019), or metabolites (Chini-Zittelli et al., 2006; Ramasamy et al., 2015; Fendiyanto et al., 2020; Fendiyanto et al., 2021) in metabolic pathways certain.

Changes in the structure of amino acid residues in CrACCase seemed to change greatly based on the residue composition of Proline, Glycine, and Pre-Proline (Figures 3, 4). Changes in protein structure residues in Proline and Glycine are related to changes in the function of an enzyme according to Sharma et al., (2018). The interaction of the CrACCase enzyme was also validated concerning the PLIP/chain D interaction in the active site of CrACCase protein and Zinc-Zinc (ZN 2 ZN) binding (Figure 5). Zinc ligands related to the role of CrACCase protein are thought to be related to regulatory functions or transcription factors that can work more actively in the presence of zinc ions. This structural and functional change resulted in the mode of action of the CrACCase protein. This bioinformatics information is important to perform in-vivo genome editing on the CrACCase in the future so that mutants with the highest TAG production or the highest biodiesel (oil body) producer can be obtained. The manipulation of the *CrACCase* gene in *Chlamydomonas reinhardtii* can be applied to other microalgae organisms with the highest lipid percentages to increase future bioenergy production by molecular biologists and biotechnologists.

5. Conclusion

The location of the mutation of the CrACCase gene, the result of genome editing using chop-chop tools, was found in the XM 001703135.1:1089 region, especially in the negative thread. The putative protein of CrACCase was predicted to have the structure of carboxyl transferase subunit of ACC, carboxyl transferase subunit of putative PCC, humanized carboxyltransferase domain of yeast Acetyl-CoA carboxylase, and Acetyl-CoA Carboxylase. Changes in frameshift mutations in the CrACCase gene result in structural changes of the functional regions of the ligand-protein binding sites at residues D:C 92, 95, 111, and 114 where these sites are zinc ion binding sites. This structural change results in a change in the function of the CrACCase protein. Manipulation of the CrACCase gene in Chlamydomonas reinhardtii can also be used as a source of information to biotechnologists and biologists to increase the production of lipids or TAG as an alternative to biodiesel or renewable bioenergy in the future.

Acknowledgments

This research was supported by the Defense Ministry of the Republic of Indonesia for funding this research through Dr. Mentari Putri Pratami, S.Si., M.Si fiscal year 2021 through LP2M, the Republic of Indonesia Defense University (RIDU) Funding. We thank Molecular Biology and Bioinformatics Laboratory, Biology Study Program, Indonesia Defense University for their guidance in insilico analysis of *CrACCase* characterization.

References

Alam F, Date A, Rasjidin R, Mobin S, Moria H and Baqui A. 2012. Biofuel from algae – is it a viable alternative?. *Procedia Eng*, **49**:221–227.

Altschul SF, Madden TL and Schäffer AA. 1997. Gapped BLAST and PSI-BLAST: a new generation of protein database search programs. *Nucleic Acids Res*, **25**:3389–3402.

Barqi WS. 2015. Extraction of oil from microalgae *Chlorella* sp. with the method of microwave assisted extraction. *JBAT*, **4(1)**: 34-41.

Barsanti L and Gualtieri P. 2006. Microalgae. CRC Press, New York.

Bellinger EG and Sigee DC. 2010. Lipid Production of Microalgae. John Willey & Sons, New York.

Bienert S, Waterhouse A and de Beer TAP. 2017. The SWISS-MODEL Repository - new features and functionality. *Nucleic Acids Res*, **45**:313-319.

Bligh EG and Dyer WJ. 1959. A rapid method for total lipid extraction and purification. *J Biochem Physiol*, **37**:911-917.

Bold HC and Wynne MJ. 1985. **Introduction to the Algae Structure and Reproduction**, second edition. Prentice-Hall Inc, New Jersey.

Bouabidi ZB, EI-Naas M and Zhang Z. 2018. Immobilization of microbial cells for the biotreatment of wastewater: a review. *Environ Chem Letter*, 2:1-15.

Brennan L and Owende P. 2010. Biofuels from microalgae-a review of technologies for production, processing, and extractions of biofuels and co-products. *Renew Sustain Energy Rev*, 14(2):557–577.

Bringezu S, Ramesohl S, Arnold K, Fischedick M and Von Geibler J. 2007. Towards a sustainable biomass strategy: what we know and what we should know. *Wuppertal*, **2**:1-16.

Brown LM, Sprague S, Jarviss EE, Roessler PG and Zeiler KG. 1994. Biodiesel from aquatic species. *IJEB*, **42**: 5726-5731.

Chini-Zittelli G, Rodolfi L, Biondi N and Tredici MR. 2006. Productivity and photosynthetic efficiency of outdoor cultures of *Tetraselmis suecica* in annular columns. *Aquaculture* **261(3)**:932–943

Chisti Y. 2007. Biodiesel from microalgae, biotechnology advances. *Biotech*, **25**: 294-306.

Cooksey KE, Gukert JB, Williams SA and Collis PR. 1987. Fluorometric determinant of the neutral lipid content of microalgal cells using nile red. *J Microbiol Met*, **6**: 333-345.

Countway P, Gast RJ, Savala P and Caron DA. 2005. Protistan diversity estimates based on 18S rDNA from seawater incubations in the Western North Atlantic. *J Eukaryot Microbiol*, **52(2)**:95–106

Demirbas MF. 2011. Biofuels from algae for sustainable development. *Appl Energy*, **88(10)**:3473–3480.

de Brevern AG, Etchebest C and Hazout S. 2000. Bayesian probabilistic approach for predicting backbone structures in terms of protein blocks. *Proteins*, **41**: 271-287.

Diaz MR, Jacobson JW, Goodwin KD, Dubar S and Fell JW. 2010. Molecular detection of harmful algal blooms (HABs) using locked nucleic acids and bead array technology. *Limnol Oceanogr Met* **8**:269–284

Duong VT, Ahmed F, Thomas-Hall SR, Quigley S, Nowak E and Schenk PM. 2015. High proteinand high lipid-producing microalgae from northern Australia as potential feedstock for animal feed and biodiesel. *Front Bioeng Biotechnol*, **3**:47-53. doi: 10.3389/fbioe.2015.00053.

Eisentraut A. 2010. Sustainable production of second-generation biofuels, potential and perspectives in major economies and developing countries. *Bioenergy*, 2:1-15.

Fendiyanto MH, Satrio RD, Suharsono, Tjahjoleksono A and Miftahudin. 2019a. Correlation among Snpb11 markers, root growth, and physiological characters of upland rice under aluminum stress. *Biodiversitas*, **20(5)**: 1243-1254. DOI; 10.13057/biodiv/d200514.

Fendiyanto MH, Satrio RD, Suharsono, Tjahjoleksono A, Hanarida I and Miftahudin. 2019b. QTL for aluminum tolerance on rice chromosome 3 based on root length characters. *SABRAO J Breed Genet*, **51**(**4**): 451-469.

Fendiyanto MH, Satrio RD and Darmadi D. 2020. Metabolic profiling and pathway analysis in red arillus of Salacca sumatrana demonstrate significant pyruvate, sulfur, and fatty acid metabolisms. *Biodiversitas*, **21**(9): 4361-4368. DOI: 10.13057/biodiv/d210955.

Fendiyanto MH, Satrio RD, Widana IDKK, Pratami MP, Nikmah IA and Darmadi D. 2021. Differential hierarchical metabolites expression of red/white *Salacca sumatrana* arillus and its molecular docking studies. *Biodiversitas*, **22(2)**: 1014-1024. DOI: 10.13057/biodiv/d220258.

Fendiyanto MH, Satrio RD, Pratami MP, Nikmah IA, Sari NIP, Widana IDKK and Darmadi D. 2021. Analysis of *Superoxide Dismutase (OsSOD)* gene expression using qRT-PCR, its morphophysiological characters, and path analysis in rice variety IR64 under aluminum stress. Intl J Agric Biol, **6(1)**: 131-138.

Galluzzi L, Penna A, Bertozzini E, Vila M, Garces E and Magnani M. 2004. Development of a real-time PCR assay for rapid detection and quantification of *Alexandrium minutum* (a dinoflagellate). *Appl Environ Microbiol*, **70(2)**:1199–1206.

Galluzzi L, Bertozzini E, Penna A, Perini F, Garcés E and Magnani M. 2010. Analysis of rRNA gene content in the Mediterranean dinoflagellate *Alexandrium catenella* and *Alexandrium taylori*: implications for the quantitative real-time PCR-based monitoring methods. *J Appl Phycol*, **22(1)**:1-9.

Ghufran A and Kordi L. 2010. Budi Daya Bioata Akuatik untuk Pangan, Kosmetik, dan Obat-Obatan. Andi, Yogyakarta.

Godhe A, Asplund ME, Härnström K, Saravanan V, Tyagi A and Karunasagar I. 2008. Quantification of diatom and dinoflagellate biomasses in coastal marine seawater samples by real-time PCR. *Appl Environ Microbiol*, **74(23)**:7174–7182.

Ghouzam Y, Postic G and de Brevern AG. 2015. Improving protein fold recognition with hybrid profiles combining sequence and structure evolution. *Bioinformatics*, **31**:3782-3789.

Halim I, Fendiyanto MH and Miftahudin M. 2021. sgRNA design for DLT gene editing using CRISPR-Cas9 and in-silico mutation prediction in Rice cv. Hawara Bunar. *IOP Conf Ser Earth Environ Sci*, **948**:1-13.

Harada A, Ohtsuka S and Horiguchi T. 2007. Species of the parasitic genus *Duboscquella* are members of the enigmatic marine alveolate group I. *Protist*, **158**: 337-347.

Hariyanti R. 1994. **Kelimpahan dan Keanekaragaman Mikroalga di Sumber Air Panas Gonoharjo Kendal** [skripsi]. Universitas Diponegoro, Semarang.

Hu Q, Sommerfeld M, Jarvis E, Ghirardi M, Posewitz M and Seibert M. 2008. Microalgal triacylglycerols as feedstocks for biofuel production: perspectives and advances. *Plant J*, **54**:621-639

Hubbard KA, Rocap G and Armbrust EV. 2008. Inter- and intraspecific community structure within the diatom genus *Pseudo-nitzschia* (Bacillariophyceae). *J Phycol*, **44(3)**:637–649.

Jones CS and Mayfield SP. 2012. Algae biofuels: versatility for the future of bioenergy. *Curr Opin Biotechnol*, **23(3)**:346–51.

Joo S, Lee S-R and Park S. 2010. Monitoring of phytoplankton community structure using terminal restriction fragment length polymorphism (T-RFLP). *J Microbiol Method*, **81**(1):61–68.

Khan SA, Hussain MZ, Prasad S and Banerjee UC. 2009. Prospects of biodiesel production from microalgae in India. *Renew Sustain Energy Rev* **13(9)**:2361–2372.

Lee RE. 1980. **Phycology**. Cambridge University Press, New York.

Medipally SR, Yusoff FMd, Banerjee S and Shariff M. 2015. Microalgae Review. *Biomed Res*, **15**:1-13. DOI:10.1155/2015/519513.

Miftahudin M, Roslim DI, Fendiyanto MH, Satrio RD, Zulkifli A, Umaiyah EI, Chikmawati T, Sulistyaningsih YC, Suharsono S, Hartana A, Nguyen HT and Gustafson JP. 2021. *OsGERLP*: A novel aluminum tolerance rice gene isolated from a local cultivar in Indonesia. *Plant Physiol Biochem*, **162**: 86-99. DOI: 10.1016/j.plaphy.2021.02.019.

Milano J, Ong HC, Masjuki HH, Chong WT and Lam MK. 2016. Microalgae biofuels as an alternative to fossil fuel for power generation. *Renew Sustainable Energy Rev*, **58**: 180-197.

Okonechnikov K, Golosova O and Fursov M. 2012. Unipro UGENE: a unified bioinformatics toolkit. *Bioinformatics*, **28(8)**: 1166-1167

Peng L, Lan CQ and Zhang Z. 2013. Evolution, detrimental effects, and removal of oxygen in microalga cultures: a review. *Environ Prog Sustain*, **32(4)**:982-988.

Peng L, Zhang Z, Cheng P, Wang Z and Lan CQ. 2016. Cultivation of *Neochloris oleoabundans* in bubble column photobioreactor with or without localized deoxygenation. *Biores Technol*, **206**:255–263.

Pratami MP, Chikmawati T and Rugayah R. 2020. Genetic diversity of *Cucumis* and *Mukia* (Cucurbitaceae) based on ISSR markers. *SABRAO J Breed Genet*, **52(2)**: 127-143.

Ramasamy P, Lee K, Lee J and Oh YK. 2015. Breaking dormancy: an energy-efficient means of recovering astaxanthin from microalgae. *Green Chem*, **17**:1226–1234.

Ratha SK and Prasanna R. 2012. Bioprospecting microalgae as potential sources of 'Green Energy'—challenges and perspectives (review). *Appl Biochem Microbiol*, **48(2)**:109–125.

Rodolfi L, Zittelli GC, Bassi N, Padovani G, Biondi N, Bonini G and Tredici MR. 2009. Microalgae for oil: strain selection, induction of lipid synthesis and outdoor mass cultivation in a low-cost photobioreactor. *Biotechnol Bioeng*, **102(1)**:100–112.

Satrio RD, Fendiyanto MH, Suharsono, Supena EDJ and Miftahudin. 2019. Identification of drought-responsive regulatory genes by hierarchical selection of expressed sequence tags and their expression under drought stress in rice. *Intl J Agric Biol*, **22(6)**: 1524-1532.

Satrio RD, Fendiyanto MH, Suharsono, Supena EDJ and Miftahudin. 2021. Genome-wide SNP discovery, linkage mapping, and analysis of QTL for morpho-physiological traits in rice during vegetative stage under drought stress. Physiol Mol Biol Plants, 27(11): 2635-2650. doi: 10.1007/s12298-021-01095-y

Scott SA, Davey MP, Dennis JS, Horst I, Howe CJ and Lea-Smith DJ. 2010. Biodiesel from algae: challenges and prospects. *Curr Opin Biotechnol*, **21**: 277–286.

Shuba ES and Kifleb D. 2018. Microalgae to biofuels: 'Promising' alternative and renewable energy. *Renew Sustain Energy Rev*, **81**:743–755.

Sharma PK, Saharia M, Srivstava R, Kumar S and Sahoo L. 2018. Tailoring microalgae for efficient biofuel production. *Front Mar Sci*, 5:382. doi: 10.3389/fmars.2018.00382

Spolaore P, Joannis-Cassan C, Duran E and Isambert A. 2006. Commercial applications of microalgae. *J Biosci Bioeng*, **101(2)**:87–96.

Söding J. 2005. Protein homology detection by HMM-HMM comparison. *Bioinformatics*, **21**:951–960.

Suali E and Sarbatly R. 2012. Conversion of Microalgae to Biofuel. *Renew Sustain Energy Rev*, **16**: 4316-4342.

Ummalyma SB, Gnansounou E, Sukumaran RK, Sindhu R, Pandey A and Sahoo D. 2017. Bioflocculation: an alternative strategy for harvesting of microalgae—an overview. *Bioresour Technol*, **242**:227–235.

Waterhouse A, Bertoni M and Bienert S. 2018. SWISS-MODEL: homology modelling of protein structures and complexes. *Nucleic Acids Res*, **46**:296-303.

Weldy CS and Huesemann M. 2007. Lipid production by Dunaliella salina in batch culture: effects of nitrogen limitation and light intensity. *J Res*, **101**:86-92.

Wilson CL and Loomis WE. 1962. **Botany**, Third edition. Holt, Rinehart and Winston Inc , New York.

Yani AP. 2003. Identifikasi jenis-jenis mikroalga di sumber air panas sungai air putih zona penyanggah Taman Nasional Kerinci Seblat di Kecamatan Lebong Utara Propinsi Bengkulu. *J Penelitian UNIB*, 9:42-44.

Yun YM, Kim DH, Oh YK, Shin HS and Jung KW. 2014. Application of a novel enzymatic pretreatment using crude hydrolytic extracellular enzyme solution to microalgal biomass for dark fermentative hydrogen production. *Bioresour Technol*, **159**:365–372.

Zhu F, Massana R, Not F, Marie D and Vaulot D. 2005. Mapping of picoeukaryotes in marine ecosystems with quantitative PCR of the 18S rRNA gene. *FEMS Microbiol Ecol*, **52**:79–92.



Potential for Crude Oil and Diesel Biodegradation by the Indigenous *Pseudomonas* sp. Strain LGMS7 Using GC-MS and GC-FID Analyses

Abdelkrim Chaida^{1,*}, Farid Bensalah¹, Belhadj Trari²

¹Laboratory of Microbial Genetics (LGM), Department of Biology, Faculty of Nature and Life Sciences, University Oran 1, 31000 Oran, Algeria; ²Laboratory of Bioactive Organic Synthesis, Department of Industrial Organic Chemistry, Faculty of Chemistry, University of Sciences and Technology of Oran Mohamed Boudiaf-USTO-MB, 31003 Oran, Algeria.

Received: August 14, 2021; Revised: December 24, 2021; Accepted: January 19, 2022

Abstract

Pollution caused by hydrocarbons in the environment is a serious global issue, especially in countries in development such as Algeria. In this context, *Pseudomonas* sp. strain LGMS7 (MT071345) previously isolated from a soil contaminated with hydrocarbons, in Algeria, was selected to evaluate its crude oil and diesel degradation capacity, individually. For this, we have used an MSM medium with 1% (v/v) of crude oil and 2% (v/v) of diesel as the sole carbon sources, individually, incubated for 27 days at room temperature (25 ± 1 °C) and 150 rpm, and analysed with GC-MS and GC-FID, respectively. Consequently, after analysing of the chromatogram, the results revealed the presence of a linear fraction of aliphatic hydrocarbons *n*-alkane (C13-C30) of average molecular weight for crude oil, with highly biodegradation efficiency of 98.50%. Nevertheless, biodegradation efficiency of 100% was recorded for the lightest molecules of the *n*-alkane fraction (C13-C30), which corresponds to the C13-C14 molecules, and for the heaviest molecules of the same *n*-alkane fraction, which corresponds to molecules C27-C30. Furthermore, biodegradation efficiency >96.00% was recorded for the C15-C26 fraction. While for diesel, biodegradation efficiency of 70% was recorded. Because of its intriguing biodegradation properties for hydrocarbons, this strain appears to be a promising bioremediation candidate for hydrocarbon-polluted soils in Algeria.

Keywords: Biodegradation; Crude oil; Diesel; GC-FID; GC-MS; Pollution

1. Introduction

Crude oil-derived hydrocarbons are the most common type of pollution in the world's environment (Ławniczak *et al.*, 2020). Their carcinogenic, mutagenic and toxic nature poses a serious problem for ecosystems and living beings (Varjani and Upasani, 2016). Algeria is a major oil producer in Africa, with a primarily fossil-fuel-based economy like oil and natural gas (Chaida *et al.*, 2021; Harrouz *et al.*, 2017). However, the consequences of such production are devastating for the environment. Regardless of the pollution source, accidental or as a result of various extraction, refining, or transport activities, it is threatening the life of living beings and endangering the purity of groundwater, a significant source for Algeria's freshwater supply, by the permeability of hydrocarbons through the soil or the sand (in the case of Sahara).

For pollution treatment, various biological and physicochemical methods can be considered. Among these methods is the microorganism-mediated bioremediation method, which is considered to be as a better bio-based approach to remove petroleum hydrocarbons from contaminated sites because it is an economical, profitable,

green, and sustainable method (Elkarmi et al., 2008; Logeshwaran et al., 2018).

Crude oil is divided into two main categories: aliphatic and aromatic hydrocarbons, which might be pronounced recalcitrant and threatening to health (Hidayat and Tachibana, 2012). Several bacterial strains can easily degrade the major crude oil's aliphatic component. However, the polycyclic aromatic hydrocarbons (PAHs) and large branched-chain fractions, on the other hand, are difficult to degrade because of their complex structures. (Hasanuzzaman *et al.*, 2007; Khan *et al.*, 2019).

Diesel, defined as a complicated hydrocarbon pollutant, consists of an aggregate of alkanes and aromatics, which are regularly stated as soil pollutants (Gallego *et al.*, 2001). The microorganisms' natural abilities to overcome the constraints of bioavailability plague the bioremediation of those pollutants. In addition, pH, nutrients, electron acceptor availability and temperature are among the environmental factors to consider (Mukherji and Vijay, 2002).

For bioremediation of crude oil-polluted sites, several bacterial strains have been reported in the literature, belonging to the genera "Alcaligenes, Brevibacillus, Paenibacillus, Stenotrophomonas,

 $^{^* \} Corresponding \ author. \ e-mail: chaida.abdelkrim@edu.univ-oran1.dz\ ; \ chaida.abdelkrim@gmail.com.$

^{**} Abbreviations: MSM: Mineral Salt Medium; NB medium: Nutrient broth medium; GC-FID: Gas chromatography-flame ionization detection; GC-MS: Gas chromatography-Mass spectrometry

Lysinibacillus, Bacillus, Delftia, Achromobacter, and Pseudomonas" (Roy et al., 2014). However, Pseudomonas sp., and Achromobacter xyloxidans have been identified as the best biodegraders of hydrocarbons. Moreover, special strategies including Gas chromatography (GC) in addition to gas chromatography-mass spectrometry (GC-MS) may be employed to evaluate crude oil's ability to degrade by comparison of abiotic and biotic control (Varjani et al., 2015).

In Algeria, studies on the biodegradation of hydrocarbons are uncommon. However, a better understanding of the mechanisms involved in the degradation of hydrocarbons by indigenous microorganisms could be extremely important for future bioremediation programs at polluted sites.

In this context, the present study highlighted a promising capacity of the indigenous bacterium *Pseudomonas* sp. strain LGMS7 (MT071345) isolated from a hydrocarbon-polluted soil in western Algeria, capable to degrade crude oil and diesel at room temperature (25 \pm 1 °C), using greater in-intensity studies techniques, including GC-MS and GC-FID, to assess degradation performance of every oil individually.

2. Materials and methods

2.1. Strains and chemicals

Pseudomonas sp. strain LGMS7 was previously isolated from a hydrocarbon-contaminated soil at Ain El Arbaa, Algeria, after enrichment in the nutrient broth medium (NB) (Chaida et al., 2021) (Fig. 1). The sequence of 16S rRNA of the strain LGMS7 has been defined and placed in the GenBank nucleotide database under the accession number (MT071345). Regarding the chemicals, the crude oil and diesel gas were purchased from an oil refinery (NAFTEC) in Arzew and a service station in Oran, western Algeria, respectively. All additional chemicals that were used, including dichloromethane, were purchased from the Sigma-Aldrich Company.



Figure 1. Hydrocarbon-contaminated soil at Ain El Arbaa region (Aïn Temouchent city), Algeria

2.2. Media composition

The mineral salt medium (MSM) used consisted of (g/l): KH₂PO₄ (0.7), NaNO₃ (2), CaCl_{2.2} H₂O (0.1), FeSO_{4.7} H₂O (0.001), Na2HPO₄ (0.9), MgSO_{4.7} H₂O (0.4), as well as 1 ml of a solution composed of different trace element consisted of (g/l): Na₂MoO_{4.2} H₂O (0.06), CuSO_{4.5} H₂O (0.5), H₃BO₄ (0.26), MnSO₄. H₂O (0.5), ZnSO_{4.7} H₂O (0.7), for a litre of distilled water (Chebbi *et al.*, 2017). To achieve a pH of 7.2, solutions of (5M)

NaOH and (6N) HCl were used. Afterwards, separately, it was followed by the addition of crude oil and diesel at a rate of 1 and 2%, respectively. The medium was autoclaved at 121 °C for 20 minutes to sterilize it.

2.3. Growth of the strain LGMS7 using diesel and crude oil as only carbon sources

We have studied the strain LGMS7's capacity to grow utilizing only carbon sources from diesel and crude oil. The experiment was conducted with an inoculum of 3% (v/v) in Erlenmeyer flask composed of 100 ml of the MSM supplemented with (1%, v/v) of crude oil and (2%, v/v) of diesel individually, for 27 days of incubation at room temperature (25 \pm 1 °C), and 150 rpm. A 600-nm optical density measurement and colony-forming units (CFUs) were used to monitor bacterial growth. The abiotic control (without the addition of strain LGMS7) was also used with the same experimental conditions. Results are defined as the mean of two replicates experiments \pm standard deviation.

2.4. Liquid-liquid extraction of crude oil and diesel

A double liquid/liquid extraction with dichloromethane (Khan *et al.*, 2005) on abiotic control (without the LGMS7 strain) and biotic control (with the LGMS7 strain) was used for the recovery of the hydrocarbons tested (Fig. 2). Centrifugation was performed individually for 20 minutes at 6000 rpm to extract the supernatant after incubation of LGMS7 strain for 27 days at room temperature (25 ± 1 °C) in MSM medium containing (1%, v/v) and (2%, v/v) crude oil and diesel, respectively. The extraction operation was conducted by inserting an equal amount of the supernatant and the dichloromethane in a separation funnel (Khan *et al.*, 2005). A series of systematic stirring followed by degassing was carried out to extract the hydrocarbons found in the supernatant and retrieve them with the extraction solvent.



Figure 2. Extraction of crude oil and diesel with dichloromethane after incubation of the samples for 27 days at room temperature and at 150 rpm. (1) Crude oil (biotic control); (2) crude oil (abiotic control); (3) diesel (biotic control); (4) diesel (abiotic control)

2.5. GC-MS analyses

GC-MS analyses were carried out to confirm the strain LGMS7's ability to degrade crude oil using a Clarus 500 GC interfaced to a Clarus 500 MS equipped with an EI source and auto-injector. TurboMass software was used for data processing (PerkinElmer, USA). The chromatography of undifferentiated polar amines has been privileged using a special column (50% methyl-50% phenyl-silicone). The column temperature was ramped from 75°C for 1min to 275 °C at 10 °C/min, during 10 min, with a total of 31

minutes per sample. Helium was the carrier gas used at a debit of 1 ml/min and was brought to a pressure of 30 Psi. Both the injector and GC-MS transfer line temperatures were 250 °C. The injector had a double-tapered liner installed during which it was set to splitless mode for two minutes following the injection (volume of injection 1ml, the division ratio of 10: 1). The electron multiplier detector and the electron ionisation energy have been set to 358 V and of 70 eV, respectively. A rate of 250 scans/sec was used to acquire spectral data with a scanning range of 30 to 600 u. The percentage of degradation (%) of crude oil was calculated as follows:

Degradation percentage (%) = 100 - (Tpb x 100 / Tpa), where Tpb: Chromatogram's total peak area (biotic control); and Tpa: Chromatogram's total peak area (abiotic control) (Varjani *et al.*, 2015).

2.6. GC-FID analyses

The biodegradation potential of diesel by the LGMS7 strain was studied using a GC Perkin Elmer Clarus 500 with HS40 "Headspace" injector coupled to FID using an HP5 30 m*0.32 ID 0.25 μ m capillary column. The data acquisition and processing system was obtained using a computer equipped with Total Chrom 6.3 software. Helium (He) was used as a carrier gas, with 2 μ l injection volume using a split injection mode with a 5: 1 split ratio. A 40 °C pre-oven temperature was used to achieve a higher peak resolution, with 10 min preserve period; ramp

as much as 200 °C for 10 mn, with a upward push in pace of 5 °C/min. The temperatures of the detector and injector were both adjusted to 250 °C. Degradation percentage (%) of diesel was calculated as follows:

Degradation percentage (%) = 100 - (Tpb x 100 / Tpa), where Tpb: Chromatogram's total peak area (biotic control); and Tpa: Chromatogram's total peak area (abiotic control) (Varjani *et al.*, 2015).

2.7. Statistical analysis

Bacterial growth determination was performed at two replicates experiments. GraphPad Prism 6 (Trial version) was performed to calculate the means and standard deviations.

3. Results

3.1. Bacterial growth

Monitoring the growth of the strain LGMS7 during 27 days of incubation at room temperature, together with non-static conditions, has demonstrated its ability to grow individually with (1%, v/v) and (2%, v/v) crude oil and diesel, respectively in MSM medium, where maximum OD was registered at 0.52 ± 0.04 (300.10⁷ CFU/ml) and 0.92 ± 0.04 (200.10⁷ CFU/ml) (Fig. 3a, b). Accordingly, the stain LGMS7 is capable of metabolizing diesel and crude oil, which are used as the only carbon sources.

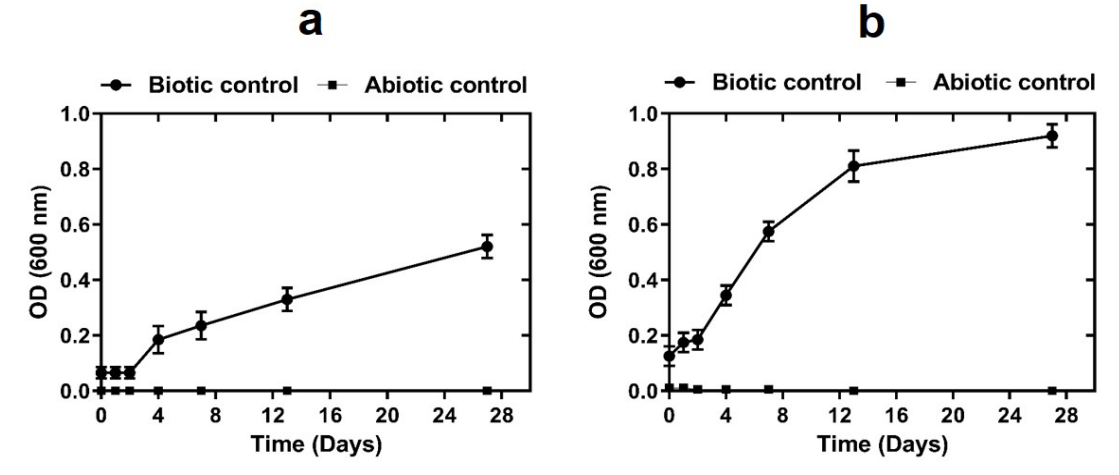


Figure 3. Growth monitoring (OD 600 nm); biotic control (●) and abiotic control (■) in the presence of (1%, v/v) of crude oil as sol carbon source (a); Growth monitoring (OD 600 nm); biotic control (●) and abiotic control (■) in the presence of (2%, v/v) of diesel as sol carbon source (b), of the strain LGMS7 for 27 days of incubation at room temperature, and 150 rpm

3.2. GC-MS analyses

Crude oil metabolizing capacity of strain LGMS7 was confirmed by GC-MS. However, examination of the obtained chromatograms revealed the presence of a linear fraction of aliphatic hydrocarbons *n*-alkane (C13-C30) of average molecular weight, i.e. with several carbon atoms of 13-30 (Table 1). Each chromatogram peak has a defined retention time that corresponds to a hydrocarbon molecule present in crude oil that was identified using mass spectrometry (MS) and a data library (Fig 4). Besides, through calculating the total peak area by integration,

which corresponds to each retention time recorded on the chromatograms of both biotic and abiotic controls, we obtained a very interesting degradation efficiency (%) of the n-alkane fraction (C13-C30), equal to 98.50%, with a degradation efficiency of 100% noted for the lightest molecules of the n-alkane fraction (C13-C30), which corresponds to the C13-C14 molecules, and for the heaviest molecules of the same n-alkane fraction, which corresponds to the C27-C30 molecules. Concerning the other C15-C26 molecules, degradation efficiency > 96.00% was recorded (Table 1, Fig. 5).

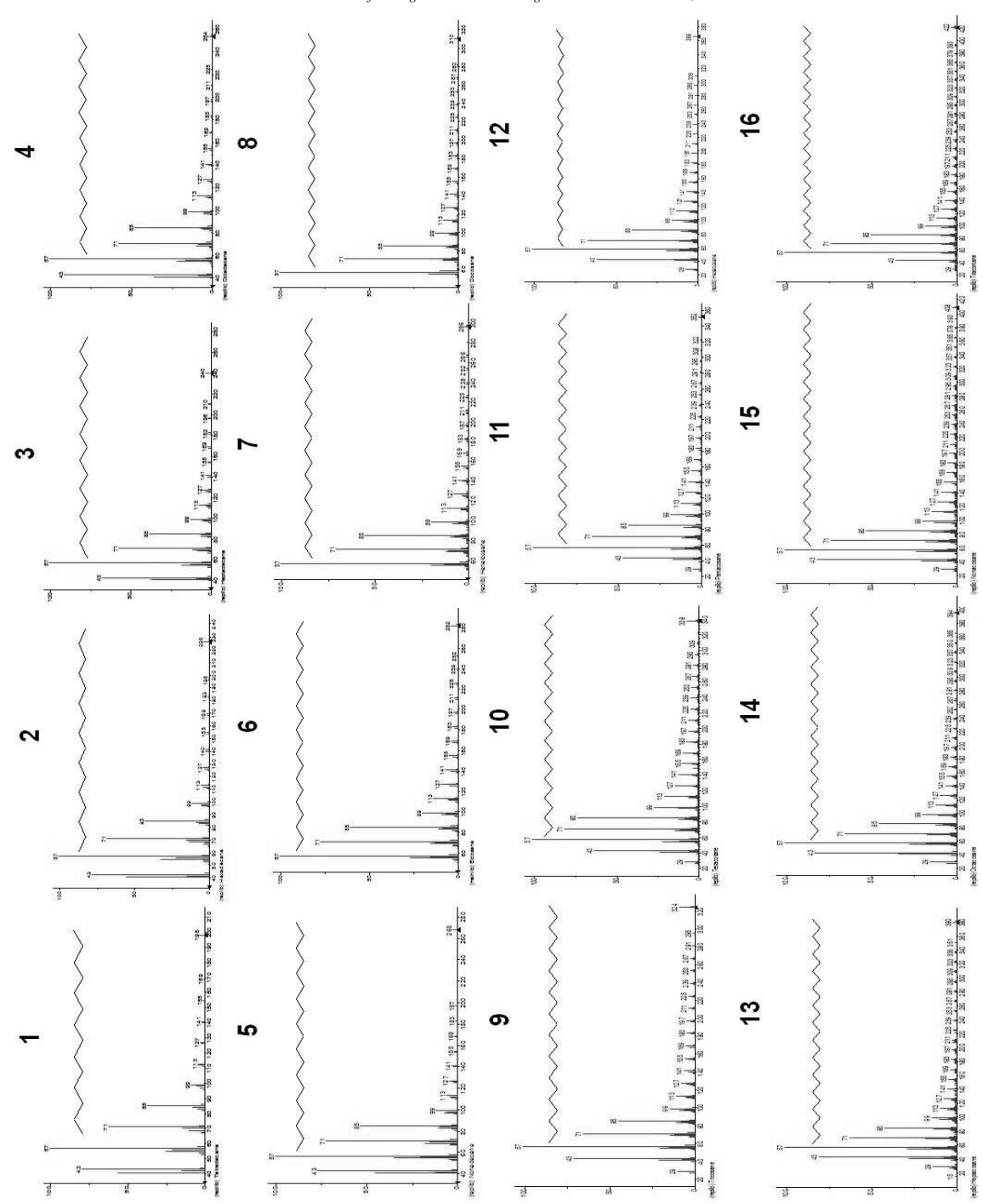


Figure 4. Mass spectrometry (MS) of the majority of components of *n*-alkanes in crude oil: Tetradecane (1), Hexadecane (2), Heptadecane (3), Octadecane (4), Nonadecane (5), Eicosane (6), Heneicosane 7), Docosane (8), Tricosane (9), Tetracosane (10), Pentacosane (11), Hexacosane (12), Heptacosane (13) Octacosane (14) Nonacosane (15), Triacontane (16)

Table 1. Degradation efficiency (%) of n-alkanes fraction of crude oil (1%, v/v) by Pseudomonas sp. strain LGMS7 after 27 days of incubation at room temperature and 150 rpm

Retention time (mn)	Molecular masse (g/mol)	Crude chemical formula	Compound	Degradation effeciency (%)
7.90	184	$C_{13}H_{28}$	Tridécane	100
9.27	198	$C_{14}H_{30}$	Tetradécane	100
10.54	212	$C_{15}H_{32}$	Pentadécane	100
11.75	226	$C_{16}H_{34}$	Hexadécane	99.074
12.90	240	$C_{17}H_{36}$	Heptadécane	97.522
13.97	254	$C_{18}H_{38}$	Octadécane	96.656
15.00	268	$C_{19}H_{40}$	Nonadécane	96.422
15.98	282	$C_{20}H_{42}$	Eicosane	96.803
16.91	296	$C_{21}H_{44}$	Heneicosane	98.125
17.82	310	$C_{22}H_{46}$	Docosane	97.985
18.68	324	$C_{23}H_{48}$	Tricosane	97.158
19.51	338	$C_{24}H_{50}$	Tetracosane	99.193
20.30	352	$C_{25}H_{52}$	Pentacosane	96.500
21.08	366	$C_{26}H_{54}$	Hexacosane	97.536
21.88	380	$C_{27}H_{56}$	Heptacosane	100
22.79	394	$C_{28}H_{58}$	Octacosane	100
23.87	408	$C_{29}H_{60}$	Nonacosane	100
25.15	422	$C_{30}H_{62}$	Triacontane	100

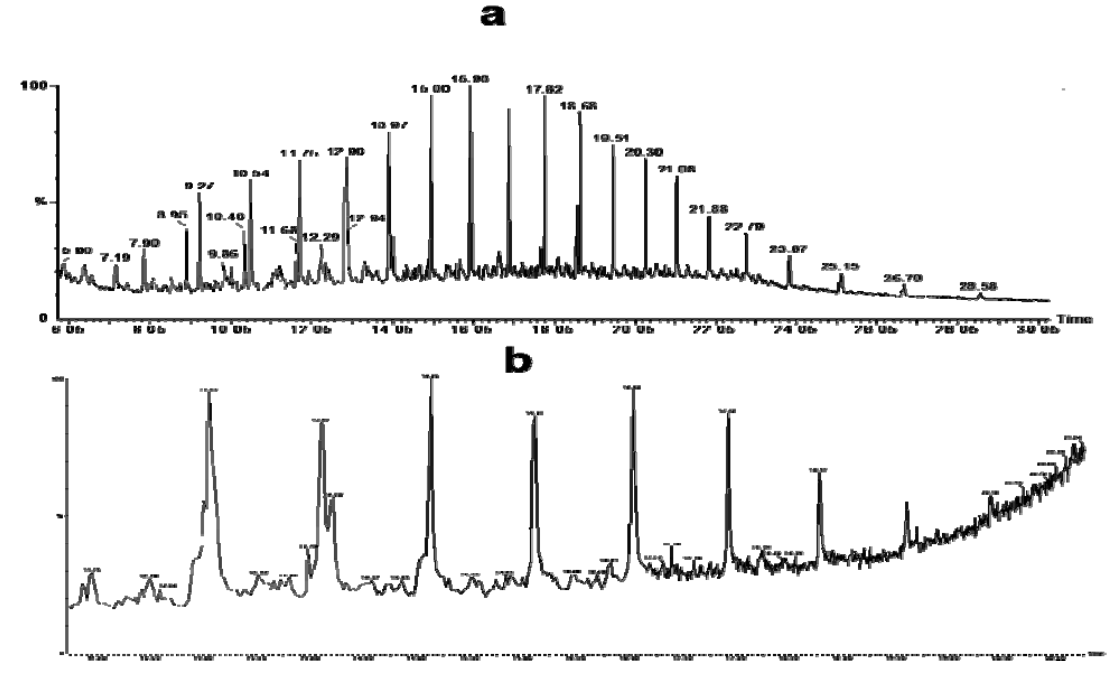


Figure 5. Crude oil (1%, v/v) analysis using GC-MS: (a) abiotic control; (b) biotic control

3.3. GC-FID analyses

GC-FID analysis confirmed strain LGMS7's ability to digest diesel oil (Fig. 6). Through calculating the total peak area by integration, we have recorded degradation efficiency (%) of 70% of the diesel fraction (Table 2). The retention times recorded on the chromatogram of the abiotic control (22.438 min, 26.233 min, 26.808 min, 29.585 min, and 32.640 min) were not recorded on the chromatogram of the biotic control. The disappearance of Table 2. Degradation efficiency (%) of diesel (2%, v/v) by *Pseudomonas* sp. strain LGMS7 after incubation period of 27 days of at room temperature and 150 rpm

the peaks is the result of total degradation of the studied fraction of diesel with an efficiency of 100%. In addition, biodegradation efficiency of 17.83%, 37.83%, 2.90%, 72.91%, 68.55% was recorded for the other compounds (Table 2). The peak recorded on the chromatogram of the biotic control at a retention time of 4.84 min, which is not recorded on the abiotic chromatogram, is probably a compound of the degradation products of diesel.

Abiotic control		Biotic control		
Retention time	peak area	Retention time	peak area	Degradation efficiency
(mn)	μV.s	(mn)	μV.s	(%)
2.60	23323.26	2.62	19164.75	17.83
3.31	386157.54	3.33	240086.53	37.83
4.51	8291158.41	4.55	8051391.46	2.90
no peak	/	4.84	8385.14	/
5.13	299386.5	5.16	81111.06	72.91
22.44	7945.57	no peak	/	100
26.23	31809.27	no peak	/	100
26.81	8456.81	no peak	/	100
29.59	29717.14	no peak	/	100
32.64	29316.84	no peak	/	100
35.46	16947.33	35.50	5330.96	68.55

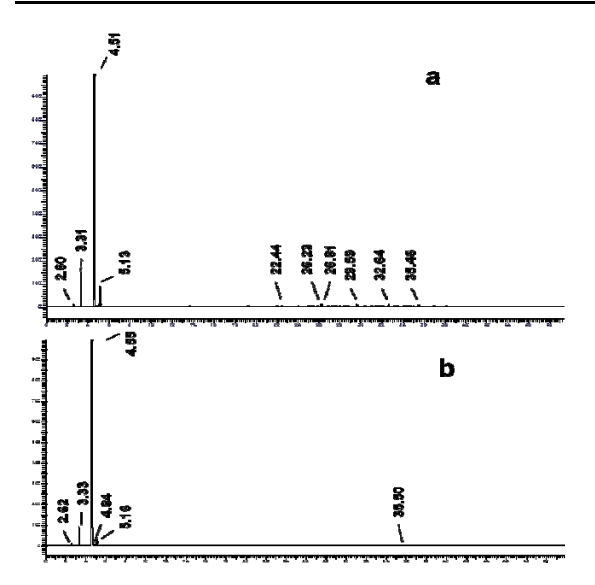


Figure 6. Diesel (2%, v/v) analysis using GC-FID: **(a)** abiotic control; **(b)** biotic control

4. Discussion

Most polluting oil appears to be used as a source of organic carbon by microbes, causing petroleum components to break down into lower molecular weight compounds (Chhatre *et al.*, 1996). Nevertheless, *n*-Alkanes are the components of aliphatic hydrocarbons that decompose the fastest, and are categorized into four

molecular mass categories: gaseous alkanes, aliphatic hydrocarbons of low molecular mass (C8-C16), aliphatic hydrocarbons of medium molecular mass (C17 - C28), and finally, aliphatic hydrocarbons of high molecular mass (> C28) (Abbasian *et al.*, 2015). Numerous studies have shown the biodegradation capacity of crude oil's *n*-alkane group by several strains of bacteria, with different degradation efficiencies, in agreement with the findings of the current study.

In this study, we discovered an intriguing crude oil degradation efficiency, by strain LGMS7 compared to the majority of studies available in the literature. We've also shown that this strain is better at biodegrading petroleum hydrocarbons than other Pseudomonas spp. For example, Varjani et al. (2015) found that the fraction (C8-C35) was degraded by 83.49%, using GC-FID analysis with a higher concentration (3%, v/v) of crude oil as the only carbon source. Likewise, Varjani and Upasani (2016) published their report showing a degradation percentage of 60.63% of the fraction (C8-C36 +) of petroleum (3%, v/v) on average, for 60 days at 37 °C in non-static conditions (180 rpm). In addition, the halotolerant Pseudomonas sp. strain NAPH6 was tested for crude oil degradation using GC-MS analysis. It was found that it was capable of metabolizing 96.2% of crude oil aliphatic group (1%, v/v), in basic medium with NaCl concentration of 30 g/l, within 20 days of incubation at 37 °C (Hentati et al., 2020). Zenati (2018) showed significant degradation of 83.68% of petroleum nalkanes (1%, v/v) by the Marinobacter hydrocaromrehtru. Furthermore, it has been reported that n-alkanes (C14 -C30) degrade faster than PAHs by Pseudomonas sp. (Sugiura et al., 1996).

On the other hand, several authors isolated and characterized bacteria from hydrocarbon-contaminated soils, capable of producing biosurfactant and degrading hydrocarbon (Chebbi et al., 2017; Ebadi et al., 2018). For instance, Ebadi et al. (2017) have proven the bioremediation efficiency of an oil-contaminted saline soil using a consortium of Pseudomonas aeruginosa, producer of biosurfactants. They discovered that using the consortium to treat polluted soils increased dehydrogenase activity significantly (approximately 2 times). In a lettuce seedling bioassay, the level of phytotoxicity in the soil was reduced by 30% after treatment compared to untreated soil. Treatment with a suitable bacterial consortium could help to mitigate the negative effects of salinity on petroleum microbial degradation. As a result, microbial remediation of saline petroleum-contaminated soils will be

In our study, crude oil degradation by *Pseudomonas* sp. strain LGMS7 at room temperature and close to the average outside soil temperature is a precondition for its *in situ* application when dealing with hydrocarbon-polluted soils using bioremediation technology, as reported by the study of Varjani and Upasani (2016).

In Algeria, only a few detailed studies have been conducted on the microbial capacity of hydrocarbon biodegradation. For instance, M'rassi et al. (2015) investigated the bacteria's' abilities to degrade both aliphatic and aromatic hydrocarbons in the contaminated soil of a refinery, in Arzew, Algeria. These authors have reported the growth of several strains related to Pseudomonas and effectively the use of an n-branched alkane like pristane, while Enterobacter, Pseudomonas, Acinetobacter, and Bacillus strains were found to be capable of degrading PAHs of high molecular mass like pyrene and benzo [a] pyrene. Accordingly, the Pseudomonas sp. strain LGM2 had the characteristic of degradation ability of both PAHs and n-alkanes, indicating that it could play a crucial role in hydrocarbon-polluted areas. Moreover, numerous bacterial strains were selected that could be used to develop and implement appropriate biological strategies for contaminated soil and refinery wastewater treatment (M'rassi et al., 2015).

Diesel pollution is a growing environmental problem. The most common sources of soil and groundwater pollution are diesel spills caused by numerous production storage issues, as well as transportation mishaps, and other issues related to damage at the level of the pipes (Lee et al., 2006). Diesel is made up of saturated hydrocarbons such as paraffin and aromatic hydrocarbons. The ability of microorganisms to metabolize diesel and use it as an energy source for growth has been documented in numerous studies in correlation with our study. In this context, Palanisamy et al. (2014) demonstrated that Acinetobacter baumannii could degrade > 99% of diesel (4%, v/v), incubated for 5 days at 37 °C and pH 7, using GC-MS analysis. According to these authors, A. baumannii can be used to effectively degrade diesel from diesel-polluted industrial waste. Ameen et al. (2016) studied the diesel degradation ability by fungi. An oildegrading fungus consortium was found to be highly effective, as evidenced by the chromatogram of the diesel fuel after an incubation period at 0 and 30 days. As a result, all of the hydrocarbons found in diesel were completely destroyed, yielding short-chain compounds.

Additionally, *Burkholderia cepacia* and *Exiguobacterium aurantiacum* were able to use diesel substrate as the only carbon source. For diesel degradation, the crops showed promising results for the *n*-alkane fraction (C9-C26). They have also shown a degradation capacity of pristane (Mohanty and Mukherji, 2008).

The strain LGMS7 has an advantage when it comes to growth over diesel (2%, v/v) as the only carbon source at room temperature (25 \pm 1 °C), which implies its ability to adapt to variations in the temperature during its growth, allows its use in situ in diesel-contaminated soil where it can resist variations in outside temperatures. In this context, Michaud et al. (2004) investigated the temperature effect on the efficiency of diesel biodegradation by two strains of bacteria. Therefore, after 60 days of growth in mineral medium containing (1%, v/v) commercial diesel, gas chromatographic analysis revealed a degradation percentage of 55.20% and 86% for strain E28 at 4° and 20 °C, respectively. While concerning the strain E60, a degradation rate of 57.66% was recorded at 4 °C and 89.2% at 20 °C. These authors suggested the future biotechnological processes in which these two bacteria could be used, directly in the form of microorganisms released on the ground in contaminated marine environments, both cold and temperate.

Additional investigations will be performed in the future to examine the LGMS7 strain's ability to degrade recalcitrant hydrocarbons like PAHs, under various stress conditions, including pH, salinity, and temperature. However, additional research will be conducted on the genes implicated in biodegradation, to fully comprehend the strain's degradation mechanisms, and consequently develop a strategy for implementing it on hydrocarbon-contaminated sites (Saadoun et al., 2020).

5. Conclusion

In the current research, we analysed the ability of the indigenous bacterium *Pseudomonas* sp. strain LGMS7 to metabolize the crude oil and diesel fuel used as only source of carbon in MSM medium at the room temperature. Interestingly, strain LGMS7 was able to degrade 98.50% of the linear fraction *n*- alkanes (C13-C30) of aliphatic hydrocarbons of crude oil (1%, v/v) and 70% of the diesel fraction (2%, v/v). Other studies will have to be carried out to assess the capacity of this strain to degrade recalcitrant hydrocarbons such as long branched-chain hydrocarbons and PAHs. This newly isolated strain, which has previously been studied for its ability to reduce surface tension and produce rhamnolipid biosurfactants, represents a promising path for the treatment of hydrocarbon-polluted sites in Algeria.

Acknowledgments

We are grateful to the chemistry department of the scientific police of the Oran police station for the GC-MS and GC-FID analyses.

References

Abbasian F, Lockington R, Mallavarapu M, Naidu R .2015. A comprehensive review of aliphatic hydrocarbon biodegradation by bacteria. *Appl. Biochem. Biotechno*, **176**: 670-699.

Ameen F, Moslem M, Hadi S, Al-Sabri AE .2016. Biodegradation of diesel fuel hydrocarbons by mangrove fungi from Red Sea Coast of Saudi Arabia. *Saudi J. Biol.*, Sci., **23**: 211-218.

Chaida A, Chebbi A, Bensalah F, Franzetti A .2021. Isolation and characterization of a novel rhamnolipid producer *Pseudomonas* sp. LGMS7 from a highly contaminated site in Ain El Arbaa region of Ain Temouchent, Algeria. *3 Biotech*, **11**: 1-15.

Chebbi A, Hentati D, Zaghden H, Baccar N, Rezgui F, Chalbi M, Sayadi S, Chamkha M .2017. Polycyclic aromatic hydrocarbon degradation and biosurfactant production by a newly isolated *Pseudomonas* sp. strain from used motor oil-contaminated soil. *Int. Biodeterior. Biodegrad*, **122**: 128-140.

Chhatre S, Purohit H, Shanker R, Khanna P .1996. Bacterial consortia for crude oil spill remediation. *Water Sci. Technol*, **34**: 187-193

Ebadi A, Olamaee M, Khoshkholgh Sima NA et al .2018. Isolation and Characterization of Biosurfactant Producing and Crude Oil Degrading Bacteria from Oil Contaminated Soils. *Iran J Sci Technol Trans Sci*, **42**: 1149–1156

Ebadi A, Sima NAK, Olamaee M, Hashemi M, Nasrabadi RG .2017. Effective bioremediation of a petroleum-polluted saline soil by a surfactant-producing *Pseudomonas aeruginosa* consortium. *J. Adv. Res.* **8**: 627-633.

Elkarmi A, Abu-Elteen K, Khader M .2008. Modeling the biodegradation efficiency and growth of *Pseudomonas alcaligenes* utilizing 2, 4-dichlorophenol as a carbon source Preand Post-exposure to UV radiation. *Jordan J. Biol. Sci*, 1:7-11

Gallego JL, Loredo J, Llamas JF, Vázquez F, Sánchez J .2001. Bioremediation of diesel-contaminated soils: evaluation of potential in situ techniques by study of bacterial degradation. *Biodegradation*, **12**: 325-335.

Harrouz A, Abbes M, Colak I, Kayisli K .2017. Smart grid and renewable energy in Algeria. Paper presented at the 2017 IEEE 6th International Conference on Renewable Energy Research and Applications (ICRERA).

Hasanuzzaman M, Ueno A, Ito H, Ito Y, Yamamoto Y, Yumoto I, Okuyama H .2007. Degradation of long-chain n-alkanes (C36 and C40) by *Pseudomonas aeruginosa* strain WatG. *Int. Biodeterior. Biodegrad*, **59**: 40-43.

Hentati D, Chebbi A, Mahmoudi A, Hadrich F, Cheffi M, Frikha I, Sayadi S, Chamkha M .2020. Biodegradation of hydrocarbons and biosurfactants production by a newly halotolerant *Pseudomonas* sp. strain isolated from contaminated seawater. *Biochem. Eng. J*, **166**: 107861.

Hidayat A, Tachibana S .2012. Biodegradation of aliphatic hydrocarbon in three types of crude oil by *Fusarium* sp. F 092 under stress with artificial sea water. *J. Environ. Sci. Technol*, **5**: 64-73.

Khan AHA, Ayaz M, Arshad M et al .2019. Biogeochemical Cycle, Occurrence and Biological Treatments of Polycyclic Aromatic Hydrocarbons (PAHs). *Iran J Sci Technol Trans Sci*, **43**: 1393–1410

Khan Z, Troquet J, Vachelard C .2005. Sample preparation and analytical techniques for determination of polyaromatic hydrocarbons in soils. *Int. J. Environ. Sci. Technol*, **2**: 275-286.

Ławniczak Ł, Woźniak-Karczewska M, Loibner AP, Heipieper HJ, Chrzanowski Ł .2020. Microbial degradation of hydrocarbons-basic principles for bioremediation: a review. *Molecules*, **25**: 856.

Lee M, Kim M, Singleton I, Goodfellow M, Lee ST .2006. Enhanced biodegradation of diesel oil by a newly identified *Rhodococcus baikonurensis* EN3 in the presence of mycolic acid. *J. Appl. Microbiol*, **100**: 325-333.

Logeshwaran P, Megharaj M, Chadalavada S, Bowman M, Naidu R .2018. Petroleum hydrocarbons (PH) in groundwater aquifers: An overview of environmental fate, toxicity, microbial degradation and risk-based remediation approaches. *Environ. Technol. Innovation*, **10**: 175-193.

M'rassi AG, Bensalah F, Gury J, Duran R .2015. Isolation and characterization of different bacterial strains for bioremediation of n-alkanes and polycyclic aromatic hydrocarbons. Environ. *Sci. Pollut. Res*, **22**: 15332-15346.

Michaud L, Giudice AL, Saitta M, De Domenico M, Bruni V .2004. The biodegradation efficiency on diesel oil by two psychrotrophic Antarctic marine bacteria during a two-month-long experiment. *Mar. Pollut. Bull.* 49: 405-409.

Mohanty G, Mukherji S .2008. Biodegradation rate of diesel range n-alkanes by bacterial cultures *Exiguobacterium aurantiacum* and *Burkholderia cepacia*. *Int. Biodeterior*. *Biodegrad*, **61**: 240-250.

Mukherji S, Vijay A .2002. Critical issues in bioremediation of oil and tar contaminated sites. Paper presented at the ACE 2002: International Conference on Advances in Civil Engineering.

Palanisamy N, Ramya J, Kumar S, Vasanthi N, Chandran P, Khan S. 2014. Diesel biodegradation capacities of indigenous bacterial species isolated from diesel contaminated soil. *J. Environ. Health Sci. Eng.*, **12**: 1-8.

Roy AS, Baruah R, Borah M, Singh AK, Boruah HPD, Saikia N, Deka M, Dutta N, Bora TC .2014. Bioremediation potential of native hydrocarbon degrading bacterial strains in crude oil contaminated soil under microcosm study. *Int. Biodeterior. Biodegrad*, **94**: 79-89.

Saadoun I, Alawawdeh M, Jaradat Z, Ababneh Q .2020. *Streptomyces* flora in chronically fuel oil-polluted soils and analysis of their alkane hydroxylase (alkB) gene by PCR. *Jordan J. Biol. Sci.*, 13: 731-734

Sugiura K, Ishihara M, Shimauchi T, Harayama S .1996. Physicochemical properties and biodegradability of crude oil. *Environ. Sci. Technol*, **31**: 45-51.

Varjani SJ, Rana DP, Jain AK, Bateja S, Upasani VN .2015. Synergistic ex-situ biodegradation of crude oil by halotolerant bacterial consortium of indigenous strains isolated from on shore sites of Gujarat, India. *Int. Biodeterior. Biodegrad*, **103**: 116-124.

Varjani SJ, Upasani VN .2016. Biodegradation of petroleum hydrocarbons by oleophilic strain of *Pseudomonas aeruginosa* NCIM 5514. *Bioresour. Technol.* **222:** 195-201.

Zenati B .2018. Biodegradation of petroleum hydrocarbons by marine bacteria: Application in the treatment of petroleum-contaminated seawater. PhD thesis, Saad Dahlab Blida 1 University, Algeria.



Preliminary Studies on the Potential Antioxidant and Antidiabetic Activities of *Sargassum polycystum* C. Agardh (Phaeophyceae, Ochrophyta)

Eldrin DLR. Arguelles*

Philippine National Collection of Microorganisms (PNCM), National Institute of Molecular Biology and Biotechnology (BIOTECH), University of the Philippine Los Baños, College, Laguna, Philippines, 4031

Received: August 19, 2021; Revised: December 25, 2021; Accepted: January 19, 2022

Abstract

Seaweeds are considered natural sources of chemical compounds with notable potent antioxidant and antidiabetic activities. The study aims to know the total polyphenolic content (TPC) and assess the antioxidant and antidiabetic activities of Sargassum polycystum for potential pharmacological use. The seaweed has a TPC of 1.149 ± 0.22 mg GAE/g. Antioxidant activity of S. polycystum is characterized by having potent scavenging activity against ABTS⁺ radical and high copper reduction capacity with IC₅₀ value of 49.50 µg GAE/ml and 20.40 µg GAE/ml, respectively, more effective than ascorbic acid (control). Assessment of the antidiabetic properties of S. polycystum was done in vitro via α -amylase and α -glucosidase inhibition assay. Results of the analysis proved that S. polycystum has potent α -amylase (IC₅₀ of 0.264 µg/ml) and α -glucosidase (IC₅₀ of 120 µg/ml) inhibition activities in collation to that of acarbose (antidiabetic drug) with IC₅₀ values of 4.81µg/ml and 6771 µg/ml, respectively. This study is a pioneering research investigation in the Philippines describing the bioactive properties of S. polycystum as renewable source of bioactive substances for inhibition of important carbohydrate degrading enzymes.

Keywords: biological activities; diabetes; marine; phenolic compounds; seaweeds

1. Introduction

Diabetes is a systemic long-term disease known for the occurrence of hyperglycemia in which there is an elevated concentration of sugar in the blood because the pancreas fails to produce enough insulin (Arguelles & Sapin, 2020a). It causes glycation (non-enzymatic) of serum proteins which leads to generation of glycation end products (Ulrich & Cerami, 2001). These end products cause major complications of diabetes such as kidney failure, stroke, and heart attack (Ulrich & Cerami, 2001). In general, medical treatments available for patients with diabetes include insulin injections and oral antidiabetic drugs. However, prolonged use of these treatments leads to lower therapeutic capacity and several side effects (Arica et al., 2017). In addition, leading carbohydrate degrading enzyme inhibitors, miglitol, and acarbose, are recently documented to produce intestinal side effects like diarrhea, bloating, and abdominal pain occurring simultaneously (Ulrich & Cerami, 2001; Arica et al., 2017). Thus, preventive antidiabetic substances with minimum side effects are needed. A therapeutic method in treatment of diabetes is to lessen the occurrence of hyperglycemia via inhibition of α-amylase (enzyme for the degradation of long-chain starch) and α-glucosidase (an enzyme responsible for oligosaccharide and disaccharide breakdown) (Zhao et al., 2017). These enzymes are responsible for regulating the postprandial blood sugar levels and are considered target enzymes for the development and synthesis of natural hypoglycemic drugs (Ulrich & Cerami, 2001). Inhibitors of these hydrolyzing enzymes impede carbohydrate degradation causing a lower absorption of glucose preventing diabetes (Ulrich & Cerami, 2001; Zhao *et al.*, 2017).

Naturally derived antidiabetic drugs are currently becoming popular because of high financial burdens and side effects that are coupled with allopathic therapy strategies for the treatment of diabetes. Antioxidants are substances that inhibit oxidation and are considered to have medicinal value in treatment of several diseases like diabetes (Arguelles et al., 2017; Rajendiran et al., 2018). Diabetes treatment using antioxidants (such as thioctic acid, tocopherol, and vitamin C) protects beta-cells against oxidative stress-induced apoptosis and prevents complications caused by the disease. Studies using streptozotocin-induced diabetic rats showed antioxidant therapy (diet supplementation) using tocopherol and vitamin C lowers the concentration of lipid peroxide and significantly increases superoxide dismutase (SOD) activity improving the health condition of the animal (Seven et al., 2004). In addition, vitamin C therapy in diabetic rats lowers the erythrocyte sorbitol levels and helps in improving the insulin resistance of the animal (Rajendiran et al., 2018). These findings suggest that dietary supplementation of antioxidants may reduce the complication of diabetes and are beneficial for diabetes treatment (Seven et al., 2004; Rajendiran et al., 2018).

_

^{*} Corresponding author. e-mail: edarguelles@up.edu.ph.

Seaweeds are marine organisms that have diverse medicinal value and are currently being tapped as candidate natural resources for bioactive substances that can be used for diabetes treatment (Arguelles, 2018; Zhao et al., 2017). Among seaweeds, brown macroalgae are reported as promising sources due to the therapeutic potential of polyphenolic compounds isolated from these organisms that exhibit antidiabetic activity (Arica et al., 2017). Sargassum polycystum C. Agardh is a brown seaweed that is taxonomically classified under the phylum Ochrophyta, and class Phaeophyceae which are commonly observed in Philippine coastal areas. This seaweed is characterized by having a large and brownish thallus with oblanceolate leaves that is usually attached to a solid substratum. The primary branch is terete with secondary branches that are arranged irregularly alternate with several proliferations. The leaves of this seaweed have percurrent midrib and serrated margins usually with vesicles that are ovoid or spherical (Trono, 1997). Phenolic compounds from this seaweed such as phlorotannins, gallic acids, ellagic acids, and phloroglucinol can activate insulin secretion and possess inhibitory properties against carbohydrate degrading enzymes which can be utilized for pharmaceutical research applications (Hwang et al., 2014; Zhao et al., 2017).

The Philippines diverse seaweed natural resource is considered underutilized and have not been widely studied as a source of bioactive ingredients for medicinal use. This study serves as a pioneering research investigation in the country assessing the bioactive properties of *S. polycystum* against carbohydrate degrading enzymes (Arguelles & Sapin, 2020a). The current investigation aims to determine

the TPC and assess the antioxidant and antidiabetic properties of S. polycystum extract for pharmacological use. The antidiabetic activities of the algal extract were assessed using the α -amylase and α -glucosidase inhibition assays while antioxidant activities of S. polycystum were analyzed using copper reduction antioxidant capacity and ABTS⁺ radical scavenging assay. In addition, correlation analysis between phenolic concentration of the macroalgal extract and the antioxidant and antidiabetic activities were established.

2. Materials and Method

2.1. Seaweed collection and sample preparation

S. polycystum was harvested on 19 January, 2020 in shallow waters in the coastal area of Laiya, (Lat. 13° 40' 26.364" N; Long. 121° 23' 48.948" E), Batangas, Philippines (Figures 1 and 2). Mature dark brown thalli of S. polycystum were collected in the sampling area. The seaweed was scrubbed using brush bristles. The seaweed was rinsed several times using sterile tap water to remove sand particles, epiphytes, and other necrotic parts present in the thalli of the alga. The cleaned thalli of S. polycystum was securely packed in polythene bags (kept inside a chilled plastic cooler) and immediately transported to the laboratory for further processing. The washed seaweed was oven-dried and pulverized before solvent extraction (Arguelles et al., 2019; Arguelles, 2020). The seaweed was identified using relevant morphotaxonomic features and taxonomic monographs of Trono (1997) and Algae Base (Guiry & Guiry, 2021).

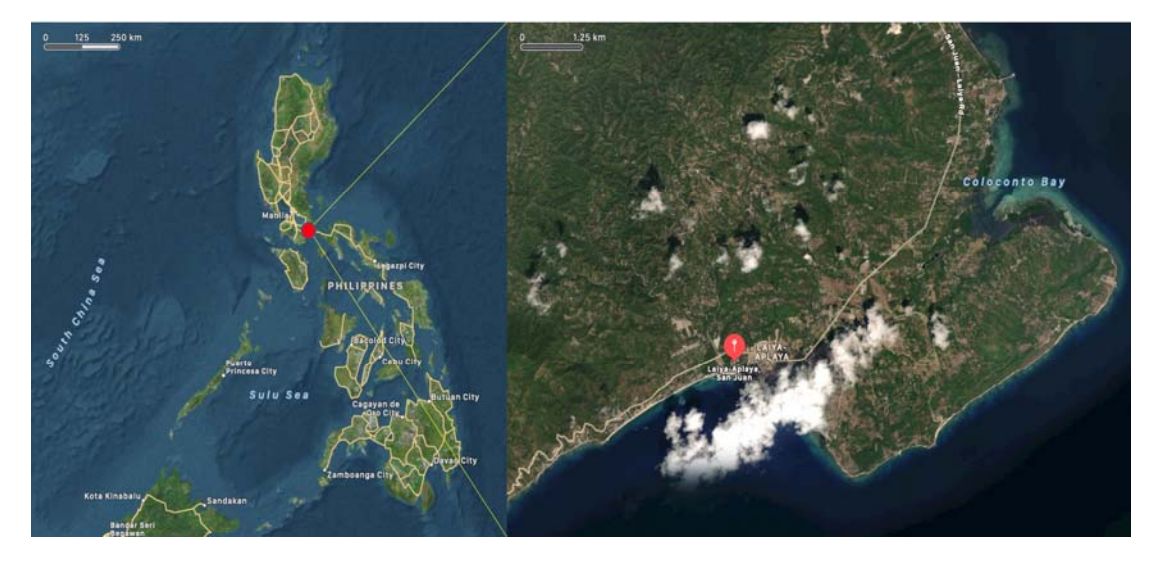


Figure 1. Location map of sampling site of Sargassum polycystum from Batangas, Philippines.



Figure 2. Thallus morphology of *Sargassum polycystum* C. Agardh.

2.2. Seaweed Extract Preparation

Powdered *S. polycystum* biomass (1 g) was immersed with 30 ml of the extraction solvent (acidified methanol, 1:80:10 v/v, HCl: CH₃OH: H₂O) and stirred for 1 h using an ultrasonic bath following the extraction protocol of Gao et al. (2002). Using a rotary evaporator (BUCHITM RotavaporTM Scholar System), the liquid soluble constituent was concentrated at 40 °C. The concentrated algal crude extract was placed in a sterile screw-capped tube and kept at 4 °C until use (Gao *et al.*, 2002; Arguelles & Sapin, 2020a). The yield extract of *S. polycystum* was calculated using the equation:

Yield (%) =
$$\frac{\text{Weight of the algal extract (g)}}{\text{Weight of the dried algal biomass (g)}} \times 100$$

2.3. Determination of the total phenolic content

The TPC of *S. polycystum* was estimated using the Folin-Ciocalteu method (Nuñez-Selles *et al.*, 2002). Initially, 0.5 ml of *S. polycystum* extract was mixed with 0.5 ml of 10% sodium carbonate and Folin-Ciocalteu's reagent. The solution was mixed via a vortex mixer until homogenous and was set aside for 5 min. The volume of the reaction mixtures was adjusted by adding 5 ml of sterile distilled water. Absorbance reading of each sample were taken using an Ultraviolet-Visible spectrophotometer at 720 nm wavelength. The TPC of *S. polycystum* was estimated using a standard gallic acid calibration curve (y = 0.0682x - 0.0214, R² = 0.997). The TPC of *S. polycystum* is reported as milligrams of gallic acid equivalent per gram of the seaweed sample (Nuñez-Selles *et al.*, 2002).

2.4. ABTS+ radical scavenging assay

The extract of *S. polycystum* was evaluated for ABTS⁺ radical scavenging property using the protocol of Re *et al.*, (1999). An aliquot (40 μ l) of the algal extract at varying phenolic concentrations and 40 μ l of the control were mixed with 3 ml of ABTS⁺ free radical mixture (with

initial optical density of 0.72 ± 0.05 at 734 nm). The reaction mixtures were mixed and stored for 5 min at normal room temperature. The absorbance of each test samples was taken at 734 nm. The effective concentrations (IC₅₀) for *S. polycystum* and the ascorbic acid (control) were determined during the analysis. The percent inhibition was computed using the equation:

ABTS⁺ Inhibition
$$(\%) = \frac{\text{Abs}_{734} (\text{control}) - \text{Abs}_{734} (\text{sample})}{\text{Abs}_{734} (\text{control})} \times 100$$

2.5. CUPRAC assay

The antioxidant capacity of S. polycystum extract for copper reduction was evaluated following the colorimetric method of Alpinar et al., (2009). Initially, 1 ml each of 0.01 M copper (II) chloride (CuCl₂), 1 M ammonium acetate buffer (pH 7), and 0.0075 M neocuproine solutions were mixed until homogenous in a test tube. An aliquot (0.5 ml) of S. polycystum extract prepared at different phenolic concentrations as well as ascorbic acid were added from the initial mixture. The total volume of the reaction mixture was adjusted up to 4.1 mL for each concentration using fresh distilled water. The reaction mixtures were placed for 30 min at ambient temperature condition. The absorbance readings of each test sample were noted at 450 nm. The effective concentrations (IC₅₀) for S. polycystum extract and the control (ascorbic acid) were determined during the analysis of copper reduction antioxidant capacity (Alpinar et al., 2009; Arguelles & Sapin, 2020c).

2.6. Alpha-amylase inhibition assay

The capacity of S. polycystum extract to inhibit αamylase was assayed in vitro conditions using the methods of Phoboo et al., (2015) with modifications. Solutions of alpha-amylase from porcine pancreas (0.5 mg/ml, Sigma A3176), 0.02 M Sodium-phosphate buffer (pH 6.9) with 0.006M NaCl and 1% starch solution were prepared. The samples of S. polycystum with different phenolic concentrations were prepared by dilution with water. In a 50 μ l of the alpha-amylase solution, 25 μ l of the sample (S. polycystum at varying phenolic concentrations) were mixed in test tubes. As for the case of the control, 25 µl of buffer was mixed with 50 µl of alpha-amylase solution. The volume was made up to 250 µl by adding 175 µl phosphate buffer. Then, 250 µl starch solution was added at timed intervals. After 20 min of incubation, the reaction was halted by adding 400 µl DNS color reagent also at timed intervals. The blank to zero the instrument consisted of 500 µl buffer and 400 µl DNS reagent. The reaction tubes were subjected to a boiling hot water bath for about 5 minutes, cooled, and further diluted with 5 ml fresh distilled water. Absorbance reading of the test mixture was noted at 540 nm wavelength. Acarbose served as the control (anti-diabetic drug) in the analysis. The inhibition was determined using the equation:

$$\alpha$$
-Amylase inhibition (%) =
$$\frac{\text{Abss40(control) - Abss40(sample)}}{\text{Abss40(control)}} \times 100$$

2.7. Alpha-glucosidase inhibition assay

The capacity of *S. polycystum* to inhibit α - glucosidase was done *in vitro* using the methods of Nair *et al.*, (2013). A mixture consisting of 75 μ l of α – glucosidase (2.5 U/ml) and 100 μ l of the different prepared phenolic

concentrations of *S. polycystum* or 100 μ l of 0.1 M phosphate buffer pH 6.8 (in case of the control) were prepared and thoroughly mixed in sterile test tubes. The volume of the test sample was adjusted to 500 μ l by adding 295 μ l buffer and 30 μ l of 10mM p-nitrophenyl- α -D-glucopyranoside (Sigma N1337). The mixtures were kept at 37 °C for 12 min after which 3 ml of 50 mM NaOH were added. The absorbance reading of the mixtures was taken at 410 nm. Acarbose served as the control (an α -glucosidase inhibitor and anti-diabetic drug) in the analysis. The α – glucosidase inhibition was determined using the equation:

2.8. Statistical Data Analyses

The assays used in this study were done in three replicates (means \pm standard deviations). The correlation analysis among antidiabetic and antioxidant activities as well as the phenolic concentrations of *Sargassum polycystum* extract were done using Pearson's correlation (R) coeeficient via Microsoft (MS) Office Excel 2021 (Arguelles & Sapin, 2020b).

3. Results and Discussion

3.1. Extraction yield and TPC

The crude extract of S. polycystum obtained from this study is brownish, which can be attributed to algal pigments such as xanthophylls, violaxanthin, carotenoids, fucoxanthin, and chlorophyll present in the crude extract (El-Sheekh et al., 2021). Extraction yield is the percentage of the crude extract that can be utilized from the sample (El-Sheekh et al., 2021). Sargassum polycystum crude extract have an extraction yield of 12.47± 0.31% which is higher as compared to that observed by Sivagnanam et al., (2015) from ethanol extracts of S. japonica (1.22 \pm 0.12%) and S. horneri (1.36±0.14%) from the coastal area of Korea. However, this extraction yield is lower than that obtained by El-Sheekh et al., (2021) from methanol and cold aqueous extracts of Taonia atomaria from Alexandria, Egypt with an extraction yield of $16.5 \pm 0.2\%$ and $13.5 \pm 0.1\%$, respectively. The results obtained in the current investigation are consistent with earlier studies (Sivagnanam et al., 2015; El-Sheekh et al., 2021), which documented that extraction yield is highly dependent on the polarity of the solvent. Generally, sample extracts that are prepared using polar solvents are observed to have the highest amount of crude extractable substances (Sivagnanam et al., 2015). Variation in the extraction yield of S. polycystum reported in this investigation can be ascribed to several factors such as sample particle size, method of extraction, and temperature used in the extraction protocol (Sivagnanam et al., 2015). Hence, optimization of the extraction condition is recommended for large-scale production of the active compound from S. polycystum.

Table 1. Extraction yield and TPC of *Sargassum polycystum* acidified methanolic extract.

Sample	Extract	Extract Yield (%)	Total Phenolic Content (mg GAE/g)
Sargassum polycystum	Acidified Methanol	12.47 ± 0.31	1.149 ± 0.22

Seaweeds are considered natural sources of biologically active chemical compounds with therapeutic uses. Polyphenols from marine macroalgae are characterized to possess potent antioxidant and antidiabetic activities. The TPC of S. polycystum is 1.149±0.22 mg GAE/g extract (Table 1). This result was comparable with previous research done by Chakraborty et al., (2017) and Fu et al., (2015) for S. polycystum with TPC of 0.37 mg GAE/g and 8.71 mg GAE/g, respectively. However, Arguelles (2020) showed that the green seaweed (Codium intricatum) has a higher TPC, which was 40.79±0.015 mg GAE/g. Cikoš et al., (2018) also reported that strains of Ascophyllum nodosum extracted using methanol showed TPC ranging from 0.51 mg GAE/g to 1.40 mg GAE/g. The differences in the TPC of several algal species could be attributed to several intrinsic and extrinsic factors such as seasonal variations, age or maturity of the alga, geographic location, tidal cycles, and salinity that can affect the metabolic profile of the macroalga (Arguelles and Sapin, 2020b,c; Arguelles, 2021a,b).

3.2. Antioxidant activities of S. polycystum extract

The antioxidant properties of S. polycystum were evaluated using CUPRAC and ABTS+ radical scavenging assays. Results showed that S. polycystum has potent antioxidant activity, more effective than ascorbic acid (control). As presented in Table 2, scavenging efficiency of the algal extract was observed to cause a dosedependent inhibition of ABTS+ free radicals. The computed effective concentration (IC₅₀) of S. polycystum extract is 49.50 µg GAE/ml which is more effective than ascorbic acid (control) with IC₅₀ value of 147.90 µg/ml (Table 2). In comparison with other known seaweeds, S. polycystum was able to exhibit potent ABTS+ radical scavenging activity more potent than those obtained from methanol extracts of Acetabularia acetabulum (IC50 of 6.30 mg/ml) and Halimeda tuna (IC₅₀ of 16.1 mg/ml) (Sivaramakrishnan et al., 2017). However, Arguelles and Sapin (2020a) reported that methanol extract of a brown macroalga, Turbinaria decurrens, has a more potent antioxidant activity than S. polycystum having extract with an IC50 value of 49.31 ug GAE/ml. Several phenolic compounds derived from seaweeds are antioxidants with excellent scavenging activity against free radical (Fu et al., 2015). These substances are capable of terminating autoxidation of free radicals by hydrogen atom donation from phenolic hydroxyl (OH) groups present in the compound (Fu et al., 2015; Arguelles et al., 2019; Arguelles & Sapin, 2020b).

Table 2. ABTS⁺ free radical scavenging activity and IC₅₀ value of phenolics from *S. polycystum* and ascorbic acid.

1							
	Phenoli	c concen	tration (ug GAE/	ml)	IC50 *	
Sample	12.5	25.0	37.5	50.0	62.5	(μg/ml)	
	ABTS ⁺	Inhibiti	on (%)			(((() () () () () () () () (
Sargassum	15.58	28.74	41.92	50.43	59.02	49.50	
polycystum	± 1.22	± 0.04	± 0.31	± 0.51	± 1.02		
	Concen	Concentration (µg/ml)					
	37.5	75.0	112.5	150.0	187.5		
	ABTS ⁺	Inhibitio	on (%)				
Ascorbic	11.70	24.56	36.70	50.87	64.53	147.90	
Acid	± 1.54	± 0.62	± 0.51	± 0.82	± 1.64		

^{*}IC₅₀ is the concentration capable of inhibiting the activity of ABTS⁺ radical by 50%. Computed via interpolation.

Table 3. Copper reduction antioxidant capacity and IC₅₀ value of phenolics from *S. polycystum* and ascorbic acid.

	Phenol	ic concen	tration (µ	ıg GAE/n	nl)	- IC ₅₀ *	
Sample	5	10	15	20	25	- 1C ₅₀ _ (μg/ml)	
	CUPRA	AC (Abso	rbance a	t 450 nm))	- (μg/IIII)	
Sargassum polycystum	0.154 ± 0.001	0.278 ± 0.008	0.402 ± 0.001	0.486 ± 0.001	0.599 ± 0.011	20.40	
	Concer	Concentration (µg/ml)					
	10	20	30	40	50		
	CUPRAC (Absorbance at 450 nm)						
Ascorbic acid	0.112 ± 0.002	0.213 ± 0.007	0.328 ± 0.004	0.429 ± 0.012	0.542 ± 0.011	46.30	

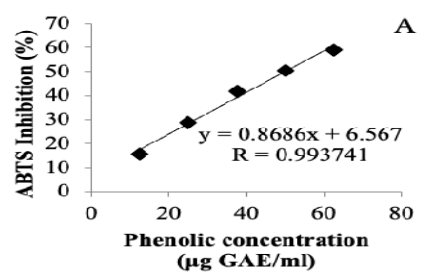
^{*} $1C_{50}$ is the concentration that shows a CUPRAC value of 0.5 at a wavelength of 450 nm. Computed via interpolation.

S. polycystum extract also exhibited copper ion reduction ability in a concentration-dependent manner (Table 3). The seaweed extract exhibited more effective antioxidant activity than ascorbic acid with IC50 of 20.40 $\mu g/ml$ and $IC_{50} = 46.30~\mu g/ml,$ respectively. The observed trend in this analysis is homologous to that observed from ABTS⁺ scavenging assay in which at 62.5 μg/ml concentration the highest ABTS+ free radical inhibition of 59.02% was noted. The copper reduction antioxidant capacity of S. polycystum is more effective than that of Turbinaria ornata (IC50 value of 24.34 µg GAE/ml) but is less potent than that of Sargassum siliquosum with IC50 of 18.50 µg GAE/ml (Arguelles & Sapin, 2020b,c). The results obtained in this antioxidant assay show that S. polycystum is capable of inhibiting oxidation via a metal chelation which can be attributed to phenolic compounds like phloroglucinols, phlorotannins, fucoxanthin, and bromophenols that are found in the algal extract (Ponnan et al., 2017; Arguelles & Sapin, 2020b,c).

3.3. Correlation analysis of antioxidant activities and phenolic content

The correlation analysis between phenolic concentration of *S. polycystum* extract and antioxidant activities using ABTS⁺ free radical scavenging and CUPRAC assay is shown in Figure 3. The analysis exhibited positive correlations among antioxidant (ABTS⁺

radical scavenging and CUPRAC assays) capacity and the phenolic concentrations of the seaweed extract with R=0.993741 and R=0.997816, respectively. It is clear from these results that phenolic compounds may serve an important function in the metal ion chelating and free-radical scavenging abilities exhibited by the algal extract. This finding is further supported by previous studies showing positive correlations between antioxidant activities and phenolic contents in several *Sargassum* species such as *S. acinarium*, *S. ilicifolium*, *S. muticum*, and *S. vulgare* (Arguelles *et al.*, 2019; Ismail *et al.*, 2020; Arguelles, 2021a).



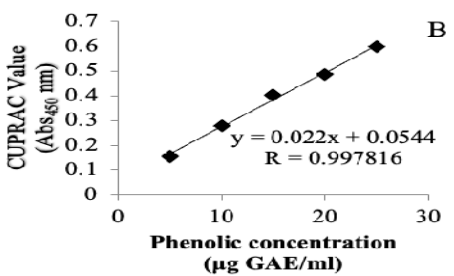


Figure 3. Correlation among phenolic concentration and antioxidant activities via (A) ABTS⁺ radical scavenging and (B) copper reduction antioxidant capacity of *S. polycystum*.

3.4. Antidiabetic activities of S. polycystum extract

The most common way of treating patients with diabetes is by preventing the occurrence of hyperglycemia. This is made possible by suppressing key carbohydrate hydrolyzing enzymes in the digestive system such as αglucosidase and α-amylase (Pirian et al., 2017; Ismail et al., 2020). The antidiabetic activities of Sargassum polycystum were evaluated by measuring the ability of the algal extract to cause inhibition of these carbohydrate hydrolyzing enzymes. The result of the α -amylase inhibitory effect of S. polycystum extract is presented in Table 4. The seaweed extract showed a more potent α amylase inhibition activity as compared to acarbose (standard antidiabetic drug) with IC50 values of 0.264 µg/ml and 4.81 µg/ml, respectively. The α-glucosidase inhibition activity of S. polycystum extract is shown in Table 5. The inhibition of various concentrations of the seaweed extract also exhibited a concentration-dependent reduction in enzyme activity. S. polycystum extract showed high inhibitory activity of α -glucosidase with an effective concentration (IC50) of 120 µg/ml. This IC50 value is considered more potent than that of acarbose, which gave an IC₅₀ of 6771 μg/ml.

Table 4. α -amylase inhibition and IC₅₀ of phenolics from *S. polycystum* in comparison to acarbose.

	Phenoli	Phenolic concentration (µg GAE/ml)				
Sample	0.1	0.2	0.3	0.4	0.5	- IC ₅₀ *
	α-gluco	sidase in	hibition	(%)		. (μg/ml)
Sargassum	11.48	31.79	60.30	72.48	79.27	0.264
polycystum	$\pm~0.20$	$\pm~0.25$	$\pm~0.20$	± 0.15	± 0.25	
	Concen	Concentration (µg/ml)				
	1.5	3.0	4.5	6.0	7.5	
	α-amylase inhibition (%)					
Acarbose**	24.01 ± 0.87	38.85 ± 2.32	47.90 ± 0.93	58.24 ± 0.43	65.43 ± 0.43	4.81

^{*} IC_{50} is the effective concentration that inhibits α -amylase activity by 50%.

Table 5. α -glucosidase inhibition and IC₅₀ of phenolics from *S. polycystum* in comparison to acarbose.

	Phenolic concentration (µg GAE/ml)					- IC ₅₀ *
Sample	25	50	75	100	125	- 1C ₅₀ - (μg/ml)
	α-gluco	sidase in	hibition	(%)		- (μg/IIII)
Sargassum polycystum	5.81 ± 0.14	14.48 ± 0.00	24.61 ± 0.00	38.61 ± 0.10	52.77 ± 0.12	120
	Concen	Concentration (µg/ml)				
	2000	4000	6000	8000	10000	
	α-gluco	sidase in	hibition	(%)		
Acarbose**	17.96 ± 1.36	31.69 ± 1.22	45.32 ± 1.90	57.26 ± 0.49	62.35 ± 0.49	6771

^{*} IC_{50} is the effective concentration that inhibits α -glucosidase activity by 50%.

The extract of S. polycystum was significantly effective in inhibiting carbohydrate hydrolyzing enzymes being more potent than acarbose (standard antidiabetic drug). The IC50 values of S. polycystum acidified methanol extract showed that the seaweed is an effective and potent inhibitor for both enzymes. Thus, showing that S. polycystum can be utilize in the control of postprandial hyperglycemia and treatment of diabetes. This result is further supported by previous studies from seaweed extracts of Turbinaria decurrens (IC50 of 2.84 µg/ml), Turbinaria ornata (IC50 of 535.6 µg/ml), and Sargassum glaucescens (IC50 of 8.9 mg/ml) with potent enzyme inhibition activities that can be utilized as antidiabetic agents (Unnikrishnan et al., 2014; Payghami et al., 2015; Arguelles & Sapin, 2020a). Polyphenolic compounds have the ability of chelating α -amylase and α -glucosidase, causing these key enzymes to chemically precipitate and have structural changes in combination with loss of biological activities. This confirms the potent carbohydrate hydrolyzing enzyme inhibition exhibited by S. polycystum extract in the current study. In addition, the diverse kinds of polyphenolic compounds (such as bromophenols, phlorotannins, p-coumaric acid, and dihydrobenzoic acid) found in the algal extract may have expressed synergistic effects, causing higher effectiveness in α-amylase and αglucosidase inhibition (Firdaus et al., 2015). The promising carbohydrate hydrolyzing enzyme inhibition properties of *S. polycystum* extract show the possible use of this macroalga as an alternative source of natural antidiabetic drugs that can be used in the regulation of hyperglycemia in the body via slow digestion and absorption (Arguelles & Sapin, 2020a).

In this study, S. polycystum extract exhibited a stronger inhibition activity in α-amylase than α-glucosidase. A possible reason for this might be that the strength of enzyme inhibition may not only depend on the number of phenolic compounds included in the algal extract but also on the composition. Previous findings have reported positive correlation between the polyphenol concentration (in the seaweed extracts) and their potent ability to cause inhibition of the carbohydrate digestive enzymes; however, high concentration of phenolic compounds of seaweed extracts are not always correlated or associated with potent α-amylase than α-glucosidase inhibition (Pirian et al., 2017; Ismail et al., 2020). This suggests that the interaction (among the chemical components of the extract) and the type of phenolic compounds present in seaweed extract may be potent to α -amylase but not so for α -glucosidase or vice versa. Thus, showing that S. polycystum extract may have a phenolic profile with specific phenolic compounds that have greater enzyme inhibition for α -amylase than for α -glucosidase.

3.5. Correlation analysis of antidiabetic activities and phenolic content

The correlation analysis among antidiabetic activities and phenolic concentration of *S. polycystum* extract via enzyme inhibition activities are shown in Figure 4. The analysis exhibited a positive correlation between antidiabetic (enzyme inhibition) activities and phenolic concentrations of the seaweed extract with R=0.93999 and R=0.99415, respectively. Such correlation supports the potential function of polyphenols in the antidiabetic properties of the algal extract. This correlation is homologous to that observed by Firdaus *et al.*, (2015) where they attributed the carbohydrate hydrolyzing enzyme inhibition activities of different *Sargassum* species extracts to their high phenolic content.

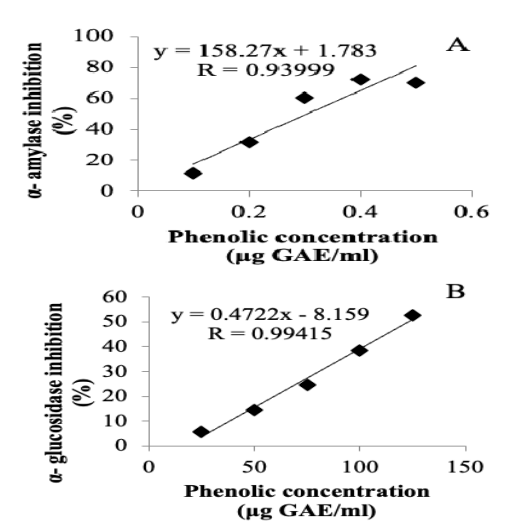


Figure 4. Correlation between phenolic concentration and antidiabetic properties via (A) α -amylase inhibition and (B) α -glucosidase inhibition activities of *S. polycystum*.

^{**}Reference α-amylase inhibitor and anti-diabetic drug.

^{**}Reference α-glucosidase inhibitor and anti-diabetic drug.

4. Conclusions

Sargassum polycystum C. Agardh contains a high amount of polyphenols and exhibited antioxidant activity characterized by having potent ABTS+ radical scavenging activity and high copper reduction capacity more effective than ascorbic acid. In addition, analysis of the antidiabetic properties of S. polycystum showed that the seaweed has potent α-amylase and α-glucosidase inhibition properties in collation to that of acarbose (antidiabetic drug) proving the potential application of S. polycystum for treatment of diabetes. This study is a pioneering research investigation in the Philippines that reported the potential antioxidant and antidiabetic properties of S. polycystum as potential source of active substances for inhibition of target carbohydrate degrading enzymes. It is recommended that investigation on the isolation, identification, and mass production of the target active substances found in S. polycystum extract should be done to further understand the mechanisms involved in other biological activities of the alga in vivo. In addition, the use of other food-grade solvents such as aqueous ethanol (at different percentages) and water as the extraction solvents in the assay is also recommended to further support safety concerns regarding the use of seaweed for pharmaceutical application.

Acknowledgement

The author acknowledges the support given by the PNCM-BIOTECH, UPLB for this research study. The author is also thankful to Mrs. Arsenia B. Sapin (Food Laboratory) for her technical assistance in the conduct of the assays needed in the study.

References

Alpinar K, Özyurek M, Kolak U, Guclu K, Aras Ç, Altun M, Celik SE, Berker KI, Bektasoglu B and Ampal R. 2009. Antioxidant capacities of some food plants wildly grown in Ayvalik of Turkey. *Food Sci Technol Res.*, **15(1)**: 59-64.

Arguelles EDLR. 2021a. Evaluation of antioxidant capacity, tyrosinase inhibition, and antibacterial activities of brown seaweed, *Sargassum ilicifolium* (Turner) C. Agardh 1820 for Cosmeceutical Application. *J Fish Environ.*, **45(1)**: 64-77.

Arguelles EDLR. 2021b. Biochemical composition and bioactive properties of *Chlorella minutissima* (Chm1) as a potential source of chemical compounds for nutritional feed supplement and disease control in aquaculture. *Curr Appl Sci Technol.*, **21(1)**: 65-77

Arguelles EDLR. 2020. Evaluation of nutritional composition and in vitro antioxidant and antibacterial activities of Codium intricatum Okamura from Ilocos Norte (Philippines). Jordan J Biol Sci., 13(3): 375-382.

Arguelles EDLR and Sapin AB. 2020a. *In vitro* antioxidant, alpha-glucosidase inhibition and antibacterial properties of *Turbinaria decurrens* Bory (Sargassaceae, Ochrophyta). *Asia-Pacific J Sci Technol.*, **25(3)**: https://so01.tci-thaijo.org/index.php/APST/article/view/240714/165247.

Arguelles EDLR and Sapin AB. 2020b. Bioprospecting of *Turbinaria ornata* (Fucales, Phaeophyceae) for cosmetic application: antioxidant, tyrosinase inhibition and antibacterial activities. *J ISSAAS.*, **26**(2): 30-41.

Arguelles EDLR and Sapin AB. 2020c. Bioactive properties of *Sargassum siliquosum* J. Agardh (Fucales, Ochrophyta) and its potential as source of skin-lightening active ingredient for cosmetic application. *J Appl Pharm Sci.*, **10(7)**: 51-58

Arguelles EDLR, Monsalud RG, and Sapin AB. 2019. Chemical composition and *in vitro* antioxidant and antibacterial activities of *Sargassum vulgare* C. Agardh from Lobo, Batangas, Philippines. *J ISSAAS.*, **25(1)**:112-122.

Arguelles EDLR. 2018. Proximate analysis, antibacterial activity, total phenolic content and antioxidant capacity of a green microalga *Scenedesmus quadricauda* (Turpin) Brébisson. *Asian J Microbiol Biotechnol Environ Sci.*, **20(1)**:150-158.

Arguelles EDLR, Laurena AC, Martinez-Goss MR and Monsalud RG. 2017. Antibacterial sctivity, total phenolic content, and antioxidant capacity of a green microalga *Desmodesmus* sp. (U-AU2) From Los Baños, Laguna (Philippines). *J Nat Stud.*, **16(2)**: 1-13

Arica SC, Ozyilmaz A, and Demirci S. 2017. A study on the rich compounds and potential benefits of algae: A review. *Pharm Innov J.*, 6(12): 42-51.

Chakraborty K, Maneesh A and Makkar F. 2017. Antioxidant activity of brown seaweeds. *J Aquat Food Prod Technol.*, **26**:406–419

Cikoš A-M, Jokic S, Šubaric D and Jerkovic I. 2018. Overview on the application of modern methods for the extraction of bioactive compounds from marine macroalgae. *Marine Drugs*, **16**: 348

El-Sheekh MM, El-Shenody RAEK, Bases EA and El-Shafay SM. 2021. Comparative assessment of antioxidant activity and biochemical composition of four seaweeds, Rocky Bay of Abu Qir in Alexandria, Egypt. *Food Sci Technol.*, **41(Suppl. 1)**: 29-40.

Firdaus M, Nurdiani R and Prihanto AA 2015. Antihyperglycemic of *Sargassum* sp. extract. In: Kim SK, Chojnacka K. (Eds.). **Marine algae extracts: Processes, products and applications**. Wiley, Weinheim, pp 381–394.

Fu CWF, Ho CW, Yong WTL, Abas F and Tan CP. 2015. Effects of phenolic antioxidants extraction from four selected seaweeds obtained from Sabah. *PeerJ PrePrints*, **3**: e1249v1.

Gao L, Wang S, Oomah BD, and Mazza G. 2002. Wheat quality: Antioxidant activity of wheat millstreams. In: Ng P, Wrigley CW. (Eds.). **Wheat Quality Elucidation**. AACC International, St. Paul, Minnesota, USA, pp 219 – 233.

Google. (n.d.). [Google Maps location of sampling site in Laiya, Batangas, Philippines]. Retrieved December 18, 2021, from https://www.google.com/maps/place/13%C2%B040'26.4%22N+1 21%C2%B023'49.0%22E/@13.729365,121.3579252,12.22z/data =!4m5!3m4!1s0x0:0x3b38fcb0886aa22!8m2!3d13.67399!4d121. 39693

Guiry M D, in Guiry M D, and Guiry G M. 2021. AlgaeBase. World-wide electronic publication, National University of Ireland, Galway. Retrieved July 19, 2021, from http://www.algaebase.org.

Hwang PA, Hung YL, Tsai YK, Chien SY and Kong ZL. 2014. The brown seaweed *Sargassum hemiphyllum* exhibits α -amylase and α -glucosidase inhibitory activity and enhances insulin release *in vitro*. *Cytotechnology*, **67**: 653–660.

Ismail GA, Gheda SF, Abo-Shady AM, and Abdel-Karim OH. 2020. *In vitro* potential activity of some seaweeds as antioxidants and inhibitors of diabetic enzymes. *Food Sci Technol.*, **40(3)**: 681-691

Iwai K. 2008. Antidiabetic and antioxidant effects of polyphenols in brown alga *Ecklonia stolonifera* in genetically diabetic KK-Ay mice. *Plant Foods Hum Nutr.*, **63(4)**: 163–169.

Nair SS, Kavrekar V and Mishra A. 2013. *In vitro* studies on alpha amylase and alpha-glucosidase inhibitory activities of selected plant extracts. *Eur J Exp Biol.*, **3(1)**:128-132.

Nuñez-Selles A, Castro HTV, Aguero JA, Gonzalez JG, Naddeo F, De Simone F and Pastrelli L. 2002. Isolation and quantitative analysis of phenolic antioxidants, free sugars and polyols from mango (*Mangifera indica* L.) stem bark aqueous decoction used in Cuba as a nutritional supplement. *J Agric Food Chem.*, **50**: 762-766

Payghami N, Jamili S, Rustaiyan A, Saeidnia S, Nikan M and Gohari AR. 2015. Alpha-amylase inhibitory activity and sterol composition of the marine algae, *Sargassum glaucescens*. *Pharmacog Res.*, 7:314-321.

Pirian K, Moein S, Sohrabipour J, Rabiei R and Blomster J. 2017. Antidiabetic and antioxidant activities of brown and red macroalgae from the Persian Gulf. *J Appl Phycol.*, **29**(6): 3151-3159.

Phoboo S, Shetty K and Abdelkhalig TEE. 2015. *In vitro* assays of anti-diabetic and anti-hypertensive potential of some traditional edible plants of Qatar. *J Med Act Plants*, **4(3-4)**: 22-29.

Ponnan A, Ramu K, Marudhamuthu M, Marimuthu R, Siva K and Kadarkarai M. 2017. Antibacterial, antioxidant and anticancer properties of *Turbinaria conoides* (J. Agardh) Kuetz. *Clin Phytoscience*, **3(1)**:1–10.

Rajendiran D, Packirisamy S and Gunasekaran K. 2018. A review on role of antioxidants in diabetes. *Asian J Pharm Clin Res.*, **11(2)**:48-53.

Re R, Pellegrine N, Proteggente A, Pannala A, Yang M and Rice-Evans C. 1999. Antioxidant activity applying an improved ABTS⁺ radical cation decolorization assay. *Free Radic Biol Med.*, **26**:1231-1237.

Sivagnanam SR, Yin S, Choi JH, Park YB, Woo HC and Chun BS. 2015. Biological properties of fucoxanthin in oil recovered from two brown seaweeds using supercritical CO₂ extraction. *Marine Drugs*, **13**:3422-3442.

Sivaramakrishnan T, Swain S, Saravanan K, Kiruba SR, Roy SD, Biswas L and Shalini B. 2017. *In vitro* antioxidant and free radical scavenging activity and chemometric approach to reveal their variability in green macroalgae from South Andaman Coast of India. *Turk J Fish Aquat Sci.*, 17: 639-648.

Seven A, Guzel S, Seymen O, Civelek S, Bolayirli M, Uncu M and Burcak G. 2004. Effects of Vitamin E supplementation on oxidative stress in streptozotocin induced diabetic rats: Investigation of liver and plasma. *Yonsei Med J.*, **45(4)**:703-710.

Trono G C. 1997. Field Guide and Atlas of the Seaweed Resources of the Philippines, First ed. Makati City: Bookmark Inc.

Ulrich P and Cerami A. 2001. Protein glycation, diabetes, and aging. Recent Prog Horm Res., 56:1-21.

Unnikrishnan P, Suthindhiran K and Jayasri M. 2014. Inhibitory potential of *Turbinaria ornata* against key metabolic enzymes linked to diabetes. *BioMed Res Int.*, 1-10.

Zhao C, Yang C, Liu B, Lin L, Sarker SD, Nahar L, Yu H, Cao H and Xiao J. 2017. Bioactive compounds from marine macroalgae and their hypoglycemic benefits. *Trends in Food Sci Technol.*, **72**:1-12.

Biodegradation of Doxycycline Hyclate by Local Purpureocillium lilacinum strain PlHN17 and Trichoderma asperellum isolate Tullur: Monitoring by Antimicrobial Activity

Fathin Fashihah Kamaruddin¹, Maslinda Musa¹, Mohd Muzamir Mahat¹, Shahrul Hisham Zainal Ariffin², Muhd Fauzi Safian¹ and Zaidah Zainal Ariffin^{1*}

¹Faculty of Applied Sciences, Universiti Teknologi MARA, 40450 Shah Alam, UiTM, Malaysia; ²School of Biosciences and Biotechnology, Faculty of Science and Technology, National University of Malaysia, 43600 Bangi, Selangor, Malaysia

Received: September 9, 2021; Revised: January 11, 2022; Accepted: January 19, 2022

Abstract

In this study, two soil fungi from ruminant farms soil that has been exposed to tetracycline antibiotic with GPS coordinate 2°59′28.8″N 101°44′00.5″E were isolated and identified. Identification was carried out based on morphological observations, macroscopic, microscopic and molecular identification, polymerase chain reactions (PCR) and sequencing. The isolated species were identified as *Purpureocillium lilacinum* strain PlHN17 (S1) and *Trichoderma asperellum* isolate Tullur (S12). Growth profiles for each of the isolated fungi were constructed and the fungi showed exponential phase from day 4 to day 5. Both fungi went through a biodegradation process and antimicrobial activity of doxycycline hyclate antibiotic residues was determined. The finding revealed *P. lilacinum* strain PlHN17 (S1) has the highest deactivation ability of doxycycline hyclate antibiotic (77.78 %) compared to *T. asperellum* isolate Tullur (75.45 %). Hence, the isolated *P. lilacinum* strain PlHN17 (S1) showed the potential as a bioremediation tool to deactivate the doxycycline hyclate antibiotic.

Keywords: Biodegradation, Doxycycline Hyclate, Purpureocillium lilacinum strain PlHN17, Trichoderma asperellum isolate Tullur

1. Introduction

Tetracyclines possess many benefits for instance a wide range of antimicrobial activity, low toxicity, and mostly oral administration. The beneficial antimicrobial properties of these antibiotics have contributed to their extensive use in therapy and prophylaxis of human infections along with the absence of major adverse side effects (Chopra and Roberts 2001; Eliopoulos et al. 2003). Doxycycline hyclate (DOXH) is a hydrochloride hemiethanol hemihydrate of doxycycline (DOX) with a molecular mass and molecular formula of 512.94 g/mol. It is more frequently used in pharmaceutical samples as it is much more soluble compared to doxycycline monohydrate. DOXH is a semisynthetic broad-spectrum tetracycline antibiotic, and it is widely used in veterinary medicine. It is also used as an animal feed supplement to prevent diseases (Kogawa and Salgado, 2013). DOXH is more active than tetracycline against many bacterial species such as Streptococcus pyogenes, enterococci, Nocardia spp and several anaerobic species. In comparison with other tetracyclines, DOXH is preferable in the treatment of certain infections such as chronic prostatitis, sinusitis, syphilis, chlamydia and pelvic inflammatory disease due to better absorption and prolonged half-life thus permitting less persistent dosage (Kogawa and Salgado, 2013). However, the increase in the use of antibiotics such as tetracyclines especially DOXH for veterinary and medical

purposes, affects the environment and human health as active antibiotics forms are excreted from the body via urine and/or feces into the environment (Javid *et al.* 2016). As a result, the overuse of these antibiotics may pollute water resources.

Tetracyclines in water and soil can cause allergies and toxicity as these compounds remain active. For example, excreted antibiotics affect almost all bacterial species in the environment and cause these species to develop resistance to these compounds (Pena *et al.* 2010). Tetracyclines are classified as the most detected antibiotics in sewage, domestic wastewater, drinking water, sludge, surface and groundwater resources. The reasons behind this are the increased usage of tetracyclines and the inefficiency to remove tetracyclines by most conventional wastewater treatment processes, which is why tetracycline is now more likely to pollute surface and groundwater resources (Javid *et al.* 2016).

The biodegradation process is crucial for overcoming the inefficiency of most conventional wastewater treatment processes in the removal of tetracycline especially DOXH. Filamentous fungi are versatile and robust organisms with enormous capabilities for biodegradation of several substrates and therefore are preferable (Carvalho *et al.* 2010). The contamination of DOXH in the soil surface and groundwater resources can be prevented by carrying out the fungal biodegradation process.

_

^{*} Corresponding author. e-mail: drzaidah@uitm.edu.my.

2. Materials and Methods

2.1. 2.1 Soil Sample Collection

Three soil samples with triplicates were collected randomly from different sites within the depth of 20 cm at Serdang with GPS coordinate 2°59'28.8"N 101°44'00.5"E where veterinary antibiotics have been used extensively. Different sites were chosen for sample collection to obtain a diverse soil fungal cultures that have been exposed to the veterinary antibiotics. The sites were the dairy cattle farm, beef cattle farm and sheep farm. A soil sample (500 g) was collected and stored in sterile plastic bags for the analysis of pH, temperature and moisture at the laboratory.

2.2. Isolation of Soil Fungi

The soil samples were serially diluted. A ten folds serial dilution was prepared from the microbial suspension. Soil with 3 and 4 dilution factors were plated on Potato Dextrose Agar (PDA) (Merck, Germany). Afterward, the PDA plates were incubated for 3 to 5 days at 28 °C. A single colony was streaked on PDA plates in order to obtain pure cultures. The pure cultures were labelled S1 and S12 respectively. The plates were incubated for 3 to 5 days and stored at 4 °C (Muthulakshmi *et al.* 2011).

2.3. Identification of Isolated Soil Fungi

The isolated soil fungi were established by morphological observations; macroscopic and microscopic. The growth, pigment production, presence of mycelium and the colony characteristics were determined via naked eye observation for macroscopic identification (Kim *et al.* 2011). The stained fungi were viewed under a light microscope (Olympus, CX12) using 1000X magnification for hyphae and conidia observation for microscopic identification.

2.4. 2.4 DNA Extraction and Amplification

Molecular identification of the isolated fungi was identified based on Mohammad et al. (2018).

2.5. Growth Profile of Isolated Fungi

The growth profile was determined based on the dry weight of the fungus. During the growth of strains in Potato Dextrose Broth (PDB) (Merck, Germany), a volume of 6 mL was withdrawn at 5 different times (48, 96, 144, 192, 240 h). The mycelia were filtered on a Whatman 125 mm filter paper and their dry cells weights were determined after drying at 70 °C for 24 hours. The growth profiles of fungi were constructed from the dry cell weights (g) plotted versus incubation time (h). The experiments were conducted in triplicate (Melgar *et al.* 2013, Mohammad *et al.* 2018).

2.6. Biodegradation of Doxycycline Hyclate Antibiotic

Four of 250 mL Erlenmeyer flasks containing 100 mL of Potato Dextrose Broth (PDB) were prepared and sterilized using autoclave. Approximately 1x10⁶ CFU/mL of spore suspension solution of the isolated fungi was inoculated into each culture flask respectively. A flask containing PDB and culture only was used as biotic control whereas a flask containing PDB with doxycycline hyclate only was used as abiotic control. All culture flasks were incubated at 28 °C on a rotary shaker at 120 rpm until the mid-exponential phase was reached. All experiments were conducted in triplicate. After the exponential phase, a

volume of 10 mL of doxycycline hyclate antibiotic (Sigma-Aldrich, USA) (final concentration 500 μg/mL) was added into each culture flask. The flasks were further incubated at 28 °C for another 96 hours on the rotary shaker at 120 rpm (C vanc arová et al. 2015). A volume of 6 mL of medium was collected as a biodegradation product. The collection of biodegradation product was carried out every 24 hours until 96 hours of incubation was achieved (Zikmundová et al. 2002). All biodegradation products and controls were proceeded for the extraction of doxycycline hyclate antibiotic residual.

2.7. Liquid-Liquid Extraction (LLE)

The biodegradation products were subjected to liquid-liquid extraction (LLE) every 24 hours of incubation time. A volume of 6 ml of sample was mixed with 40 mL of extraction solution, 0.1 M of McIlvaine buffer-EDTA and vortexed for 60 seconds before placing it into an ultrasonic bath for 10 minutes. A volume of 10 ml of ethyl acetate: nheptane (50:50) was added into the tube. The tube was shaken for 2 minutes to create two layers and left for 10 minutes. A volume of 1 ml of the organic phase supernatant was transferred into a microcentrifuge tube and dried using Hypervac vacuum concentrator (VC2200) (Gyrozen, Korea).

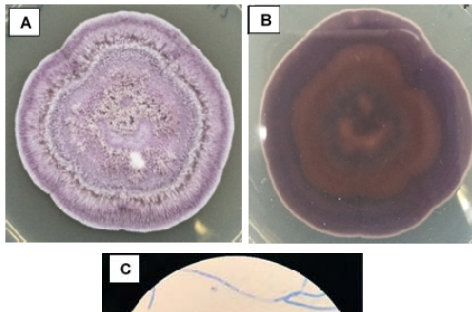
2.8. Residual Antimicrobial Activity Assay of Doxycycline Hyclate

Antimicrobial assay was performed to evaluate the activity of doxycycline hyclate antibiotic residual after biodegradation process. *Bacillus subtilis* strain ATCC6633 which is a Gram-positive bacterial strain and susceptible to tetracyclines was used for antimicrobial activity assay. The antimicrobial assay was carried out by using well diffusion techniques. The bacteria were grown in Mueller-Hinton Broth (MHB) (Oxoid, UK) overnight and diluted to 10⁸ cfu/mL based on 0.5 McFarland turbidity standard. Doxycycline hyclate antibiotic (30 μg/mL) as a positive control and 70 % ethanol and sterile DMSO as negative controls. The plates were incubated overnight at 37 °C. The zones of inhibition produced by each well were measured and recorded. This assay was done in triplicate (Mohammad *et al.* 2018).

3. Results and Discussion

3.1. Identification of Isolated Fungus

Two fungal species were successfully isolated from the soil that had been exposed to veterinary antibiotics. The species were identified by morphological and molecular identifications as *P. lilacinum* strain PlHN17 (Isolate S1) and *T. asperellum* isolate Tullur (Isolate S12). Morphologically, the reproductive characteristics can be observed from the 1000X magnification. Isolate S1 (Figure 1) has similar microscopic images with the one reported by de Sequeira *et al.* (2017) which resembled *P. lilacinum*. Conidiophores verticillate with two or four phialides which have a swollen basal portion tapering into a short distinct neck. Meanwhile, the conidia are hyaline and ellipsoidal to fusiform (de Sequeira *et al.* 2017).



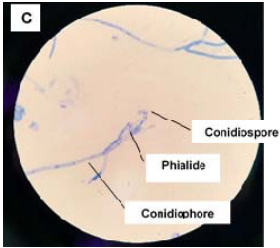
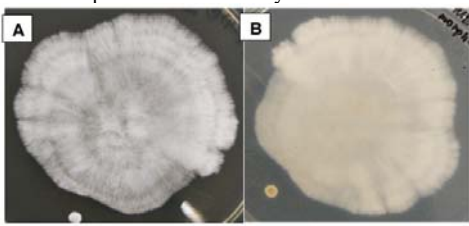


Figure 1. Macroscopic observations of isolate S1 after 5 days of incubation (A: Front view; B: Reverse view) and microscopic observation of isolate S1 under 1000X total magnification (C) using light microscope (Olympus, CX12)

The macroconidia of isolate S12 are oval, large and cumulative over the conidiophores as reported by Samuels *et al.* (1999) that resembled *T. asperellum* (Figure 2). The isolated fungal species were from two different genera, and both species were normally found in soil.



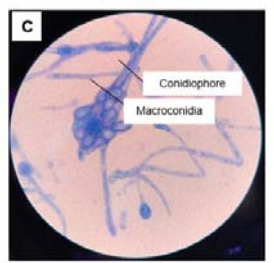


Figure 2. Macroscopic observations of isolate S12 after 5 days of incubation (A: Front view; B: Reverse view) and microscopic observation of isolate S12 under 1000X total magnification (C) using light microscope (Olympus, CX12)

Table 1. Summary of NCBI Blast of the isolated fungi

The molecular identification was carried out by DNA barcoding using the ITS region sequencing. The ITS rDNA sequences were compared to those in the databases by using NCBI-BLAST. Sequence analysis of the ITS regions of the nuclear encoded rDNA revealed significant alignments of 100% with the isolated fungal species. According to NCBI-BLAST, *P. lilacinum* strain PIHN17 and *T. asperellum* isolate Tullur have query length of 571 and 585 base pairs respectively (NCBI 2019). The query length of both isolates was similar to the finding from the agarose gel electrophoresis conducted which revealed that both isolates relatively are 600 base pairs in length (Figure 3, Table 1)

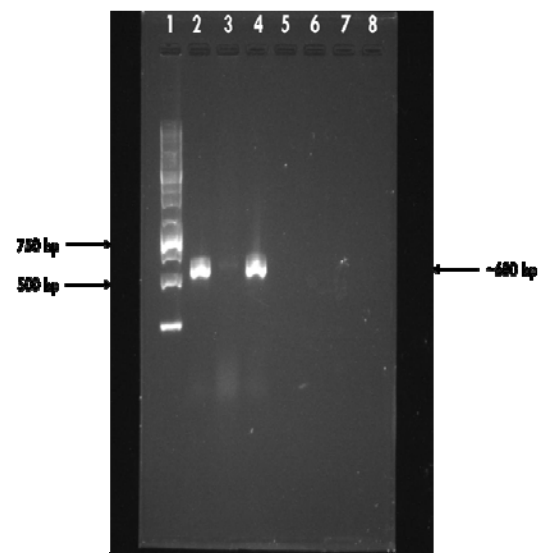


Figure 3. Agarose gel electrophoresis (1%) of genomic DNA of the fungi isolates (S1 and S12) amplified with ITS1 and ITS4 primers. Lane 1: 1kb DNA ladder marker (Solis Biodyne), Lane 2: Isolate S1 and Lane 4: Isolate S12.

	•	C					
Isolate	Description	Max Score	Total Score	Query Cover	E Value	Identity	Accession
S1	Purpureocillium lilacinum strain PIHN17 internal transcribed spacer 1, partial sequence	889	889	81%	0.0	100%	MH483732.1
S12	Trichoderma asperellum isolate Tullur internal transcribed spacer 1, partial sequence	837	903	87%	0.0	100%	MN396441.1

3.2. Growth Profile of The Identified Soil Fungi

The growth profiles of two isolated fungal species were constructed (Figure 4). Based on the graph plotted, the exponential or log phase of the isolated fungi occurred from day 4. *P. lilacinum* strain PlHN17 showed exponential growth on day 4 of incubation and the

stationary phase began on day 6 in PDB which is faster than in Karanja deoiled cake liquid medium (Sharma *et al.* 2016). *T. asperellum* isolate Tullur was an intermediate growing fungus since the exponential phase occurred on day 1 to day 4 of incubation and experienced stationary phase on day 5 which is agreeable with Saranya *et al.* (2020).

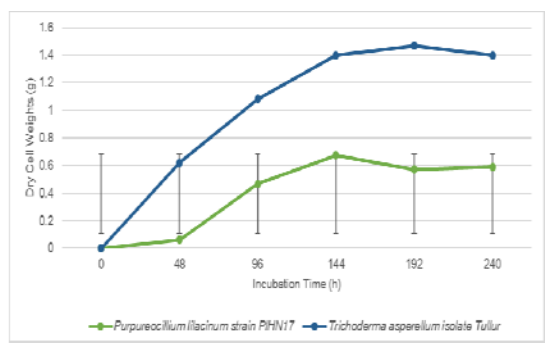


Figure 4. Growth profiles of the isolated fungal species in triplicates after 10 days of incubation.

3.3. Antimicrobial Activity of Doxycycline Hyclate

Both isolated fungal species were subjected to undergo the biodegradation assay of doxycycline hyclate antibiotic. Thus, the ability of fungi to degrade antibiotics, doxycycline hyclate in this case, could be better studied as different fungal strains were being tested. The percentage of inhibition was calculated by dividing the inhibition zone diameter of the doxycycline hyclate residues with the inhibition zone diameter of the abiotic control. The diameter of abiotic control served as a control in which no degradation of doxycycline hyclate antibiotic occurred. Both isolated fungal species exhibited good degradation activity as the percentage of inhibition of doxycycline hyclate antibiotic residues against *Bacillus subtilis* strain ATCC6633 decreased after 96 hours of incubation (Figure 5).

Generally, doxycycline hyclate went through epimerization and this reaction can occur at C-4 and C-6 positions thus resulting in degradation products which are 4-epidoxycycline (4-EDOX), 4,6-epidoxycycline (4,6-EDOX) and 2-acetyl-2-decarboxiamidodoxycycline (ADDOX) (de Barros et al. 2018). Genera Purpureocillium has the ability of parasitizing fungi, nematodes, and arthropods by enzymatic penetration through cellulase, glucanase, laccase, leucinoxin, lipase, pectinase, protease, chitinase or xylanase release which are involved in the infection process (Moreno-Gavíra 2020). Suda et al. (2012) reported that the laccase-HBT system facilitated the elimination of doxycycline as it was completely eliminated after 0.25 h. A study by Xie et al. (2016) observed the production of proteolytic enzymes and carbohydrate hydrolases (Xie et al. 2016) such as chitinases and serine proteases by P. lilacinum. Moreover, P. lilacinum has the ability to synthesize heterogenous biologically active secondary metabolites including polyketides and non-ribosome-synthesized peptides (Xie et al. 2016).

In our finding, *T. asperellum* isolate Tullur showed a 75.45 % degradation of doxycycline hyclate antibiotic. *T. asperellum* strain BPLMBT1 was reported to produce laccase with excellent temperature and pH stabilities (Shanmugam *et al.* 2020). Research by Zafra et al. (2015) observed a 78 % of phenanthrene degradation by *T. asperellum* after 14 days in soil contaminated with 1000 mg kg⁻¹ of phenanthrene. The results of the research revealed the potential of *T. asperellum* to be used in a bioremediation process and served as evidence that *T.*

asperellum was considered a promising and effective PAH-degrading microorganism (Zafra et al. 2015).

In this study, *P. lilacinum* strain PIHN17 exhibited the highest degradation ability (77.78 %) to degrade doxycycline hyclate (Figure 5). With a prolonged incubation period, doxycycline hyclate antibiotic could be completely removed due to its rapid growth that leads to a high level of mycelia mass production and therefore high level of degradation. To date, no research has been conducted to study the degradation or transformation of doxycycline hyclate antibiotic by using *P. lilacinum* strain PIHN17 and *T. asperellum* isolate Tullur.

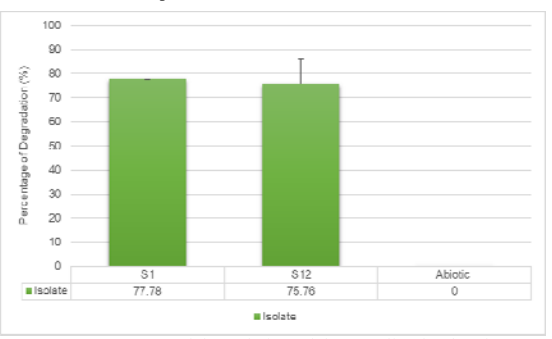


Figure 5. Percentage of degradation of doxycycline hyclate by Purpureocillium lilacinum strain PIHN17 (S1) and Trichoderma asperellum isolate Tullur (S12) in triplicates after 96 hours of incubation.

4. Conclusions

The isolated fungal species were identified morphologically and molecularly as *P. lilacinum* strain PIHN17 and *T. asperellum* isolate Tullur. *P. lilacinum* showed the highest degradation ability (77.78 %) to degrade doxycycline hyclate antibiotic. Hence, the isolated *P. lilacinum* showed a potential bioremediation tool to degrade doxycycline hyclate antibiotic.

Acknowledgements

This work is supported by Fundamental Research Grant Scheme (FRGS), 600-IRMI FRGS 5/3 (197/2019).

References

C'vanc'arová M, Moeder M, Filipová A and Cajthaml T. (2015). Biotransformation of fluoroquinolone antibiotics by ligninolytic fungi--metabolites, enzymes and residual antibacterial activity. *Chemosphere* **136**: 311–320.

Carvalho T C de, Polizeli A M, Turatti I C C, Severiano M E, Carvalho C de, Ambrósio S R *et al.* (2010). Screening of filamentous fungi to identify biocatalysts for lupeol biotransformation. *Molecules* **15(9)**: 6140–6151.

Chopra I and Roberts M. (2001). Tetracycline antibiotics: Mode of action, applications, molecular biology, and epidemiology of bacterial resistance. *Microbiol. Mol. Biol. Rev.* **65(2)**: 232–260.

de Barros J O, Kogawa A C and Salgado H R N. (2018). Short-term stability study of doxycycline tablets by high performance liquid chromatography, spectrophotometry in the ultraviolet region and turbidimetry. *J. Pharmcol. Clin. Trials* **1(1)**: 43–49.

de Sequeira D C M, Menezes R C, Oliveira M M E, Antas P R Z, De Luca P M, Oliveira-Ferreira J and Borba C M. (2017). Experimental hyalohyphomycosis by *Purpureocillium lilacinum*:

Outcome of the infection in C57BL/6 murine models. Front. Microbiol. 8: 1617.

Eliopoulos G M, Eliopoulos G M and Roberts M C. (2003). Tetracycline therapy: Update. *Clin. Infect. Dis.* **36(4)**: 462–467.

Javid A, Mesdaghinia A, Nasseri S, Mahvi A H, Alimohammadi M and Gharibi H. (2016). Assessment of tetracycline contamination in surface and groundwater resources proximal to animal farming houses in Tehran, Iran. *J. Environ. Health Sci.* 14(4).

Kim J Y, Yeo S H, Baek S Y and Choi H S. (2011). Molecular and morphological identification of fungal species isolated from bealmijang meju. *J. Microbiol. Biotechnol.* **21(12)**: 1270–1279.

Kogawa A C and Salgado H R. (2013). Quantification of doxycycline hyclate in tablets by HPLC-UV method. *J. Chromatogr. Sci.* **51(10)**: 919-925.

Melgar G Z, Assis F V S de, Rocha L C da, Fanti S C, Sette L D and Porto A L M. (2013). Growth curves of filamentous fungi for utilization in biocatalytic reduction of cyclohexanones. *Glob. J. Sci. Front. Res* **13(5)**.

Mohammad N S, Safian M F, Zainal Ariffin S H and Zainal Ariffin Z. (2018). Biotransformation of nitrofurans antibiotics by Aspergillus species -residual antibacterial activity. *Malays. J. Biochem. Mol. Biol.* 2: 28–33.

Moreno-Gavíra A, Huertas V, Diánez F, Sánchez-Montesinos B and Santos M. (2020). *Paecilomyces* and its importance in the biological control of agricultural pests and diseases. *Plants* 9.

Muthulakshmi, C., Gomathi, D., Kumar, D. G., Ravikumar, G., Kalaiselvi, M., & Uma, C. (2011). Production, Purification and Characterization of Protease by *Aspergillus flavus* under Solid State Fermentation. *Jordan J Biol Sci*, 4(3).

Pena A, Albert-Garcia J R, Silva L J G, Lino C M and Calatayud J M. (2010). Photo-induced fluorescence of magnesium derivatives of tetracycline antibiotics in wastewater samples. *J. Hazard. Mater.* **179(1)**: 409–414.

Samuels G J, Lieckfeldt E and Nirenberg H I. (1999). *Trichoderma asperellum*, a New species with warted conidia, and redescription of *T. viride*. *Sydowia* **51(1)**: 71–88.

Saranya N, Suganya E, Narayanasamy S, Sivaprakasam S, Sivasubramanian V, Pandian S and Selvaraj R. (2020). 3-level Box–Behnkenoptimization of hexavalent chromium reduction by chromate resistant *Trichoderma asperellum* cells from simulated and industrial effluent. *Environ. Technol. Innov.*, **19**, 101024.

Sharma A, Sharma S, Mittal A. et al. (2016). Evidence for the involvement of nematocidal toxins of *Purpureocillium lilacinum* 6029 cultured on Karanja deoiled cake liquid medium. *World J Microbiol Biotechnol* 32: 82.

Shanmugam S, Krishnaswamy S, Chandrababu R, Veerabagu U, Pugazhendhi A and Mathimani T. (2020). Optimal immobilization of *Trichoderma* asperellum laccase on polymer coated Fe₃O₄@SiO₂ nanoparticles for enhanced biohydrogen production from delignified lignocellulosic biomass. *Fuel* **273**: 117777.

Suda T, Hata T, Kawai S, Okamura H and Nishida T. (2012). Treatment of tetracycline antibiotics by laccase in the presence of 1-hydroxybenzotriazole. *Bioresour. Technol.* **103(1)**: 498–501.

Xie J, Li S, Mo C, Xiao X, Peng D, Wang G and Xiao Y. (2016). Genome and transcriptome sequences reveal the specific parasitism of the nematophagous *Purpureocillium lilacinum* 36-1. *Front. Microbiol.* 7:1084

Zafra G, Moreno-Montaño A, Absalón Á E and Cortés-Espinosa D V. (2015). Degradation of polycyclic aromatic hydrocarbons in soil by a tolerant strain of *Trichoderma asperellum*. *Environ. Sci. Pollut*. Res. **22(2)**: 1034–1042.

Zikmundová M, Drandarov K, Bigler L, Hesse M and Werner C. (2002). Biotransformation of 2-benzoxazolinone and 2-hydroxy-1,4-benzoxazin-3-one by endophytic fungi isolated from *Aphelandra tetragona*. *Appl. Environ. Microbiol.* **68(10)**: 4863–4870

Utility of SPC25 as a Biological Biomarker in Colorectal Adenocarcinoma

AbdulFattah Salah Fararjeh*

 $Department\ of\ Medical\ Laboratory\ Analysis,\ Faculty\ of\ Science,\ Al-Balqa\ Applied\ University,\ Al-salt,\ Jordan\ Al-salt,\ Medical\ Laboratory\ Analysis,\ Faculty\ of\ Science,\ Al-Balqa\ Applied\ University,\ Al-salt,\ Medical\ Laboratory\ Al-salt,\ Medical\ Medical\ Laboratory\ Al-salt,\ Medical\ Medical\ Laboratory\ Al-salt,\ Medical\ Medical\ Al-salt,\ Medical\

Received: October 9, 2021; Revised: December 14, 2021; Accepted: December 28, 2021

Abstract

Spindle pole body component 25(SPC25) is involved in a variety of biological processes, including carcinogenesis. However, no research has been done on the clinical importance of SPC25 in colorectal adenocarcinoma (COAD). The goal of this work was to investigate the mRNA level of SPC25 in COAD and normal tissues, as well as its diagnostic and prognostic usefulness. The mRNA level of SPC25 was examined in colorectal adenocarcinoma (COAD) using Gene Expression Profiling Interactive Analysis (GEPIA), Firebrowse, Gene Expression Omnibus (GEO), Oncomine and The Cancer Genome Atlas (TCGA) databases. To examine the diagnostic significance of SPC25, we use receiver operating characteristic (ROC) plotter. SPC25 was upregulated in several type of cancers, and the highest expression was in COAD cohort study. SPC25 was higher in tumor COAD tissues in comparison to normal tissues (p value <0.001). High level of SPC25 at mRNA level was associated with tumor stage (p value= 0.045) and lymph node (p value= 0.019). Patients with high SPC25 had poor overall survival and disease free survival. In ROC analysis, SPC25 was shown to be a highly diagnostic biomarker in COAD with Area value =0.548 and p value= 4.5e-2. SPC25 was elevated in COAD and was found to be an independent predictor of worse Overall Survival and Disease free survival in patients with COAD. Therefore, SPC25 is a useful biomarker for diagnostic and prognostic COAD patients.

Keywords: SPC25, COAD, Overall survival, TCGA

1. Introduction

Colorectal adenocarcinoma cancer (COAD) continues to be the leading cause of cancer-related death worldwide, with a high annual incidence of cancer per population (Jemal et al., 2011; Sung et al., 2021). In general, liver metastasis affects roughly 30 % of COAD patients, while more than half of individuals acquire metastasis at particular sites after identification of a tumor stage (Cardona et al., 2013; Mayo et al., 2011). Genetic mutations, epigenetic alterations, and environmental variables all have a role in development of COAD. COAD is more common in those between the ages of 40 and 50; however, it is becoming more common among younger people (Karunanithi & Levi, 2018). chemotherapy, and radiotherapy are the most common treatments for COAD today; nonetheless, in metastatic cases, the 5-year overall survival rate is less than 10%(Jiang, Yang, Yuan, & Liu, 2018). As a result, it is necessary to discover a critical gene involved in the development of COAD in order to design appropriate diagnostics and successful treatment strategies for COAD patients.

Spindle pole body component 25 (SPC25) is a part of a nuclear division cycle 80 complex (Ndc80) controls the interaction of kinetochore protein with microtubules.; it plays an important function in chromosomal segregation (F. Chen et al., 2020; Tooley & Stukenberg, 2011;

Ustinov, Korshunova, & Gudimchuk, 2020). Several theories have been postulated that fault in chromosomal segregation causes genetic instability, which links to cancer development (Raaijmakers & Medema, 2014). Recent studies have reported the role of SPC25 in cancer progression in several type of malignancies; prostate cancer, hepatocellular carcinoma, breast cancer, gastric cancer and lung cancer (J. Chen, Chen, Yang, & Dai, 2018; Cui, Hu, Fan, Tan, & Tang, 2018; Wang et al., 2019; Yang, Sun, Song, Yang, & Liu, 2020; B. Zhang et al., 2020). Blood samples from those with mild cognitive impairment showed considerably increased SPC25 expression, indicating that it may serve as a biomarker for alzheimer's disease, according to a cell-based assay (X. Zhang, Li, Shen, & Lau, 2018). However, no definitive research has been done on the link between SPC25 gene expression and CROAD clinical diagnosis and disease prognosis.

In this study, the potential role of SPC25 as a diagnostic and prognostic biomarker was verified by using several bioinformatics tools; TCGA xena browser, GEPIA, Oncomine and GEO databases. For the first time, we report on the differential expression of SPC25 in COAD and its relationship to prognosis.

^{*} Corresponding author. e-mail: Fararjehas@bau.edu.jo.

2. Material and Methods

2.1. Expression profile of SPC25 in colorectal adenocarcinoma cancer (COAD) using GEPIA.

GEPIA (http://gepia.cancer-pku.com) is an interactive web-based program that delivers RNA sequencing data based on TCGA and GTEx, with roughly 10,000 tumor samples and 9,000 normal samples. We used the Expression DIY functionality to find the SPC25 gene, then selected Boxplot from the Expression DIY menu, with Colorectal cancer (COAD) added to the Datasets list. Then, automatically, Log scale, Jitter size, and Matched normal data were all established.

2.2. Expression profile of SPC25 in COAD using Oncomine and TCGA databases

Oncomine — a cancer microarray dataset-providing server that grants access to about 800 datasets from numerous study cohorts. (http://www.oncomine.org). In addition, TCGA-BC cohort by UCSC (University of California at Santa Cruz, CA, USA) Cancer Genomics Browser (https://xenabrowser.net/) assisted the collection of data of 300 COAD tissue samples in link to clinicopathological parameters.

We searched for "TCGA colon cancer (COAD) in Search for a study, then Genomic was selected for the Data Type, and the desired SPC25 gene was added; finally, Gene Expression was checked as a dataset.

2.3. Gene expression Omnibus database

We used GEO datasets website (https://www.ncbi.nlm.nih.gov.com) looking for a study on profile of mRNA in colorectal cancer. We then download the GSE156720 dataset which examines the expression of mRNAs between 3 pairs of colorectal tumor tissues and normal tissues. This study reported significantly up-

regulated as well as down-regulated mRNAs and lncRNAs in CRC tissues compared with their matched non-tumoral tissues.

2.4. Receiver operating characteristic (ROC) Plotter

By using the RNA sequencing data of over 1500 COAD patients, the ROC plotter (http://www.rocplot.org/) was able to expect the relationship between gene expression and therapeutic response.

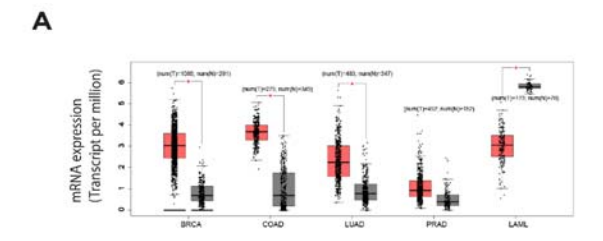
2.5. Statistical analysis

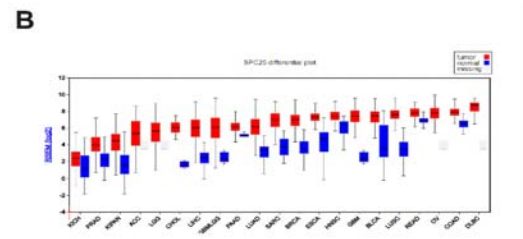
SPSS version 18.0 was used to analyze the data (SPSS, Inc., Chicago, IL, USA). One-way ANOVA, as well as chi-squared tests, were used to analyze the association between STARD3 and BC clinicopathological parameters. Statistical significance was defined as *p < 0.05 and **p < 0.001.

3. Results

3.1. SPC25 is overexpressed in colorectal cancer than in other types of cancer

The GEPIA web-based RNA expression tool was used to determine the SPC25 mRNA expression in different types of human malignancies (n = 5) in contrast to neighboring normal tissues (Figure 1 A). When compared to other kinds of human cancer, colorectal cancer (COAD) had the greatest level of SPC25 expression. Furthermore, based on firebrowse when compared to nearby normal colorectal tissues, SPC25 was upregulated in colorectal carcinoma tissues (Figure 1 B). SPC25 mRNA levels were elevated in primary colorectal tissues (n=286) more than normal tissues (n=41) when we used the UALCAN website. Altogether, SPC25 mRNA expression was shown to be greater in COAD tissues than in normal tissues.





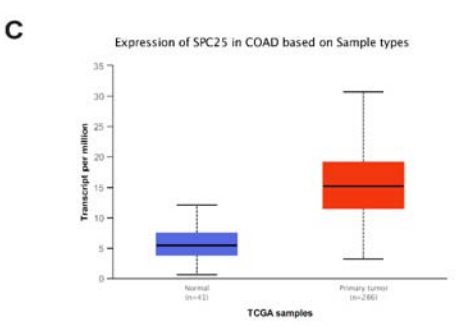


Figure 1 Expression level of SPC25 in different types of cancers. A) The graph was created from the GEPIA, B) Firebrowse webpages, which indicates the expression of SPC25 at the mRNA level in several types of malignancies. The red box indicates the expression of SPC25 in tumor tissues, and the gray box indicates the expression of SPC25 in normal tissues. C) SPC25 expression in COAD using UALCAN database, the blue box indicates the normal tissues (n=41) and the red box indicates the primary COAD tissues (n=286) the p value <1E-12.

3.2. SPC25 expression based on Oncomine and GEO databases

With solid, peer-reviewed analytic methodologies and a rich collection of analysis functions that compute gene expression signatures, the Oncomine Platform delivers solutions for individual researchers and multinational corporations. We analyzed the mRNA level of SPC25 in different types of colorectal cancer. Overexpression of SPC25 in COAD has been found in eight studies (Figure 2 A/B). 1; Rectal Adenocarcinoma vs. Normal Gaedcke/ 2; Colon Adenoma vs. Normal Sabates-Bellver Colon/ 3; Colorectal Carcinoma vs. Normal Skrzypczak / 4; Cecum Adenocarcinoma vs. Normal TCGA Colorectal / 5; Colon Adenocarcinoma vs. Normal TCGA Colorectal/ 6; Colon Mucinous Adenocarcinoma vs. Normal TCGA Colorectal / 7: Rectal Adenocarcinoma vs. Normal TCGA Colorectal /8; Rectal Mucinous Adenocarcinoma vs. Normal TCGA Colorectal.

To confirm these results, we downloaded RNA seq data from GEO microarray datasets based on transcriptome analysis to identify the expression level of SPC25 in colorectal cancer (GSE156720) was performed on 3 pairs of colorectal tumor tissues and normal tissues. Total RNA was extracted and Samples labeling and array hybridization were done based on the Agilent One-Color Microarray-Based Gene Expression Analysis protocol

(Agilent Technology). All the three tumor tissues had high level of SPC25 in comparison to the adjacent normal tissues, the (Figure 2 C), shows the average mRNA level for the three tumor tissues and the three normal tissues.

3.3. Association of SPC25 with COAD clinicopathological features

Next, relationship between SPC25 and COAD clinicopathological parameters have been analyzed from COAD-TCGA dataset (Table 1). High level of SPC25 was significantly associated with tumor stage (p=0.045) and lymph node status (p=0.019). No significant association had been found with tumor size or radiation therapy or height or weight of the patients.

Patients with high level of SPC25 mRNA had poor overall survival (OS) and disease-free survival (DFS); however, better overall survival and disease-free survival are predicted by low levels of SPC25. (Figure 2 D/E).

We created a ROC curve utilizing SPC25 expression data from colorectal adenocarcinoma tissues using ROC plotter to explore the diagnostic utility of SPC25 gene. SPC25 was found to have a high clinical utility in separating COAD normal from tumor tissues, as shown in (Figure 2 F), with an AUC of 0.548, a true positive rate of 0.56, and a false positive rate of 0.53, and a p value of 4.5e-2.

Clinicopathological characteristics	Variables	SPC25 mRNA low	SPC25 mRNA high	P-value
Height	≤168 cm	48	54	0.339
	VS	46	44	
	≥169cm			
Weight	≤82kg	52	56	0.172
	VS	53	42	
	≥83kg			
Tumor size	T1 &T2	25	125	0.197
	vs	26	95	
	T3&T4			
Tumor stage	Stage I & II	74	73	0.045*
	VS	72	45	
	Stage III& IV			
Node	N0	73	72	0.019*
	N1	41	16	
	N2	27	21	
Radiation therapy	No	126	4	0.285
	Yes	97	1	

Table 1: Clinicopathological features of colorectal cancer with high vs low SPC25 mRNA expression based on TCGA database. Clinicopathological parameters were assessed using Chi-square analysis. * p < 0.05, ** p < 0.001.

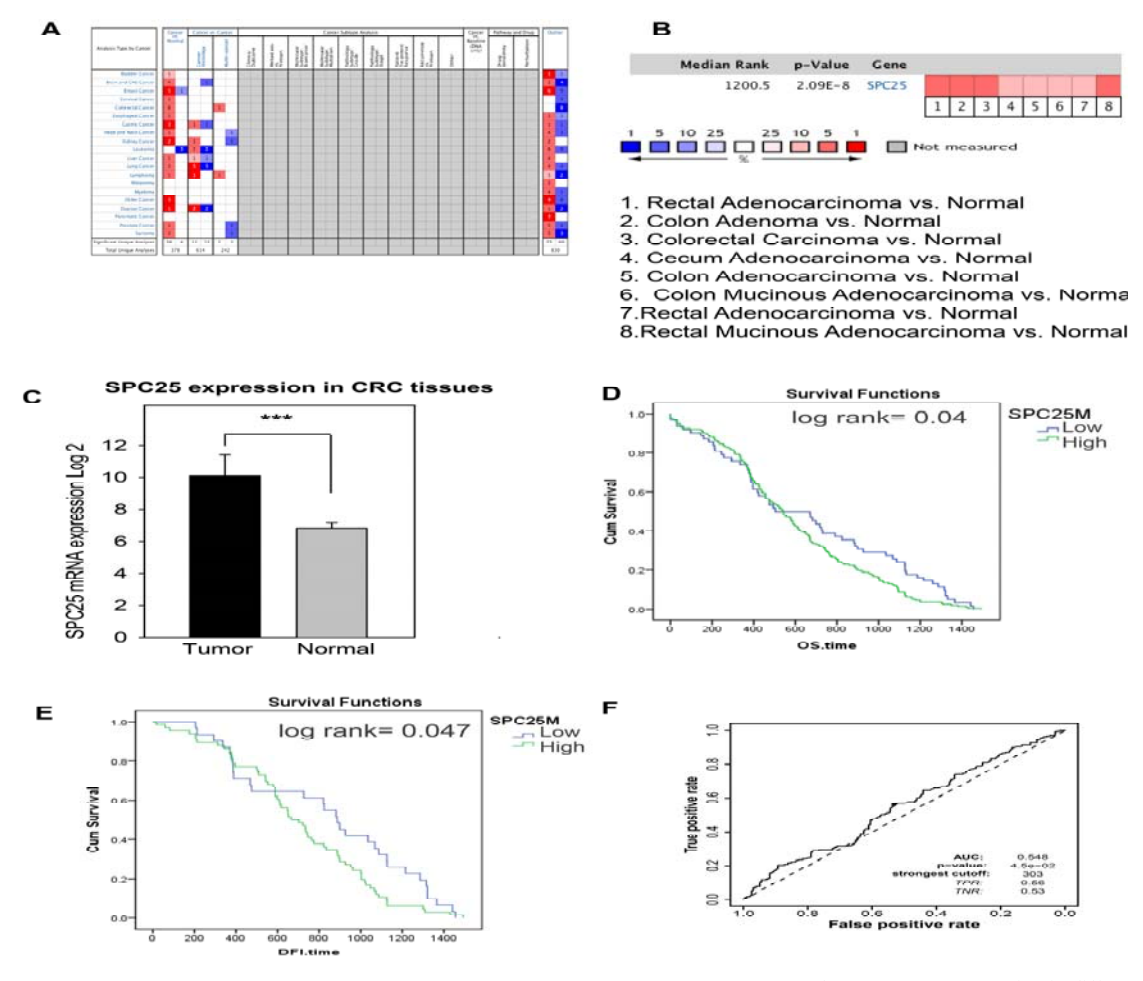


Figure 2 Oncomine, GEO analysis and the prognostic significance of SPC25 in CAOD. A) The SPC25 gene expression in different types of malignancies based on Oncomine database. B) SPC25 mRNA expression in COAD subtypes is compared; high expression is indicated by a red, whereas low expression is indicated by a blue. C) SPC25 in colorectal adenocarcinoma based on GEO analysis. D&E) Survival analysis of SPC25 in COAD patients. F) ROC analysis for true positive rare vs false positive rate.

4. Discussion

SPC25 is a component of the Ndc80 complex that regulates the segregation of mitotic chromosomes during mitosis (Tooley & Stukenberg, 2011). During the mitotic process, SPC25, can form a dimer with SPC24 to control microtubule-kinetochore binding. chromosomal arrangement, and spindle checkpoint initiation (Sun, Lee, Xu, & Kim, 2010). Ndc80 was found to be overexpressed in several type of human cancers (Liu et al., 2016; Xing, Wu, Chen, & Feng, 2016). SPC25 was observed to play an important role in thyroid cancer development, and it has been discovered to be a new prognostic biomarker for lung cancer and hepatocellular carcinoma (Yin, Meng, Zhou, Chen, & Song, 2017; Zhou et al., 2017; Zhu et al., 2015). In the current study, we focused on SPC25 and investigate the prognostic significant and expression pattern in patients with colorectal adenocarcinoma. Per our information, this is the first research to examine the SPC25 expression at mRNA in COAD.

Recently, SPC25 was upregulated in hepatocellular carcinoma and breast cancer, and was associated with poor overall survival (Wang et al., 2019; Yang et al., 2020). Furthermore, SPC25 was discovered to be an effective

diagnostic marker for distinguishing between normal and HCC tissues. Upregulation of SPC25 in lung adenocarcinoma can increase cancer stem cell characteristics and indicate poor survival in patients with lung adenocarcinoma. In lung adenocarcinoma, knocking down SPC25 harmed cancer stem cell characteristics (J. Chen et al., 2018). SPC25 knockdown was also found to increase prostate cancer cell death in a new study (Cui et al., 2018).

The expression pattern and prognostic value of SPC25 in COAD were investigated using the GEPIA and TCGA databases in this study. We found that SPC25 at mRNA level was upregulated in several types of cancers using GEPIA database and firebrowse webpage in comparison to the normal tissues. The highest expression was found to be in COAD. These findings could point to SPC25's oncogenic function in colorectal cancer. More research is needed to determine the molecular involvement of SPC25 in CRC.

Using TCGA RNA sequencing data, the potential prognostic significance of SPC25 was assessed in this work. According to the results, SPC25 expression was observed to be higher in stages III&IV than in stages I&II. SPC25 levels were similarly higher in N2 stage COAD samples than in N0 stage COAD samples, according to

these findings. Patients with COAD who had low SPC25 expression had a longer OS free survival time than those who had high SPC25 expression, according to a Kaplan Meier analysis. To the best of our knowledge, this is the first study to show that SPC25 is implicated in COAD prediction.

Previously, SPC25 knockdown decreased cell proliferation and resulted in a decrease in the number of PCa cells in the S phase and an increase in the number of cells in the G2/M phase, according to the results of the SPC25 loss of function experiment. Furthermore, knocking down SPC25 enhanced PCa apoptosis. SPC25 has several functional roles in regulating cell proliferation, apoptosis, invasion, the involvement of tissue factor in cancer, transforming growth factor signaling, and the Sumoylation pathway in PCa, according to bioinformatics studies (Cui et al., 2018).

5. Conclusion

In conclusion, the current study's findings imply that SPC25 is a predictive and diagnostic biological marker for COAD patients, and that it may have a unique oncogenic role in colon cancer.

Acknowledgements

Not applicable.

Funding

Not applicable.

References

- Cardona, K., Mastrodomenico, P., D'Amico, F., Shia, J., Gonen, M., Weiser, M. R., D'Angelica, M. I. (2013). Detailed pathologic characteristics of the primary colorectal tumor independently predict outcome after hepatectomy for metastases. *Ann Surg Oncol*, 20(1), 148-154. doi:10.1245/s10434-012-2540-y
- Chen, F., Zhang, K., Huang, Y., Luo, F., Hu, K., & Cai, Q. (2020). SPC25 may promote proliferation and metastasis of hepatocellular carcinoma via p53. *FEBS Open Bio*, 10(7), 1261-1275. doi:10.1002/2211-5463.12872
- Chen, J., Chen, H., Yang, H., & Dai, H. (2018). SPC25 upregulation increases cancer stem cell properties in non-small cell lung adenocarcinoma cells and independently predicts poor survival. *Biomed Pharmacother*, 100, 233-239. doi:10.1016/j.biopha.2018.02.015
- Cui, F., Hu, J., Fan, Y., Tan, J., & Tang, H. (2018). Knockdown of spindle pole body component 25 homolog inhibits cell proliferation and cycle progression in prostate cancer. *Oncol Lett,* 15(4), 5712-5720. doi:10.3892/ol.2018.8003
- Jemal, A., Bray, F., Center, M. M., Ferlay, J., Ward, E., & Forman, D. (2011). Global cancer statistics. *CA Cancer J Clin*, 61(2), 69-90. doi:10.3322/caac.20107
- Jiang, W., Yang, W., Yuan, L., & Liu, F. (2018). Upregulation of AKIP1 contributes to metastasis and progression and predicts poor prognosis of patients with colorectal cancer. *Onco Targets Ther*, 11, 6795-6801. doi:10.2147/OTT.S151952
- Karunanithi, S., & Levi, L. (2018). High-fat diet and colorectal cancer: myths and facts. *Future Oncol*, 14(6), 493-495. doi:10.2217/fon-2017-0578

- Liu, B., Yao, Z., Hu, K., Huang, H., Xu, S., Wang, Q., . . . Ren, J. (2016). ShRNA-mediated silencing of the Ndc80 gene suppress cell proliferation and affected hepatitis B virus-related hepatocellular carcinoma. *Clin Res Hepatol Gastroenterol*, 40(3), 297-303. doi:10.1016/j.clinre.2015.08.002
- Mayo, S. C., Heckman, J. E., Shore, A. D., Nathan, H., Parikh, A. A., Bridges, J. F., . . . Pawlik, T. M. (2011). Shifting trends in liver-directed management of patients with colorectal liver metastasis: a population-based analysis. *Surgery*, *150*(2), 204-216. doi:10.1016/j.surg.2011.06.013
- Raaijmakers, J. A., & Medema, R. H. (2014). Function and regulation of dynein in mitotic chromosome segregation. *Chromosoma*, 123(5), 407-422. doi:10.1007/s00412-014-0468-7
- Sun, S. C., Lee, S. E., Xu, Y. N., & Kim, N. H. (2010). Perturbation of Spc25 expression affects meiotic spindle organization, chromosome alignment and spindle assembly checkpoint in mouse oocytes. *Cell Cycle*, 9(22), 4552-4559. doi:10.4161/cc.9.22.13815
- Sung, H., Ferlay, J., Siegel, R. L., Laversanne, M., Soerjomataram, I., Jemal, A., & Bray, F. (2021). Global Cancer Statistics 2020: GLOBOCAN Estimates of Incidence and Mortality Worldwide for 36 Cancers in 185 Countries. *CA Cancer J Clin*, 71(3), 209-249. doi:10.3322/caac.21660
- Tooley, J., & Stukenberg, P. T. (2011). The Ndc80 complex: integrating the kinetochore's many movements. *Chromosome Res*, 19(3), 377-391. doi:10.1007/s10577-010-9180-5
- Ustinov, N. B., Korshunova, A. V., & Gudimchuk, N. B. (2020). Protein Complex NDC80: Properties, Functions, and Possible Role in Pathophysiology of Cell Division. *Biochemistry (Mosc)*, 85(4), 448-462. doi:10.1134/S0006297920040057
- Wang, Q., Zhu, Y., Li, Z., Bu, Q., Sun, T., Wang, H., . . . Cao, X. (2019). Up-regulation of SPC25 promotes breast cancer. *Aging (Albany NY)*, 11(15), 5689-5704. doi:10.18632/aging.102153
- Xing, X. K., Wu, H. Y., Chen, H. L., & Feng, H. G. (2016). NDC80 promotes proliferation and metastasis of colon cancer cells. *Genet Mol Res*, 15(2). doi:10.4238/gmr.15028312
- Yang, X., Sun, H., Song, Y., Yang, L., & Liu, H. (2020). Diagnostic and prognostic values of upregulated SPC25 in patients with hepatocellular carcinoma. *PeerJ*, 8, e9535. doi:10.7717/peerj.9535
- Yin, H., Meng, T., Zhou, L., Chen, H., & Song, D. (2017). SPC24 is critical for anaplastic thyroid cancer progression. *Oncotarget*, 8(13), 21884-21891. doi:10.18632/oncotarget.15670
- Zhang, B., Zhou, Q., Xie, Q., Lin, X., Miao, W., Wei, Z., . . . Chen, X. (2020). SPC25 overexpression promotes tumor proliferation and is prognostic of poor survival in hepatocellular carcinoma. *Aging (Albany NY)*, 13(2), 2803-2821. doi:10.18632/aging.202329
- Zhang, X., Li, J., Shen, F., & Lau, W. Y. (2018). Significance of presence of microvascular invasion in specimens obtained after surgical treatment of hepatocellular carcinoma. *J Gastroenterol Hepatol*, 33(2), 347-354. doi:10.1111/jgh.13843
- Zhou, J., Yu, Y., Pei, Y., Cao, C., Ding, C., Wang, D., . . . Niu, G. (2017). A potential prognostic biomarker SPC24 promotes tumorigenesis and metastasis in lung cancer. *Oncotarget*, 8(39), 65469-65480. doi:10.18632/oncotarget.18971
- Zhu, P., Jin, J., Liao, Y., Li, J., Yu, X. Z., Liao, W., & He, S. (2015). A novel prognostic biomarker SPC24 up-regulated in hepatocellular carcinoma. *Oncotarget*, 6(38), 41383-41397. doi:10.18632/oncotarget.5510

Modeling and Allometric Analysis of two Butterfly Species of the Genus *Colotis*

Ali Elkarmi^{1,*} and Lina Shaheen²

¹ Biology and Biotechnology Department, Faculty of Science, Hashemite University, Zarqa, Jordan; ² Physical and Life Sciences Department, King's Academy, Madaba-Manja, Jordan

Received: September 13, 2021; Revised: November 13, 2021; Accepted: December 28, 2021

Abstract

A sample (282) of two butterfly species Colotis phisadia (144) and Colotis chrysonome (138) was collected and allometric analysis in addition to growth models were used to analyze the morphology and growth of these two species. The objective of this study is to find out if it is feasible to use allometry and growth models as tools to differentiate between these two species. Butterflies were randomly collected and measured for maximum body length, body width, wing length, wing width and head diameter. Two growth models were used: the Von Bertalanffy growth model and Gompertz. The results indicate that the two butterfly species have different allometric parameters indicating significant differences in morphology and the feasibility of using allometry for this purpose while the growth models showed large similarities in the growth of these two species.

Keywords: Modeling, Allometry, Growth Models, Colotis Spp.,

1. Introduction

Colotis phisadiaphisadia (GODART 1819) belongs to family Pieridae sub-family Pieridae (Katbeh-Bader et al., 2004); it is common in Jordan and in tropical Africa and Arabia but limited to the Dead Sea area in Jordan. It is characterized by an intermediate size, white, yellow or orange wing ground color with black or greenish markings. Colotis chrysonome (KLUG 1829) belongs to family Pieridae sub-family Pieridae (Katbeh-Bader et al., 2004), an Afrotropical species and known as the Golden Arab. Tropical oases in southern part of the Dead Sea are typical localities for this butterfly (Larsen and Nakamura, 1983). Maeruacrassifouaas is a food source (Katbeh-Bader et al., 2004), and fluctuation in the number of this butterfly is dependent on this food source (Walker and Bittaway, 1987). The legs are equally developed (Korshunov and Gorbunov, 1995), and the larvae are Green in color, with markings and stripes.

Palmer et al. (2019) conducted a study of the scaling and allometry of butterfly wing patterns. Their results indicated that the color patterns showed that the positions and size of the pattern elements scaled isometrically with wing size. Mirth et al. (2016) carried out a study on the allometry and size control to analyze the evolution of morphological scaling relationships. They indicated that allometric studies and population genetics provide a mechanism for the understanding of evolution and allometry. Wolfe et al. (2010) showed that limb evolution in butterfly members of the families Nymphalidae and Riodinidae are likely evolved reduced forelimbs in parallel. Kunte (2007) analyzed the allometry of proboscis

lengths using Costa Rican butterflies. He stated that a strong positive relationship exists between proboscis length in relation to body size and handling time per flower on nectar plants. Garcia-Barros(2006) showed that the evidence for intra-specific allometry between the traits investigated and egg weight varied among the species, indicating that the slope of such relationship may be a specific feature. Steppan (2000) calculates the allometric relationships of dried forewings of ten butterfly species to the butterflies' gross morphological parameters. He concluded that the distal regions of the wings are stiffer against forces applied to the ventral side. Akand et al. (2017) examined the morphometric variations in the species of two sub-families of butterflies of the family Lycaenid. They stated that there were differences between the two subfamilies and can be used as good indicators to identify the species more correctly. Bai et al. (2015) carried out a geometric morphometric study of the wing shapes of the butterfly Pierisrapae. They concluded that there are significant differences in the forewings and hindwings of the butterfly.

The purpose of this study which is the first in Jordan is to examine the feasibility of using growth models and allometric parameters to differentiate between two butterfly species and to examine the differences in the growth and allometry of two species belonging to the same genus.

2. Method

2.1. Study area and species

The two species are found in the area of the Dead Sea, Wadi Arabah and sometimes Aqaba (Katbeh-Bader et al.,

^{*} Corresponding author.e-mail: karmi@hu.edu.jo.

2004), and the male is characterized by a pale salmon-pink ground color on the upper side of the forewing. Its base is spotted with bluish-grey scales that extend outwards and are merged with a black patch that occupies the apex of the cell (Borroret al., 1981). Its hindwing is white with a base dotted with bluish-grey. The female is very variable, but resembles the male in markings (Borroret al., 1981).

2.2. Collection and analyses

A total of (282) butterflies (Colotis phisadia (144) and Colotis chrysonome(138) were collected and the maximum body length (BL), body width (BW), wing length (WL), wing width (WW) and head diameter (HD) were measured using a digital caliper accurate to $10~\mu m$ (E-Base, MC 02050282-I, China). The following figure shows the locations of the above measurements.

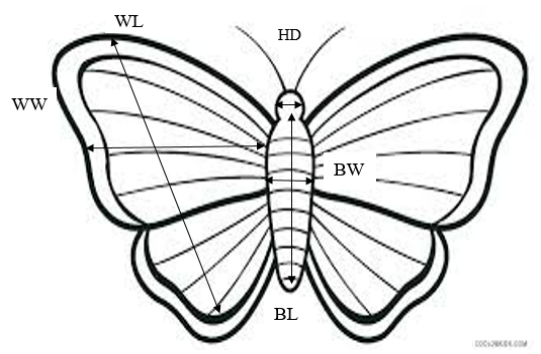


Figure 1. Locations of the measurements carried out on the butterfly

Allometric analyses was carried out using nonlinear regression analysis of the parameters BL and BW; WL and WW; BL and HD; BW and HD; BL and WL; BW and WW. All measured parameters were analyzed using the equation:

$$Y = A*X^b$$

Where b is the allometric coefficient and A reflects the ratio of \mathbf{Y}/\mathbf{X}

All calculations were carried out using STATISTICA software for windows (StatSoft, USA).

Utilizing body length as a measure of growth the Von Bertalanffy's growth model:

$$BL(t) = L_{max}(1 - A * e^{(-kt)})$$

and the Gompertz growth model:

$$BL(t) = L_{max}e^{(-A * e(-kt))}$$

were used, where BL is the body length, L_{max} is the theoretical maximum body length, A is a constant that indicates the ratio between the maximum body length and minimum body length, and k is the growth coefficient. The variables L_{max} , A and K were calculated using the Quasi-Newton method for nonlinear estimates (Ostle and Mensing, 1975) and STATISTICA software for windows version 10 (StatSoft, USA).

3. Results

There are significant differences between the allometric results of *Colotis phisadia* from *Colotis chrysonome*. The allometric results between body length and body width of *Colotis phisadia* showed that the constants A=17.1335 and

b= 0.4779 while those of *Colitis chrysono*me were A=6.0028 and b=0.8684. Moreover, the results between body length and head diameter of *Colotis phisadia* were A=17.1583 and b=0.5811 while those for *Colotis chrysonome* were A=5.6481 and b=1.0333. Table (1) shows the results of all the allometric analyses between all parameters. Furthermore, the results indicated that there is no allometric relationship between body width and wing length; and body width and wing width of *Colotis phisadia* while there was a clear allometric relationship between these parameters for *Colotis chrysonome* (table 1).

Figures (2-7) show the results (in mm) between body length and body width, wing length and length width; and body length and head diameter of both butterfly species.

There is almost always a difference in the results of the allometric measurements between both species, and in some cases the allometric coefficient (b) is less than one in the case of *Colotis phisadia* and slightly more than one in the case of *Colotis chrysonome*.

The results of the growth models although show slight differences between both species as in the growth coefficient k calculated by the Von Bertalanffy's model (k=0.1463 for Colotis phisadia and k=0.0933 for Colotis chrysonome) and by Gompertz model (k=0.1879 for Colotis phisadia and k=0.1109 for Colotis chrysonome) (table 2); these slight differences indicate that the growth of both species is similar but not identical. The other parameters shown in table (2) are for the theoretical maximum length of the butterfly and the relationship between the minimum and maximum length (constant A).

Table 1. Allometric results of *Colotis phisadia* and *Colotis chrysonome*

	Colotis phisadia	Colotis chrysonome
Body Length-Body	A=17.1336	A=6.0028
Width	b=0478	b=0.8684
Wing Length-Wing	A=1.0481	A=0.6498
Width	b=0.9239	b=0.9872
Body Length-Wing	A=0.3273	A=0.4050
Width	b=1.2461	b=1.2049
Body Length-Wing	A=0.3333	A=0.7457
Length	b=1.3227	b=1.1898
Body Width-Wing	A=0.0006	A=0.1909
Length	b=2.5138	b=1.0972
Body Width-Wing	A=0.0001	A=0.10633
Width	b=2.4835	b=1.1181
Body Length-Head	A=17.1583	A=5.6482
Diameter	b=0.5811	b=1.0333
Wing Length-Head	A=19.7542	A=5.8906
Diameter	b=0.4283	b=0.8086

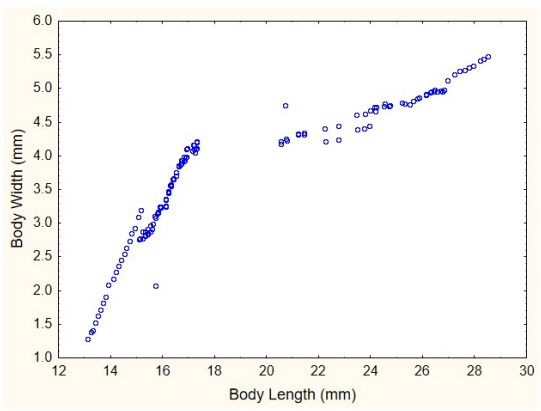


Figure 2: Measurements of body length and width of *Colotis phisadia*

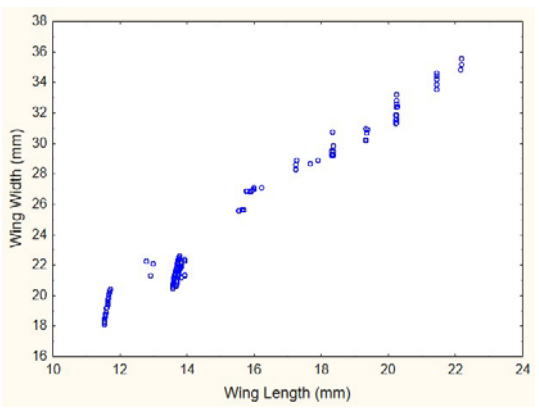


Figure 3: Measurements of wing length and width of *Colotis phisadia*

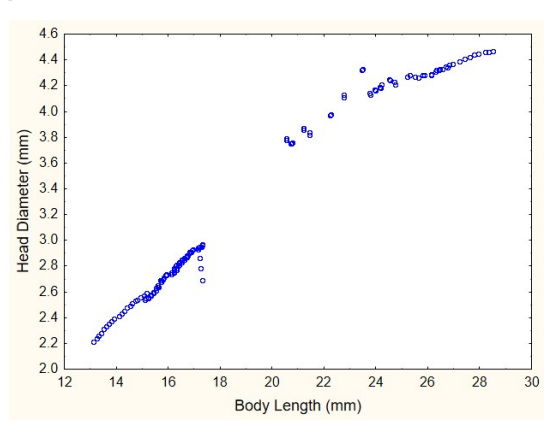


Figure 4: Measurements of body length and head diameter of *Colotis phisadia*

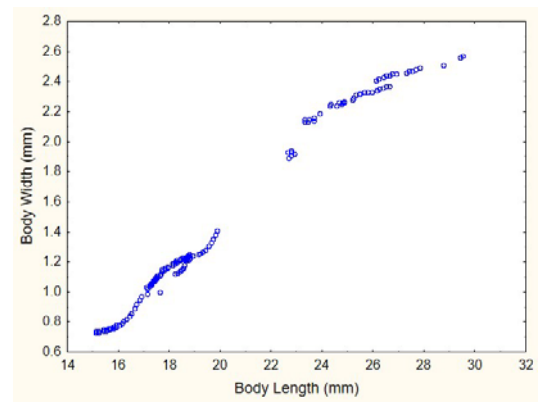


Figure 5: Measurements of body length and width of *Colotis chrysonome*

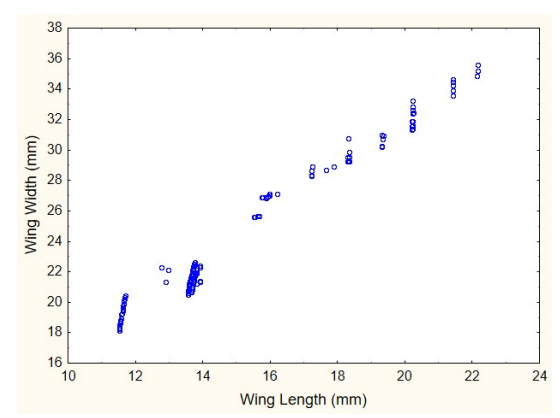


Figure 6: Measurements of wing length and width of *Colotis chrysonome*

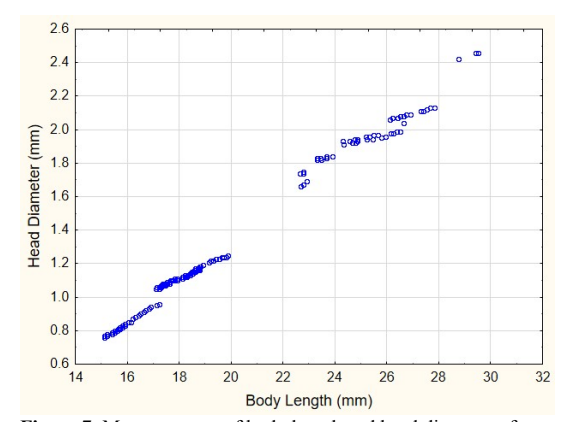


Figure 7: Measurements of body length and head diameter of *Colotis chrysonome*

Table 2. Results of the Von Bertalanffy's and Gompertz models

	Colotis phisadia	Colotis chrysonome
Von Bertalanffy's		
L_{max}	29.5	30.1
A	0.6047	0.5478
k	0.1463	0.0933
Gompertz		
L_{max}	29.3	30.3
A	0.8711	0.7601
k	0.1879	0.1109

4. Discussion

There are clear differences in the allometry of the two species of the butterflies. This can be attributed to differences in the genetic material of both species. These differences were enough to result in different allometric coefficients. Benitez et al. (2013) conducted an allometric research and concluded that the differences in sexual dimorphism of wing shape may be influenced by natural selection demonstrating the occurrence of two clearly different genetic materials. Ramirez-Ponce et al. (2017) showed that allometry can be explained within a framework of natural or sexual selection. Akandet al. (2017) results confirm the findings of this research. They showed that it is possible to differentiate between species since significant differences in forewing length, hind wing length, body length and antenna lengthMorphometry existed in the species of the subfamilies Polyommatinae and Theclinae. The results of Chazotet al. (2015) showed that microhabitat has determined wing shape evolution, and a common selective force connects sexual dimorphism of forewing shape and color pattern. According to Owen (2012), morphometric analysis can be useful for species identification and classification. He stated that astrongmethod is to combine morphometric genetic methods, especially to in the areas of systematic and

Kunte (2007) examined proboscis length in butterflies using allometric approach showing a strong positive relationship between relative proboscis length and handling time per flower. Elkarmi and Ismail (2007) stated that allometry can be used to differentiate between two populations of the same species of *Melanoides tuberculata* living in hot and in cold waters.

The two models used showed similar but not identical results indicating that there are similarities in the growth patterns of the two butterfly species even though the morphology and allometric parameters differ. This can be explained by the closeness of the genetic material between the two species.

The limited number of studies using growth models to examine the difference between two species makes it difficult to assess our results. From these few studies, Tschinkelet al., (2003) concluded that growth models can be used to study the changes in body size and shape occurring during the course of evolution. Palmer (1983) research indicated that models can be used to study the relationship between body growth and predator size, prey size and prey species. Elkarmi and Ismail (2006a, 2006b and 2007) used Bertalanffy's and Richards' growth models to study the growth of the gastropods and limpets.

In conclusion, our results indicated that allometric analyses proved to be a useful tool to study the morphology of two species belonging to the same genus. Models of growth, however, can be used to show the closeness of the species in the growth patterns not the differences between them. Both methods are useful in the areas of environmental and taxonomy studies.

References

Akand, S., Bashar, M., Rahman, S., and Khan, H. 2017. Morphometric variations in the species of two subfamilies of Lycaenid butterflies (Lepidoptera: Lycaenidae) of Bangladish. *J. Biodivers. Conser. Bioresour. Manag.*, **3(1)**: 9-15.

Bai, W., Ma, L., Xu, S., and Wang, G. 2015. A geometric morphometric study of the wing shapes of *Pieris rapae* (Lepidoptera: Pieridae) from the Qinling Mountains and adjacent regions: An environmental and distance-based consideration. *Fla. Entomol.*, **98(1)**: 162.

Benitez, H., Brani, R., Parra, L., Sanzana, M., and Sepulveda-Zuniga, E. 2013. Allometric and non- allometric patterns in sexual dimorphisim discrimination of wing shape in *Ophionintricatus*: Might two male morphotypes coexist? *J. Insect Sci.*, 13(143): 1-10.

Borrer, D., De Long, D. and Triplehorn, C.1981. *An Introduction to the Study of Insects*. Sanders College Publishing, Philadelphia.

Chazot, N., Panara, S., Zilberman, N., Blandin, P., Le Poul, Y., Cornette, R., Elias, M., and Debat, V. 2015. Morpho morphometrics: Shared ancestry and selection drive the evolution of wing size and shape in Morpho butterflies. *Evol.; Int. J. Org. Evol.*, DOI: 10.1111/evo. 12842.

Elkarmi, A. and Ismail, S. 2006a. Allometry of the Gastropod *Melanopsispraemorsa* (Thiaridae: Prosobranchia) From Azraq Oasis, Jordan. *Pak. J. Biol. Sci.*, **9(7)**: 1359-1363.

Elkarmi, A. and Ismail, S. 2006b. Population structure and shell morphometrics of the gastropod *Theoduxusmacri* (Neritidae:Prosobranchia) from Azraq Oasis, *Jordan. Pak. J. Biol. Sci.*, **9 (3):** 549-552.

Elkarmi, A. and Ismail, S. 2007. Growth models and shell morphometrics of two populations of *Melanoides tuberculate* (Thiaridae) living in hot springs and freshwater pools. *J. Limnol.*, **66(2)**: 90-96.

Garcia-Barros, E. 2006. Within and between species scaling in the weight, water, carbon and nitrogen contents of eggs and neonate larvae of twelve satyrine butterflies (Lepideoptera: Nymphalidae). *Eur. J. Entomol.*, **103**: 559-568.

Ismail, N., and Elkarmi. A. 1999. Age, Growth and Shell Morphometrics of the limpet *Cellana Radiata*(Born, 1778) from the Gulf of Aqaba, Red Sea. *Jpn. J. Malac.* **58(2)**:61-69.

Katbeh, B., Amr, Z., Abu Baker, M., and Isma'el, S. 2003. The butterflies of Jordan. *J. Res. Lepid.*. **37**:11-26.

Korshunov, Y. and Gorbunov, P. 1995. **Butterflies of the Asian** part of Russia. *Ural University Press, Ekaterinburg*: 1-202.

Kovac, V., G. H. and Francis, M. P. 1999. Morphometry of the stone loach, *Barbatulabarbatula*: do mensural characters reflect the species' life history thresholds? *Environ. Biol. Fishes*, **56**:105-115.

Kunte, K. 2007. Allometry and functional constraints on proboscis lengths in butterflies. *Funct. Ecol.*, 21: 982- 987.

Larsen, T.and Nakamura, I. 1983. The butterflies of east Jordan. *Entomol.'s Gaz.*, **34**: 135-208.

Mirth, C., Frankino, W., and Shingleton, A. 2016. Allometry and size control: What can studies of body size regulation teach us about the evolution of morphological scaling relationships? *Curr. Opin. Insect Sci...* 13:93-98.

Ostle, B and Mensing, R. W.1975. Statistics in Research. Iowa State University Press, Iowa, USA.

Owen, R.2012. Applications of Morphometrics to the Hymenoptera, Particularly Bumble Bees (Bombus, Apidae), Christina Wahl (Ed.), **Morphometrics**, ISBN: 978-953-51-0172-7.

Palmer, R., MsKenna, K., and Nijhout, H. 2019. Morphological morals: The scaling of allometry of butterflies' wing patterns. Integrative and Comparative Biology. Symposium: Allometry, Scaling and Ontogeny of Forum, DOI: 10. 1093/icb/icz123.

Ramirez-Ponce, A., Garfias- Lozano, G., and Contreraz- Ramos, A. 2017. The nature of allometry in an exaggerated trait: The postocular flange in *Platyneutomus*weele (Insecta: Megaloptera). *PLoS ONE*, 12(2): DOI: 10. 1371.

Steppan, S. 2000. Fexural stiffness patterns of butterfly wings (Papilionoidea). *J. Res. Lepid.*, 35: 61-77.

Tschinkel, W., Alexander, S., Storz, M., and Storz, S. 2003. Allometry of workers of the fire ant, Solenopsisinvicta. *J. Insect Sci.*. **3**:2.

Walker, D.andBittaway, A. 1987. Insects of Eastern Arabia. MacMillan Publishers, London.

Wolfe, J., Oliver, J., and Monteiro, A. 2010. Evolutionary reduction of the first thoracic limb in butterflies. *J. Insect Sci.*, **11(66):** 1-9.



Evaluation of Coffee Pulp Waste from Coffee Cultivation Areas in Indonesia as Iron Booster

Roy Hendroko Setyobudi^{1,2}, Manar Fayiz Mousa Atoum³, Damat Damat^{1,*} Erkata Yandri², Yogo Adi Nugroho⁴, Mardiana Sri Susanti⁵, Satriyo Krido Wahono⁶, Wahyu Widodo¹, Lili Zalizar¹, Ahmad Wahyudi¹, Elfi Anis Saati¹, M. Maftuchah¹, Zahid Hussain⁷, Dwi Yono⁴, Soni Sisbudi Harsono⁸, Rangga Kala Mahaswa⁹, Herry Susanto², Praptiningsih Gamawati Adinurani¹⁰, Ida Ekawati¹¹, Ahmad Fauzi¹, and Susi Mindarti¹

¹University of Muhammadiyah Malang, Malang 65145, East Java Indonesia; ²Darma Persada University, Special Capital Region of Jakarta 13450, Indonesia; ³The Hashemite University, 13133 Zarqa, Jordan; ⁴IPB University, Bogor 16680, West Java, Indonesia; ⁵Aura Statistics Consultant, Malang 65141, East Java, Indonesia; ⁶Research Center for Food Technology and Processing - National Research and Innovation Agency Republic of Indonesia (PRTPP – BRIN), Special Region of Yogyakarta 55861, Indonesia; ⁷The University of Agriculture Peshawar, 25130 Khyber Pakhtunkhwa, Pakistan; ⁸University of Jember, Jember 68121, East Java, Indonesia; ⁹Universitas Gadjah Mada, Special Region of Yogyakarta 55281, Indonesia; ¹⁰Merdeka University of Madiun, Madiun 63133, East Java, Indonesia; ¹¹Wiraraja University, Sumenep 69451, East Java, Indonesia.

Received: June 2, 2022; Revised: June 30, 2022; Accepted: July 6, 2022

Abstract

The research aimed to reduce the amount of coffee pulp (CP) as a pollutant and turn it into Coffee Cherry Fluor (CCF) as a functional food. CCF is expected to serve a function as a non-heme iron source to treat anemia. Further, reusing CP should be able to boost the circulation of economy. Six CP samples from three Arabica coffee areas (highlands of Mount Batur, Mount Ijen, and Mount Arjuno) in Indonesia were compared to La Boite CCF, a commercial product made in Brazil. Variables observed were iron contents which is determined by Inductively Coupled Plasma Optical Emission Spectrometer, vitamin C contents as enhancers by Iodimetric titration, total phenol contents as inhibitors by Folin-Ciocalteu method, tannin contents by spectrophotometry method, lignin contents by Van Soest method, total plant count by ISO 4833-1, and antioxidant capacity by IC 50 in the DPPH scavenging assay. Sample disparity significance was statistically determined by ANOVA, followed by Tukey test at 95 %. Sample resemblance with La Boite CCF was tested using Principal Coordinates Analysis (PCoA) and then presented in Heat Map. Conclusively, Mengani CCF and Mengani CP Estate samples are similar to La Boite CCF regarding vitamin C and inhibitor contents. It is suggested to reduce the temperature of the artificial drying device in Mengani. Further research should cover heavy metal contents, proximate analysis, and the detail of amino acid contents as research observed variables; expanding this research *in vivo* to study non-heme Fe's bioavailability should also be conducted.

Keywords: Anemia booster, Coffee cherry flour, Economy circular, Environmentally friendly, Functional food, Herbal medicine, Waste to food, Waste management

1. Introduction

Coffee (*Coffea* L.) owns worldwide popularity – in early morning work calls, casual gatherings, or smalls meeting; it has often been a go-to drink loved by many people. As a commodity, coffee is responsible for the livelihoods of over 125 × 10⁶ people globally. According to Fairtrade Foundation, coffee is one of the most widely-traded tropical agricultural products, 80 % of which is produced by 25 × 10⁶ smallholders (Atabani *et al.*, 2019; Chala *et al.*, 2018; Gill, 2021a; Lestari *et al.*, 2022; Nurul *et al.*, 2022; Wachamo, 2017). Concurring with this opinion, several researchers have declared that coffee is the most traded commodity only second to edible oil (Blinová *et al.*, 2017; Corro *et al.*, 2014; Das and

Venkatachalapathy, 2016; Ijanu *et al.*, 2020; Padmapriya *et al.* 2013; Poole *et al.*, 2017).

In large cities throughout the globe, coffee is more of a lifestyle than just a drink, which makes the coffee business essential for corporations (Felton, 2019; Gill, 2021a and b). The rank in the world's big-five coffee companies in 2021 is (fifth) by McCafe (owned by McDonald's Corporation), (fourth) by Costa Coffee (owned by The Coca-Cola Company), (third) by Tim Hortons (owned by Restaurant Brands International Inc.), (second) by Dunkin' Donuts (owned by Inspire Brands), and (first) by Starbucks Corporation (Gill, 2021b). The facts have proven that coffee positively influences the economy (Gil 2021a; Shumeta and D'Haese, 2018) and social (Felton, 2019; Viartasiwi and Trihartono, 2020) globally. Further benefits of drinking coffee for dental health (Dewanti *et al.*, 2020; Purwanto *et al.*, 2020) and physical health

(Bizzo et al., 2015; DeMelo Pereira et al., 2020; Susilowati et al., 2020; Wachamo et al., 2017) are also indicated.

Ironically, the concerns about poor waste management in local coffee producers is also a focus given by many researchers (Corro et al., 2014; Das and Venkatachalapathy, 2016; Genanaw et al. 2021; Geremu et al., 2016; Novita, 2012, 2016). Coffee Pulp (CP) and Coffee Husk (CH) contain toxic substances, e.g., caffeine, alkaloids, tannins and polyphenolics (Chala et al., 2018; Dzung et al., 2013; Ijanu et al., 2020; Padmapriya et al., 2013) that shall bring negative impact towards the environment (Beyene et al., 2012; Carmen et al., 2020; Genanaw et al., 2021; Dzung et al., 2013; Lestari et al., 2022; Novita, 2012).

To illustrate the wet coffee processing, the amount of 1 t green bean, 2 t CP, 22 730 L liquid waste containing 80 kg Biological Oxygen Demand (BOD), and 0.28 t silver skin waste are made out of 5.5 t coffee cherry (Novia, 2012). In those local production sites, solid CP and CH are simply piled up at roadsides and riverbanks, while liquid Waste goes down the drains directly heading to rivers (Novia 2012; Novia et al. 2021; Setyobudi et al., 2019, 2021a) – such treatments in handling so much pollutant are dire threats for soil and water bodies.

As a part of solving the problems above, several experts (Chala et al., 2018; Novita, 2012, 2016; Novita et al., 2021; Padmapriva et al., 2013, 2015; Setvobudi et al., 2021a, 2021b, Syarif et al. 2012) recommended biogas digester to process liquid coffee waste before discharge. Employing a biogas digester should result in double benefits: a renewable energy source for coffee production (i.e., drying, lighting, power) and organic solid and liquid fertilizers for coffee cultivation (Abdullah et al., 2020; Novia et al., 2021; Setyobudi et al. 2021a, 2021b; Susanto et al., 2020). Various types of the digester are advised by certain experts: Mulato and Suharyanto (2010) utilized a floating drum in Indonesia; Centro Nacional de Investigación del Café (CENICAFE) developed a Modular Anaerobic Treatment System (MATS) for coffee farms in the Colombian mountains (Bermeo-Andrade et al., 2020); Hernández-Sarabia et al. (2021) proposed tubular, or bag biodigester (Taiwan type - PVC 1005 geomembrane) in Colombia; Bombardiere (2006) reported the use of thermophilic Continuous Stirred Tank Reactor (CSTR) in Mexico. Rattan et al. (2015) suggest Upflow Anaerobic Hybrid Reactor-continuous (UAHR) and intermittent aeration system. Expressly, some researchers agreed to choose Upflow Anaerobic Sludge Blanket (UASB) digester type (Ijanu et al., 2019; Sengupta et al., 2020); Bruno and Oliveira (2008) even emphasized how twostage digester had better performance compared to the onestage. On the other hand, Adinurani et al. (2015), and Hendroko et al. (2013) were also on the side of two-stage, considering the acidic characteristic of liquid coffee waste (Genanaw et al. 2021; Novita, 2012, 2016; Rattan et al. 2015).

With simple technology, another way out is turning CP and CH into coffee cherry tea or cascara (from Spanish "cáscara," meaning husk or skin and pulp of a coffee cherry). There is nothing new about this since traditional beverages from coffee cherries have been consumed in Yemen (called Qishr), Ethiopia (Hashana), Bolivia (Sultana), and Costa Rica (Cáscara) (Ota, 2018). Studies

on cascara have also been conducted (Ariva et al., 2018; Arpi et al., 2018; Heeger et al., 2017; Muzaifa et al., 2021; Nafisah and Widyaningsih, 2018; Novita et al. 2021; Pua et al., 2021; Zeckel et al. 2020). However, Setyobudi et al. (2019 and 2021a) concluded its inefficiency in solving the problem since CP and CH solid waste remained after being steeped in hot water.

Andrew Fedak and Dan Belliveau proposed to turn CP and CH into Coffee Cherry Flour (CCF) (Cheatham, 2019; WIPO-PCT, 2014). Damat et al. (2019), Elba et al. (2017), Mindarti et al. (2020), Moreno et al., 2019, and Rosas-Sánchez et al. (2021) have discussed CCF's positive impacts on its fibre content, while Setyobudi et al. (2019 and 2021a) advised CCF to be an iron (Fe) source. The latter, after reviewing a considerable amount of data, discovered that CP and CH contained Fe between (4.3 to 50) mg 100 g⁻¹ (Anna et al., 2019; Avinash et al., 2017; Elias, 1979; Hermosa et al., 2014; Iriondo-DeHond et al. 2020; Kayhanian and Tchobanoglous, 2016; Marín-Tello et al., 2020, Setyobudi et al., 2018, 2019, 2021a; Wich, 2015; Zupancic and Grile, 2012). Setyobudi et al. (2019) have also summed up that the Fe contents in CP and CH are higher than in sweet leaf or star gooseberry [Sauropus androgynus L. (Merr)], leaf of cassava or manioc [Manihot esculenta (Crantz)], leaf of papaya or papaw (Carica papaya L.), Indian mustard or vegetable mustard (Brassica juncea L.), tomato (Solanum lycopersicum L.), and wild carrot [Daucus carota subsp. Sativus (Hoffm.) Schubl. & G. Martens.]; they are even higher than in Indonesia's currently most-studied haemoglobin boosters: drumstick tree (Moringa oleifera L.) of (5.57 to 6.28) mg 100 g⁻¹, date-palm (Phoenix dactylifera L.) of (4.06 to 7.06) mg 100 g⁻¹, and spinach (Spinacia oleracea L.) of (2.7 mg to 3.9 mg) 100 g⁻¹ (DKBM Indonesia, 2017; Hamzah and Jusuf, 2019; Rania et al., 2014; USDA, 2018).

Setyobudi *et al.* (2021a) determined that the CCF of arabica coffee in Kintamani, Bali, Indonesia, met the requirement better than Brazilian commercial products despite its relatively lower Fe content, presumably due to the Inceptisol soil (Asfimanto *et al.*, 2013; Nurul *et al.*, 2022) that contains low Fe (Nandini and Narendra, 2012).

Following up Setyobudi *et al.* (2021a), CP potentials as Fe-source CCF in three coffee areas in Indonesia, were examined in this research, aimed to (i) minimize CP and CH pollutant potentials, (ii) encourage prosperity for coffee farmers and producers, and (iii) provide Fe nonheme source for haemoglobin booster due to the relatively high chance of anemia (Milman, 2011; Muhammadong *et al.* 2021; Nurbadriyah, 2019), especially in Indonesia (Bukhari *et al.*, 2020; Ellie *et al.*, 2012; Nurbadriyah, 2019; Yuniastuti, 2014).

2. Materials and Methods

2.1. Sample collection

Three dried coffee CP samples were obtained from three indigenous *Coffea arabica* L. areas in Indonesia: Ijen Farm at the side of Mount Ijen, Bondowoso, East Java (7°57'59.55 "S 114°01'14.37 "E), Karangploso Farm downhill Mount Arjuno, Malang, East Java (7°52'13.80" S 112°34'54.44" E), and Mengani Farm at the slope of Mount Batur, Mengani, Bali (8° 17' 16.63" S 115° 15'

0.61" E). Varied enormously in particle sizes (Figure 1), all the samples were collected within February and July 2018, then dried and homogeneously ground and sieved before analysis. The CCF commercial product serving as a comparator had been made in Brazil, acquired from La Boite, a store in Manhattan, 724 11th Avenue, New York, NY 10019, in May 2018.



Figure 1. The appearance of dried coffee pulps (A), Four coffee cherry flour produced from Mengani (B), Karang Ploso (C), Ijen (D), and the La Boitê commercial product (E).

2.2. Observed Variables and Statistical Analysis

Sample materials are organized as follows: (i) Ijen CP, (ii) Karangploso CP, (iii) La Boite CCF, (iv) Mengani CCF, (v), Mengani CP-Est., (vi) Mengani CP-SP, (vii) Mengani CP-Hay.

Notes:

- CP = coffee pulp
- CCF = coffee cherry flour
- Mengani CP-Est. refers to CP collected from the industrial-scale coffee processor owned by the Arabica Coffee Factory Estate of Mengani.
- Mengani CP-SP refers to CP collected from small-scale processors owned by farmers in Mengani.
- Mengani CP-Hay refers to CP collected from the storage room of the Arabica Coffee Factory Estate of Mengani, packed in plastic bags, and stored at room temperature for 15 mo.

Setyobudi *et al.* (2021a) have listed the Fe non-heme booster agents in CCF-covering vitamin (Vit.) C, Vit. A, amino acid, dan reducing sugars. The observed variables in this study were the amounts of Fe and enhancer agent (Vit. C), inhibitors agents (total phenol, tannin, and lignin), of 2,2-diphenyl-1-picrylhydrazyl (DPPH) scavenging assay, and of total plate count (TPC). Using GLM-ANOVA to diverge the samples' statistical significance and employing Tukey test at 95 % scale, the data were presented in box plot and vertical bar chart (Adinurani, 2016; Mishra and Homa. 2019).

Two analysis steps were conducted to determine the samples' similarity to the comparator (La Boite's CCF). Firstly, the seven observed variables were summed up through Principal Coordinates Analysis (PCoA) – also known as Multidimensional Scaling (MDS) – using Dissimilarity Analysis and Representation for Windows (DARwin) 6.0.010 software (Nasibeh 2019; Perrier *et al.*, 2003; Perrier and Jacquemoud-Collet, 2006). Then the Neighbor-Joining and Hierarchical Clustering results were laid out in a Heat Map (DeBoer, 2015; Tomanek and Schröder, 2018; Zhao *et al.*, 2014) by activating the feature Style > Conditional Formatting > Color Scales on Microsoft Excel 2010. The vector values were established

from 2 (the highest score, light yellow) to -2 (the lowest score, dark red).

2.3. Analysis of Fe

To analyze the Fe content, an Inductively Coupled Plasma Optical Emission Spectrometer (ICP-OES) Varian-730-ES by Varian Inc. under Agilent Technologies (Palo Alto, USA) was exercised. A total of 5 g CCF per sample was treated with dry-ashing procedures involving hydrochloric acid dilution to extract the minerals then studied in duplicates and replicated at least twice (Xianden et *al.*, 2016).

2.4. Analysis of Vitamin C

The Iodimetric method (AOAC, 1995) was used in Vit. C content analysis. A total of 5 g CCF per sample was diluted in a 100 mL marked flask. The dilutions were then filtered, and 25 mL of each was then mixed with a few drops of starch and quickly titrated with 0.01N sodium thiosulfate to blue color. Vit. C content was calculated on Equation (1):

Note: V 12 = Iodium volume (mL), NFp = Dilution factor, W s = Sample weight (g)

2.5. Analysis of Total Phenol

Following the procedures detailed in Almey et al. (2010), a total of 5 g CCF per sample was extracted with 5 mL of 85 % methanol in a test tube, centrifuged/vortex mixed in 3 000 rpm (1 rpm = 1/60 Hz) for 15 min and filtered. Each filtrate was then diluted to 5 mL, 0.4 mL of which was added to 0.4 mL of Folin-Clocaften reagent in a test tube, vortex mixed, and rested for 6 min. Next, 4.2 mL of 5 % sodium carbonate solution (Na₂CO₃) was added to each before vortex mixed and incubated at room temperature for 90 min. Absorbance was computed on $\lambda max = 760$ nm using Merck Perkin Elmer Lambda 25 UV-V Spectrophotometer. Standard curve construction followed by diluting gallic acid in 85 % methanol of various concentrations ranging between (0 to 100) mg L⁻¹. Total phenol content was calculated on the linear regression equation of gallic acid as in Equation (2):

$$y = ax + b \tag{2}$$

2.6. Analysis of Tannin

A total of 0.25 g CCF per sample was diluted in 20 mL of boiling aqua dest and filtered after a few minutes. Each filtrate was then diluted to 50 mL, 1 mL of which was added to 2 mL of 0.02 M FeCl₃ in 0.02 M HCl solution and 2 mL of 0.0015 M K₃[Fe(CN)₆] in a 25 mL flask, then further diluted to its maximum limit. A blank solution was employed to check the absorbance, recorded on λ max = 744.6 nm using Hitachi U 2010 Spectrophotometer UV-V (Arapitsas, 2012).

2.7. Analysis of Lignin

Finding (1 g) the Acid Detergent Fiber (ADF) and the Neutral Detergent Fiber (PDF) rates of the samples is essential in estimating the lignin contents. Next, each sintered glass containing ADF was put on a petri dish, soaked in 20 mL of 72 % H₂SO₄ (stir for thorough coverage), and let sit for 2 h. After being heated in an oven of 1 000 °C for 8 h and rested overnight, every sample was laid in an exicator for 30 men and then weighed (a g)

before reheating up to 5 000 °C for 2 h. Once cooled, it returned to the exicator for 30 min and then weighed (b g). Total lignin content was evaluated based on Equation (3) (Van Soest *et al.*, 1991):

Lignin Content =
$$\underline{a - b} \times 100 \%$$
 (3)
Sample weighed (1 g)

2.8. Analysis of Antioxidants

A total of 200 mg CCF per sample was suspended in 20 mL of 80 % (V V^{-1}) methanol and homogenized for 30 s, an amount of 1 mL of which was then mixed with 0.4 mL of hexane before homogenized for another 30 s. After centrifuging at 3 000 g for 10 min at 25 °C, the supernatant was discharged from the tube, followed by washing with hexane twice. The methanol extract was then filtered with 0.45 m millipore mesh before being used for the DPPH (2,2- diphenyl-1-picrylhydrazyl) scavenging assay.

Antioxidant activity was measured by obtaining the IC 50 (50 % inhibitory concentration) in the DPPH scavenging assay. The sample extract was dissolved to produce solutions with concentrations between 100 mg L^{-1} to 1 300 mg L^{-1} . A volume of 50 μL of 0.15 mM DPPH was mixed with 30 μL of the sample, then incubated in darkness for 30 min before the absorbance was measured using a spectrophotometer at a wavelength of 517 nm. As a control, 4.9 mL of DPPH solution was mixed with 0.1 mL of methanol, and the absorbance was measured at the same wavelength. Inhibition percentage was calculated based on Equation (4) (Xie and Schaich, 2014):

% inhibitation =
$$\frac{Control\ absorbance - Sample\ absorbance}{Control\ absorbance} \times 100\ \%$$

2.9. Analysis of Total Plate Count (TPC)

A total of 25 g CCF per sample was added to 225 mL of Butterfield's Phosphate Buffered solution and homogenized for 2 min, an amount of 1 mL was mixed in 9 mL of distilled water to obtain dilutions 10^{-2} , 10^{-3} , and 10^{-4} sequentially. Next, 1 mL of each suspension was inoculated to a petri dish containing liquid agar and incubated at 37 °C for 2 d. TPC was noted using Colony Counter (ISO, 2013; Yunita *et al.*, 2015).

3. Result and Discussion

3.1. Iron (Fe) Content.

Iron (Fe) is only a particularly essential micronutrient in red blood cells forming during the haemoglobin synthesis process (Achmad, 2000; Elstrott *et al.*, 2020; Ogawa *et al.*, 2020); Fe is only obtainable externally from food or supplement. Found in all types of bodily cells, this substance also plays a vital role in various biochemical reactions. Fe is also found in enzymes involved in electron distribution (cytochrome), oxygen activation, and oxygen distribution (haemoglobin and cytochrome) (Musallam and Taher, 2018; Seriki *et al.*, 2017). Further, Fe is required in forming lymphocyte cells to build immunity, while transferrin and lactoferrin – proteins that absorb and deliver iron throughout the body – also work to prevent infection (Kell *et al.*, 2020; Winarsi, 2007).

The non-heme Fe contents in CCF and CP from three coffee cultivation areas compared to one in La Boite CCF are presented in Figure 2.

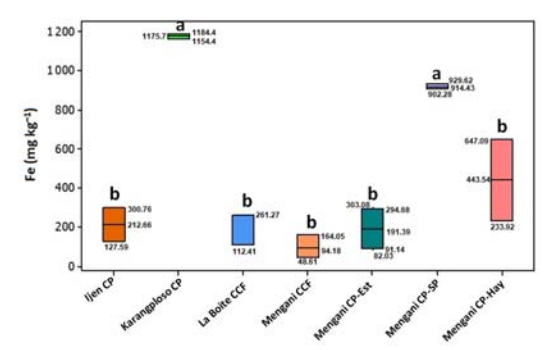


Figure 2. Box-plot of Fe contents in samples from three coffee cultivation areas.

Tukey test sorted the seven samples into two groups: (i) Karangploso CP and Mengani CP-SP, while (ii) Ijen CP, La Boite CCF, Mengani CCF, Mengani CP-Est, and Mengani CP-Hay. Relevant to the purpose of finding the highest Fe content was group (i), considering human body absorption towards non-heme Fe is relatively low – between 5 % and 10 % – compared to heme Fe which goes between 10 % and 30 % (Jumadi 2020; Nurbadriyah, 2019; Setyobudi *et al.*, 2019, 2021a; Yuniastuti, 2014).

However, the authors were uncertain about the validity of Fe contents in group (i), i.e. [(91.43 to 117.47) mg 100 kg⁻¹]. Setyobudi et al. (2019, 2021a) reviewed 12 references to find out that the highest Fe content in CP and CH should only be 50 mg 100 kg-1 (Kayhanian et al., 2016). The two samples in the group (i) were presumably contaminated by iron and rust flakes from worn-out mini pulper equipment in small-scale coffee processors. Such Fe contaminants may be formed since small-scale coffee processors typically use little water in the wet process. Hendarto (personal communication, 2020), and Sariadi (2012) admitted that the water used was of (7 to 9) m³ t⁻¹ cherry. Assari (2021, personal communication) even verified that Kopilos, a small coffee processor in Karangploso, unused water in the pulping process. The facts defy Yahmadi (1972) information that the traditional wet process should involve water of (16 to 18) m³ t⁻¹ cherry, and the Ministry of Agriculture of Indonesia – Menteri Pertanian (2012) data that one required (10 to 30) m³ t⁻¹ cherry, and Dadi et al., (2018) finding of (15 to 20) m³ t⁻¹ cherry. Arabica Coffee Factory Estate of Mengani used water of (16 to 25) m³ t⁻¹ cherry in its pulping process (Hendarto, 2020, personal communication).

The water utilization in the wet process pollutes rivers and soils (Campos *et al.*, 2021; Ijanu *et al.*, 2020; Novita, 2012, 2016). Novia (2012, 2016) and Syarif *et al.* (2012) recommended wet-process technology based on clean production by reducing the amount of water up to 3 m³ t⁻¹ cherry to cut the pollution down, resulting in the increase of environmentally disadvantageous BOD and COD formed in liquid waste. This situation requires appropriate technology to reduce the amount of BOD and COD without additional water which is applicable to small-scale coffee processors (Campos *et al.*, 2021; Fereja *et al.*, 2020; Gururaj *et al.* 2021; Ijamu *et al.* 2000).

As for Fe pollutant, it must be cut off due to the harms. Fe content of higher than 20 mg 100 kg⁻¹ can cause stomachache, constipation, nausea, vomiting, and loss of consciousness towards the human. Too much iron can trigger hemochromatosis (Jumadi 2020, Naruki *et*

al. 2010). Disorders like hemosiderosis or hemochromatosis are due to progressive iron deposition in the liver, pancreas, and joints (Arora and Kapoor, 2012; Naruki et al., 2010; Yuniastuti, 2014). Fenton reaction – where an electron of Ferro ion is transferred to HOOH molecule to create ferri ion and hydroxyl radical destructive towards cell protein (Naruki et al., 2010; Yuniastuti, 2014) – is next in the chain.

Figure 2 demonstrates how Fe contents in La Boite CCF and Mengani CCF are similar to those reported in Setyobudi et al. (2021a). Mengani CCF has the lowest Fe content of all samples for two probable reasons. (i) Inceptisol soil of Mount Batur, Bali, contains low iron (Nandini and Narendra, 2012), and (ii) CP drying process in Mengani Est. employs an artificial heater at 80 °C for 15 h (Setyobudi et al., 2021a). Arista et report on how boiling and steaming significantly decreased the Fe in beetroot (Beta vulgaris L.var Rubra), as well as Syarfaini et al. (2017); Wahyani and Rahmawati (2021) results on the Fe decreased due to heating and long processing time in sweet potato (Ipomoea batatas L.) and sorghum (Sorghum bicolor (L.) - based cookies, supported the latter cause. It also shows that CP-Hay stored in plastic bags at room temperature for 18 mo contains more Fe than the other four fresh samples; this data is convenient for maintaining CCF production even during off-seasons. Another point is that precisely in Mengani, Bali, four different rates of Fe are recorded - getting a consistent amount of certain content has been one of the obstructions faced by the herbal medicine industry.

Further revealed in Figure 2 that Fe contents in the group (ii)'s CP are generally equal to the control and therefore fitting for Fe-source CCF. The Fe values of [(9.42 to 44.35) mg 100 kg⁻¹] are higher than what is contained in sweet leaf, leaf of cassava, leaf of papaya, vegetable mustard, and wild carrot (Setyobudi *et al.*, 2019) and also higher than the currently most-studied haemoglobin-booster ingredients *i.e.*, drumstick tree, datepalm, and spinach [(2.7 to 7.06) mg 100 kg⁻¹] (DKBM Indonesia, 2017; Hamzah and Jusuf, 2019; Rania *et al.*, 2014; USDA, 2018).

3.2. Vitamin C Content.

Vit. C (ascorbic acid) as an enhancer works by reducing non-heme's Ferri (Fe³⁺) into Ferro (Fe²⁺) in the small intestine to make it 2 to 4 times easier to absorb. In addition to the role mentioned above, it also helps prevent haemosiderin from forming and distributing transferrin in plasma to ferritin in the liver. Focusing on transfers, it carries iron to all body parts, including the marrow, where haemoglobin is produced (Agusmayanti *et al.*, 2020; Conner *et al.*, 2012; Jumadi, 2020; Wulandari, 2015).

Not only Vit. C, other kinds of acid -e.g., citric acid, malic acid, and tartaric acid - also have the ability to enhance iron, as reported by Yuniastuti (2014), Jumadi (2020), and Susiloningtyas (2012). CP dan CH was said to contain citric acid (Shankaranand and Lonsane 1994). Ginz *et al.* (2020) noted that sucrose and reduction sugar were the main precursors to these acids, of which contents in CP had been confirmed by Setyobudi *et al.* (2021a). The Vit. C contents in CCF and CP from three coffee plantations compared to one in La Boite CCF are detailed in Figure 3.

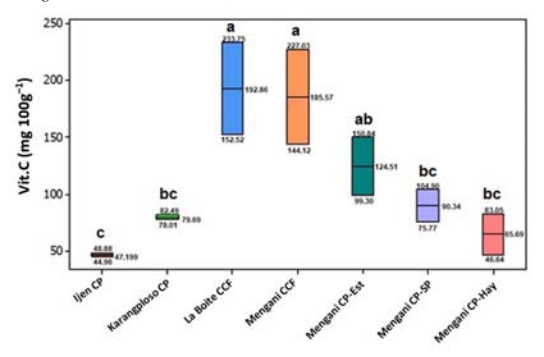


Figure 3. Box-plot of Vitamin C contents in samples from three coffee cultivations areas

Referring to the Tukey result, Vit. C content in Mengani CCF is equal to one in control, putting it in the first and second places of all samples – Mengani CP-Est is in the third, while Ijen CP is in the last. It has been elaborated in Setyobudi *et al.* (2021a) that Vit. C in Mengani CCF (and Mengani CP-Est) was lower than in La Boite CCF due to the drying method (equipment drying at 80 °C for 15 h). Some researchers on cascara (dried CP and CH for herbal drink, the basic component of CCF) suggested convection oven drying at 45 °C for 32 h (Ariva *et al.*, 2020) or sun-drying at 30 °C to 35 °C for 2 wk to 3 wk (Nafisah and Widyaningsih, 2018). Almatsier (2009) explained that Vit. C started to degrade at approximately 35 °C, yet argued by Rahmadi and Bohari (2018) that it should be 50 °C.

Although the figure puts Karangploso CP, Mengani CP-Est, and Mengani CP-Hay on equal footing, the Vit, is convincing that plastic-bagged CP-Hay stored at room temperature reduces the Vit. C content is consistent with Jumadi (2020) statement that Vit. C reduction occurred in food storing.

The high Fe contents in Karangploso CP and Mengani CP-SP (Figure 2) are diverged by their Vit. C contents (Figure 3). It is apparent that poor control over the drying process in small-scale coffee processors is the problem. Despite meeting the requirements (Alakali *et al.*, 2015; Ariva *et al.*, 2020; Nafisah and Widyaningsih, 2018; Rahmadi and Bohari, 2018; Setyobudi *et al.* 2021a) of sundrying on tropical drying floors at 22.67 °C to 37.90 °C (Jaisyurahman *et al.* 2019; Setiawan *et al.*, 2014), human resource needed to toss CP or CH every 1 h to 2 h his likely unavailable. To top it up, inconsistent sunlight related to ultraviolet and infrared exposures further oxidize Vit. C (Zhou *et al.*, 2016). Vit. C reduction was also reported in the drying process of drumstick tree leaves (Gernah and Sengev, 2011; Mbah *et al.*, 2012).

The low Vit. C content in Ijen CP (4. 72 mg 100 kg $^{-1}$) emphasizes the difficulty small-scale coffee processors face in maintaining it. At the same time, Sukartiningsih (2011) declared that the cascara of fresh before-ripe Arabica coffee in Ijen contains Vit. C of (275.7 to 651.2) mg 100 g $^{-1}$.

3.3. Total Phenol Content.

To sustain, plants perform primary as well as secondary metabolism. In addition to food, primary metabolites – such as carbohydrates, protein, fat, vitamin, and mineral – also act as precursors of the secondary metabolism for self-defense against biotic and abiotic harms in a plant's habitat (Erb and Kliebenstein, 2020;

Goyal *et al.*, 2012; Mazid *et al.* 2011; Vladimir-Knežević *et al.*, 2012). Basically, pericarp, exocarp, and mesocarp of coffee beans, CP, and CH exist to protect the beans; therefore, secondary metabolites should be found there

Esquivel and Jimenez (2012) and Martínez and Clifford (2000) confirmed it with their findings, stating four main polyphenolic compounds – flavan-3-ol, hydroxycinnamic acid, flavonoid, and anthocyanin – were identified in Arabica coffee cherry. Ramirez-Coronel *et al.*, (2004) and Ramirez-Martinez (1988) also noted the presence of phenolic compounds – chlorogenic acid (5-caffeoylquinic acid), epicatechin, is chlorogenic acid I, II, and III, catechin, rutin, and protocatechuic acid – in the coffee pulp.

Gillooly et al., (1984); Jumadi (2020); Lesjak and Srai, (2019); Susiloningtyas (2012); Wahyani and Rahmawati (2021); and Yuniastuti (2014) agreed that phenol compounds were Fe inhibitors. Although Phenol consists of three hydroxyl groups bonded to triple valence iron in chelation, which can reduce iron bioavailability (Lesjak and Srai, 2019; Wahyani and Rahmawati, 2021; Yuniastuti, 2014), phenolic compounds are known to be beneficial to treat cardiovascular diseases, colon cancer, liver disorders, and diabetes (Pandey and Rizvi, 2009). Other researchers also pointed out phenolic compounds' capacity to combat various diseases associated with oxidative stress (Arts and Hollman, 2005; Lesiak and Srai, 2019) and exhibit antioxidant, anti-inflammatory, and anticlastogenic activities (Lambert et al., 2005). More researchers (e.g., de Melo Pereira et al., 2020; de la Rosa et al., 2019; Dorsey and Jones, 2017; Geremu et al., 2016; Huang et al., 2010; Ifadah et al. 2021; Lestari et al., 2022; Vladimir-Knežević et al., 2012) encouraged the use of phenolic compounds to maintain health. The total phenol contents in CCF and CP from three coffee cultivation areas compared to one in La Boite CCF are depicted in Figure 4.

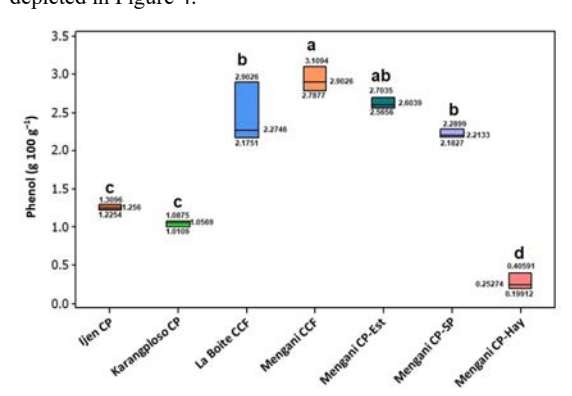


Figure 4. Box-plot of total Phenol contents in samples from three coffee cultivation areas

Tukey test sorted the seven samples into three groups: (i) Mengani CCF with the highest content, followed respectively by (ii) La Boite CCF, Mengani CP-Est, and Mengani CP-SP; Ijen CP and Karangploso CP; while (iii) Mengani CP-Hay with the lowest content. The result shows that plastic-bagged CP-Hay stored at room temperature reduces Vit. C content (see Figure 3) but also phenol compounds. The second group may be the best Fe source regarding inhibitor presence for iron absorption, but

the first group is better concerning phenol benefits. The degrading amount of total Phenol in CCF due to cooking is another point since heating triggers the enzymatic oxidation process (Shabri dan Rohdiana, 2016). Diniyah and Lee (2020) and Xu and Chang (2008) reported total phenol damage due to soaking, steaming, and boiling. Nurhayati *et al.* (2021) recorded chlorogenic acid damage after heating. Ifadah *et al.* (2021), Mulyawanti (2020) noted anthocyanin damage. All those findings are consistent with the data on temperature limit of 50 °C (Budilaksana and Andaka, 2016; Hayati *et al.* 2012; Kwartiningsih *et al.*, 2016; Sudarmi *et al.* 2015).

3.4. Tannin Content.

Several researchers (Schmidl and Labuza, 2000; Susiloningtyas, 2012; Yuniastuti, 2014) trusted Tannin as an iron absorption inhibitor. However, Arpi *et al.* (2018), Jumadi (2020), and Lesjak and Srai (2019) disregarded its importance, especially when Vit. C was there. Other researchers (Esquivel and Jimenez, 2012; Kumari and Jain, 2012; Woldesenbet *et al.*, 2015) even regarded Tannin anti-nutrient since when bounding with protein, it forms insoluble complex compounds that block the protein's digestive ability (Chung *et al.*, 1998; Suarni, 2009).

Suarni and Subagio (2013) and Suarni and Firmansyah (2007) considered Tannin a unique nutrient with both positive and negative effects. A phenolic compound, Tannin is a natural antioxidant that bounds free radicals (Suarni and Subagio, 2013; Suarni and Firmansyah, 2007; Tandon and Rai, 2007) that can act as an astringent, antidiarrhoea, anti-microbial activities (Chung et al. 1998; Hagerman, 2002; Malaggia et al. 2012), anti-carcinogen and anti-mutagen (Chung et al., 1998). It can also reduce the incidence of several human diseases such as cardiovascular diseases, colon cancer, liver disorders, and diabetes (Rasouli et al., 2017; Tandon and Rai, 2007). Another quality is exerting other physiological effects, such as accelerating blood clotting, reducing blood pressure, decreasing the serum lipid level, producing liver necrosis, and modulating immune responses (Chung et al., 1998; Tandon and Rai, 2007).

The total Tannin contents in CCF and CP from three coffee cultivation areas compared to one in La Boite CCF is presented in Figure 5.

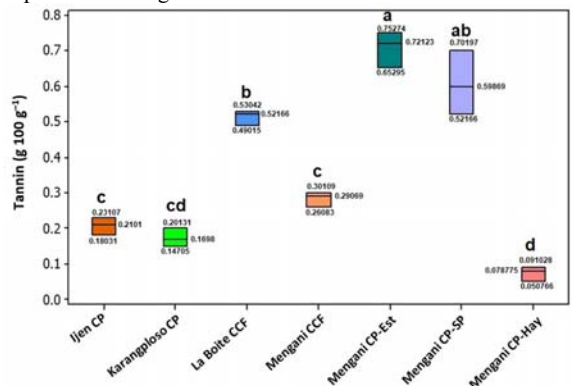


Figure 5. Box-plot of Tannin contents in samples from three coffee cultivation areas.

Tukey test sorted the seven samples into three groups: Mengani CP-Est, Mengani CP-SP, and La Boite CCF in the first; Ijen CP dan Mengani CCF were in the second; while Karangploso CP dan Mengani CP-Hay were in the third. Mengani CP-Est contains the highest Tannin, followed by Mengani CP-SP. Mengani CP-Hay is of the lowest, which matches the lowest total Phenol content in Figure 4.

The Tannin content in control is relatively the same as in Mengani CP-SP but higher than in Mengani CCF. Such discrepancy in the same farming area has been problematic in herbal medicine.

3.5. Lignin Content.

While some researchers agreed that fibre acts as a Fe inhibitor (Cook et al., 1983; Fernandez and Phillips, 1982; Gillooly et al., 1984; Jumadi, 2000; Reinhold et al., 1981; Suarni and Firmansyah, 2016; Rufaizah, 2011; Wahyani and Rahmawati 2021; Yuniastuti, 2014), but Schmidl dan Labuza (2000) deduced that its effect on iron absorption is relatively lower than tannin dan phytic acid. Monnier et al. (1980) found that pectin inhibited the absorption of inorganic iron, not cellulose. Yet, Fernandez and Phillips (1982) reported that lignin and psyllium mucilage had a pronounced capacity to bind ferrous iron in vitro, whereas cellulose and pectin were much less potent. Although support has been on lignin's side (Plalt and Clydesdale, 1987; Reinhold et al., 1981).

The total lignin contents in CCF and CP from three coffee cultivation areas compared to one in La Boite CCF is depicted in Figure 6.

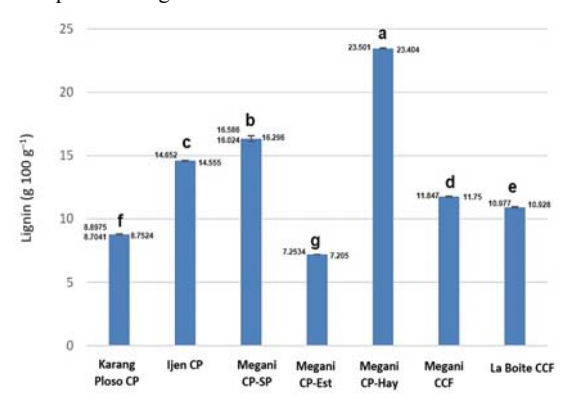


Figure 6. Bar-chart of Lignin from samples from three coffee plantations

In Figure 6, the highest lignin content is recorded by Mengani CP-Hay, whereas the lowest is by Mengani CP-Est. The control's content is in the lowest third, less than one of Mengani CCF.

Lignin may be an iron inhibitor, but Cook et al. (1983), Jumadi (2020), Kelsay et al. (1979), and Reinhold et al. (1981) said that Vit. C. (ascorbic acid) dan citric acid should be able to compensate for their weakness. It is vital since high dietary fibre intake helps diminish the chances of heart disease and obesity while lowering high blood pressure, maintaining ideal sugar content in the blood, and preventing colon cancer. Furthermore, in the case of cardiovascular conditions (coronary heart), fibre binds bile acids to reduce cholesterol in the blood (Damat et al., 2019; Elba et al. 2017; Mindarti et al. 2020; Wahyani and Rahmawati 2021). Furthermore, as insoluble dietary fibre,

lignin thickens food mass in the digestive system, and it is adequate to prevent digestive ailments such as hemorrhoids, diverticulosis, and colon cancer (Damat *et al.*, 2019; Mindarti *et al.* 2020). Astawan and Wresdiyati (2004), Dreher (2018), Fung-Jou *et al.* (1998), Harbone (1996), Huang *et al.* (2010), Kritchevsky and Bonfield (2012), Soliman (2019), Suarni and Firmansyah (2007), Veronese *et al.* (2018), and Yahia *et al.* (2019) were therefore in unison that lignin is an antioxidant compound.

3.6. Antioxidant Capacity

Three plant bioactive compounds found in CP – total Phenol, Tannin, and Lignin – have been discussed in the previous sub-sections. The antioxidant capacity of the DPPH scavenging assay outcome is revealed in Figure 7 to complement.

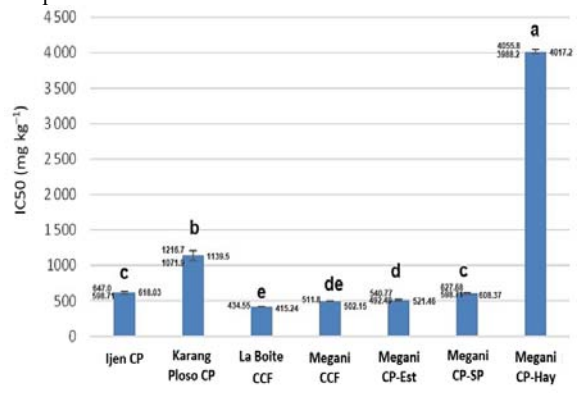


Figure 7. Bar-chart of IC-50 in samples from three coffee cultivation areas.

The figure generally sorts the seven samples into four groups. The lowest ratio, Mengani CP-Hay, is in the first. Karangploso CP is in the second. Ijen CP and Mengani CP-SP are in the third. The highest ratios – Mengani CP-Est, Mengani CCF, and La Boite CCF – are fourth. It goes along with Nurhayati *et al.* (2021) finding that the higher the total phenol rate is, the higher the antioxidant activity will be. Mengani CCF comes with the highest total phenol rate (followed by La Boite CCF, Mengani CP-Est, and Mengani CP-SP, respectively) in Figure 4, akin to Fig. 7, where La Boite CCF has the highest IC-50 (followed by Mengani CCF, Mengani CP-Est, and Mengani CP-SP respectively). As of the lowest total phenol content in Figure 4, Mengani CP-Hay also holds the lowest IC-50 result in Figure 7.

Figure 7 is key to the double purpose of this research—in addition to non-heme Fe, natural antioxidant contents in CP are also revealed. Since synthetic antioxidants (such as butylated hydroxytoluene and butylated hydroxyanisole) have recently been reported to be harmful to human health, the search for effective and non-toxic natural compounds with natural antioxidant activity should be feasible (Amarowicz *et al.* 2012; Felter *et al.*, 2021; Xu *et al.*, 2021). Figure 7 also supports the findings of Damat *et al.*, (2019), Lestari *et al.*, (2022); and Moreno *et al.*, (2019) that CP has a positive effect on antioxidant capacity.

3.7. Total Plate Count

Total Plate Count (TPC) is a means to find the hygienic rates of CP as a CCF source, which result is disclosed in Figure 8.

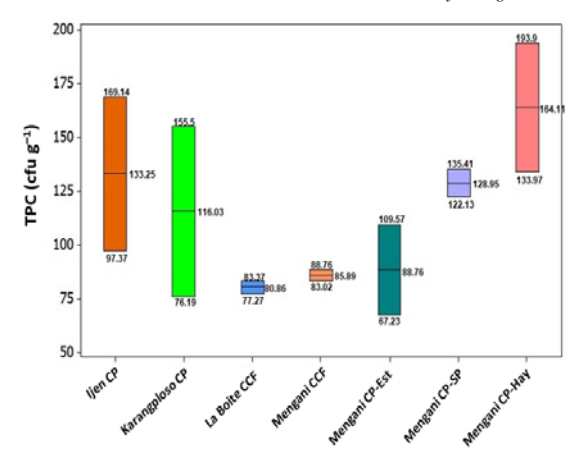


Figure 8. Box plot TPC in samples from three coffee cultivation areas.

Referring to the figure, the highest rate of TPC is in Mengani CP-Hay. Apparently, plastic-bagged CP-Hay stored at room temperature does not protect the goods from organism contamination. The following highest rates – meaning the least hygienic ones – go to Ijen CP, Karangploso CP, and Mengani CP-SP, respectively. The data illustrates that small coffee processor units are currently incapable of applying hygienic work. Due to the low TPC rate, the cleanest product is La Boite CCF, followed by Mengani CCF and Mengani CP-Est, respectively.

3.8. Principal Coordinates Analysis (PCoA) and Heat Map

The authors summed up the results of seven observed variables (Figure 2 to Figure 8) applied to six different CP samples to find the most similar one to the control. Employing PCoA (MDS) through DARwin 6.0.010 software program (Perrier and Jacquemoud-Collet, 2006), the dendrogram was then visualized in the form of a Heat Map and included in Figure 9.

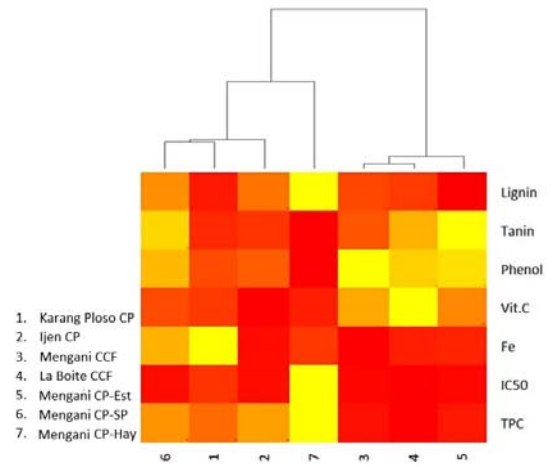


Figure 9. Heat Map of seven observed variable results of seven CP samples

Three groups are formed based on the objects' Euclidean distance: Mengani CP-Hay is in the first; Karangploso CP, Ijen CP, and Mengani CP are in the second; Mengani CP-Est, Mengani CCF, and La Boite CCF are in the third. Since Mengani CP-Est and Mengani

CCF are in the same group as La Boite CCF, this means that they are the most similar samples to the control.

4. Conclusion and Recommendation

Two samples with the highest degrees of similarity to the control (La Boite CCF) are Mengani CCF and Mengani CP-Est. The authors recommend improving the drying system for Mengani CCF and Mengani CP-Est since high temperatures presumably damaged some observed variables. Furthermore, further investigation on Fe contaminant in Karangploso CP and Mengani CP-SP samples should also be conducted to prevent it from happening.

Following up on this research, the authors suggest applying other observed variables to the samples mentioned above, such as heavy metal content, proximate analysis, and detailed amino acid content. This *in vitro* research should also expand too as *in vivo*.

Acknowledgments

The authors sadly acknowledge that Yogo Adhi Nugroho, one of the authors of this article, passed away on June 30, 2021, after a fight against COVID-19. We sincerely appreciate his enthusiasm and dedication to the writing of this manuscript. The authors are grateful for the provision of research materials: (i) Ricky Hendarto Setyobudi and Fitri Ramli (Mengani CP and CCF), (ii) Dr. Soni Sisbudi Harsono (Ijen CP), (iii) Pandu Prabowo (Karangploso CP), and (iv) Yohannes Kohar Whisnu Wardhana (La Boite CCF).

References

Adinurani PG, Setyobudi RH, Nindita A, Wahono SK, Maizirwan M, Sasmito A, Nugroho YA, Liwang T. 2015. Characterization of *Jatropha curcas* Linn. capsule husk as feedstock for anaerobic digestion. *Energy Procedia* **65**: 264 – 273. https://doi.org/10.1016/j.egypro.2015.01.046

Adinurani PG. 2016. **Design and analysis of agrotrial data: Manual and SPSS**. Plantaxia, Yogyakarta, Indonesia

Abdullah K, Uyun AS, Soegeng R, Suherman E, Susanto H, Setyobudi RH, Burlakovs J and Vincēviča-Gaile Z. 2020. Renewable energy technologies for economic development. *E3S Web of Conf.*, **188(00016)**: 1–8.

https://doi.org/10.1051/e3sconf/202018800016

Achmad DS. 2000. **Nutrition science for students and professionals in Indonesia volume I.** Dian Rakyat Publisher, Jakarta. Indonesia.

Agusmayanti R., Farich A, and Anggraini A. 2020. Vitamin C can increase hemoglobin levels in anemic pregnant women. *Jurnal Kebidanan Malahayati*. **6(3)**: 342–348,

https://doi.org/10.33024/jkm.v6i3.1731

Alakali JS, Kucha CT, and Rabiu IA. 2015. Effect of drying temperature on the nutritional quality of *Moringa oleifera* leaves. *Afr. J. Food Sci.*, **9(7)**: 395–399.

https://doi.org/10.5897/AJFS2014.1145

Almatsier. 2009. **Basic principles of nutrition**. Gramedia Pustaka Utama. Jakarta, Indonesia.

Almey A, Khan AJ, Zahir S, Suleiman M and Aisyah RK. 2010. Total phenolic content and primary antioxidant activity of methanolic and ethanolic extract of aromatic plants'leaves. *Int. Food Res. J.*, **17**:1077–1088.

Amarowicz R, Naczka M and Shahidi F. 2012. Antioxidant activity of crude tannins of canola and rapeseed hulls. *J. Am. Oil Chem. Soc.*, 77 (9-J9465): 957–961.

https://doi.org/ 10.1007/s11746-000-0151

Anna B, Haryanto A, Hasanudin U, Iryani DA, Telaumbanua M and Herák D. 2019. Sustainable management of coffee fruit waste biomass in ecological farming systems at West Lampung, Indonesia. *IOP Conf. Ser. Earth Environ. Sci.* **345(012007)**:1–10. https://doi.org/10.1088/1755-1315/345/1/012007

AOAC. 1995. **Official methods of analysis** 16th Ed. Association of Official Analytical Chemists. Washington DC, USA.

Arapitsas P. 2012. Hydrolyzable tannin analysis in food. *Food Chem.*, **135(3):**1708-1717. https://doi.org/10.1016/j.foodchem.

Arista DPK, Lestari I and Rahayuningsih CK. 2018. Changes in iron (Fe) content in red beets (*Beta vulgaris* L.) by boiling and steaming. *Analis Kesehatan Sain*. **7(1):** 524–526

Ariva AN, Widyasanti A and Nurjanah S. 2020. The effect of drying temperature to the quality of cascara tea from arabica pulp (Coffea arabica). Jurnal Teknologi dan Industri Pertanian Indonesia. 12(1):21–28.

https://doi.org/10.17969/jtipi.v12i1.15744

Arora S and Kapoor RK. 2012. Iron metabolism in humans: An overview. In: Arora S (Ed.), Chapter 1, **Iron Metabolism**. *InTech*, Croatia. pp 1–22. https://doi.org/10.5772/39031

Arpi N, Rasdiansyah, Widayat HP and Foenna RF. 2018. Utilization of Arabica coffee (*Coffea arabica* L.) pulp waste into coffee pulp juice with the addition of lime (*Citrus aurantifolia*) and lemon (*Citrus limon*) juice: A feasibility study. *Jurnal Teknologi dan Industri Pertanian Indonesia.*, **10** (**02**): 33–39. https://doi.org/10.17969/jtipi.v10i2.12593

Arts IC and Hollman PC. 2005. Polyphenols and disease risk in epidemiologic studies. *Am J Clin Nutr.* **81 (1 Suppl):**317S–325S. https://doi.org/10.1093/ajcn/81.1.317S

Asfimanto WA, Nurlambang T and Waryono T. 2013. Effect of physical condition and cultivation on the quality coffee in Kintamani and Gayo. Fakultas FMIPA, Universitas Indonesia, Jakarta. (https://nanopdf.com/queue/pengaruh-kondisi-fisik-dan-budidaya-terhadap-kualitas-kopi-di_pdf?queue_id=-

Astawan M and Wresdiyati T. 2004. **Healthy diet with fiber foods**. Tiga Serangkai Pustaka Mandiri Publisher, Solo, Indonesia.

1&x=1644534641&z=MTU4LjE0MC4xNjMuNDU=).

Atabani AE, Al-Muhtaseb AH, Kumar G, Saratale GD, Aslame M, Khan HA, Saidg Z and Mahmoudh E. 2019. Valorization of spent coffee grounds into biofuels and value-added products: Pathway towards integrated bio-refinery. *Fuel*. 254,115640. https://doi.org/10.1016/j.fuel.2019.115640

Avinash SN, Srinivasamurthy CA, Bhaskar S and Prakash NB. 2017 Characterization, extraction and foliar spray of fortified humic acid on quality of capsicum. *Int. J. Curr. Microbiol. Appl. Sci.* 6(10): 2265–2272.

https://doi.org/10.20546/ijcmas.2017.610.268

Bermeo-Andrade H, Bahamón-Monje AF, Aragón-Calderón R, Beltrán-Vargas Y and Gutiérrez-Guzmán N. 2020. Is coffee (Coffea arabica L.) quality related to a combined farmer-farm profile? Sustainability 12 (9518): 1–14.

https://doi.org/10.3390/su12229518

Beyene A, Kassahun Y, Addis T, Assefa F, Amsalu A, Legesse W, Kloos H and Triest L. 2012. The impact of traditional coffee processing on river water quality in Ethiopia and the urgency of adopting sound environmental practices. *Environ. Monit. Assess.* **184**: 7053–7063. https://doi.org/10.1007/s10661-011-2479-7.

Bombardiere YE. 2006. The potential of anaerobic digestion technology to treat coffee waste in Huatusco, Mexico. Thesis. Ohio University, USA

Bizzo MLG, Farah A, Kemp JA and Scancetti LB. 2015. Highlights in the history of coffee science related to health. In: Preedy VR (Ed). **Coffee in Health and Disease Prevention**. Academic Press. Cambridge, Massachusetts, USA. pp. 11–17. https://doi.org/10.1016/B978-0-12-409517-5.00002-4

Blinová L, Sirotiak M, Bartošová A and Soldán M. 2017. Review: Utilization of waste from coffee production. *Research Papers Faculty of Materials Science and Technology Slovak Uniersity of Technology.* **25(40)**:91–101.

https://doi.org/10.1515/rput-2017-001

Bruno M and Oliveira RAD. 2008. Anaerobic treatment of waste from coffee pulping in up-flow anaerobic sludge blanket (UASB) in two-stage. International Proceedings. FCAV-UNESP, Brazil.

Budilaksana F and Andaka G. 2016. Extraction of anthocyanin dyes from rambutan fruit hulls extract (*Nephelium lappaceum* L.) as natural food coloring substitute for synthetic dyes (extraction temperature variables and extraction time). *Jurnal Inovasi Proses*, 1 (1): 54–57

Bukhari A, Firdaus H, Rahmawati M, Sheryl SN and Prisilia MC. 2020. Non-nutritional and disease-related anemia in Indonesia: A systematic review. *Asia Pac. J. Clin. Nutr.* (supplement). 29: S.41–S.54.

Campos RC, Pinto VRA, Melo LF, da Rocha SJS and Coimbra JS. 2021. New sustainable perspectives for coffee wastewater and other by-products: A critical review. *Future Foods* **4(100058)**:1–10. https://doi.org/10.1016/j.fufo.2021.100058

Carmen MT, Lorena ZC, Alexander VA, Amandio V and Raúl S. 2020. Coffee pulp: An industrial by-product with uses in agriculture, nutrition and biotechnology. *Rev. Agric. Sci.*, **8**: 323–342. https://dx.doi.org/10.7831/ras.8.0_323

Chala B, Oechsner H, Latif S and Müller J. 2018. Biogas potential of coffee processing waste in Ethiopia. *Sustainability* **10(2678)**: 1–14. https://doi.org/10.3390/su10082678

Cheatham R. 2019. Well hello, coffee cherry flour. Foodscape Informer. https://www.foodscapefinds.com/content/2019/3/9/well-hello-coffee-cherry-flour

Chung KT, Wong TY, Wei CI, Huang YW, and Lin Y. 1998. Tannins and human health: A review. Crit Rev Food Sci Nutr. 38(6):421–64. https://doi.org/10.1080/10408699891274273

Conner TA, McQuade C, Olp J and Pai AB. 2012. Effect of intravenous vitamin C on cytokine activation and oxidative stress in end-stage renal disease patients receiving intravenous iron sucrose. *Biometals*. **25**, 961–969. https://doi.org/10.1007/s10534-012-9562-6

Cook JD, Noble NL, Morek TA, Lynch SR and Petersburg SJ. 1983. Effect of fiber on nonheme iron absorption. Gastroenterology., 85(6):1354–1358

Corro G, Pal U and Cebada S. 2014. Enhanced biogas production from coffee pulp through deligninocellulosic photocatalytic pretreatment. *Energy Sci. Eng.*, **2(4)**: 177–187.

https://doi.org/10.1002/ese3.44

Dadi D, Mengistie E, Terefe G, Getahun T, Haddis A, Birke W, Beyene A, Luis P and Van der Bruggen B. 2018. Assessment of the effluent quality of wet coffee processing wastewater and its influence on downstream water quality. *Ecohydrol Hydrobiol* **18(2):**201–211. https://doi.org/10.1016/j.ecohy d.2017.10.007

Damat D, Angriani R, Setyobudi RH and Soni P. 2019. Dietary fiber and antioxidant activity of gluten-free cookies with coffee cherry flour addition. *Coffee Sci*, **14(4)**: 493–500.

Das A and Venkatachalapathy N. 2016. Profitable exploitation of coffee pulp- a review. *Int. J. Appl. Nat. Sci.*, **5(1):** 75–82.

DeBoer M. 2015. Understanding the heat map. Cartographic perspectives.

https://doi.org/10.14714/CP80.1314

https://cartographicperspectives.org/index.php/journal/article/view/cp80-deboer/1419

de la Rosa LA, Moreno-Escamilla JO, Rodrigo-Garcia J, Alvarez-Parrilla E. 2019. Phenolic compounds. In: Yahia E and Carrillo-Lopez A (Eds.). Chapter 12. **Postharvest Physiology and Biochemistry of Fruits and Vegetables**, 1st edition. Elsevier, Netherland. pp.253–271. https://doi.org/10.1016/B978-0-12-813278-4.00012-9

de Melo Pereira GV, Neto DPC, Magalhães Júnior AI, Prado FG, Pagnoncelli MGB, Karp SG and Soccol CR. 2020. In: Toldrá F (Ed.). Chapter 3 - Chemical Composition and Health Properties of Coffee and Coffee By-Products. Adv Food Nutr Res., 91: 65–96. https://doi.org/10.1016/bs.afnr.2019.10.002

Dewanti IDAR, Lestari PE, Budirahardjo R, Setyorini D, Yani RWE, Wibisono S and Mel M. 2019. The effect of steeping robusta coffee beans on monocytes: expression of il-1 β and tnf- α against Streptococcus mutans. Coffee Sci., 14(4): 477–483

Diniyah N and Lee SH. 2020 Phenolic composition and antioxidant potential of legumes -A review. *Jurnal Agroteknologi* **14(1)**:91–102. https://doi.org/10.19184/j-agt.v14i01.17965

DKBM Indonesia 2017 List of Indonesian food composition

http://staffnew.uny.ac.id/upload/132318122/pendidikan/DKBMIn donesia

Dorsey BM and Jones MA. 2017. Healthy components of coffee processing by-products. In: Galanakis CM (Ed.). Chapter 2. **Handbook of Coffee Processing By-Products Sustainable Applications**. Academic Press, Cambridge, Massachusetts, USA. pp. 27–62. https://doi.org/10.1016/B978-0-12-811290-8.00002-5

Dreher ML. 2018. **Dietary fiber in health and disease**. Springer Nature Switzerland

Dzung NA, Dzung TT and Khanh VTP. 2013. Evaluation of coffee husk compost for improving soil fertility and sustainable coffee production in rural central highland of Vietnam. *Resources and Environment*, **3(4)**:77–82.

https://doi.org/10.5923/j.re.20130304.03.

Elba CC, Ana RBL and Eva CV. 2017. Coffee berry processing by-product valorization: Coffee parchment as a potential fiber source to enrich bakery goods. *J Food Nutr Popul Health.*, **1(2):**1–7.

Elías L. 1979. Chemical composition of coffee-berry by-products. In: Braham J and Bressani R. (Eds.). **Coffee Pulp: Composition, Technology, and Utilization**. Institute of Nutrition of Central America and Panama, Ottawa, Canada. p. 11–16.

Ellie SS, Sun K, de Pee S, Kraemer K, Jee-Hyun R, Moench-Pfanner R, Sari M, Bloem MW and Semba RD. 2012. Relationship of maternal knowledge of anemia with maternal and child anemia and health-related behaviors targeted at anemia among families in Indonesia. *Matern Child Health J.* 16: 1913–1925. https://doi.org/10.1007/s10995-011-0938-y

Elstrott, B. Khan, L., Olson S, Raghunathan V, DeLoughery T and Shatzel JJ. 2020. The role of iron repletion in adult iron deficiency anemia and other diseases. *Eur J Haematol.* **104**:153–161. https://doi.org/10.1111/ejh.13345

Erb M and Kliebenstein DJ. 2020. Plant secondary metabolites as defenses, regulators, and primary metabolites: The blurred functional trichotomy. *Plant Physiol.*, **184(1)**, 39–52. https://doi.org/10.1104/pp.20.00433

Esquivel P and Jiménez VM. 2012. Functional properties of coffee and coffee by-products. *Food Res. Int.* **46(2)**: 488-495. https://doi.org/10.1016/j.foodres.2011.05.028

Felter SP, Zhang X and Thompson C. 2021. Butylated hydroxyanisole: Carcinogenic food additive to be avoided or harmless antioxidant important to protect food supply? *Regul. Toxicol. Pharmacol.*, **121** (104887): 1–8.

https://doi.org/10.1016/j.yrtph.2021.104887

Felton E. 2019. Filtered: Coffee, the Café and the 21st-Century City. Routledge Publisher, London

Fereja WM, Tagesse W, and Benti G. 2020. Treatment of coffee processing wastewater using *Moringa stenopetala* seed powder: Removal of turbidity and chemical oxygen demand. *Cogent Food & Agriculture*, 6(1816420): 1–14.

https://doi.org/10.1080/23311932.2020.1816420

Fernandez R and Phillips SF. 1982. Components of fiber bind iron in vitro. *Am J Clin Nutr.*, **35**:100–106.

https://doi.org/10.1093/ajcn/35.1.100.

Fung-Jou L., Li-Hsueh C and Rung-Jiun G. 1998 Free radical-scavenging properties of lignin, *Nutr Cancer.*, **30:1**, 31–38. https://doi.org/10.1080/01635589809514637

Genanaw W, Kanno GG, Derese D and Aregu MB. 2021. Effect of wastewater discharge from coffee processing plant on river water quality, Sidama region, south Ethiopia. *Environ. Health Insights.*, **15**: 1–12.

https://doi.org/10.1177/1178630221106104

Geremu M, Tola YB and Sualeh A. 2016. Extraction and determination of total polyphenols and antioxidant capacity of red coffee (*Coffea Arabica* L.) pulp of wet processing plants. *Chem. Biol. Technol.*, **3(25):**1–6. https://doi.org/10.1186/s40538-016-0077-1

Gernah DI and Sengev IA. 2011. Effect of processing on some chemical properties of the leaves of drumstick tree (*Moringa oleifera*). Niger. Food J. 29(1):70–77.

Gill V. 2021a. 15 Largest coffee companies in the world in 2021. https://finance.yahoo.com/news/15-largest-coffee-companies-world-122455780.html

Gill, V. 2021 b. 5 Largest coffee companies in the world in 2021.

https://www.insidermonkey.com/blog/5-largest-coffee-companies-in-the-world-in-2021-944121/

Gillooly M, Bothwell TH, Charlton RW, Torrance JD, Bezwoda WR, MacPhail AP, Derman DP, Novelli L, Morrall P, and F. Mayet F. 1984. Factors affecting the absorption of iron from cereals. *Br J Nutr.*, **51(1)**: 37–46.

https://doi.org/10.1079/BJN19840007

Ginz M, Balzer HH, Bradbury AGW and Maier HG. 2000. Formation of aliphatic acids by carbohydrate degradation during roasting of coffee. *Eur. Food Res. Technol.* **211 (6)**: 404–410. https://doi.org/10.1007/s002170000215

Goyal S, Lambert C, Cluzet S, Mérillon JM and Ramawat KG. 2012. Secondary metabolites and plant defence. In: Mérillon J ad Ramawat K (eds). Plant defence: Biological control. Progress in Biological Control, vol 12. Springer, Dordrecht. Switzerland. https://doi.org/10.1007/978-94-007-1933-0 5

Gururaj A, Kumar BM, Achyuth KN and Manoj BR. 2021. Coffee processing wastewater management: An overview. *J. Eng Res. Reports.*, **20(11)**: 52–61.

https://doi.org/10.9734/JERR/2021/v20i1117405

Hamzah H and Jusuf NR. 2019. Analysis of ferrum content (Fe) in kelor leaves (*Moringa oleifera* Lam) with the height growing areas in Baubau. *Indo. J. Chem.* Res. 6, 88–93.

https://doi.org/10.30598//ijcr.2019.6-has

Harbone JB. 1996. **Phytochemical methods: A guide to modern ways of analysing plants.** Padmawinata K and Soedino I (Transl.) 2nd Edition. Penerbit ITB, Bandung, Indonesia.

Hayati EK, Budi US, and Hermawan R. 2012. Total anthocyanin compound concentration rosella flower (*Hibiscus sabdariffa* L.) petals extract: Effect temperature and pH. *Jurnal Kimia* 6 (2): 138–147

Hagerman AE. 2002. **Tannin handbook**. Department of Chemistry and Biochemistry, Miami University.

Heeger A, Kosińska-Cagnazzo A, Cantergiani E and Andlauer W. 2017. Bioactives of coffee cherry pulp and its utilisation for production of cascara beverage. *Food Chem.* **221**: 969–975. https://doi.org/10.1016/j.foodchem.2016.11.067

Hendroko R, Wahyudi A, Wahono SK, Adinurani PG, Salundik S and Liwang T. 2013. Bio-refinery study in the crude Jatropha oil process: Co-digestion sludge of crude Jatropha oil and capsule husk *Jatropha curcas* Linn. as biogas feedstock. *Int. J. Technol.* **4(3)**: 202–208. https://doi.org/10.14716/ijtech.v4i3.115

Hermosa B, Duarte VA and Schwan RF. 2014. Utilization of coffee by-products obtained from semi-washed process for production of value-added compounds. *Bioresour. Technol.* **166:** 142–150. https://doi.org/10.1016/j.biortech.2014.05.031

Hernández-Sarabia M, Sierra-Silva J, Delgadillo-Mirquez L, Ávila-Navarro J and Carranza L. 2021. The potential of the biodigester as a useful tool in coffee farms. *Appl. Sci.* **11 (6884)**: 1-12 https://doi.org/10.3390/app11156884

Huang WY, Cai YZ, and Zhang Y. 2010. Natural phenolic compounds from medicinal herbs and dietary plants: potential use for cancer prevention. *Nutr Cancer.*, **62**:1–20. https://doi.org/10.1080/01635580903191585

Ifadah RA, Wiratara PRW and Afgani CA. 2021. Scientific review: Anthocyanins and their health benefits. *Jurnal Teknologi Pengolahan Pertanian*, **3 (2)**: 11–21.

Ijanu EM, Kamaruddin MA and Norashiddin FA. 2020. Coffee processing wastewater treatment: A critical review on current treatment technologies with a proposed alternative. *Appl. Water Sci.*, **10**: !-11.

https://doi.org/10.1007/s13201-019-1091-9

Iriondo-DeHond A, Iriondo-DeHond M and Dolores del Castillo M. 2020. Applications of compounds from coffee processing byproducts. *Biomolecules* **10** (1219): 1–20.

http://dx.doi.org/10.3390/biom10091219

ISO. 2013. ISO 4833-1:2013 - Microbiology of the food chain — Horizontal method for the enumeration of microorganisms Part 1: Colony count at 30 °C by the pour plate technique https://www.iso.org/standard/53728.html

Jaisyurahman U, Wirnas D, Trikoesoemaningtyas and Purnamawati H. 2019. Effect of high-temperature conditions to rice growing and yield. *J. Agron. Indonesia* **47(3):**248–254.

https://dx.doi.org/10.24831/jai.v47i3.24892

Jumadi. 2020. The effect of iron biofortified maize on haemoglobin and erythrocyte level of Wistar rat anemia. PhD Dissertation. Universitas Hasanudin, Makasar, Indonesia.

http://digilib.unhas.ac.id/uploaded_files/temporary/DigitalCollecti on/YTBhMjg4YTZhN2ZjZTFkNzlhMDNINWQ0Y2VkYjQ5NGI vYzcxNjIzYQ==.pdf

Kayhanian M and Tchobanoglous G. 2016. Energy recovery by anaerobic digestion process. In: Goswani DY and Kreith F (Eds.). **Handbook of Energy Efficiency and Renewable Energy**, 2nd Edition, Section IV-48. CRC Press. Boca Raton, Florida, USA. p 1529–1580.

Kell DB, Heyden EL and Pretorius E. 2020. The biology of lactoferrin, an iron-binding protein that can help defend against viruses and bacteria. *Front. Immunol.*, **11(1221)**: 1–15 https://doi.org/10.3389/fimmu.2020.01221

Kelsay JL, Behall KM, and Prather ES. 1979. Effect of fiber from fruits and vegetables on metabolic responses of human subjects. II. Calcium, magnesium, iron, and silicon balances. *Am J Clin Nutr.*, **32**:1876–1880. https://doi.org/10.1093/ajcn/32.9.1876.

Kritchevsky D and Bonfield CT. 2012. **Dietary fiber in health and disease**. Vol. 427. Springer Science & Business Media Vol. 247. Boston, USA.

Kumari M and Jain S. 2012. Tannins: An antinutrient with positive effect to manage diabetes. *Res.J.Recent Sci.* 1(12): 1–8.

Kwartiningsih E, Prastika KD and Triana DL. 2016. Extraction and stability test of anthocyanins from super red dragon fruit hulls (*Hylocereus costaricensis*). Proceedings of the National Seminar Chemical Engineering "The Struggle" of Chemical Technology Development for Processing of Indonesian Natural Resources, 17 Maret 2016. UPN Veteran Yogyakarta, Indonesia. pp. B6.1–B6.6

Lambert JD, Hong J, Yang GY, Liao J, and Yang CS. 2005. Inhibition of carcinogenesis by polyphenols: evidence from laboratory investigations. *Am J Clin Nutr.* **81 (1 Suppl):**284S–291S. https://doi.org/10.1093/ajcn/81.1.284S

Lesjak M and Srai SKS. 2019. Role of dietary flavonoids in iron homeostasis. *Pharmaceuticals* (Basel, Switzerland), **12(3)**: 119: 1-21. https://doi.org/10.3390/ph12030119

Lestari W, Hasballah K, Listiawan MY, Sofia S. 2022. Coffee by-products as the source of antioxidants: A systematic review. *F1000 Research*. **11(220)**:1–12.

https://doi.org/10.12688/f1000research.107811.1

Malaggia LP, Sangia MS, and Paedonga JJE. 2012. Determination of tannin content and activity test of avocado seed extract (*Presea americana* Mill.). *Jurnal MIPA Unsrat Online* 1(1):5–10

Marín-Tello C, Zelada-Castillo L, Vásquez-Arqueros A, Vieira A and R. Siche R. 2020. Coffee pulp: An industrial by-product with uses in agriculture, nutrition and biotechnology. *Rev. Agric. Sci.*, **8:** 323–342. https://doi.org/10.7831/ras.8.0_323.

Martínez JRR and Clifford MN. 2000. Coffee pulp polyphenols: An overview. In: Sera T, Soccol CR., Pandey A, and Roussos S (eds). **Coffee Biotechnology and Quality**. Springer, Dordrecht. Swiszerland https://doi.org/10.1007/978-94-017-1068-8_47

Mazid M, Khan TA, and Mohammad. 2011. Role of secondary metabolites in defense mechanisms of plants., *Biol. Med.* **3 (2)** Special Issue: 232–249.

Mbah BO, Eme PE, and Paul AE. 2012. Effect of drying techniques on the proximate and other nutrient composition of *Moringa oleifera* leaves from two areas in eastern Nigeria. *Pak. J. Nutr.* 11(11): 1044–1048.

Menteri Pertanian. 2012. Regulation number 52/Permentan/Ot.140/9/2012 concerning guidelines for handling postharvest coffee. Kementerian Pertanian Republik Indonesia,

Milman N. 2011. Anemia—still a major health problem in many parts of the world!. *Ann Hematol* **90**: 369–377. https://doi.org/10.1007/s00277-010-1144-5

Mindarti S, Zalizar L, Damat, Saati EA and Fajriani S. 2020. Characterization of fiber fraction, physical and chemical properties of coffee flour (*Coffea* sp.) as functional foodstuff for diabetes mellitus patient. *IOP Conf. Ser. Earth Environ. Sci.* 462 (012017):1–10. https://doi.org/10.1088/1755-1315/462/1/012017

Mishra P and Homa P. (Eds). 2019. Essentials of statistics in agriculture sciences. Apple Academic Press. Waretown, USA.

Monnier L. Colette C, Aquirre L and Mirouze J. 1980. Evidence and mechanism for pectin-reduced intestinal inorganic iron absorption in idiopathic hemochromatosis. *Am J Clin Nutr.* **33**:1225–1232. https://doi.org/10.1093/ajcn/33.6.1225

Moreno J, Cozzano S, Pérez AM, Arcia P and Curutchet A. 2019. Coffee pulp waste as a functional ingredient: Effect on salty cookies quality. *J. Food Nutr. Res.*, **7(9):** 632–638. https://doi.org/10.12691/jfnr-7-9-2

Muhammadong J, Sirajuddin S, Djide MN and Mallongi A. 2021. Improving body weight of female Wistar rats anemia by using iron biofortified maize. *Curr Res Nutr Food Sci.*, **9(1):** 184–189. http://dx.doi.org/10.12944/CRNFSJ.9.1.18

Mulato S and Suharyanto E. 2010. Case study of biogas production from plant-based materials and animal manure resources available in the coffee farm. Proceedings of 22th International Conference on Coffee Science, 2010. Bali, Indonesia. ASIC. 3-8 October 2010.

Mulyawanti I, Budijanto S and Yasni S. 2018. Stability of anthocyanin during processing, storage and simulated digestion of purple sweet potato pasta. *Indones. J. Agric. Sci.*, **19(1)**: 1–8. https://doi.org/10.21082/ijas.v19n1.2018.p1-8

Musallam KM and Taher AT. 2018. Iron deficiency beyond erythropoiesis: Should we be concerned? *Curr Med Res Opin* **34(1)** 81–93. 10.1080/03007995.2017.1394833

Muzaifa M, Rahmi F and Syarifudin. 2021. Utilization of coffee by-products as profitable foods - A mini review. *IOP Conf. Ser. Earth Environ. Sci.* **672(012077)**:1–9. https://doi.org/10.1088/1755-1315/672/1/012077

Nafisah D and Widyaningsih TD. 2018. Study of drying method and brewing ratio in process of making cascara tea from Arabica coffee (*Coffea arabika L.*). Jurnal Pangan dan Agroindustri. **6(30)**: 37–47

Nandini R and Narendra BH. 2012. Critical land characteristics of former eruption of Mount Batur in Bangli district, Bali. *Jurnal Penelitian Hutan dan Konservasi Alam*, **9(3)**:199–211

Naruki S, Astuti M, Marsono Y and Raharjo S. 2010. Oxidative effect of Na Fe EDTA fortificant in sweet soy sauce as fortification vehicle, on biological system (rats). *Agritech*, **30(4)**: 237, 242

Nasibeh A.M. 2019. How to use DarWin software to draw a tree and do PCoA. https://www.youtube.com/watch?v=FB2B7nunEIM

Novita E. 2012. Process design in robusta coffee agroindustry using modified wet processing technology based on clean production. PhD Dissertation. Sekolah Pascasarjana, Institut Pertanian Bogor, Indonesia.

https://repository.ipb.ac.id/handle/123456789/55728?show=full

Novita, E. 2016. Biodegradability simulation of coffee wastewater using instant coffee. *Agric Agric Sci Procedia.*, **9**: 217–229. https://doi.org/10.1016/j.aaspro.2016.02.138

Novita E, Marhaenanto B and Sujarwo MW. 2016. Anaerobic process temperature control system for handling coffee processing liquid waste. Prosiding seminar nasional APTA (Asosiasi Profesi

Teknologi Agroindustri 26–27 October 2016, Jember, Indonesia pp. 401–406.

Novita E, Khotijah, Purbasari D and Pradana HA. 2021. The application of cleaner production in Wulan coffee agroindustry Maesan sub district Bondowoso regency. *Jurnal Teknik Pertanian Lampung* **10(2)**: 263–273. http://dx.doi.org/10.23960/jtep-l.v10.i2.263-273

Nurbadriyah WD. 2019. **Iron deficiency anemia**. Deepublish publisher, Yogyakarta. Indonesia.

Nurhayati, Belgis M, and Neilasari DA. 2021. Physicochemical characteristics and preferences of cascara made from Robusta var. Tugu Sari and BP 42. *Jurnal Ilmiah Inovasi*. **20(2)**:28–33.

Nurul A, Epriyani C, Kurnia A, Ramadhan K, Hidayat SG and Apriyantono A. 2022. **Kintamani Bali Arabica coffee profile**. In: Nurul A and Apriyantono A (eds). AE Publishing, Malang, Indonesia

Ogawa, C, Tsuchiya K and Maeda K. 2020. Reticulocyte hemoglobin content. *Clin. Chim. Acta* **504**: 138–145. https://doi.org/10.1016/j.cca.2020.01.032

Ota K. 2018. Coffee as a global beverage before 1700. J. Int. Econ. Stud. 3: 43-55

Padmapriya R, Tharian JA and Thirunalasundari T. 2013. Coffee waste management—an overview. *Int J Curr Sci* **9**:83–91

Padmapriya R, Tharian JA, and Thirunalasundari T. 2015. Original research article treatment of coffee effluent by *Moringa oleifera* seed. *Int J Curr Microbiol Appl Sci* **4(1)**:288–295

Pandey KB and Rizvi SI. 2009. Plant polyphenols as dietary antioxidants in human health and disease. *Oxid. Med. Cell. Longev.*, **2(5)**: 270–278. https://doi.org/10.4161/oxim.2.5.9498

Perrier X., Flori A and Bonnot F. 2003. Data analysis methods. In: Hamon P, Seguin M, Perrier X, and Glaszmann JC (Eds.). **Genetic Diversity of Cultivated Tropical Plants**, Science Publishers, Enfield. USA. pp 43–76.

Perrier X and Jacquemoud-Collet JP. 2006. DARwin software https://darwin.cirad.fr/

Poole R, Kennedy OJ, Roderick P, Fallowfield JA, Hayes PC and Parkes J. 2017. Coffee consumption and health: Umbrella review of meta-analyses of multiple health outcomes. *BMJ* **359**(**5024**): 1–17

http://dx.doi.org/10.1136/bmj.j5024

Plalt SR and Clydesdale FM. 1987. Mineral binding characteristics of lignin, guar gum, cellulose, pectin, and neutral detergent fiber under simulated duodenal pH conditions.. *J. Food Sci.* **52(5)**: 1121–1439. https://doi.org/10.1111/j.1365-2621.1987.tb14096.x

Pua A, Xian W, Choo D, Goh RMV, Liu SQ, Cornuz M, Ee KH, Sun J, Lassabliere B and Yua B. 2021. A systematic study of key odourants, non-volatile compounds, and antioxidant capacity of cascara (dried *Coffea arabica* pulp). *LWT* **138 (110630)**: 1–13. https://doi.org/10.1016/j.lwt.2020.110630

Purwanto P, Sagita YA, Lestari PE, Praharani D, Jani Y and Yaro A. 2020. Inhibition of *Candida albicans* growth by steeping freeze-dried robusta ground coffee. *Coffee Sci.*15, (e151638): 1–6. https://doi.org/10.25186/cs.v15i.1638

Rahmadi A. dan Bohari. 2018. **Functional food antioxidant efficacy**. Mulawarman University Press. Samarinda, Indonesia

Ramirez-Coronel MA, Marnet N, Kolli VSK, Roussos S, Guyot S, and Augur C. 2004. Characterization and estimation of proanthocyanidins and other phenolics in coffee pulp (*Coffea arabica*) by thiolysis— high-performance liquid chromatography. *J. Agric. Food Chem.* **52(5)**: 1344–1349.

https://doi.org/10.1021/jf035208t

Ramirez-Martinez JR. 1988. Phenolic compounds in coffee pulp: Quantitative determination by HPLC. *J. Sci. Food Agric.* **43(2)**: 135–144. https://doi.org/10.1002/jsfa.2740430204

Rania M.A.M., Fageer A.S.M, Eltayeb M.M and Ahmed IAM. 2014. Chemical composition, antioxidant capacity, and mineral extractability of Sudanese date palm (*Phoenix dactylifera* L.) fruits. *Food Sci Nutr.* **2(5)**: 478–489.

Rasouli H, Farzei M, and Khodarahmi R. 2017. Polyphenols and their benefits: A review. *Int. J. Food Prop.*, **20(issue sup. 2)**: 1700–1741. https://doi.org/10.1080/10942912.2017.1354017

Rattan S, Parande AK, Nagaraju VD and Ghiwari GK. 2015. A comprehensive review on utilization of wastewater from coffee processing. *Environ Sci Pollut Res Int.* **22(9):**6461–6472. https://doi.org/10.1007/s11356-015-4079-5.

Reinhold JG, Garcia JS, Garzon P. 1981. Binding of iron by fiber of wheat and maize, *Am. J. Clin. Nutr.* **34(7)**:1384–1391, https://doi.org/10.1093/ajcn/34.7.1384

Rosas-Sánchez GA, Hernández-Estrada ZJ, Suárez-Quiroz ML, González-Ríos O and Rayas-Duarte P. 2021. Coffee cherry pulp by-product as a potential fiber source for bread production: A fundamental and empirical rheological approach. *Foods.*, **10(4)**, **742**: 1–12.

https://doi.org/10.3390/foods10040742

Rufaizah U. 2011. Utilization of sorghum flour (*Sorghum bicolor* L. Moench.) in making snack bars high in food fiber and source of iron for young girls. Under graduated thesis IPB, Bogor, Indonesia.

Sariadi. 2011. Processing of coffee liquid waste by batch electrocoagulation method. *Jurnal Teknologi.*, **11(2)**: 72–76.

Schmidl MK and Labuza TP. 2000. Essentials of functional foods. Aspen Publ. Maryland, USA.

Shumeta Z and D'Haese M. 2018. Do coffee farmers benefit in food security from participating in coffee cooperatives? Evidence from southwest Ethiopia coffee cooperatives. *Food Nutr Bull.*, **39(2)** 266–280. https://doi.org/10.1177/0379572118765341.

Sengupta B, Priyadarshinee R., Roy A, Banerjee A, Malaviya A, Singh S, Mandal T and Kumar A. 2020. Toward sustainable and eco-friendly production of coffee: Abatement of wastewater and evaluation of its potential valorization. *Clean Technol. Environ. Policy* 22: 995–1014. https://doi.org/10.1007/s10098-020-01841-y

Seriki SA, Adebayo O and Odetola AO, 2017. Iron: From dietary sources to utilization in the body. *Glob J Nano.*, **3(3-555615)**: 1-6. https://doi.org/00610.19080/GJN.2017.03.555615.

Setiawan MD, Tamrin and Lanya B. 2014. The performance test of mechanical rack grain dryer with three environmental conditions. *Jurnal Teknik Pertanian Lampung* **3(1)**: 91–102

Setyobudi RH, Wahono SK, Adinurani PG, Wahyudi A, Widodo W, Mel M, Nugroho YA, Prabowo B and Liwang T. 2018. Characterisation of arabica coffee pulp - hay from Kintamani - Bali as prospective biogas feedstocks. *MATEC Web Conf.* **164 (01039)**: 1–13. https://doi.org/10.1051/matecconf/201816401039

Setyobudi RH, Zalizar L, Wahono SK, Widodo W, Wahyudi A, Mel M, Prabowo B, Jani Y, Nugroho YA, Liwang T and Zaebudin A. 2019. Prospect of Fe non-heme on coffee flour made from solid coffee waste: Mini review. *IOP Conf. Ser. Earth Environ. Sci.*, **293** (012035):1–24. https://doi.org/10.1088/1755-1315/293/1/012035.

Setyobudi RH, Yandri E, Nugroho YA, Susanti MS, Wahono SK, Widodo W, Zalizar L, Saati EA, Maftuchah M, Atoum MFM, Massadeh MI, Yono D, Mahaswa RK, Susanto D, Damat D, Roeswitawati D, Adinurani PG and Mindarti S. 2021a. Assessment on coffee cherry flour of Mengani Arabica Coffee,

Bali, Indonesia as iron non-heme source. *Sarhad J. Agric.*, **37(Special issue 1)**: 171–183.

https://dx.doi.org/10.17582/journal.sja/2022.37.s1.171.183

Setyobudi RH, Yandri E, Atoum MFM, Nur SM, Zekker I, Idroes R, Tallei TE, Adinurani PG, Vincēviča-Gaile Z, Widodo W, Zalizar L, Van Minh N, Susanto H, Mahaswa RK, Nugroho YA, Wahono SK, and Zahriah Z. 2021b. Healthy-smart concept as standard design of kitchen waste biogas digester for urban households. *Jordan J. Biol. Sci.*, **14(3)**, 613–620. https://doi.org/10.54319/jjbs/140331

Shabri and Rohdiana D. 2016. Optimization and characterization of green tea polyphenol extract from various solvents. *Jurnal Penelitian Teh dan Kina.*, **19** (1): 57–66

Shankaranand VS and Lonsane BK. 1994. Coffee husk: An inexpensive substrate for production of citric acid by *Aspergillus niger* in a solid-state fermentation system. *World J. Microbiol. Biotechnol.* **10:** 165–168. https://doi.org/10.1007/BF00360879

Soliman GA. 2019. Dietary fiber, atherosclerosis, and cardiovascular disease. *Nutrients*, **11(1155):**1–11. https://doi.org/10.3390/nu11051155

Suarni. 2009. Potential of corn flour and sorghum as a substitute for wheat in processed products. *Iptek Tanaman Pangan.*, **4** (2): 181–193

Suarni and Firmansyah IU. 2007. Structure, nutrient composition and processing technology of sorghum. Balai Penelitian Tanaman Serealia, Maros, Indonesia.

Suarni and Subagio H. 2013. Prospects of developing corn and sorghum as functional food sources. *Jurnal Penelitian dan Pengembangan Pertanian.***32** (3): 47–55.

Sudarmi, Subagyo P, Susanti A, and Sri AW. 2015. Dragon fruit hulls extraction as natural dyes. Proceedings of the National Seminar Chemical Engineering the Struggle of Chemical Technology Development for Processing of Indonesian Natural Resources, 17 March 2016. UPN Veteran Yogyakarta, Indonesia. pp. G10.1–G10.5

Sukatiningsih. 2011. The encapsulation of antioxidant extract of coffee husk using a combination of gum arabic and tapioca is oxidized as a capsule material. Research Report. University of Jember.

http://repository.unej.ac.id/bitstream/handle/123456789/58861/Su katiningsih_unggulan_boptn_129.pdf?sequence=1

Susanto H, Setyobudi RH, Sugiyanto D, Nur SM, Yandri E, Herianto H, Jani Y, Wahono SK, Adinurani PA, Nurdiansyah Y and Yaro A. 2020. Development of the biogas-energized livestock feed making machine for breeders. *E3S Web of Conf.*, **188 (00010)**: 1–13.

https://doi.org/10.1051/e3sconf/202018800010

Susiloningtyas I. 2012. Giving iron (Fe) in pregnancy. *Majalah Ilmiah Sultan Agung* **50 (128):** 1–27

Susilawati IDAA, Suryono S, Purwanto P, Burlakovs J and Yaro A. 2020. Coffee protects cardiovascular health by maintaining the structure of coronary arterial wall intimal collagen. *Coffee Sci.* **15(e151637)**: 1–6. https://doi.org/10.25186/.v15i.1637.

Syarfaini S, Satrianegara MF, Alam S and Amriani A. 2017. Analysis of nutritional content of purple sweet potato biscuits (*Ipomoea batatas* L. Poiret) as an alternative to improve nutrition in the community. *Al-Sihah: The Public Health Science Journal*, **9(2):** 138–152. https://doi.org/10.24252/as.v9i2.3763

Syarief R, Novita E, Noor E, and Mulato S. 2012. Smallholder coffee processing design using wet technology based on clean production. *Journal of Applied Sciences in Environmental Sanitation*, **7 (2)**: 93–102.

Tandon M and Rai SN. 2007. Tannins and human health: Nutraceuticals effect of tannin and its monomers. Animal Nutrition Division, National Dairy Research Institute, India

Tomanek DP and Schröder J. 2018. Value added heat map. Springer Nature. Switzerland

USDA. 2018 (United States Department of Agriculture, Agricultural Research Service). National nutrient database for standard reference legacy release.

(https://ndb.nal.usda.gov/ndb/foods/show/11457).

Van Soest PJ, Robertson JB and Lewis BA, 1991. Methods for dietary fiber, neutral detergent fiber, and nonstarch polysaccharides in relation to animal nutrition. *J. Dairy Sci.***74(10)**:3583–3597. https://doi.org/10.3168/jds.S0022-0302(91)78551-2

Veronese N, Solmi M, Caruso MG, Giannelli G, Osella AR, Evangelou E, Maggi S, Fontana L, Stubbs B and Tzoulaki I. 2018. Dietary fiber and health outcomes: An umbrella review of systematic reviews and meta-analyses. *Am. J. Clin. Nutr.*, **107(3)**: 436–444, https://doi.org/10.1093/ajcn/nqx082

Viartasiwi N and Trihartono A. 2020 Café in small towns: A picture of the weakening social engagement. *Coffee Sci.* **15(e151687)**:1–6. https://doi.org/10.25186/cs.v15i.1687.

Vladimir-Knežević S, Blažeković B, Štefan MB and Babac M. 2012. Plant polyphenols as antioxidants influencing the human health. In: Rao V. (Ed.). Chapter 9. **Phytochemicals as Nutraceuticals**. IntechOpen Limited, London, UK. pp. 155–180. https://doi.org/10.5772/27843

Wahyani AD and Rahmawati YD. 2021. Analysis of food fiber and iron content in sorghum flour substitution cookies as alternative food for anemia teenage princess. *Jurnal Kesehatan Masyarakat STIKES Cendekia Utama* 8(2): 227–237

Wachamo HL. 2017. Review on health benefit and risk of coffee consumption. *Med Aromat Plants* **6(4-1000301):** 1–12. https://doi.org/10.4172/2167-0412.1000301

Wich D. 2015. Coffee flour: New potential ingredient?

https://raypeatforum.com/community/threads/coffee-flour-new-potential-ingredient.7194

Winarsi H. 2007. **Natural antioxidants and free radicals**. Kanisius Publisher, Yogyakarta, Indonesia.

WIPO – PCT. 2014. WO2014/158267A1. The coffee cherry flour compositions and methods for their preparation. World Intelectual Property Organization International Bureau Patent Cooperation Treaty. (https://patents.google.com/patent/WO2014158267A1/en)

Woldesenbet AG, Woldeyes B, and Chandravanshi BS. 2015. Wet coffee processing waste management practice in Ethiopia. *Asian Journal of Science and Technology.*, **6(5):** 1467–1471

Wulandari P. 2015. Honey to prevent iron deficiency anemia in pregnancy. *Majority* **4(3)**: 90–95.

Xiandeng H, Amais RS, Jones BT and Donati GL. 2016. Inductively coupled plasma optical emission spectrometry. Wiley Online Library.

https://doi.org/10.1002/9780470027318.a5110.pub3

Xie J and Schaich K. 2014. Re-evaluation of the 2,2-Diphenyl-1-picrylhydrazyl free radical (DPPH) assay for antioxidant activity. *J. Agric. Food Chem.*, **62(19)**: 4251–4260.

https://doi.org/10.1021/jf500180u

Xu B and Chang S. 2008. Effect of soaking, boiling, and steaming on total phenolic content and antioxidant activities of cool season food legumes. *Food Chem*, **110** (1): 1–13.

https://doi.org/10.1016/j.foodchem.2008.01.045

Xu X., Liu A, Ares SHI, Martínez-Larrañaga MR, Wang X, Martínez M, Anadón A, and Martínez, MA. 2021. Synthetic phenolic antioxidants: Metabolism, hazards and mechanism of action. *Food Chem.* **353**, 129488.

https://doi.org/10.1016/j.foodchem.2021.129488

Yahmadi M. 1972. **Coffee Cultivation and Processing.** Balai Penelitian Perkebunan Bogor Sub Balai Penelitian Budidaya Jember. Jember, Indonesia.

Yahia EM, García-Solís P and Celis MEM. 2019. Contribution of fruits and vegetables to human nutrition and health. Chapter 2. **Postharvest Physiology and Biochemistry of Fruits and Vegetables**. Science Direct. Elsevier, Amsterdam. Netherlands. pp. 19–45. https://doi.org/10.1016/B978-0-12-813278-4.00002-6.

Yuniastuti A. 2014. Micromineral nutrition and health. Unnes Press, Semarang, Indonesia.

Yunita M, Hendrawan Y and Yulianingsih R. 2015. Microbiological quantitative analysis of Garuda Indonesia Aviation Food (Aerofood ACS) based on TPC (total plate count) using the Pour Plate Method. *Jurnal Keteknikan Pertanian Tropis dan Biosistem.* 3(3):237–248.

Zeckel S, Susanto PC and Erfiani NMD. 2020. Market potential of cascara tea from Catur village Kintamani Bali. Proceeding I-CFAR (International Conference on Fundamental and Applied Research). Bali, Indonesia, 7 October 2019. pp 331–338.

Zhao S, Guo Y, Sheng Q and Shyr Y. 2014. Advanced heat map and clustering analysis using heatmap3. Biomed Res. Int. Special Issue Advances in Computational Genomics. Article ID 986048: 1–6. https://doi.org/10.1155/2014/986048

Zhou L, Cao Z, Bi J, Yi J, Chen Q, Wu X, dan Zhou M. 2016. Degradation kinetics of total phenolic compounds, capsaicinoids and antioxidant activity in red pepper during hot air and infrared drying process. *Int J Food Sci Technol.*, **51(4):** 1365–2621. 10.1111/ijfs.13050.

Zupancic GD and Grile V. 2012. Anaerobic treatment and biogas production from organic waste. In: Sunil, K. and A. Bharti (Eds.). Chapter 1. **Management of Organic Waste**. IntechOpen Limited, London, UK. pp. 3–28. https://doi.org/10.5772/32756.



Jordan Journal of Biological Sciences

Infraspecific identity of the wild *Brassica nigra* (L.) Koch. using morphological, cytogenetics and molecular (nuclear and chloroplast) approaches

Wafaa M. Amer¹, Mahmoud A. Shoulkamy², Hadeer D. Abd El-Baset^{2,*} and Ahmed M. Faried³

¹Botany and Microbiology Department, Faculty of Science, Cairo University, Giza, Egypt (wamer@sc.cu.edu.eg); ²Botany and Microbiology Department, Faculty of Science, Minia University, Minya, Egypt; ³Botany and Microbiology Department, Faculty of Science, Assiut University, Assiut, Egypt.

Received: December 10, 2020; Revised: May 20, 2021; Accepted: June 30, 2021

Abstract

Egyptian flora is still hosting the wild diploid *Brassica nigra* (L.) Koch. (Brassicaceae); as one of the most important wild crop relatives of the cultivated *Brassica* crops. Despite the field and herbarium observations indicating that the populations of this species showed considerable morphological diversity, the taxonomic identity of these variations is not yet resolved. This study covered the morphology, the cytogenetics and the genome diversity at the intraspecies level to resolve the taxonomic identity and their genetic relationships. Nine representative populations were morphologically investigated using 70 macro-and micro-morphological characters. The morphological results confirmed the presence of two varieties (var. *bracteolata* and var. *nigra*), and three forms, while the chromosome investigation revealed the presence of 2n=16), with notable karyotyping diversity among the studied varieties where satellite was observed on the chromosome pair no. "6" distinguished var. *bracteolata* from var. nigra. The retrieved accession numbers of the chloroplast (rps, ropC & trnK) and nuclear (ITS) markers have been deposited in the EMBL/GenBank/DDBJ nucleotide sequence data libraries; then compared with that of *B. nigra* from Gene-Bank database search via Basic Local Alignment Search Tool (BLAST). The constructed cladogram based on molecular markers supported the morphological and cytological results and confirmed the presence of the two varieties (*bracteolata* and *nigra*). This study recommends combining different taxonomic approaches in resolving the taxonomic identity of morphologically different wild *B. nigra* populations.

Keywords: Brassica nigra - Nuclear marker (ITS)- Chloroplast markers- Chromosome number- Karyotyping- infraspecific diversity-morphological diversity.

1. Introduction

Brassicaceae (Cruciferae) is a monophyletic family, distributed in temperate areas of all continents except Antarctica, species of this family retain high diversity in Irano-Turanian, Mediterranean, and West N. American regions (El Rabiai, 2015; Taiyan et al., 2001). Brassicaceae is highly homoplasious in its morphological characters, which seems to play a limited role in resolving the phylogenetic affinities at the generic and family levels (Al-Shehbaz et al., 2006). It includes 3977 species (351 genera), in which the genus Brassica contains species with unique agricultural potentialities and wide-utilization range (Amer et al., 2019; Rakow, 2004; Song et al., 1988). The generic boundary of this genus needs revision (Felger et al., 2015).

In Egyptian flora, Brassicaceae is one of the four largest families, which is represented by 53 genera and 103 species (Boulos, 1995; Boulos, 1999). Genus *Brassica* in Egypt represented by five species from about 80 accepted *Brassica* species worldwide. These species are: *B. nigra* (L.) Koch, *B. rapa* L. and *B. tournefortii* Gouan, *B. deserti*

Danin & Hedge and *B. juncea* (L.) Czernj. & Coss. (Boulos, 2009). This genus shows a high level of phenotypic variations with and within the wild Egyptian populations (Amer *et al.*, 2019).

Genus Brassica L. received the attentions of taxonomists due to its great economic importance as oil seed and vegetable crops (Amer et al., 2019; Warwick, 2011). Brassica nigra (L.) Koch. (Black Mustard) is widely cultivated as a chief source of edible oil, mustard and medicine (Tsunoda, 1980; Vaughan, 1977). It also possesses several agronomic potentialities as a pillar of the basic Brassica triangle for the diploid genome including B. oleracea, B. nigra and B. rapa, with 2n=18, 16 and 20; respectively and their shared hybrids (Schranz et al., 2002) and crossbreeding (Pires et al., 2004). Nevertheless, the study of chromosome numbers at the species level was carried out decades ago (Karpechenko, 1922). Later, the identity of the individual chromosome attains great attention. Brassica nigra harbors unique genomic ancestor genes in the genus Brassica (Yang et al., 2002).

The taxonomic identity of the infraspecific taxa of *Brassica nigra* in Egypt is still unresolved. However, it

^{*} Corresponding author e-mail: hadeerdahy44@gmail.com.

was identified as three varieties namely var. bracteolata (Fisch. & Mey.) Spach, var. torulosa Alef. and var. turgida Alef. (Täckholm, 1974); while (Boulos, 1999, 2009) considered these varieties as synonyms of B. nigra (L.) Koch. Later, Amer et al., (2019) studied the macro- and micro morphological characters of the infraspecific diversity of B. nigra (represented by 26 populations). The study revealed the presence of two distinctive varieties var. bracteolata and var. nigra and the later represented by two phenotypic forms. To date, the genetic variation, karyotyping, and molecular identity of this species at the infraspecific level are not yet investigated. Cytotaxonomy is the application of chromosome karyotyping in taxonomy (Greilhuber and Ehrendorfer, 1988), which can clarify the hereditary relationship along with the studied species or populations, and enable understanding their divergence (Guerra, 2008). The study of genetic variation of B. nigra accessions has significant implications in the crop improvement programs despite that the genome sequencing of B. nigra is still in progress (Negi et al., 2004; Jiang et al., 2015); and little is known about the magnitude and the genetic diversity among its wild population (Gomez-Campo, 1978; Roy, 1978).

Nowadays, the assessment of genetic diversity and DNA identity was performed by using molecular markers to overcome the morphological diversity within certain taxa (Ruangsuttapha *et al.*, 2007; Li *et al.*, 2012). The nuclear ribosomal DNA (nrDNA) is a universal molecular marker which harbors both highly variable and conserved regions (Simon *et al.*, 2012). Bailey *et al.* (2006) reported that the plants and animals' phylogeny was estimated using the internal transcribed spacer (ITS); those ranges from 500-700 bp in angiosperms (Baldwin *et al.*, 1995).

In plants, the chloroplast genome is of conserved genome compared to the mitochondria and nuclear genomes, so it is commonly used for genome identity (Haider, 2011). The highly conserved regions are interrupted by introns and non-coding cpDNA regions (Clegg, 1993); The variability in these regions can be utilized in the systematic studies even at lower taxonomic levels (Haider, 2011). Seol *et al.* (2015) reported that the *Brassica nigra* (accession no. KT878383) was a circular, measured 153633 bp with a pair of inverted repeat regions.

The present work aimed to: (1) Assess the morphological variation and its relationship to chromosome number variation within the infraspecific taxa (varieties and/or forms) of *B. nigra*. (2) Identify the molecular identity of the studied taxa using ITS and

chloroplast markers. (3) Determine the genetic diversity within and between these taxa. (4) Check genotypic/karyotypic identity of these. (5) Identify the similarity between the status of Egyptian taxa and others available in the database.

2. Materials and Methods

2.1. Plant materials

Fresh *Brassica nigra* specimens were collected from different geographical regions during flowering and fruiting seasons, then grouped morphologically and represented in this study by 9 populations. Locations of the collected populations, for the *Brassica nigra* var. *nigra* Form 1, var. *nigra* Form 2 and var. *bracteolata* each represented by three populations collected from different localities (Table 1). The pollen grains of the collected populations were examined morphologically using Scanning Electron Microscope (by a Joel 1200 EX II SEM at 20 kv). The studied populations were identified based on the 70 macro-and micro-morphological characters as outlined in Table (2), according to (Amer *et al.*, 2019).

Table (1): Geographic locations of the studied *Brassica nigra* populations.

St.	Localities	GPS Coo	ordinates	
No.	Localities	N	Е	Associated Field
1	Assuit –Dairout	27° 34' 3.348"	30° 48' 7.085"	Alfalfa
2	Sohag –Tema	26° 53' 41.863"	31° 26' 33.989"	Wheat
3	Minya – Samalot	28° 19 40.130"	30° 42 9.552"	Alfalfa
4	Minya – Matai	28° 23 58.125"	30° 46 14.230"	Lentil
5	Minya – Maghagha	28° 37' 38.189"	30° 49' 8.758"	Alfalfa
6	Minya – Abo Qorkas	27° 52 3.226"	30° 48 0.528"	Wheat
7	Beni Suef	29° 04' 22.45"	31° 05′ 27.33	Wheat
8	El Giza	30°18' 33.14	31°10′ 91.44	Wheat
9	Monufia - Ashmoon	30°12' 39"	30° 57' 23"	Wheat

 $\textbf{Table 2.} \ \textbf{The spectrum of} \ \textit{Brassica nigra } \ \textbf{macro-\& micro-morphological features in the studied} \ \ \textbf{9 populations}.$

Characters	var. nigra						var. bracteolata		
	Form 1.1	Form 1.2	Form 1.3	Form 2.1	Form 2 .2	Form 2.3	Bract. 1	Bract.2	Bract. 3
Stem:									
Sculpture by SEM (Striate=0 & not so =0)	1	1	1	1	1	1	0	0	0
Presence of verrucate cuticular deposits by SEM (Dense =1 & spare =0)	0	0	0	0	0	0	1	1	1
Basal (Radical) leaf:									
Shape (Pinnatisect =1 & not so =0)	1	1	1	1	1	1	1	1	1
Margin Shape (Serrate=1 & not so =0)	1	1	1	0	0	0	0	0	0
Margin regularity (Regular=1 & Irregularly=0)	1	1	1	0	0	0	0	0	0
Petiole (Petiolate =1 & sessile =0)	1	1	1	1	1	1	1	1	1
Leaf Length (Up to 75 cm=1 & up to 50 cm=0)	1	1	1	0	0	0	0	0	0
Shape (Oblong ovate= 1 & not so 0)	1	1	1	1	1	1	1	1	1
Stomata shape (Kidney =1 & not so 0)	1	1	1	1	1	1	1	1	1
Apex (Acute=1 & not so =0)	1	1	1	1	1	1	0	0	0
Segmentation lobes (3-7 lobes=1 & not so =0)	1	1	1	0	0	0	0	0	0
Width of the upper lobe (up to 5 cm=1 & less than 5 cm=0)	1	1	1	1	1	1	0	0	0
Hairy allover =1 & not so =0	1	1	1	0	0	0	0	0	0
Hairy midrib=1 & not so =0	1	1	1	1	1	1	0	0	0
Stomata position by SEM (On raised ridges=1 & not so=0)	1	1	1	1	1	1	0	0	0
Upper (Cauline) leaf:									
Shape (Ovate =1 & not so =0)	1	1	1	1	1	1	1	1	1
Apex (Acute =1 & not so =0)	1	1	1	1	1	1	1	1	1
Margin (Denticulate=1 & not so =0)	0	0	0	1	1	1	1	1	1
Petiole (Petiolate =1 & sessile =0)	1	1	1	1	1	1	1	1	1
Segmentation lobes (more than 2 =1 & not more than 2 =0)	1	1	1	0	0	0	1	1	1
Upper lobe L mm (Up to $2.5 = 1 & \text{not so } = 0$)	1	1	1	0	0	0	0	0	0
Upper lobe W mm ((Up to 15 = 1 & more than 15 = 0)	0	0	0	1	1	1	0	0	0
Sepal:									
Sepal L mm (From 4-6 mm=1 & not so =0)	1	1	1	1	1	1	1	1	1
Sepal W mm (Up to 1.5 mm = 1 & not so = 0	1	1	1	1	1	1	1	1	1
Shape (Linear=1 & not so =0)	1	1	1	1	1	1	1	1	1
Surface (Hairy =1 & Glabrous =0)	0	0	0	0	0	0	0	0	0
No. of main veins (3 veins=1 & others=0)	1	1	1	1	1	1	1	1	1
Apex (Obtuse=1 & others =0)	1	1	1	1	1	1	1	1	1
Margin (Entire=1 & others =0)	1	1	1	1	1	1	1	1	1
Petal:									
Petal L mm (Up to 14 mm=1 & less than 14 mm=0)	1	1	1	0	0	0	0	0	0
Petal W mm (Up to 6 mm=1 & less than 6 mm=0)	0	0	0	1	1	1	1	1	1
Petal blade L mm (Up to 9 mm=1 & less than 9 mm=0)	1	1	1	1	1	1	0	0	0
Shape of claw (Filiform=1 & not so =0)	1	1	1	1	1	1	1	1	1
Petal surface (Glabrous=1 & Hairy=0)	1	1	1	1	1	1	1	1	1
No. of main veins in petal (Up to 9=1 & less than 9=0)	0	0	0	1	1	1	1	1	1
Apex (Obtuse=1 & others =0)	1	1	1	1	1	1	1	1	1
Margin (Entire=1 & others =0)	1	1	1	1	1	1	1	1	1

492 © 2022 Jordan Journal of B	iologica	ıl Science	es. All rig	thts reserv	ed - Volun	ne 15, Num	ber 3		
Filament L mm (Up to 7mm=1 & less than 7mm=0)	1	1	1	1	1	1	1	1	1
Filament W mm (Up to 0.5mm=1 & less than 0.5 mm=0)	1	1	1	1	1	1	1	1	1
Stamen shape (Linear =1 & not so =0)	1	1	1	1	1	1	1	1	1
Stamen surface (Glabrous=1 & Hairy=0)	1	1	1	1	1	1	1	1	1
Anther:									
Anther L mm (Up to 3mm=1 & less than 3mm=0)	1	1	1	1	1	1	0	0	0
Anther W mm (Up to 1.0 mm=1 & less than 1mm=0)	1	1	1	1	1	1	0	0	0
Anther shape (Oblong=1 & not so=0)	1	1	1	1	1	1	1	1	1
Anther apex (Obtuse=1 & not so=0)	1	1	1	1	1	1	1	1	1
Stigma shape (Capitate=1 & not so =0)	1	1	1	1	1	1	1	1	1
Pedicle									
Pedicle L mm (equal or more than 10=1 & not so=0)	1	1	1	0	0	0	1	1	1
Flower bract:									
Surface (Hairy=1 & Glabrous=0)	1	1	1	0	0	0	0	0	0
Bract venation (Reticulate=1 & not so=0)	1	1	1	1	1	1	1	1	1
Bract margin (Dentate=1 & not so=0)	1	1	1	1	1	1	0	0	0
Apex (Acute=1 & not so=0)	1	1	1	1	1	1	1	1	1
Shape (Ovate=1 & not so=0)	1	1	1	1	1	1	0	0	0
Length cm (Up to 3.5cm=1 & less than 3.5cm=0)	1	1	1	0	0	0	0	1	0
Fruit:									
Fruit L mm (Up to 35mm=1 & more than 35mm=0)	1	1	1	1	1	1	0	0	0
Fruiting part L mm (Up to 20mm=1 & more than 20mm=0)	1	1	1	0	0	0	0	0	0
Fruit peak L mm (Up to 15mm=1 & less than 15mm=0)	1	1	1	1	1	1	0	0	0
Number of seeds/ fruit (Up to 12=1 & more than 12=0)	1	1	1	1	1	1	0	0	0
Surface (Hairy=1 & Glabrous= 0)	0	0	0	0	0	0	0	0	0
Receptacle shape (Flat=1 & not so= 0)	1	1	1	1	1	1	1	1	1
Pollen using SEM:									
Pollen shape (Oblate=1 & not so=0)	1	1	1	1	1	1	0	0	0
Number of colpi (3=1 & not so =0)	1	1	1	1	1	1	1	1	1
Pollen sculpture (Reticulate=1& not so=0)	1	1	1	1	1	1	1	1	1
Endexine sculpture (Warty=1 & not so=0)	1	1	1	0	0	0	1	1	1
Muri-wall (Dense warty=1 & not so=0)	1	1	1	1	1	1	0	0	0
Muri-pattern (Regular=1 & irregular =0)	1	1	1	0	0	0	1	1	1
Polar Axis (P) μm (Equal or less than 20=1 & more than 20=0)	1	1	1	1	1	1	0	0	0
Equatorial Axis $\ L\ \mu m$ (More than 30=1 & less than 30=0)	1	1	1	0	0	0	1	1	1
$P/\:E\:\:\mu m\:\:$ (More than 0.5 =1 & equal or less than 0.5=0)	0	0	0	1	1	1	1	1	1
Colpus Length $\ L\ \mu m$ (More than 22 =1 & equal or less than 22=0)	1	1	1	1	1	1	0	0	0

SEM: Scanning Electron Microscope.

2.2. Chromosome counting

Seeds from ten individual plants were randomly selected from each population of the studied three infraspecific taxa (varieties and Forms1 & 2), for chromosome counting. Ten seeds/taxa were soaked in distilled water for 2 hours, then germinated at 20°C in the dark chamber. Then root tips of about 1.5 cm length were treated at room temperature for 4 hours with colchicine

(C22H25NO6, 0.05 %) then washed by distilled H2O. Overnight fixation was carried out in a freshly prepared farmer's fixative (ethanol/glacial acetic acid, 3: 1). Then, root tips were hydrolyzed using 1 N HCl at 64 C for five minutes. Slides were prepared using 45% acetic acid for squashing the root tips and stained with Aceto-orcein solution. Chromosome counting was visualized in the clearly ten observable cells during the mitotic metaphase.

2.3. Data analysis and karyotyping

In order to prepare the karyotype and ideogram, the chromosome counting was carried out on metaphase cells using the light microscope (Nikon Eclipse EG00 microscope at initial magnification of 2.5X). Ten clearly observable/cells, of the well-spread chromosomes were photographed, using the high-resolution automated karyotyping software processing (Leica CW4000). The two arms of each chromosome were measured, the short arm length (p), the long arm length (q) and the total chromatid length (TL) was calculated (p+q) for each chromosome. The relative chromosome length (RL) was $(\frac{TL}{sumTL} \times 100),$ mean (MRL)/chromosome pair to calculate the relative length of each chromosome pair. The centromeric index (CI) was estimated using the equation $\frac{P}{TL} \times 100$ and the mean centromeric index (MCI) was calculated/ each

centromeric index (MCI) was calculated/ each chromosome pair, which used for determining the centromere position (metacentric chromosome when the CI ranges between 45.0 and 50.0; submetacentric CI ranges from 35 to 44; subterminal for CI less than 35 and telocentric when CI was zero) as reported by (Hassan and Gawad, 2013). It was found more appropriate to use the relative length expressed in percentage of the total length of the complement (Rothfels and Siminovitch, 1958).

2.4. Plant genomic DNA extraction

To study the molecular identity using the DNA markers (nuclear ITS and chloroplast), the total genomic DNA was extracted from fresh young leaves that were grounded in liquid nitrogen, following the steps of CTAB protocol (Doyle, 1991). The extracted DNA pellet washed with 70% alcohol, dried at room temperature, and dissolved in TE buffer.

2.5. Polymerase Chain Reaction (PCR)

The complete ITS region of the ribosomal DNA was amplified with plant specific primer pair ITS-p5/ITS-u4 (Cheng *et al.*, 2016), while the three chloroplast marker-intergenic spacers were amplified using three plastid primer pairs (rps7 & rpsl2.1), (rpoC1 intron.1 & 2) and (trnK intron.1 &2), according to (Haider and Wilkinson, 2011), the sequences of the used primers are given in Table (3).

Amplification was carried out using a thermal cycler (Thermo Hybaid, USA). The PCR mixture (25 μL) contained dNTPs (200 μM), KCL (50 mM), Tris-HCl (10 mm; pH 9.0), MgCl₂ (1.5 mM), 0.1% Triton® X-100, 0.5 μM /primer, one unit of Taq DNA Polymerase (Promega), and template DNA (50 ng). The PCR program was 94 °C (4 min), 34 cycles of 30 s at 94 °C, 40 s at 55 °C and 52°C for both of the rps7 & rps12.1 primer and 1 min (72 °C), the final step was 10 min at 72 °C. The developed PCR products were run in a 1.5% agarose gel with ethidium bromide and visualized under ultraviolet transilluminator.

2.6. Sequencing of amplified DNA

Sequencing reactions were performed in a MJ Research PTC-225 Peltier Thermal Cycler using a ABI PRISM BigDyeTM Terminator Cycle Sequencing Kits with AmpliTaq DNA polymerase (FS enzyme; Applied Biosystems), according to the Sigma laboratory protocol supplied by the manufacturer. Single-pass sequencing was

performed on each template using primers. The fluorescent-labeled fragments were purified from the unincorporated terminators with BigDye XTerminator™ purification protocol. The PCR products were re-loaded in dis. H2O and subjected to electrophoresis in an ABI 3730xl sequencer (Applied Biosystems), then sequence was achieved by Clone Manager 9 (Sci-Ed, Cary, NC, USA). The obtained sequences were aligned by CLUSTAL W (Thompson et al., 1994). Similarities in nucleotide sequence were determined using BLAST, version 2.0 (National Center for Biotechnology Information databases); jModelTest 0.1.1 program was used to find the model of sequence evolution that fitting the data (Posada, 2008). Neighbor-Joining method NJ was used for phylogenetic analyses (Saitou and Nei, 1987) with the Maximum Composite Likelihood method (Felsenstein, 1992) in MEGA 6.0 (Tamura et al., 2013).

3. Results

3.1. Morphological features

The morphological investigations of the collected 9 populations using the 70 macro-and micro-morphological characters (Table 3), confirming the presence of two varieties namely var. *bracteolata* and var. *nigra*. The fruit peak and trichomes are the differential characters delimiting the studied taxa, the differential key is:

Leaves glabrous, fruit peak up to 1/4 fruit length

..... var. bracteolata

Leaves hairy, fruit peak up to 1/2 fruit length

..... var. nigra

2- Basal leaves to 30 cm, hairs on all over the surface Form 1

Basal leaves to 75 cm, hairs found only on leaf mid-rips Form 2

The retrieved heat map based on the detected morphological characters (Table 2 & Figure 1), showing two hierarchical clusters each/variety, one of them including the six populations of var. *nigra* (Form 1 & Form 2) indicating that the phenotypic features are distinctive to the infraspecific level.

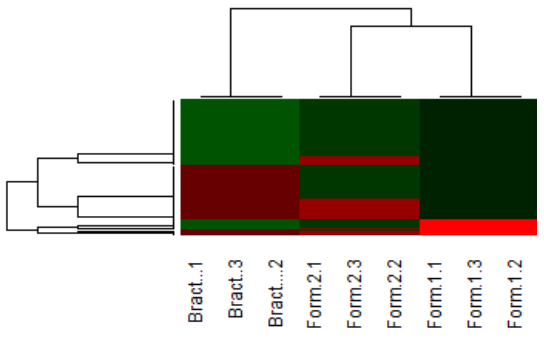


Figure 1. Heat map with hierarchical clustering of the 9 studied *Brassica nigra* populations (1-9; X-axis), Y-axis representing 70 micro-& macro-morphological characters. Red indicates a high level of expression; green represents a low level of expression; increasing color intensity is directly proportional with the value of the studied character. Using "R" software for windows version 3.5.1. (Bract. 1,2 & 3: var. *bracteolata*. Form 1.1,1.2 & 1.3: var. *nigra* Form 1 and Form 2.1,2.2 & 2.3: var. *nigra* Form 2). Cytogenetics (chromosome number and karyotyping):

Chromosome count of *Brassica nigra* (ten well-spread root cells/ population) in the mitotic metaphase revealed that all populations have the same diploid chromosome number (2n=16) as shown in Figure (2). Chromosomes were observed in metaphase and the karyotyping of the chromosome pairs were arranged in descending order (from 1 - 8; Figure 3), while the karyotyping measures as short arm (p), long arm (q) and total lengths (TL), the mean relative length (MRL), the mean centromeric index (MCI) were taken for each chromosome/taxa (Table 4).

The retrieved results showed that Chromosomes of B. nigra are small in size, the total genomic length was 27.05 μm in var. nigra Form 1, 25.13 μm in var. nigra Form 2, while the smallest value (24.6 µm) was in var. bracteolata. Moreover, the chromosomes are highly variable referring to their mean relative length (MRL; Fig. 4 and Table 4). The chromosome pair no. "1" is the longest among the studied taxa, its length ranges from 4.85 µm in var. nigra Form 1 to 4.53 µm in var. bracteolate, and its mean relative length (MRL) ranges from 17.93% in var. nigra Form 1 to 18.70% in var. nigra Form 2. The shortest chromosome pair is the chromosome pair number 8, its length ranges from 2.11 µm to 2.13 µm in var. nigra Form 1 and 2, respectively. The mean relative length (MRL) ranges from 7.80% to 8.62% for var. nigra Form 1 and var. bracteolate; respectively (Table 4).

The observed eight chromosome pairs are variable referring to their mean centromeric index (MCI), classifying the chromosomes based on the centromere position into two types: metacentric and acrocentric (Figure 5 and Table 4). The chromosome pairs 1-4 are metacentric while chromosomes 5-8 are acrocentric in all the studied taxa. Satellite was observed on the chromosome pair no. "6" distinguished var. bracteolata from var. nigra (Figure 6).

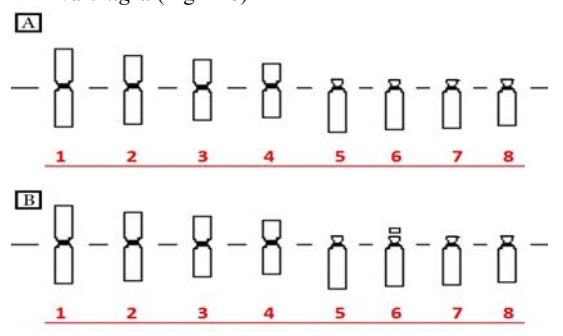


Figure (6): Idiogram of haploid set of chromosomes of *B. nigra* showing metacentric (1-4) and acrocentric (5-8) chromosomes. A: var. *nigra* Forms1 and 2 (without satellite); B: var. *bracteolata* (has satellite in chromosome no. 6).

3.2. Molecular identity

3.2.1. Amplification of internal transcribed spacer (ITS) nrDNA genes:

The amplified products of PCR using ITS-p5 and ITS-u4 plant specific primers showed one monomorphic band of c. 650 bp for the three representative populations/taxa (varieties and forms; Fig. 7). These amplified fragments were sequenced; var. *bracteolata* the length of the ITS region was 630 bp, and notable base divergence recorded in var. *nigra* Form 1 (652 bp) reached 656 bp in var.

nigra Form 2, 161 bp for the 5.8S nrDNA gene and 197-216 bp for the ITS2 region.

3.2.2. Amplification of chloroplast markers:

3.2.2.1. Rps intergenic spacer:

Using rps7 & rps12.2 universal primers, single monomorphic band c. 400 bp was produced as PCR product of three representative populations in each studied taxa (Fig. 7). The amplified fragments were subjected to DNA sequencing. The length of rps region varied from 369 bp in var. 494racteolate, 371 bp in var. nigra Form 1 to 372 bp in var. nigra Form 2.

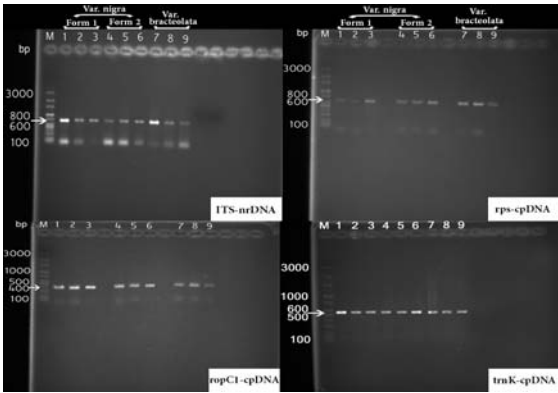


Figure 7. Agarose gel-electrophoresis of PCR amplification bands. M: DNA ladder (100 bp - 3000 bp). Lanes (1-9): amplicons of targeted locus in the studied 9 populations of var. *bracteolata* and var. *nigra*; denoting the close genetic affinity between the studied populations.

3.2.2.2. ropC1 intron:

The PCR products of ropC1 intron amplification show bands c. 620 bp for the populations/studied taxa (Fig. 7). The amplified fragments were subjected to DNA sequencing. The length of ropC1 intron varied form 612 bp in var. 494racteolate, 618 bp in var. nigra Form 1 to 620 bp in var. nigra Form 2.

3.2.2.3. trnK intron:

The amplified products of PCR using trnK intron 1 and trnK intron 2 primers revealed one monomorphic band with about 550 bp in all the studied taxa (Fig. 7). The amplified fragments were subjected to DNA sequencing, the length of trnK intron varied form 568 bp in var. bracteolata, 587 bp in var. nigra Form 1 to 556 bp in var. nigra Form 2.

3.2.3. Molecular authentication:

Accession numbers of nucleotide sequences for the ITS region and the three studied barcodes (chloroplast noncoding regions) were obtained from complete sequence data that have been deposited in EMBL/GenBank/DDBJ nucleotide sequence data libraries. The sequences of the studied B. nigra taxa were submitted to Gene-Bank database with accession numbers outlined in Table (5), then compared with that of B. nigra retrieved from Gene-Bank database search via Basic Local Alignment Search Tool (BLAST) as outlined in Table (5). The constructed cladogram of ITS region and the three studied chloroplast non coding regions are the same, each exhibited two branches each representing variety, one for variety bracteolata and the other cluster including the two Forms (Form 1 & Form 2) of the variety nigra (Fig. 8).

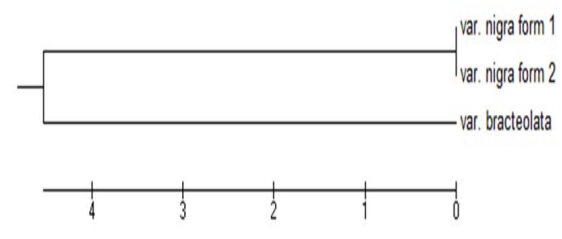


Figure 8. Cladogram showing varieties of *Brassica nigra* based on the nucleotide sequences of ITS region and three chloroplast regions (using Mega 6 program); denoting the genomic similarity of Forms 1 &2.

4. Discussion

The combined morphological data (70 characters) retrieved from the studied wild *Brassica nigra* populations (Table 3), and the developed consensus tree (Fig. 1), delimited all the morphological diversity under two distinct varieties var. *bracteolata* and var. *nigra*. This study distinguished the later variety into two Forms (Form 1 & Form 2), by their basal leaves up to 75 cm in Form 2 and 30 cm in Form 1); while var. *bracteolata* was identified earlier in the Egypt (Täckholm, 1974). The observed quantitative morphological (phenotypic) variations at the infraspecific level of *B. nigra* may be induced by the natural selection as claimed by (Österberg *et al.*, 2002).

Table 3. The oligonucleotide sequences of forward and reverse primers used during this study.

Primers	Sequence
Forward primer ITS-	5'-CCTTATCAYTTAGAGGAAGGAG-3'
p5	
Reverse primer ITS-	5'-RGTTTCTTTTCCTCCGCTTA-3'
u4	
Forward primer	5'-GGTGAAAATCTCATGTACG-3'
rps7&rpsl2.1.1	
Reverse primer	5'-TTTCTAGCGATTCACATGG-3'
rps7&rpsl2.1.2	
Forward primer	5'-GAGTAACATGAAGCTCAG-3'
rpoC1 intron.1	
Reverse primer	5'-GTTTCCTTCATCCGGCT-3'
rpoC1 intron.2	
Forward primer trnK	5'-GTCTACATCATCGGTAGAG-3'
intron.1	
Reverse primer trnK	5'-CAACCCAATCGCTCTTTTG-3'
intron.2	

The morphological diversity of the studied *B. nigra* taxa, is not reflected to its chromosome number, where all these taxa are similar (2n=16; Fig. 2 & Table 4). This indicated that the studied wild populations were diploid *Brassica* (genome BB). Identification of this BB genome in Egypt will be of future applicability in breeding programs of *Brassica* crops (Westman *et al.*, 1999), as source of the drought tolerant genes (Groat, 2003; Pradhan *et al.*, 2011), and its importance extended to the evolutionary lineages of both of the *nigra* and the *rapa/oleracea* lineages used in crop improvement (Yang *et al.*, 2002). The observed chromosome number in the *B. nigra* taxa was reported earlier (Nakayama and Fukui, 1997).

 Table 4. The karyotype features of studied Brassica nigra taxa.

var. nigra Form 1						
Chromosome number	рμш	q μm	p+q μm	MRL%	MCI%	CP
1	2.4	2.45	4.85	17.93	49.48	metacintric
2	1.99	2.39	4.38	16.19	45.43	metacintric
3	1.97	2.4	4.37	16.16	45.08	metacintric
4	1.89	2.35	4.24	15.67	44.58	metacintric
5	0.15	2.3	2.45	9.06	6.12	acrocentric
6	0.15	2.25	2.4	8.87	6.25	acrocentric
7	0.15	2.1	2.25	8.32	6.67	acrocentric
8	0.11	2	2.11	7.80	5.21	acrocentric
Total genome length			27.05			
var. nigra Form 2						
Chromosome number	рμш	q μm	p+q μm	MRL%	MCI%	CP
1	2.3	2.4	4.7	18.70	48.94	metacintric
2	1.91	2	3.91	15.56	48.85	metacintric
3	1.87	1.95	3.82	15.20	48.95	metacintric
4	1.74	1.87	3.61	14.37	48.20	metacintric
5	0.13	2.25	2.38	9.47	5.46	acrocentric
6	0.14	2.2	2.34	9.31	5.98	acrocentric
7	0.14	2.1	2.24	8.91	6.25	acrocentric
8	0.13	2	2.13	8.48	6.10	acrocentric
Total genome length			25.13			
var. bracteolata						
Chromosome number	рμт	q μm	p+q μm	MRL%	MCI%	CP
1	2.21	2.32	4.53	18.41	48.79	metacintric
2	1.79	1.99	3.78	15.37	47.35	metacintric
3	1.77	1.9	3.67	14.92	48.23	metacintric
4	1.75	1.9	3.65	14.84	47.95	metacintric
5	0.1	2.26	2.36	9.59	4.24	acrocentric
6	0.15	2.2	2.35	9.55	6.38	acrocentric
7	0.14	2	2.14	8.70	6.54	acrocentric
8	0.12	2	2.12	8.62	5.66	acrocentric
Total genome length			24.6			

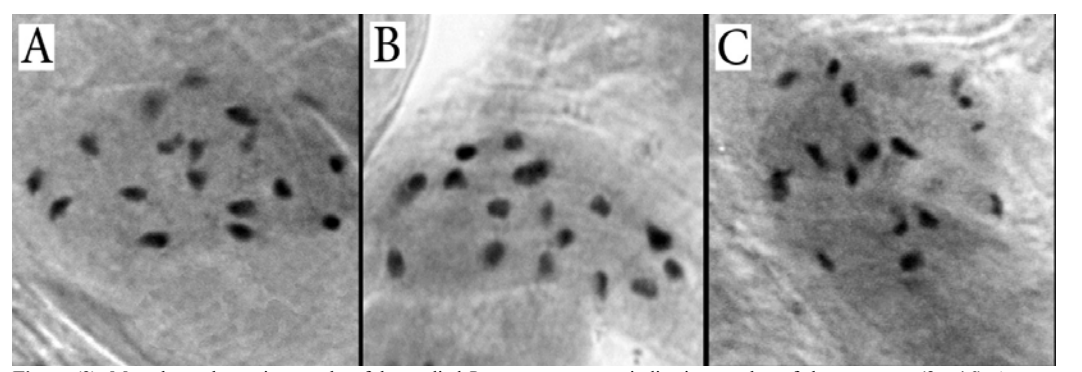


Figure (2): Metaphase photomicrographs of the studied *Brassica nigra* taxa indicating number of chromosomes (2n=16). A: var. *nigra* Form 1, B: var. *nigra* Form 2 and C: var. *bracteolata*

The observed karyotype analysis (Table 4; Figs 3,4 & 5) showed that the chromosomes are small in size; this result was supported by (Schmidt and Bancroft, 2011).

The small-size chromosome as in *Brassica nigra*, makes its karyotyping study challenging (Kulak *et al.*, 2002), however, some studies have provided information about

chromosome morphology of the B genome (Cheng and Heneen, 1995; Fukui et al., 1998; Hasterok and

Mahszynska, 1997; Lan *et al.*, 1991; Maćkowiak and Heneen, 1999; Robbelen, 1960; This *et al.*, 1990).

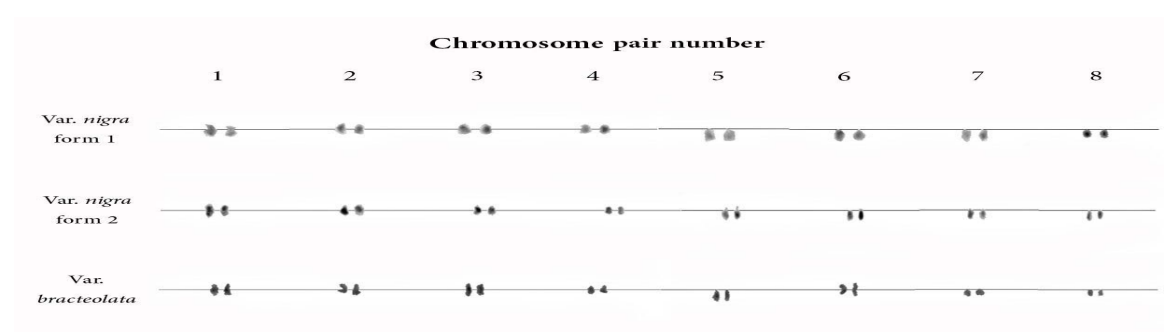


Figure (3): Karyotypes of the Brassica nigra taxa.

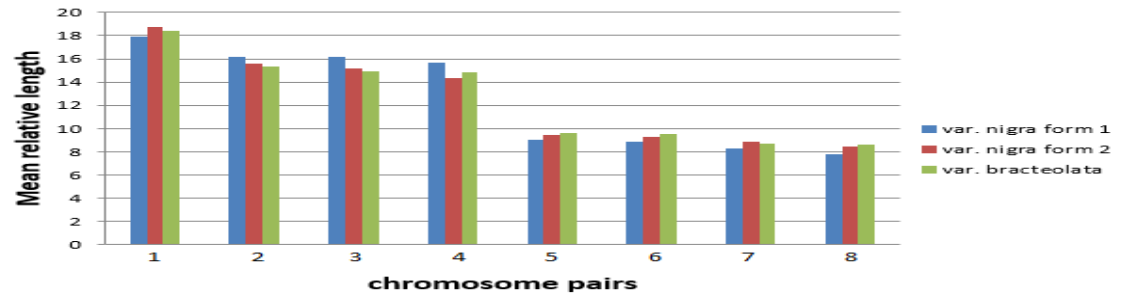


Figure (4): Mean relative length (MRL) of each chromosome pair in the studied B. nigra taxa.

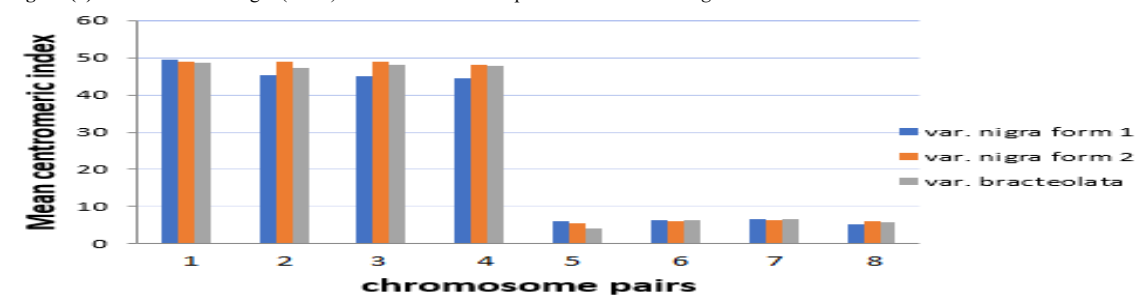


Figure 5. Mean centromeric index (MCI) of each chromosome pair in the studied B. nigra taxa.

The karyotyping of the studied *B. nigra* taxa showed chromosomes features distinguished between the studied varieties, referring to their mean relative length (MRL), the longest chromosome (chromosome no. 1; MRL ranges from 17.93% in var. *nigra* Form "1" to 18.70% in var. *nigra* Form "2"), where var. *bracteolata* is characterized by an intermediate value (18.41%); similar observation was noticed in the shortest chromosome (chromosome no. 8; Table 4 & Fig. 4). Consistent results were reported in *B. nigra* using the Fish technique (Wang *et al.*, 2017). This observed infraspecific chromosomal variability in the studied *B. nigra* taxa indicated that each taxon retains its genotypic identity.

However, the achieved results (Table 4 & Fig. 5), showed variable mean centromeric index (MCI), classifying the chromosomes into two types: metacentric and acrocentric in all the studied taxa. Wang *et al.*, (2017), reported that all chromosomes of *B. nigra* are metacentric with an arm ratio of 1.12–1.49.

The karyotyping (Fig. 6) indicates the presence of satellite in the chromosome pair no. "6" which characterizes var. bracteolata from var. nigra. The presence of satellite was supported by Wang et al., (2017), who found that the satellites were abundant in the whole genome of B. nigra; in the same study he reported the

presence of 6 satellite repeats in metaphase cells of *B. nigra* root tips. Cheng and Heneen (1995) and Fukui *et al.* (1998) noticed the presence of three nucleolar chromosome pairs with satellites in mitotic divisions, while similar observation was reported during meiotic divisions of *B. nigra* by Maćkowiak and Heneen (1999). Only two pairs of chromosomes to be satellited in mitotic divisions were reported by other studies (Robbelen, 1960; This *et al.*, 1990) and in meiotic divisions (Lan *et al.*, 1991; Sikka, 1940). Accordingly, it is expected that satellite associations among the nucleolar chromosomes were predominate during diakinesis in *B. nigra* (Maćkowiak and Heneen 1999).

The data retrieved from the nuclear DNA marker (ITS, Fig. 7) and the chloroplast DNA markers (rps, ropC & trnK; Table 5 & Fig. 7), showed that the genetic divergence of var. bracteolata is higher than that of var. nigra the divergence is more notable in ITS region. This is attributed to the rate of evolution (limited deletionsinsertion and point mutation) of chloroplast genome being much lower than that in the nuclear genome (Zhu et al., 2021). The obtained nuclear data (Table 5) elucidate the phylogenetic relationship between the studied wild taxa and that from other geographic regions; Zhu et al., (2021) reported that several studies used the chloroplast genome

to study the phylogenetic relationships in family Brassicaceae. The congruent data of the nuclear and chloroplast markers enhance the author to support treating these identified morphological taxa as distinct varieties not as synonyms. This postulation was supported by Yang et al., (2002), who reported that the chloroplast noncoding region between trnD & trnT and that between trnT & trnF are useful for studying the interspecific relationships among angiosperms. The achieved results for the cpDNA markers reveal the intraspecific polymorphisms in Egyptian wild B. nigra taxa, is a useful tool for conservation and as marker assisted Brassica breeding programs, as reported by Sarin et al. (2015). The detected low divergence between the two forms of var. nigra (Table 5 & Fig. 8) indicate that these forms were recently diversified; relevant data were reported by Mummenhoff et al., 2001) in section Lepia (Brassicaceae), and other Brassica species (Zhu et al., 2021).

The studied 9 populations of wild *B. nigra* were collected from different localities along the Nile valley and

Delta (Table 1), showing that the identified varieties are not correlated with geographical distribution, which could be explained by adaptive mechanism of natural selection (Österberg *et al.*, 2002).

The authentication of the molecular data in the GenBank confirmed that the chloroplast marker showed that 100% similarity to the accession number (KT878383; Table 5), with *var. nigra* Form "1" and Form "2". Moreover, the current results obtained using chloroplast DNA of *Brassica nigra* from Egypt as part from its native range, this range include North African and Mediterranean region (Mummenhoff *et al.*, 2001). These results may help to identify the species distribution range. The population origin and distribution range can be achieved by using chloroplast DNA and also for population genetics/ phylogeographic analyses (Oduor *et al.*, 2015).

Table 5. Authentication of the studied B. nigra taxa compared to the GenBank data.

Studied Taxa Name Accession numbers		- BLAST Result	Accession numbers retrieved	Locus	Similarity %
		- DLAST Result	from database	Locus	Sillilarity 70
	MN480491	Brassica nigra clone 136	KX709349 (South Korea)	ITS	97.99%
var. bracteolata	MN869001	Chloroplast complete genome	KT878383 (Korea)	rps	99.68%
	MN886246	Chloroplast complete genome	KT878383 (Korea)	ropC	93.50%
	MN886249	Chloroplast complete genome	KT878383 (Korea)	trnK	95.74%
	MN480492	Clone 133	KX709348 (South Korea)	ITS	98.60%
F 1	MN869002	Chloroplast complete genome	KT878383 (Korea)	rps	100%
var. nigra Form 1	MN886247	Chloroplast complete genome	KT878383 (Korea)	ropC	98.84%
	MN886250	Chloroplast complete genome	KT878383 (Korea)	trnK	98.91%
	MN480493	Clone 95	KX709346 (South Korea)	ITS	98.40%
var. nigra Form 2	MN869003	Chloroplast complete genome	KT878383 (Korea)	rps	100%
	MN886248	Chloroplast complete genome	KT878383 (Korea)	ropC	99.42%
	MN886251	Chloroplast complete genome	KT878383 (Korea)	trnK	98.94%

Finally, this study recommends the application of multidiscipline approach in taxonomy to resolve the identity of the infraspecific level for the *Brassica nigra*, which possesses morpho-plasticity and wide geographic range crop similar to many wild plants' relatives.

References

Al-Shehbaz IA, Beilstein MA and Kellogg EA. 2006. Systematics and phylogeny of the Brassicaceae (Cruciferae): an overview. *Plant Syst. Evol.*, **259**: 89-120.

Amer W, Shoulkamy M, Faried A and El-Baset A. 2019. Autotaxonomy of *Brassica nigra* (L.) Koch (Brassicaceae) in Egypt. *Egypt. J. Bot.*, **59**: 439-450.

Bailey CD, Koch MA, Mayer M, Mummenhoff K, O'Kane Jr SL, Warwick SI, Windham MD and Al-Shehbaz IA. 2006. Toward a global phylogeny of the Brassicaceae. *Mol Biol Evol.*, **23**: 2142-2160.

Baldwin BG, Sanderson MJ, Porter JM, Wojciechowski MF, Campbell CS and Donoghue MJ. 1995. The ITS region of nuclear ribosomal DNA: a valuable source of evidence on angiosperm phylogeny. *Ann. Missouri Bot. Gard.*, 247-277.

Boulos L. 1995. **Flora of Egypt**. Checklist. *Al-Hadara Publishing, Cairo, Egypt*. 287 pp..

Boulos L. 1999. **Flora of Egypt**, 1 (Azollaceae–Oxalidaceae). *Al-Hadara Publishing, Cairo, Egypt.* 418 pp.

Boulos L. 2009. **Flora of Egypt checklist**, revised annotated edition. *Al-Hadara Publishing*, *Cairo*: 198-201.

Cheng B and Heneen W. 1995. Satellited chromosomes, nucleolus organizer regions and nucleoli of *Brassica campestris* L., *B. nigra* (L.) Koch, and *Sinapis arvensis* L. *Hereditas*, **122**: 113-118.

Cheng T, Xu C, Lei L, Li C, Zhang Y and Zhou S. 2016. Barcoding the kingdom Plantae: new PCR primers for ITS regions of plants with improved universality and specificity. *Mol. Ecol. Resour.*, **16**: 138-149.

Clegg MT. 1993. Chloroplast gene sequences and the study of plant evolution. *PNAS*, **90**: 363-367.

Doyle J. 1991. **DNA protocols for plants**. Molecular techniques in taxonomy. Springer, pp. 283-293.

El Rabiai G. 2015. Systematic consideration of petiole anatomy of some taxa of Brassicaceae in Libya. *BRI*, **8**: 36-40.

Felger R, Herbarium F, Rutman S and Malusa J. 2015. Ajo Peak to Tinajas Altas: A Flora of Southwestern Arizona Part 11. Eudicots: Brassicaceae and Burseraceae. *Phytoneuron*: 1-48.

Felsenstein J. 1992. Phylogenies from restriction sites: a maximum-likelihood approach. *Evolution*, **46**: 159-173.

Fukui K, Nakayama S, Ohmido N, Yoshiaki H and Yamabe M. 1998. Quantitative karyotyping of three diploid *Brassica* species by imaging methods and localization of 45S rDNA loci on the identified chromosomes. *Theor. Appl. Genet.*, **96**: 325-330.

Gomez-Campo C. 1978. **Studies on Cruciferae**. IV. Chorological notes. Anales.

Greilhuber J and Ehrendorfer F. 1988. Karyological approaches to plant taxonomy. *ISI atlas of science. Anim. Plant Sci (USA)*.

Groat CM. 2003. The sodium chloride tolerance of *Brassica nigra*. Dissertation, University of California

Guerra M. 2008. Chromosome numbers in plant cytotaxonomy: concepts and implications. *Cytogenet. Genome Res.*, **120**: 339-350.

Haider N. 2011. Chloroplast-specific universal primers and their uses in plant studies. *Biol. Plant.*, **55**: 225-236.

Haider N and Wilkinson M. 2011. A set of plastid DNA-specific universal primers for flowering plants. *Russ. J. Genet.*, **47**: 1066.

Hassan NA and Gawad M. 2013. Morphological karyotype analysis of eleven pomegranate cultivars. *Am Eurasian J Agric Environ Sci*, **13**: 1562-1567.

Hasterok R and Mahszynska J. 1997. Analiza cytogenetyczna wybranych gatunków Brassica. Materiały z I Krajowej Konferencji "*Hod. Rośl.*". Poznań.

Jiang J, Wang Y, Zhu B, Fang T, Fang Y and Wang Y. 2015. Digital gene expression analysis of gene expression differences within Brassica diploids and allopolyploids. *BMC Plant Biol.*, **15**: 22.

Karpechenko G. 1922. The number of chromosomes and genetic correlation of cultivated Cruciferae. *Bull. Appl. Bot. Gen. Plant Breed.*, 13: 3-14.

KULAK S, HASTEROK R and MALUSZYNSKA J. 2002. Karyotyping of *Brassica* amphidiploids using 5S and 25S rDNA as chromosome markers. *Hereditas*, **136**: 144-150.

Lan Z, Luo P, Zhou H and Zhang X. 1991. Comparison of the karyotype of some *Brassica* species. *J. Sichuan Univ. Nat. Sci. Edition*, **28**: 3-44.

Li Y, Liu Z, Wang Y, Yang N, Xin X, Yang S and Feng H. 2012. Identification of quantitative trait loci for yellow inner leaves in Chinese cabbage (*Brassica rapa* L. ssp. pekinensis) based on SSR and SRAP markers. *Sci. Hortic.*, **133**: 10-17.

Maćkowiak M and Heneen W. 1999. Meiotic karyotypes of the B genomes of *Brassica nigra* and *B. carinata*. *Hereditas*, **130**: 131-135

Mummenhoff K, Brüggemann H and Bowman J. 2001. Chloroplast DNA Phylogeny and Biogeography of Lepidium (Brassicaceae). *Am. J. Bot.*, **88**: 2051-2063.

Nakayama S and Fukui K. 1997. Quantitative chromosome mapping of small plant chromosomes by improved imaging on CHIAS II. *Genes Genet. Syst.*, **72**: 35-40.

Negi M, Sabharwal V, Bhat S and Lakshmikumaran M. 2004. Utility of AFLP markers for the assessment of genetic diversity within *Brassica nigra* germplasm. *Plant Breed.*, **123**: 13-16.

Oduor AM, Gómez JM, Herrador MB and Perfectti F. 2015. Invasion of *Brassica nigra* in North America: distributions and origins of chloroplast DNA haplotypes suggest multiple introductions. *Biol. Invasions*, 17: 2447-2459.

Österberg MK, Shavorskaya O, Lascoux M and Lagercrantz U. 2002. Naturally occurring indel variation in the *Brassica nigra* COL1 gene is associated with variation in flowering time. *Genetics*, **161**: 299-306.

Pires JC, Zhao J, Schranz ME, Leon EJ, Quijada PA, Lukens LN and Osborn TC. 2004. Flowering time divergence and genomic rearrangements in resynthesized *Brassica* polyploids (Brassicaceae). *Biol. J. Linn. Soc.*, **82**: 675-688.

Posada D. 2008. jModelTest: phylogenetic model averaging. *Mol. Biol. Evol.*, **25**: 1253-1256.

Pradhan A, Nelson MN, Plummer JA, Cowling WA and Yan G. 2011. Characterization of *Brassica nigra* collections using simple sequence repeat markers reveals distinct groups associated with geographical location, and frequent mislabelling of species identity. *Genome*, **54**: 50-63.

Rakow G. 2004. Species origin and economic importance of *Brassica*. **Brassica**. Springer, pp. 3-11.

Robbelen G. 1960. Beitrage zur analyse des *Brassica* genomes. *Chromosoma*, **11**: 205-228.

Rothfels K and Siminovitch L. 1958. An air-drying technique for flattening chromosomes in mammalian cells grown in vitro. *Stain Technol.*, **33**: 73-77.

Roy N. 1978. A study on disease variation in the populations of an interspecific cross of *Brassica juncea* L. x *B. napus* L. *Euphytica*, **27**: 145-149.

Ruangsuttapha S, Eimert K, Schröder M-B, Silayoi B, Denduangboripant J and Kanchanapoom K. 2007. Molecular phylogeny of banana cultivars from Thailand based on HAT-RAPD markers. *Genet. Resour. Crop Evol.*, **54**: 1565-1572.

Saitou N and Nei M. 1987. The neighbor-joining method: a new method for reconstructing phylogenetic trees. *Mol. Biol. Evol.*, 4: 406-425

Sarin B, Martín JP, Kaula BC and Mohanty A. 2015. Chloroplast DNA variations in wild *Brassicas* and their implication in breeding and population genetics studies. *Scientifica*, **2015**.

Schmidt R and Bancroft I. 2011. Genetics and Genomics of the Brassicaceae. Springer.

Schranz ME, Quijada P, Sung SB, Lukens L, Amasino R and Osborn TC. 2002. Characterization and effects of the replicated flowering time gene FLC in *Brassica rapa*. *Genetics*, **162**: 1457-1468.

Seol YJ, Kim K, Kang SH, Perumal S, Lee J and Kim CK. 2015. The complete chloroplast genome of two *Brassica* species, *Brassica nigra* and *B. oleracea*. *Mitochondrial DNA A: DNA Mapp. Seq. Anal.*, **28**: 167-168.

Sikka S. 1940. Cytogenetics of Brassica hybrids and species. *Genetics*, **40**: 441-474.

Simon UK, Trajanoski S, Kroneis T, Sedlmayr P, Guelly C and Guttenberger H. 2012. Accession-specific haplotypes of the internal transcribed spacer region in *Arabidopsis thaliana*—a means for barcoding populations. *Mol. Biol. Evol.*, **29**: 2231-2239

Song K, Osborn T and Williams P. 1988. *Brassica* taxonomy based on nuclear restriction fragment length polymorphisms (RFLPs). *Theor. Appl. Genet.*, **75**: 784-794.

Täckholm V. 1974. Students' flora of Egypt, 2nd. Cairo University, Egypt, 888.

Taiyan Z, Lianli L, Guang Y and Al-Shehbaz IA. 2001. Flora of China, Brassicaceae (Cruciferae). 8: 1-193.

Tamura K, Stecher G, Peterson D, Filipski A and Kumar S. 2013. MEGA6: molecular evolutionary genetics analysis version 6.0. *Mol. Biol. Evol.*, **30**: 2725-2729.

This P, Ochoa O and Quiros C. 1990. Dissection of the *Brassica nigra* genome by monosomic addition lines. *Plant Breed.*, **105**: 211-220.

Thompson JD, Higgins DG and Gibson TJ. 1994. CLUSTAL W: improving the sensitivity of progressive multiple sequence alignment through sequence weighting, position-specific gap penalties and weight matrix choice. *Nucleic Acids Res.*, **22**: 4673-4680.

Tsunoda S. 1980. **Eco-physiology of wild and cultivated formsin** *Brassica* **and allied genera**. Brassica crops and wild allies.[I]. 109-120.

Vaughan J. 1977. A multidisciplinary study of the taxonomy and origin of *Brassica* crops. *BioScience*, **27**: 35-40.

Wang GX, He QY, Macas J, Novák P, Neumann P, Meng DX, Zhao H, Guo N, Han S and Zong M. 2017. Karyotypes and distribution of tandem repeat sequences in *Brassica nigra* determined by fluorescence in situ hybridization. *Cytogenet. Genome Res.*, **152**: 158-165.

Warwick S. 2011. Brassicaceae in agriculture. In 'Genetics and genomics of the Brassicaceae'.(Eds R Schmidt, I Bancroft) **Plants Genetics and Genomics**: Crops and Models Series, Vol. 9. Springer: Berlin.

Westman AL, Kresovich S and Dickson MH. 1999. Regional variation in *Brassica nigra* and other weedy crucifers for disease reaction to *Alternaria brassicicola* and *Xanthomonas campestris pv. campestris*. *Euphytica*, **106**: 253-259.

Yang YW, Tai P-Y, Chen Y and Li WH. 2002. A study of the phylogeny of *Brassica rapa*, *B. nigra*, *Raphanus sativus*, and their related genera using noncoding regions of chloroplast DNA. *Mol. Phylogenet. Evol.*, **23**: 268-275.

Zhu B, Qian F, Hou Y, Yang W, Cai M and Wu X. 2021. Complete chloroplast genome features and phylogenetic analysis of Eruca sativa (Brassicaceae). *PLOS ONE*, **16**: e0248556.



Jordan Journal of Biological Sciences

Molecular Genetic Identificatin of Plants of the Genus Artemisia L. Growing in Southern Regions of Kazakhstan

Zhanar Rakhimberdiyeva¹, Anar Kaliyeva^{1,*}, Ahmet Aksoy², Bekbossyn Kassymbayev³, Galiya Medeuova¹

¹Kazakh National Women's Teacher Training University, 99 Aiteke bi St., Almaty, Republic of Kazakhstan; ²Akdeniz Üniversitesidisabled, 07070 Konyaalti, Antalya, Turkey; ³Kazakh National Agrarian University, 8 Albay St., Almaty, 050010, Republic of Kazakhstan

Received: August 2, 2021; Revised: September 30, 2021; Accepted: October 9, 2021

Abstract

The purpose of this research study is to carry out a molecular genetic identification of the plant species of the genus Artemisia L. growing in Southern Kazakhstan. Such methods as barcoding, PCR analysis, sequencing and electrophoresis were involved. In the course of DNA barcoding, universal plastidial markers for plants were used: rbcL, matK and trnH-psbA. Three samples of Artemisia L. plants were studied for further determination of genetic relationship between species, and identification thereof. Molecular genetic passportization was done based on the obtained results. Molecular genetic analysis enabled identification of the species-level for Artemisia L. samples, and selection of the most promising plants. It was demonstrated that all samples belong to the same species, namely Artemisia annua L. The longest genetic distance between contrast samples is 0.9%. The advised methodology may serve as a model for genetic passportization of resource plant species, as well as an approach to assessing the state of gene pools in population.

Keywords: genetic analysis; molecular markers; DNA markers; genetic passportization; Artemisia L.

1. Introduction

Botany being part of the biodiversity conservation system and the source of new technologies, currently represents one of the priority areas for scientific development. Fundamental research is in full swing worldwide addressing the issues of systematics, floristics, and genetics for rational use and protection of plants (Pavlov, 1961; Aubakirova et al., 2014; Chen et al., 2010; Graham et al., 2010).

In consideration of highly informative content of DNA molecules, a number of molecular genetic analyses of cultivated plants using molecular markers, known as DNA markers, is rapidly on the rise in the global scientific practice (Drobot and Matveeva, 2015; Leonova, 2015; Chase, 2003). Such methods of DNA molecular analysis can be used for genetic passportization of plant varieties instead of the low-informative methods of protein marker analysis (Cho et al., 2004; Hajibabaei et al., 2007; Kaliyeva et al., 2015).

At present, the molecular or DNA marker detection technologies have become a relevant standard for plant identification, and are increasingly and widely used around the world (Valentini et al., 2009). Their introduction provides for accurate and quick identification of genetic diversity of populations, subspecies, species, as well as differentiation of higher taxonomic ranks: genus and family. Besides, it makes it possible to create the genetic fingerprints of varieties and, from the cost perspective, to determine economically valuable criteria as early as at the initial stage of selection at the level of DNA (Delabays et al., 2001; Graham et al., 2010). Such methods can become

the basis for genetic passportization of varieties, lines and hybrids of various cultivated plants. Study and conservation of plant genetic resources, including medicinal plants, is the key aspect of sustainable development of agroindustry in any country. The loss of such resources and, consequently, of genetic diversity, represents a harsh reality of today (Mezhnina and Urbanovich, 2016; Rzepka-Plevneš et al., 2009).

Among the most effective and inexpensive methods for detecting intraspecific polymorphism are such analyses as ISSR (Inter Simple Sequence Repeats, with its primer comprising a microsatellite sequence); SSR (Simple Sequence Repeats: microsatellite markers); and SNP (Single Nucleotide Polymorphism). SNP analysis is the most informative of them, and it is likely to experience wide acceptance in genetic testing and breeding of cultivated plants. It is acknowledged, that different types of markers are suitable for studying polymorphism both within one species and within higher taxonomic ranks (genus, family, etc.) (Omasheva et al., 2016; Sukhareva and Kuluev, 2018; Pavlov, 1961).

A range of papers discuss that rbcL gene of the chloroplast genome can be used for phylogenetic analysis (Cai et al., 2017; Alrawashdeh, 2011; Ferreira et al., 2005; Kavrakova et al., 2015). RbcL gene underwent in-depth research, and is now widely used in the phylogenetic analysis of plants (Omasheva et al., 2016; Boronnikova, 2009; von Cräutlein et al., 2011). The resolution of this gene is quite low. In this respect, for the purposes of the phylogenetic analysis, it is used in conjunction with other markers, such as matK and trnH-psbA.

MatK gene is one of the fastest evolving plastidial genes of plants; and together with other markers used in

barcoding, it is responsible for increasing resolution in line with the plant identification (Pavlov, 1961; Hall, 1999; Kaliyeva et al., 2014).

TrnH-psbA gene represents the most variable fragment of plastidial DNA, and can be successfully used for the phylogenetic analysis of plants (Chen et al., 2010; PS et al., 2017).

Passportization of varieties is particularly required for the purposes of certification and commercial distribution of seeds. Besides, the methods underlying genetic passportization can be successfully adapted by plant breeders in their breeding activities: for instance, for early detection of genetic markers of valuable phenotypic properties, as well as for consolidation and preservation of achievements in selection. The methods of genetic passportization are used worldwide, as well as in seed production and control of purchased seed lots in terms of their compliance with the declared grade because fraud is not uncommon there.

Methods of electrophoretic determination polymorphism of proteins for passportization of cultivated plant varieties are still popular in Russia and in other countries (Omasheva et al., 2016; Mower et al., 2007). Nonetheless, protein markers are currently considered obsolete owing to a great number of drawbacks. They are more and more seldom used in the course of genetic analysis of cultivated plants (Kanukova et al., 2019). More promising for genetic passportization of agricultural plants are considered DNA markers-based methods. There is an obvious shift in passportization of varieties from the protein polymorphism analysis to a system enabling detection of polymorphic DNA loci in Russia over the past few years (Drobot and Matveeva, 2015; Oladosu et al., 2015). Unfortunately, in the present-day Russia, selection of cultivated plants often takes place solely on the grounds of phenotypic. Owing to this, the creation of new varieties takes long. In order to improve efficiency of breeding activities and reduce the time required to create a variety, application of advanced methods of genetic analysis seems relevant.

ITS2-amplicon sequencing based on a new generation of NGS sequencing technology is the most preferred method for DNA barcoding of plant compounds. This method enables management of highly degraded DNA in the multicomponent plant compounds, and makes it possible to determine species membership for all ingredients in multicomponent phyto preparations (Leonova, 2015). Various studies focused on the genetic transformation containing rol B and rol C genes (Chase, 2003). Random amplified polymorphic DNA (RAPD) markers were applied in a number of studies to investigate genetic variability of wild medicinal plants growing in Jordan. In order to plot a dendrogram and similarity matrix, 10 primers displaying polymorphous bands were used (Trifonova et al., 2016). ISSR amplification was applied to study polymorphisms of microsatellite sequences in genome, and to estimate genetic diversity (Kaliyeva et al., 2015).

One of the immediate priority of public health service is to extend the range of medicines used by introducing new plant products into traditional medicine. Long-term medical practice proves that phyto preparations are not inferior in terms of their effectiveness to synthetic analogues for treatment of a number of diseases, and given the absence of side effects and contraindications, they are even superior to synthetic analogues.

Among various medicinal plant species growing in Kazakhstan, *Artemisia L*. genus is of particular interest. The plants of this genus stand out from other medicinal plants used in traditional and folk medicine. It is famous for its anti-inflammatory, hypolipidemic, antimalarial, antitumor, bronchodilating, anticonvulsant properties (Kocherina and Chesnokov, 2016; Boyko, 2013). In accordance with the obtained patent, the method for extraction of essential oil from *Artemisia porrecta* was demonstrated (Rakhimberdiyeva et al., 2020). Essential oil obtained from *Artemisia L*. has a bactericidal and bacteriostatic action, and provides an antimicrobial effect in treating inflammatory airway diseases.

The first round of clinical trials with regard to the extract from Artemisia L. plants proved the effectiveness of this agent to treat SARS-CoV-2, i.e., the American scientists succeeded in stopping the spread of the virus in cells in laboratory conditions using the plant. The study outcome was published on the bioRxiv website. Artemisia annua is widely used in a number of countries to treat tropical malaria, and waseven proved helpful to treat SARS-CoV-1, the virus that caused an outbreak of SARS in the years of 2002-2003. The scientists confirmed that in the form of hot aqueous solution, the extract manifests antiviral activity against SARS-CoV-2. Moreover, Artemisia L. plants are active against the virus after its penetration into cells. In the future, the researchers will have to continue the trials in order to understand whether it is possible to create a drug based on the ground in powder dried leaves of the plant. According to their assumptions, the drug can become an inexpensive and safe remedy against a new coronavirus, and can find its application in the cases when vaccination is constraint (Balandina, 2021).

Molecular genetic identification of artemisia species shall ensure the selection of the economically important ones and selection thereof. Passportization of rare relict plant species is another compulsory step to implement gene pool conservation of these species at the population level

The purpose of this research was to conduct a molecular genetic identification of the plant species of Artemicia L. genus growing in South Kazakhstan – Artemisia karatavica (Krasch. & Abolin ex Poljakov), Artemisia cina Berg ex Poljak., and Artemisia porrecta (Krasch. ex Poljakov) – by molecular marking their genomes at the population level to assess the state of population gene pool.

2. Materials and Methods

The molecular genetic research study was conducted in 2019.

The material for the study comprised three species of Artemicia L. genus: Artemisia karatavica Krasch. & Abolin ex Poljakov (Artemisia karatavica), Artemisia cina Berg ex Poljak. (Artemisia cina) and Artemisia porrecta Krasch. ex Poljakov (Artemisia porrecta) from the family Asteraceae. The collection of plants took place in various areas of vegetation in the Turkestan region of Kazakhstan: Shardarinsky district (Komsomol village); Baydibek district (Shakpak village); Aryssky district (Darmino

village). The collected study samples entered their flowering stage.

DNA purification. For the purposes of purification, there were used three samples of each species of Artemisia L: Artemisia karatavica Krasch. & Abolin ex Poljakov (Artemisia karatavica), Artemisia cina Berg ex Poljak. (Artemisia cina), and Artemisia porrecta Krasch. ex Poljakov (Artemisia porrecta). Genomic DNA was purified from the aboveground parts of Artemisia L. using CTAB and TE buffers (Sukhareva and Kuluev, 2018) of certain modifications. 100 mg of leaves were pulverized in a cooled pounder in presence of 1 ml of extraction buffer (100 mM Tris-HCl pH 8.0; 20 mM EDTA, pH 8.0; 1, 4M NaCl, 2% CTAB, PVP and 2-mercaptoethanol were added before use to reach the resulting concentration of 2 and 0.2% respectively). The resulting homogenate was incubated at 60°C for 30 minutes, and then extracted with chloroform. 0.5 volumes of 5M of chloride of sodium and 2 volumes of ethanol were added into a water phase. The compound was incubated at 4°C for 15-20 minutes, and then centrifuged for 15 minutes at 13000 g. The sediment of DNA was washed with 70% ethanol, and dissolved in 100 µl double-distilled water. DNA was treated with RNA. The assessment of DNA quality and amount was done by electrophoresis with 1% agarose gel in 1xTAE buffer, and by absorption at wavelengths of 260 and 280 nm by spectrophotometry employing Nanodrop 2000 (Thermo Scientific, USA).

DNA barcoding: The following markers were used to barcode DNA of artemisia: two plastidial DNA genes (rbcL and matK), and one spacer region (trnH2/psbA) (Hajibabaei et al., 2007).

Amplification of PCR of 20 µl in volume was done in Eppendorf Vapo.protect Mastercycler thermal cycler (USA) and containing as follows: 2 µl of 10xTAQ buffer (750 mM TrisHCl, pH 8.8, 200 mM (NH4)2SO4, 0.1% Tween 20), 2.5 µl of 25 mM MgCl₂, 0.4 µl of 10 mM compound of deoxynucleotide triphosphates (dNTP), 0.4 µl of 10 mM direct and reverse oligonucleotides of one of the markers, 12.3 µl of deionized sterile water and 1 TAQ polymerase unit. The concentration of genomic DNA was 40-60 ng/20 µl. The annealing point was selected depending on the marker sequence. The synthesis was carried out at the following temperature: one cycle at 94°C for 4 minutes; 35 cycles consisting of the following stages: 94°C for 30 seconds, 57°C for 30 seconds, 72°C for 1 minute; and the final cycle at 72°C for 10 min.

DNA quality and quantity testing was done by electrophoresis with 1.4% agarose gel in 1xTAE buffer (0.04 M-Tris HCl, 0.02 M CH₃COONa, 0.01 M EDTA, pH 8.0). 1.4 g of agarose per 100 ml of 1xTAE buffer was measured to prepare 1.4% agarose gel. The agarose mixed with buffer was boiled in a microwave oven at high power to complete the dissolution of agarose. The compound was cooled down to 40-50°C, and then 7 μl of ethidium bromide was added into 10 mg/ml concentration, stirred and poured into a reservoir. Dividing strips were placed in the reservoir to form wells needed for sample application. Then the gel was cooled to its hardening.

At the end of the amplification program, 5 μ l of each PCR reaction were tested by electrophoresis with 1% agarose gel containing ethidium bromide, and visualized in UV light using BioRad gel documentation system. The

remnants of PCR reaction were cleared through GeneJet PCR Purification Kit column (Thermo Scientific, USA). Once purified, PCR concentration of the product was measured. At that, per every sequencing reaction there were taken 10 to 20 ng depending on the product length.

The quality of DNA samples was also tested by PCR amplification of 18S ribosomal DNA using the primers as follows:

5'-GAGAAACGGCTACCACATCCAAGG-3'; 5'-rCCATGCACCACCACCATAGAATC-3'.

The assumed amount of product reached 870-bp. PCR was done in the resulting volume of 25 μl, containing 0.2 μm of deoxyribonucleotide triphosphate, 0.2 μm of each primer, 0.5 UTaqDNA polymerase (Thermo Scientific, USA), 2.5 μm, and 40 ng of DNA in 1xTAQ Buffer with (NH₄)₂SO₄ (750 Mm of Tris-HCl, pH 8.8, at 25°C, 200 μm of (NH₄)₂SO₄ and 0.1% (v/v) Tween 20). Amplification: initial denaturation at 94°C for 2 min; 25 cycles at 94°C for 30 sec, annealing at 67°C for 15 sec, and synthesis at 72°C for 15 sec. The final elongation was done at 72°C for 10 min.

Sequencing was done by ABIPrizm 310 genetic analyzer (Applied Biosystems, USA) according to the instruction manual. The comparison of nucleotide sequences was accomplished using DNAMAN and BioEdit software complexes (Delabays, 1997).

Selection of markers and PCR conditions. Three ISSR markers were used to assess genotypes. The material for the assessment comprised 10 samples. In all further experiments, DNA with the indicators of absorption relation ranging from 1.68 to 1.87 at wavelengths of 260/280 was used (SmartSpecPlus spectrophotometer, Bio-Rad).

PCR was done in the volume of 20 μ l containing 2 μ l 10xTAQ of the buffer (750 Mm of TrisHCl, pH 8.8, 200 μ m (NH₄)₂SO₄, 0.1% of Tween 20), 2.5 μ l of MgCl₂, 0.4 μ l of 10 mM compound of deoxyribonucleotide triphosphate (dNTP), 0.8 μ l 10 mM of oligonukleotid of the used marker, 12.7 μ l of deionized sterile water and 1xTAQ of polymerase. The concentration of genomic DNA was 40-60 ng/20 μ l. Amplification was done according to the following sequence: one cycle at 94°C for 2 minutes; 35 cycles consisting of the following stages: 94°C for 40 sec, 44°C for 45sec, 72°C for 1.5 minutes; and the final cycle at 72°C for 15 min.

Electrophoresis of the amplification products obtained using ISSR-PCR was done with 2% agarose gel. After staining with ethidium bromide, UV visualization followed using BioRad gel documentation system. In order to control the amplified DNA, GeneRulerTM 1kb (Fermentas, USA) marker was used.

Phylogenetic analysis. Sequence alignment was achieved using UGENE software. Plotting of genetic trees using nucleotide DNA barcoding sequences was done in NCBI-blast module.

When measuring the genetic distance, the maximum likelihood technique or maximum composite likelihood technique was used.

Only DNA fragments of good reproduction in repeated experiments were taken into account. The intensity of the fragments was disregarded. The obtained data were computer-processed using PopGen32 software, as well as the specialized GenAlEx6 macros for MS Excel.

3. Results

At the outcome of sequencing three samples of *Artemisia L*. the nucleotide sequences of rbcL, matK and trnH-psbA for each sample were obtained (Figure 1). Numbers 1 to 3 in the figure are rbcL, matK and trnH-psbA samples respectively.

When comparing the nucleotide sequences of rbcL gene with the known sequences of rbcL from NCBI genetic database, the studied samples formed a cluster containing eudicots of the greatest genetic affinity with various species of *Artemisia L*. (Figure 2).

1 2 3	TACTGATATCTTGGCAGCATTTCGAGTAACTCCTCAACCT	40 40 40
1 2 3	GGAGTTCCGCCTGAAGAAGCAGGGGCCGCAGTAGCTGCCG	80 80 80
1 2 3	AATCTTCTACTGGTACATGGACAACTGTGTGGACCGATGG	120 120 120
1 2 3	ACTTACGAGCCTTGATCGTTACAAAGGGCGATGCTATGGA	160 160 160
1 2 3	ATTGAG.CCTGTTCCTGG	177 178 177

Figure 1. Comparison of nucleotide sequences of rbcL for three samples of Artemisia L.

Comparison of the nucleotide sequences of rbcL for three studied samples was done with the sequences of NCBI database (National Center for Biotechnology Information).

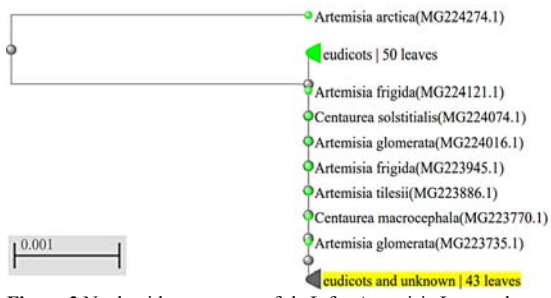


Figure 2. Nucleotide sequences of rbcL for Artemisia L. samples

Note: marked in yellow is the cluster containing the studied samples.

When comparing the nucleotide sequences of matK gene of 286bp in the first and third samples, the sequences proved to be identical. The second sample in matK sequence contained deoxycytidine and deoxyadenosine in positions 265 and 266 respectively (Figure 3).

1	GATTCTTTCTCCATGAGTGTCATAATTGGGATAGTCTTATTACTTCAATT	50
2		50
3		50
1	CARAGAAAGTTAGTTCTTCTTTTCAAAAAGAAAAAACAGATTATTCTTC	100
2		100
3		100
1	TTCCTATATACTTTTCATGTATGTGAATATGAATCTGGCTTCCTCTTTCT	150
2		150
3		150
1	CCGTAACCAGTCTTCTCACTTACGATCAACATCTTCTGGAGCCCTTATTG	200
2		200
3		200
1	AACGAATAAATTTCTATGGAAAAATAGAGCATCTTGCAGAAGTCTTTGTC	250
2		250
3		250
1	AGGTCTTTTCAAGCATATTTATGGTTGTTCAAAGAT	286
2	ca	286
3		286

Figure 3. Comparison of nucleotide sequences of matK for three samples of Artemisia L.

Based on the analysis of matK nucleotide sequences of the studied samples, it was possible to plot the phylogenetic tree with a genetic distance relative to the known species of the international genetic database NCBI (Figure 4).



Figure 4.Nucleotide sequences of matK for Artemisia L. samples. Note: marked in yellow are the studied samples.

The outcome of the phylogenetic analysis proves that the studied samples form monophyletic groups with different species of *Artemisia L.* genus.

At the outcome of the analysis of three samples of trnH-psbA sequence of 255-bp. no variations were recorded. The sequences of three samples are identical (Figure 5).



Figure 5.Comparison of nucleotide sequences trnH-psbA for three samples of Artemisia L.

Phylogenetic analysis of the studied samples using trnH-psbA sequence versus the known sequences from NCBI database revealed the genetic distance between different *Artemisia L*. species (Figure 6). Genetic distance (GD) is a measure of genetic divergence between species, or between populations within one species.



Figure 6. Nucleotide sequences of trnH-psbA for Artemisia L. samples.

Note: marked in yellow are the studied samples.

There exists a multitude of parameters worth taking into account when measuring genetic distances. In the simplest scenario, the genetic distance between two populations of the same species can be determined based on the difference in frequencies of occurrence of a particular feature.

The genetic distance between samples was determined by cross-linking nucleotide sequences of three genetic markers for each sample. The genetic distance reached 0.9% between the second and first, as well as between the second and third samples. The distance between the first and third samples was equal to zero.

The identification results for the studied samples using matK and rbcL markers from the international BOLD database (BARCODE OF LIFE DATA SYSTEM) for DNA barcoding revealed that the greatest overlap for the studied samples was with *Artemisia annua L* species.

(Figure 7).

The study evaluated the population structure, genetic diversity, and relationships of Artemisia annua germplasm across Iran using 18 IRAP primers. RTN-based markers are being newly used, and are yet to be exploited fully. This approach can provide comprehensive information about the level of genetic diversity and population structure of Artemisia annua which could be useful for conservation and management of Artemisia annua germplasm genetic resource base. Single IRAP primer Tnt1.OL16 revealed more distinguished contribution in defining the genetic diversity of the studied taxon's or species and their segregation. These results revealed that the genetic diversity of the Iranian Sweet Artemisia annua is insufficient, and that makes it uniformly a distinct population for extraction of artemisinin (Valizadeh et al., 2021).



Figure 7.Identification of the studied samples in BOLD database.

Based on DNA barcoding results, the samples of Artemisia karatavica Krasch. & Abolin ex Poljakov, Artemisia cina Berg ex Poljak.

H. Artemisia porrecta Krasch. ex Poljakov proved the greatest affinity with Artemisia annua species. The identification of the results in DNA barcoding database demonstrated the greatest overlap with Artemisia annua species for three samples.

Upon purification of the genomic DNA, its quality analysis was measured by a spectrophotometer (NanoDrop 2000C) and by electrophoresis with 1% agarose gel in a triple track sequence (Figure 8).

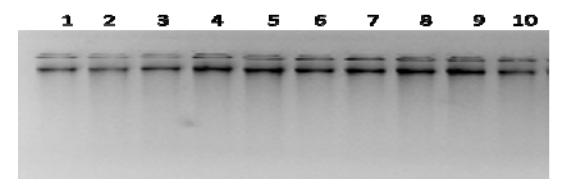


Figure 8.Electrophoresis of genomic DNA with 1% agarose gel (Tracks 1 to 3 correspond to sample 1; tracks 4 to 6 to sample 2; tracks 7 to 10 to sample 3).

In order to prove absence of inhibitors in DNA preparations purified in accordance with the modified protocol (Sukhareva and Kuluev, 2018), a pilot PCR analysis was undertaken using oligonucleotides specific to 18S gene of the ribosomal RNA. The electrophoretogram of the products of PCR analysis of the ribosomal DNA of artemisia prove absence of reaction inhibitors in the resulting DNA preparations (Figure 9).

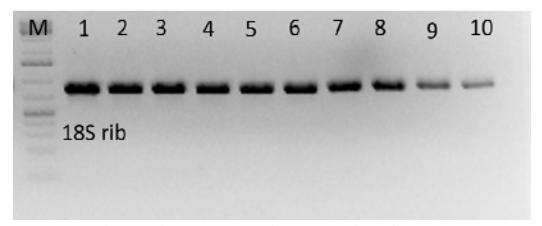


Figure 9. Electrophoretogram of PCR product from 18S gene

(Tracks 1 to 10 correspond to PCR products of 18S gene fragment of the ribosomal RNA for the studied samples; M is DNA marker of GeneRulerTM 1kb).

The following stage of the sequenced products analysis of involved primers 274 and 275 complementary to different microsatellites (Figures 10-12).

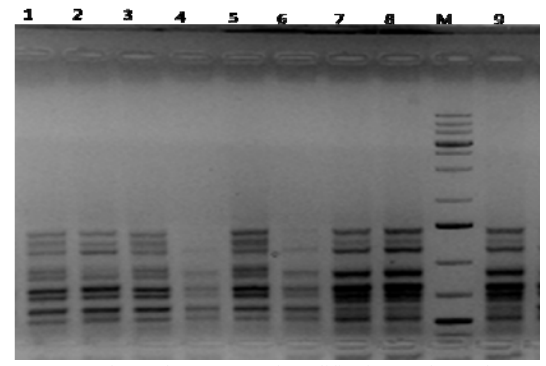


Figure 10. Electrophoretogram of amplification products when using primer 274

(Tracks 1 to 3 correspond to sample 1; tracks 4 to 6 correspond to sample 2; tracks 7 to 9 correspond to sample 3; M is DNA marker of GeneRulerTM 1kb).

The results of analysis proved that all artemisia samples are genetically related under primer 274.

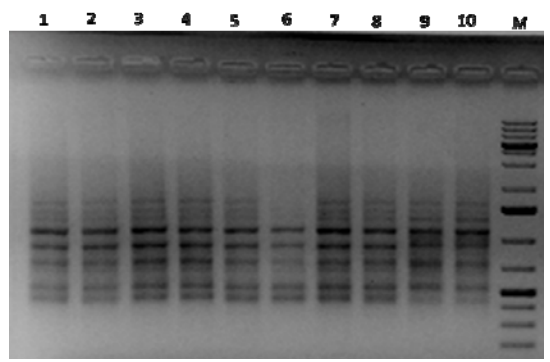


Figure 11. Electrophoretogram of amplification products when using primer 275

(Tracks 1 to 3 correspond to sample 1; tracks 4 to 6 to sample 2; tracks 7 to 10 to sample 3; M is DNA marker of GeneRulerTM 1kb).

The analysis of amplification results proved that the studied artemisia samples were not genetically different under primers 274 and 275. PCR analysis revealed no genetic variability among the studied samples.

4. Discussion

This research study was based on the classical approach to molecular and genetic passportization of resource plant species which includes the stages as follows: selection of effective methods to analyse polymorphism of DNA, collection of material, determination of effective primers, molecular and genetic analysis using PCR, identification of DNA markers, monomorphic and polymorphic DNA fragments, compilation of a molecular genetic formula, barcode and genetic passport (Dilshad et al., 2015). The last three stages, i.e. compilation of a molecular genetic formula, barcode and genetic passport, which are often used for the certification purposes of commercial varieties of agricultural plants, were not involved into this study owing to a different scope of research tasks.

DNA barcoding based on sequencing of standard DNA fragments, especially mitochondria and chloroplasts, is widely used in molecular systematics of organisms (Kondratenko, 2015). The methods used in this study, i.e. DNA barcoding, sequencing, phylogenetic analysis and final control of the results by PCR, altogether helped to reveal polymorphism of the greater part of the genome of the plant species under study. These methods are stable, and provide clearly visible results.

DNA banks are created and integrated with the already existing herbarium collections, seed banks, and plant collections in botanical gardens (Kanukova et al., 2019). The methods described above and the results obtained at this stage of the study were carried out using three medicinal species of Artemisia L. of a high pharmaceutical potential and growing in the South Kazakhstan. Particularly this approach to the analysis of DNA polymorphism is considered promising for the purposes of identification of the genetic mechanisms responsible for adapting population systems in a heterogeneous environment. The content of DNA in plants is determined in more than 10 thousand species (Chen et al., 2010). In the course of this research, DNA sequences of three pharmaceutically significant resource species among the plants of Kazakhstan were sequenced for the very first time, and the absence of genetic variability among the studied samples was proved. On the grounds of comparison of the obtained results with the standards of the international base BOLD, DNA sequences of Artemisia karatavica Krasch. & Abolin ex Poljakov, Artemisia cina Berg ex Poljak., and Artemisia porrecta Krasch. ex Poljakov displayed the greatest affinity with Artemisia annua species.

Relatively small size of the nuclear genome facilitates molecular studies of resource plants (Kavrakova et al., 2015). In the course of molecular genetic analysis of *Artemisia L.*, from the samples of various geographical vegetation in Southern Kazakhstan, a set of amplification products specific to 18S gene of the ribosomal RNA was obtained. The vast majority of amplified DNA fragments were polymorphic.

The number of amplicons in total sampling of plants varied depending on the primer, i.e. from 9 (primer 275) to 11 (primer 274), with their sizes not exceeding the size of 1 kb.

The level of polymorphism of ISSR markers in this species was 0.9%. The number of rare amplicons (DNA fragments with a frequency of \leq 0.05) was null in the studied Artemisia L samples.

The search for rare alleles is quite important, since these rare alleles are most valuable for development of measures aimed at preservation of natural populations, and are important for passportization of populations within this species. Consequently, in the future, the assessment of genetic polymorphism of a wider range of geographically diverse plant samples of *Artemisia L*. species would be of significant practical interest, and important in terms of assessing diversity of wild plants species.

For the purposes of molecular genetic passportization, there were selected most informative ISSR primers, with the help of which effective ISSR markers for the species under study were identified and identification of the molecular markers was done (Figures 2, 4, 6). The molecular markers selected for passportization and

identification of resources for these valuable medicinal plants were visualized by way of a genetic divergency tree. When plotting it, the so-called generic, species-related or polymorphic PCR fragments of DNA were used.

Many researchers follow the protocol to purify DNA from various organs of the plant, which would not consume much time and would minimize contamination of the purified DNA (Omasheva et al., 2016; Cai et al., 2017). At that, the principal property of a molecular marker - its length - was determined using DNA marker GeneRulerTM 1kb.

This approach to describing genomes of various plants is applicable to both homogeneous plant varieties and heterogeneous natural populations. For the purposes of genetic passportization of the studied populations, the number of molecular markers involved can be further extended. Thus, numerous research papers focused on the study of genetic diversity of plants in Perm Region suggested to take 10 to 12 markers. This made it possible to passportize plants, and apply molecular genetic formula to them (Kostylev et al., 2015).

The genetic divergence tree discussed in our studies, as well as molecular genetic formula and barcode (Mezhnina and Urbanovich, 2016), enabled identification of affinity of both plant raw material and plant samples not just upto the genus and species, but also to the group of populations or one specific population. The principle advantage of the discussed method of genetic expertise is the mechanism of generalization of molecular genetic analysis data by determining the identification markers reflecting most of the genome of the studied species. The visualization of results was proposed in a generalized way by means of the genetic divergency tree, with PCR analysis of amplicons, introducing, along with conventional indicators, the description of state for every pharmaceutically significant population and introducing the specifics of its gene pool.

Currently, artemisinin and its derivatives are used in combination therapy for the treatment of malaria (Haynes R.K., 2006), as well as for the treatment of a number of oncological and viral diseases (Effert T., 2007). All these scientific undertakings prove again that further research is required for the species of Artemisia L. (Zhokhova et al., 2019; Kalko, 2015; Kondratenko, 2015; Urbanovich, 2007, Lyzhin and Savelieva, 2018; Sukhareva and Kuluev, 2018; Levin et al., 2003).

5. Conclusion

Artemisia is an economically important medicinal plant. In particular, essential oils extracted from artemisia are used in manufacturing perfumes and antiseptic agents. The species identification of artemisia ensures selection of important species and further selection activities. The search and study of various types of artemisia contributes to identification of species advantageous in view of glycosides or alkaloids content, which is crucial for pharmaceutical industry.

The World Health Organization (WHO) welcomes innovations around the world including repurposing drugs, traditional medicines and developing new therapies in the search for potential treatments for COVID-19. WHO recognizes that traditional, complementary and alternative medicine has many benefits, and Africa has a long history of traditional medicine and practitioners that play an

important role in providing care to the peoples. Medicinal plants such as *Artemisia annua* are being considered as possible treatments for COVID-19 and should be tested for efficacy and adverse side effects. The Africans should use the medicines tested to the same standards as the peoples in other countries. Even if the medicinal products derived from traditional sources are natural, establishing their efficacy and safety through rigorous clinical trials is critical (World Health Organization. Africa, 2020).

Artemisinin derived from the medicinal plant *Artemisia* sp. is an effective antimalarial medicinal product. In 2015, the Nobel Prize was awarded to the findings of effectiveness of artemisinin as a potent antimalarial medication. Due to the limited market and low extraction of artemisinin, the economical way of increasing its production lies in increasing the amount of *Artemisia sp.* through various biotechnological techniques, inclusive of genetic transformation. (Bushra Hafeez Kiani, 2016).

Molecular genetic identification of artemisia species was not accomplished in Kazakhstan previously. The description of species is based on botanical properties. Molecular genetic analysis of Artemisia L. (rbcL, matK, trnH-psbA) displayed complete identification of Artemisia karatavica Krasch. & Abolin ex Poljakov and Artemisia porrecta Krasch. ex Poljakov samples, as well as the genetic distance between these samples and Artemisia cina Berg ex Poljak. being 0.9%. Comparison of DNA barcoding results with the available database proved the greatest overlap of the studied samples with Artemisia annua L species, which may be due to insufficient study of the species. The issues related to the origin of each plant species, because of the complexity of the process, represent quite a laborious scientific challenge. Among the most promising techniques to study genetic purity is the analysis of variability of highly polymorphic genetic systems. The large number of polymorphic markers identified in the course of decoding the genome of any particular plant species is a powerful tool to analyze the gene pool, and its main properties, dynamics and geography. Numerous studies focusing on polymorphic systems of nuclear and mitochondrial genomes led to the development of a new section of genomics ethnogenomics. Nowadays, accumulation of data on polymorphism of autosomal microsatellite loci, microsatellites and mitochondrial genome variability in various populations worldwide is a task of paramount importance.

According to the available research finding, there is a tendency towards depletion of the gene pool among the studied populations of Artemisia L. Molecular analysis of highly polymorphic fragments of the genome in rare relict plant species discussed in the scientific sources represents the base to approach their molecular genetic passportization. The principle of compiling and recording a genetic formula relies on identification of DNA markers using ISSR and PCR methods to analyze DNA polymorphism. It covers most of the plant genomes, and there are few genetically studied plant species suitable for genetic passportization. The new approach to recording the data contains detailed information about the identification of molecular marker, including plant species, molecular marker type, its size, and properties of the studied part of the genome by indicating the analysis technique of DNA polymorphism and the number or sequence of primer.

Such approach to genetic passportization is of high resolution, and provides stable visual results, as well as adaptive to automation.

Data availability statement:

The data that support this study are available in the article and accompanying online supplementary material.

Conflict of Interest statement:

The authors declare no conflicts of interest

References

Alrawashdeh, I. (2011). Genetic variability in a medicinal plant artemisia judaica using random amplified polymorphic DNA (RAPD) markers. *International Journal of Agriculture and Biology*, 13, 1560–8530.

Aubakirova, K., Omasheva, M., Ryabushkina, N., Tazhibaev, T., Kampitova, G., & Galiakparov, N. (2014). Evaluation of five protocols for DNA extraction from leaves of Malus sieversii, Vitis vinifera, and Armeniaca vulgaris. *Genetics and Molecular Research*, 13(1), 1278–1287. https://doi.org/10.4238/2014.february.27.13

Balandina, A. 2021. It kills secondary infections: could Artemisia help fight COVID-19? Gazeta.ru: January13, 2021.

Boronnikova, S. V. (2009). Molekulyarnoye markirovaniye i geneticheskaya pasportizatsiya resursnykh i redkikh vidov rasteniy s tsel'yu optimizatsii sokhraneniya ikh genofondov [Molecular labeling and genetic certification of resource and rare plant species in order to optimize the conservation of their gene pools]. Agrarnyy vestnik Urala, 2, 57-59.

Boyko, E. V. (2013). Mikromorfologiya semyanok vidov roda artemisia (anthemideae – asteraceae) [Micromorphology of seeds of species of the genus Artemisia L. (Asteraceae)]. Turczaninowia, 16(2), 91–105. http://turczaninowia.asu.ru/article/view/724

Kiani, B. H., Suberu, J. (2016). Cellular engineering of Artemisia annua and Artemisia dubia with the rol ABC genes for enhanced production of potent anti-malarial drug artemisinin. Malaria Journal, 252: May. 04, 2016.

Cai, C., Zhu, G., Zhang, T., & Guo, W. (2017). High-density 80 K SNP array is a powerful tool for genotyping G. hirsutum accessions and genome analysis. *BMC Genomics*, *18*(1). https://doi.org/10.1186/s12864-017-4062-2

Chase, M. W. (2003). Molecular Systematics, GISH and the Origin of Hybrid Taxa in Nicotiana (Solanaceae). *Annals of Botany*, 92(1), 107–127. https://doi.org/10.1093/aob/mcg087

Chen, S., Yao, H., Han, J., Liu, C., Song, J., Shi, L., Zhu, Y., Ma, X., Gao, T., Pang, X., Luo, K., Li, Y., Li, X., Jia, X., Lin, Y., & Leon, C. (2010). Validation of the ITS2 Region as a Novel DNA Barcode for Identifying Medicinal Plant Species. *PLoS ONE*, *5*(1), e8613. https://doi.org/10.1371/journal.pone.0008613

Cho, Y., Mower, J. P., Qiu, Y.-L., & Palmer, J. D. (2004). Mitochondrial substitution rates are extraordinarily elevated and variable in a genus of flowering plants. *Proceedings of the National Academy of Sciences*, 101(51), 17741–17746. https://doi.org/10.1073/pnas.0408302101

Delabays, N. (1997). Biologie de la reproduction chez l'Artemisia annua L. et génétique de la production en artémisinine: contribution à la domestication et à l'amélioration génétique de l'espèce [PhD Thesis]. Lausanne University.

Delabays, N., Simonnet, X., & Gaudin, M. (2001). The Genetics of Artemisinin Content in Artemisia annua L. and the Breeding of

High Yielding Cultivars. Current Medicinal Chemistry, 8(15), 1795–1801. https://doi.org/10.2174/0929867013371635

Dilshad, E. Cusido, R. M. Ramirez Estrada, K. Bonfill, M. and Mirza, B. 2015. Genetic Transformation of Artemisia carvifolia Buch with rol Genes Enhances Artemisinin Accumulation. PloS One, 10(10), e0140266.

https://doi.org/10.1371/journal.pone.0140266

Drobot, E. A., Matveeva, N. A. (2015). In vitro of the plant of the genus Artemisia L. as producers of biologically active compounds. *Agrobiodiversity for improving nutrition, health and life quality*, 127-130.

Ferreira, J. F. S., Laughlin, J. C., Delabays, N., & de Magalhães, P. M. (2005). Cultivation and genetics of Artemisia annuaL for increased production of the antimalarial artemisinin. *Plant Genetic Resources*, 3(2), 206–229. https://doi.org/10.1079/pgr200585

Graham, I. A., Besser, K., Blumer, S., Branigan, C. A., Czechowski, T., Elias, L., Guterman, I., Harvey, D., Isaac, P. G., Khan, A. M., Larson, T. R., Li, Y., Pawson, T., Penfield, T., Rae, A. M., Rathbone, D. A., Reid, S., Ross, J., Smallwood, M. F., & Segura, V. (2010). The Genetic Map of Artemisia annua L. Identifies Loci Affecting Yield of the Antimalarial Drug Artemisinin. *Science*, 327(5963), 328–331. https://doi.org/10.1126/science.1182612

Hajibabaei, M., Singer, G., Hebert, P., Hickey, D. (2007). DNA Barcoding: how it complements taxonomy, molecular phylogenetic and population genetics. *Trends in Genetics*, 23(4), 167-72. https://doi.org/10.1016/j.tig.2007.02.001

Hall, T. A. (1999). BioEdit: a user-friendly biological sequence alignment editor and analysis program for windows 95/98/NT. *Nucleic Acids Symposium Series*, 41, 95-98.

Kaliyeva, A. N., Dyuskaliyeva, G. U., Zhexembiyev, R. K., Medeuova, G. D., & Tileubayeva, Z. S. (2015). Anatomical, Morphological and Biochemical Analysis of Medicinal Species Agrimonia L. Growing at South-east of Kazakhstan. *Biosciences Biotechnology Research Asia*, 12(2), 1709–1717. https://doi.org/10.13005/bbra/1834

Kaliyeva, A. N., Dyuskaliyeva, G., Newsome, A., Zhexembiyev, R., & Medeuova, G. D. (2014). Biological Features of Medicinal Plants of Agrimonia L. in South Eastern Kazakhstan. *Modern Applied Science*, 9(5). https://doi.org/10.5539/mas.v9n5p63

Kalko, G.V. 2015. Dnk-markery dlya otsenki geneticheskikh resursov yeli i sosny [DNA markers in assessment of the genetic resources of spruce and pine]. Proceedings of the St. Petersburg Forestry Research Institute, 4: 19-34.

Kanukova, K. R., Gazaev, I. Kh., Sabanchieva, L. K., Bogotova, Z. I., Appaev, S. P. (2019). *Dnk-markery v rasteniyevodstve* [DNA markers in crop production]. *Proceedings of the Kabardino-Balkar Scientific Center of the Russian Academy of Sciences*, 6(92), 220-232. https://doi.org/10.35330/1991-6639-2019-6-92-220-232

Kavrakova, Z. B., Mamadjusufova, M., Kosumbekova, F. A., Nasyrova, F. Ju. (2015). Rard- i ssr analiz vnutri- i mezhvidovogo polimorfizma vidov roda aegilops l., proizrastayushchikh v razlichnykh prirodno- klimaticheskikh zonakh tadzhikistana [RARD- i SSR interspecies analysis of AEGILOPS L. growing in different natural and climate zones of Tadzhikistan]. Kishovarz, 3, 16–19.

Kocherina, N. V., Chesnokov, Yu. V. (2016). Programmnoye obespecheniye dlya geneticheskogo kartirovaniya i analiza assotsiatsiy markerov / priznakov [Software for genetic mapping and analysis of marker/trait associations]. Vegetable crops of Russia, 1, 3-9. https://doi.org/10.18619/2072-9146-2016-1-3-9

Kondratenko, E.I. 2015. Tsitogeneticheskiye i molekulyarnobiologicheskiye metody analiza rasteniy «Cytogenetic and molecular biological methods of plant analysis: education and study guide». Astrakhan: Astrakhan University Publishing House.

Kostylev, P. I., Krasnova, E. V., Redkin, A. A., Repkina, N. V., Mukhina, J. M., Dubina, E. V. (2015). Sort risa Magnat, sozdannyy s pomoshch'yu biotekhnologii [Variety of Magnat rice created through biotechnology]. Dostizheniya nauki i tekhniki APK, 29(3), 10-12.

Leonova, I. N. (2015). Genetic control of resistance to fungal diseases in soft wheat with introgressions from Triticum timipheevii [PhD Thesis]. Novosibirsk: ITC SB RAS.

Levin, R. A., Wagner, W. L., Hoch, P. C., Nepokroeff, M., Pires, J. C., Zimmer, E. A., & Sytsma, K. J. (2003). Family-level relationships of Onagraceae based on chloroplast rbc L and ndh F data. *American Journal of Botany*, 90(1), 107–115. https://doi.org/10.3732/ajb.90.1.107

Lyzhin, A. S., Savelieva, N. N. (2018). Genotipirovaniye sortov yabloni po allelyam S-lokusa (samonesovmestimost') [Genotyping of apple varieties by alleles of the S-locus (self-incompatibility)]. Innovative Science, 8-3, 38-40.

Mezhnina, O. A., Urbanovich, O. Yu. (2016). *Identifikatsiya* sortov zemlyaniki sadovoy (Fragaria ananassa) s pomoshch'yu SSR-markerov [Identification of garden strawberry varieties (Fragaria ananassa) using SSR markers]. *Molecular and applied genetics*, 20, 37-45.

Mower, J. P., Touzet, P., Gummow, J. S., Delph, L. F., & Palmer, J. D. (2007). Extensive variation in synonymous substitution rates in mitochondrial genes of seed plants. *BMC Evolutionary Biology*, 7(1), 135. https://doi.org/10.1186/1471-2148-7-135

Oladosu, Y., Rafii, M. Y., Abdullah, N. et al. (2015). Genetic variability and diversity of mutant rice revealed by quantitative traits and molecular markers. *Agrociencia*, 49(3), 249–266.

Omasheva, M. E., Pozharsky, A. S., Maulenbay, A. D., Ryabushkina, N. A., Galikarpov, N. N. (2016). SSR genotyping of Kazakhstani apple varieties: identification of alleles associated with resistance to highly destructive pathogens. *Biotechnology Theory and practice*. http://dx.doi.org/10.11134/btp.2.2016.4

Omasheva, M. Y., Pozharskiy, A. S., Maulenbay, A. D., Ryabushkina, N. A., Galiakparov, N. N. (2016). SSR-genotyping of Kazakh apple varieties: identification of alleles associated with resistance to highly destructive pathogens. *Eurasian Journal of Applied Biotechnology*, 2, 46-58.

Pavlov, N. V. (1961). Flora of Kazakhstan. Vol. IX. Alma-Ata: Publishing House of the Academy of Sciences of the Kazakh ASSR, pp. 76-131.

PS, S., SV, A. M., Prakash, C., MK, R., Tiwari, R., Mohapatra, T., & Singh, N. K. (2017). High Resolution Mapping of QTLs for Heat Tolerance in Rice Using a 5K SNP Array. *Rice*, *10*(1), 28. https://doi.org/10.1186/s12284-017-0167-0

Rakhimberdiyeva, Zh. Sh., Kaliyeva, A. N., Karzhaubekova, Zh. Zh., Ghemedzhieva, N. G. (2020). Patent №6236. For utility model. Method for extracting essential oil from Artemisia porrecta Krasch. ex. Poljakov.

Rzepka-Plevneš, D., Smolik, M., Urbanek, K., & Jadczak, D. (2009). Morphological and Genetic Variability in Some Artemisia Species. *Acta Horticulturae*, 830, 687–694. https://doi.org/10.17660/actahortic.2009.830.99

Sukhareva, A. S., Kuluev, B. R. (2018). *DNK-markery dlya geneticheskogo analiza sortov kul'turnykh rasteniy* [DNA markers for genetic analysis of the cultivated plant varieties]. *Biomika*, 10(1), 69-84. https://doi.org/10.31301/2221-6197.bmcs.2018-15

Sukhareva, A. S., Kuluev, B. R. (2018). *Dnk-markery dlya geneticheskogo analiza sortov kul'turnykh rasteniy* [DNA markers for genetic analysis of the cultivated plant varieties]. *Biomika*, 10(1), 69-84. https://doi.org/10.31301/2221-6197.bmcs.2018-15

Trifonova, A. A., Filyushin, M. A., Kochieva, E. Z., Kudryavtsev, A. M. (2016). Analiz yadernykh speyserov its1/its2 i vtorichnoy struktury gena 5.8s rrnk u endemichnogo vida bellevalia sarmatica (pall. Ex georgi) woronow i rodstvennykh vidov podsemeystva scilloideae [Analysis of nuclear spacers ITS1/ITS2 and secondary structure of 5.8S gene of rRNA in the endemic species Bellevalia sarmatica and related species of Scilloideae subfamily]. Genetics, 52(5), 1-6. https://doi.org/10.7868/S0016675816050118

Urbanovich, O.Yu. 2007. Otsenka geneticheskogo raznoobraziya genofonda plodovykh kul'tur i razrabotka metodov DNK-identifikatsii i genotipirovaniya ikh sortov i vidov [Assessment of genetic diversity of the gene pool of fruit crops and development of methods for DNA identification and genotyping of their varieties and species [PhD Thesis]. Minsk.

Valentini, A., Pompanon, F., & Taberlet, P. (2009). DNA barcoding for ecologists. *Trends in Ecology & Evolution*, 24(2), 110–117. https://doi.org/10.1016/j.tree.2008.09.011

Valizadeh, N., Holasou, H.A., Mohammadi, S. A., Khawar, Kh. M. (2021). Molecular Insights Into the Genetic Diversity and Population Structure of Artemisia Annua L. As Revealed by Insertional Polymorphisms. This work is licensed under a Creative Commons Attribution 4.0 International License. Read Full License. https://doi.org/10.21203/rs.3.rs-683992/v1.

Von Cräutlein, M., Korpelainen, H., Pietiläinen, M., & Rikkinen, J. (2011). DNA barcoding: a tool for improved taxon identification and detection of species diversity. *Biodiversity and Conservation*, 20(2), 373–389. https://doi.org/10.1007/s10531-010-9964-0

Zhokhova, E.V., Rodionov, A.V., Povydysh, M.N., Goncharov, M.Yu., Protasova, Ya.A., Yakovlev, G.P. 2019. Sovremennoye sostoyaniye i perspektivy ispol'zovaniya dnk-shtrikhkodirovaniya i dnk-fingerprintinga dlya analiza kachestva lekarstvennogo rastitel'nogo syr'ya i lekarstvennykh rastitel'nykh preparatov [Current state and trends of using DNA barcoding and fingerprinting for quality analysis of medicinal plant raw materials and herbal medicinal products]. Advances in Modern Biology, 139(1): 25-40.

Efferth, T. 2007. Antiplasmodial and antitumor activity of artemisinin from bench to bedside. Planta Med., 73: 299–309.

Haynes, R.K. 2006. From artemisinin to new artemisinin antimalarials: biosynthesis, old and new derivatives, stereochemistry and medicinal chemistry requirements. Curr Top Med Chem., 6: 509–37.

World Health Organization. Africa 2020. WHO supports scientifically-proven traditional medicine.

Jordan Journal of Biological Sciences

Response Surface Method for Optimizing the Biosynthesis of Silver Nanoparticles Using *Talaromyces stipitatus* and Their Antimicrobial Activity

Nada M. Elmayah*, Amira A. El-Fallal, Mohamed I. Abou-Dobara, Mahmoud E. Khalifa

Department of Botany and Microbiology, Faculty of Science, Damietta University, New Damietta, Egypt.

Received: May 29, 2021; Revised: August 16, 2021; Accepted: October 4, 2021

Abstract

Central composite design (CCD) as one of response surface designs was employed to optimize the biosynthesis process of silver nanoparticles (AgNPs). In this design, fungal cell-free filtrate of *Talaromyces stipitatus* was applied as a biosource for the biosynthesis of AgNPs. Different variables with five levels were used to optimize AgNPs biosynthesis. Independent variables were concentration of silver nitrate (AgNO3; mmole), temperature (°C), time, pH and ratio of AgNO3 to cell free extract. While dependent variable was peak intensity of surface plasmon resonance (SPR) at wavelength 420 nm. The predicted optimal setup parameters were AgNO3 concentration of 7 mmol, temperature of 25 °C, time of 91.2 hr, pH of 8 and ratio of AgNO3 solution to cell-free extract of 2:1. The characteristics of biosynthesized AgNPs were revealed using Fourier transform infrared spectroscopy (FTIR), dynamic light scattering (DLS), zeta potential, energy dispersive x-ray analysis (EDX), and transmission electron microscopy (TEM). Biosynthesized AgNPs appeared to be spherical, with mean size of 13.95 nm and zeta potential of 9.85 mV. Biosynthesized AgNPs were also examined for their antimicrobial properties against selected bacterial and fungal pathogens including *Staphylococcus aureus*, *Bacillus cereus*, *Pseudomonas aeruginosa*, *Klebsiella pneumoniae*, *Aspergillus flavus*, *A. niger*, *Fusarium oxysporum* and *Alternaria alternata*.

Keywords: Nanoparticles, silver, Talaromyces stipitatus, antibacterial, antifungal,

1. Introduction

Nanotechnology is identified as the control or transformation of a substance at the nano scale, normally at sizes extending from 1 to 100 nm. Nanomaterials and nanoparticles (NPs) are considered the fundamental components of nanotechnology (Phanjom & Ahmed, 2017). Owing to the fact that the features of transformed substances (at the nano scale) vary greatly from those of their macro scale original forms. NPs have peculiar physicochemical properties, i.e., high reactivity, larger surface area and unique particle morphology (Siddiqui et al., 2015). In the early stage of substance transformation into the nano scale, the properties remain almost unchanged. Afterwards, minor variations arise until eventually drastic shifts in properties are noted when dimensions decrease to the nano scale, below 100 nm (Bhushan, 2017). The term "nano" is a prefix for one billionth (10⁻⁹) and has its origin from the Latin word "nanos", meaning tiny.

Nanomaterials are generally obtained through two approaches; bottom-up and top-down. In the bottom-up approach, the process begins with a bulk material that gets split into smaller particles via chemical, mechanical or other (top-down) energy forms. The second approach (bottom-up) is to synthesize the substance by chemical

reactions from atomic or molecular precursors that gradually grow in size (Ahumada et al., 2019). Metal NPs are of significant scientific importance in bridging the gap between the bulk structures and atomic structures. Silver nanoparticles (AgNPs), a remarkable type of metallic NPs, have become more widespread and are currently used in several fields, including food storage and industry, in addition to medicine as they have effective antimicrobial activities (Vega-Baudrit et al., 2019).

AgNPs biosynthesis is a bottom-up strategy that depends mainly on reduction and oxidation reactions (Majeed et al., 2019; El-Zahed et al., 2021). For the synthesis of AgNPs, several preparation strategies with diverse processes have been proposed including chemical, physical, and biological approaches (Ahumada et al., 2019; Baker et al., 2015). Green nanotechnology has risen in popularity on account of the current surge in the creation of environmentally friendly technologies, leading to an evolution of diverse studies on natural reducing agents utilized in NPs synthesis (Bhatnagar et al., 2019). The biological approach or green synthesis system, called nanobiotechnology, is usually classified as a modern nanotechnology (Basavegowda & Lee, 2014).

In the production of AgNPs, bio-extracts from microorganisms can function as reducing and/or capping agents. Combinations of biomolecules included in these extracts, such as enzymes, amino acids, vitamins,

_

^{*} Corresponding author. e-mail: Nada_elmayah.20@yahoo.com.

polysaccharides and proteins, can help in reducing Ag⁺ ions (Collera-Zúñiga et al., 2005; Jagadeesh et al., 2004; Kate et al., 2020).

Given the drawbacks of utilizing classical experimental optimization methods, by employing statistical experimental design and response surface method (RSM) to optimize all of the influencing factors, the drawbacks of a single factor optimization procedure may be eliminated (Baş & Boyacı, 2007). RSM has been commonly used to achieve the optimal conditions required for several biotechnological processes by assessing the interaction impact of model variables (Guo et al., 2016).

In the present study, a fungal cell-free extract was applied to biosynthesis of ecofriendly and low-cost AgNPs. The effect of different factors influencing AgNPs production was optimized using central composite design (CCD) as one of RSM. This method provided us little number of trial-and-error runs is usually performed. Reports on using this experimental design and also *Talaromyces stipitatus* fungus in green synthesis of AgNPs are rare.

2. Materials and methods

2.1. Chemicals

Different culture media for routine culturing of fungal and bacterial strains were purchased from Difco Laboratories (Detroit, Mich., USA); silver nitrate (AgNO₃) was provided by Panreac Quimica (S.L.U, Barcelona, Spain); and HNO₃ (0.1 M), NaOH (0.1 M) solution used in pH measurements and all other chemicals were purchased from Oxoid Ltd. (Hampshire, UK).

2.2. Instruments

Several instruments used in this study included Ultraviolet Spectrum (origin: JASCO, model: V-630); Infrared Spectrum (origin: JASCO, model: FT/IR-4100 type A), Zeta Potential Analyzer (origin: Malvern Instruments Ltd, model: Malvern Zetasizer Nano-zs90), Transmission Electron Microscope (TEM) (model: JEOL JEM-2100); Energy-dispersive X-ray spectroscopy (EDS)

(Oxford instrument, model: Oxford X-Max 20), and a pH meter.

2.3. The fungal strain used for biosynthesis of AgNPs

The fungal strain used in this research was previously isolated from Lake Burullus, Egypt and identified as *Talaromyces stipitatus* by Botany and Microbiology Department, Faculty of Science, Damietta University, using classical morphological methods and confirmed by sequencing the internal transcribed spacer (ITS) region using universal primers ITS4 and ITS5 (White et al., 1990).

2.4. Preparation of fungal extract

Cell-free fungal filtrate of *T. stipitatus* was prepared to be applied in the biosynthesis of AgNPs. Firstly, to obtain fungal biomass, 250 ml Erlenmeyer flasks containing 100 ml of nitrate medium (0.35% yeast extract, 1% peptone, 0.35% potassium nitrate, and 1.5% glucose) (Hamedi et al., 2017) were inoculated with 5-day old discs of *T. stipitatus* and grown at 30°C for 7 day. For extracellular biosynthesis of AgNPs, wet fungal biomass was shaken for 72 h in 100 ml of sterilized distilled water at 150 rpm and 30° C. The cell-free filtrate was collected by filtration through Whatman filter paper no. 1.

2.5. Designing experiments for optimizing AgNPs production Talaromyces stipitatus

To prepare AgNPs, cell-free filtrate and AgNO₃ solution (1mM) were mixed and incubated at 30°C with agitation (150 rpm) for 120 hours in the dark. Initially, development of brown color is considered as an indication for the biosynthesis of AgNPs. A set of experiments were designed based on CCD changing the independent variables (temperature, reaction time, concentration of AgNO₃, and ratio of cell free extract and AgNO₃) considering absorbance at wavelength 420 nm as response (Table 1). Design was built with a total of 32 runs, and SPR intensity was recorded for each run.

Table 1. The different variables and their levels used for optimization of AgNPs biosynthesis by Talaromyces stipitatus.

	Independent variable (actual value)							
	A	В	С	D	E			
Level (coded value)	concentration of AgNO ₃ (mmol)	Temperature (C°)	Time of reaction (day)	pН	ratio of AgNO ₃ solution to cell free extract			
-2 (-α)	1	20	1	5	3:1			
-1	3	25	2	6	2:1			
0	5	30	3	7	1:1			
1	7	35	4	8	1:2			
2(+α)	9	40	5	9	1:3			

In 32 CCD-designed runs, there were 16 factorial runs included as cubic points, and 6 center points as replication runs used for pure error clarification. In addition, 8 axial runs were incorporated as star points of the proposed CCD. The alpha star points were set to a value of 2, so as to provide a rotatable design for experiments. The response was represented and indicated as "Peak intensity" of the

SPR which obtained by measuring the absorbance of 32 produced AgNPs samples at 420 nm.

The analysis of results and the building of experimental design were created using graphical and statistical analysis software (Design Expert ®, Version 11.0.0) and all experiments were carried out in triplicates. The first step in performing the statistical analysis using a multivariate optimization was to construct a regression model between

the intensity of the SPR (target response) and the experimental factors as the model's independent variables.

Different linear and polynomial regression models and various statistical parameters such as Sequential p-value, Lack of Fit p-value and squared correlation coefficient (R²) as "Adjusted R²" and "Predicted R²" were tested to select the best regression model.

The following second order polynomial equation was applied to calculate the relationship between different variables and the response:

$$Y = \beta_0 + \sum \beta_i X_i + \sum \beta_{ii} X_i^2 + \sum \beta_{ij} X_i X_j$$
 (eq.1)

where Y is the expected response, Xi, Xi^2 , and Xj are variables with coded values, $\beta0$ is the constant, βi is the linear effect, βii is the squared effect, and βij is the interaction effect.

2.6. Characterization of AgNPs

Nanoparticle size, morphology and shape were studied using TEM (Zhang et al., 2016). The particle size and zeta potential in liquid suspension were measured at 25°C using a Zeta Potential Analyzer. Energy-dispersive X-ray spectroscopy (EDX) was used as a standard approach for defining and quantifying elemental composition of samples. To estimate the functional components of synthesized AgNPs, Fourier transform infrared (FTIR) spectrum was analyzed.

2.7. Antibacterial activity

Potential antibacterial activity of biosynthesized AgNPs against Gram-positive bacteria such as Staphylococcus aureus ATCC25923 and Bacillus cereus ATCC6633, and Gram-negative bacteria like Pseudomonas aeruginosa ATCC27853 and Klebsiella pneumoniae ATCC33495 was firstly checked using the disk diffusion method.

First, 0.5 McFarland (1.5*10⁸ CFU/mL) of overnight pathogenic bacterial cultures were prepared. The bacterial growth was then inoculated into molten Mueller Hinton (MH) agar, resulting in a final concentration of tested strains of approximately 10⁶ cfu/ml. After solidification, 15 mm-diameter pores were made on agar plates and 200 μL of AgNPs (50, 100, 200 μg/ml) were added in each pore. Also, solutions of AgNO₃ (1 mmole), fungal cell-free filtrate of *T. stipitatus* and standard commercial antibiotic disks were used as controls. Following an incubation period of 24 h at 37° C, diameters of inhibition zone were

assessed in millimeters (mm). The tests were all performed in triplicate.

Using a broth microdilution methodology, the biosynthesized NPs were experimented for their minimum inhibitory concentrations (MIC) against pathogenic bacteria. AgNPs (64 g/ml) solution was serially diluted by Mueller-Hinton (MH) broth to get concentrations (32, 16, 8, 4, 2, 1, 0.5, 0.25 g/ml). In this experiment, bacterial inocula (final concentration of 106 CFU/ml) were placed in wells of a microtiter plate and different controls were included, i.e., culture media, cultures inoculated with tested strains, and culture media supplemented with AgNPs solely without inocula. The microtiter plate was kept at 37 °C for 24h, then the bacterial turbidity was measured spectrophotometrically and growth confirmed by re-culturing on MH agar plates. MIC values were determined by taking the lowest concentration leading to no growth on plates. The trials were carried out in two repetitions.

2.8. Antifungal activity

Antifungal activity of AgNPs against Aspergillus flavus Link ex Fries group, Aspergillus niger van Tiegh, Fusarium oxysporum f. sp. lycopersici Fol4287 and Alternaria alternata Fr. Keissler was carried out on PDA media. Tested fungal strains were obtained from Botany and Microbiology Department, Faculty of Science, Damietta University.

PDA plates supplemented with different AgNPs concentrations (1, 2, 4, 8, 16, 32 and 64 mg/l), with fluconazole (0.01 g/ml) as an antifungal agent (positive control) and without any treatment (negative control) were used. Each treatment was replicated. Disks (6 mm in diameter) of 7-day old fungal were placed upside-down in the center of the plates, incubated for 5 days and the radial growth was measured.

3. Results and discussion

3.1. Optimization of AgNPs production using response surface methodology

Table 2 shows 32 CCD-designed runs with the results of response as SPR intensity.

Table 2. Details of the 32 runs performed using central composite design (CDD) to optimize the biosynthesis of AgNPs.

	A	В	С	D	E	Absorbance Intensity*	
Run	Concentration of AgNO ₃ (mmole)	Temperature (°C)	Time (day)	pН	ratio of gNO ₃ to cell free extract	_ 1110113113	
1	-1	1	1	-1	1	0.204831	
2	-1	1	-1	-1	-1	0.361102	
3	-1	1	1	1	-1	0.432689	
1	0	0	0	0	0	0.418252	
;	-1	-1	1	1	1	0.214648	
j	1	-1	-1	1	1	0.229373	
,	0	2	0	0	0	0.480851	
	1	1	1	-1	-1	0.713129	
	0	0	0	0	2	0.426267	
0	1	1	-1	1	-1	0.543788	
1	0	0	0	2	0	0.874823	
2	0	-2	0	0	0	0.429624	
3	0	0	0	0	0	0.474823	
4	-2	0	0	0	0	0.261278	
5	1	-1	1	1	-1	0.747416	
6	0	0	2	0	0	0.134135	
7	-1	-1	-1	1	-1	0.418703	
8	0	0	0	0	0	0.408007	
9	0	0	-2	0	0	0.267079	
0	0	0	0	0	0	0.408007	
1	0	0	0	0	0	0.200634	
2	1	1	-1	-1	1	0.388326	
3	0	0	0	0	0	0.409437	
4	0	0	0	-2	0	0.866519	
5	1	1	1	1	1	0.318729	
6	1	-1	-1	-1	-1	0.433972	
7	1	-1	1	-1	1	0.535898	
8	-1	1	-1	1	1	0.353926	
9	2	0	0	0	0	0.701836	
0	-1	-1	-1	-1	1	0.260633	
1	-1	-1	1	-1	-1	0.196726	
2	0	0	0	0	-2	0.411167	

^{*} The absorbance intensity of the SPR at 420 nm.

A quadratic model was proposed on the basis of these statistics to establish a correlation between the experimental variables and the response, as indicated in table 3. In this case, quadratic model was the highest order polynomial selection where the additional terms are significant and the model is not aliased; cannot be accurately fit with the design and should generally not be considered for analysis.

Table 3. Fit statistics of the quadratic model.

Std. Dev.	0.1209	R ²	0.8555
Mean	0.4227	Adjusted R ²	0.5927
C.V. %	28.60	Predicted R ²	-1.6546
		Adeq Precision	7.0880

[:] R² = Correlation Coefficient

Adequate precision (Adeq. Precision) seems to be another statistical indicator for our model validation and can be a measure of the ratio of signal to noise. In our model, ratio of 7.088 indicates an adequate signal (greater than 4), as the precision acceptance cut-off value. This model can be utilized to navigate the design space.

The computed parameters for the quadratic full model (FM), which included all experimental variables, were

AgNO₃ concentration (A), temperature (B), time of reaction (C), pH (D) and proportion of AgNO₃ to cell free extract (E) and their binary and self-interactions. The final equation with reference to coded factors was represented by the following equation in which SPR intensity of AgNPs (Y) was the response [eq (2)]:

SPR Intensity =0.407063 + 0.0978537 * A + 0.0159002 * B + 0.00451479 * C + 0.00755262 * D + -0.0546234 * E - 0.0152828 * AB + 0.0665739 * AC + -0.0392933 * AD + -0.0369248 * AE + -0.0206107 * BC -0.0125729 * BD + -0.0142894 * BE + -0.00242869 * CD + -0.0181592 * CE + -0.0444174 * DE + 0.00322165 * A^2 + -0.00335823 * B^2 + -0.0670159 * C^2 + 0.1005 * D^2 + -0.0124884 * E^2 (eq.2)

This equation with regard to coded factors may be applied to predict response for different levels of each factor and determine the relative importance of the components by contrasting the factor coefficients. For each factor, when all other factors are maintained constant, the coefficient estimate provides the predicted change in response per unit change in factor value. Based on Eq. 2, the sign of coefficient is negative for the ratio of AgNO3 to cell free extract (factor E) and positive for the other four variables (AgNO3 concentration, temperature, reaction time, and pH). This indicates that the ratio of AgNO3 to cell free extract (factor E) reversely affect AgNPs biosynthesis, whereas AgNO3 concentration (factor A), temperature (factor B), reaction time (factor C), and pH

(factor D) have direct effect on AgNPs formation. Temperature effect of SPR intensity could be due to improving the formation rate of AgNPs. Increasing pH beneficially influence the intensity of SPR probably as a result of increasing the ionisation of active functional groups, the reduction capability of the extract and subsequently the formation of AgNPs. Raising AgNO3 concentration results in improving AgNPs formation as indicated by darkening in solution and increased SPR peak intensity. Also, increasing reaction time increased AgNPs formation.

On the contrary, increasing AgNO₃ concentration while decreasing the volume of cell free extract resulted in an increasing in the AgNPs SPR intensity. Several studies indicated that for better AgNPs formation, excess silver ion is required in the biological /green synthesis approach (Dada et al., 2018). The SPR intensity decreased in a high volume of fungal cell-free extracts because of the high amounts of the reducing agents, that could promote AgNPs precipitation (Yakovlev & Golubeva, 2014).

As seen in Eq. (2), the positive sign of AgNO₃ concentration*time implied a direct influence of their interaction on AgNPs formation and quality as indicated by SPR intensity, whereas the negative sign of the other interaction reflects their reverse influence on AgNPs biosynthesis. The analysis of variance (ANOVA) was performed and results are presented in Table 4.

Table 4. ANOVA and model performance of full quadratic model.

	•					
Source	Sum of Squares	Df	Mean Square	F-value	p-value	
Model	0.9518	20	0.0476	3.26	0.0242	Significant
A- AgNO ₃ conc.	0.2298	1	0.2298	15.72	0.0022	
B- temperature	0.0061	1	0.0061	0.4151	0.5326	
C- time	0.0005	1	0.0005	0.0335	0.8582	
D- pH	0.0014	1	0.0014	0.0937	0.7653	
E- ratio	0.0716	1	0.0716	4.90	0.0489	
AB	0.0037	1	0.0037	0.2557	0.6231	
AC	0.0709	1	0.0709	4.85	0.0499	
AD	0.0247	1	0.0247	1.69	0.2202	
AE	0.0218	1	0.0218	1.49	0.2474	
BC	0.0068	1	0.0068	0.4650	0.5094	
BD	0.0025	1	0.0025	0.1730	0.6854	
BE	0.0033	1	0.0033	0.2235	0.6456	
CD	0.0001	1	0.0001	0.0065	0.9374	
CE	0.0053	1	0.0053	0.3610	0.5602	
DE	0.0316	1	0.0316	2.16	0.1697	
A^2	0.0003	1	0.0003	0.0208	0.8879	
B ²	0.0003	1	0.0003	0.0226	0.8831	
\mathbb{C}^2	0.1317	1	0.1317	9.01	0.0120	
D^2	0.2963	1	0.2963	20.27	0.0009	
\mathbb{E}^2	0.0046	1	0.0046	0.3130	0.5871	
Residual	0.1608	11	0.0146			
Lack of Fit	0.1160	6	0.0193	2.16	0.2082	not significant
Pure Error	0.0448	5	0.0090			-
Cor Total	1.11	31				

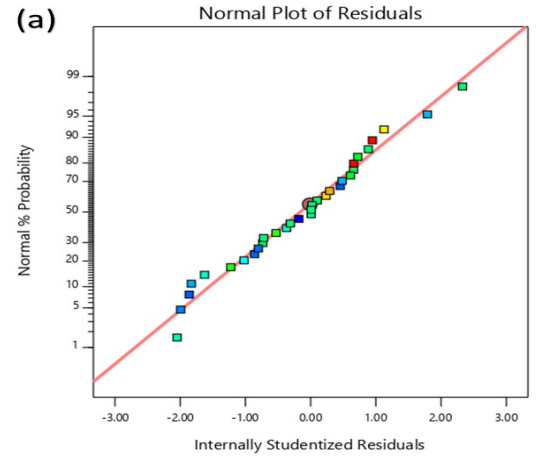
DF = Degree of Freedmen, F = Fisher-ratio.

Model terms are considered significant when the P-value is less than 0.0500 whereas values larger than 0.1000

imply that they are not significant. A, E, AC, C², and D² are significant model terms in this situation.. In addition,

the normal residual probability and the internally studied residual vs. the expected response (SPR intensity) are two more ways that may be used to assess the validity of the models. According to Figure 1 (a), for all the outstanding values reflected along the straight line with small value of

deviations and proves the normality of errors-distribution. Figure 1(b) presents the relation of residual vs. predicted SPR intensity, the residual is randomly distributed in both sides of zero line and also lie in a range that is less than the allowable range of $\pm 3\sigma$.



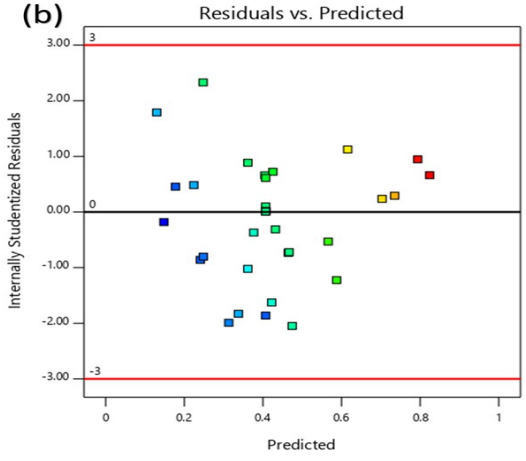


Figure 1. Normal probability plot of internally studentized residuals for the quadratic model for SPR intensity (a) and plot of residual versus predicted SPR intensity (b).

Using the three-dimensional (3D) response surface plots, the effect of different tested factors (independent variables) on the AgNPs SPR intensity (dependent variable) was studied (Figure 2). The graphs show SPR intensity as response surface, versus two factors that may show binary interactions. The other factors were set constant at the central level. Figure 2 (a) demonstrates that AgNO₃ concentration (A) has a greater influence on SPR intensity than time (C), since the surface slope is steeper in the direction of AgNO₃ concentration axis than towards time axis. Furthermore, temperature (B) has a greater influence on SPR intensity than ratio (E) (e). The surface slope obtained for temperature × AgNO₃ concentration was less steep than that obtained for time × concentration of AgNO₃ (Figure 2 (a, b)). AgNPs formation was

improved at alkaline pH, as predicted and shown in Figure 2 (c). As shown in Figure 2 (d), AgNO₃ concentration (A) versus the ratio (E) was the steepest slope of the surface plots confirming that using amounts of AgNO₃ larger than the amount of cell-free filtrate improves the biosynthesis of AgNPs. It can be viewed in Figure 2 (f) that the interaction of time × pH is more complex since more curvature in the 3D plot surface was noted. Finally, because all of the produced surfaces are smooth in each plot and both factors have a comparable influence on the SPR intensity, there is no abnormal interaction between variables. Data obtained by the 3D response surface plots are in accordance with those obtained from quadratic model equation.

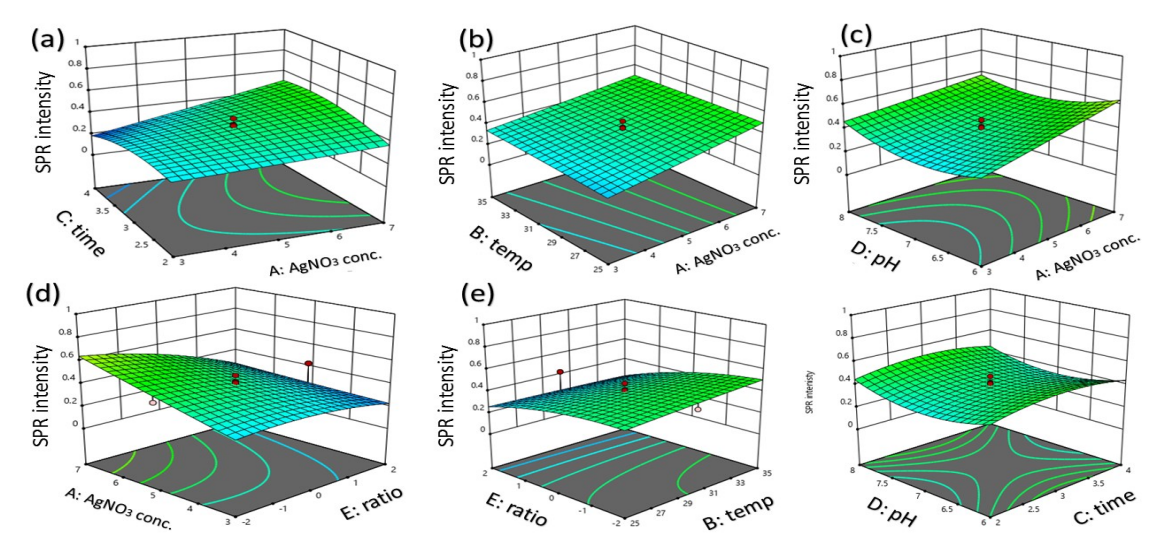


Figure 2. Three-dimensional response surface plots of independent factors effect [time-AgNO₃ concentration(a)], [temperature-AgNO₃ concentration (b)], [AgNO₃ concentration -pH (c)], [AgNO₃ concentration -ratio (d)], [ratio-temperature (e)], and [pH-time (f)] on the SPR intensity of AgNPs Optimal condition of AgNPs biosynthesis by T. stipitatus

To get maximum SPR intensity and thus obtaining high amounts of AgNPs, the predicted optimal conditions were determined to be: AgNO $_3$ concentration= 7mmol, temperature = 25°C, time= 91.2 hr, pH=8, ratio of AgNO $_3$ solution to cell free extract is 2:1. Some synthesized samples of AgNPs were prepared under these optimal conditions to verify the accuracy of this prediction as shown in Figure 3.

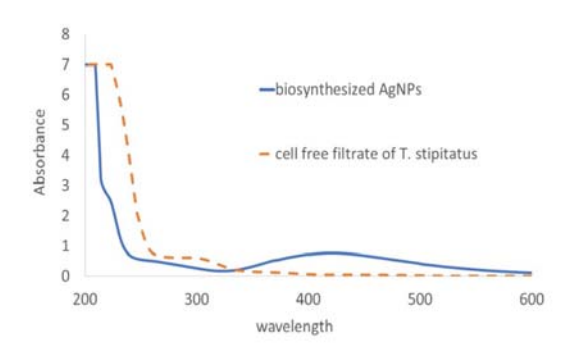


Figure 3. UV-Vis absorption spectra, showing the SPR peak, of synthesized AgNPs using cell free extract of *T. stipitatus*.

3.2. Characterization of synthesized silver nanoparticles

As shown in Figure 4, the biosynthesized AgNPs varied in size from 6.89 nm 23.64 nm and had spherical shapes. The average size of AgNPs based on different taken images is 13.95 nm. The size of AgNPs observed in TEM images is comparable with that obtained in previous studies focusing on AgNPs biosynthesis (Sharma et al.,

2018); especially by fungi belonging to the same family of *Talaromyces* (Rose et al., 2019).

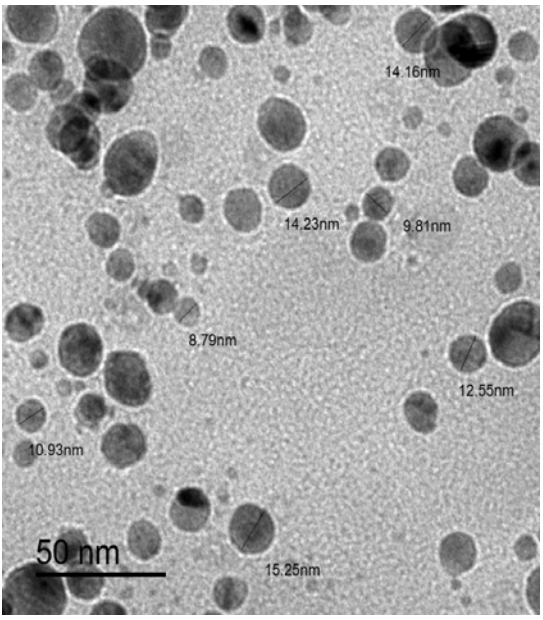


Figure 4. Transmission electron microscopy (TEM) micrograph of spherical AgNPs, biosynthesized by *Talaromyces stipitatus*.

In EDX analysis, the energy dispersive spectrum indicated the existence of elemental silver (Figure 5). As previously reported, at 3 keV, the sharp peak marked the presence of metallic silver (Femi-Adepoju et al., 2019). Also, the appearance of other EDX peaks for C, O, Na, k and Mo is probably due to the content of used cell-free filtrate.

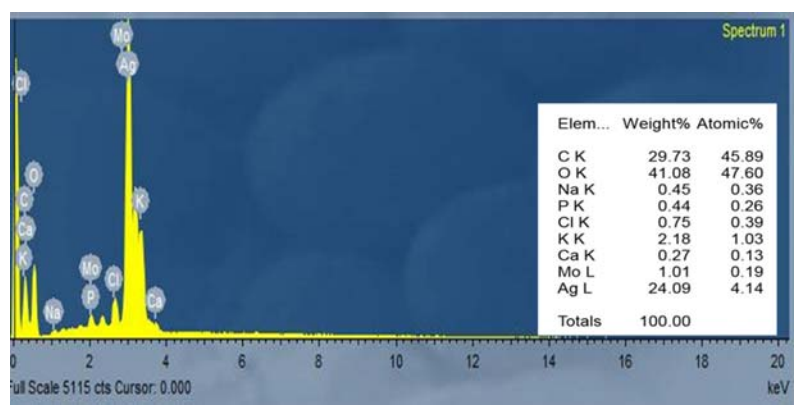
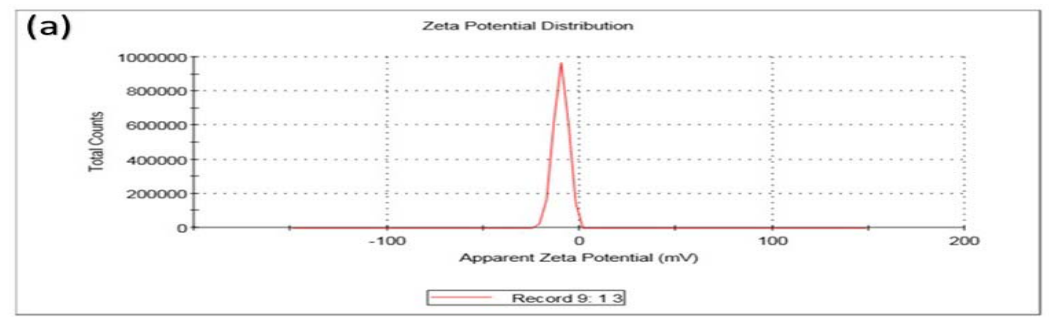


Figure 5. EDX spectrum of AgNPs biosynthesized by Talaromyces stipitatus filtrate.

The zeta potential, a measure indicator of NPs stability, was indicated to be 9.85 mV (Figure 6 (a)). NPs having a zeta potential of 0 to 10 mV are considered to be near to neutral state (Asha & Narain, 2020). The zeta potential

value might be attributed to biomolecules contained in the employed cell-free fungal filtrate capping (Raja et al., 2017).



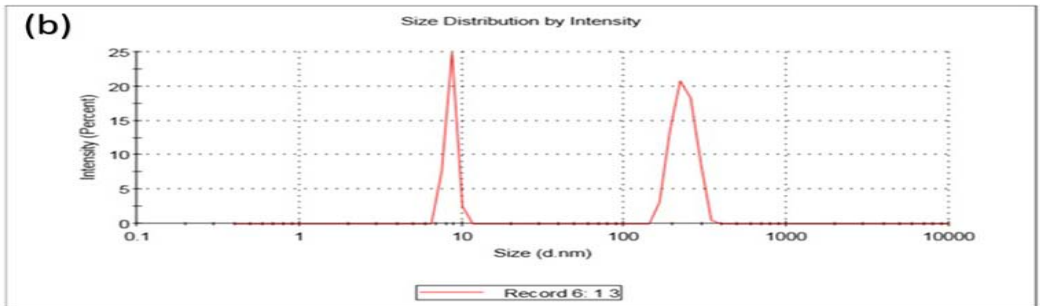


Figure 6: DLS and Zeta potential measurement using Zetasizer; (a): Zeta potential and (b) Size Distribution chart, determined by intensity, using DLS for AgNPs sample biosynthesized by *Talaromyces stipitatus*

Using dynamic light scattering (DLS), the size distribution profile of AgNPs biosynthesized by *T. stipitatus* is presented in Figure 6 (b). The distribution curve shows two different peaks that represent different particle sizes with average size of 58.22 (d. nm). In fact, the size of 65% of particles was 232.1 d.mn, whereas that of remaining 35 % was 8.562 d. nm. It is considered that DLS measures the hydrodynamic radius, not the absolute radius. This measure depends on the velocity of the Brownian motion which is transformed into particle size using the Stokes-Einstein relationship (Zhang et al., 2016).

FTIR analysis was performed to identify the compounds and functional groups responsible for the reduction of Ag⁺ ions and capping of NPs. In Figure 7, the FTIR spectrum of biosynthesized AgNPs showed several

noticeable peaks at 3408.57, 2142.53, 1623.77, 1395.25, 1038.48 and 623.85 cm⁻¹. The existence of band peak at 3408.57 cm⁻¹ might be due to the presence of N-H stretching. The presence of silver nanomaterials in the composition of biosynthesized AgNPs is demonstrated by a clear band at 1623 cm⁻¹ (Owaid et al., 2018). Also, the C-O stretching mode is responsible for the vibrations at 1,395 and 2,142 cm⁻¹ (El-Naggar et al., 2014). Moreover, the band at 1038 cm⁻¹ correspond to the amine's C-N stretching vibrations. The existence of a proteinaceous capping agent that inhibits NPs from aggregating has been suggested as a possible explanation for the stability of AgNPs produced using cell-free filtrates (Saifuddin et al., 2009).

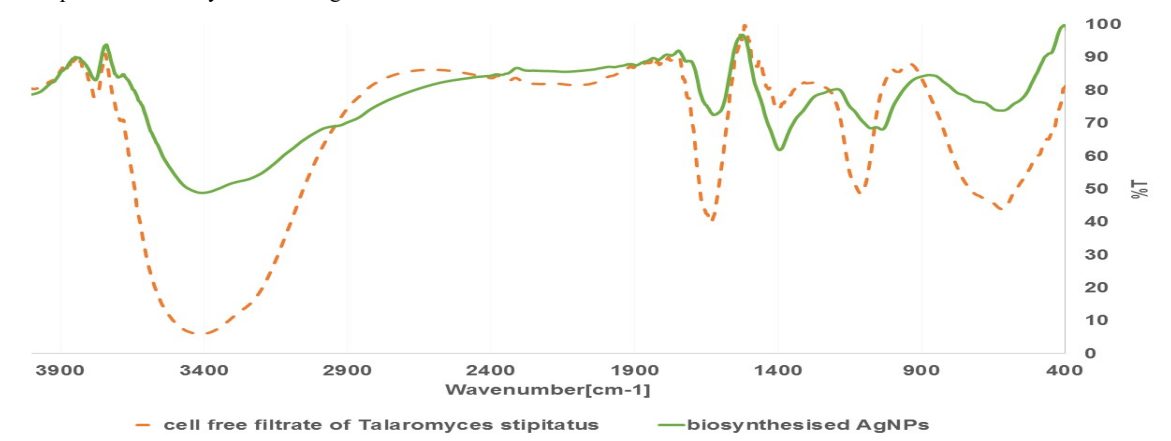


Figure 7. FTIR spectrum of AgNPs biosynthesized by Talaromyces stipitatus

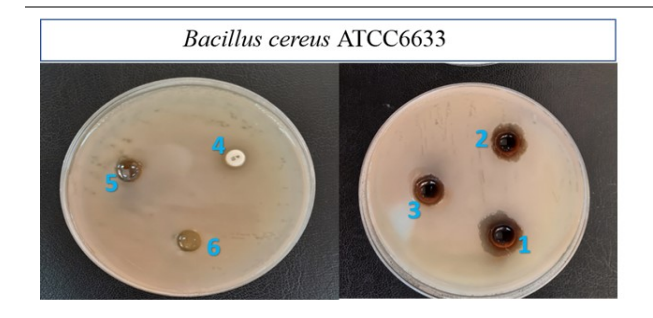
3.3. Antibacterial activity:

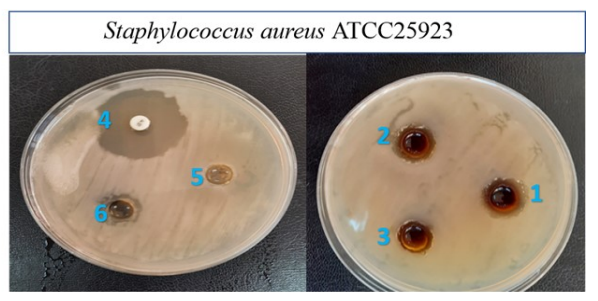
AgNPs synthesized by *T. stipitatus* were evaluated for their antibacterial activity by disk diffusion method and results were recorded in Table 5 and shown in

Supplementary Figure 1. The MIC values were 4, 8, 16 and 8 μg/ml for *B. cereus*, *S. aureus*, *K. pneumoniae* and *P. aeruginosa*, respectively. The antibacterial activity results against *B. cereus* ATCC6633 was similar to that reported by Nour El-Dein et al., (2021).

Table 5. Inhibition effect of silver nanoparticles against selected pathogenic bacteria

	Diameter of inhibition (mm, mean)								
Treatment	Bacillus cereus ATCC6633	Staphylococcus aureus ATCC25923	Klebsiella pneumoniae ATCC33495	Pseudomonas aeruginosa ATCC27853					
200 μg/ml AgNPs	19.11	16.1	19.15	18.36					
100 μg/ml AgNPs	16.71	15.3	15.3	14.16					
50 μg/ml AgNPs	12.63	12.86	12.84	11.43					
Penicillin G	10.36	30.1	17.81	8.2					
AgNO ₃ (1 mmole)	10.06	12.01	15.1	12					
cell free filtrate of Talaromyces stipitatus	-	-	-	-					





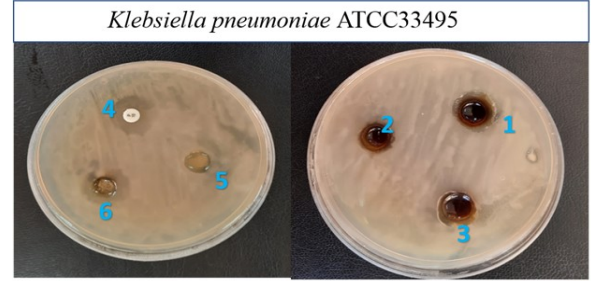




Figure 8. Inhibition zone of AgNPs against B. cereus ATCC6633, S. aureus ATCC25923, P. aeruginosa ATCC27853 and K. pneumoniae ATCC33495

note: (1) 200 μ g/mL AgNPs, (2) 100 μ g/mL AgNPs, (3) 50 μ g/mL AgNPs, (4) Penicillin G, (5) AgNO₃ (1m. mole) and (6) cell free filtrate of *T. stipitatus* treatments

3.4. Antifungal activity:

The effect of different AgNPs concentrations on fungal growth was tested and data recorded and shown in Table 6 and Supplementary Figure 2. AgNPs synthesized by *T. stipitatus* appeared to be a promising control agent against

A. flavus Link ex Fries group and A. niger van Tiegh as the growth diameter was reduced in rates comparable with the positive control, the antifungal compound fluconazole (0.01g/ml).

Table 6. Inhibition effect of silver nanoparticles against some fungi.

	Radial growth (mm) *			
Treatment	Fusarium oxysporum f. sp. lycopersici Fol4287	Alternaria alternata Fr. Keissler	Aspergillus flavus Link ex Fries group	Aspergillus niger van Tiegh
Negative control – without any treatment	64	64	82	85
Positive control -with antifungal compound-fluconazole (0.01g/ml)	54	24	71	79
1 mg/l of AgNPs	63	55	78	85
2 mg/l of AgNPs	62	52	77	82
4 mg/l of AgNPs	61	50	75	80
8 mg/l of AgNPs	60	47	73	78
16 mg/l of AgNPs	60	45.5	70	76
32 mg/l of AgNPs	59	45	65	72
64 mg/l of AgNPs	58	43	64	65

^{*}mean

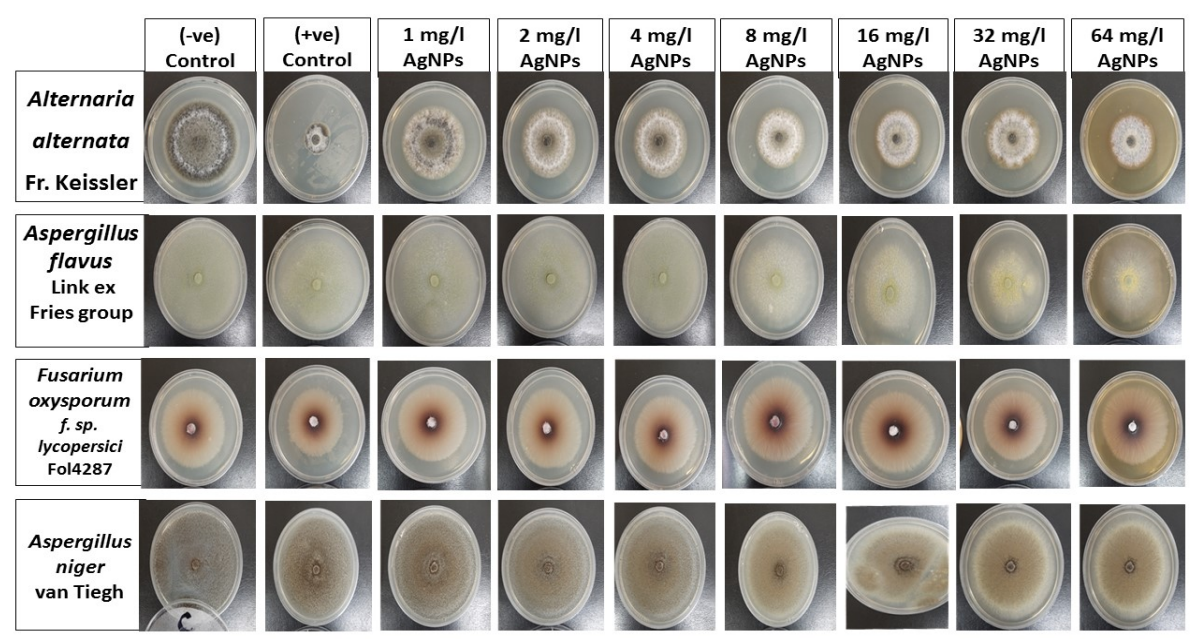


Figure 9. Visual radial growth for inhibitory effect of AgNPs against *Aspergillus* niger van Tiegh, *Aspergillus flavus* Link ex Fries group, *Alternaria alternata* Fr. Keissler and *Fusarium oxysporum* f. sp. lycopersici Fol4287. note: AgNPs concentrations (1, 2, 4, 8, 16, 32 and 64 mg/L) and controls; Negative control: without any treatment and positive control: with antifungal compound-fluconazole (0.01g/ml).

4. Conclusion

T. stipitatus fungus was used as a green source for the biosynthesis of AgNPs. Fungal cell-free filtrate, including the metabolites, may work as reducing and capping reagent in the process of AgNPs biosynthesis. It helps stabilizing the produced AgNPs by converting Ag+ ions to Ag°. Different factors including temperature, pH, and time of reaction may affect this process. Therefore, in the current study, CCD was used for optimizing AgNPs biosynthesis process. Five factors were evaluated in the optimization process of NPs biosynthesis by fungal cell-free filtrate, i.e., concentration of AgNO3 (mmole), temperature (°C), time, pH and ratio of AgNO3 to cell free extract. Using CDD, the optimal conditions were predicted to be: AgNO3 concentration= 7mmol, temperature = 25°C, time= 91.2 hr, pH=8, ratio of AgNO3 solution to cell

free extract is 2:1. Biosynthesized AgNPs were spherical with average size of 13.95nm and hydrodynamic radius average of 58.22(d. nm). The biosynthesized AgNPs were negatively charged with a charge equal to -9.85 mV as determined by zeta potential analyzer. The presence of silver metal in obtained AgNPs was confirmed using EDX and functional groups present in the fungal cell-free filtrate that may be responsible for reducing Ag ions and keeping the NPs stable FTIR estimated. Finally, the antimicrobial activity of biosynthesized AgNPs were tested and showed promising results. Also, future studies on the effect of combinations of AgNPs with known antibiotics should be considered to increase the benefit of applying both agents together. To our awareness, this is the first study on optimization of biosynthesis AgNPs by T. stipitatus fungus using CCD as one of response surface method.

Acknowledgement

Our sincere appreciation and gratitude to every member of the Department of Botany and Microbiology at the Faculty of Science, Damietta University, and special thanks to Mohamed M. El-Zahed for his support in this research.

Reference

- Ahumada M., Suuronen E.J., Alarcon E.I. (2019) Biomolecule Silver Nanoparticle-Based Materials for Biomedical Applications. In: Martínez L., Kharissova O., Kharisov B. (eds) **Handbook of Ecomaterials**. Springer, Cham. https://doi.org/10.1007/978-3-319-68255-6 161
- Asha, A. B., & Narain, R. (2020). Nanomaterials properties. In: R. Narain, **Polymer Science and Nanotechnology** (pp. 343-359). Elsevier. doi:https://doi.org/10.1016/B978-0-12-816806-6.00015-7
- Baker, S., Mohan Kumar, K., Santosh, P., Rakshith, D., & Satish, S. (2015). Extracellular synthesis of silver nanoparticles by novel *Pseudomonas veronii* AS41G inhabiting Annona squamosa L. and their bactericidal activity. *Spectrochim. Acta A Mol. Biomol. Spectrosc.*, **136**, 1434–1440.
- https://doi.org/10.1016/j.saa.2014.10.033
- Baş, D., & Boyacı, İ. H. (2007). Modeling and optimization I: Usability of response surface methodology. *J Food Eng.*, **78(3)**, 836–845. https://doi.org/10.1016/j.jfoodeng.2005.11.024
- Basavegowda, N., & Lee, Y. R. (2014). Synthesis of Gold and Silver Nanoparticles Using Leaf Extract of *Perilla Frutescens* A Biogenic Approach. *J Nanosci Nanotechnol.*, *14*(6), 4377–4382. https://doi.org/10.1166/jnn.2014.8646
- Bhatnagar, S., Kobori, T., Ganesh, D., Ogawa, K., & Aoyagi, H. (2019). Biosynthesis of Silver Nanoparticles Mediated by Extracellular Pigment from *Talaromyces purpurogenus* and Their Biomedical Applications. *Nanomaterials*, *9*(7), 1042. https://doi.org/10.3390/nano9071042
- Bhushan, B. (2017). **Springer Handbook of Nanotechnology**. Springer Berlin Heidelberg. https://doi.org/10.1007/978-3-662-54357-3
- Collera-Zúñiga, O., García Jiménez, F., & Meléndez Gordillo, R. (2005). Comparative study of carotenoid composition in three mexican varieties of *Capsicum annuum L. Food Chem.*, 90(1–2), 109–114. https://doi.org/10.1016/j.foodchem.2004.03.032
- Dada, A. O., Adekola, F. A., Adeyemi, O. S., Bello, O. M., Oluwaseun, A. C., Awakan, O. J., & Grace, F.-A. A. (2018). Exploring the Effect of Operational Factors and Characterization Imperative to the Synthesis of Silver Nanoparticles. In: Silver Nanoparticles Fabrication, Characterization and Applications. InTech. https://doi.org/10.5772/intechopen.76947
- El-Naggar, N. E.-A., Abdelwahed, N. A. M., & Darwesh, O. M. M. (2014). Fabrication of Biogenic Antimicrobial Silver Nanoparticles by *Streptomyces aegyptia* {NEAE} 102 as Eco-Friendly Nanofactory. *J Microbiol Biotechnol.*, **24(4)**, 453–464. https://doi.org/10.4014/jmb.1310.10095
- El-Zahed, M. M., Baka, Z., Abou-Dobara, M. I., & El-Sayed, A. (2021). In Vitro Biosynthesis and Antimicrobial Potential of Biologically Reduced Graphene Oxide/Ag Nanocomposite at Room Temperature. *J microbiol biotechnol food sci.*, *10*(6), e3956–e3956.

- Femi-Adepoju, A. G., Dada, A. O., Otun, K. O., Adepoju, A. O., & Fatoba, O. P. (2019). Green synthesis of silver nanoparticles using terrestrial fern (*Gleichenia pectinata* (Willd.) C. Presl.): characterization and antimicrobial studies. *Heliyon*, **5(4)**, e01543. https://doi.org/10.1016/j.heliyon.2019.e01543
- Guo, X., Zhang, Q., Ding, X., Shen, Q., Wu, C., Zhang, L., & Yang, H. (2016). Synthesis and application of several sol–gelderived materials via sol–gel process combining with other technologies: a review. *J Sol-Gel Sci Technol.*, **79(2)**, 328–358. https://doi.org/10.1007/s10971-015-3935-6
- Hamedi, S., Ghaseminezhad, M., Shokrollahzadeh, S., & Shojaosadati, S. A. (2017). Controlled biosynthesis of silver nanoparticles using nitrate reductase enzyme induction of filamentous fungus and their antibacterial evaluation. *Artif Cells Nanomed Biotechnol.*, **45(8)**, 1588–1596. https://doi.org/10.1080/21691401.2016.1267011
- Jagadeesh, B. H., Prabha, T. N., & Srinivasan, K. (2004). Activities of β-hexosaminidase and α-mannosidase during development and ripening of bell capsicum (Capsicum annuum var. variata). Plant Sci., 167(6), 1263–1271. https://doi.org/10.1016/j.plantsci.2004.06.031
- Kate, S., Sahasrabudhe, M., & Pethe, A. (2020). Biogenic Silver Nanoparticle Synthesis, Characterization and its Antibacterial activity against Leather Deteriorates. *Jordan J Biol Sci.*, *13*(4), 493–498.
- Majeed, M. I., Bhatti, H. N., Nawaz, H., & Kashif, M. (2019). Nanobiotechnology: Applications of Nanomaterials in Biological Research. In: Shahid ul-Islam (Ed.), **Integrating Green Chemistry and Sustainable Engineering** (pp. 581–615). John Wiley & Sons, Inc. https://doi.org/10.1002/9781119509868.ch17
- Nour El-Dein, M. M., Baka, Z. A. M., Abou-Dobara, M. I., El-Sayed, A. K., & El-Zahed, M. M. (2021). Extracellular Biosynthesis, Optimization, Characterization and Antimicrobial Potential of *Escherichia Coli* D8 Silver Nanoparticles. *J microbiol biotechnol food sci.*, 10(4), 648–656.
- Owaid, M. N., Naeem, G. A., Muslim, R. F., & Oleiwi, R. S. (2018). Synthesis, Characterization and Antitumor Efficacy of Silver Nanoparticle from *Agaricus bisporus* Pileus, Basidiomycota. *Walailak J Sci & Tech. (WJST)*, *17*(2), 75–87. https://doi.org/10.48048/wjst.2020.5840
- Phanjom, P., & Ahmed, G. (2017). Effect of different physicochemical conditions on the synthesis of silver nanoparticles using fungal cell filtrate of *Aspergillus oryzae* ({MTCC} No. 1846) and their antibacterial effect. *Adv Nat Sci: Nanosci Nanotechnol.*, 8(4), 45016. https://doi.org/10.1088/2043-6254/aa92bc
- Raja, S., Ramesh, V., & Thivaharan, V. (2017). Green biosynthesis of silver nanoparticles using *Calliandra haematocephala* leaf extract, their antibacterial activity and hydrogen peroxide sensing capability. *Arab J Chem.*, *10*(2), 253–261. https://doi.org/10.1016/j.arabjc.2015.06.023
- Rose, G. K., Soni, R., Rishi, P., & Soni, S. K. (2019). Optimization of the biological synthesis of silver nanoparticles using *Penicillium oxalicum* GRS-1 and their antimicrobial effects against common food-borne pathogens. *Green Processing and Synthesis*, 8(1), 144–156. https://doi.org/10.1515/gps-2018-0042
- Saifuddin, N., Wong, C. W., & Yasumira, A. A. N. (2009). Rapid Biosynthesis of Silver Nanoparticles Using Culture Supernatant of Bacteria with Microwave Irradiation. *J Chem.*, **6(1)**, 61–70. https://doi.org/10.1155/2009/734264

Sharma, G., Nam, J.-S., Sharma, A., & Lee, S.-S. (2018). Antimicrobial Potential of Silver Nanoparticles Synthesized Using Medicinal Herb *Coptidis rhizome. Molecules*, **23(9)**, 2268. https://doi.org/10.3390/molecules23092268

Siddiqui, M. H., Al-Whaibi, M. H., Firoz, M., & Al-Khaishany, M. Y. (2015). Role of Nanoparticles in Plants. In: Nanotechnology and Plant Sciences (pp. 19–35). Springer International Publishing. https://doi.org/10.1007/978-3-319-14502-0 2

Vega-Baudrit, J., Gamboa, S. M., Rojas, E. R., & Martinez, V. V. (2019). Synthesis and characterization of silver nanoparticles and their application as an antibacterial agent. *Int J Biosens Bioelectron.*, **5(5)**. https://doi.org/10.15406/ijbsbe.2019.05.00172

White, T. J., Bruns, T., Lee, S., and Taylor, J. (1990). Amplification and direct sequencing of fungal ribosomal RNA genes for phylogenetics, In: M. A. Innis, D. H. Gelfand, J. J. Sninsky, and T. J. White (Eds.), **PCR Protocols: A Guide to Methods and Applications**, (New York, NY: Academic Press), 315–322. doi: 10.1016/b978-0-12-372180-8.50042-1

Yakovlev, A. V, & Golubeva, O. Y. (2014). Synthesis Optimisation of Lysozyme Monolayer-Coated Silver Nanoparticles in Aqueous Solution. *J Nanomaterials*, **2014**, 1–8. https://doi.org/10.1155/2014/460605

Zhang, X.-F., Liu, Z.-G., Shen, W., & Gurunathan, S. (2016). Silver Nanoparticles: Synthesis, Characterization Properties, Applications, and Therapeutic Approaches. *Int J Mol Sci.*, *17*(9), 1534. https://doi.org/10.3390/ijms17091534.

Jordan Journal of Biological Sciences

Anti-malarial Effect of *Momordica charantia* Involved Modulation of Cytokine Mediated via GSK3β Inhibition in *Plasmodium berghei*- Infected Mice

Mayada Hussain Ali^{1,2}, Izyanti Ibrahim^{3,*}, Malina Jasamai⁴,Noor Embi⁵, Hasidah Sidek⁵

¹ Faculty of Science and Technology, Universiti Kebangsaan Malaysia, Bangi 43600 UKM, Selangor, Malaysia.; ² Institute of Genetic Engineering and Biotechnology for Postgraduate Studies, University of Baghdad, Iraq.; ³ Faculty of Science and Technology, Universiti Kebangsaan Malaysia, Bangi 43600 UKM, Selangor, Malaysia; ⁴ Faculty of Pharmacy, Universiti Kebangsaan Malaysia, Malaysia; ⁵ Faculty of Science and Technology, Universiti Kebangsaan Malaysia, Bangi 43600 UKM, Selangor, Malaysia.

Received: June 20, 2021; Revised: December 19, 2021; Accepted: January 4, 2021

Abstract

Increasing resistance of malarial parasites to current anti-malarials has led to efforts to explore use of medicinal plants as immunomodulators to target the host. *Momordica charantia(MC)* is an Asian dietary fruit with different pharmacological activities. GSK3 is known to be pivotal in the controlling of cytokine inflammatory response. Present investigation involves evaluation of MC aqueous extract for its anti-malarial activity and to elucidate whether its mechanism involves inhibition of GSK3 β . Akt and NF- κ B in the action of MC on GSK3 were evaluated. Our *in vitro* studies using *Plasmodium falciparum* 3D7 culture revealed that MC suppressed parasite growth with a selectivity index exceeding 10. Intra-peritoneal administration of the aqueous extract into P. *berghei* NK65-infected mice resulted in a dose-dependent manner and improved median survival time. The selected doses of MC into infected mice resulted in significant increase in the levels (7.2 and 2.7fold) of phosphorylated GSK3 β and Akt respectively in liver. Decreased phosphorylation of NF- κ B (2.0fold) in MC-treated infected mice was observed. MC decreased levels of the serum pro-inflammatory cytokines IFN- γ (2.7fold), TNF- α (4.9fold), while the anti-inflammatory cytokine level IL-10 was increased (2.3fold). Our findings demonstrate that anti-malarial effect of MC involved cytokine modulation mediated via inhibition of GSK3 β in P. *berghei*- infected mice.

Keywords: Malaria, Momordica charantia, Glycogen synthase kinase-3β, P. berghei, inflammatory cytokines

1. Introduction

Malaria caused by *Plasmodium* parasites is still one of the most common and deadly human infectious diseases. WHO has estimated 229 million malaria cases in 87 endemic countries and responsible for 409 000 deaths distributed in African, Western Pacific regions, South-East Asia, Eastern Mediterranean and Americas in 2019 (WHO, 2020). The increasing of parasite resistance to available anti-malarial drugs is occurring at an alarming rate (Deu, 2017); besides, malaria is a life-threatening disease. Thus, alternative therapeutic modalities for this disease are urgently needed. The infection with P. falciparum can progress if left untreated. As a result, a new anti-malarial compound with a novel mechanism is urgently required. The potential use of medicinal plants for inflammationrelated conditions offers an attractive strategy for antimalarial drug discovery efforts (Bekono et al., 2020).

One example of medicinal plant, *Momordica charantia* (MC) belongs to the Cucurbitaceae family and is a traditional dietary fruit. Pharmacological activities associated with *M. charantia* extracts include anti-diabetic, anti-cancer, anti-inflammation, anti-fungal, anti-bacterial,

and parasites infections as well as, has immunomodulatory effects (Saeed et al., 2018). M. charantia modulated transcription factor (NF-κB) activity as a potential target to prevent insulin resistance and diabetes (Yang et al., 2014). Akanji et al. (2016) have reported that the leaf extract of M. charantia has shown anti-malarial activity, though the mechanism is not yet elucidated. M. charantia contains momordenol and momordicilin capable to binding of glycogen synthase kinase (GSK3), which have been reported as GSK3 inhibitors based on in silico docking and binding studies and can be potentially used as an antidiabetic compounds via activation of insulin signaling (Hazarika et al., 2012). GSK3 is a serine / threonine kinase initially identified as the kinase which phosphorylates of glycogen synthase in skeletal muscle (Embi et al., 1980). Which is now recognized as a target for the regulation of cytokine production and the dysregulation of this kinase is implicated in many diseases and inflammation-related conditions (Hoffmeister et al., 2020). Dai et al. (2012) showed that GSK3β inhibition by lithium chloride (LiCl) reduced neuronal degeneration in cerebral malaria via Akt activation. Our own work showed the curcumin had anti-malarial effect with mechanism GSK3\beta inhibition (Ali et al., 2017). We investigate the

 $^{^{}st}$ Corresponding author e-mail: izzy@ukm.edu.my.

anti-malarial effect of M. charantia aqueous extract using a murine model of malarial infection to elucidate whether the mechanism of action involves GSK3 β inhibition.The findings will provide further insight on the potential of M. charantia as a plant-based immunomodulator for malarial therapeutics.

2. Materials and Methods

2.1. Plant Collection and Aqueous Extract Preparation

M. charantia fruit was obtained from the Agriculture Department of Lekir, Perak, Malaysia. The voucher specimen of fruit (UKMB 40346) was deposited from Universiti Kebangsaan Malaysia (UKM) botanist. The extract was prepared according to Abas et al. (2014), with some modifications. The fruit was dried in an oven at 60°C for 24 hour and ground using an electric grinder. The distilled water was added to dried powdered using reflux extraction after which it was filtered by Whatman filter paper no.1(Whatman International, UK). The crude extract was stored at -80°C refrigerator overnight before freezedrying (Labconco, USA) then stored at -20°C in a labelled amber glass until used in experiments.

2.2. High Performance Liquid Chromatography (HPLC)

2.2.1. Standard quercetin preparation

A standard solution was prepared by weighing 10 mg of quercetin (Sigma, USA) dissolved in HPLC grade methanol to acquire the final concentration of 1000 $\mu g/mL$ as a stock, which is then used to prepare five different concentrations of the standard.

2.2.2. Liquid chromatography instrument and conditions

The system of HPLC was Waters C18 column (4.6 mm \times 250 mm), equipped with software, UV detector with wavelength 369 nm. The mobile phase was [methanol: 0.1% ortho-phosphoric acid (65%:35% v/v)] (Sanghavi *et al.*, 2014), at flow rate 1 mL/min. Standard quercetin and *M. charantia* aqueous extract (20 μ L) were each injected automatically to get the standard peaks.

2.3. In vitro Anti-plasmodial Assay

P. falciparum 3D7 (chloroquine-sensitive) strain was obtained from MR4, USA. Parasites were cultured in RPMI 1640 medium and incubated 37°C, 5% CO₂. The parasite lactate dehydrogenase (pLDH) assay was used to evaluate the anti-plasmodial activity of M. charantia aqueous extract on P. falciparum growth and conducted based on Makler et al. (1993). The serially diluted concentrations of M. charantia aqueous extract or control drug chloroquine were each inoculated with parasitized red blood cells of P. falciparum (2% parasitemia, 2% hematocrit) in 96-microtiter plate wells. The parasitized red blood cells were used as a positive control while noninfected cells were used as a negative control. After the incubation period of M. charantia aqueous extract with parasitic culture at 37°C for 48 hours, the plate was frozen at - 20°C for 24 hours. The cycles of freezing and thawing were applied to lyse the red blood cells.

Absorbance readings were measured after 1 hour of adding Malstat reagent, using a microplate reader (Optima, Germany), at a wavelength of 650 nm. The pLDH experiment was performed in triplicate and three replicate readings for each concentration were recorded. IC50 values (concentration of extract or drug inhibited 50% of growth) were determined.

2.4. Cytotoxicity Assay

3-(4, 5-dimethylthiazol-2-yl)-2, 5- diphenyltetrazolium bromide (MTT) assay in vitro was carried out by Mosmann, (1983) to evaluate the cytotoxicity of the M. charantia aqueous extract on Vero cells. The cells used were purchased from ATCC, USA. The cells seeded at a density of 1×10^4 cells/mL into 96- microtiter plate were incubated for 48 hour following treatment with serial dilutions of M. charantia aqueous extract. The wells containing culture medium with cells were used as positive control. MTT reagent was then added to each well and the plate incubated for 3h. The medium was replaced with DMSO to dissolve the formazan. The microplate reader (Optima, Germany) was used to measure the absorbance at 540 nm. The cytotoxicity assay was performed in triplicate, and three replicate readings for each concentration were recorded IC50 values were determined.

2.5. Selectivity Index (SI)

Selectivity index was calculated using the following formula:

$$SelectivityIndex = \frac{IC_{50} MTT}{IC_{50} PLDH}$$

2.6. The Parasite and Experimental Mice

P. bergei NK65 (chloroquine-sensitive) strain of was obtained from MR4, USA. ICR male mice (6-7 weeks old), weighing approximately 25 ± 5 g were obtained from the Animal House Complex, (UKM). The experimental animals were housed in plastic cages, distilled water and fed *ad libitum*. The mice were acclimated for a week before the experiments. The animal studies permission was obtained from UKM Animal Ethics Committee (UKMAEC).

2.6.1. In vivo anti-malarial test

The test followed depended on Peters (1975) method to determine anti-malarial activities of M. charantia aqueous extract in infected mice. The mice (6 groups/ 6 mice) were inoculated on day 0 intraperitoneally (ip) with 0.2 ml of blood an inoculated 2 x 10⁷ P. berghei-infected erythrocytes. Three hours later, the mice were injected with either 0.85% saline (control group) or CQ (10 mg/ kg bw), LiCl (100 mg / kg bw), or treated with (50, 75 or 100 mg / kg bw) of M. charantia aqueous extract (test groups), for four consecutive days. Blood smears were prepared from mice tail. The dried slides were observed under microscope (100 x magnification) (Leica DM750, England), using immersion oil. On day 4 post- infection, the parasitemia percentage was calculated and the mice survivability was recorded up to day 30. The percentage of chemosuppression was calculated by the formula:

2.7. Western Analysis

Western blotting was used to determine GSK3 β (Ser9), Akt (Ser473) and NF- κ B (Ser536) phosphorylation state. Protein extraction was conducted according to Lee (2007); the liver homogenized with protein extraction buffer and Bradford assay was used to detect protein concentrations (Bradford, 1976). The SDS-PAGE was used to separate the protein samples (Laemmli, 1970). The proteins were electro-transferred onto a nitrocellulose membrane. The membrane was then blocked with 3% BSA (Towbin *et al.*, 1979). After overnight incubation with the primary antibody, the membrane was incubated with secondary antibody for 2 hours at room temperature (Cell Signaling, USA). Chemiluminescent Substrate Kit (Thermo Scientific, USA) was used to detect immunoreactive bands.

2.8. Analysis of Cytokine

Three major cytokines determined in the sera of infected and treated mice at day- 4 post infection include the pro-inflammatory cytokines Tumor necrosis factor (TNF- α), Interferon (*IFN*- γ) and anti- inflammatory cytokine Interleukin (IL-10). Enzyme- linked immunosorbent assay (ELISA) kit (Qiagen, Germany) was

used to measure the cytokines based on the instructions of manufacturer.

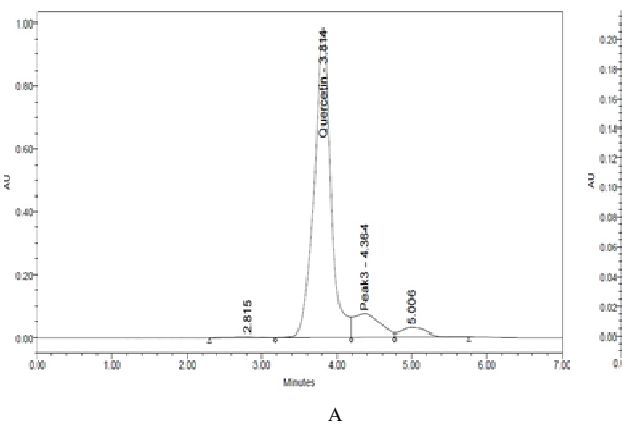
2.9. Statistical Analysis

All results are expressed as means \pm standard deviation (SD), and IC₅₀ values were estimated by non-linear regression fitted to the growth curve using GraphPad Prism5 (Graph Pad Software, California). Rank test (Kaplan-Meier analysis) were analyzed using Graph Pad Prism 5 using One-Way Analysis of Variance (ANOVA) with Tukey post-hoc test to determine the significance of data (p<0.05) between the test groups and control.

3. Results

3.1. Identification of Quercetin in M. charantia Aqueous Extract

HPLC has been performed to quantify quercetin in the M. charantia aqueous extract. The linearity of standard quercetin was estimated by linear calibration curve, quercetin exposed good linearity with correlation coefficient of $R^2 = 0.9977$. The HPLC chromatogram of M. charantia extract showed extract peak at retention time 2.417 within 2 minutes, and the quercetin peak positively identified was separated depending on the retention time (Fig. 1).



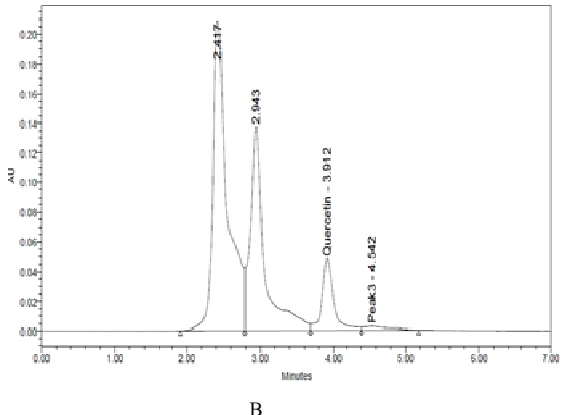


Figure 1. A: HPLC chromatogram of standard quercetin, B: HPLC chromatogram of *M. charantia* aqueous extract. Column: wavelength:369 nm; C18; Flow rate:1 mL/min.

3.2. In vitro Anti-plasmodial Activity and Cytotoxicity Assav

M. charantia aqueous extract against P. falciparum 3D7 exhibited moderate anti-plasmodial activity at IC_{50} value of $41.46 \pm 1.31 \, \mu g/mL$. The IC_{50} values in vitro were classified by Kvist et al. (2006). Further, M. charantia aqueous extract showed no cytotoxicity against Vero cells based on Tanamatayaratab et al. (2012) classification at IC_{50} value exceeding 1000 $\mu g/mL$ (Table 1).

Table 1. Anti-plasmodial activity against *P. falciparum* 3D7 and cytotoxicity assay of the *M. charantia* aqueous extract *in vitro*

Extract/drug	Cytotoxic activity IC ₅₀ MTT (µg/mL)	Anti-plasmodial activity IC ₅₀ (μg/mL)	Selectivity Index (SI)
M.charantia aqueous extract	>1000	41.46 ± 1.31	>10
Chloroquine (CQ)	44.00 ± 1.66	0.038 ± 0.02	>10

The results based on $IC_{50} \pm SD$.

3.3. In vivo Four-Day Suppressive Test

Administration mice with *M. charantia* aqueous extract following injection with *P. berghei*- infected erythrocytes for four consecutive days exhibited dose-dependent manner. *M. charantia* at doses 50, 75 and 100 mg/kg bw inhibited the parasite development by 57.90 \pm 2.90%, 60.90 \pm 2.71% and 70.20 \pm 2.13%, respectively (Table 2).

The groups treated with M. charantia aqueous extract showed a prolonged median survival time than the control group with a recorded median survival time of 16 days (Fig. 2). The growth inhibition and the mice survival were improved with increased M. charantia aqueous extract doses. Meanwhile, the chloroquine suppressed parasitaemia growth by $94.27 \pm 0.22\%$ and the mice survived within the observation period 30 days (Table 2). These results indicated that the M. charantia aqueous extract has anti-malarial activity by suppression of parasitemia development and prolonging the mice survival.

Table 2. Anti-malarial activity of *M. charantia* aqueous extract against *P. berghei* NK65 infected mice *in vivo*

Drug/extract	Doses (mg/kg/bw)	Parasitemia percentage on day 4(%)	Median survival time (days)
	50	57.90± 2.90*	18
M. Charantia	75	60.90± 2.71*	21
aqueous extract	100	70.20± 2.13*	22
Chloroquine			
(anti- malarial drug control)	10	94.27± 0.22*	>30
LiCI (GSK3 Inhibitor)	100	57.7± 1.34*	20
0.85% NaCL (control)	0.2 ml	-	16

The results demonstrated chemosuppressive \pm SD refers to significant value (p<0.05). *Significant different with control.

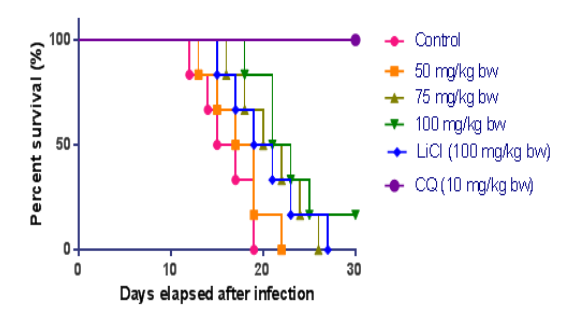


Figure 2. Kaplan-Meier survival curve of *M. charantia* aqueous extract and control groups.

3.4. M. charantia Aqueous Extract Increases Phosphorylation Levels of Akt (Ser473) and GSK3 β (Ser9) in Malarial Infected Mice

Based on our data, administration of the effective dose (75 mg/kg bw) of M. charantia aqueous extract into infected mice increased phosphorylation levels of Akt and GSK3 β in host liver by 2.7 fold, 7.2 fold (Fig. 3 and Fig. 4) respectively, compared with non-treated infected mice (control). In addition, LiCI increased the phosphorylation level of GSK3 β in mice by 9.3 fold. The present investigation revealed that the M. charantia aqueous extract involves activation of Akt and potential inhibition GSK3 β .

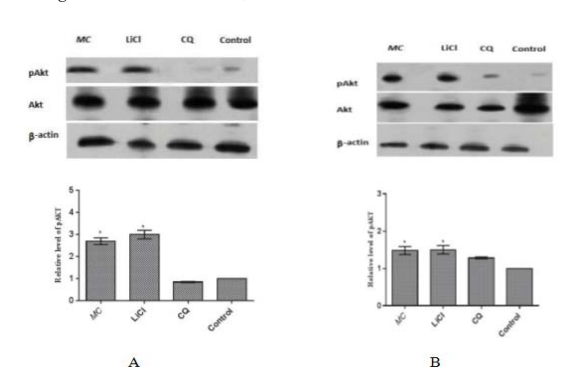


Figure 3. Phosphorylation levels of Akt (A) in *P. berghei*-infected mice (B) in non-infected mice. The results represented as a mean (fold) \pm SD for treated groups as compared with control (p<0.05). *M. charantia* aqueous extract (*MC*), Lithium chloride (LiCl), chloroquine (CQ).

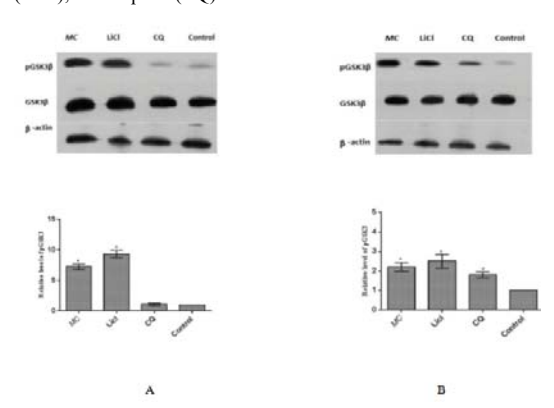


Figure 4. Phosphorylation levels of GSK3 β (A) in *P. berghei*-infected mice (B) in non-infected mice. The results represented as a mean (fold) \pm SD for treated groups as compared with control (p<0.05). *M. charantia* aqueous extract (*MC*), Lithium chloride (LiCl), chloroquine (CQ).

3.5. M. charantia Aqueous Extract Decreases Phosphorylation Level of NF- кВ (Ser536) in Malarial Infected Mice

Our Western blotting experiments indicated that infected mice treated with *M. charantia* aqueous extract were decreased phosphorylation of NF-κB liver by 2.0 fold as compared with infected mice without treatment (Fig. 5). The decrease phosphorylation was also comparable in the LiCl-treated mice by 1.6 fold. The aforementioned results revealed that the *M. charantia* aqueous extract caused inhibition of NF-κB mediated via inhibition GSK3β.

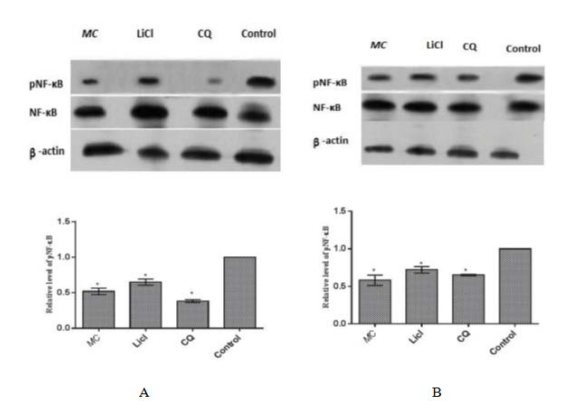


Figure 5. Phosphorylation levels of NF- κ B (A) in *P. berghei*-infected mice (B) in non-infected mice. The results represented as a mean (fold) \pm SD for treated groups as compared with control (p<0.05). *M. charantia* aqueous extract (*MC*), Lithium chloride (LiCl), chloroquine (CQ).

3.6. M. charantia Aqueous Extract Regulates the Proand Anti-inflammatory Cytokines Levels in Malarial Infected Mice

Our outcomes presented that the infected mice treated with M. charantia aqueous extract significantly decreased IFN- γ , TNF- α levels by 2.7, 4.9 fold respectively, whilst significantly increased IL-10 level by 2.3 fold as compared with non-treated infected mice (Fig. 6). These findings proved that the M. charantia aqueous extract modulated the pro- and anti-inflammatory cytokines levels via inhibition of host GSK3 β . Moreover, the $IFN-\gamma$, TNF- α levels decreased by 4.7, 3.9 fold respectively, and IL-10 level increased by 2.0 fold in infected mice treated with LiCl, compared with non-treated infected mice.

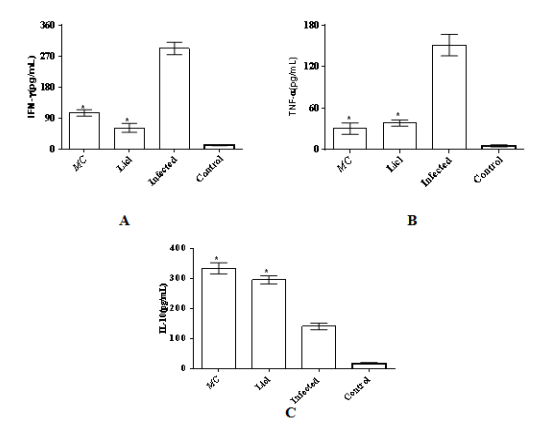


Figure 6. Pro-inflammatory and anti-inflammatory cytokines (A) IFN- γ , (B) TNF- α , and (C) IL-10 levels. The results represented as a mean (fold) \pm SD for treated groups as compared with control (p<0.05). *M. charantia* aqueous extract (*MC*), Lithium chloride (LiCl).

4. Discussion

M. charantia is better known for its anti- diabetic properties and even now extensively used as traditional remedy for diabetes in many parts of world. Nevertheless, M. charantia has been shown to have anti-plasmodial effect in previous reports (Olasehinde et al., 2014). In

another study, leaf extract of M. charantia has been shown with anti-malarial activity (Akanji et al. 2016), though, the mechanism of action is not yet elucidated. Even though, the plant is known to contain many phytochemicals such as saponins, steroids, alkaloid, flavonoids, phenolic compounds, triterpenes, protein and polysaccharides (Saeed et al., 2018). It is worth mentioning that this plant is also reported to contain several bioactive compounds, e.g. momordenol, momordicilin and quercetin which are known to exhibit GSK3- inhibitory properties (Hazarika et al., 2012; Svobodova et al., 2017). The pathology of major diseases such as neurological disorders, cancer, diabetes and malaria are associated with increased GSK3 activity (Wang et al., 2014). Our previous finding that LiCI (an inhibitor of GSK3) exhibited chemosuppressive effects in a murine model of malarial infection (Zakaria et al., 2010). We evaluated whether anti-malarial effect of M. charantia also involved GSK3 inhibition. Here we have shown that the anti-malarial effect of M charantia aqueous extract involved cytokine modulation mediated via inhibition of GSK3\beta in p. berghei- infected mice. Recently, pharmacological studies utilize traditional medicinal plants as a source of immunomodulation instead of therapeutic drugs for their side effects (Slimani et al., 2020). M potential plantcharantia is thus a based immunomodulator to address malarial infection as adjunctive therapy (Tcheghebe et al., 2016). Parasite resistance to anti-malarial drugs is a prime health concern. The anti-malarial activity of plant extracts is due to the presence of active compounds may occur in the form of alkaloids, flavonoids and triterpenoids. In addition, the main participating factor of increasing anti-plasmodial activity is related with synergistic effect of the active compounds and enhancing anti-malarial of herbal plants (Okello & Kang 2019).

In this study, we employed *M charantia* aqueous extract with quercetin as a marker, and it is possible that the cytokines- modulation effect seen here is attributed to the GSK3 inhibitory action of quercetin and/ or bioactive compounds in *M. charantia* described earlier. Quercetin is a flavonol belonging to flavonoid group normally present in vegetables and fruits. It exhibits many biological activities including anti-diabetic, anti-inflammation, anti-bacterial and anti-viral activities (Mondal & Rahaman 2020); it also suppresses parasite growth and provide antimalarial agent (Abu-Lafi *et al.*, 2020). Quercetin is believed to have GSK3-inhibitory activities based on in silico docking and binding studies (Johnson *et al.* 2011).

Our results demonstrated that *M. charantia* aqueous extract caused phosphorylation of host GSK3β and Akt. Akt is a serine/threonine kinase as an upstream kinase involved inactivation (phosphorylation) of GSK3 to regulate immune response and inflammation (Wang *et al.* 2011). This suggests that inhibition of GSK3 after treatment with *M. charantia* aqueous extract could be mediated through Akt activation. Han *et al.* (2018) reported the potential mechanism of action of *M. charantia* to manage the diabetes and glucose homeostasis which involved phosphorylation of Akt, GSK3β and other signalling pathways in diabetic mice by cucurbitane triterpenoids isolated from *M. charantia* fruit. GSK3 is a known downstream component of the PI3K/Akt pathway, which is recognized to play an essential role in the control

of the inflammatory response to pathogenic infection (Cortés-Vieyra et al., 2021), and as a regulator of many components of the innate and adaptive immune system (Matteis et al., 2016). It has a plausible therapeutic target in inflammation and management of diseases (Rippin & inkelman 2021). However, the inhibitors of GSK3 potentially used against malaria-pathogen (Osolodkin et al., 2011). IFN-γ and TNF-α levels were decreased, while, IL-10 level was increased upon treatment with M. charantia aqueous extract, meaning that the anti- malarial effects of M. charantia aqueous extract modulate inflammatory cytokines elicited via inhibition host GSK3B. Modulating of GSK3 activation is differentially controlling pro and anti-inflammatory cytokines production through NF-κB (downstream of GSK3β) regulation (Patel & Werstuck 2021) to reduce the pathogenesis. A previous study on bacterial infection in mice has shown that M. charantia modulates cytokines production by inhibiting NF-kB activation (Huang et al., 2015). Our finding exhibited inhibition of NF-κB activation in infected mice treated with M. charantia aqueous extract as a result of M. charantia aqueous extract and implicated phosphorylated GSK3\(\beta\). The results of this study, presented that the M. charantia suppressed the growth of P. falciparum culture in vitro and P. berghei NK65 in vivo. M. charantia is capable of potential inhibition of the host GSK3ß activity and modulates proand anti-inflammatory cytokines. Moreover, continuous usage of *M. charantia* may be useful in malaria treatment. In addition, the results confirm the importance of GSK3 as a main player to mange the pathogenic infection includes malaria and inflammation related-conditions.

5. Conclusion

The research reiterates GSK3 β as a target for malaria therapeutics and the importance of the kinase in inflammatory processes during infection. *M. charantia* aqueous extract in malaria is believed to have dual roles: anti-parasitic effect on the one hand (from *in vitro* experiments) and immunomodulatory effect on the other (from *in vivo* studies). This present study provides evidence on the potential of *M. charantia* as a plant-based immunomodulator to address malarial infection which may lead to more discovery efforts for potential anti-malarial plant extracts with novel mechanism of action.

Acknowledgment

This research was supported by grants from University Kebangsaan Malaysia (UKM).

References

Abas R, Othman F and Thent C. 2014. Protective effect of *Momordica charantia* fruit extract on hyperglycaemia-induced cardiac fibrosis. *Oxid Med Cell Longev*, **2014**: 1–8.

Abu-Lafi S. Akkawi M. Al-Rimaw F. Abu-Remeleh Q and Lutgen P. 2020. Morin, quercetin, catechin and quercitrin as novel natural antimalarial candidates. *Pharm Pharmacol Int J*, **8**: 184-190

Akanji C, Mojisola C, Taiwo E and Ola O. 2016. The antimalaria effect of *Momordica charantia* L. and *Mirabilis jalapa* leaf extracts using animal model. *J Med Plants Res*, **10**: 344–350.

Ali A, Sudi S, Basir R, Embi N and Sidek M. 2017. The antimalarial effect of curcumin is mediated by the inhibition of glycogen synthase kinase-3β. *J Med Food*, **20**: 152–161.

Bekono B. Ntie-Kang F. Onguéné P. Lifongo L. Sipp W. Fester K and Owono L. 2020. The potential of anti-malarial compounds derived from African medicinal plants: a review of pharmacological evaluations from 2013 to 2019. *Malar J*, **19**: 1-35

Bradford M. 1976. A rapid and sensitive method for the quantitation of microgram quantities of protein utilizing the principle of protein-dye binding. *Anal Biochem*, 72: 248–254.

Corte' s-Vieyra R. Silva-Garcı'a O. Go'mez-Garcı'a A. Gutie'rrez-Castellanos S. A' lvarez-Aguilar C and Aguirre V. 2021. Glycogen synthase kinase 3β modulates the inflammatory response activated by bacteria, viruses, and parasites. *Front Immunol*, **12**: 1-13.

Dai M, Freeman B, Shikani H, Bruno P, Collado J, Macias R, Reznik S, Davies P, Spray D, Tanowitz H, Weiss L and Desuisseaux M. 2012. Altered regulation of Akt signaling with murine cerebral malaria, effects on long-term neuro-cognitive function, restoration with lithium treatment. *Plos One*, 7: 1-15.

Deu E. 2017. Proteases as antimalarial targets: strategies for genetic, chemical, and therapeutic validation. *Febs J*, **284**: 2604–2628.

Embi N, Rylatt D and Cohen P. 1980. Glycogen Synthase Kinase-3 from rabbit skeletal muscle. *Eur J Biochem*, **107**: 519–527.

Han J, Tuan N, Park M, Quan K, Oh J, Heo K, Na M and Myung C. 2018. Cucurbitane triterpenoids from the fruits of *Momordica charantia* improve insulin sensitivity and glucose homeostasis in streptozotocin-induced diabetic mice. *Mol Nutr Food Res*, **62**: 1-11

Hazarika R, Parida P, Neog B and Yadav R. 2012. Binding energy calculation of GSK-3 protein of human against some anti-diabetic compounds of *Momordica charantia* linn (Bitter melon). *Bioinformation*, **8**: 251–254.

Hoffmeister L. Diekmanny M. Brand K and Huber R. 2020. GSK3: A kinase balancing promotion and resolution of inflammation. *Cells*, **9**: 1-34.

Huang C, Tsai H, Huang J, Li Y, Chyuan H, Chuang T and Tsai J. 2015. Inhibitory effects of wild bitter melon leaf extract on *Propionibacterium* acnes-induced skin inflammation in mice and cytokine production *in vitro*. *Food Funct*, **6**: 2550–2560.

Johnson J, Rupasinghe S, Stefani F, Schuler M and Mejia E. 2011. Citrus flavonoids luteolin, apigenin, and quercetin inhibit glycogen synthase kinase- 3β enzymatic activity by lowering the interaction energy within the binding cavity. *J Med Food* , **14**: 325–333.

Kvist L, Christensen S, Rasmussen H, Mejia K and Gonzalez A. 2006. Identification and evaluation of peruvian plants used to treat malaria and leishmaniasis. *J Ethnopharmacol*, **106**: 390–402.

Laemmli U. 1970. Cleavage of structural proteins during the assembly of the head of bacteriophage T4. *Nature*, **227**: 680–685.

Lee C. 2007. Protein extraction from mammalian tissues. *Methods in Mol Biol*, **362**: 385–389.

Makler M, Ries J, Williams J, Bancroft J, Piper R, Gibbins B and Hinrichs D. 1993. Parasite lactate dehydrogenase as an Assay for *Plasmodium falciparum* drug sensitivity. *Am J Trop Med Hyg*, **48**: 739–741.

Matteis S, Napolitano R and Carloni S. 2016. GSK-3 β and its unexpected role in immunity, inflammation and cancer. *J Hematol Oncol and ogy*, 1: 1-6.

Mondal S and Rahaman S. 2020. Flavonoids: A vital resource in healthcare and medicine. *Pharm Pharmacol Int J*, **8**: 91-104.

Mosmann T. 1983. Rapid colorimetric assay for cellular growth and survival: application to proliferation and cytotoxicity assays. *J Immunol Methods*, **65**: 55–63.

Okello D and Kang, Y. 2019. Exploring antimalarial herbal plants across communities in Uganda based on electronic data. *Evid Based Complement Alternat Med*, **2019**: 1-27.

Olasehinde I, Ojurongbe O, Adeyeba O, Fagade E, Valecha N, Ayanda O, Ajayi A and Egwari L. 2014. *In vitro* studies on the sensitivity pattern of *Plasmodium falciparum* to anti-malarial drugs and local herbal extracts. *Malar J*, **13**: 1-11.

Omoregie E and Pal A. 2016. Antiplasmodial, antioxidant and immunomodulatory activities of ethanol extract of *Vernonia amygdalina del*. leaf in swiss mice. *Avicenna J Phytomed*, **6**: 236–247.

Osolodkin D, Zakharevich N, Palyulin V, Danilenko V and Zefirov N. 2011. Bioinformatic analysis of glycogen synthase kinase 3: human versus parasite kinases. *Parasitology*, **138**: 725–735.

Patel S and Werstuck G. 2021. Macrophage function and the role of GSK3. *Int. J. Mol. Sci.*, 22:1-13.

Peters W. 1975. The chemotherapy of rodent malaria, XXII. the value of drugresistant strains of *P. berghei* in screening for blood schizontocidal activity. *Ann Trop Med Parasitol*, **69**: 155–171.

Rippin I and Finkelman H. 2021. Mechanisms and therapeutic implications of GSK-3 in Treating Neurodegeneration. *Cells*, **10**: 1-21.

Tanamatayaratab P, Sotanaphunb U and Poobrasert O. 2012. Thai plants from Doi Tung: brine shrimp lethality, antioxidative activity and combination effect with L-ascorbic acid. *Nat Prod Res*, **26**: 919–925.

Tcheghebe T, Timoléon M, Seukep J and Tatong N. 2016. Ethnobotanical uses, phytochemical and pharmacological profiles, and cultural value of *Momordica chlarantia* Linn: an overview. *Gjmpr*, **4**: 23–39.

Towbin H, Staehelin T and Gordon J. 1979. Electrophoretic transfer of proteins from polyacrylamide gels to nitrocellulose sheets: procedure and some applications. *Proc Natl Acad Sci U S A*, **76**: 4350-4354.

Wang H, Brown J and Martin M. 2011. Cytokine glycogen synthase kinase 3: a point of convergence for the host inflammatory response. *Cytokine*, **53**: 130–140.

Wang H, Kumar A, Lamont R and Scott D. 2014. GSK3β and the control of infectious bacterial diseases. *Trends Microbiol*, **22**: 208-217

WHO. 2020. Word Malaria Report. Geneva, Switzerland. World Health Organisation. https://reliefweb.int/report/world/world-malaria-report-2020 (Apr. 3, 2021).

Saeed F, Afzaal M, Niaz B, Arshad U, Tufail T, Hussain B and Javed A. 2018. Bitter melon (*Momordica charantia*): a natural healthy vegetable. *Ijfp*, **21**: 1270-1290.

Sanghavi N, Bhosale D and Malode Y. 2014. RP-HPLC method development and validation of quercetin isolated from the plant *Tridax procumbens* L. *Jsir Journal*, **3**: 594–597.

Slimani W, Zerizer S and Kabouche Z. 2020. Immunomodulatory and Anti-Arthritic Activities of *Stachys circinata*. *Jordan J Biol Sci.* 13:183-189.

Svobodova B, Barros L, Calhelha R, Heleno S, Jose M, Walcott S, Bittova M and Kuban V. 2017. Bioactive properties and phenolic profile of *Momordica charantia* L . medicinal plant growing wild in trinidad and tobago. *Ind Crops Prod*, **95**:365-373.

Yang S, Choi M, Park E, Rhee J, Lee Y, Oh W, Park W and Park C. 2014. Preventive effects of bitter melon (*Momordica charantia*) against insulin resistance and diabetes are associated with the inhibition of NF- κ B and JNK pathways in high-fat-fed oletf rats. *J Nutr Biochem*, **26**: 234-240.

Zakaria A, Embi N and Sidek M. 2010. Suppression of *Plasmodium berghei* parasitemia by LiCI in an animal infection model. *Trop Biomed*, **27**: 624 - 631.

Jordan Journal of Biological Sciences

Short Communication

Assessing Factors that Shape Neonatal Gut Microbiota in Erbil Province/Iraq

Muayad Ahmed Mahmud*

Department of Medical Laboratory Technology, Shaqlawa Technical College, Erbil Polytechnic University, Erbil-Iraq
Received: Feb 1, 2022; Revised: April 17, 2022; Accepted April, 19, 2022

Abstract

Bifidobacteria and Lactobacilli are considered the initial microbial species to colonize the gastrointestinal tract in the human host. In this study, we investigated the influence of delivery mode, feeding style, infant sex, mother's age, number of siblings, and birthplace on the prevalence of Lactobacillus and Bifidobacteria in the gut of 20 newborns aged 1-3 weeks in Erbil. Fecal samples from infants and breast milk from mothers were examined for the presence of Bifidobacteria and Lactobacilli using selective culture media (BSM and MRS respectively). The results showed that breast milk samples (95%) contained the two bacterial genera, but only 30% of the stool samples contained Lactobacillus (p = 0.0037) and 50% of them contained Bifidobacteria (p > 0.005). Babies who were strictly on breast milk had a significantly higher chance of harboring Bifidobacteria (p = 0.0003) and Lactobacilli (p = 0.0034) in their feces than those who were given both breast milk formula milk. Babies born by caesarian section had a lesser chance to have Lactobacillus in their gut compared to those who were naturally born via the birth canal (p = 0.009). Baby sex, mother's age, number of siblings, and birthplace did not affect the prevalence of Bifidobacteria. Our results suggest that the feeding type and delivery mode are the most crucial factors affecting the composition of both Lactobacillus and Bifidobacteria in the newborn's gut.

Keywords: Bifidobacteria, intestinal flora, Lactobacilli, microbe-host interaction, probiotic.

1. Introduction

Gut microbiota involves numerous microbial populations that are associated with the human host in a symbiotic relationship. Microbiota applies a substantial influence on host health through its role in the regulation of physiology, immune responses, and nutritional status (Fraher, O'Toole, & Quigley, 2012). Disturbance in the gut microbiome is thought to be associated with several diseases including obesity, diabetes, cancers, inflammatory bowel diseases, gout, depression, arthritis, and others (Ding et al., 2019). It has been found that the diversity of gut microbiota among ethnic groups is associated with eco-geographical factors including lifestyle and dietary habit (Nakayama et al., 2015).

Initial establishment of the gut microbiota starts straight after a baby's birth (Soto et al., 2014; West, Dzidic, Prescott, & Jenmalm, 2017). Later, a complex microbiota composition will develop depending on the dietary nature. It is estimated that over 1000 species of bacteria exists in the intestine of an adult human (Qin et al., 2010). The influence of intestinal bacteria can be harmful, beneficial, or neutral on human health (Liang, Leung, Guan, & Au, 2018; Tlaskalova-Hogenova et al., 2011). Bifidobacterium and Lactobacillus are thought to be the most beneficial bacteria to human health and are expected to contribute to physiological functions (Soto et al., 2014; Tanaka & Nakayama, 2017). Recently published studies of metagenomics on the functionality and composition of the microbiome in infant gut suggest that

there is a link between compositional features of the infant gut microbiota and intestinal diseases in infants or other illnesses such as metabolic disorders, inflammatory bowel disease and asthma which could manifest during adulthood (Milani, Duranti, & Bottacini, 2017).

Factors that contribute to shaping the compositions of Bifidobacteria and Lactobacillus in the neonatal gut include delivery mode, feeding type, gestational time, birthplace, antibiotic use, farm residence, number of siblings, and presence of furry pets at home (Penders *et al.*, 2006; Vandenplas *et al.*, 2020). Vaginally delivered infants are expected to acquire their mother's vaginal microflora, but the passing mechanism is still not clear. After delivery, the diversity of infants' gut microflora depends on feeding style and breast feeding is expected to promote colonization of a distinctive microbial profile (Hoang, Levy, & Vandenplas, 2021; Madan *et al.*, 2016).

Infants born through vagina delivery are colonized with gut microbiota immediately after birth, while babies born through Cesarean section might require a long time to acquire these intestinal bacteria (Dunn, Jordan, Baker, & Carlson, 2017). The development of microbiota is modulated and driven by dietary compounds in breast milk which support the colonization of certain microbes (Rodriguez et al., 2015; Tanaka & Nakayama, 2017). Breastfeeding is thought to enhance colonization of gut Bifidobacteria and Lactobacillus, while formula-milk promotes high diversity of gut microbiota leading to a strong competition among different microbial taxa (Backhed et al., 2015; Elsen, Garssen, Burcelin, &

^{*} Corresponding author e-mail: muayad.mahmud@epu.edu.iq.

Verhasselt, 2019). Globally, there is a rising interest in the role of gut microbiota in neonatal health and in Iraq; there is a lack of empirical studies focusing on neonatal gut microbiota. The private health sector particularly in the Kurdistan Region is increasingly expanding, but this is associated with a high caesarean delivery rate (25.4%) which is to be higher than the WHO's recommended rate (15%) (Shabila, 2017). In the current study, the role of delivery mode, feeding type, baby's gender, mother's age, number of previous birth, and birthplace were examined to determine the prevalence of Lactobacillus and Bifidobacteria in the gut. Breast milk, infant stool sample, and five types of commercially available probiotic supplements were thoroughly examined to investigate the possibility of transferring probiotic quality from mothers to newborns. The study will provide a better understanding of factors that may affect the development of the gastrointestinal microbiome in newborns.

2. Methodology

2.1. Ethical approval

This study was approved by the Clinical Research Ethics Committee of the Erbil General Directorate of Health/ the Ministry of Health KRG-Iraq, and their regulations were properly followed. Mothers of newborn participants were provided with written informed consent and the research guidelines (consent form attached).

2.2. Bacterial isolation and identification

Quality control strains of Lactobacillus and Bifidobacteria were prepared using commercially available probiotics including; Entero Junior (Italy), Lactoflor- Kids (Bulgaria), ProIBS (Germany), Advanced Probiotic (USA), and Probiodex (Italy).

During one month (between December 2020 and January 2021), fecal samples from 20 newborns aged 3 weeks and approximately 10 ml of their mothers' breast milk were collected using sterile Eppendorf tubes at the Maternity Teaching Hospital-Erbil. Samples were properly labeled and quickly transferred on ice to the lab for culturing and identification. Briefly, quality control strains of Lactobacillus and Bifidobacteria were prepared by transferring 5 grams from each of the above mentioned probiotic sources separately to 45 ml of sterilized BHI broth (Brain Heart Infusion Broth, Thermo Scientific, USA) in order to promote the growth of lyophilized bacteria. Simultaneously, 5 grams from newborns' fecal sample and 5 ml from mothers' breast milk sample were separately transferred to 45 ml of sterilized BHI (Brain Heart Infusion Broth, Thermo Scientific, USA). Tubes containing inoculated BHI were incubated under anaerobic conditions using an anaerobic jar (Oxoid AnaeroJar 2.5L, UK) at 37°C for 48 hours. After the incubation time, homogenate was prepared from each BHI tube and diluted using tenfold dilution. From appropriate dilutions, an amount of 0.1 ml was taken and spread on sterile MRS agar (de Man, Rogosa, and Sharpe, Oxoid-UK) for Lactobacillus, and on BSM agar (Bifidus Selective Medium, Merck- Germany) for Bifidobacteria. After inoculation, plates were kept under anaerobic conditions using an anaerobic jar at 37°C for 48 hours.

To identify colonies of Lactobacillus and Bifidobacteria, we followed the guidelines of

manufacturers of the two selective medias (MRS and BSM). Colonies of Lactobacillus appeared white, large and embedded in MRS Agar, while Bifidobacteria appeared purple/brown on BSM. For additional purification, 10-15 colonies which showed characteristics of Lactobacillus and Bifidobacteria were sub cultured on MRS and BSM respectively. Gram stain and KOH test, Catalase Test and Spore Staining were carried out for all the Lactobacillus and Bifidobacterium suspected colonies. Briefly, a drop of KOH (3%) solution was added on a glass slide and part of a suspected colony from freshly cultured bacteria was thoroughly mixed to make a dense suspension. After constant stirring, isolates which have not become thick and stringy products were selected since Bifidobacterium and Lactobacillus species are Grampositive cells. This was followed by a routine gram stain procedure (Gram stain kit-010221, Diapath- Italy) using cells from the same colony. The catalase test was conducted by adding one drop of 3% Hydrogen Peroxide (3% H2O2) on 48 hours old cultures on a clean glass slide. When the formation of oxygen bubbles happened, the catalase test was considered a positive reaction. Sporestaining was performed using Schaeffer and Fulton Spore Stain Kit (Merck- Germany). Only non-endospore forming isolates were considered for subsequent examination.

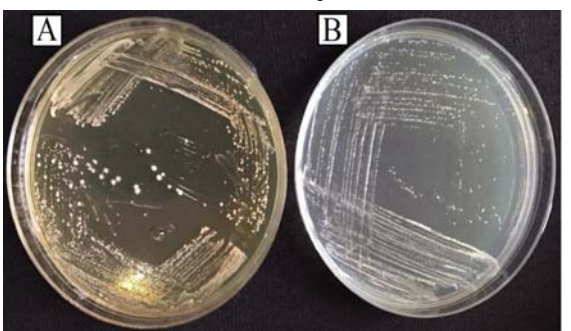


Figure 1: Colony morphology of Lactobacillus and Bifidobacterium on MRS (A) and BSM (B) agar respectively after 48 hours of incubation at 37C under anaerobic conditions.

2.3. Statistical analysis

Association between the abundance of Lactobacillus and Bifidobacteria in mothers' breast milk and their newborns' gut was examined using Chi-square test. Regression analysis was used to examine the influence of independent variables including delivery mode, feeding type, baby's gender, mother's age, number of previous birth, and birthplace on the abundance of the two bacterial genera in newborns' feces. Statistical tests were performed in SPSS (SPSS Statistics V22-IBM) using a p-value that is less than 0.05 considered as the level of significance.

3. Results

Quality control strains of Lactobacillus and Bifidobacterium species were successfully isolated from four probiotic sources; Lactoflor- Kids (Bulgaria), ProIBS (Germany), Advanced Probiotic (USA), and Probiodex (Italy). One of the sources (Entero Junior, Italy) did not harbor any of the two bacterial genera.

Twenty mothers participated in this study, and their babies included 9 females (45%) and 11 males (55%). Twelve of the babies were delivered by SC (60%), while 8

(40%) of them were delivered through the birth canal. Apart from one baby born at home, the rest (95%) were born in the hospital. All the babies were on breast milk, but 10 of them (50%) were on both breast and formula milk. Among mothers who contributed to the study, 11

(55%) had zero or one more pregnancy in the past while the other 9 (45%) had 3 or more pregnancies in the past. All the mothers and babies were neither on antibiotics nor on probiotic/food supplements. Most of the babies (95%) were born at no lesser than 37 weeks, but only one of them was born at 36 weeks of pregnancy and its medical history was showing no abnormality. Premature babies who were born at lesser than 36 weeks of pregnancy and those who have been identified with congenital birth defects were excluded from the study.

There were statistically significant differences in the prevalence rate of Lactobacillus and Bifidobacteria between breast milk and stool samples; stool samples of babies who were born via birth canal and C-section; stool samples of babies who were strictly on breast milk and babies who were fed both breast milk and formula milk (table 1).

Generally, most of breast milk samples contained both Lactobacillus and Bifidobacteria, but only one of the stool samples found to contain these bacterial genera. It was found that 19 (95%) of the breast milk samples were positive for both Lactobacillus and Bifidobacteria except one of the breast milk samples neither supported the growth of Lactobacillus nor Bifidobacteria. Only six (30%) of the stool samples contained Lactobacillus.

Delivery mode had influence on the prevalence of the two bacterial genera in the babies' stool. There was a remarkable difference in the prevalence of Lactobacillus between naturally born babies and those were delivered via C-section, but the difference in the prevalence of Bifidobacteria was not found to be significant. Babies who were born via the birth canal had a higher prevalence of Lactobacillus (65%) and Bifidobacteria (75%) compared to other babies who were born via C-section (8.3% and 33.3% respectively).

Stool samples from babies who were strictly on breast milk showed a higher prevalence of Lactobacillus (60%) and Bifidobacteria (90%) compared to babies who were fed the two milk types (0% and 10% respectively).

There were no differences in the prevalence of Bifidobacteria in the stool content between male and female babies. Although stool samples from female babies had slightly lesser prevalence of Lactobacillus species (11.1%) compared to male babies (45.5), the difference was statistically not significant.

Table 1. The Chi square (X^2) was set at 95% confidence interval and one degree of freedom. Two-tailed P value was selected and stated in four digits.

Characteristics	For Lactobacillus				For Bifidobacteria					
Characteristics	Positive	Negative	N	X2	P value	Positive	Negative	N	X2	P value
Breast milk	19	1	20	4.33	0.037	19	1	20	1.647	0.199
Baby stool sample	6	14	20	4.33	0.037	10	10	20	1.647	0.199
Strictly on breast milk	6	4	20	8.571	0.003	9	1	20	12.8	0.000
Breast milk plus formula milk	0	10	20	-	-	1	9	20	12.8	0.000
Birth canal	5	3	20	6.706	0.010	6	2	20	3.33	0.068
C-Section	1	11	20	6.706	0.010	8	4	20	3.33	0.068
Female	1	8	20	2.78	0.095	5	4	20	0.202	0.653
Male	5	6	20	2.78	0.095	5	6	20	0.202	0.653

4. Discussions

A good understanding of the initial development of the neonatal intestinal ecosystem can be the key to the prevention or modification of several important diseases including Necrotizing enterocolitis (NEC), hematopoietic abnormalities, intraventricular hemorrhage and chronic lung diseases (Ding et al., 2019; Elsen et al., 2019; George Kerry et al., 2018; Tanaka & Nakayama, 2017). Adhesion and colonization of probiotic bacteria, such as Lactobacilli and Bifidobacteria in the gastrointestinal tract of the host, is believed to be one of the essential features required for delivering their health benefits (Costa & Weese, 2019; George Kerry et al., 2018; Rinninella et al., 2019). Probiotics of the human gut start to establish at a very early stage of life (Dunn et al., 2017; Tanaka & Nakayama, 2017). The majority of mothers (95%) who contributed to the study have possessed the two bacterial species in their breast milk; one of the milk samples did not contain any of the two bacterial species. Although it was not clear what could have contributed to the absence of essential probiotic bacteria in breast milk, the bacteria could have become inactivated during the transportation.

Five commercial probiotic supplements were used in the study to prepare quality control strains of Bifidobacteria and Lactobacillus. Four out of five contained the bacterial species just as the manufactural description. Although all the products used in this study had at least 6 months of validity or longer (some up to 2 years) left before the expiry date, the reason for the absence of Lactobacillus in Entero Junior (Italy) could be due to improper storage.

Although most of breast milk samples were rich in the two bacterial species, only 30% of the fecal samples from their babies supported the growth of Lactobacillus and only 50% of them contained viable Bifidobacteria. The prevalence of both bacterial species was generally low in the fecal samples, and this is not in agreement with what was found by Martin *et al.* (2012) that breastfeeding is expected to transfer bacteria particularly bile salt resistant anaerobes such as Bifidobacteria and Lactobacillus from the mother to babies; and there they can colonize neonatal out.

Various factors can affect the early establishment of gut microbiota including delivery mode (vaginal or cesarean delivery), feeding type (breast milk and/or formula milk), cessation of milk feeding, antibiotic usage, timing, and type of the introduction of solid foods, location and other mother's related factors (Tanaka & Nakayama, 2017). The prevalence of both Lactobacillus and Bifidobacteria can also be influenced indirectly through the ecosystem changes of intestinal flora due to intrinsic factors such as genetics and infections or extrinsic factors such as dietary intake and medications (Abrahamsson, Sinkiewicz, Jakobsson, Fredrikson, & Björkstén, 2009). For example, half of the newborn participants (50%) who participated in the study were taking both breast milk and formula milk. Lactobacillus prevalence was significantly higher in the infants who were solely fed on breast milk than those who were taking both breast and formula milk while Bifidobacterium prevalence did not differ significantly between the two feeding regimes. Studies suggest that breastfeeding infants are expected to receive bacterial flora which exists in their mothers' milk (Abrahamsson et al., 2009) particularly during the first month of lactation (Collado, Laitinen, Salminen, & Isolauri, 2012). Some studies suggest that formula milk induces the growth of various bacterial species in infants' guts (Ho et al., 2018), and this might explain strong competition with Lactobacillus and Bifidobacteria.

Interestingly, the prevalence of both Bifidobacteria and Lactobacillus was significantly higher in naturally born infants than what was found in those who were born via Csection. Only 40% of the babies were born via birth canal while the rest were born through C-section. Babies who were delivered via birth canal generally their stool samples were rich with the two studied bacteria, but only a few sample (8.3% and 33.3% respectively) of stool samples of babies who were born via C-section contained Lactobacillus and Bifidobacteria. It has been well established that babies are free of probiotic bacteria in the mother's womb and their microbial flora starts to establish only during and after the birth (Sanz, 2011; Tanaka & Nakayama, 2017). Women's vagina contains a large number of normal flora including Lactobacillus species (Dunn et al., 2017) which can help passing many of these bacteria to a newborn's body and hence their gastrointestinal tracts (Martin et al., 2012). Although vaginal swab is recommended for babies who are born via CS (Dominguez-Bello et al., 2016), this procedure was not followed in the studied hospital. These results support the results of previous studies in this field that CS-born babies have poorer flora in their GIT (Hoang et al., 2021).

Other factors such as maternal age, surgical history, social history, obstetrical history, and the number of pregnancies did not associate with the prevalence of Bifidobacteria and Lactobacillus in the infant stool sample. Female infants had a slightly lesser prevalence rate (11.1%) of Lactobacillus compared to male babies (45.5%), but the difference was not (table 1). Although sex differences in gut microbiota have been found in adults (Kim, Unno, Kim, & Park, 2020), the current study did not find a significant influence of gender on compositions of the neonatal gut Lactobacillus and Bifidobacteria.

5. Conclusion

In conclusion, these findings suggest that environmental factors, particularly feeding type and delivery mode, can greatly impact the microbiota composition of newborns. Infants who are born via CS have little chance to obtain Lactobacillus in their gut. Although breast milk is rich in many important microbiotas it becomes less useful when is used along with artificial formula milk. Because of the important roles are played by probiotics in the infants' health, our results support previous studies that administration of probiotic supplements might be recommended for infants with poor gut microbiota which could be due to the mode of delivery and feeding practices.

Acknowledgements

I would like to express my sincere gratitude to the Ministry of Health/ KRG Iraq and the management of Maternity Teaching Hospital-Erbil for their valuable collaboration. I would also like to thank Ms. Ahlam Hami and Ms. Rayan Taha for helping with sample collections.

References

Abrahamsson, T. R., Sinkiewicz, G., Jakobsson, T., et al. 2009. Probiotic lactobacilli in breast milk and infant stool in relation to oral intake during the first year of life. *J Pediatr Gastroenterol Nutr.*, **49** (3), pp. 349-354.

Backhed, F., Roswall, J., Peng, Y., et al. 2015. Dynamics and Stabilization of the Human Gut Microbiome during the First Year of Life. *Cell Host Microbe*, **17** (**5**), pp. 690-703.

Collado, M. C., Laitinen, K., Salminen, S., et al. 2012. Maternal weight and excessive weight gain during pregnancy modify the immunomodulatory potential of breast milk. *Pediatr Res*, **72** (1), pp. 77-85.

Costa, M., & Weese, J. S. 2019. Methods and basic concepts for microbiota assessment. *Vet J*, **249** pp. 10-15.

Ding, R. X., Goh, W. R., Wu, R. N., et al. 2019. Revisit gut microbiota and its impact on human health and disease. J Food Drug Anal, 27 (3), pp. 623-631.

Dominguez-Bello, M. G., De Jesus-Laboy, K. M., Shen, N., et al. 2016. Partial restoration of the microbiota of cesarean-born infants via vaginal microbial transfer. *Nat Med*, **22** (3), pp. 250-253.

Dunn, A. B., Jordan, S., Baker, B. J., et al. 2017. The Maternal Infant Microbiome: Considerations for Labor and Birth. MCN Am J Matern Child Nurs, 42 (6), pp. 318-325.

Elsen, L. W. J. v. d., Garssen, J., Burcelin, R., et al. 2019. Shaping the Gut Microbiota by Breastfeeding: The Gateway to Allergy Prevention? *Front Pediatr*, 7 pp. 47.

Fraher, M. H., O'Toole, P. W., & Quigley, E. M. 2012. Techniques used to characterize the gut microbiota: a guide for the clinician. *Nat Rev Gastroenterol Hepatol*, **9** (6), pp. 312-322.

George Kerry, R., Patra, J. K., Gouda, S., et al. 2018. Benefaction of probiotics for human health: A review. *Journal of Food and Drug Analysis*, **26 (3)**, pp. 927-939.

Ho, N. T., Li, F., Lee-Sarwar, K. A., et al. 2018. Meta-analysis of effects of exclusive breastfeeding on infant gut microbiota across populations. *Nat Commun*, 9 (1), pp. 4169.

Hoang, D. M., Levy, E. I., & Vandenplas, Y. 2021. The impact of Caesarean section on the infant gut microbiome. *Acta Paediatr*, **110 (1)**, pp. 60-67.

Kim, Y. S., Unno, T., Kim, B. Y., et al. 2020. Sex Differences in Gut Microbiota. World J Mens Health, 38 (1), pp. 48-60.

Liang, D., Leung, R. K., Guan, W., et al. 2018. Involvement of gut microbiome in human health and disease: brief overview, knowledge gaps and research opportunities. *Gut Pathog*, **10** pp. 3.

Madan, J. C., Hoen, A. G., Lundgren, S. N., *et al.* 2016. Association of Cesarean Delivery and Formula Supplementation With the Intestinal Microbiome of 6-Week-Old Infants. *JAMA Pediatr*, **170** (3), pp. 212-219.

Martin, V., Maldonado-Barragan, A., Moles, L., *et al.* 2012. Sharing of bacterial strains between breast milk and infant feces. *J Hum Lact*, **28** (1), pp. 36-44.

Milani, C., Duranti, S., & Bottacini, F. 2017. The First Microbial Colonizers of the Human Gut: Composition, Activities, and Health Implications of the Infant Gut Microbiota. *Microbiology and molecular biology reviews: MMBR*, **81** (4), pp. e00036-00017

Nakayama, J., Watanabe, K., Jiang, J., et al. 2015. Diversity in gut bacterial community of school-age children in Asia. Sci Rep, 5 pp. 8397.

Penders, J., Thijs, C., Vink, C., et al. 2006. Factors influencing the composition of the intestinal microbiota in early infancy. *Pediatrics*, **118** (2), pp. 511-521.

Qin, J., Li, R., Raes, J., et al. 2010. A human gut microbial gene catalogue established by metagenomic sequencing. *Nature*, **464** (7285), pp. 59-65.

Rinninella, E., Raoul, P., Cintoni, M., et al. 2019. What is the Healthy Gut Microbiota Composition? A Changing Ecosystem across Age, Environment, Diet, and Diseases. *Microorganisms*, 7 (1).

Rodriguez, J. M., Murphy, K., Stanton, C., et al. 2015. The composition of the gut microbiota throughout life, with an emphasis on early life. *Microb Ecol Health Dis*, **26** pp. 26050.

Sanz, Y. 2011. Gut microbiota and probiotics in maternal and infant health. *Am J Clin Nutr*, **94** (6 Suppl), pp. 2000S-2005S.

Shabila, N. P. 2017. Rates and trends in cesarean sections between 2008 and 2012 in Iraq. *BMC Pregnancy Childbirth*, **17** (1), pp. 22.

Soto, A., Martin, V., Jimenez, E., et al. 2014. Lactobacilli and bifidobacteria in human breast milk: influence of antibiotherapy and other host and clinical factors. *J Pediatr Gastroenterol Nutr*, **59** (1), pp. 78-88.

Tanaka, M., & Nakayama, J. 2017. Development of the gut microbiota in infancy and its impact on health in later life. *Allergol Int*, **66** (**4**), pp. 515-522.

Tlaskalova-Hogenova, H., Stepankova, R., Kozakova, H., et al. 2011. The role of gut microbiota (commensal bacteria) and the mucosal barrier in the pathogenesis of inflammatory and autoimmune diseases and cancer: contribution of germ-free and gnotobiotic animal models of human diseases. *Cell Mol Immunol*, 8 (2), pp. 110-120.

Vandenplas, Y., Carnielli, V. P., Ksiazyk, J., et al. 2020. Factors affecting early-life intestinal microbiota development. *Nutrition*, **78** pp. 110812.

West, C. E., Dzidic, M., Prescott, S. L., et al. 2017. Bugging allergy; role of pre-, pro- and synbiotics in allergy prevention. *Allergol Int*, **66** (**4**), pp. 529-538.

ubscription

Jordan Journal of

Biological Sciences

 ${\bf An\ International\ Peer-Reviewed\ Research\ Journal}$



William Co.
Zarga - Jordan

Name:			الاسم:			
Specialty:			التخصص:			
Address:			العنوان:			
صندوق البريد:						
المدينة: الرمز البريدي:						
Country:			الدولة:			
رقم الهاتف Phone:						
رقم الفاكس: Fax No.:						
E-mail:			البريد الإلكتروني:			
طريقة الدفع: Method of payment:						
Amount Enclosed:						
Signature:			التوقيع:			
Cheque should be paid to Deanship of Research and Graduate Stu	ıdies – The I	Hashemite	University.			
	One Y	ear Subscrip	otion Rates			
I would like to subscribe to the Journal	Inside Jordan Outside Jordan					
For	Individuals	JD10	\$70			
☐ One year			*			
☐ Two years	Students	JD5	\$35			
☐ Three years	Institutions	JD 20	\$90			
Correspondence						
Subscriptions and sales:						
The Hashemite University P.O. Box 330127-Zarqa 13115 – Jorda Telephone: 00 962 5 3903333 Fax no.: 0096253903349 E. mail: jjbs@hu.edu.jo	n					

المجلة الأردنية للعلوم الحياتية Jordan Journal of Biological Sciences (JJBS)

http://jjbs.hu.edu.jo

المجلة الأردنية للعلوم الحياتية: مجلة علمية عالمية محكمة ومفهرسة ومصنفة، تصدر عن الجامعة الهاشمية وبدعم من صندوق دعم البحث العلمي والإبتكار – وزراة التعليم العالي والبحث العلمي.

هيئة التحرير

رئيس التحرير

مساعد رئيس التحرير

الدكتور مهند عليان مساعدة الجامعة الهاشمية، الزرقاء، الأردن

الأعضاء:

الاستاذ الدكتور ليث ناصر العيطان جامعة العلوم و التكنولوجيا الأربنية

الأستاذ الدكتور وسام محمد هادي الخطيب الجامعة البرموك

الاستاذ الدكتور نضال احمد عودات جامعة البلقاء التطبيقية

الأستاذ الدكتور خالد محمد خليفات جامعة مؤتة

الأستاذ الدكتورة منار فايز عتوم

الجامعة الهاشمية، الزرقاء، الأردن

الأستاذ الدكتورة طارق حسن النجار الجامعة الأرينية / العقية

الاستاذ الدكتور عبد اللطيف علي الغزاوي المجامعة الهاشمية

فريق الدعم:

المحرر اللغوي

الدكتور شادي نعامنة

ترسل البحوث الى العنوان التالى:

رئيس تحرير المجلة الأردنية للعلوم الحياتية

الجامعة الهاشمية

ص.ب, 330127, الزرقاء, 13115, الأردن

هاتف: 0096253903333

E-mail: jjbs@hu.edu.jo, Website: www.jjbs.hu.edu.jo

تنفيذ وإخراج

م. مهند عقده









للعلوم الحياتية

قمكمه قيمالا قيملا قليم

تحدر بدعم من حندوق دعم البحث العلمي و الابتكار

